

**Mimicking developmental biology to regenerate  
the intervertebral disc**

**Frances Bach**

Mimicking developmental biology to regenerate the intervertebral disc  
Frances Bach  
PhD thesis, Utrecht University, Faculty of Veterinary Medicine, the Netherlands

ISBN: 978-90-393-6944-9

Cover: Ary Bekx, beeld van iStock  
Layout: Frances Bach, Mieke de Wit  
Printing: GVO drukkers & vormgevers B.V., Ede

Copyright © F.C. Bach, 2018. All rights reserved. No part of this thesis may be reproduced, stored in a retrieval system of any nature or transmitted in any form or by any means, without prior written consent of the author. The copyright of the articles that have been published has been transferred to the respective journals.

# **Mimicking developmental biology to regenerate the intervertebral disc**

Regeneratie van de tussenwervelschijf door de ontwikkelingsbiologie  
na te bootsen

(met een samenvatting in het Nederlands)

## **Proefschrift**

ter verkrijging van de graad van doctor aan de Universiteit Utrecht op gezag  
van de rector magnificus, prof.dr. G.J. van der Zwaan, ingevolge het besluit van  
het college voor promoties in het openbaar te verdedigen op donderdag  
22 maart 2018 des middags te 2.30 uur

door

**Frances Claudine Bach**

geboren op 8 november 1985 te Zwolle

**Promotoren:**

Prof.dr. B.P.Meij

Prof. dr. K.Ito

**Copromotor:**

Dr. M.A. Tryfonidou

Publication of this thesis was financially supported by generous gifts from the Dutch Arthritis Foundation (IDiDAS, LLP-12, LLP-22), AOSpine International (SRN2011\_11, Consortium award 109933), Elanco Animal Health BeNeLux, Royal Canin Nederland B.V., Annafonds te Leiden, Nederlandse Vereniging voor Matrix Biologie, Stichting Nederlandse Databank Gezelschapsdieren, Boehringer Ingelheim Animal Health, Greiner Bio-One BV, and Merck Millipore.

# Contents

<b>Chapter 1</b>	General introduction, aims and outline of this thesis	<b>7</b>
<b>Part I. Notochordal cell-based therapies</b>		
<b>Chapter 2</b>	The species-specific regenerative effects of notochordal cell-conditioned medium on chondrocyte-like cells derived from degenerated human intervertebral discs	<b>33</b>
<b>Chapter 3</b>	Soluble and pelletable factors in porcine, canine, and human notochordal cell-conditioned medium: implications for IVD regeneration	<b>57</b>
<b>Chapter 4</b>	Notochordal-cell derived extracellular vesicles exert regenerative effects on canine and human nucleus pulposus cells	<b>85</b>
<b>Chapter 5</b>	Biologic IVD repair by Notochordal Cell Matrix: from bench towards bedside	<b>109</b>
<b>Part II. Growth factor-based therapies</b>		
<b>Chapter 6</b>	Intradiscal application of rhBMP7 does not induce regeneration in a canine model of spontaneous intervertebral disc degeneration	<b>147</b>
<b>Chapter 7</b>	Bone morphogenetic protein-2, but not mesenchymal stromal cells, exert regenerative effects on canine and human nucleus pulposus cells	<b>171</b>
<b>Chapter 8</b>	Link-N: the missing link towards intervertebral disc repair is species-specific	<b>193</b>
<b>Chapter 9</b>	Increased caveolin-1 in intervertebral disc degeneration facilitates repair	<b>221</b>
<b>Part III. What can we learn from developmental biology?</b>		
<b>Chapter 10</b>	The paracrine feedback loop between vitamin D <sub>3</sub> (1,25(OH) <sub>2</sub> D <sub>3</sub> ) and PTHrP in prehypertrophic chondrocytes	<b>249</b>
<b>Chapter 11</b>	IHH and PTHrP are implicated in degeneration of the intervertebral disc	<b>285</b>
<b>Chapter 12</b>	Summarizing discussion	<b>323</b>
<b>Addendum</b>	Dutch summary/Nederlandse samenvatting	<b>339</b>
	List of abbreviations	<b>347</b>
	Acknowledgements/Dankwoord	<b>351</b>
	Curriculum vitae	<b>357</b>

## **This thesis is based on the following publications:**

- 1) **Bach FC**, Willems N, Penning LC, et al. 2014. Potential regenerative treatment strategies for intervertebral disc degeneration in dogs. *BMC Vet Res* 10: 3-6148-10-3. 12. **Q1 – IF 1.777**
- 2) **Bach FC**, de Vries SA, Krouwels A, et al. 2015. The species-specific regenerative effects of notochordal cell-conditioned medium on chondrocyte-like cells derived from degenerated human intervertebral discs. *Eur Cell Mater* 30: 132-46. **Q1 – 4.560**
- 3) **Bach FC**, de Vries SA, Riemers FM, et al. 2016. Soluble and pelletable factors in porcine, canine and human notochordal cell-conditioned medium: Implications for IVD regeneration. *Eur Cell Mater* 32: 163-180. **Q1 – IF 4.633**
- 4) **Bach FC**, Libregts SFWM, Creemers LB, et al. 2017. Notochordal-cell derived extracellular vesicles exert regenerative effects on canine and human nucleus pulposus cells. *Oncotarget* 8 (51): 88845-88856 **Q1 – 5yIF: 5.415**
- 5) Willems N, **Bach FC**, Plomp SG, et al. 2015. Intradiscal application of rhBMP-7 does not induce regeneration in a canine model of spontaneous intervertebral disc degeneration. *Arthritis Res Ther* 17: 137-015-0625-2. **Q2 – IF: 3.979**
- 6) **Bach FC**, Miranda-Bedate A, van Heel FW, et al. 2017. Bone morphogenetic protein-2, but not mesenchymal stromal cells, exert regenerative effects on canine and human nucleus pulposus cells. *Tissue Eng Part A* 23: 233-242. **Q1 – 5yIF: 4.451**
- 7) **Bach FC**, Laagland L, Grant MP, et al. 2017. Link-N: the missing link towards intervertebral disc repair is species-specific. *PLoS ONE* 12(11): e0187831. **Q1 – 5yIF: 3.543**
- 8) **Bach FC**, Zhang Y, Miranda-Bedate A, et al. 2016. Increased caveolin-1 in intervertebral disc degeneration facilitates repair. *Arthritis Res Ther* 18: 59-016-0960-y. **Q2 - 4.121**
- 9) **Bach FC**, Rutten K, Hendriks K, et al. 2014. The paracrine feedback loop between vitamin D(3) (1,25(OH)(2)D(3)) and PTHrP in prehypertrophic chondrocytes. *J Cell Physiol* 229: 1999-2014. **Q1 – IF 3.839**

**General introduction, aims and outline of this thesis**

**Emerging regenerative treatment strategies for  
intervertebral disc degeneration**

Part of this chapter has been published as:

**Potential regenerative treatment strategies for intervertebral disc degeneration in dogs**

Frances C. Bach<sup>1</sup>, Nicole Willems<sup>1</sup>, Louis C. Penning<sup>1</sup>, Keita Ito<sup>2,3</sup>, Björn P. Meij<sup>1</sup>, Marianna A. Tryfonidou<sup>1</sup>

<sup>1</sup>Department of Clinical Sciences of Companion Animals, Faculty of Veterinary Medicine, Utrecht University, Utrecht, the Netherlands

<sup>2</sup>Department of Biomedical Engineering, Eindhoven University of Technology, Eindhoven, the Netherlands

<sup>3</sup>Department of Orthopedics, University Medical Centre Utrecht, Utrecht, the Netherlands

*Published as 'highly accessed' invited review, BMC Veterinary Research (2014) 10*

# 1

## Low back pain and intervertebral disc degeneration

The intervertebral disc (IVD) arises from the embryonic notochord and mesenchyme and develops into a complex tissue that permits movement between vertebrae and provides flexibility and integrity to the spine<sup>1</sup>. The IVD consists of the vertebral endplates (EPs), the annulus fibrosus (AF), and the nucleus pulposus (NP) (Figure 1). The AF contains concentric lamellae mainly composed of collagen type I, elastin fibers, and fibroblast-like cells. Together with the hyaline cartilage EPs, it encloses the bean-shaped NP<sup>2,3</sup>. By enabling diffusion and permeability, the EPs play an essential role in NP nutrient delivery, since the latter has no direct blood supply<sup>2</sup>. The NP contains a highly hydrated gelatinous matrix, mainly composed of proteoglycan and collagen type II<sup>2</sup>. Cations, which are attracted to the negatively charged proteoglycans, create a strong osmotic gradient that draws water molecules into the NP<sup>2</sup>. During early development, the NP contains a relatively large amount of cells and a small amount of extracellular matrix (ECM), whereas the ECM/cell ratio is high in the healthy, mature NP<sup>3,4</sup>. In the young and healthy NP, notochordal cells (NCs) are the main cell type present. During IVD maturation, vacuolated NCs are replaced by non-vacuolated CLCs and in the transitional NP, a mixture of chondrocyte-like cells (CLCs) and NCs is present. In early IVD degeneration, CLCs are the main cell type present in the NP (Figure 1). In the human NP, the replacement of NCs by CLCs already starts during childhood.

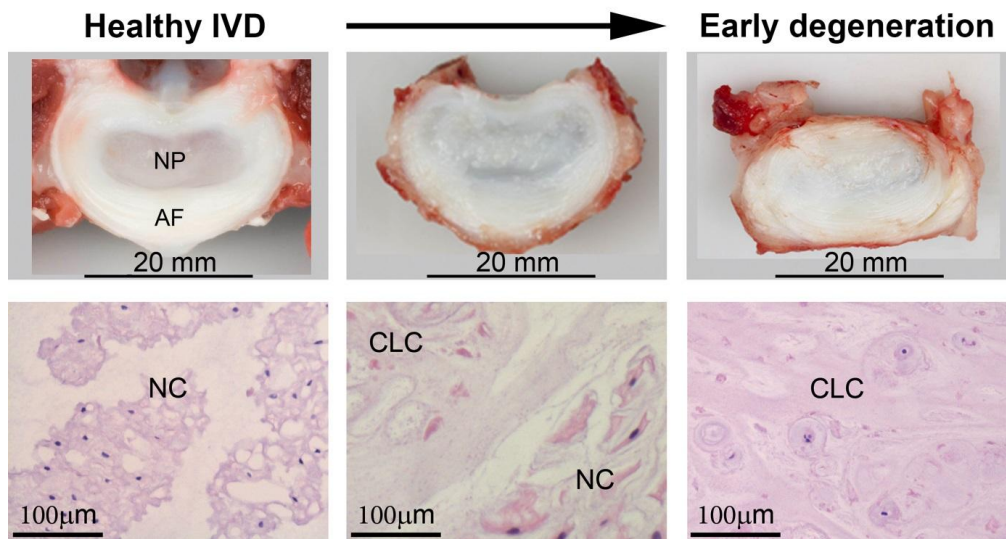


**Figure 1. The transition from a healthy to an early degenerated canine intervertebral disc.** Macroscopic and microscopic images showing a healthy intervertebral disc (IVD) (left), and the transition (middle) into an early degenerated IVD (right). The healthy IVD (upper left) consists of a well-distinguished lamellar annulus fibrosus (AF) and a bean-shaped nucleus pulposus (NP). During disc degeneration, the distinction between AF and NP becomes less clear (upper middle and right). In the healthy canine NP, notochordal cells (NCs) are the main cell type present (lower left), whereas in the transitional NP, a mixture of chondrocyte-like cells (CLCs) and NCs is present (lower middle). In early canine IVD degeneration, CLCs are the main cell type present in the NP (lower right).

Degeneration of the IVD is marked by changes in cell number and cell type, but is also characterized by changes in the biochemical composition and mechanical integrity<sup>2,4</sup>. The glycosaminoglycan (GAG, a proteoglycan side chain) content decreases and catabolic matrix metalloproteinase (MMP) activity and disorganized collagen content increases - the latter creating a more rigid IVD matrix<sup>2,5</sup>. Matrix repair is impaired in the avascular IVD, resulting in weakening and increased vulnerability to damage by physiologic loading. A vicious circle of continuous damage and inadequate repair develops, leading to disc degeneration rather than healing. Once the degenerative process starts, it is progressive<sup>6</sup>. The decrease in GAG content, and subsequent dehydration, causes a decrease in disc height<sup>7</sup>. Compressive forces cause increased loading on the AF, generating a concave bending load on the AF and EPs. This change in the direction of loading forces is considered to be responsible for AF tearing, EP fracturing, and/or disc herniation. Herniation usually occurs on the dorsal side, because the ventral part of the AF is two to three times thicker than the dorsal part and because the vertebral column is normally more flexed than extended, resulting in higher tension in the dorsal part than in the ventral part<sup>2</sup>.

Like humans, dogs suffer from spontaneous IVD degeneration with similar characteristics and therefore, the dog is considered to be a suitable animal model for IVD degeneration in humans<sup>8</sup>. In both species, IVD degeneration can be asymptomatic, however, symptoms (humans) or clinical signs (dogs) may arise from the degenerated IVD itself and/or surrounding tissues (bone, cartilage, ligaments, neural tissue) ultimately leading to IVD disease. In dogs, IVD disease due to degeneration is a relatively common reason for euthanasia<sup>8</sup>. IVD degeneration impairs the function of the spinal unit (IVD, EPs, ligaments, facet joints and vertebral body), causing secondary osteoarthritic changes, bone sclerosis/spondylosis, and neurological signs and deficits due to spinal cord or nerve root compression<sup>9</sup>. Owners of dogs may report unilateral or bilateral lameness or paresis/paralysis, toe dragging, low tail or neck carriage, difficulties with rising, sitting or lying down, reluctance to jump or climb, urinary or fecal incontinence, and hyperesthesia or self-mutilation<sup>10</sup>. Furthermore, pain is evoked by pressure applied to the affected spinal region during the clinical examination by veterinary specialists<sup>10</sup>.

Dog breeds can be divided into chondrodystrophic (CD) and non-chondrodystrophic (NCD) breeds based on their physical appearance which coincides with a different clinical representation. In CD dog breeds (*e.g.* Beagles and Dachshunds), IVD disease typically develops in the cervical (C2-C6) or thoracolumbar (T11-L3) spine at about 3-7 years of age<sup>5</sup>. These CD dog breeds have short bowlegs due to disrupted endochondral ossification, which has strongly been linked with IVD degeneration<sup>5</sup>. NCD dog breeds, especially large breeds, can also develop IVD disease, but in the caudal cervical (C5-T1) or lumbosacral (L6-S1) spine at about 6-8 years of age, mostly due to trauma or "wear and tear"<sup>5,8</sup>. The macroscopic, histopathological, and biochemical changes as well as the diagnostics and treatment of IVD disease are rather similar in NCD and CD dogs<sup>5,8</sup>. Typically, in mature healthy CD dogs, histological examination of the IVD shows clear evidence of degeneration in the NP, but a completely normal lamellar structure of the AF<sup>11</sup>. Excessive loading may ultimately lead to failure of the lamellar structure and rupture of the AF resulting in NP herniation. However, sequestration of the NP in the spinal canal through an AF rupture may induce further IVD degeneration. In NCD dogs, bulging of the IVD due to gradual degeneration of both the NP and AF is often encountered.

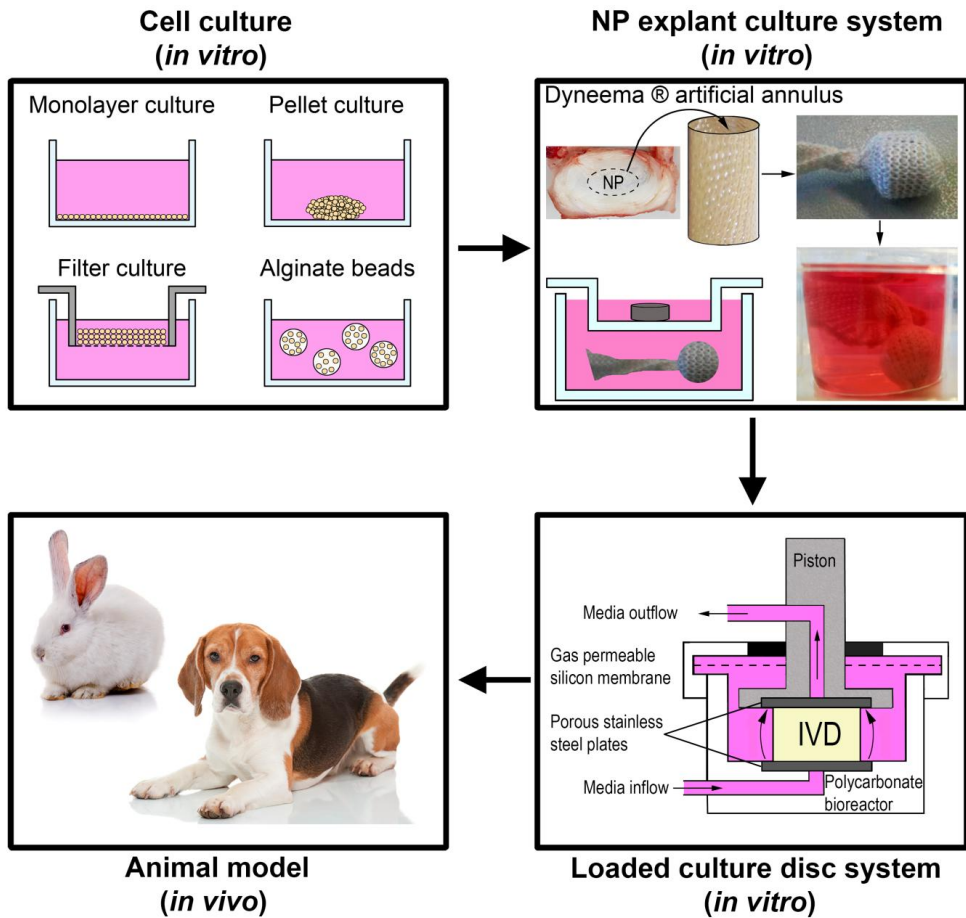


**Figure 2. Regenerative treatment strategies for intervertebral disc (IVD) degeneration.** Upper left: *in vitro* cell cultures: monolayer (2D), pellet cell culture (3D), filter cell culture (3D), and cell-containing alginate beads (3D). Upper right: the *in vitro* nucleus pulposus (NP) explant culture system, in which the NP is cultured in an artificial annulus system. As the artificial annulus may be buoyant, a stainless steel cylinder is added to keep the NP submerged. Lower right: the *in vitro* loaded culture disc system, in which intact IVD explants are cultured under loading conditions with preservation of biological and structural integrity. Lower left: *in vivo* animal models, e.g., the rabbit, in which IVD degeneration is often experimentally induced, and the Beagle (chondrodystrophic dog breed), which develops spontaneous IVD degeneration from 1 year of age (right). Pictures of the rabbit and Beagle are obtained from Depositphotos (<http://depositphotos.com>).

Current treatments for IVD disease in both humans and dogs focus on alleviating pain and include physiotherapy, anti-inflammatory/analgesic medication, and surgery. The aim of surgery for IVD disease is to relieve the compression of neural structures, and procedures in dogs include removal of the NP (nucleotomy) through fenestration of the AF alone or combined with partial removal of the vertebral roof (laminectomy) or vertebral body (ventral decompression)<sup>12</sup>. Above mentioned therapies may resolve neurological deficits and reduce pain (although in many cases insufficient), but they do not lead to repair of the

degenerated IVD. In fact, long-term medication can cause side-effects, surgery can lead to spinal instability and adjacent segment disease, and recurrence of IVD disease may occur<sup>12</sup>. Therefore, there is increasing interest in regenerative therapies aimed at the biological repair of the degenerated IVD, including cell-based strategies and the use of growth factors or gene therapy. The specific aim of these therapies is to repair the degenerated disc matrix and in this way, restore the biomechanical function of the IVD<sup>13, 14</sup>. Research in the field of regenerative medicine increases our understanding of disease processes and findings may ultimately be translated into therapeutic interventions for both veterinary and human patients. The focus of this chapter is to discuss potential regenerative treatment strategies for IVD degeneration, with specific emphasis on cell-based strategies.

## Models to develop new regenerative treatment strategies for IVD degeneration

Regenerative treatment options are developed *in vitro* and then extrapolated to *in vivo* animal models before being used in the clinic. Commonly used *in vitro* cell culture models are 2D monolayer and 3D cell pellet/micro-aggregate culture, filter cell culture, or alginate bead cell culture (Figure 2). A major disadvantage of these *in vitro* models, however, is that the native tissue environment is lost during cell isolation, which might affect cell behaviour<sup>15</sup>. Thus, cell culture experiments may not adequately represent the *in vivo* situation, and care should be taken when interpreting the results of such studies. For this reason, tissue explant systems have been developed, in which an environment is created that more accurately resembles the *in vivo* situation<sup>16</sup>. However, a drawback of NP explants is that swelling pressure is no longer balanced by the AF and hyperosmolarity within the NP is difficult to maintain, which results in NP tissue swelling. A special fiber jacket (artificial annulus) has been developed to mimic the AF in the so-called NP explant system, creating a physiological model to test the efficacy of regenerative therapies for IVD degeneration<sup>15, 17</sup>. To mimic the *in vivo* situation even closer, whole organ culture bioreactor systems, *e.g.* the loaded culture disc system, have been developed, in which intact IVD explants, including AF, NP, and EPs, are kept alive under loading conditions for as long as six weeks with preservation of biological and structural integrity<sup>18, 19</sup>. The last step for validating regenerative medicine treatment strategies involves the use of *in vivo* animal models. Models based on mice, rats, rabbits, goats, and dogs with experimentally induced IVD degeneration have often been used<sup>20</sup>, but these animals, with the exception of dogs, do not spontaneously develop IVD degeneration and disease. Interestingly, some *in vivo* IVD regeneration studies have been performed with laboratory dogs with experimentally induced IVD degeneration<sup>21-26</sup>. To our knowledge, dogs with naturally occurring IVD degeneration have not been widely used, even though it is recognized that CD dog breeds are a suitable animal model of spontaneous IVD degeneration<sup>8, 13</sup>. Only recently, one study investigated the (regenerative) effect of intradiscally injected mesenchymal stromal cells (MSCs) in NCD canine patients with spontaneously developed IVD disease<sup>27</sup>.

# 1

## Regenerative treatment options

### Cell-based therapies

The synthesis of healthy NP matrix can be stimulated by means of growth factors and/or gene therapy. However, since cell viability is impaired in the degenerated IVD, stimulation of the remaining cells may be insufficient to achieve repair<sup>13</sup>. Cell-based therapies may overcome this problem (Figure 3). Thus far, cell-based treatment strategies have mainly used CLCs, MSCs, and NCs<sup>13</sup>. These cell types are discussed below with regard to their characteristics, effectiveness, benefits, and drawbacks.

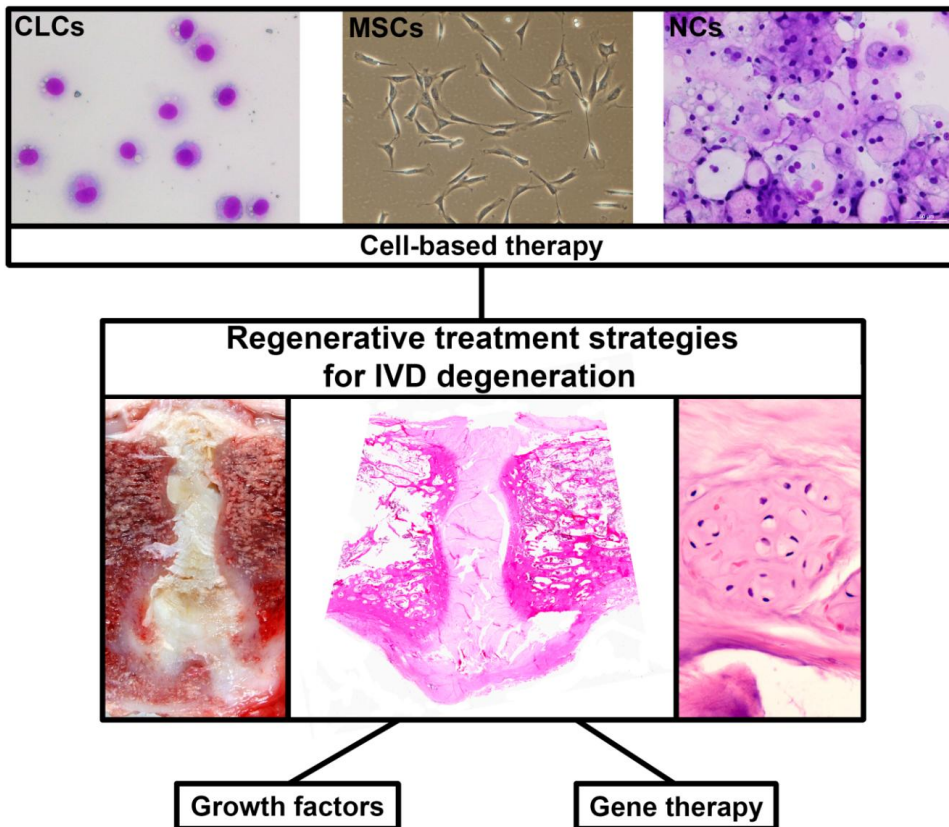


**Figure 3. Regenerative treatment options for intervertebral disc (IVD) degeneration: cell-based therapy, growth factors, and gene therapy.** Cell-based treatment strategies have mainly used chondrocyte-like cells (CLCs), mesenchymal stromal (stem) cells (MSCs), and notochordal cells (NCs). The lower images show a severely degenerated IVD macroscopically (left) and on haematoxylin & eosin staining (middle and right). The lower right image shows a cluster of CLCs, which are frequently observed in (severely) degenerated IVDs.

### *Chondrocyte-like cells (CLCs)*

The cells found in the human adult and degenerating NP are similar, but not identical, to articular chondrocytes and are therefore termed chondrocyte-like cells<sup>28</sup>. Insertion of autologous and allogeneic CLCs in the NP has been shown to retard IVD degeneration in various species without inducing any appreciable host-versus-graft response<sup>21, 29, 30</sup>. This is in line with the notion that the IVD is immune privileged due to its avascularity<sup>31</sup> and the expression of Fas ligand (FasL), which induces apoptosis of invading Fas-bearing T-cells<sup>24, 32</sup>.

Although CLCs have regenerative potential, the severity of IVD degeneration can limit their regenerative capacity. Degenerated CLCs may lose specific characteristics (e.g. their chondrogenic potential), making them less suitable for tissue engineering purposes. CLC transplantation has its limitations because these cells can only be obtained from herniated discs, cell numbers are low, and extensive expansion before transplantation is needed<sup>33</sup>. Preconditioning expanding CLCs with AF cells, however, improved the performance of CLCs in a rabbit IVD degeneration model<sup>34</sup>. Also, co-culture of CLCs with MSCs enhanced the biological activity and viability of CLCs *in vitro*, as evidenced by increased cell proliferation and matrix synthesis<sup>33, 35-40</sup>. The latter is consistent with the well-known beneficial effect of MSCs on articular chondrocytes<sup>41</sup>.

### *Mesenchymal stromal (stem) cells (MSCs)*

NP-derived cells are of limited availability<sup>42</sup> and, therefore, current regenerative strategies focus on stem cells, particularly MSCs. MSCs are emerging as a leading cellular therapy for several diseases, since they can easily be isolated from a variety of tissues, including bone marrow, adipose and synovial tissue, muscle, placenta, and umbilical cord blood. MSCs can differentiate into different cell types, such as osteoblasts, adipocytes, chondrocytes, myocytes, and neural cells<sup>43, 44</sup>, depending on their environment<sup>6</sup>. In addition, MSCs have immunosuppressive properties and secrete trophic/growth factors (anti-apoptotic, stimulation of proliferation and differentiation) that support regenerative processes<sup>44-46</sup>. The unique combination of these properties makes MSCs highly suitable for tissue replacement therapies.

*In vivo* intradiscally injected MSCs have been shown to maintain their viability and proliferate within the IVD<sup>47</sup>. Bone marrow-derived stem cell (BMSC) transplantation was found to counteract IVD degeneration and/or increase the proteoglycan content of IVDs in experimental rabbit and mouse models<sup>6, 31, 48-51</sup>. Adipose-derived stem cell (ASC) and BMSC delivery has also been shown to promote disc regeneration in an experimentally induced IVD degeneration in (Beagle<sup>24</sup>) dogs<sup>25</sup>. In addition, MSCs may be responsible for sustaining the IVD immune privilege by differentiating into cells expressing FasL<sup>24</sup>. The optimal number of BMSCs for intradiscal delivery (4 weeks after NP aspiration) was estimated in Beagles, based on the survival rate and apoptosis of CLCs in BMSC-injected IVDs<sup>26</sup>. In IVDs injected with 10<sup>6</sup> MSCs, the microenvironment and ECM abundance was maintained, whereas the injection of fewer cells (10<sup>5</sup> MSCs) resulted in fewer viable cells and the injection of more cells (10<sup>7</sup> MSCs) resulted in more apoptotic cells<sup>26</sup>. The intradiscal injection of 2 x 10<sup>6</sup> BMSCs in NCD dogs with spontaneously developed degenerative IVD disease, however, did not have evident regenerative effects<sup>27</sup>. The latter can be attributed to methodological aspects, including cell concentration and injection volume, the size of the needle and the pressure applied to the IVD during injection.

1 Despite the overall promising experimental studies and clinical trials, there is uncertainty about the chondrogenic differentiation of MSCs. Can MSCs differentiate into CLCs instead of hyaline articular chondrocytes? MSCs have been reported to undergo chondrocytic differentiation and form repair tissue that resembles hyaline cartilage during *in vitro* studies or after transplantation into the NP<sup>31, 52</sup>. Morphologically, both articular cartilage and NP tissue consist of chondrocyte(-like cells) surrounded by ECM, but there are considerable differences in composition and biomechanical function<sup>53</sup>. Properly differentiated MSCs should therefore express notochord/NP specific marker genes, *e.g.* Paired Box Protein 1 (PAX1) and Forkhead box F1 (FOXF1) and have a proteoglycan:collagen ratio closer to that of NP tissue than that of hyaline articular cartilage<sup>53-57</sup>.

Healthy and degenerated NPs of various species, including dogs, have been reported to contain multipotent NP progenitor cells (NPPCs)<sup>9, 28, 58, 59</sup>. These NPPCs express genes typical for stem cells, but differ from MSCs in the higher expression of the *Nanog* “stemness” gene<sup>9</sup>. NPPCs are able to differentiate into the chondrogenic lineage *in vitro*, and to survive in the aneural, avascular, hypoxic NP<sup>9, 14</sup>. Thus, NPPCs might be appropriate for developing regenerative strategies to treat IVD degeneration.

#### *Notochordal cells (NCs)*

The notochord is a mesodermal, curved rod-like structure that defines the primitive axis of the body and serves as the center of development of the axial skeleton during embryogenesis. Notochordal signals generate a mesenchymal peri-notochordal sheath, which eventually gives rise to the AF, EPs, and vertebral bodies<sup>7</sup>. The notochord condenses within the primitive AF to form the NP<sup>1, 4</sup>. The composition of the NP changes as the IVD matures: the number of cells of notochordal origin decreases and the smaller CLCs increase in number<sup>4</sup> (Figure 1). NCs are characterized by their morphology: they are large and have cytoplasmic vesicles, the content and function of which are still debated<sup>7</sup>. NCs are usually found in clusters and secrete matrix rich in proteoglycan and collagen type II<sup>2</sup>. They have considerable regenerative potential and restorative capacity for other cells (CLCs and MSCs), which makes them an interesting focus for regenerative strategies.

Loss of the NC population is associated with the development of IVD degeneration<sup>60</sup>, and thus restoring the NC population may help to delay or even reverse IVD degeneration<sup>14</sup>. The NC population undergoes species-specific changes<sup>4, 7</sup>. Most studies report that in humans, NCs disappear when they are about 7-10 years of age, whereas the age of onset of disc degeneration is 30–50 years<sup>7</sup>. This means that CLCs also reside in healthy human IVDs. However, in dogs, NCs are replaced by CLCs at about 1 year of age in CD breeds, but remain the predominant cell type until middle/old age in NCD breeds<sup>4, 5, 14</sup>. In general, NCs are not present in degenerated canine IVDs.

Interestingly, intradiscal MSC injection increased the number of NCs and matrix deposition in murine degenerated IVDs<sup>31</sup>. This suggests that MSCs can promote NC proliferation and/or prevent NC apoptosis and that the anabolic NC function can be stimulated by MSCs. Taking into consideration the recently described NPPC population (which shows stem cell characteristics) in healthy and degenerated IVDs, it is tempting to hypothesize that NPPCs may be in cross-talk with resident NCs and have a functional role in the differentiation and maintenance of NCs.

The question arises: What is the role of NCs in the IVD degeneration process and hence their potential function in IVD regeneration? The NCs may have a dual regenerative role: they may instruct CLCs and/or replenish by differentiating into CLCs. NCs may serve as 'organizer' cells, influencing the surrounding NP-cell homeostasis to maintain NP integrity. It seems reasonable to consider NCs as a potential source of growth factors that stimulate NP matrix synthesis<sup>61-65</sup>, given the signaling role of the notochord during embryonic development<sup>42</sup>. NC-conditioned medium (NCCM; medium in which NCs or NC-containing tissue is cultured for four days and comprises NC-secreted soluble factors) has the potential to increase NP GAG production and/or cell proliferation *in vitro* and *in vivo*<sup>63-69</sup>. Furthermore, both NCCM and CLC+NC co-culture stimulate the *in vitro* differentiation of MSCs into a NP-like phenotype with a high chondrogenic matrix production<sup>37, 40, 43, 61, 62, 68, 70, 71</sup>. NCs may maintain the young NP phenotype by secreting factors that suppress cell death<sup>72</sup> and by influencing genes that regulate IVD anabolic activity and matrix protection<sup>73</sup>. Attempts have been made to identify, isolate, and/or synthesize the bioactive factors in NCCM for use in therapeutic interventions<sup>63</sup>. NCCM may exert its effects in several ways: through extracellular matrix components such as GAGs<sup>74</sup> and/or through growth factors. Factors that were already found are connective tissue growth factor (CTGF)<sup>66, 75</sup>, transforming growth factor- $\beta_1$  (TGF- $\beta_1$ ), Wnt-induced soluble protein 2, insulin-like growth factor binding protein 7, and angiopoietin-like 7<sup>66</sup> in canine NCCM, and CTGF<sup>76</sup>, alpha-2-macroglobulin, clusterin, and tenascin<sup>62</sup> in porcine NCCM. Affirmatively, CTGF has been shown to promote matrix production, proliferation, differentiation, and cell migration and to inhibit apoptosis, effects that prevent the development of IVD degeneration<sup>66, 75, 77, 78</sup>.

The exact mechanism how NCs exert their trophic effects remains to be determined. NCs contain large vacuoles, which may be related to extracellular vesicles (EVs). Recently, EVs, small lipid bilayer-enclosed particles released by all cell types, have attracted attention as potential targets for the development of regenerative therapies<sup>79</sup>. EVs serve in intercellular signaling, since they are protective carriers for biologically active molecules (*e.g.* mRNA, microRNA, DNA, protein, lipid). They are either formed by direct budding from the cell membrane or by fusion of endosomal-derived multivesicular bodies with the cell membrane<sup>80</sup>. The EV membrane contains proteins and lipids that enable cell adherence. Interaction between EVs and target cells can occur via several routes: direct fusion with the plasma membrane, thereby releasing their cargo, ligand binding at a receptor located at the plasma membrane for pathway activation, or endocytosis and fusion with intracellular compartments<sup>81, 82</sup>. Also, soluble factors can bind to the EV membrane for transport towards target cells<sup>83</sup>. In above mentioned ways, EVs play an important role in tissue (patho)physiology and may transport regenerative factors towards diseased tissue. It remains to be elucidated what role EVs play in degeneration and regeneration of the IVD. Specifically, NC-derived EVs are of interest from a developmental and therapeutic perspective.

Moreover, NCs are also considered to be 'progenitors' of the CLC population. It is much debated whether the chondrification of the maturing IVD is due to the differentiation of NCs into a CLC-like phenotype (stem cell function) or apoptosis of the NCs followed by invasion of CLCs from other locations, *e.g.* the EPs and/or inner AF<sup>28, 60</sup>. There are several arguments for and against the notion that NCs are CLC progenitor cells. The first argument that disputes the progenitor function is the considerable difference in cell morphology and size of CLCs

1 (17-23  $\mu\text{m}$ ) and NCs (25-85  $\mu\text{m}$ )<sup>1,7</sup>. Secondly, NCs and NCCM are both able to stimulate the migration of EP chondrocytes<sup>84</sup>, which makes the NC organizer function more likely than the progenitor function. Thirdly, two cell types have been detected in the developing notochord: large vacuolated cells, resembling NCs, and smaller non-vacuolated cells, resembling CLCs<sup>85</sup>. Thus, the presumed origin of NP tissue, i.e. the notochord, seems to contain cells that appear similar to those detected in the NP itself. Fourthly, the gene expression profile is different in NCs and CLCs, which also opposes the progenitor function status of NCs<sup>86</sup>. Fifthly, the self-renewal of NCs occurs infrequently and is not unlimited, aspects that oppose the stem/progenitor cell function<sup>60</sup>. Lastly, *Brachyury* expression - often considered a marker for NCs and required for the differentiation of mesoderm into notochord<sup>3</sup> - was not detected in the human adult NP, which may argue against the hypothesis that both NC and CLCs are derived from the notochord<sup>87</sup>. The expression of this NC marker can, however, simply be lost during (trans)differentiation of NCs into CLCs.

In contrast, there are several arguments in favor of the NC progenitor theory. Firstly, NCs decrease and CLCs increase in number during ageing and disc degeneration, which could be explained by the transformation of NCs into CLCs<sup>1</sup>. Histological and automated live cell-imaging studies of degenerated IVDs show that NCs can differentiate into cells morphologically similar to CLCs<sup>60,88</sup>. Secondly, NCs have the ability to renew themselves *in vitro*<sup>60</sup>. Thirdly, chondrocyte volumes can vary about 10-fold in the growth plate, which counteracts the argument that the differences in cell size are too large for NCs to be a progenitor for CLCs. This variation in cell morphology and size can be explained by different maturation stages and/or cell function<sup>1,3</sup>. Porcine NCs have been shown to exhibit a significant variation in cell morphology, size, and number<sup>89</sup>, implying that NC morphology can change with time. Fourthly, it is known from growth plate chondrocytes that, within a single cell population, cells of different sizes and/or location can express different gene profiles, which could explain the difference in gene expression profiles between NCs and CLCs<sup>1,3</sup>. In fact, gene expression of NCs and CLCs showed substantial overlap, and *Brachyury* expression remained constant during IVD degeneration when NCs were replaced by CLCs<sup>60,90</sup>. Fifthly, NCs and CLCs have been shown to synthesize proteoglycans at the same rate<sup>60</sup>, which indicates that they have a comparable capacity to produce matrix. In contrast, others found that NCs synthesized proteoglycans at significantly greater rates than CLCs<sup>91</sup>. However, in this study, the CD dogs (donors of the CLCs) were older and had a higher disc degeneration grade than the NCD dogs (donors of the NCs), which could have influenced the study outcomes. Sixthly, trace lineage studies indicate that both NCs and CLCs are derived from the embryonic notochord, suggesting that NCs are precursors of CLCs<sup>92,93</sup>. Lastly, there is as yet no marker that is homogeneously and uniquely expressed within a specific population (NC or CLC) and, therefore, it is impossible to state that both cells of notochordal and mesenchymal origin are present within the IVD<sup>1,3</sup>.

There are some points of interest concerning the design of experiments investigating NC-based regenerative strategies for the treatment of IVD degeneration. Some species retain NCs throughout life, whereas others lose them during development and ageing, which may considerably influence experimental outcomes. Most studies report that NCs are present in skeletally mature non-chondrodystrophic dogs, pigs, ferrets, rabbits, rats, and mice<sup>4,5,7,42</sup>, whereas in chondrodystrophic dogs, goats, horses, cows, and sheep, they disappear before skeletal maturity is reached<sup>4,5,7,94</sup>. In contrast, others favor the hypothesis that in all animal

species, including humans, NCs remain in the NP throughout life, although their phenotype may change with age and disease<sup>3</sup>. It is important that inter-species differences are taken into consideration and that research results are interpreted with care. Furthermore, NC isolation has the disadvantage of a low purity or yield<sup>60</sup>, which is further complicated by the lack of specific markers for NCs<sup>7</sup>. *Brachyury*, and *Cytokeratin 8* or *19* have been proposed as NC markers<sup>3,95,96</sup> but they are not very specific and show interspecies variation<sup>90</sup>. Additional obstacles are the slow growth of NCs and their sensitivity to the external environment<sup>60</sup>. It is essential that culture conditions are optimized, so that NCs do not lose their characteristics. Thus far, culture media pH, glucose concentration, osmolality, and O<sub>2</sub> and CO<sub>2</sub> percentages have been shown to affect maintenance of the NC-phenotype in culture<sup>78,97</sup>.

### Growth factors

Stimulation of cell proliferation and/or healthy matrix synthesis with exogenous growth factors alters IVD homeostasis either by inhibiting catabolic and/or by stimulating anabolic processes<sup>98</sup>. Several growth factors have been tested *in vitro* and most have been shown to successfully decrease cell apoptosis and/or to enhance chondrogenic matrix production, and/or to direct MSC differentiation towards an NP-like phenotype. Growth factors have also been proven effective *in vivo* in animal models, but often with experimentally induced instead of spontaneously developed IVD degeneration (Table 1).

The half-life and solubility of growth factors, the proper carrier, and the presence of inhibitors need to be taken into consideration when growth factors are used in regenerative strategies<sup>98</sup>. Since the NP is a confined, avascular space, the injected factor may be retained for a long time. Some factors have been shown to bind to the ECM and metabolic changes following a single growth factor injection might be sustained, potentially leading to long-lasting effects<sup>98</sup>. If a growth factor has a short half-life, it can be administered by sustained delivery systems. Since degenerated discs contain relatively few cells, the injection of growth factors may not produce an optimal therapeutic effect<sup>98</sup>. Combined cell- and growth factor-based therapy may solve this problem.

Taken together, a therapeutic approach to IVD degeneration involving enhanced tissue repair by exogenous growth factors may be clinically important, but more research is needed to address the efficacy, duration of action, safety, and adverse effects of the growth factors administered *in vivo*.

### Gene therapy

In gene therapy-based regenerative medicine, messenger RNA can be degraded to decrease the expression level of relevant genes or exogenous genes can be inserted into cells by means of (non-) viral vectors to increase gene expression<sup>99</sup>. Once the transferred gene is functional, the genetically modified cells can produce the desired product (*e.g.* a specific growth factor) in a continuous fashion with long-lasting effects<sup>100</sup>. Major barriers to the clinical use of gene therapy, however, include transfection efficiency, the creation of long-term effects, the difficulty of controlling cell proliferation and translation, ectopic transfection, disease transmission, patient-specific dose responses, immune reactions against viral proteins, possible side effects, and ethical issues<sup>101,102</sup>. For these reasons, gene therapy for IVD regeneration has not been used in a clinical setting yet to our knowledge.

# 1

## Drawbacks of regenerative treatment strategies for IVD degeneration

Regenerative treatment strategies have some drawbacks. Firstly, early identification of IVD degeneration is essential to prevent the occurrence of IVD disease. Early IVD degeneration can be detected by means of MRI, but this diagnostic tool is typically only used when clinical signs are profound. In the case of early IVD degeneration with minor clinical signs, there is the ethical issue of whether the risks of an intradiscal injection are not higher than the benefit that may be expected from the novel regenerative treatment<sup>103, 104</sup>. Secondly, several cell- and growth factor-based regenerative treatment strategies have been tested *in vitro* and *in vivo* in animal models with experimentally induced IVD degeneration, which may not be representative for spontaneous IVD degeneration. As CD breed dogs have proven a suitable animal model of naturally occurring IVD degeneration<sup>8, 13</sup>, we advocate using this model to assess the (side) effects of novel regenerative treatments. NP tissue from CD and NCD dogs show differences in gene expression profiles<sup>14</sup> and, therefore, future studies should aim at determining whether CD and NCD dogs also respond differently on IVD regenerative treatments. Thirdly, the performed regenerative IVD studies show halting of degeneration (by increased disc height, proteoglycan or water content, and improved clinical status of patients during follow-up), but it is not known whether the cell-based IVD treatment strategies were actually able to regenerate NP tissue. Therefore, a critical analysis of study results is important, *e.g.* by assessing how close the regenerated IVD resembles a healthy IVD. Fourthly, the severity of IVD degeneration possibly influences the therapeutic effect of injected cells and/or growth factors, since CLCs from degenerated IVDs may have lost their chondrogenic potential. Additionally, the effect of injected cells/growth factors may differ between early and severely degenerated IVDs<sup>105</sup>.

Regenerative treatment strategies aim to treat the degenerative process at an earlier stage. As such, they are developed based on minimally invasive concepts, and are primarily provided through injection into the IVD. However, clinicians are concerned that injectable treatments may cause side effects. There are several examples reported within this context. Cell leakage after intradiscal BMSC injection has been reported to induce osteophyte formation in a rabbit IVD degeneration model<sup>106</sup>. Furthermore, the dose of growth factor to be used needs to be fine-tuned. For example, intradiscal injection of bone morphogenetic protein-2 (BMP-2) induced degenerative changes<sup>107</sup> and weekly intradiscal treatment with growth and differentiation factor-5 (GDF-5) or insulin-like growth factor-1 (IGF-1) resulted in inflammatory reactions in the adjacent vertebrae and connective tissue infiltrates in the NP, causing the IVD to collapse<sup>108</sup>. The latter was also noted in IVDs injected with saline and may have been caused by multiple needle insertions<sup>108</sup>. Also, misplacement of recombinant gene therapy products has been associated with lower extremity paralysis after intradiscal injection, and with paraesthesia, systemic illness, and death after epidural injection<sup>109, 110</sup>. Furthermore, the sudden acceleration of the cell reproductive cycle by growth factor or gene therapy treatment has been linked with chromosomal translocations or tumorigenesis<sup>33</sup>. Lastly, a meta-analysis demonstrated that treatment of a degenerated IVD with cells and biomaterials showed better results on disc height restoration and MRI T2 signal intensity than treatment with cells or biomaterial alone. However, none of the treatments could fully restore the disc height or achieve the same MRI T2 signal intensity as the healthy disc<sup>111</sup>.

## Regenerative treatments in human patients

Nearly three-quarters of the human population will be affected by low back pain at some stage in their lives<sup>23</sup>. While this condition is multifactorial, IVD degeneration is one of its major causes, involved in at least 40% of chronic back pain cases<sup>112</sup>. As no effective therapies to retard or reverse disc degeneration have yet been devised, there is huge interest in potential regenerative treatments for human patients. Therefore, over the past few years, several human clinical phase I (safety) and II (efficacy) cell-based trials have been initiated.

In the Euro Disc study, CLCs were obtained from 112 human patients with IVD herniation who underwent discectomy, subsequently culture-expanded and after 12 weeks percutaneously re-injected into the IVD<sup>23</sup>. Interim analysis revealed that human patients receiving autologous CLC transplantation experienced a greater pain reduction after 2 years and had a higher IVD fluid content on MRI than patients who did not undergo CLC transplantation after discectomy<sup>23</sup>. Ten human patients with lumbar IVD disease treated with an intradiscal BMSC injection showed diminished pain and disability and a significantly elevated IVD water content (MRI) at the 1-year follow-up<sup>113</sup>. The same research group is currently performing a clinical study on the treatment of IVD disease with allogeneic BMSCs in twenty-four human patients (<http://clinicaltrials.gov/show/NCT01860417>). Furthermore, another phase II clinical trial enrolled 100 human patients with a single painful, degenerated lumbar IVD and treated them with immuno-selected and culture-expanded MSCs at two different dosages delivered in a hyaluronic acid-based hydrogel and compared that to hydrogel alone. Interim analysis of 50% of the patients after 6 months follow-up indicated a greater reduction in low back pain and an improvement in function in patients receiving  $6 \times 10^6$  MSCs compared with control patients. The MRI status of the injected IVD, however, was not affected by the treatment. No cell-related safety issues were encountered in this trial, although the patients receiving  $18 \times 10^6$  MSCs showed a higher incidence of adverse effects (<http://clinicaltrials.gov/show/NCT01290367>). Another study tested the effect of intradiscally injected allogeneic placental tissue extract on 30 human patients with degenerated IVDs (<https://clinicaltrials.gov/show/NCT02379689>), but no results are available yet. Lastly, several human growth factor-based phase I/II clinical trials were started to evaluate the safety, tolerability, and preliminary effectiveness of intradiscal delivery of growth and differentiation factor-5 (GDF-5) as compared with placebo (sterile water/vehicle control) in human patients with early lumbar disc degeneration in the United States, Australia, and the Republic of Korea. Clinical and safety outcomes in these trials are the development of adverse events and the neurological status of patients (<http://clinicaltrials.gov/show/NCT00813813>, [NCT01124006](http://clinicaltrials.gov/show/NCT01124006), [NCT01158924](http://clinicaltrials.gov/show/NCT01158924), and [NCT01182337](http://clinicaltrials.gov/show/NCT01182337)).

## One Medicine

Over the past few years, both human and veterinary medicine have recognized the importance of the 'One Medicine' concept: bringing together human and animal health for new medical solutions, advantageous for humans as well as animals. Dogs are the only animals that spontaneously develop IVD disease that is diagnosed and treated, both medically and surgically, in the same way as in humans. Our research group has previously

1 shown that the gross pathology, histopathology, GAG content, and MMP-2 activity of human and canine IVDs were similar in all different stages of IVD degeneration<sup>8</sup>. Only some differences between human and canine IVDs were found, such as the absence of growth plates in developing human vertebrae, thicker cartilaginous endplates and more pronounced endplate irregularities in humans with increasing severity of IVD degeneration<sup>8</sup>. Although the canine IVDs were smaller than the human IVDs, the ratio of NP area/IVD area was similar in the two species<sup>8</sup>. These facts indicate that human and canine IVD degeneration is comparable at many different levels and that humans and dogs can benefit from each other by being a suitable model for the other species. Human and canine patients with IVD degeneration can thus be used as a study population to investigate the mechanisms of degeneration and potential regenerative treatments, which is beneficial for both species and suits the 'One Medicine' concept.

## Conclusions

Cell-based or growth factor-based regenerative treatment of the degenerated IVD seems promising. Clinical indications for intradiscal injections are (a) treatment of discogenic pain without severe compression and/or neurologic deficits and (b) treatment of the adjacent degenerated discs during decompressive spinal surgery. Percutaneous intradiscal injection has been shown to be technically feasible and safe in canines<sup>21-23</sup>. This altogether paves the way for prospective phase I-II clinical trials of minimally invasive cell- or growth factor-based treatment in canine patients with spontaneously developed IVD disease. New strategies need to concentrate on enhancing the cell-based regenerative potential by growth factors, including those that are specifically secreted by the NCs.

## Aims and outline of this thesis

The main aim of this thesis is to develop regenerative treatment strategies for intervertebral disc degeneration by mimicking developmental biology. To achieve this, three different approaches are followed (Part I-III, Figure 4).

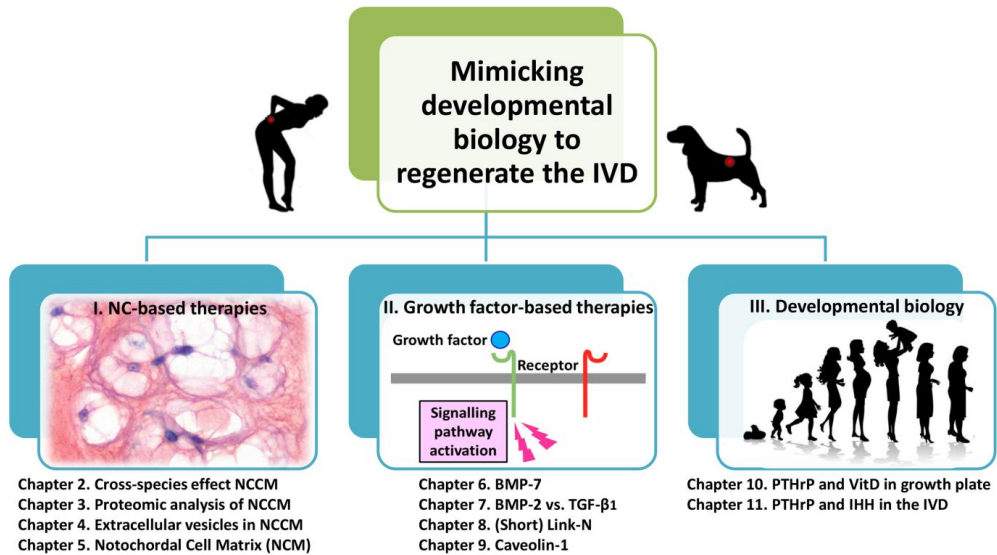


**Figure 4. Schematic representation of the outline of this thesis.** IVD: intervertebral disc, NC: Notochordal cell, NCCM: Notochordal cell-conditioned medium, BMP: Bone Morphogenetic Protein, TGF: Transforming growth factor, PTHrP: Parathyroid hormone-related protein, IHH: Indian Hedgehog, VitD: Vitamin D. Developmental biology picture modified from <http://www.richardsonthebrain.com/developmental-biology>

### Part I – Notochordal cell-based therapies

During IVD maturation, the main cell type in the NP shifts from NCs to CLCs<sup>4</sup>, suggesting that NCs play a role in maintaining tissue health. In line with this, NCs secrete bioactive factors with regenerative potential upon CLCs<sup>63-69</sup>. In Part I of this thesis, the unique regenerative potential of NCs and their secreted factors is employed for the development of a treatment strategy for IVD degeneration. During initial development, these strategies preferably employ non-human donors due to easy availability of their NC-rich NP tissue. To increase the success of translating these strategies for clinical application, **Chapter 2** delineates whether NC-secreted factors of different species have a cross-species regenerative effect on human CLCs from early degenerated IVDs *in vitro*. As a follow-up step, **Chapter 3** aims to identify the specific NC-secreted substances that stimulate IVD regeneration by performing mass spectrometry on porcine, canine, and human NCCM. Furthermore, to determine whether the effect of NCCM is mediated by soluble and/or pelletable factors, porcine and canine NCCM is separated in a soluble (NCCM-S; peptides and proteins) and pelletable (NCCM-P; protein aggregates and EVs) fraction by ultracentrifugation, and tested on bovine and canine CLCs from early degenerated IVDs *in vitro*. Moreover, **Chapter 4** aims to purify NC-secreted

1 EVs from porcine NCCM through size exclusion chromatography, ultracentrifugation or density gradient centrifugation. The isolated EVs are quantitatively analyzed by high-resolution flow cytometry and their biologic effect is determined on canine and human CLCs from early degenerated IVDs *in vitro* and compared with NCCM-derived proteins and unfractionated NCCM.

Since identification of the regenerative NC-secreted factors may be time consuming and cumbersome, **Chapter 5** focuses on a straightforward approach for IVD regeneration, by applying whole NC-derived matrix (NCM) derived from healthy porcine NPs. The first aim of this chapter is to determine the (regenerative) effects of NCM on canine and human CLCs from early degenerated IVDs *in vitro*. Additionally, as a first step towards translation from bench to bedside, the effect of NCM is tested on mildly (spontaneously) and more severely (induced) degenerated canine IVDs *in vivo*. For clinical IVD repair, however, NCM stimulation alone may not be sufficient, since cell viability is impaired in the degenerated IVD<sup>13</sup>. Therefore, the second aim of this chapter is to determine the effects of MSCs, alone and combined with NCM, on degenerated canine IVDs *in vivo*.

## Part II – Growth factor-based therapies

Part II of this thesis explores the potency of growth factors (expected to stimulate cell proliferation and/or healthy ECM synthesis) to translate this treatment strategy towards a clinical application for IVD disease. **Chapter 6** aims to determine the effects of bone morphogenetic protein-7 (BMP7), which has been shown to stimulate matrix production by IVD cells *in vitro*<sup>114, 115</sup> and in animal models of induced IVD degeneration *in vivo*<sup>116-118</sup>, in a spontaneous canine IVD degeneration model. For this purpose, canine CLCs are cultured with BMP7 *in vitro* and BMP7 is intradiscally injected into early degenerated canine IVDs *in vivo*. Given that growth factors differ in their biologic effects at the IVD level, **Chapter 7** studies the differential effects of transforming growth factor- $\beta_1$  (TGF- $\beta_1$ ) and bone morphogenetic protein-2 (BMP2) on canine and human CLCs from early degenerated IVDs *in vitro*. As a step towards preclinical translation, treatment with BMP2 alone and combined with MSCs is further investigated by seeding the canine CLCs in albumin-based hydrogels with/without BMSCs (50:50) in control or BMP2-supplemented culture medium.

**Chapter 8** investigates the growth factor-like properties of Link-N, which stabilizes proteoglycan aggregates in cartilaginous tissues, on human, bovine and canine CLCs from early degenerated IVDs. Link-N has been shown to facilitate regeneration in rabbit<sup>119</sup>, human<sup>120-122</sup>, and bovine<sup>120, 121, 123</sup> IVD cells by inducing Smad1 (BMP) signaling<sup>119</sup>. Dogs with IVD disease could possibly benefit from Link-N treatment, but Link-N has not been tested on canine IVD cells. Therefore, the aim this chapter is to determine whether Link-N is also effective in canine CLCs. This will facilitate translation of Link-N into the clinic using the dog as an *in vivo* large animal model for both canine and human IVD regeneration.

Lastly, **Chapter 9** aims to determine the role of the membrane protein caveolin-1 in IVD degeneration. As a scaffolding protein, caveolin-1 can influence several signaling pathways<sup>124</sup> and TGF- $\beta$  receptors have been demonstrated to co-localize with caveolin-1<sup>125</sup>. Therefore, this chapter explores whether caveolin-1 facilitates IVD repair by enhancing TGF- $\beta$  signaling in the IVD employing murine caveolin-1 null IVDs. Additionally, canine and human

CLCs from early degenerated IVDs are either treated with caveolin-1 scaffolding domain peptide and/or silenced for caveolin-1.

### **Part III – What can we learn from developmental biology?**

Longitudinal bone growth occurs at the growth plate, a highly organized structure that contains proliferating and differentiating chondrocytes. These chondrocytes undergo a maturation process involving hypertrophy followed by apoptosis, thereby facilitating bone formation<sup>126, 127</sup>. Some changes that occur in osteoarthritis and IVD degeneration resemble the processes that occur during growth plate chondrocyte differentiation<sup>128-130</sup>. Understanding the processes behind chondrocyte differentiation is crucial, and the growth plate can be used to study this<sup>126, 127, 131</sup>. Vitamin D<sub>3</sub>, PTHrP, and IHH are all known to play an essential role in growth plate chondrocyte proliferation and differentiation<sup>132-134</sup>, but their role in the IVD is yet unknown. For this reason, Part III of this thesis aims to better understand their involvement in the postnatal IVD, thereby supplying therapeutic clues for the development of a regenerative treatment for IVD disease.

To further elucidate the role of vitamin D<sub>3</sub> and PTHrP in chondrocytes, **Chapter 10** first investigates the possible existence of a paracrine feedback loop between vitamin D<sub>3</sub> and PTHrP in the growth plate. Second, this chapter aims to determine whether vitamin D<sub>3</sub> and/or PTHrP could be used to prevent hypertrophic chondrocyte differentiation in degenerative cartilaginous tissues. For this purpose, chondrogenic ATDC5 cells treated with vitamin D<sub>3</sub> or PTHrP, Col2-pd2EGFP transgenic mice, and primary Col2-pd2EGFP growth plate chondrocytes isolated by FACS are analyzed *in vitro*. For a better understanding of the role of the PTHrP/IHH feedback loop at the IVD level, the expression of PTHrP, IHH and related receptors is explored in the healthy until severely degenerated canine and human IVD in **Chapter 11**. Lastly, the functional effect of IHH and PTHrP is studied on canine CLCs from early degenerated IVDs *in vitro*.

Conclusions, limitations and future perspectives of this thesis are discussed in **Chapter 12**.

# References

1. Risbud MV, Schaer TP, Shapiro IM. 2010. Toward an understanding of the role of notochordal cells in the adult intervertebral disc: From discord to accord. *Dev Dyn* 239: 2141-2148.
2. Bergknut N, Smolders LA, Grinwis GC, et al. 2013. Intervertebral disc degeneration in the dog. part 1: Anatomy and physiology of the intervertebral disc and characteristics of intervertebral disc degeneration. *Vet J* 195: 282-291.
3. Risbud MV, Shapiro IM. 2011. Notochordal cells in the adult intervertebral disc: New perspective on an old question. *Crit Rev Eukaryot Gene Expr* 21: 29-41.
4. Hunter CJ, Matyas JR, Duncan NA. 2004. Cytomorphology of notochordal and chondrocytic cells from the nucleus pulposus: A species comparison. *J Anat* 205: 357-362.
5. Smolders LA, Bergknut N, Grinwis GC, et al. 2013. Intervertebral disc degeneration in the dog. part 2: Chondrodystrophic and non-chondrodystrophic breeds. *Vet J* 195: 292-299.
6. Sakai D, Mochida J, Yamamoto Y, et al. 2003. Transplantation of mesenchymal stem cells embedded in atelocollagen gel to the intervertebral disc: A potential therapeutic model for disc degeneration. *Biomaterials* 24: 3531-3541.
7. Hunter CJ, Matyas JR, Duncan NA. 2003. The notochordal cell in the nucleus pulposus: A review in the context of tissue engineering. *Tissue Eng* 9: 667-677.
8. Bergknut N, Rutges JP, Kranenburg HJ, et al. 2012. The dog as an animal model for intervertebral disc degeneration? *Spine (Phila Pa 1976)* 37: 351-358.
9. Erwin WM, Islam D, Eftekarpour E, et al. 2013. Intervertebral disc-derived stem cells: Implications for regenerative medicine and neural repair. *Spine (Phila Pa 1976)* 38: 211-216.
10. Meij BP, Bergknut N. 2010. Degenerative lumbosacral stenosis in dogs. *Vet Clin North Am Small Anim Pract* 40: 983-1009.
11. Bergknut N, Meij BP, Hagman R, et al. 2013. Intervertebral disc disease in dogs - part 1: A new histological grading scheme for classification of intervertebral disc degeneration in dogs. *Vet J* 195: 156-163.
12. Smolders LA, Kingma I, Bergknut N, et al. 2012. Biomechanical assessment of the effects of decompressive surgery in non-chondrodystrophic and chondrodystrophic canine multisegmented lumbar spines. *Eur Spine J* 21: 1692-1699.
13. Sakai D, Nakai T, Mochida J, Alini M, Grad S. 2009. Differential phenotype of intervertebral disc cells: Microarray and immunohistochemical analysis of canine nucleus pulposus and anulus fibrosus. *Spine (Phila Pa 1976)* 34: 1448-1456.
14. Smolders LA, Meij BP, Onis D, et al. 2013. Gene expression profiling of early intervertebral disc degeneration reveals a down-regulation of canonical wnt signaling and caveolin-1 expression: Implications for development of regenerative strategies. *Arthritis Res Ther* 15: R23.
15. van Dijk BG, Potier E, Ito K. 2013. Long-term culture of bovine nucleus pulposus explants in a native environment. *Spine J* 13: 454-463.
16. Urban JP, Maroudas A. 1981. Swelling of the intervertebral disc in vitro. *Connect Tissue Res* 9: 1-10.
17. van Dijk B, Potier E, Ito K. 2011. Culturing bovine nucleus pulposus explants by balancing medium osmolarity. *Tissue Eng Part C Methods* 17: 1089-1096.
18. Gantenbein B, Grunhagen T, Lee CR, et al. 2006. An in vitro organ culturing system for intervertebral disc explants with vertebral endplates: A feasibility study with ovine caudal discs. *Spine (Phila Pa 1976)* 31: 2665-2673.
19. Illien-Junger S, Gantenbein-Ritter B, Grad S, et al. 2010. The combined effects of limited nutrition and high-frequency loading on intervertebral discs with endplates. *Spine (Phila Pa 1976)* 35: 1744-1752.
20. Alini M, Eisenstein SM, Ito K, et al. 2008. Are animal models useful for studying human disc disorders/degeneration? *Eur Spine J* 17: 2-19.
21. Ganey T, Libera J, Moos V, et al. 2003. Disc chondrocyte transplantation in a canine model: A treatment for degenerated or damaged intervertebral disc. *Spine (Phila Pa 1976)* 28: 2609-2620.
22. Meisel HJ, Siodla V, Ganey T, et al. 2007. Clinical experience in cell-based therapeutics: Disc chondrocyte transplantation A treatment for degenerated or damaged intervertebral disc. *Biomol Eng* 24: 5-21.
23. Hohaus C, Ganey TM, Minkus Y, Meisel HJ. 2008. Cell transplantation in lumbar spine disc degeneration disease. *Eur Spine J* 17 Suppl 4: 492-503.
24. Hiyama A, Mochida J, Iwashina T, et al. 2008. Transplantation of mesenchymal stem cells in a canine disc degeneration model. *J Orthop Res* 26: 589-600.
25. Ganey T, Hutton WC, Moseley T, Hedrick M, Meisel HJ. 2009. Intervertebral disc repair using adipose tissue-derived stem and regenerative cells: Experiments in a canine model. *Spine (Phila Pa 1976)* 34: 2297-2304.
26. Serigano K, Sakai D, Hiyama A, et al. 2010. Effect of cell number on mesenchymal stem cell transplantation in a canine disc degeneration model. *J Orthop Res* 28: 1267-1275.
27. Steffen F, Smolders L, Roentgen A, Bertolo A, Stoyanov J. 2017. Bone marrow-derived mesenchymal stem cells as autologous therapy in dogs with naturally occurring intervertebral disc disease: Feasibility, safety and preliminary results. *Tissue Eng Part C Methods*, Epub ahead of print.
28. Henriksson HB, Brisby H. 2013. Development and regeneration potential of the mammalian intervertebral disc. *Cells Tissues Organs* 197: 1-13.
29. Nomura T, Mochida J, Okuma M, Nishimura K, Sakabe K. 2001. Nucleus pulposus allograft retards intervertebral disc degeneration. *Clin Orthop Relat Res* (389): 94-101.

30. Nishimura K, Mochida J. 1998. Percutaneous reinsertion of the nucleus pulposus. an experimental study. *Spine (Phila Pa 1976)* 23: 1531-9.
31. Yang F, Leung VY, Luk KD, Chan D, Cheung KM. 2009. Mesenchymal stem cells arrest intervertebral disc degeneration through chondrocytic differentiation and stimulation of endogenous cells. *Mol Ther* 17: 1959-1966.
32. Takada T, Nishida K, Doita M, Kurosaka M. 2002. Fas ligand exists on intervertebral disc cells: A potential molecular mechanism for immune privilege of the disc. *Spine (Phila Pa 1976)* 27: 1526-1530.
33. Watanabe T, Sakai D, Yamamoto Y, et al. 2010. Human nucleus pulposus cells significantly enhanced biological properties in a coculture system with direct cell-to-cell contact with autologous mesenchymal stem cells. *J Orthop Res* 28: 623-630.
34. Okuma M, Mochida J, Nishimura K, Sakabe K, Seiki K. 2000. Reinsertion of stimulated nucleus pulposus cells retards intervertebral disc degeneration: An in vitro and in vivo experimental study. *J Orthop Res* 18: 988-997.
35. Yamamoto Y, Mochida J, Sakai D, et al. 2004. Upregulation of the viability of nucleus pulposus cells by bone marrow-derived stromal cells: Significance of direct cell-to-cell contact in coculture system. *Spine (Phila Pa 1976)* 29: 1508-1514.
36. Gaetani P, Torre ML, Klinger M, et al. 2008. Adipose-derived stem cell therapy for intervertebral disc regeneration: An in vitro reconstructed tissue in alginate capsules. *Tissue Eng Part A* 14: 1415-1423.
37. Lu ZF, Zandieh Doulabi B, Wuisman PI, Bank RA, Helder MN. 2007. Differentiation of adipose stem cells by nucleus pulposus cells: Configuration effect. *Biochem Biophys Res Commun* 359: 991-996.
38. Mochida J. 2005. New strategies for disc repair: Novel preclinical trials. *J Orthop Sci* 10: 112-118.
39. Svanvik T, Henriksson HB, Karlsson C, et al. 2010. Human disk cells from degenerated disks and mesenchymal stem cells in co-culture result in increased matrix production. *Cells Tissues Organs* 191: 2-11.
40. Yang SH, Wu CC, Shih TT, Sun YH, Lin FH. 2008. In vitro study on interaction between human nucleus pulposus cells and mesenchymal stem cells through paracrine stimulation. *Spine (Phila Pa 1976)* 33: 1951-1957.
41. Acharya C, Adesida A, Zajac P, et al. 2012. Enhanced chondrocyte proliferation and mesenchymal stromal cells chondrogenesis in coculture pellets mediate improved cartilage formation. *J Cell Physiol* 227: 88-97.
42. McCann MR, Bacher CA, Seguin CA. 2011. Exploiting notochord cells for stem cell-based regeneration of the intervertebral disc. *J Cell Commun Signal* 5: 39-43.
43. Chen S, Emery SE, Pei M. 2009. Coculture of synovium-derived stem cells and nucleus pulposus cells in serum-free defined medium with supplementation of transforming growth factor-beta1: A potential application of tissue-specific stem cells in disc regeneration. *Spine (Phila Pa 1976)* 34: 1272-1280.
44. Bartholomew A, Sturgeon C, Siatskas M, et al. 2002. Mesenchymal stem cells suppress lymphocyte proliferation in vitro and prolong skin graft survival in vivo. *Exp Hematol* 30: 42-48.
45. Meirelles Lda S, Fontes AM, Covas DT, Caplan AI. 2009. Mechanisms involved in the therapeutic properties of mesenchymal stem cells. *Cytokine Growth Factor Rev* 20: 419-427.
46. Tse WT, Pendleton JD, Beyer WM, Egalka MC, Guinan EC. 2003. Suppression of allogeneic T-cell proliferation by human marrow stromal cells: Implications in transplantation. *Transplantation* 75: 389-397.
47. Crevensten G, Walsh AJ, Ananthakrishnan D, et al. 2004. Intervertebral disc cell therapy for regeneration: Mesenchymal stem cell implantation in rat intervertebral discs. *Ann Biomed Eng* 32: 430-434.
48. Sakai D, Mochida J, Iwashina T, et al. 2006. Regenerative effects of transplanting mesenchymal stem cells embedded in atelocollagen to the degenerated intervertebral disc. *Biomaterials* 27: 335-345.
49. Zhang YG, Guo X, Xu P, Kang LL, Li J. 2005. Bone mesenchymal stem cells transplanted into rabbit intervertebral discs can increase proteoglycans. *Clin Orthop Relat Res* (430): 219-226.
50. Sakai D, Mochida J, Iwashina T, et al. 2005. Differentiation of mesenchymal stem cells transplanted to a rabbit degenerative disc model: Potential and limitations for stem cell therapy in disc regeneration. *Spine (Phila Pa 1976)* 30: 2379-2387.
51. Chun HJ, Kim YS, Kim BK, et al. 2012. Transplantation of human adipose-derived stem cells in a rabbit model of traumatic degeneration of lumbar discs. *World Neurosurg* 78: 364-371.
52. Jin ES, Min J, Jeon SR, Choi KH, Jeong JH. 2013. Analysis of molecular expression in adipose tissue-derived mesenchymal stem cells: Prospects for use in the treatment of intervertebral disc degeneration. *J Korean Neurosurg Soc* 53: 207-212.
53. Steck E, Bertram H, Abel R, et al. 2005. Induction of intervertebral disc-like cells from adult mesenchymal stem cells. *Stem Cells* 23: 403-411.
54. Bertolo A, Mehr M, Aebli N, et al. 2012. Influence of different commercial scaffolds on the in vitro differentiation of human mesenchymal stem cells to nucleus pulposus-like cells. *Eur Spine J* 21 Suppl 6: S826-38.
55. Richardson SM, Hughes N, Hunt JA, Freemont AJ, Hoyland JA. 2008. Human mesenchymal stem cell differentiation to NP-like cells in chitosan-glycerophosphate hydrogels. *Biomaterials* 29: 85-93.
56. Minogue BM, Richardson SM, Zeef LA, Freemont AJ, Hoyland JA. 2010. Characterization of the human nucleus pulposus cell phenotype and evaluation of novel marker gene expression to define adult stem cell differentiation. *Arthritis Rheum* 62: 3695-3705.
57. Thorpe AA, Binch AL, Creemers LB, Sammon C, Le Maitre CL. 2016. Nucleus pulposus phenotypic markers to determine stem cell differentiation: Fact or fiction? *Oncotarget* 7: 2189-2200.
58. Sakai D, Nakamura Y, Nakai T, et al. 2012. Exhaustion of nucleus pulposus progenitor cells with ageing and degeneration of the intervertebral disc. *Nat Commun* 3: 1264.
59. Huang S, Leung VY, Long D, et al. 2013. Coupling of small leucine-rich proteoglycans to hypoxic survival of a progenitor cell-like subpopulation in rhesus macaque intervertebral disc. *Biomaterials* 34: 6548-6558.

60. Kim JH, Deasy BM, Seo HY, et al. 2009. Differentiation of intervertebral notochordal cells through live automated cell imaging system in vitro. *Spine (Phila Pa 1976)* 34: 2486-2493.
61. Korecki CL, Taboas JM, Tuan RS, Iatridis JC. 2010. Notochordal cell conditioned medium stimulates mesenchymal stem cell differentiation toward a young nucleus pulposus phenotype. *Stem Cell Res Ther* 1: 18.
62. Purmessur D, Schek RM, Abbott RD, et al. 2011. Notochordal conditioned media from tissue increases proteoglycan accumulation and promotes a healthy nucleus pulposus phenotype in human mesenchymal stem cells. *Arthritis Res Ther* 13: R81.
63. Abbott RD, Purmessur D, Monsey RD, Iatridis JC. 2012. Regenerative potential of TGFbeta3 + dex and notochordal cell conditioned media on degenerated human intervertebral disc cells. *J Orthop Res* 30: 482-488.
64. Aguiar DJ, Johnson SL, Oegema TR. 1999. Notochordal cells interact with nucleus pulposus cells: Regulation of proteoglycan synthesis. *Exp Cell Res* 246: 129-137.
65. Erwin WM, Inman RD. 2006. Notochord cells regulate intervertebral disc chondrocyte proteoglycan production and cell proliferation. *Spine (Phila Pa 1976)* 31: 1094-1099.
66. Matta A, Karim MZ, Isenman DE, Erwin WM. 2017. Molecular therapy for degenerative disc disease: Clues from secretome analysis of the notochordal cell-rich nucleus pulposus. *Sci Rep* 7: 45623.
67. Potier E, de Vries S, van Doeselaar M, Ito K. 2014. Potential application of notochordal cells for intervertebral disc regeneration: An in vitro assessment. *Eur Cell Mater* 28: 68-81.
68. de Vries SA, Potier E, van Doeselaar M, et al. 2015. Conditioned medium derived from notochordal cell-rich nucleus pulposus tissue stimulates matrix production by canine nucleus pulposus cells and bone marrow-derived stromal cells. *Tissue Eng Part A* 21: 1077-1084.
69. de Vries SA, van Doeselaar M, Meij BP, Tryfonidou MA, Ito K. 2016. The stimulatory effect of notochordal cell-conditioned medium in a nucleus pulposus explant culture. *Tissue Eng Part A* 22: 103-110.
70. Allon AA, Butcher K, Schneider RA, Lotz JC. 2012. Structured coculture of mesenchymal stem cells and disc cells enhances differentiation and proliferation. *Cells Tissues Organs* 196: 99-106.
71. Xie LW, Fang H, Chen AM, Li F. 2009. Differentiation of rat adipose tissue-derived mesenchymal stem cells towards a nucleus pulposus-like phenotype in vitro. *Chin J Traumatol* 12: 98-103.
72. Mehrkens A, Matta A, Karim MZ, et al. 2017. Notochordal cell-derived conditioned medium protects human nucleus pulposus cells from stress-induced apoptosis. *Spine J* 17: 579-588.
73. Erwin WM, Islam D, Inman RD, Fehlings MG, Tsui FW. 2011. Notochordal cells protect nucleus pulposus cells from degradation and apoptosis: Implications for the mechanisms of intervertebral disc degeneration. *Arthritis Res Ther* 13: R215.
74. Purmessur D, Cornejo MC, Cho SK, et al. 2015. Intact glycosaminoglycans from intervertebral disc-derived notochordal cell-conditioned media inhibit neurite growth while maintaining neuronal cell viability. *Spine J* 15: 1060-1069.
75. Erwin WM, Ashman K, O'Donnell P, Inman RD. 2006. Nucleus pulposus notochord cells secrete connective tissue growth factor and up-regulate proteoglycan expression by intervertebral disc chondrocytes. *Arthritis Rheum* 54: 3859-3867.
76. Gantenbein B, Calandriello E, Wuertz-Kozak K, et al. 2014. Activation of intervertebral disc cells by co-culture with notochordal cells, conditioned medium and hypoxia. *BMC Musculoskelet Disord* 15: 422-2474-15-422.
77. Erwin WM. 2008. The notochord, notochordal cell and CTGF/CCN-2: Ongoing activity from development through maturation. *J Cell Commun Signal* 2: 59-65.
78. Erwin WM, Las Heras F, Islam D, Fehlings MG, Inman RD. 2009. The regenerative capacity of the notochordal cell: Tissue constructs generated in vitro under hypoxic conditions. *J Neurosurg Spine* 10: 513-521.
79. Malda J, Boere J, van de Lest CH, van Weeren P, Wauben MH. 2016. Extracellular vesicles - new tool for joint repair and regeneration. *Nat Rev Rheumatol* 12: 243-249.
80. Thery C, Zitvogel L, Amigorena S. 2002. Exosomes: Composition, biogenesis and function. *Nat Rev Immunol* 2: 569-579.
81. Thery C, Ostrowski M, Segura E. 2009. Membrane vesicles as conveyors of immune responses. *Nat Rev Immunol* 9: 581-593.
82. Mulcahy LA, Pink RC, Carter DR. 2014. Routes and mechanisms of extracellular vesicle uptake. *J Extracell Vesicles* 3: 10.3402/jev.v3.24641. eCollection 2014.
83. Yanez-Mo M, Siljander PR, Andreu Z, et al. 2015. Biological properties of extracellular vesicles and their physiological functions. *J Extracell Vesicles* 4: 27066.
84. Kim KW, Ha KY, Lee JS, et al. 2009. Notochordal cells stimulate migration of cartilage end plate chondrocytes of the intervertebral disc in in vitro cell migration assays. *Spine J* 9: 323-329.
85. Zavala G, Vazquez-Nin GH. 2000. Analysis of nuclear ribonucleoprotein structures during notochordal cell differentiation and maturation in chick embryos. *Anat Rec* 259: 113-123.
86. Chen J, Yan W, Setton LA. 2006. Molecular phenotypes of notochordal cells purified from immature nucleus pulposus. *Eur Spine J* 15 Suppl 3: S303-11.
87. Vujovic S, Henderson S, Presneau N, et al. 2006. Brachyury, a crucial regulator of notochordal development, is a novel biomarker for chordomas. *J Pathol* 209: 157-165.
88. Yang F, Leung VY, Luk KD, Chan D, Cheung KM. 2009. Injury-induced sequential transformation of notochordal nucleus pulposus to chondrogenic and fibrocartilaginous phenotype in the mouse. *J Pathol* 218: 113-121.
89. Guehring T, Urban JP, Cui Z, Tirlapur UK. 2008. Noninvasive 3D vital imaging and characterization of notochordal cells of the intervertebral disc by femtosecond near-infrared two-photon laser scanning microscopy and spatial-volume rendering. *Microsc Res Tech* 71: 298-304.

90. Minogue BM, Richardson SM, Zeef LA, Freemont AJ, Hoyland JA. 2010. Transcriptional profiling of bovine intervertebral disc cells: Implications for identification of normal and degenerate human intervertebral disc cell phenotypes. *Arthritis Res Ther* 12: R22.
91. Cappello R, Bird JL, Pfeiffer D, Bayliss MT, Dudhia J. 2006. Notochordal cell produce and assemble extracellular matrix in a distinct manner, which may be responsible for the maintenance of healthy nucleus pulposus. *Spine (Phila Pa 1976)* 31: 873-83.
92. Choi KS, Cohn MJ, Harfe BD. 2008. Identification of nucleus pulposus precursor cells and notochordal remnants in the mouse: Implications for disk degeneration and chordoma formation. *Dev Dyn* 237: 3953-3958.
93. McCann MR, Tamplin OJ, Rossant J, Seguin CA. 2012. Tracing notochord-derived cells using a noto-cre mouse: Implications for intervertebral disc development. *Dis Model Mech* 5: 73-82.
94. Hoogendoorn R. 2005. Notochordal cells in mature caprine intervertebral discs. *European Cells and Materials* 10: 59.
95. Gilson A, Dreger M, Urban JP. 2010. Differential expression level of cytokeratin 8 in cells of the bovine nucleus pulposus complicates the search for specific intervertebral disc cell markers. *Arthritis Res Ther* 12: R24.
96. Rutges J, Creemers LB, Dhert W, et al. 2010. Variations in gene and protein expression in human nucleus pulposus in comparison with annulus fibrosus and cartilage cells: Potential associations with aging and degeneration. *Osteoarthritis Cartilage* 18: 416-423.
97. Rastogi A, Thakore P, Leung A, et al. 2009. Environmental regulation of notochordal gene expression in nucleus pulposus cells. *J Cell Physiol* 220: 698-705.
98. Masuda K. 2008. Biological repair of the degenerated intervertebral disc by the injection of growth factors. *Eur Spine J* 17 Suppl 4: 441-451.
99. Nishida K, Doita M, Takada T, et al. 2006. Sustained transgene expression in intervertebral disc cells in vivo mediated by microbubble-enhanced ultrasound gene therapy. *Spine (Phila Pa 1976)* 31: 1415-1419.
100. Nishida K, Kang JD, Gilbertson LG, et al. 1999. Modulation of the biologic activity of the rabbit intervertebral disc by gene therapy: An in vivo study of adenovirus-mediated transfer of the human transforming growth factor beta 1 encoding gene. *Spine (Phila Pa 1976)* 24: 2419-2425.
101. Maerz T, Herkowitz H, Baker K. 2013. Molecular and genetic advances in the regeneration of the intervertebral disc. *Surg Neurol Int* 4: S94-S105.
102. Fassett DR, Kurd MF, Vaccaro AR. 2009. Biologic solutions for degenerative disk disease. *J Spinal Disord Tech* 22: 297-308.
103. Niemansburg SL, van Delden JJ, Dhert WJ, Bredenoord AL. 2013. Regenerative medicine interventions for orthopedic disorders: Ethical issues in the translation into patients. *Regen Med* 8: 65-73.
104. Carragee EJ, Don AS, Hurwitz EL, et al. 2009. 2009 ISSLS prize winner: Does discography cause accelerated progression of degeneration changes in the lumbar disc: A ten-year matched cohort study. *Spine (Phila Pa 1976)* 34: 2338-2345.
105. Ho G, Leung VY, Cheung KM, Chan D. 2008. Effect of severity of intervertebral disc injury on mesenchymal stem cell-based regeneration. *Connect Tissue Res* 49: 15-21.
106. Vadala G, Sowa G, Hubert M, et al. 2012. Mesenchymal stem cells injection in degenerated intervertebral disc: Cell leakage may induce osteophyte formation. *J Tissue Eng Regen Med* 6: 348-355.
107. Huang KY, Yan JJ, Hsieh CC, Chang MS, Lin RM. 2007. The in vivo biological effects of intradiscal recombinant human bone morphogenetic protein-2 on the injured intervertebral disc: An animal experiment. *Spine (Phila Pa 1976)* 32: 1174-1180.
108. Walsh AJ, Bradford DS, Lotz JC. 2004. In vivo growth factor treatment of degenerated intervertebral discs. *Spine (Phila Pa 1976)* 29: 156-163.
109. Wallach CJ, Kim JS, Sobajima S, et al. 2006. Safety assessment of intradiscal gene transfer: A pilot study. *Spine J* 6: 107-112.
110. Vadala G, Sowa GA, Kang JD. 2007. Gene therapy for disc degeneration. *Expert Opin Biol Ther* 7: 185-196.
111. Mehrkens A, Muller AM, Valderrabano V, Scharen S, Vavken P. 2012. Tissue engineering approaches to degenerative disc disease—a meta-analysis of controlled animal trials. *Osteoarthritis Cartilage* 20: 1316-1325.
112. Freemont AJ. 2009. The cellular pathobiology of the degenerate intervertebral disc and discogenic back pain. *Rheumatology (Oxford)* 48: 5-10.
113. Orozco L, Soler R, Morera C, et al. 2011. Intervertebral disc repair by autologous mesenchymal bone marrow cells: A pilot study. *Transplantation* 92: 822-828.
114. Imai Y, Miyamoto K, An HS, et al. 2007. Recombinant human osteogenic protein-1 upregulates proteoglycan metabolism of human annulus fibrosus and nucleus pulposus cells. *Spine (Phila Pa 1976)* 32: 1303-9; discussion 1310.
115. Masuda K, Takegami K, An H, et al. 2003. Recombinant osteogenic protein-1 upregulates extracellular matrix metabolism by rabbit annulus fibrosus and nucleus pulposus cells cultured in alginate beads. *J Orthop Res* 21: 922-930.
116. Masuda K, Imai Y, Okuma M, et al. 2006. Osteogenic protein-1 injection into a degenerated disc induces the restoration of disc height and structural changes in the rabbit anular puncture model. *Spine (Phila Pa 1976)* 31: 742-754.
117. An HS, Takegami K, Kamada H, et al. 2005. Intradiscal administration of osteogenic protein-1 increases intervertebral disc height and proteoglycan content in the nucleus pulposus in normal adolescent rabbits. *Spine (Phila Pa 1976)* 30: 25-32.
118. Chubinskaya S, Kawakami M, Rappoport L, et al. 2007. Anti-catabolic effect of OP-1 in chronically compressed intervertebral discs. *J Orthop Res* 25: 517-530.

119. Wang Z, Weitzmann MN, Sangadala S, Hutton WC, Yoon ST. 2013. Link protein N-terminal peptide binds to bone morphogenetic protein (BMP) type II receptor and drives matrix protein expression in rabbit intervertebral disc cells. *J Biol Chem* 288: 28243-28253.
120. Gawri R, Antoniou J, Ouellet J, et al. 2013. Best paper NASS 2013: Link-N can stimulate proteoglycan synthesis in the degenerated human intervertebral discs. *Eur Cell Mater* 26: 107-19.
121. Gawri R, Ouellet J, Onnerfjord P, et al. 2014. Link N is cleaved by human annulus fibrosus cells generating a fragment with retained biological activity. *J Orthop Res* 32: 1189-1197.
122. Petit A, Yao G, Rowas SA, et al. 2011. Effect of synthetic link N peptide on the expression of type I and type II collagens in human intervertebral disc cells. *Tissue Eng Part A* 17: 899-904.
123. Mwale F, Demers CN, Petit A, et al. 2003. A synthetic peptide of link protein stimulates the biosynthesis of collagens II, IX and proteoglycan by cells of the intervertebral disc. *J Cell Biochem* 88: 1202-1213.
124. Okamoto T, Schlegel A, Scherer PE, Lisanti MP. 1998. Caveolins, a family of scaffolding proteins for organizing "preassembled signaling complexes" at the plasma membrane. *J Biol Chem* 273: 5419-5422.
125. Mayoral R, Valverde AM, Llorente Izquierdo C, et al. 2010. Impairment of transforming growth factor beta signaling in caveolin-1-deficient hepatocytes: Role in liver regeneration. *J Biol Chem* 285: 3633-3642.
126. Brochhausen C, Lehmann M, Halstenberg S, et al. 2009. Signalling molecules and growth factors for tissue engineering of cartilage-what can we learn from the growth plate? *Journal of tissue engineering and regenerative medicine* 3: 416-29.
127. Nilsson O, Marino R, De Luca F, Phillip M, Baron J. 2005. Endocrine regulation of the growth plate. *Hormone research* 64: 157-65.
128. Dreier R. 2010. Hypertrophic differentiation of chondrocytes in osteoarthritis: The developmental aspect of degenerative joint disorders. *Arthritis Res Ther* 12: 216.
129. Zhang W, Chen J, Zhang S, Ouyang HW. 2012. Inhibitory function of parathyroid hormone-related protein on chondrocyte hypertrophy: The implication for articular cartilage repair. *Arthritis Res Ther* 14: 221.
130. Rutges JP, Duit RA, Kummer JA, et al. 2010. Hypertrophic differentiation and calcification during intervertebral disc degeneration. *Osteoarthritis Cartilage* 18: 1487-1495.
131. Denison TA, Koch CF, Shapiro IM, Schwartz Z, Boyan BD. 2009. Inorganic phosphate modulates responsiveness to 24,25(OH)2D3 in chondrogenic ATDC5 cells. *J Cell Biochem* 107: 155-62.
132. Kato Y, Shimazu A, Iwamoto M, et al. 1990. Role of 1,25-dihydroxycholecalciferol in growth-plate cartilage: Inhibition of terminal differentiation of chondrocytes in vitro and in vivo. *Proc Natl Acad Sci U S A* 87: 6522-6526.
133. Klaus G, Meinhold-Heerlein R, Milde P, Ritz E, Mehls O. 1991. Effect of vitamin D on growth cartilage cell proliferation in vitro. *Pediatr Nephrol* 5: 461-466.
134. Drissi H, Pouliot A, Kooloos C, et al. 2002. 1,25-(OH)2-vitamin D3 suppresses the bone-related Runx2/Cbfa1 gene promoter. *Exp Cell Res* 274: 323-333.

# Supplementary File 1. Growth factors tested *in vivo* in animal models with IVD degeneration

1

Growth factor	Mechanism of action	Animal model, Induction of degeneration	Treatment dose; duration Control treatment	GAG content of NP	Histo(patho)logy	MRI/radiograph
<b>BMP-2</b>	Differentiation signalling factor; anabolic	17 rabbits <sup>1</sup> AF tearing	0.1 mg (in 0.1 mL); 12 wks Control: saline	ND	Vascularity, fibroblast proliferation, inflammation	Degenerative changes; disc space narrowing/irregularity, subchondral sclerosis, osteophytes, EP hypertrophy ND
<b>BMP-7/ OP-1</b>	Differentiation signalling factor; anabolic	34 rats <sup>2</sup> Compression 90 rabbits <sup>3</sup> AF puncture 16 rabbits <sup>4</sup> AF puncture 54 rabbits <sup>5</sup> Chondroitinase 24 rabbits <sup>6</sup> None	0.2 µg (in 1 µL); 4 wks Control: saline 100 µg (in 10 µL); 2, 4, 8, 12, 24 wks Control: lactose 100 µg (in 10 µL); 8 wks Control: lactose 100 µg (in 10 µL); 6, 8, 12, 16 wks Control: lactose 2 µg (in 10 µL); 2, 4, 8 wks Control: saline	ND + + + + (only significant at 2 wks)	ECM content + (NS) NP size + Total histological scores (AF fibers, NP cellularity and matrix) + ND Some BMP-7-treated IVDs with abundant matrix ND	ND DH +, MRI score + MRI T2W/intensity + (NS) DH + MRI T2W/intensity + DH + DH +
<b>BMP-14/GDF-5</b>	Differentiation signalling factor; anabolic	16 mice <sup>7</sup> Compression 16 rabbits <sup>8</sup> AF puncture	8 ng (in 8 µL); 1, 4 wks Control: saline 10 ng, 1 or 100 µg (in 10 µL); 12 wks. Control: puncture alone, puncture + PBS	ND ND ND	DH +, PC + (NS) Collagen 2, aggrecan expr. (NP) Total histological score (AF fibers, NP cellularity and ECM) at 100 µg + (vs. puncture alone)	ND DH + (only significant at 1 and 100 µg) MRI scores + (all doses, NS) MRI T2W/intensity + (all doses) ND
<b>FGF</b>	Signalling factor; anabolic	10 mice <sup>7</sup> Compression	8 ng (in 8 µL); 1, 4 wks Control: saline	ND	Cell density in middle/inner AF + (NS)	ND
<b>IGF-1</b>	Insulin-like activity; anabolic	16 mice <sup>7</sup> Compression	8 ng (in 8 µL); 1, 4 wks Control: saline	ND	DH1, inner annular fibrochondrocytes, and PC + (all NS)	ND
<b>Link-N</b>	Smad signalling	28 rabbits <sup>9</sup> AF puncture	100 µg (in 10 µL); 12 wks Control: saline	+ (NS)	Less signs of IVD degeneration (NS)	DH +
<b>P2K</b>	Peptide, possibly regulating TGFβ signalling	14 rabbits <sup>5,4</sup> AF puncture	10 µg (in 15 µL); 12 wks Control: lactose	+	Less signs of IVD degeneration ECM content +	DH + MRI scores + MRI T2W/intensity +
<b>PRP</b>	Plasma fraction with highly concentrated growth factor levels	36 rabbits <sup>10</sup> NP aspiration 128 rabbits <sup>11</sup> NP aspiration	20 µL gelatin hydrogel microspheres (GHM) impregnated with PRP (sustained release); 2, 4, 8 wks. Control: PBS-GHM 20 µL GHM impregnated with PRP (sustained release); 2, 4, 8 wks. Control: PBS-GHM	ND ND	Less signs of IVD degeneration PG expression + (NS) Less apoptotic NP cells	ND DH +, MRI scores + MRI T2W/intensity + (NS)
<b>Simvastatin</b>	Stimulates BMP-2 pathway	30 rats <sup>13</sup> AF puncture	20 µL PRP; 12 wks Control: PBS PEG gel with 10 µg simvastatin; 2 wks. Control: PEG gel	ND + (NS)	CLC number +, Histological scores not different Total histological scores (AF fibers, NP cellularity and ECM) +	DH + MRI T2W/intensity + (NS) MRI scores + MRI T2W/intensity +
<b>TGFβ</b>	Signalling factor; anabolic	19 mice <sup>7</sup> Compression	1.6 ng (in 8 µL); 1, 4 wks Control: saline	ND	PC + (NS)	ND

1

+: significantly better/higher than in the control group; AF, annulus fibrosus; BMP, bone morphogenetic protein; DH, disc height; ECM, extracellular matrix; EP, end plate; FGF, fibroblast growth factor; GAG, glycosaminoglycan; GDF-5, growth and differentiation factor-5; GHM, gelatin hydrogel microspheres; IGF-1, insulin-like growth factor 1; MRI, magnetic resonance imaging; ND, not done; NP, nucleus pulposus; NS, not significant; OP-1, osteogenic protein-1; P2K, Peniel 2000; PC, percentage proliferating cells; PG, proteoglycan; PRP, platelet rich plasma; TGF $\beta$ , transforming growth factor- $\beta$ ; T2W, T2-weighted; wks, weeks.

## References

- Huang KY, Yan JJ, Hsieh CC, Chang MS, Lin RM. 2007. The in vivo biological effects of intradiscal recombinant human bone morphogenetic protein-2 on the injured intervertebral disc: An animal experiment. *Spine (Phila Pa 1976)* 32: 1174-1180.
- Kawakami M, Matsumoto T, Hashizume H, et al. 2005. Osteogenic protein-1 (osteogenic protein-1/bone morphogenetic protein-7) inhibits degeneration and pain-related behavior induced by chronically compressed nucleus pulposus in the rat. *Spine (Phila Pa 1976)* 30: 1933-1939.
- Masuda K, Imai Y, Okuma M, et al. 2006. Osteogenic protein-1 injection into a degenerated disc induces the restoration of disc height and structural changes in the rabbit anular puncture model. *Spine (Phila Pa 1976)* 31: 742-754.
- Miyamoto K, Masuda K, Kim JG, et al. 2006. Intradiscal injections of osteogenic protein-1 restore the viscoelastic properties of degenerated intervertebral discs. *Spine J* 6: 692-703.
- Imai Y, Okuma M, An HS, et al. 2007. Restoration of disc height loss by recombinant human osteogenic protein-1 injection into intervertebral discs undergoing degeneration induced by an intradiscal injection of chondroitinase ABC. *Spine (Phila Pa 1976)* 32: 1197-1205.
- An HS, Takegami K, Kamada H, et al. 2005. Intradiscal administration of osteogenic protein-1 increases intervertebral disc height and proteoglycan content in the nucleus pulposus in normal adolescent rabbits. *Spine (Phila Pa 1976)* 30: 25-31; discussion 31-2.
- Walsh AJ, Bradford DS, Lotz JC. 2004. In vivo growth factor treatment of degenerated intervertebral discs. *Spine (Phila Pa 1976)* 29: 156-163.
- Chujo T, An HS, Akeda K, et al. 2006. Effects of growth differentiation factor-5 on the intervertebral disc--in vitro bovine study and in vivo rabbit disc degeneration model study. *Spine (Phila Pa 1976)* 31: 2909-2917.
- Mwale F, Masuda K, Pichika R, et al. 2011. The efficacy of link N as a mediator of repair in a rabbit model of intervertebral disc degeneration. *Arthritis Res Ther* 13: R120.
- Nagae M, Ikeda T, Mikami Y, et al. 2007. Intervertebral disc regeneration using platelet-rich plasma and biodegradable gelatin hydrogel microspheres. *Tissue Eng* 13: 147-158.
- Sawamura K, Ikeda T, Nagae M, et al. 2009. Characterization of in vivo effects of platelet-rich plasma and biodegradable gelatin hydrogel microspheres on degenerated intervertebral discs. *Tissue Eng Part A* 15: 3719-3727.
- Obata S, Akeda K, Imanishi T, et al. 2012. Effect of autologous platelet-rich plasma-releasate on intervertebral disc degeneration in the rabbit anular puncture model: A preclinical study. *Arthritis Res Ther* 14: R241.
- Zhang H, Wang L, Park JB, et al. 2009. Intradiscal injection of simvastatin retards progression of intervertebral disc degeneration induced by stab injury. *Arthritis Res Ther* 11: R172.14. Kwon YJ, Lee JW, et al. 2013. Anabolic effects of Peniel 2000, a peptide that regulates TGF-beta1 signaling on intervertebral disc degeneration. *Spine (Phila Pa 1976)* 38:49-58.
- Kwon YJ, Lee JW, Moon EJ, et al. 2013. Anabolic effects of peniel 2000, a peptide that regulates TGF-beta1 signaling on intervertebral disc degeneration. *Spine (Phila Pa 1976)* 38: E49-58.

## Part I – Notochordal cell-based therapies





### **The species-specific regenerative effects of notochordal cell-conditioned medium on chondrocyte-like cells derived from degenerated human intervertebral discs**

Frances C. Bach<sup>1</sup>, Stefan A.H. de Vries<sup>2</sup>, Anita Krouwels<sup>3</sup>, Laura B. Creemers<sup>3</sup>, Keita Ito<sup>2,3</sup>, Björn P. Meij<sup>1</sup>, Marianna A. Tryfonidou<sup>1</sup>

<sup>1</sup>Department of Clinical Sciences of Companion Animals, Faculty of Veterinary Medicine, Utrecht University, Utrecht, the Netherlands

<sup>2</sup>Orthopedic Biomechanics, Department of Biomedical Engineering, Eindhoven University of Technology, Eindhoven, the Netherlands

<sup>3</sup>Department of Orthopedics, University Medical Centre Utrecht, Utrecht, the Netherlands

## Abstract

2

During intervertebral disc (IVD) maturation, the main cell type shifts from notochordal cells (NCs) to chondrocyte-like cells (CLCs). NCs secrete factors with regenerative potential, making them an interesting focus for regenerative treatments. During initial development, these strategies preferably employ non-human donors due to easy availability of their NC-rich nucleus pulposus (NP) tissue. To increase the success of translating these strategies for clinical application, this study aimed to delineate whether NC-secreted factors of different species have a regenerative effect on human CLCs. Human, canine, and porcine NC-rich NP tissue and NC-conditioned medium (NCCM) were analysed biochemically and histologically. Human CLC micro-aggregates from degenerated IVDs were cultured in human, canine, or porcine NCCM. Collagen, glycosaminoglycan (GAG), and DNA content was determined and histology was performed. Canine and porcine NPs were richer in NCs than human NPs. Human NPs contained the highest collagen content, whereas the DNA and GAG content of canine NPs was significantly higher than that of human or porcine NPs. NCCM from all species significantly increased the DNA and GAG content of the human CLC micro-aggregates. Porcine and canine NCCM were significantly more potent than human NCCM in inducing GAG deposition, whereas only human NCCM induced collagen type II production. Secreted factors from human, canine, and porcine NC-rich NPs exerted regenerative effects on human CLCs, indicating a cross-species effect. Bioactive compound(s) are present in NCCM of different species that may reverse human IVD degeneration, supporting further research into strategies based on NC-technology employing canine or porcine models for their translation into humans.

## Introduction

Low back pain affects nearly 75% of the human population at some stage in their lives<sup>1</sup>. Consequently, low back pain is a serious socioeconomic burden: in the US, the total cost exceed \$100 billion per year<sup>2</sup>. Degeneration of the intervertebral disc (IVD) has been associated with low back pain. The IVD arises from the embryonic notochord and mesenchyme and is situated between the vertebrae, where it transmits loads and allows stable multi-directional spinal mobility<sup>3,4</sup>. The healthy IVD consists of the annulus fibrosus (AF) and nucleus pulposus (NP). Degeneration of the IVD is a complex, multifactorial process that is characterized by changes in the cell phenotype and composition of the extracellular matrix. During IVD degeneration, the glycosaminoglycan (GAG, a proteoglycan side chain) and water content decreases in the NP, changing the biomechanical environment of the IVD cells. Because of the changed IVD matrix, diffusion of nutrients becomes impaired, which further deteriorates the health of the IVD cells and healthy matrix synthesis. Since the avascular IVD exhibits inadequate matrix repair, a vicious circle develops in which the IVD weakens and experiences increased vulnerability to damage by physiologic loading<sup>5,6</sup>.

Current medical, physiotherapeutic, and surgical treatments for IVD disease aim at reducing neurological deficits and pain, rather than IVD repair. For this reason, regenerative strategies like gene-, growth factor- or cell-based therapies, that try to biologically repair the degenerated IVD, have gained increasing interest<sup>7,8</sup>. They either aim at increasing the cell numbers by cell transplantation and/or by stimulating proliferation of the resident cells or matrix anabolism. Thus far, several growth factors and peptides (e.g. bone morphogenetic protein, Link-N) have been shown to promote cell proliferation and/or matrix formation *in vitro* and/or *in vivo* in animal models with experimentally induced IVD degeneration<sup>9-13</sup>. In addition, cell-based treatments using mesenchymal stromal cells (MSCs), articular chondrocytes and chondrocyte-like cells (CLCs) derived from the NP<sup>8,14,15</sup> have been tested. To date, however, only a limited number of regenerative therapies have entered the clinical phase as a treatment for human IVD degeneration (e.g. the Mesoblast study (allogeneic mesenchymal precursor cell (MPC) transplantation), <http://clinicaltrials.gov/show/:NCT00813813> (recombinant human growth and differentiation factor-5 (rhGDF-5)), NCT01640457 (NOVOCART® disc plus autologous disc chondrocyte transplantation), NCT01771471 (allogenic juvenile chondrocytes (NuQu) transplantation), NCT01643681 (autologous adipose tissue derived MSC transplantation), NCT02338271 (autologous adipose tissue derived MSC transplantation), and the study by Mochida *et al.*, 2015: MSC-activated chondrocyte-like CLC transplantation)<sup>16</sup>.

During IVD maturation, a transition in cell phenotype takes place from large, vacuolated notochordal cells (NCs) to smaller, non-vacuolated CLCs<sup>17</sup>. During this process, the vacuolated NCs obtain a transitional phenotype, i.e. they maintain their size but do not contain vacuoles. Thereafter, they obtain a morphology of rounded CLCs. Early NC loss in certain species (e.g. chondrodystrophic dogs) coincides with the onset of IVD degeneration. NC-conditioned medium (NCCM, containing factors secreted by NCs) and NC:CLC co-culture stimulate *in vitro* differentiation of MSCs into a NP-like phenotype<sup>18-20</sup>, protect the NP from apoptosis<sup>21,22</sup>, and/or increase CLC proliferation and GAG production<sup>3,18,23-26</sup>. In addition, NCs significantly stimulate CLC activity and GAG production<sup>27</sup> and produce more GAGs than CLCs<sup>28</sup>. NCs have also been described to exert potential symptom modifying actions, e.g.

2

anti-inflammatory, anti-neurogenic and anti-angiogenic effects by secreting factors as sonic hedgehog, noggin, connective tissue growth factor and chondroitin sulfate<sup>29-31</sup>. Thus, NCs secrete factors with auspicious potential, making them an interesting target for regenerative and/or symptom modifying therapies<sup>7</sup>. NC-based regenerative strategies are being developed using canine non-chondrodystrophic (NCD) and porcine donors because of easy availability of their NC-rich NP tissue<sup>7</sup>. Although regenerative effects of canine and porcine NC-secreted factors on human CLCs/MSCs have been demonstrated in several studies<sup>19, 20, 22, 23</sup>, the impact of human NC-secreted factors has never been determined, most probably due to limited availability of human NC-rich NP tissue. It is, however, important to define if the human CLC response to homologous human NC-secreted factors is superior to canine and porcine NC-secreted factors. Therefore, the main aim of this study was to delineate whether secreted factors from NC-rich NP tissue from different species have a differential regenerative effect on human CLCs derived from degenerated IVDs. For this purpose, human, canine, and porcine NC-rich NP tissue was cultured to generate NCCM. Given the differences in life span and in NC-maintenance with ageing between these species, it is impossible to account for the ageing effect and distinguish it from the species-specific NCCM effect. Human CLCs derived from degenerated IVDs (Thompson grade III) were isolated and after expansion cultured in human, canine, or porcine NCCM using a micro-aggregate culture system and compared with CLCs cultured in basal and chondrogenic culture medium.

## Materials and methods

### NC-rich NP tissue sources

IVD tissue (Thompson grade I) was collected from 12 human, 13 canine, and 7 porcine donors. IVDs from human donors between 20 weeks of gestation and 3 months of age (postnatal) were obtained during a standard postmortem diagnostic procedure in which part of the spine was collected within 48 hours after death, as approved by the scientific committee of the Pathology department of the University Medical Centre Utrecht. Anonymous use of redundant tissue for research purposes is a standard treatment agreement with patients in the University Medical Centre Utrecht (Local Medical Ethical Committee (METC) number 12-364). The material was used in line with the code 'Proper Secondary Use of Human Tissue' as installed by the Federation of Biomedical Scientific Societies. Complete canine spines (18-23 months of age) were collected from NCD dogs that had been euthanized in unrelated research studies (approved by the Utrecht University Animal Ethics Committee). Complete porcine spines (3 months of age) were collected from the slaughterhouse in accordance with local regulations. IVDs from all donors were opened under sterile conditions and NP tissue was collected by precise separation from the AF and cartilaginous endplates.

### DNA and extracellular matrix content of human, canine and porcine NC-rich NP tissue

#### *Collagen, DNA and GAG content*

NC-rich NPs from 4 human (22 weeks of gestation, 3 days, 5 days and 3 months of age), 21 canine (18-23 months of age), and 6 porcine (3 months of age) donors were used for histological and biochemical analysis. The human, canine, and porcine NP tissue (naturally

hydrated) was weighted using a microbalance. Papain digestion solution (pH 6, 200 mM  $\text{H}_2\text{NaPO}_4 \cdot 2 \text{H}_2\text{O}$  (21254, Boom B.V., Meppel, the Netherlands), 10 mM EDTA (100944, Merck Millipore, Amsterdam, the Netherlands), 10 mM cysteine HCl (C7880, Sigma-Aldrich, Saint Louis, USA), and 10 mM papain (P3125, Sigma-Aldrich, Saint Louis, USA)) was added to each NP, followed by overnight incubation at 60°C. The collagen content of NC-rich NP tissue was assessed using a hydroxyproline (HYP) assay<sup>32</sup>. Papain-digested NP samples were lyophilized for 1 hour (Savant SpeedVac® System AES 2010 Concentrator) and hydrolysed overnight at 108°C in 4 M NaOH (106498, Merck Millipore, Amsterdam, the Netherlands) in demineralized water. The samples were then centrifuged (15 seconds at 14000g) and incubated for 20 minutes with chloramine T reagent (2426, Merck Millipore, Amsterdam, the Netherlands). Thereafter, freshly prepared dimethylaminobenzaldehyde (DMAB; 103058, Merck Millipore, Amsterdam, the Netherlands) was added and the samples were incubated for 20 minutes at 60°C. The absorbance (570 nm) was read using a microplate reader (Model 3550, Bio-Rad, Veenendaal, the Netherlands). A linear standard line was generated with hydroxyproline (104506, Merck Millipore, Amsterdam, the Netherlands). The collagen content in the samples was calculated by multiplying the hydroxyproline content by 7.5<sup>32</sup>). The DNA content per mg wet NP tissue was measured using the Qubit® dsDNA High Sensitivity Assay Kit (Q32851, Invitrogen, Paisley, UK) according to the manufacturer's instructions. To quantify the GAG content per mg wet NP tissue, a dimethyl methylene blue (DMMB) assay was performed<sup>33</sup>. Immediately after DMMB (341088, Sigma-Aldrich, Saint Louis, USA) was added, the absorbance (540/595 nm) was measured using a microplate reader. The GAG content was calculated using a chondroitin sulphate (C4384, Sigma-Aldrich, Saint Louis, USA) standard line with polynomial properties.

#### *Safranin O/Fast Green staining*

NP tissue was fixed in 4% neutral buffered formaldehyde (4286, Klinipath B.V., Duiven, the Netherlands) for 24 hours at room temperature (RT) and embedded in paraffin. Five  $\mu\text{m}$  sections were mounted on Microscope KP+ slides (KP-3056, Klinipath B.V., Duiven, the Netherlands) and deparaffinized through xylene (two times 5 minutes) and graded ethanol (96%, 80%, 70%, 60%; 5 minutes each), followed by one PBS rinse. The sections were subjected to Mayer's hematoxylin (3870, J.T.Baker® Chemicals - Avantor Performance Materials, Center Valley, USA) for 10 seconds and rinsed with demineralized water for 5 minutes. Subsequently, the sections were counterstained with filtered 0.4% Fast Green (F7252, Sigma-Aldrich, Saint Louis, USA) for 4 minutes, subjected to 1% acetic acid for two times 3 minutes, and stained with 0.125% aqueous Safranin O (58884, Sigma-Aldrich, Saint Louis, USA) for 7 minutes. The sections were then dehydrated with 100% ethanol (2 minutes) and xylene (two times 5 minutes) and mounted (Vectamount, H5000, Vector Laboratories, Burlingame, USA).

#### *Collagen type I and II immunohistochemistry*

For collagen type II immunohistochemistry (IHC), the sections were deparaffinized (see previously). Thereafter, they were blocked for 10 minutes with 0.3%  $\text{H}_2\text{O}_2$  (51008600.9025, Boom B.V., Meppel, the Netherlands) and washed three times for 5 minutes with PBS + 0.1% Tween (PBST0.1%). Antigen retrieval was performed with 1 mg/mL pronase (11459643001, Roche Diagnostics, Almere, the Netherlands) and 10 mg/mL hyaluronidase (H3506, Sigma-Aldrich, Saint Louis, USA) in PBS for 30 minutes at 37°C. After washing with PBST0.1%, the sections were blocked with 5% BSA in PBS for 30 minutes at 37°C. Thereafter,

2

they were incubated overnight at 4°C with collagen type II mouse monoclonal antibody (0.4 µg/mL, II-II6B3, DSHB, Iowa city, IA) in 5% BSA in PBS. In control staining, the first antibody was substituted with normal mouse IgG<sub>1</sub> (0.4 µg/mL; 3877, Santa Cruz Biotechnology, Heidelberg, Germany). These negative controls showed no staining. The next day, the sections were washed with PBST0.1% before the secondary antibody (EnVision+ System-HRP Goat Anti-Mouse, K4001, Dako, Glostrup, Denmark) was applied for 60 minutes at RT. After washing with PBS, the sections were incubated with the liquid DAB substrate chromogen system (K3468, Dako, Glostrup, Denmark) for 10 minutes and counterstained with Hematoxylin QS solution (H3404, Vector Laboratories, Burlingame, USA) for 1 minute. Thereafter, they were washed with tap water for 10 minutes and dehydrated with graded ethanol (70%, 80%, 96%, 100%) and xylene (two times 5 minutes) and mounted. For collagen type I IHC, the same procedures were followed with the Anti-Collagen I antibody (0.1 µg/mL, ab6308, Abcam, Cambridge, UK).

## Generation and analysis of species-specific NCCM

### *Generation of NCCM*

Conditioned medium was generated from NC-rich NP tissue (Thompson grade I) of 10 human, 4 canine and 4 porcine donors (Table 1). The NP tissue was cultured for 4 days (1 gram tissue/30 mL) in hgDMEM+Glutamax (31966, Invitrogen, Paisley, UK) with 1% P/S (P11-010, GE Healthcare Life Sciences, Eindhoven, the Netherlands) at 37°C, 5% CO<sub>2</sub> and 5% O<sub>2</sub> (hypoxic; 6 human donors and all canine/porcine donors) or 21% O<sub>2</sub> (normoxic; 4 human donors) using a Sanyo MCO-18M incubator. After 4 days, the NP tissue was removed and the NC-conditioned medium was filtered through a 70 µm cell strainer. The filtrate was sequentially centrifuged at 200g and 500g (two times ten minutes, 4°C) to remove (dead) cells and debris. Thereafter, the supernatant containing the cell-free conditioned medium was concentrated using a 3 kDa Amicon Ultra-15 Centrifugal filter tube (Merck Millipore, Amsterdam, the Netherlands) at 4000g (45 minutes, 4°C). All substances with a molecular weight > 3 kDa were resuspended in fresh hgDMEM+Glutamax and stored in aliquots at -70°C until use. Per canine and porcine donor, about 100 mL NCCM was generated from all harvested NPs. The human NPs, however, were very small and only 2-3 NPs were available per donor, resulting on average in 1 mL NCCM per donor. Due to volume limitations, the hypoxic NCCM of 4 human donors (20-21 weeks of gestation) were pooled (two times two donors, Table 1) to perform the complete *in vitro* study design. Eventually, 4 normoxic (all separate) and 4 hypoxic (2 separate and 2 pooled) human NCCM donors were used in the culture experiments.

### *Collagen, GAG, and protein concentration of species-specific NCCM*

Filtrated, cell(debris)-free NCCM from 7 human (21 weeks of gestation – 3 months of age), 7 canine (18-23 months of age), and 7 porcine (3 months of age) donors were biochemically analysed. A HYP and DMMB assay were performed as described above. To determine the NCCM protein concentration, the Qubit® Protein Assay Kit (Q33211, Invitrogen, Paisley, UK) was used according to the manufacturer's instructions.

**Table 1. Human, canine and porcine notochordal cell-conditioned medium (NCCM) donor characteristics**

Species	HX/NX	Thompson grade	Level	Donor number	n	Donor age	Life span (years)
Human	HX	1	L2-L5	1	2 (pooled)	20 weeks of gestation	80
				2	2 (pooled)	21 weeks of gestation	
				3	1	1 days	
				4	1	6 days	
Human	NX	1	L2-L5	5	1	2 days	80
				6	1	3 days	
				7	1	5 days	
				8	1	3 months	
Canine	HX	1	Whole spine (C2-S1)	1	1	18 months	10-15
				2	1	23 months	
				3	1	20 months	
				4	1	18 months	
Porcine	HX	1	Whole spine (C2-S1)	1	1	3 months	10-20
				2	1	3 months	
				3	1	3 months	
				4	1	3 months	

NCCM was generated from NC-rich NP tissue of 10 human, 4 canine and 4 porcine donors. *n*: number of individuals from which NP tissue was used to generate NCCM; HX: NCCM generated under hypoxic (5% O<sub>2</sub>) conditions; NX: NCCM generated under normoxic (21% O<sub>2</sub>) conditions. The species life span of the canine and porcine donors depends upon the breed.

### ***In vitro* micro-aggregate culture of human CLCs derived from degenerated IVDs**

CLCs of 3 human donors (two females and one male, age range 47-63 years) were obtained from IVDs scored as Thompson grade III. These IVDs were obtained during a standard *postmortem* diagnostic procedure in which part of the spine was collected within 48 hours after death, as approved by the scientific committee of the Pathology department of the University Medical Centre Utrecht. Anonymous use of redundant tissue for research purposes is a standard treatment agreement with patients in the University Medical Centre Utrecht (Local Medical Ethical Committee (METC) number 12-364). The material was used in line with the code 'Proper Secondary Use of Human Tissue' as installed by the Federation of Biomedical Scientific Societies. The CLCs were expanded in expansion medium containing hgDMEM+Glutamax with 10% FBS (Gibco 16000-044, Life Technologies, Bleiswijk, the Netherlands), 1% P/S, 0.1 mM Ascorbic acid 2-phosphate (A8960, Sigma-Aldrich, Saint Louis, USA), 10<sup>-9</sup> M dexamethasone (AD1756, Sigma-Aldrich, Saint Louis, USA) and 1 ng/mL bFGF (PHP105, AbD Serotec, Puchheim, Germany) at 21% O<sub>2</sub>, 5% CO<sub>2</sub>, 37°C. Medium was changed twice weekly. After the CLCs reached 90% confluence in P2, they were pooled and micro-aggregates of 35,000 cells were formed (day 0). In the experimental setup, human CLCs were pooled (a) due to volume limitations of the available human NCCM and (b) in order to specifically assess the effect of donor-specific NCCM on a representative human CLC population that was derived from degenerated IVDs. The pooled CLCs were plated in low-adherence cell-repellent surface 96-well plates (650970, CELLSTAR® Greiner Bio-one, Alphen a/d Rijn, the Netherlands) in 50 µL basal culture medium: hgDMEM+Glutamax with 1% P/S, 1% ITS+ premix (354352, Corning Life Sciences, Amsterdam, the Netherlands), 0.04 mg/mL L-proline (P5607, Sigma-Aldrich, Saint Louis, USA), 0.1 mM Ascorbic acid 2-phosphate, and

1.25 mg/mL Human Serum Albumin (HSA, Sanquin Research, Amsterdam, the Netherlands). The 96-well plates were centrifuged at 50g for 5 minutes to induce micro-aggregate formation. The next day, basal culture medium was replaced with either basal culture medium for the negative control micro-aggregates, chondrogenic culture medium (basal culture medium supplemented with 10 ng/mL human recombinant TGF- $\beta_1$  (240-B, R&D Systems, Inc., Minneapolis, USA)) for the positive control micro-aggregates or human/canine/porcine NCCM supplemented with 1% P/S, 1% ITS+ premix, 0.04 mg/mL L-proline, 0.1 mM ascorbic acid 2-phosphate, and 1.25 mg/mL HSA. The micro-aggregates were cultured for 28 days in 21% O<sub>2</sub>, 5% CO<sub>2</sub>, 37 °C.

### **Cell proliferation and extracellular matrix production of the human CLC micro-aggregates**

#### *The effect of washing NCCM-treated micro-aggregates*

Given that NCCM contains a high GAG concentration which could attach to the micro-aggregates (resulting into a false positive high GAG content), human CLC micro-aggregates cultured for 7 days in canine NCCM ( $n = 4$ ) were 0, 1, 2, or 3 times incubated in 1 mL Hanks Balanced Salt Solution (HBSS, 14024, Life Technologies, Bleiswijk, the Netherlands) for 1 minute to determine whether washing decreased the measured GAG content of the micro-aggregates.

#### *Collagen, DNA and GAG content*

At day 28, the collagen content, and at day 0, 14, and 28, the DNA and GAG content of the human CLC micro-aggregates were determined as described above ( $n = 8-16$  per condition). The micro-aggregates were washed three times with 1 mL HBSS to remove any residual (conditioned) medium, lyophilized for 1 hour, and stored (-20 °C) until use. GAG release into the NCCM culture medium could not be determined due to extremely high NCCM GAG concentrations compared with the GAG release by the micro-aggregates.

#### *Histology*

At day 28, the micro-aggregates were fixed for 24 hours in 4% neutral buffered formaldehyde containing 1% eosin (115935, Merck Millipore, Amsterdam, the Netherlands) to be able to detect them during the cutting process. The next day, the micro-aggregates were embedded in one drop 2.4% alginate (A2033, Sigma-Aldrich, Saint Louis, USA) and paraffin. Five  $\mu\text{m}$  sections were stained with Safranin O/Fast Green as described above, preceded by incubation in citrate (100244, Merck Millipore, Amsterdam, the Netherlands) buffer (10 mM, 0.05% Tween, pH 6) for 15 minutes at RT to ensure alginate removal. IHC staining for collagen type I and II was performed as described previously. For collagen type X immunohistochemistry, antigen retrieval was performed with 0.5% pepsin in PBS (S3002, Dako, Glostrup, Denmark) for 20 minutes at 37°C and 10 mg/mL hyaluronidase in PBS (30 minutes, 37°C). The sections were blocked at RT with Dual Endogenous Enzyme-Blocking Reagent (S2003, Dako, Glostrup, Denmark) and goat serum (5 and 30 minutes, respectively). Thereafter, the sections were incubated overnight at 4°C with 1:50 diluted primary Collagen Type X antibody (2031501005, Quartett, Berlin, Germany). In control staining, the primary antibody was substituted with normal mouse IgG<sub>1</sub> (4  $\mu\text{g}/\text{mL}$ ; 3877, Santa Cruz Biotechnology, Heidelberg, Germany). These negative controls showed no staining. The next day, sections were washed with PBST0.1% before the secondary antibody (EnVision+ System-HRP Goat Anti-Mouse, K4001, Dako, Glostrup, Denmark) was applied (30

minutes, RT). After washing with PBS, the sections were incubated with the liquid DAB substrate chromogen system, counterstained with Hematoxylin QS solution, washed with tap water, dehydrated and mounted (see above).

### Gene expression of the human CLC micro-aggregates

In order to study the transcriptional response of CLCs to NCCM at day 7, micro-aggregates ( $n = 6$  per condition) were frozen in liquid nitrogen and crushed using pestles (P9951-901, Argos Technologies, Elgin, USA). RNA was extracted with the RNeasy® Micro kit (74004, Qiagen, Valencia, USA) according to the manufacturer's instructions. A DNase (RNase-Free DNase Set, 79254, Qiagen, Valencia, USA) step was included to ensure DNA removal. The quality of the isolated RNA was assessed with an Agilent 2100 Bioanalyzer and RNA Nanochip kit (5067-1511, Agilent Technologies, Amstelveen, the Netherlands). cDNA was synthesized using the iScript™ cDNA Synthesis Kit (170-8891, Bio-Rad, Veenendaal, the Netherlands) according to the manufacturer's instructions. Primer sequences were designed using PerlPrimer (<http://perlprimer.sourceforge.net>) or obtained from previous work (Supplementary File 1). M-fold was used to check for secondary structure formation<sup>34</sup>. Primer uniqueness and specificity was determined using BLAST<sup>35</sup>. Annealing temperatures were established by performing a temperature gradient PCR on a 16-fold dilution series. The four most stably expressed reference genes (TATAA-box binding protein (*TBP*), hypoxanthine-guanine phosphoribosyltransferase (*HPRT*), succinate dehydrogenase subunit A (*SDHA*) and tyrosine 3-monooxygenase/tryptophan 5-monooxygenase activation protein, zeta polypeptide (*YWHAZ*)) were chosen to normalize gene expression of the target genes (aggrecan (*ACAN*), a disintegrin and metalloproteinase with thrombospondin motifs 5 (*ADAMTS5*), Bcl2-like-protein (*BAX*), B-cell CLL/lymphoma 2 (*BCL-2*), caspase-3 (*CASP3*), collagen type I (*COL1A1*), collagen type II (*COL2A1*), collagen type X (*COL10A1*), cyclin D1 (*CCND1*) and matrix metalloproteinase 13 (*MMP13*)). RT-qPCR was performed using the iQT™ SYBR Green Supermix Kit (Bio-Rad, Veenendaal, the Netherlands) and the CFX384 Touch™ Real-Time PCR Detection System (Bio-Rad, Veenendaal, the Netherlands). For determination of relative quantitative gene expression, the Normfirst ( $E^{\Delta\Delta Cq}$ ) method was used. For each target gene, the Cq-value of the test sample and the calibrator sample was normalized to the mean Cq-value of the reference genes:  $\Delta Cq = Cq_{\text{mean ref}} - Cq_{\text{target}}$ . Cq-values of the negative control micro-aggregates were used as calibrator. Secondly, the  $E^{\Delta Cq}$ -value for the test and calibrator sample was calculated. In this formula, E indicates the amplification efficiency of the target/reference gene.  $E^{\Delta\Delta Cq}$  was calculated by normalizing the  $E^{\Delta Cq}$ -value of the test sample to the one of the calibrator:  $E^{\Delta\Delta Cq} = E^{\Delta Cq \text{ test}} - E^{\Delta Cq \text{ calibrator}}$ . For each target gene, the mean n-fold changes and standard deviations in gene expression were calculated.

### Statistical analysis

All statistical analyses were performed using IBM SPSS statistics 22. First, the data were examined for normal distribution using a Shapiro Wilks test. A Kruskal Wallis and Mann-Whitney U test were performed on non-normally distributed data, whereas general linear regression models based on ANOVAs were used for normally distributed data. All tests were followed by a Benjamini & Hochberg False Discovery Rate *post-hoc* test for multiple comparisons. A  $p$ -value < 0.05 was considered significant.

## Results

### Analysis of human, canine and porcine NC-rich NP tissue and species-specific NCCM

To characterise the species-specific NP tissue where the NCCM was generated from, the histological phenotype of the NC-rich NP tissue was determined. It appeared comparable in all human donors under 3 months. Healthy canine and porcine NP tissue contained considerably more typical large, vacuolated NCs than human NP tissue, which contained large areas of extracellular matrix with relatively few cells (Figure 1). Scattered throughout the human NP, cells with a transitional phenotype (large, non-vacuolated cells) or CLC phenotype (small, non-vacuolated cells with little cytoplasm) were present. NCs were only scarcely present and were predominantly positioned in cell clusters.

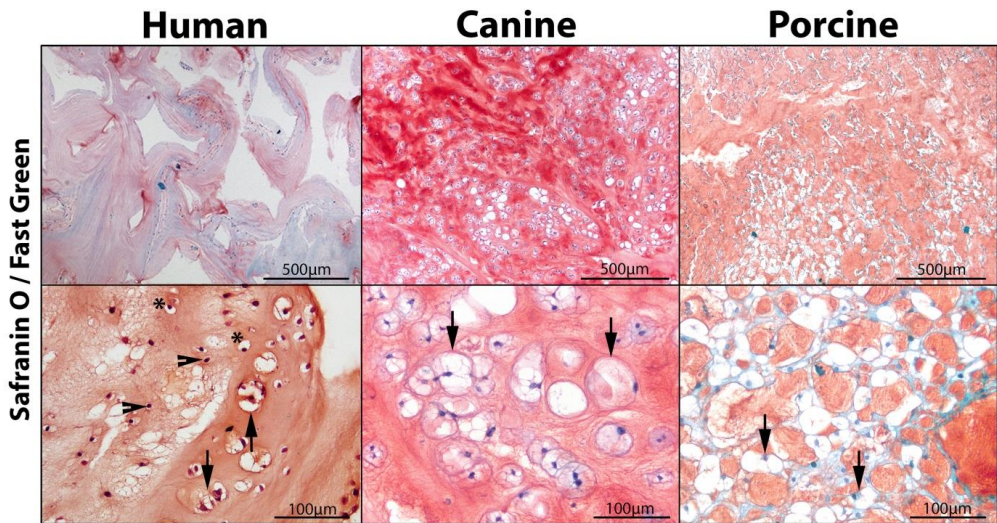


**Figure 1. Canine and porcine nucleus pulposus (NP) tissue contains typical notochordal cells (NCs), whereas human NP tissue contains more cells with a transitional phenotype and chondrocyte-like cells (CLCs).** Safranin O/Fast Green staining of representative human (3 days of age), canine (18 months of age) and porcine (3 months of age) NP tissue obtained from IVDs with Thompson grade I. The lower panel shows the NP cellular phenotype in more detail. Arrows indicate typical large vacuolated NCs, arrowheads indicate typical smaller non-vacuolated CLCs and stars indicate the transitional cell phenotype found in human NP tissue.

The GAG and DNA content per mg wet canine NC-rich NP tissue was significantly higher than that of human and porcine NC-rich NP tissue (Figure 2a;  $p < 0.05$ ). The GAG content corrected for the DNA content of the human, canine and porcine NP tissue, however, was comparable for all species (data not shown). NC-rich human NP tissue contained significantly more collagen (per mg wet NP weight and per  $\mu\text{g}$  DNA of the NP) than NC-rich canine and porcine NP tissue (Figure 2b;  $p < 0.05$ ). In line with these results, the GAG/collagen ratio was significantly lower in the human than in the canine and porcine NC-rich NP (Figure 2c;  $p < 0.05$ ). Canine NC-rich NP tissue contained significantly more collagen per mg wet tissue than porcine NC-rich NP tissue ( $p < 0.01$ ), but not more collagen per DNA content of the NP (Figure 2b). Additionally, there was no statistically significant difference in the GAG/collagen ratio between canine and porcine NC-rich NPs (Figure 2c). In the foetal human NP tissues,

the GAG:collagen ratio was 3.4:1, which equals a GAG:hydroxyproline ratio of 25:1. The latter is in line with previous findings in healthy 2- to 5-year-old human donors, in which the NP GAG:hydroxyproline ratio was 25:1, whereas it was 2:1 in the AF and 3:1 in the cartilagenous endplate<sup>36</sup>. Collagen type II protein was abundantly present in the extracellular matrix of the NP of all donors, regardless the donors species and age, whereas collagen type I was not expressed within the NP (Figure 3). Thus, in the present study, human NP tissue was successfully separated from AF tissue and that solely the effect of species-specific NP-secreted factors was compared, without interference from AF and/or endplate-secreted substances.

The protein and GAG concentration of human and porcine NCCM was comparable and significantly lower than that of canine NCCM (Figure 2d;  $p < 0.05$ ). Collagen was undetectable in NCCM of all tested species (data not shown).

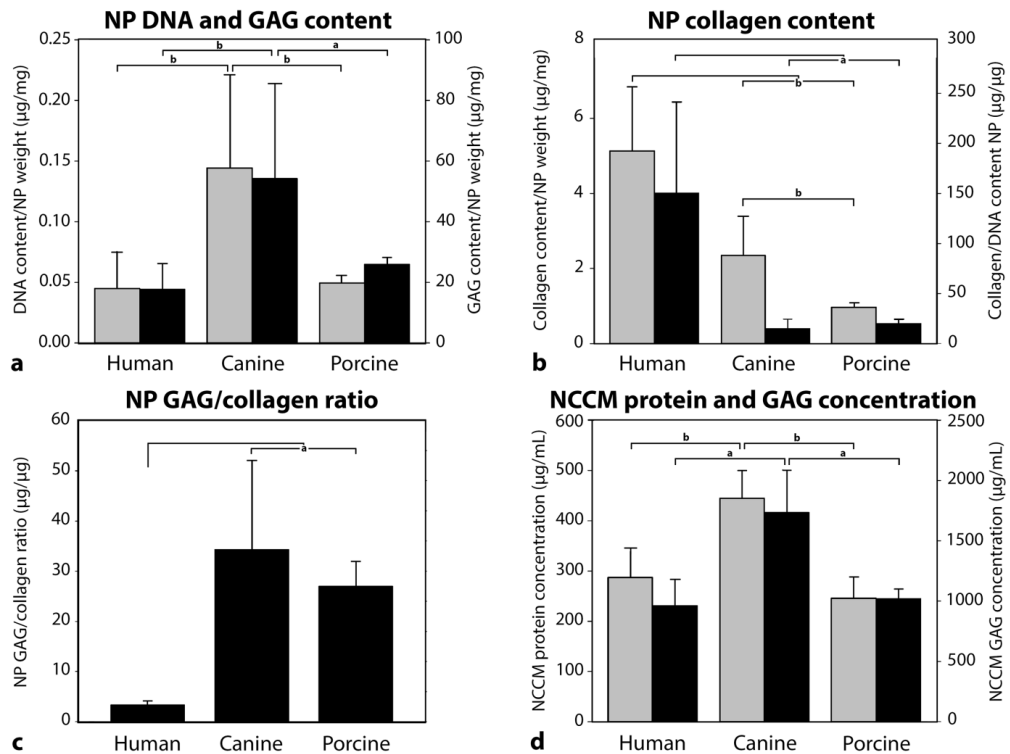


**Figure 2. Canine nucleus pulposus (NP) tissue contains the highest DNA and GAG content, whereas human NP tissue contains the highest collagen content.** Biochemical differences between human, canine, and porcine NC-rich NP tissue (Thompson grade I) and NC-conditioned medium (NCCM). (a) The DNA (grey bar) and GAG (black bar) content (mean±SD) of NC-rich human, canine and porcine NP tissue. (b) The collagen content (mean±SD) of NC-rich human, canine and porcine NP tissue per mg wet NP weight (grey bar) and per DNA content of the NP tissue (black bar). (c) The GAG/collagen ratio (mean±SD) of NC-rich human, canine and porcine NP tissue. (d) The protein (grey bar) and GAG (black bar) concentration (mean±SD) of human, canine and porcine NCCM. a:  $p < 0.05$ ; b:  $p < 0.01$ ;  $n = 4$  (human), 21 (canine) and 6 (porcine) for NC-rich NP tissue and  $n = 7$  (all species) for NCCM analysis.

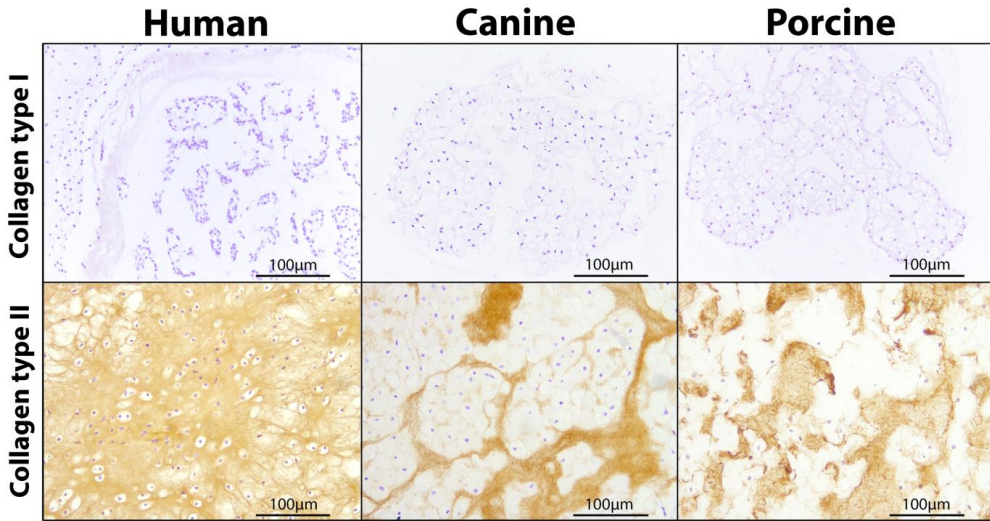


**Figure 3. Human, canine and porcine nucleus pulposus (NP) tissue contains collagen type II but no collagen type I protein.** Collagen type I and II protein expression of representative human (foetal, 21weeks of gestation), canine (18 months of age) and porcine (3 months of age) NPs obtained from IVDs with Thompson grade I.

#### ***In vitro* effects of species-specific NCCM on human CLCs derived from degenerated IVDs**

Since NCCM contains a high GAG concentration that could attach to the outer layer of the micro-aggregates (resulting in an overestimation of the micro-aggregate GAG content), micro-aggregates were washed (1 minute in 1 mL HBSS) to investigate whether this would result into a lower GAG content. Washing the micro-aggregates one or two times resulted into a significantly lower GAG/DNA content ( $p < 0.05$ ; Figure 4g). There was no significant difference in GAG/DNA content between micro-aggregates that were washed two or three times.

No significant differences were detected in DNA, GAG and GAG/DNA content of micro-aggregates cultured in human NCCM generated under normoxic (NX) and hypoxic (HX) conditions (Figure 4a-c), suggesting that oxygen status during NCCM generation does not result into a differential biologic activity on human CLCs. Therefore, the results of these two NCCM conditions were pooled in the rest of the study. The DNA content of the human CLC micro-aggregates decreased over time in every culture condition, except for canine NCCM ( $p < 0.05$ ; Figure 4d). Although not as distinct as TGF- $\beta_1$  treatment, NCCM from all species significantly increased the DNA content of the micro-aggregates compared with controls ( $p < 0.001$ ; Figure 4d). The DNA content of the micro-aggregates cultured in human NCCM was significantly lower than those cultured in canine and porcine NCCM ( $p < 0.05$ ; Figure 4d). NCCM from all species significantly increased the GAG and GAG/DNA content of the micro-aggregates compared with untreated CLCs ( $p < 0.001$ ; Figure 4e and 4f). Although not as potent as TGF- $\beta_1$  treatment, canine and porcine NCCM were significantly more potent than human NCCM in inducing GAG deposition by human CLCs ( $p < 0.001$ , Figure 4e and 4f).

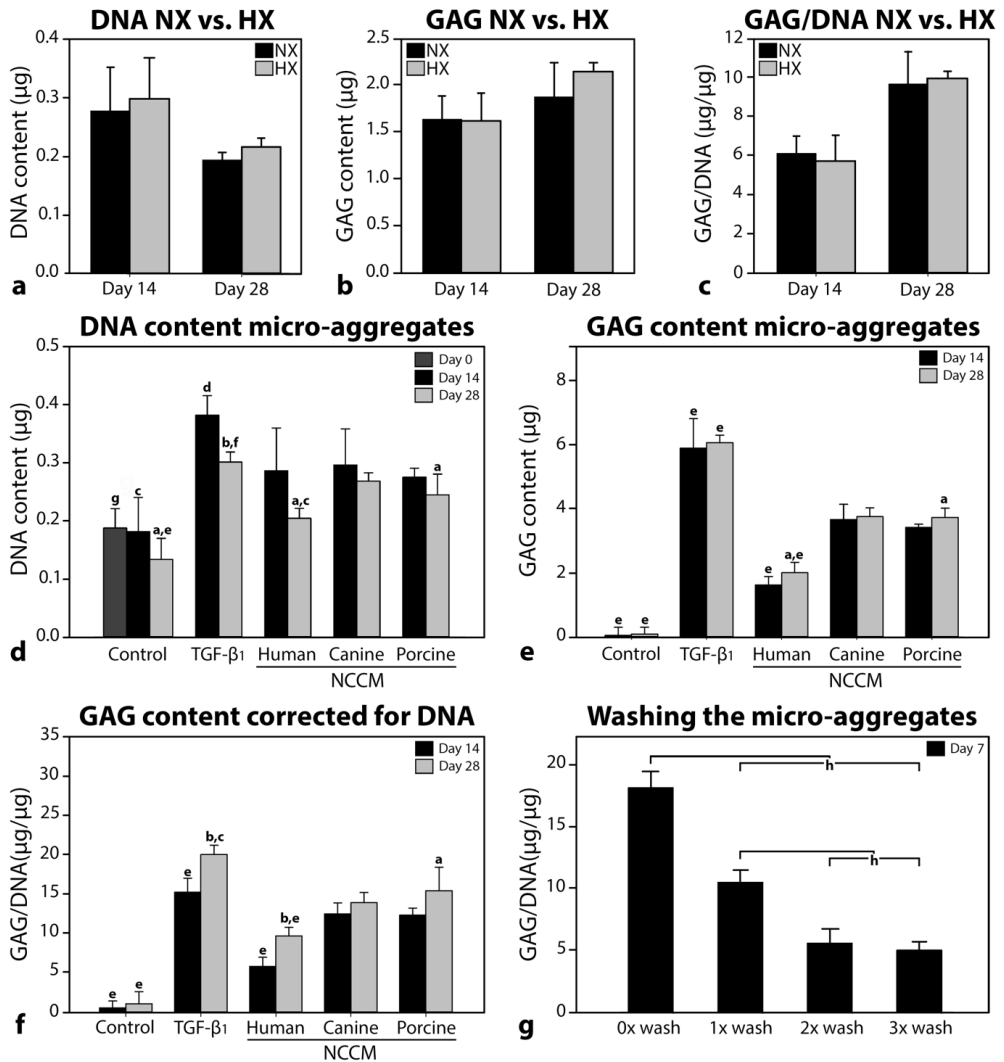


**Figure 4.** NC-conditioned medium (NCCM) derived from human, canine and porcine donors exerts regenerative effects on human chondrocyte-like cells (CLCs) derived from degenerated intervertebral discs (IVDs). Cell proliferation and matrix production of human CLCs derived from degenerated IVDs cultured in micro-aggregates in basal culture medium (control), chondrogenic culture medium (with 10 ng/mL TGF-β<sub>1</sub>) and NC-conditioned medium (NCCM) of different species. (a-c) DNA, GAG and GAG/DNA content (mean+SD) of human CLC micro-aggregates cultured in human NCCM generated under normoxic (NX, 21% O<sub>2</sub>) or hypoxic (HX, 5% O<sub>2</sub>) conditions for 28 days. *n*=4 per condition. (d-f) DNA, GAG and GAG/DNA content (mean+SD) of human CLC micro-aggregates at day 14 and 28 of culture. *n*=8-16 per condition. (g) GAG/DNA content (mean+SD) of human CLC micro-aggregates cultured in canine NCCM for 7 days washed 0, 1, 2 or 3 times with 1 mL PBS. *n*=4. Human: human NCCM (NX and HX, pooled); Canine: canine NCCM (HX); Porcine: Porcine NCCM (HX); a, b: significant difference between day 14 and 28 in this condition (*p*<0.05 and *p*<0.01, respectively); c, d, e: significant difference between this condition and all other conditions at this time point (*p*<0.05, *p*<0.01, and *p*<0.001, respectively); f: significantly different compared with porcine NCCM (*p*<0.001); g: significantly different from the TGF-β<sub>1</sub>, human, canine and porcine NCCM condition at day 14 and the TGF-β<sub>1</sub> condition at day 28; h: *p*<0.05.

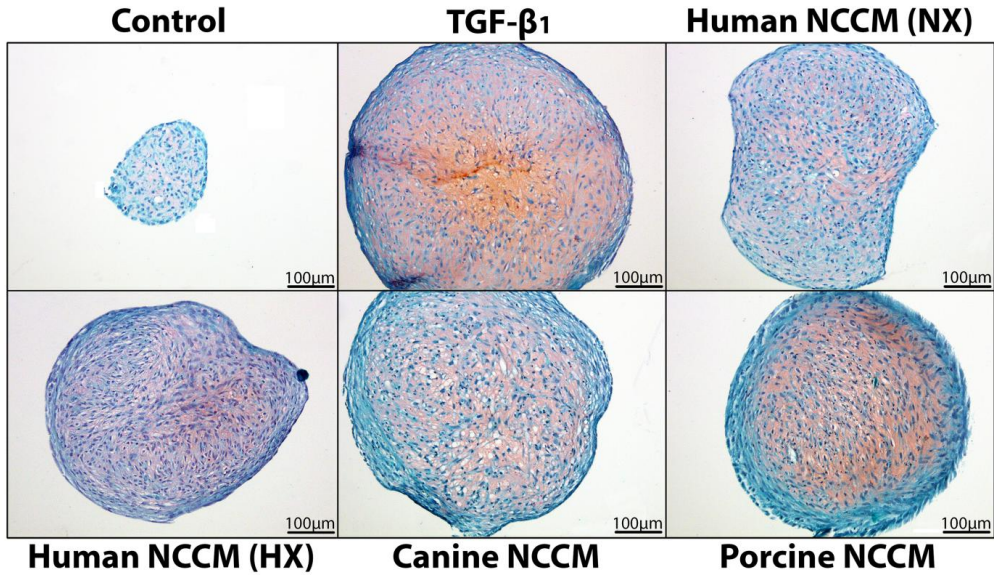


**Figure 5.** NC-conditioned medium (NCCM) derived from human, canine and porcine donors induces GAG deposition in human chondrocyte-like cells (CLCs) derived from degenerated intervertebral discs (IVDs). Safranin O/Fast Green staining of human CLCs derived from degenerated IVDs cultured in micro-aggregates in basal culture medium (control), chondrogenic culture medium (with 10 ng/mL TGF- $\beta_1$ ) and NC-conditioned medium (NCCM) of different species for 28 days. Red staining indicates GAG-rich matrix deposition. NX: Human NCCM generated under normoxic conditions (21% O<sub>2</sub>); HX: Human NCCM generated under hypoxic conditions (5% O<sub>2</sub>). Canine and porcine NCCM was generated under hypoxic conditions.

Safranin O/Fast Green staining indicated that GAGs were present in all NCCM-treated micro-aggregates (Figure 5). A fibrotic rim that did not stain positive for GAGs was visible around the micro-aggregates treated with TGF- $\beta_1$ , canine and porcine NCCM, but was less prominent in human NCCM (Figure 5). In line with these results, *COL1A1* gene expression was significantly increased in these conditions compared with human NCCM and controls ( $p < 0.001$ ; Figure 6a). Moreover, collagen type I protein was abundantly present in TGF- $\beta_1$ -treated micro-aggregates, and in lower amounts in canine and porcine NCCM-treated micro-aggregates (Figure 6b). The HYP assay was not sensitive enough to determine the collagen content of the micro-aggregates.

Although the micro-aggregates that were cultured in NCCM of all species demonstrated an increased GAG content (Figure 4e), *ACAN* and *COL2A1* gene expression was not upregulated in these conditions compared with controls at day 7 (Figure 6a). While *COL2A1* gene expression was significantly increased in the TGF- $\beta_1$ -treated micro-aggregates ( $p < 0.001$ ; Figure 6a), only human NCCM-treated micro-aggregates contained some collagen type II protein (Figure 6b). Furthermore, no significant differences were encountered for gene expression of *CCND1* (proliferation marker), *ADAMTS5* (extracellular matrix degradation), *CASP3* (apoptosis marker), *BCL-2* (anti-apoptosis marker) and *BAX* (apoptosis marker) (data not shown). *MMP13* (extracellular matrix degradation) gene expression was significantly upregulated in the TGF- $\beta_1$ -, porcine-, and human NCCM-treated micro-aggregates compared with controls ( $p < 0.05$ ), whereas collagen type 10 (*COL10A1*, marker of hypertrophy) gene

expression was only detected in the TGF- $\beta_1$ -treated micro-aggregates (data not shown). In contrast, collagen type X protein was not detected in the micro-aggregates treated with TGF- $\beta_1$  or NCCM regardless of the donor species (Figure 6b).

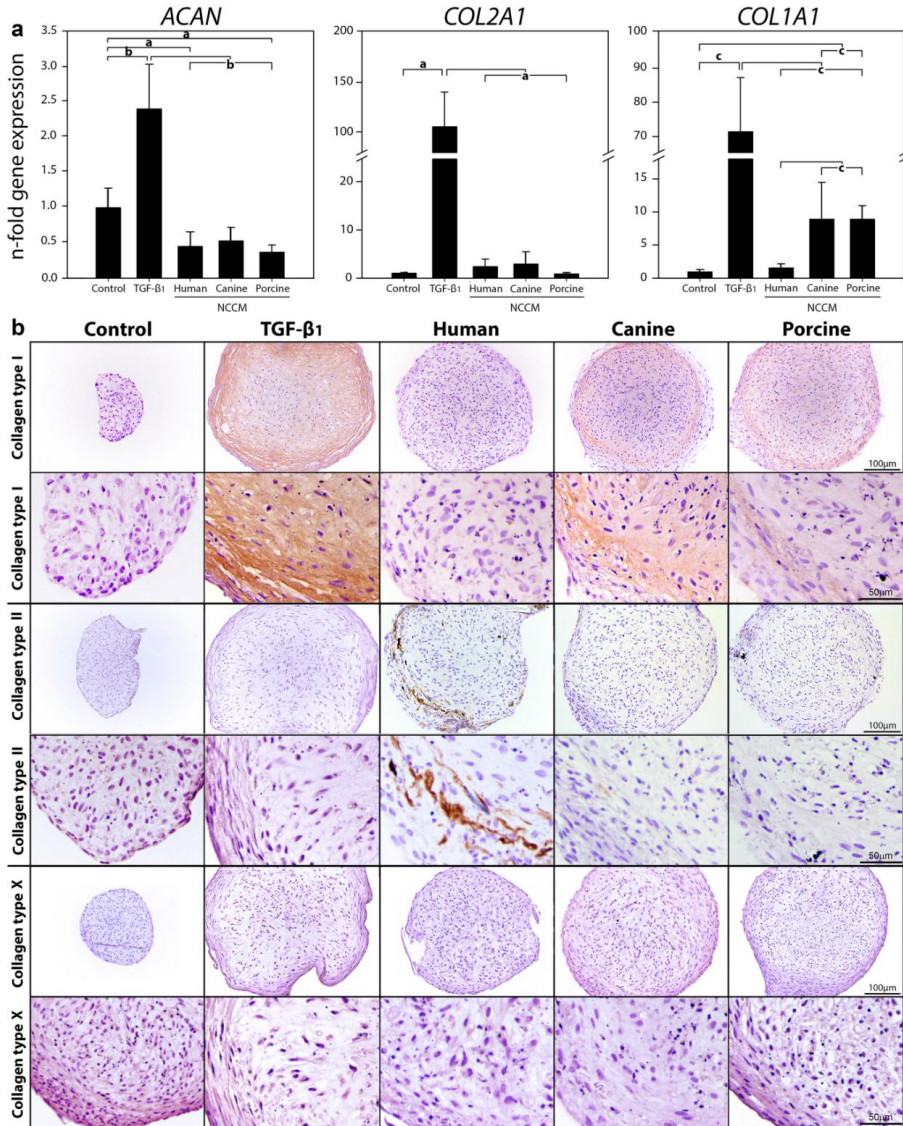


**Figure 6.** Both canine and porcine NC-conditioned medium (NCCM) induces collagen type I production, whereas only human NCCM induces collagen type II production in human chondrocyte-like cells (CLCs) derived from degenerated intervertebral discs (IVDs). Extracellular matrix production of human CLCs derived from degenerated IVDs cultured in micro-aggregates in basal culture medium (control), chondrogenic culture medium (with 10 ng/mL TGF- $\beta_1$ ) and NCCM of different species. (a) Relative *ACAN*, *COL2A1* and *COL1A1* gene expression (mean+SD) of the micro-aggregates at day 7. The control micro-aggregates were set at 1.  $n=6$  per condition. a:  $p<0.05$ ; b:  $p<0.01$ ; c:  $p<0.001$ . (b) Immunohistochemical staining for collagen type I, II and X at day 28. Human: human NCCM (NX and HX samples pooled); Canine: canine NCCM (HX); Porcine: Porcine NCCM (HX).

The GAG/DNA content of the micro-aggregates that were cultured in canine and porcine NCCM was significantly higher than those cultured in human NCCM ( $p < 0.001$ ; Figure 7a). When the GAG/DNA content of the micro-aggregates was corrected for the DNA content (an indirect measure for cell number) of the NP tissue from which the NCCM was generated, porcine NCCM was more, and canine NCCM was less potent in increasing GAG deposition ( $p < 0.01$ , Figure 7b). Also when the GAG/DNA content of the micro-aggregates was corrected for the protein and GAG concentration of species-specific NCCM, porcine NCCM was significantly more potent than human and canine NCCM ( $p < 0.01$ , Figure 7c and 7d).

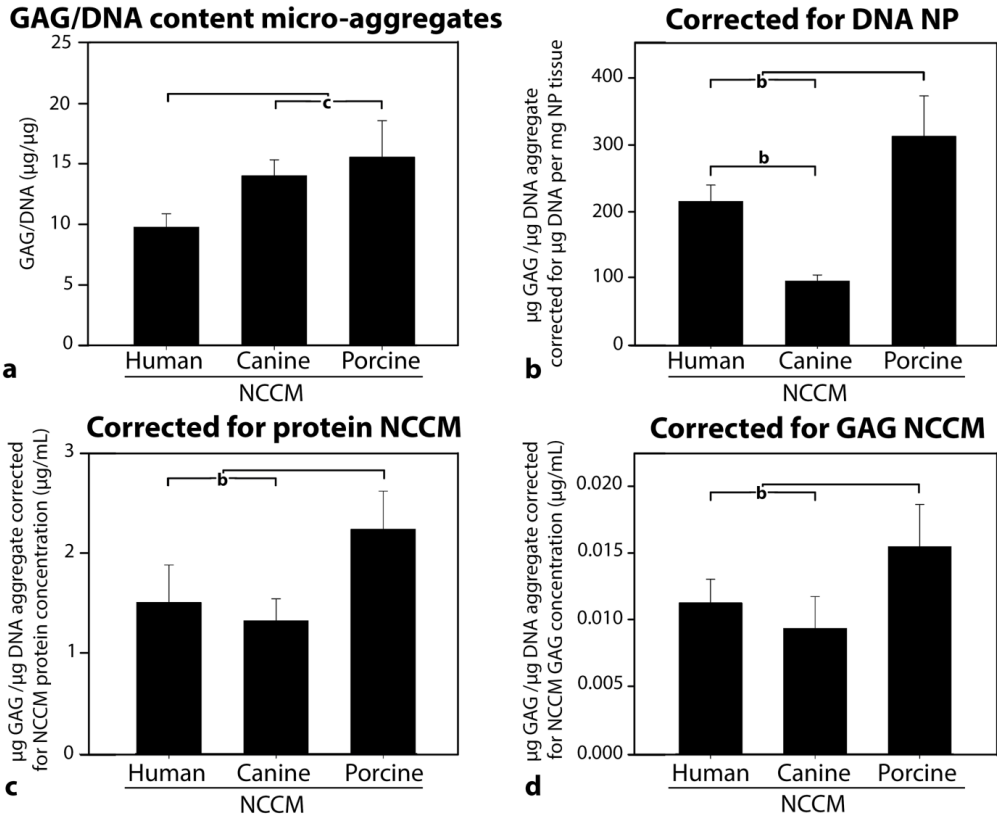


**Figure 7. The regenerative effect of porcine NC-conditioned medium (NCCM) is more potent than that of canine and human NCCM when corrected for nucleus pulposus (NP) or NCCM characteristics.** GAG/DNA content of micro-aggregates derived from human CLCs derived from degenerated IVDs cultured in micro-aggregates in NCCM of different species for 28 days. (a) GAG/DNA content (mean+SD) of micro-aggregates cultured in species-specific NCCM. (b) Corrected for the DNA content of the NP tissue from which the NCCM was generated. (c) Corrected for the donors NCCM protein concentration. (d) Corrected for the donors NCCM GAG concentration.  $n=8$  per condition. a:  $p < 0.05$ ; b:  $p < 0.01$ ; c:  $p < 0.001$ ; Human: human NCCM (NX and HX samples pooled); Canine: canine NCCM (HX); Porcine: Porcine NCCM (HX).

## Discussion

### Differential deposition of extracellular matrix by species-specific NCCM

Canine and porcine NC-secreted factors have already shown promising potential for IVD regeneration<sup>19, 20, 22, 23</sup>. The impact of human NC-secreted factors and the differential effects of xenogeneic NCCM on human CLCs, however, have never been investigated. The present study was, to our knowledge, the first to test the regenerative potential of human NCCM. Furthermore, this study sought to identify whether NC-secreted factors of different species exerted a differential regenerative effect on human CLCs derived from degenerated IVDs. This study demonstrates a cross-species effect of bioactive NC-secreted factors on human CLCs derived from degenerated IVDs. NCCM of all species, generated under identical conditions on the basis of wet NP weight, increased CLC cell numbers and GAG deposition, but canine and porcine NCCM appeared more potent than human NCCM.

Although the IVD is an avascular hypoxic structure and several studies have demonstrated that NCs respond superior to hypoxic than normoxic culture conditions<sup>37, 38</sup>, no difference in regenerative potential was found between human NCCM generated under HX or NX conditions. Unpublished work by our group indicates that also no difference in biologic activity was established between canine NCCM that was generated under NX or HX conditions. In agreement with our studies, previous work demonstrating the regenerative potential of porcine and canine NC-secreted factors have used NCCM generated under HX<sup>20, 23</sup> and NX<sup>19, 21, 24-26, 39</sup> conditions. Altogether, this may imply that oxygen status during NCCM generation does not result in a differential biologic activity of NC-secreted factors on human CLCs.

Matrix deposition by the degenerated CLCs could have been transcriptionally induced, but we cannot exclude the possibility that GAGs from the NCCM were incorporated in the deposited CLC matrix. Although increased GAG deposition was encountered in all NCCM-treated micro-aggregates and, albeit limited, collagen type II deposition was present in the human NCCM-treated micro-aggregates at day 28, gene expression of *ACAN* and *COL2A1* was not upregulated at day 7. In line with our findings, expression of extracellular matrix-related genes is also not increased in porcine NCCM-treated cultures at day 2 (porcine CLCs)<sup>39</sup>, 7 (human CLCs)<sup>23</sup> and 28 (bovine CLCs)<sup>3</sup>. In contrast, an increased expression of extracellular matrix-related genes is encountered in canine NCCM-treated bovine CLCs after 1 day<sup>26</sup> and canine CLCs after 28 days of treatment<sup>18</sup>. Human MSCs treated with porcine NCCM also demonstrate an increased expression of extracellular matrix-related genes at day 21<sup>20</sup>. In the above mentioned studies, different cell types (CLC or MSC) and different species for cell culture/NCCM generation were used. Also, NCCM was generated in different ways (culture medium, additives, days of generation, whole NP tissue or only NCs), and the cells were cultured using different systems and/or conditions, which hampers the comparison of results. Altogether, NCCM achieves regenerative effects by transcriptional regulation of anabolic matrix genes and we may have missed this time-window at 7 days of NCCM culture.

TGF- $\beta_1$  treatment induced undesirable fibrotic (re)differentiation of the CLCs, confirmed by a fibrotic rim around the micro-aggregates and increased collagen type I deposition, while even after 28 days of culture there was no evident collagen type II deposition. NCCM

2 exerted a species-specific anabolic effect on human CLCs derived from degenerated IVDs. While porcine and canine NCCM were more potent in inducing GAG and collagen type I matrix deposition, only human NCCM induced collagen type II deposition. These differences imply that not only quantitative but also qualitative differences in bioactive factors may be present in human compared with canine or porcine NCCM. Also, the bioactive substances in NCCM may be present in a suboptimal concentration. Therefore, future work should aim at the identification of GAG and collagen type II inducing factors in human, canine and porcine NCCM. Combinatory strategies with an optimal balance between bioactive NC-secreted factors may induce optimal NP matrix production. Moreover, the identified species-specific NC-secreted factors may also improve articular cartilage repair, in which GAG and collagen type II production is desirable.

### **Species-specific NP properties may influence the observed regenerative capacity of NCCM**

In this study, phenotypical and biochemical differences between species of NP tissue and NCCM were established, which may account for the observed differential regenerative potency of species-specific NCCM. Numerous typical large, vacuolated NCs were encountered in all canine and porcine NPs<sup>17, 40, 41</sup>, but in very limited numbers in human NPs. Humans lose their NCs at about 6-10 years of age<sup>17</sup>, but in the present study, NCs were only scarcely present in foetal NPs. Only few cells with mainly a transitional or CLC phenotype were present in foetal human NP tissue, indicating that the NCs gradually obtained a mature phenotype<sup>42</sup>. Previous studies also reported mixed NC:CLC populations in foetal human NPs<sup>43, 44</sup>. Specific conditions (*e.g.* hyperglycaemia) have been shown to cause premature NC apoptosis<sup>45</sup>. In the present study, human NC-rich NPs were obtained from non-viable individuals with specific disorders and/or anomalies, which may have influenced the health of the NP tissue and the presence of NCs within these NPs together with the gestation age of the donors. Inherently, the limited presence of NCs may have affected the regenerative potential of human NCCM in this study.

Overall, canine and porcine NCCM were equally potent and more potent than human NCCM in inducing CLC matrix production. However, when taking into account the cellularity (DNA content) of the NP tissue from which the NCCM was generated or the NCCM protein or NCCM GAG concentration, porcine NCCM appeared more potent than canine NCCM. The latter may have been influenced by the differences in lifespan and age (canine: 18-23 months, porcine: 3 months) of the donor species, which may translate into a differential regenerative effect related to NC-physiology. Hence, porcine NCCM may have exerted a relatively more potent regenerative effect than canine NCCM because of the young age of the porcine donors. Since all species have a different life span and lose their NCs at different ages, it would have been a challenge to find 'comparable' interspecies donors. Thus, it is impossible to distinguish species from aging effects of the NCCM. The ageing effect could be circumvented by employing healthy prenatal tissues at a species-specific developmental stage immediately after the development of the IVD. Nevertheless, from a practical point of view, canine and porcine NC-rich NP tissue is more easily available than human NC-rich NP tissue and both exerted a significant regenerative effect on human CLCs. Therefore, canine and in particular porcine donors are suitable for the development of NC-based technologies, in which the NC-secreted bioactive factors can be identified, isolated and eventually synthesized in a human recombinant form.

### Limitations of the study

The first limitation of this study is that passage 2 (P2) CLCs were used. Cell expansion for one or more passages likely induced dedifferentiation of the CLCs, a well-known phenomenon for articular chondrocytes<sup>46, 47</sup>. Since dedifferentiated CLCs could respond differently than freshly isolated CLCs (P0), future studies should determine the effect of (species-specific) NCCM on P0 CLCs and explants. In order to overcome the sample volume limitations of the human NCCM (about 1 mL human NCCM was generated per donor), CLCs derived from IVDs with Thompson grade III from three human donors were pooled in order to assess a representative degenerated CLC population. For this reason, the regenerative effect of species-specific NCCM was also not tested on CLCs derived from human IVDs with other degeneration grades or on CLCs derived from other species. Furthermore, the human CLC micro-aggregates were cultured under normoxic conditions. CLCs may respond more pronounced to the bioactive NC-secreted factors under hypoxic than normoxic conditions given the hypoxic nature of the NP<sup>48, 49</sup>. Therefore, further research under hypoxic conditions is necessary to confirm the obtained results with CLCs from several donors with different IVD degeneration grades. Lastly, it remains to be elucidated if other (symptom modifying) markers were affected by NCCM treatment than the ones measured in the present study, e.g. anti-inflammatory/neurogenic/ angiogenic markers<sup>31</sup>.

### Clinical relevance

The present study showed that human, canine, and porcine NC-secreted factors exerted regenerative effects on human CLCs isolated from degenerated IVDs. Future studies should concentrate on how NCs communicate with CLCs and which (species-specific) NC-secreted factors induce the regenerative effects. Once the bioactive NC-secreted factors have been identified and isolated, synthetic human recombinant products can be developed and their safety and efficacy can be determined. Since canine and porcine NC-secreted factors have a considerable regenerative potential and NC-rich NP tissue from these species is more easily available than human NC-rich NP tissue, canine or porcine NC-based regenerative treatments with synthetic human recombinant products have a promising potential for successful translation into humans.

### Conclusions

This study demonstrated a cross-species effect of human, canine, and porcine NC-secreted factors. NCCM derived from all these species exerted regenerative effects on human CLCs derived from degenerated IVDs in terms of GAG deposition and cell numbers. No difference in regenerative potential was found between human NCCM generated under hypoxic or normoxic conditions. The qualitative and quantitative differences in species-specific NP tissue and NCCM resulted into a differential regenerative effect on human CLCs. Given that canine and porcine NC-rich NP tissue is more easily available than human NC-rich NP tissue and that both canine and porcine NC-secreted factors exerted regenerative effects on human CLCs, canine and in particular porcine donors are suitable to delineate the underlying bioactive substances resulting into IVD regeneration. Once the canine/porcine bioactive NC-secreted factors have been identified and isolated, synthetic human recombinant products can be developed and tested *in vitro* and *in vivo*. Combinatory

strategies with an optimal balance between species-specific bioactive NC-secreted factors may further improve healthy NP matrix production.

## **Acknowledgements**

The authors would like to thank Ferdi van Heel for assistance in cell culturing and analysis.

## References

1. Hohaus C, Ganey TM, Minkus Y, Meisel HJ. 2008. Cell transplantation in lumbar spine disc degeneration disease. *Eur Spine J* 17 Suppl 4: 492-503.
2. Katz JN. 2006. Lumbar disc disorders and low-back pain: Socioeconomic factors and consequences. *J Bone Joint Surg Am* 88 Suppl 2: 21-24.
3. Potier E, de Vries S, van Doeselaar M, Ito K. 2014. Potential application of notochordal cells for intervertebral disc regeneration: An in vitro assessment. *Eur Cell Mater* 28: 68-81.
4. Risbud MV, Schaer TP, Shapiro IM. 2010. Toward an understanding of the role of notochordal cells in the adult intervertebral disc: From discord to accord. *Dev Dyn* 239: 2141-2148.
5. Bergknut N, Smolders LA, Grinwis GC, et al. 2013. Intervertebral disc degeneration in the dog. part 1: Anatomy and physiology of the intervertebral disc and characteristics of intervertebral disc degeneration. *Vet J* 195: 282-291.
6. Colombini A, Lombardi G, Corsi MM, Banfi G. 2008. Pathophysiology of the human intervertebral disc. *Int J Biochem Cell Biol* 40: 837-842.
7. Bach FC, Willems N, Penning LC, et al. 2014. Potential regenerative treatment strategies for intervertebral disc degeneration in dogs. *BMC Vet Res* 10: 3-6148-10-3.
8. Gilbert HT, Hoyland JA, Richardson SM. 2013. Stem cell regeneration of degenerated intervertebral discs: Current status (update). *Curr Pain Headache Rep* 17: 377-013-0377-0.
9. Chujo T, An HS, Akeda K, et al. 2006. Effects of growth differentiation factor-5 on the intervertebral disc--in vitro bovine study and in vivo rabbit disc degeneration model study. *Spine (Phila Pa 1976)* 31: 2909-2917.
10. Huang KY, Yan JJ, Hsieh CC, Chang MS, Lin RM. 2007. The in vivo biological effects of intradiscal recombinant human bone morphogenetic protein-2 on the injured intervertebral disc: An animal experiment. *Spine (Phila Pa 1976)* 32: 1174-1180.
11. Kwon YJ, Lee JW, Moon EJ, et al. 2013. Anabolic effects of peniel 2000, a peptide that regulates TGF-beta1 signaling on intervertebral disc degeneration. *Spine (Phila Pa 1976)* 38: E49-58.
12. Mwale F, Masuda K, Pichika R, et al. 2011. The efficacy of link N as a mediator of repair in a rabbit model of intervertebral disc degeneration. *Arthritis Res Ther* 13: R120.
13. Masuda K, Imai Y, Okuma M, et al. 2006. Osteogenic protein-1 injection into a degenerated disc induces the restoration of disc height and structural changes in the rabbit anular puncture model. *Spine (Phila Pa 1976)* 31: 742-754.
14. Yim RL, Lee JT, Bow CH, et al. 2014. A systematic review of the safety and efficacy of mesenchymal stem cells for disc degeneration: Insights and future directions for regenerative therapeutics. *Stem Cells Dev* 23: 2553-2567.
15. Henriksson H, Hagman M, Horn M, Lindahl A, Brisby H. 2012. Investigation of different cell types and gel carriers for cell-based intervertebral disc therapy, in vitro and in vivo studies. *J Tissue Eng Regen Med* 6: 738-747.
16. Mochida J, Sakai D, Nakamura Y, et al. 2015. Intervertebral disc repair with activated nucleus pulposus cell transplantation: A three-year, prospective clinical study of its safety. *Eur Cell Mater* 29: 202-12.
17. Hunter CJ, Matyas JR, Duncan NA. 2004. Cytomorphology of notochordal and chondrocytic cells from the nucleus pulposus: A species comparison. *J Anat* 205: 357-362.
18. de Vries SA, Potier E, van Doeselaar M, et al. 2015. Conditioned medium derived from notochordal cell-rich nucleus pulposus tissue stimulates matrix production by canine nucleus pulposus cells and bone marrow-derived stromal cells. *Tissue Eng Part A* 21(5-6): 1077-1084.
19. Korecki CL, Taboas JM, Tuan RS, Iatridis JC. 2010. Notochordal cell conditioned medium stimulates mesenchymal stem cell differentiation toward a young nucleus pulposus phenotype. *Stem Cell Res Ther* 1: 18.
20. Purmessur D, Schek RM, Abbott RD, et al. 2011. Notochordal conditioned media from tissue increases proteoglycan accumulation and promotes a healthy nucleus pulposus phenotype in human mesenchymal stem cells. *Arthritis Res Ther* 13: R81.
21. Erwin WM, Islam D, Inman RD, Fehlings MG, Tsui FW. 2011. Notochordal cells protect nucleus pulposus cells from degradation and apoptosis: Implications for the mechanisms of intervertebral disc degeneration. *Arthritis Res Ther* 13: R215.
22. Mehrkens A, Karim MZ, Kim S, et al. 2013. Canine notochordal cell-secreted factors protect murine and human nucleus pulposus cells from apoptosis by inhibition of activated caspase-9 and caspase-3/7. *Evid Based Spine Care J* 4: 154-156.
23. Abbott RD, Purmessur D, Monsey RD, Iatridis JC. 2012. Regenerative potential of TGFbeta3 + dex and notochordal cell conditioned media on degenerated human intervertebral disc cells. *J Orthop Res* 30: 482-488.
24. Aguiar DJ, Johnson SL, Oegema TR. 1999. Notochordal cells interact with nucleus pulposus cells: Regulation of proteoglycan synthesis. *Exp Cell Res* 246: 129-137.
25. Erwin WM, Inman RD. 2006. Notochord cells regulate intervertebral disc chondrocyte proteoglycan production and cell proliferation. *Spine (Phila Pa 1976)* 31: 1094-1099.
26. Erwin WM, Ashman K, O'Donnell P, Inman RD. 2006. Nucleus pulposus notochord cells secrete connective tissue growth factor and up-regulate proteoglycan expression by intervertebral disc chondrocytes. *Arthritis Rheum* 54: 3859-3867.
27. Gantenbein-Ritter B, Chan SC. 2012. The evolutionary importance of cell ratio between notochordal and nucleus pulposus cells: An experimental 3-D co-culture study. *Eur Spine J* 21 Suppl 6: S819-25.
28. Saggese T, Redey P, McGlashan SR. 2015. Same-species phenotypic comparison of notochordal and mature nucleus pulposus cells. *Eur Spine J* 24(9):1976-1985.

29. Cornejo MC, Cho SK, Giannarelli C, Iatridis JC, Purmessur D. 2015. Soluble factors from the notochordal-rich intervertebral disc inhibit endothelial cell invasion and vessel formation in the presence and absence of pro-inflammatory cytokines. *Osteoarthritis Cartilage* 23: 487-496.
30. Gantenbein B, Calandriello E, Wuertz-Kozak K, et al. 2014. Activation of intervertebral disc cells by co-culture with notochordal cells, conditioned medium and hypoxia. *BMC Musculoskelet Disord* 15: 422-2474-15-422.
31. Purmessur D, Cornejo MC, Cho SK, Hecht AC, Iatridis JC. 2013. Notochordal cell-derived therapeutic strategies for discogenic back pain. *Global Spine J* 3: 201-218.
32. Neuman RE, Logan MA. 1950. The determination of hydroxyproline. *J Biol Chem* 184: 299-306.
33. Farndale RW, Sayers CA, Barrett AJ. 1982. A direct spectrophotometric microassay for sulfated glycosaminoglycans in cartilage cultures. *Connect Tissue Res* 9: 247-248.
34. Zuker M. 2003. Mfold web server for nucleic acid folding and hybridization prediction. *Nucleic Acids Res* 31: 3406-3415.
35. Altschul SF, Madden TL, Schaffer AA, et al. 1997. Gapped BLAST and PSI-BLAST: A new generation of protein database search programs. *Nucleic Acids Res* 25: 3389-3402.
36. Mwale F, Roughley P, Antoniou J. 2004. Distinction between the extracellular matrix of the nucleus pulposus and hyaline cartilage: A requisite for tissue engineering of intervertebral disc. *Eur Cell Mater* 8: 58-64.
37. Erwin WM, Las Heras F, Islam D, Fehlings MG, Inman RD. 2009. The regenerative capacity of the notochordal cell: Tissue constructs generated in vitro under hypoxic conditions. *J Neurosurg Spine* 10: 513-521.
38. Omlor GW, Nerlich AG, Tirlapur UK, Urban JP, Guehring T. 2014. Loss of notochordal cell phenotype in 3D-cell cultures: Implications for disc physiology and disc repair. *Arch Orthop Trauma Surg* 134: 1673-1681.
39. Boyd LM, Chen J, Kraus VB, Setton LA. 2004. Conditioned medium differentially regulates matrix protein gene expression in cells of the intervertebral disc. *Spine (Phila Pa 1976)* 29: 2217-2222.
40. Smolders LA, Bergknut N, Grinwis GC, et al. 2013. Intervertebral disc degeneration in the dog. part 2: Chondrodystrophic and non-chondrodystrophic breeds. *Vet J* 195: 292-299.
41. Hunter CJ, Matyas JR, Duncan NA. 2003. The notochordal cell in the nucleus pulposus: A review in the context of tissue engineering. *Tissue Eng* 9: 667-677.
42. Purmessur D, Guterl CC, Cho SK, et al. 2013. Dynamic pressurization induces transition of notochordal cells to a mature phenotype while retaining production of important patterning ligands from development. *Arthritis Res Ther* 15: R122.
43. Rutges JP, Nikkels PG, Oner FC, et al. 2010. The presence of extracellular matrix degrading metalloproteinases during fetal development of the intervertebral disc. *Eur Spine J* 19: 1340-1346.
44. Shen J, Shi Q, Lu J, et al. 2013. Histological study of chordoma origin from fetal notochordal cell rests. *Spine (Phila Pa 1976)* 38: 2165-2170.
45. Won HY, Park JB, Park EY, Riew KD. 2009. Effect of hyperglycemia on apoptosis of notochordal cells and intervertebral disc degeneration in diabetic rats. *J Neurosurg Spine* 11: 741-748.
46. Bekkers JE, Saris DB, Tsuchida AI, et al. 2014. Chondrogenic potential of articular chondrocytes depends on their original location. *Tissue Eng Part A* 20: 663-671.
47. Veilleux NH, Yannas IV, Spector M. 2004. Effect of passage number and collagen type on the proliferative, biosynthetic, and contractile activity of adult canine articular chondrocytes in type I and II collagen-glycosaminoglycan matrices in vitro. *Tissue Eng* 10: 119-127.
48. Yang SH, Hu MH, Sun YH, Lin FH. 2013. Differential phenotypic behaviors of human degenerative nucleus pulposus cells under normoxic and hypoxic conditions: Influence of oxygen concentration during isolation, expansion, and cultivation. *Spine J* 13: 1590-1596.
49. Feng G, Li L, Liu H, et al. 2013. Hypoxia differentially regulates human nucleus pulposus and annulus fibrosus cell extracellular matrix production in 3D scaffolds. *Osteoarthritis Cartilage* 21: 582-588.
50. Spillekom S, Smolders LA, Grinwis GC, et al. 2014. Increased osmolarity and cell clustering preserve canine notochordal cell phenotype in culture. *Tissue Eng Part C Methods* 20: 652-662.

**Supplementary File 1. Primers used for quantitative PCR of the micro-aggregate samples**

Genes	Forward sequence 5' → 3'	Reverse sequence 5' → 3'	Amplicon size	Annealing temp (°C)
<b>Reference genes</b>				
<i>HPRT</i>	TATTGTAATGACCAGTCAACAG	GGTCCTTTTCACCAGCAAG	192	60
<i>SDHA</i>	TGGGAACAAGAGGGCATCTG	CCACCAGTGCATCAAATTCATG	86	58
<i>TBP</i>	TGCACAGGAGCCAAGAGTGAA	CACATCACAGCTCCCCACCA	132	63.5
<i>YWHAZ</i>	ACTTTTGGTACATTGTGGCTTCAA	CCGCCAGGACAACCAGTAT	94	64
<b>Target genes</b>				
<i>ACAN</i>	CAACTACCCGGCCATCC	GATGGCTCTGTAATGGAACAC	160	63.5
<i>ADAMTS5</i>	GCCAGCGGATGTGCAAGC	ACACTTCCCCGGACGCAGA	130	62.5
<i>BAX</i>	GGACGAACTGGACAGTAACATGG	GCAAAGTAGAAAAGGGCGACAAC	150	60
<i>BCL-2</i>	ATCGCCTGTGGATGACTGAG	CAGCCAGGAGAAATCAAACAGAGG	125	64
<i>CASP3</i>	CAGTGGAGGCCGACTTCTTG	TGGCACAAGCGACTGGAT	102	58
<i>CCND1</i>	AGTCTCTGTGCTGCGAAGTGAAAC	AGTGTTCAATGAAATCGTGCGGGGT	480	65
<i>COL1A1</i>	TCCAACGAGATCGAGATCC	AAGCCGAATTCCTGGTCT	191	61
<i>COL2A1</i>	AGGGCCAGGATGTCCGGCA	GGGTCCCAGTTCTCCATCT	195	63.5
<i>COL10A1</i>	CACTACCCAACCAAGACA	CTGGTTTCCCTACAGCTGAT	225	61
<i>MMP13</i>	TCCAGGAATTGGTGATAAAGTAGA	CTGGCATGACGCGACAATA	123	64

All primers were designed in-house using Perlprimer, except for *BAX*<sup>1</sup>, *BCL-2*<sup>1</sup>, *CASP3*<sup>2</sup>, *MMP13*<sup>3</sup> and *CCND1*<sup>4</sup> which were obtained from the literature.

**References**

1. Porichi O, Nikolaidou ME, Apostolaki A, et al. 2009. BCL-2, BAX and P53 expression profiles in endometrial carcinoma as studied by real-time PCR and immunohistochemistry. *Anticancer Res* 29: 3977-3982.
2. Ho YT, Lu CC, Yang JS, et al. 2009. Berberine induced apoptosis via promoting the expression of caspase-8, -9 and -3, apoptosis-inducing factor and endonuclease G in SCC-4 human tongue squamous carcinoma cancer cells. *Anticancer Res* 29: 4063-4070.
3. Ito TK, Ishii G, Chiba H, Ochiai A. 2007. The VEGF angiogenic switch of fibroblasts is regulated by MMP-7 from cancer cells. *Oncogene* 26: 7194-7203.
4. Wen W, Ding J, Sun W, et al. 2010. Suppression of cyclin D1 by hypoxia-inducible factor-1 via direct mechanism inhibits the proliferation and 5-fluorouracil-induced apoptosis of A549 cells. *Cancer Res* 70: 2010-2019.



### **Soluble and pelletable factors in porcine, canine, and human notochordal cell-conditioned medium: implications for IVD regeneration**

Frances C. Bach<sup>1</sup>, Stefan A.H. de Vries<sup>2</sup>, Frank M. Riemers<sup>1</sup>, Janneke Boere<sup>3,4,5</sup>, Ferdi W.M. van Heel<sup>1</sup>, Marina van Doeselaar<sup>2</sup>, Soenita Goerdayal<sup>6</sup>, Peter G.J. Nikkels<sup>7</sup>, Karin Benz<sup>8</sup>, Laura B. Creemers<sup>5</sup>, Maarten A.F.M. Altelaar<sup>6</sup>, Björn P. Meij<sup>1</sup>, Keita Ito<sup>2,5</sup>, Marianna A. Tryfonidou<sup>1</sup>

<sup>1</sup>Department of Clinical Sciences of Companion Animals, Faculty of Veterinary Medicine, Utrecht University, Utrecht, the Netherlands

<sup>2</sup>Orthopedic Biomechanics, Department of Biomedical Engineering, Eindhoven University of Technology, Eindhoven, the Netherlands

<sup>3</sup>Department of Biochemistry and Cell Biology, Faculty of Veterinary Medicine, Utrecht University, Utrecht, the Netherlands

<sup>4</sup>Department of Equine Sciences, Faculty of Veterinary Medicine, Utrecht University, Utrecht, the Netherlands

<sup>5</sup>Department of Orthopedics, University Medical Centre Utrecht, Utrecht, the Netherlands

<sup>6</sup>Biomolecular Mass Spectrometry and Proteomics, Bijvoet Center for Biomolecular Research, Utrecht Institute for Pharmaceutical Sciences and The Netherlands Proteomics Centre, Utrecht University, Utrecht, the Netherlands

<sup>7</sup>Department of Pathology, University Medical Centre Utrecht, Utrecht, the Netherlands

<sup>8</sup>TETEC AG, Reutlingen, Germany

## Abstract

During intervertebral disc (IVD) maturation, notochordal cells (NCs) are replaced by chondrocyte-like cells (CLCs) in the nucleus pulposus, suggesting that NCs play a role in maintaining tissue health. Affirmatively, NC-conditioned medium (NCCM) exerts regenerative effects on CLC proliferation and extracellular matrix (ECM) production. The aim of this study was to identify NC-secreted substances that stimulate IVD regeneration. By mass spectrometry of porcine, canine, and human NCCM, 149, 170, and 217 proteins were identified, respectively, with 66 proteins in common. Mainly ECM-related proteins were identified, but also organelle-derived and membrane-bound vesicle proteins. To determine whether the effect of NCCM was mediated by soluble and/or pelletable factors, porcine and canine NCCM were separated in a soluble (NCCM-S; peptides and proteins) and pelletable (NCCM-P; protein aggregates and extracellular vesicles) fraction by ultracentrifugation, and tested on bovine and canine CLCs *in vitro*, respectively. In each model, NCCM-S exerted a more pronounced anabolic effect than NCCM-P. However, glycosaminoglycan (GAG) uptake from the medium into the carrier gel prevented more definite conclusions. While the effect of porcine NCCM-P on bovine CLCs was negligible, canine NCCM-P appeared to enhance GAG and collagen type II deposition by canine CLCs. In conclusion, porcine and canine NCCM exerted their anabolic effects mainly through soluble factors, but also the pelletable NCCM factors showed moderate regenerative potential. Although the regenerative potential of NCCM-P should not be overlooked, future studies should focus on unraveling the protein-based regenerative mechanism from NCCM produced from isolated NCs, *e.g.* by NCCM fractionation and pathway blocking studies.

## Introduction

Low back pain in humans is associated with intervertebral disc (IVD) degeneration<sup>1, 2</sup>. The IVD consists of a hydrated nucleus pulposus (NP), mainly composed of proteoglycan (PG) and collagen type II, circumferentially confined by the annulus fibrosus (AF) in which collagen type I is most prominent. The PG's negative charges attract water into the NP, but its swelling is restricted by the AF. This gives rise to high osmotic pressure, crucial for sustaining compressive loads in the healthy IVD. IVD degeneration is a complex, multifactorial process and is characterized by replacement of proteoglycans and collagen type II by a fibrous and dysfunctional tissue high in collagen type I. Current treatment methods aim to alleviate pain without addressing the underlying mechanism of IVD degeneration. Therefore, cell- or growth factor-based regenerative strategies have gained increased attention<sup>3-6</sup>. Although several regenerative strategies, e.g. allogeneic mesenchymal precursor cell (<https://clinicaltrials.gov/ct2/show/NCT01290367>)/autologous disc chondrocyte (NCT01640457) transplantation or growth factor application (NCT00813813) have entered the clinical trial phase, no effective regenerative therapy for IVD degeneration is yet clinically available.

In the field of IVD regeneration, notochordal cells (NCs) have gained increasing interest because of their potential regenerative and protective properties<sup>7</sup>. NCs are large, vacuolated cells and are only present in the NP of fetal and young human individuals. They disappear at approximately 10 years of age, leaving the chondrocyte-like cells (CLCs) as the primary cell type in the NP. This process precedes the onset of IVD degeneration, suggesting that NCs play a role in maintaining tissue health. The regenerative effect of NC-secreted factors present in NC-conditioned medium (NCCM) was demonstrated previously on CLCs<sup>8, 9</sup> and MSCs<sup>10-12</sup>, with clear cross-species activity<sup>13</sup>. Furthermore, porcine NCCM exerted a regenerative effect on bovine NP explants<sup>14</sup>, suggesting that NCCM can also stimulate cells in their native tissue.

The use of NCCM itself, however, is not a clinical option; only small volumes can be injected in the IVD, which is likely insufficient to induce a long-term regenerative response. Therefore, identification and subsequent synthetic production of the biologically active factors in NCCM is more appealing. Up to date, only few studies reported on the potential biologically active NCCM factors. Connective tissue growth factor (CTGF) was found in canine<sup>15</sup> and porcine<sup>16</sup> NCCM and alpha-2-macroglobulin, clusterin and tenascin were detected in porcine NCCM<sup>11</sup>.

Initial identification of NCCM's active factors has focused on proteomics, but extracellular vesicles (EVs) have not been considered yet. EVs are a heterogeneous group of small, membrane-enclosed particles (~40 nm to ~5 µm), actively released by cells from various tissue types<sup>17, 18</sup>. EVs play an active role in intercellular signalling, since they can express receptor ligands or can be vehicles of signalling molecules. Previous studies indicated that EVs influence various processes, such as pathogenesis of diseases<sup>19</sup> and tissue regeneration<sup>20</sup>. As such, it was hypothesized that EVs can also be secreted by NCs and may be involved in maintaining healthy NP tissue. The aim of the current study was to identify whether soluble (peptides and proteins) or pelletable (protein aggregates and EVs) factors

are responsible for the anabolic effects of NCCM on CLCs. We hypothesized that both the soluble and pelletable factors contribute to the anabolic effects of NCCM.

## Material and Methods

### Sources of NC-rich NP tissue and generation of NCCM

Thompson grade I IVDs were collected from 5 porcine, 16 canine, and 3 human donors. Porcine spines (3 months of age, C1-S1) were collected from the local abattoir. Canine spines (16-38 months of age, C1-S1) were collected from mixed breed non-chondrodystrophic (NCD) dogs euthanized in unrelated research studies, approved by the Utrecht University Animal Ethics Committee. IVDs from human donors (L2-L5) between 20 weeks of gestation and 2 days of age (postnatal) were obtained during standard postmortem diagnostic procedures, approved by the scientific committee of the Pathology department of the University Medical Centre Utrecht. Anonymous use of redundant tissue for research purposes is a standard treatment agreement with patients in the University Medical Centre Utrecht (Local Medical Ethical Committee (METC) number 12-364). The material was used in line with the code 'Proper Secondary Use of Human Tissue' installed by the Federation of Biomedical Scientific Societies.

### Generation of NCCM

Conditioned medium from porcine ( $n=5$ ), canine ( $n=8$ ), and human ( $n=3$ ) NC-rich NP tissue (NCCM+) was generated by culturing NP tissue for 4 days (1 gram tissue/30 mL) in hgDMEM+Glutamax (31966, Invitrogen) with 1% P/S (P11-010, GE Healthcare Life Sciences) at 37 °C, 5% CO<sub>2</sub> and 5% O<sub>2</sub><sup>13</sup>. After 4 days, NP tissue was removed and NC-conditioned medium was filtered through 70 µm cell strainers. The filtrate was sequentially centrifuged at 200g and 500g (two times ten minutes, 4°C) to remove (dead) cells and debris. Thereafter, the supernatant (cell-free conditioned medium) was concentrated using a 3 kDa Amicon Ultra-15 Centrifugal filter tube (Merck Millipore) at 4000g (45 minutes, 4°C). All substances with a molecular weight >3 kDa were resuspended in fresh hgDMEM+Glutamax and stored in aliquots at -70°C until use. To determine whether the porcine and canine NCCM+ effects were NC-specific, negative control conditioned media (NCCM-) were generated by re-culturing the NP tissue in the presence of 5% fetal bovine serum (FBS, Gibco 16000-044, Life Technologies); the latter results in loss of vacuolated-NC morphology<sup>21</sup>. NP tissue was cultured for 18 days with medium changes twice a week, until no more vacuoles were observed. Subsequently, the NP tissue was washed twice to remove FBS components, and cultured for 4 days in hgDMEM+Glutamax with 1% P/S to generate NCCM-. NCCM- was centrifuged, filtered and stored similar to NCCM+.

### Proteomic analysis of porcine, canine, and human NCCM

NCCM+ from 5 porcine, 5 canine, and 3 human donors were deglycosylated overnight at 37°C with 20 U PGNaseF (V4831, Promega). Protein digestion was performed with filter aided sample preparation (FASP)<sup>22</sup> with a buffer containing 8 M urea in 1 mM Tris-HCl at pH 8.0 and pH 8.5; using filters with cutoff of 10 kD (MRCPR010, YM-10, Microcon). Proteins were reduced with 10 mM DTT (43815, Sigma-Aldrich) alkylated with 200 mM iodoacetamid (I625-5G, Sigma-Aldrich) and digested first for four hours with 2 mg/ml LysC (Lysyl Endopeptidase, 129-02541, Wako) in a ratio of 1:50 and overnight with 0.1 µg/µL trypsin

(V5280, Promega) in a ratio of 1:50. The digested samples were desalted using Oasis HLB 96 well  $\mu$ elution plate (186001828BA, Waters). Finally, samples were dried and reconstituted in 40  $\mu$ L of 10% formic acid/5% DMSO.

Reversed phase nLC-MSMS analysis was performed using a Proxeon EASY-nLC 1000 (Thermo Scientific)<sup>23</sup>. Mass spectra were acquired using Q-Exactive Plus mass spectrometer (Thermo Scientific)<sup>24</sup> at a resolution of 35,000 with a scan range from 375 to 1600 m/z. Dynamic exclusion was set at 10 seconds. Raw data files were analysed using Proteome Discoverer (version 1.4.1.14, Thermo Scientific)<sup>24</sup>. Data were searched against the SwissProt version 2014-12 for *Sus scrofa*, *Canis familiaris* or *Homo sapiens*.

Protein profile analysis was performed with R 3.2.2<sup>25</sup>, using preprocessCore<sup>26</sup>, biomaRt<sup>27</sup>, and VennDiagram<sup>28</sup> packages. For each species, the obtained peptide spectrum match (PSM) values were filtered for each protein on missing or low values. For canine and porcine, the sum of the PSM values for any protein was set at > 5 for at least 4 out of 5 samples and for human, the sum was set at > 4 for at least 2 out of 3 samples. The PSM values of filtered proteins were log transformed and quantile normalized. Each sample was plotted against the species mean to assess data distribution (Figure 1). To compare the profiles of the different species, filtered proteins were given a HGNC gene name using the Uniprot, Ensembl, and HGNC databases and annotation results were manually curated. Per species, gene name lists were compared using a venn diagram and the different overlapping sets were analyzed using toppgene (ToppFun) analysis<sup>29</sup>. Enriched GO Cellular Component terms were remapped to common ancestors within the GO Cellular Component term using GO.db version 3.2.2<sup>30</sup>.

### Separation of the soluble and pelletable NCCM fraction

To unravel whether the biologically active factors in NCCM+ were present in the soluble (NCCM-S) or pelletable (NCCM-P) fraction, ultracentrifugation was performed<sup>17</sup>. 37 mL porcine and canine NCCM was ultracentrifuged at 10,000g (30 minutes, 8,700 rpm; RCF average 10,016g; RCF max 13,648g;  $\kappa$ -factor 2543.1) and 100,000 g (65 minutes, 23,000 rpm; RCF average 70,002g; RCF max 95,389g;  $\kappa$ -factor 363.9) at 4 °C (Beckman Coulter Optima L-90K ultracentrifuge, SW28 rotor). After 100,000g ultracentrifugation, the supernatant containing soluble factors (NCCM-S) was aliquoted and stored at -70°C until use. The 100,000g pellet, containing EVs and protein aggregates, was suspended in 246  $\mu$ L PBS supplemented with 0.2% EV-free bovine serum albumin (BSA, A9418, Sigma-Aldrich) (6.7  $\mu$ L PBS/0.2% BSA per mL NCCM) and stored at -70°C until use. The PBS/0.2% BSA was depleted from EVs by ultracentrifugation O/N at 100,000g. Directly prior to use for culture, aliquots of the pelletable factors (dissolved in PBS/0.2% BSA) were thawed rapidly for maximal functional preservation<sup>18</sup>. Thereafter, in order to yield NCCM-P, 6.7  $\mu$ L of the 100,000g pellet was added to 1 mL basal culture medium (hgDMEM+Glutamax with 1% P/S, 1% ITS+ premix (354352, Corning Life Sciences), 0.04 mg/mL L-proline (P5607, Sigma-Aldrich), 0.1 mM ascorbic acid 2-phosphate, and 1.25 mg/mL BSA. The EV content of NCCM-P was hereby similar to NCCM+.

### Biochemical analysis of NCCM and its fractions

The protein concentration of NCCM+, NCCM-, NCCM-S, and NCCM-P (porcine  $n=4$ , canine  $n=8$ ) was assessed using the Qubit<sup>®</sup> Protein Assay Kit (Q33211, Invitrogen) according to the

manufacturer's instructions. In addition, a dimethyl methylene blue (DMMB) assay<sup>31</sup> was performed to determine the glycosaminoglycan (GAG) concentration.

### ***In vitro* culture of bovine and canine CLCs in pelletable and soluble fractions of NCCM**

Bovine CLCs ( $n=4$  repeats, CLCs from 2 donors pooled per repeat, 2-2.5 years of age, Thompson grade II) were harvested from caudal IVDs obtained from the local abattoir, and chondrodystrophic (CD) canine CLCs ( $n=4$ , 3-10 years of age, Thompson grade III) were harvested from IVDs of dogs euthanized in unrelated research studies, approved by the Utrecht University Animal Ethics Committee. NPs were enzymatically digested with 0.1% pronase (10165921001, Roche Diagnostics) for 90 minutes and subsequently with 0.025% collagenase type II (LS004177, Worthington) for 16 hours at 37°C.

Bovine CLCs were suspended in 1.2% alginate (180947, Sigma-Aldrich) beads of approximately 20  $\mu\text{L}$  at  $3 \times 10^6$  cells/mL<sup>32</sup>. Empty (no cell-containing) and CLC-containing beads were cultured for 28 days at 37°C, 5% CO<sub>2</sub> and 5% O<sub>2</sub> in basal medium or in porcine NCCM+, NCCM-, NCCM-S or NCCM-P (four different porcine NCCM donors), each with the same supplements as basal culture medium.

Given that canine CLCs did not thrive in alginate beads<sup>33</sup>, an albumin-based hydrogel was used<sup>34</sup>. Canine CLCs from four donors were pooled to assess the effect of donor-specific NCCM on a representative canine CLC population. Passage 2 CLCs were incorporated in 40  $\mu\text{L}$  hydrogels composed of chemically activated albumin cross-linked by polyethylene glycol spacers<sup>35</sup> ( $3 \times 10^6$  cells/mL hydrogel). The albumin- and hyaluronic acid-containing hydrogels were cultured for 28 days at 37°C, 5% CO<sub>2</sub> and 5% O<sub>2</sub> in basal culture medium with/without 10 ng/mL TGF- $\beta_1$  (240-B, R&D Systems), or in canine NCCM+, NCCM-, NCCM-S, or NCCM-P (eight different canine NCCM donors), each with the same supplements as basal medium. Unlike bovine CLCs, canine CLCs do not produce a considerable amount of GAGs if no growth factor is supplemented to the culture medium. Therefore, a positive control (10 ng/mL TGF- $\beta_1$ ) was used to show that the canine CLC donors were able to produce GAGs if a proper stimulus was provided, *e.g.* in case these donors would not respond to NCCM. Since the hydrogel bound GAGs present in NCCM, empty hydrogels were cultured along for each NCCM-/NCCM+/NCCM-S/NCCM-P donor to be able to correct for this.

Gene expression profiling (RT-qPCR; canine  $n=8$ ) was performed at day 4, the DNA content (dsDNA High Sensitivity Assay Kit, Q32851, Invitrogen) and GAG content (DMMB assay; porcine NCCM-treated bovine CLCs  $n=4$  and canine NCCM-treated canine CLCs  $n=8$  *in duplo*) were determined at day 0 and 28, and Safranin O/Fast Green staining and collagen type I and II immunohistochemistry (porcine NCCM-treated bovine CLCs  $n=3-4$  and canine NCCM-treated canine CLCs  $n=4-8$ ) were performed at day 28<sup>13</sup>. For gene expression profiling, four reference genes (*GAPDH*, *HPRT*, *RPS19* and *SDHA*) were chosen to normalize gene expression of the target genes *ACAN*, *ADAMT5*, *BAX*, *BCL-2*, *CASP3*, *COL1A1*, *COL2A1*, *COL10A1*, *CCND1*, *FOXF1*, *KRT8*, *KRT18*, *KRT19*, *MMP13*, *T*, and *VEGF*. Primer sequences are depicted in Supplementary File 1. The DMMB assay was done with the following modifications: papain and DMMB solution pH was adjusted to 6.8 and guanidinium chloride was used to mask hyaluronic acid.

### Testing fresh versus frozen pelletable NCCM factors *in vitro*

To determine whether freezing the pelletable factors affected their biological effect, micro-aggregates of 35,000 CD canine CLCs were generated<sup>13</sup>. CLCs have more easy access to the pelletable factors in this culture model compared with hydrogels. The micro-aggregates were cultured in low-adherence 96-well plates (650970, CELLSTAR® Greiner Bio-one) at 37°C, 5% CO<sub>2</sub> and 5% O<sub>2</sub> for 7 days and were treated with basal culture medium (control), freshly generated, non-frozen NCCM-P (P1x fresh; kept at 4°C for maximum 4 days) or canine NCCM-P that was frozen at -70°C for maximum 4 days (P1x frozen). To determine whether a higher concentration pelletable factors would exert a more pronounced effect, fresh and frozen pelletable factors were also applied in a 10 times higher concentration than present in NCCM+ (NCCM-P10x fresh and NCCM-P10x frozen, respectively). The same CD canine CLC donors as used in the hydrogel experiment and 4 different NCD canine NCCM donors were used for this part of the study. Gene expression profiling (RT-qPCR;  $n=8$ ) was performed at day 4 and the DNA and GAG content of the micro-aggregates ( $n=8$ ) was determined at day 7 as described above.

### Statistical analysis

Statistical analyses were performed using IBM SPSS statistics 22. Data were examined for normal distribution using a Shapiro Wilks test. Kruskal Wallis and Mann-Whitney U test were performed on non-normally distributed data and one-way ANOVA on normally distributed data. Benjamini & Hochberg False Discovery Rate *post-hoc* tests were performed to correct for multiple comparisons. In all tests, a  $p$ -value < 0.05 was considered significant.

## Results

### Proteomic analysis of porcine, canine, and human NCCM+

NCCM+ from 5 porcine, 5 canine, and 3 human donors was subjected to mass spectrometry and bioinformatic analysis. Log<sub>2</sub>-values of the number of PSMs plotted against the log<sub>2</sub>-values of the mean PSM number for each protein showed a wider distribution for canine NCCM, indicating a higher inter-donor variability than porcine and human NCCM (Figure 1). Raw pre-filtered protein profiles for porcine, canine and human NCCM contained respectively 737, 847, and 779 Uniprotids of which 153, 178, and 217 were left after filtering. These were annotated to 149, 170, and 217 different HGNC gene names for porcine, canine, and human, respectively, and were used for profile comparisons (Table 1). The three species had 66 of these proteins in common. A large fraction of the proteins was derived from organelles (22%, Figure 1) and macromolecular protein complexes (24%). Furthermore, a considerable amount of extracellular matrix (ECM) (16%) and membrane-bound vesicle proteins (10%) was found in NCCM from all species.

Pathway analysis (Reactome, V55) of all common proteins revealed various processes involved in ECM and its structure (Table 2). The GAG-, collagen-, hyaluronic acid- and integrin-binding pathways were significantly covered, as well as the structural molecule activity and protein complex binding pathways. Other detected pathways contained growth factor- and enzyme-binding proteins.

Due to the presence of specific collagens (e.g. type III, V and XV) in porcine and human, but not in canine NCCM, pathways involved in the assembly of collagen fibrils, biosynthesis and formation were significantly covered by proteins present in human and porcine NCCM (Table 3). Also, proteins from platelet-involved pathways were found in these two species (Table 3). Analysis of proteins common in human and canine NCCM demonstrated pathways related to glucose metabolism (Table 4). Furthermore, due to the presence of decorin and biglycan, dermatan sulfate and chondroitin sulfate biosynthesis pathways were significantly covered in human and canine NCCM (Table 4). Both canine and porcine NCCM (Table 5) contained proteins involving tubulin-related pathways. Furthermore, several pathways with proteins present in only human, porcine, or canine NCCM were detected (Tables 6-8). In porcine (Table 6) and human NCCM (Table 8), proteins related to complement binding pathways were detected. Lastly, proteins from axon guidance-related pathways were present in NCCM from all species (Table 3 and 7).

A significant number of proteins involved with transcription factor (e.g. Activator protein 1 (AP-1) and paired box gene 4 (PAX4)) binding sites were found in NCCM from all species (Table 9). Furthermore, proteins (predicted to be) targeted by miRNA29 were found in human and porcine NCCM (Table 10).

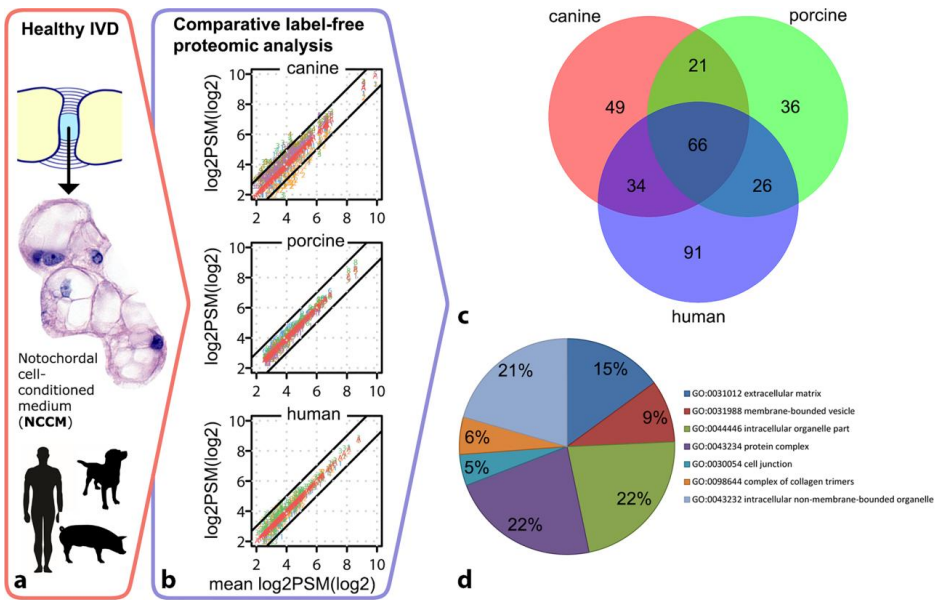


**Figure 1. Proteomic analysis of porcine, canine, and human notochordal cell (NC)-conditioned medium (NCCM).** (a) NCCM was generated from NC-rich nucleus pulposus (NP) tissue of porcine ( $n=5$ ), canine ( $n=5$ ), and human ( $n=3$ ) donors. (b) Log<sub>2</sub> values of the number of peptide spectrum matches (PSM) plotted against the average number of PSMs for each protein show a higher inter-donor variability for canine NCCM than for porcine and human NCCM. (c) The number of proteins discovered in porcine, canine, and human NCCM, and their combinations. (d) Cell and/or matrix origins of the 66 proteins in common to all three species NCCM.

***In vitro* culture of bovine CLCs in porcine NCCM**

Porcine NCCM and its fractions were analysed for their protein and GAG concentration (Figure 2a). NCCM-S contained a similar protein concentration as NCCM+, whereas the protein concentration of NCCM-P was significantly lower than that of NCCM+, NCCM-S and NCCM- ( $p<0.05$ ). The NCCM- protein concentration was significantly lower than that of NCCM+ ( $p<0.05$ ). Also the GAG concentration of NCCM+ and NCCM-S was comparable, and both were significantly higher than that of NCCM-P and NCCM- ( $p<0.05$ ). Although few GAGs were present in NCCM-, its GAG concentration was still significantly higher than that of NCCM-P ( $p<0.05$ ).

After 28 days, bovine CLC-containing alginate beads cultured in porcine NCCM (fractions) were analysed for DNA and GAG content and histology and compared with controls. Empty alginate beads did not bind GAGs (not shown). Although CLCs proliferated and formed clusters in all conditions, no statistically significant differences in DNA content were found between conditions (Figure 2b). The GAG and GAG/DNA content was, however, significantly increased for culture in NCCM+ and NCCM-S compared to control medium ( $p<0.05$ ), whereas it was not increased for NCCM- or NCCM-P (Figure 2c and 2d). The increased GAG content in NCCM+ and NCCM-S-treated beads was confirmed by Safranin O/Fast Green staining (Figure 2e). Immunohistochemical staining showed no collagen type I deposition in any condition. Collagen type II, however, was deposited in all conditions: only in the pericellular region in the control- and NCCM-P-treated alginate beads, but more abundant after NCCM+, NCCM-S, and NCCM- treatment.

***In vitro* culture of canine CLCs in canine NCCM**

Canine NCCM and its fractions were analysed for their protein and GAG concentration (Figure 3a). The protein and GAG concentration of canine NCCM+ and NCCM-S was significantly higher than that of NCCM- and NCCM-P, whereas the protein and GAG concentration of NCCM-P was significantly lower than that of NCCM- ( $p<0.001$ , Figure 3a).

After 4 days of culture, gene expression profiling was performed on the canine CLC-containing hydrogels and after 28 days of culture, the hydrogels were analysed for DNA and GAG content and histology. The DNA content and *CCND1* (a marker for cell proliferation) expression of the TGF- $\beta_1$ -treated hydrogels was significantly increased compared with all other conditions ( $p<0.05$ , Figure 3b and 4f). Furthermore, NCCM+ and NCCM-S-treated hydrogels showed a significantly increased DNA content compared with controls, and NCCM+ treatment showed a significantly increased DNA content compared with NCCM-P and NCCM- treatment ( $p<0.05$ , Figure 3b). *CCND1* expression was significantly lower in NCCM-P-treated CLCs than in NCCM-/NCCM+/NCCM-S-treated CLCs ( $p<0.05$ , Figure 4f).

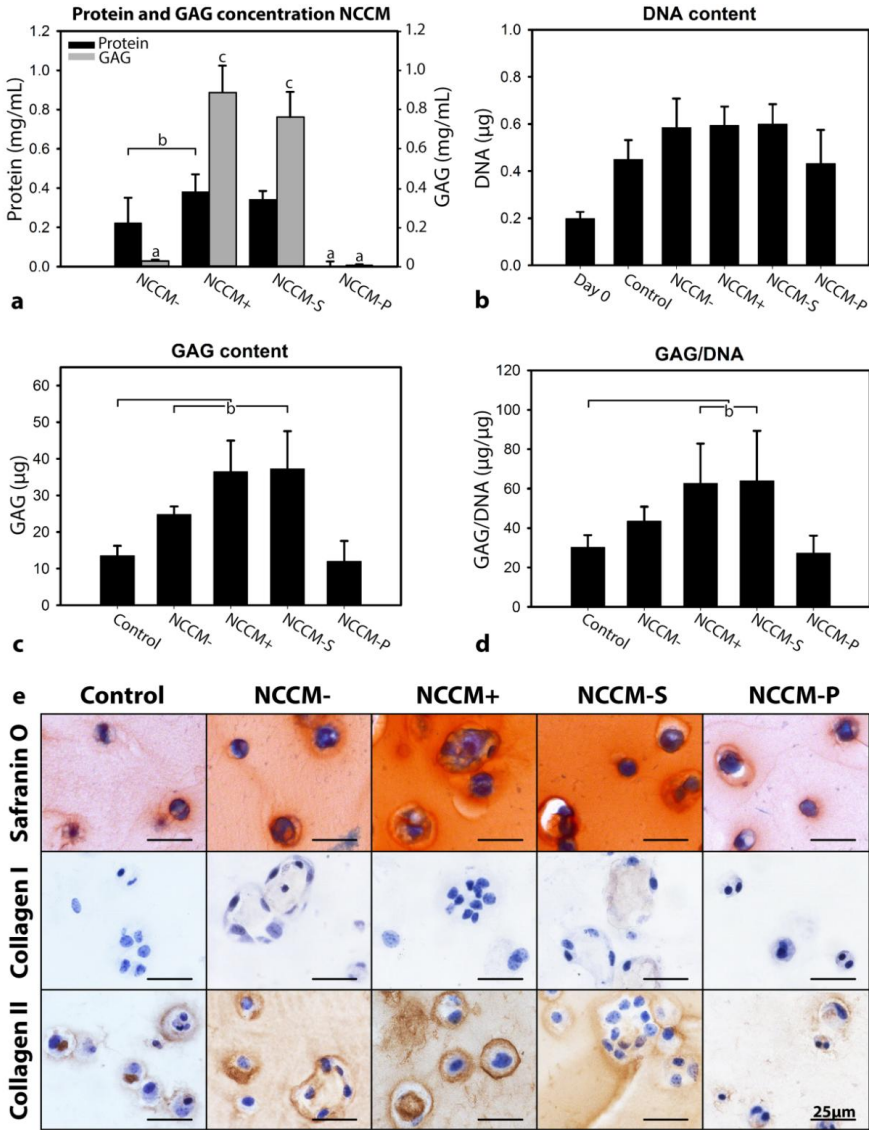


**Figure 2. Soluble factors derived from porcine NC-conditioned medium (NCCM) exert anabolic effects on bovine chondrocyte-like cells (CLCs) derived from caudal intervertebral discs (IVDs).** Cell proliferation and matrix production of bovine CLCs cultured in alginate beads in basal culture medium (control), NCCM from dedifferentiated NCs (NCCM-), NCCM from healthy NCs (NCCM+), and the soluble (NCCM-S) and pelletable (NCCM-P) fraction of NCCM+, which were separated by ultracentrifugation. (a) Protein (black) and glycosaminoglycan (GAG, grey) concentration (mean + SD) of porcine NCCM (fractions). (b-d) DNA, GAG and GAG/DNA content (mean + SD) of bovine CLC alginate beads at day 28. (e) Safranin O/Fast Green staining and collagen type I and II immunohistochemistry of bovine CLC alginate beads at day 28. a: significant difference between this condition and all other conditions ( $p < 0.05$ ); b: significant difference between these conditions ( $p < 0.05$ ); c: significant difference between this condition and all other conditions except for the other condition indicated with 'c' ( $p < 0.05$ );  $n = 4$ .

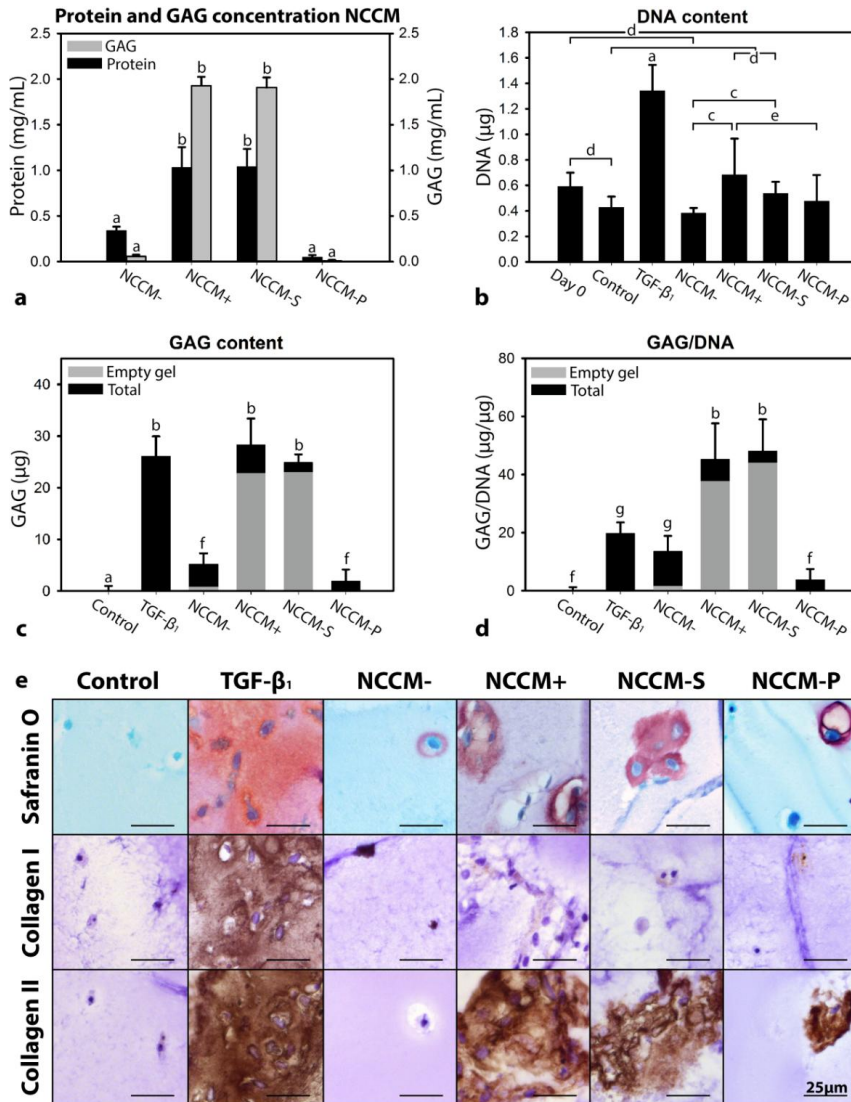


**Figure 3.** Both soluble and pelletable factors derived from canine NC-conditioned medium (NCCM) exert anabolic effects on canine chondrocyte-like cells (CLCs) derived from degenerated intervertebral discs (IVDs). Cell proliferation and matrix production of canine CLCs cultured in hydrogels in basal culture medium (control), basal culture medium supplemented with 10 ng/mL TGF-β<sub>1</sub>, NCCM from dedifferentiated NCs (NCCM-), NCCM from healthy NCs (NCCM+), and the soluble (NCCM-S) and pelletable (NCCM-P) fraction of NCCM+, which were separated by ultracentrifugation. **(a)** Protein (black) and glycosaminoglycan (GAG, grey) concentration (mean + SD) of canine NCCM (fractions). **(b-d)** DNA, GAG, and GAG/DNA content (mean + SD) of canine CLC hydrogels at day 28. The grey colour in the black bars indicates the level of GAGs present in cell-free NCCM-treated hydrogels for these conditions. **(e)** Safranin O/Fast Green staining and collagen type I and II immunohistochemistry of canine CLC hydrogels at day 28. Significant differences are indicated for non-corrected data (not corrected for empty gels). a: significant difference between this condition and all other conditions ( $p < 0.001$ ); b: significant difference between this condition and all other conditions except for the other condition indicated with 'b' ( $p < 0.001$ ); c, d, e: significant difference between these conditions with  $p < 0.001$ ,  $p < 0.01$ , and  $p < 0.05$ , respectively; f and g: significant difference between this condition and all other conditions with  $p < 0.01$  and  $p < 0.05$ , respectively;  $n = 8$  for DNA and GAG content and  $n = 4-8$  for histology.

Using the DMMB assay, empty (no cell-containing) hydrogels were found to incorporate a large amount of NCCM-derived GAGs, indicated by the grey bars in Figure 3c. The GAG content of the control hydrogels was significantly lower than that of all other conditions ( $p < 0.001$ , Figure 3c). TGF- $\beta_1$ , NCCM+ and NCCM-S treatment induced the highest total GAG content of the CLC-containing hydrogels: significantly higher than after NCCM- and NCCM-P treatment ( $p < 0.001$ , Figure 3c). The GAG content of the NCCM-P-treated hydrogels was significantly lower than that of the hydrogels treated with NCCM- ( $p < 0.01$ , Figure 3c). The total GAG/DNA content of NCCM+ and NCCM-S-treated hydrogels was the highest, followed by hydrogels treated with TGF- $\beta_1$ , NCCM-, NCCM-P and basal culture medium, respectively ( $p < 0.05$ , Figure 3d). Safranin O/Fast Green staining indicated that most GAGs were deposited in the TGF- $\beta_1$ -treated hydrogels, followed by NCCM+ and NCCM-S-treated hydrogels (Figure 3e). Collagen type I deposition was only induced by TGF- $\beta_1$  treatment, not by NCCM fractions (Figure 3e). Collagen type II was mostly deposited in NCCM+, NCCM-S, and TGF- $\beta_1$ -treated hydrogels, but also some collagen type II was present in NCCM-P-treated hydrogels (Figure 3e). Affirmatively, at gene expression level, TGF- $\beta_1$  treatment significantly induced *ACAN*, *COL1A1* and *COL2A1* mRNA compared with all other conditions ( $p < 0.05$ , Figure 4a-c). In contrast, NCCM (fractions) did not influence *COL2A1* expression compared with controls (Figure 4a-c). NCCM-P inhibited *ACAN* expression and NCCM- and NCCM+ induced *COL1A1* expression compared with controls ( $p < 0.05$ , Figure 4a-c). *COL10A1* expression was not detected in any condition (data not shown).

Furthermore, TGF- $\beta_1$  treatment significantly reduced *ADAMTS5* expression compared with all other conditions, whereas NCCM- significantly induced *ADAMTS5* expression compared with controls and NCCM-P ( $p < 0.05$  Figure 4d). NCCM+ induced even more *ADAMTS5* expression than NCCM- and NCCM-S increased *ADAMTS5* expression compared with NCCM-P ( $p < 0.05$ , Figure 4d). *MMP13* expression was significantly decreased by TGF- $\beta_1$  treatment compared with controls, whereas NCCM-S reduced *MMP13* expression compared with controls, NCCM+ and NCCM-P ( $p < 0.05$ , Figure 4e). Expression of the notochordal marker *T* was not detected regardless the culture condition (data not shown), whereas expression of notochordal marker *KRT8* was significantly higher in micro-aggregates treated with NCCM+ than in micro-aggregates treated with NCCM-P, NCCM-, TGF- $\beta_1$  and the negative controls ( $p < 0.05$ , Figure 4g). Expression of NP marker *KRT18* was significantly increased in micro-aggregates treated with basal culture medium, NCCM+, NCCM-S, and NCCM-P compared with TGF- $\beta_1$ -treated micro-aggregates ( $p < 0.05$ , Figure 4h). *KRT19* expression was significantly increased by NCCM-P and NCCM-S treatment compared with controls ( $p < 0.05$ , Figure 4i). Additionally, NCCM+, NCCM-S, and NCCM-P treatment significantly increased the expression of this NP marker compared with NCCM- and TGF- $\beta_1$  treatment ( $p < 0.05$ , Figure 4i). In contrast, *FOXF1* expression was not influenced by the culture conditions (Figure 4j). Expression of the angiogenic marker *VEGF* was significantly higher in micro-aggregates treated with NCCM- than in all other conditions ( $p < 0.05$ , Figure 4j). Furthermore, *VEGF* expression was significantly decreased by NCCM-P treatment compared with control, TGF- $\beta_1$  and NCCM-S treatment ( $p < 0.05$ ). Apoptosis-related genes (*BAX*, *BCL2*, *CASP3*) were not differentially expressed between the conditions (data not shown).

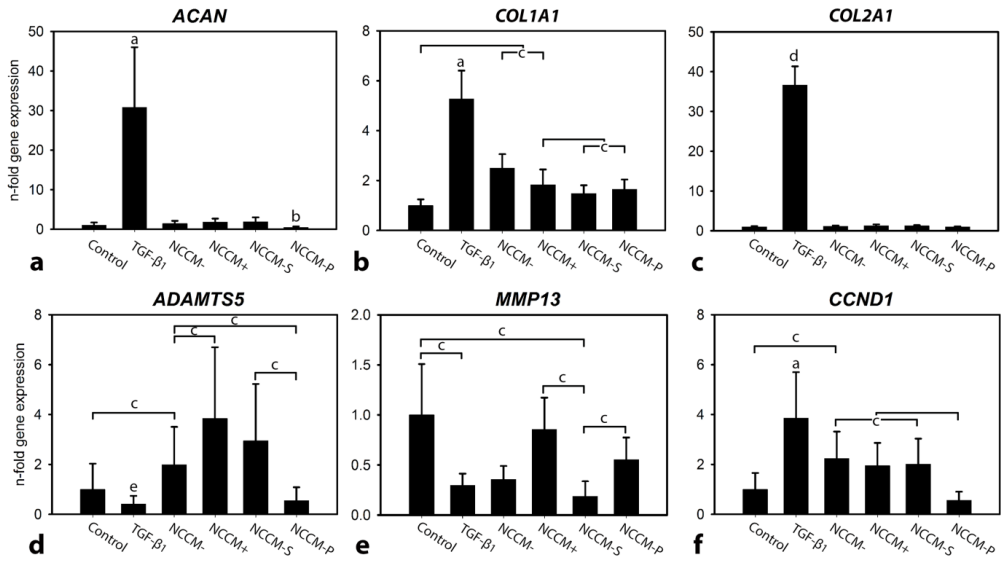


**Figure 4.** Only the soluble factors present in canine NC-conditioned medium (NCCM) stimulate expression of genes related to cell proliferation of canine chondrocyte-like cell (CLC), but none of the NCCM (fractions) effects expression of genes related to matrix production. Target gene expression levels of canine CLCs cultured in hydrogels in basal culture medium (control), basal culture medium supplemented with 10 ng/mL TGF- $\beta_1$ , NCCM from dedifferentiated NCs (NCCM-), NCCM from healthy NCs (NCCM+), and the soluble (NCCM-S) and pelletable (NCCM-P) fraction of NCCM+, which were separated by ultracentrifugation. (a-k) Relative *ACAN*, *COL1A1*, *COL2A1*, *ADAMTS5*, *MMP13*, *CCND1*, *KRT8*, *KRT18*, *KRT19*, *FOXF1*, and *VEGF* gene expression (mean + SD) of the hydrogels at day 4. The control hydrogels were set at 1. a: significant difference between this condition and all other conditions ( $p < 0.05$ ); b: significant difference between this condition and all other conditions except control ( $p < 0.05$ ); c: significant difference between these conditions and all other conditions ( $p < 0.05$ ); d: significant difference between this condition and all other conditions ( $p < 0.01$ ); e: significant difference between this condition and all other conditions except NCCM-P ( $p < 0.05$ );  $n = 8$ .

### Fresh versus frozen pelletable factors present in canine NCCM

Gene expression profiling of CD canine CLC micro-aggregates cultured in basal culture medium (control), 1x concentrated fresh (non-frozen) and frozen NCCM-P and 10x concentrated fresh (non-frozen) and frozen NCCM-P was performed at day 4. Due to donor variability, high standard deviations were obtained (Figure 5a). At day 7, the DNA content of all micro-aggregates was significantly decreased compared with day 0 ( $p < 0.01$ , Fig 5b). The GAG and GAG/DNA content of the controls was significantly lower than that of the micro-aggregates treated with 1x and 10x concentrated NCCM-P ( $p < 0.01$ , Fig 5b). Moreover, the GAG and GAG/DNA content of the micro-aggregates treated with 10x concentrated NCCM-P was significantly higher than that of the micro-aggregates treated with 1x concentrated NCCM-P ( $p < 0.01$ , Fig 5b), indicating a concentration-dependent effect, which could be repeated with frozen NCCM-P. This indicates that freezing the pelletable factors for a short period (1 hour-4 days) at  $-70^\circ\text{C}$  in EV-depleted PBS/0.2%BSA did not affect their biological effect.

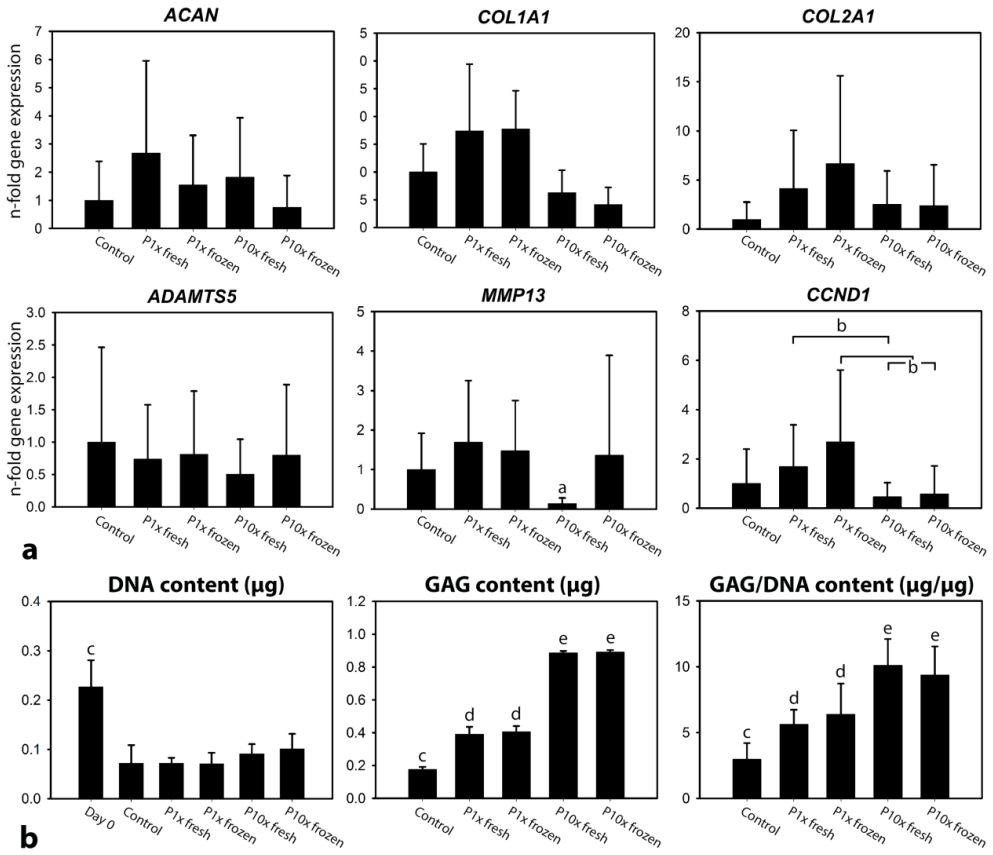


**Figure 5. Frozen canine pelletable NCCM factors exert comparable anabolic effects as freshly applied (non-frozen) pelletable NCCM factors, while a ten times higher concentration of pelletable factors induces a more pronounced effect on canine chondrocyte-like cell (CLC) matrix production.** Target gene expression levels and DNA and glycosaminoglycan (GAG) content of canine CLCs cultured in micro-aggregates in basal culture medium (control), or 1x concentrated freshly generated, non-frozen NCCM-P (P1x fresh), 1x concentrated NCCM-P frozen f at -70 °C (P1x frozen), 1x concentrated freshly generated, non-frozen NCCM-P (P10x fresh) and 10x concentrated frozen NCCM-P (P10x frozen). (a) Relative *ACAN*, *COL1A1*, *COL2A1*, *ADAMTS5*, *MMP13* and *CCND1* gene expression (mean + SD) of the micro-aggregates at day 4. The control micro-aggregates were set at 1. (b) DNA, GAG and GAG/DNA content (mean + SD) of the canine CLC micro-aggregates at day 7. a: significant difference between this condition and all other conditions ( $p < 0.05$ ); b: significant difference between these conditions ( $p < 0.05$ ); c: significant difference between this condition and all other conditions ( $p < 0.01$ ); d: significant difference between this condition and all other conditions except for the other condition indicated with 'd' ( $p < 0.01$ ); e: significant difference between this condition and all other conditions except for the other condition indicated with 'd' ( $p < 0.01$ );  $n = 8$ .

## Discussion

### NCCM exerts cross-species anabolic effects on CLCs

Porcine, canine, and human NC-secreted factors have already shown potential for IVD regeneration<sup>8, 10, 11, 13, 14, 16</sup>. With a clinical directive in mind, the aim of this study was to delineate underlying bioactive NC-secreted substances (with the focus on proteins and EVs) resulting in IVD regeneration. The present study shows that porcine and canine NCCM+ have the potential to exert a regenerative effect on bovine and canine CLCs, respectively. Secreted factors from healthy NCs (NCCM+) exerted a more pronounced anabolic effect and induced higher notochord/nucleus pulposus specific marker expression in CLCs than the secreted factors from dedifferentiated NCs (NCCM-), indicating that this was related to preservation of the NC phenotype<sup>21</sup>.

### Proteomic analysis reveals many common proteins in porcine, canine, and human NCCM

Since previous findings indicated regenerative effects of porcine, canine, and human NCCM on human CLCs<sup>13</sup>, the main focus of the proteomic analysis of this study was on common proteins discovered in NCCM from all three species. A considerable part of the detected proteins consisted of ECM, e.g. proteoglycans, collagens and keratins, and organelle-derived proteins. However, specific growth factors, potentially responsible for NCCM's regenerative effect, were not identified, which is in contrast with previous studies in which CTGF was identified in canine<sup>15</sup> and porcine<sup>16</sup> NCCM. This discrepancy may be due to the method of NCCM generation. Whereas the previous studies produced NCCM from isolated NCs, in the current study, NCCM was generated from NC-rich NP tissue. Potential growth factors secreted by NCs may therefore be overshadowed by large quantities of proteins released during NP tissue incubation. In line with previous findings<sup>11</sup>, however, clusterin and alpha-2-macroglobulin were detected in all the species' NCCM, and tenascin in human and canine NCCM. These matricellular proteins may have protective effects for NP cells. Furthermore, class 3 semaphorins were identified in canine (SEMA3C, SEMA3E) and porcine (SEMA3C) NCCM. SEMA3C is suggested to play a role in innervation and vascularisation of degenerated human IVDs and has been linked to back pain<sup>36</sup>. The finding of SEMA3C and SEMA3E in canine and porcine NCCM derived from healthy NPs, however, may also support an inhibitory role of semaphorins in nerve and blood vessel growth<sup>37</sup>.

The proteins in common to all three species and upstream bioinformatics analysis provide new insights into IVD (patho)physiology, including transcriptional gene regulation. For example, proteins related to transcription factor binding sites AP-1 and PAX4 were identified. AP-1 is a downstream target of the mitogenic activated protein (MAP) kinase signaling pathway and regulates chondrogenic differentiation<sup>38</sup>. In healthy porcine, canine, and human NP tissue, GAG synthesis may be regulated in an AP-1/growth factor-dependent manner, given that BMP2 and TGF- $\beta$  induced the expression of the GAG synthesis enzyme  $\beta$ 1,3-glucuronosyl transferase 1 in rat NP cells via - amongst others - AP-1<sup>39</sup>. PAX4 has been mainly studied in the pancreas<sup>40, 41</sup> whereas its role in bone/cartilaginous tissues is unexplored. PAX1 and PAX9, however, are known to be associated with axial and limb skeleton development<sup>42</sup> and vertebral body and cartilage formation<sup>43</sup>. Furthermore, the current study also demonstrates that proteins related to miR-29a/b/c were present in porcine and human NCCM+. The miR-29 family negatively regulates TGF- $\beta$  and canonical Wnt signalling<sup>44, 45</sup>, exerts anti-fibrotic effects<sup>46</sup>, and acts across development and

progression of osteoarthritis<sup>44</sup>. In the IVD, the role of the miR-29 family has not been investigated yet, but based on knowledge from other tissues it could also be involved in ECM production.

Taken together, many common proteins were identified in porcine, canine, and human NCCM. Mainly ECM and organelle-derived proteins, but no specific growth factors were detected. Furthermore, in porcine and human NCCM, platelet- and complement system-related proteins were identified. Possibly these proteins were identified as a result of blood contamination explained by the technically challenging harvesting of NP tissue rather than being a biologically relevant finding. Hence, it may be beneficial for future studies to focus on comparative proteomic analysis of porcine, canine, and human NCCM generated from isolated NCs, without interfering ECM proteins.

### **Pelletable NCCM factors exert a moderate anabolic effect on canine CLCs**

Proteomic analysis revealed that NCCM+ contained a considerable amount of membrane-bound vesicle proteins. In functional studies, the effect of NCCM-P (containing EVs and protein aggregates) was determined on CLCs. In bovine CLCs, the effect of porcine NCCM-P factors was negligible. In contrast, canine NCCM-P factors increased, in a concentration-dependent manner, the canine CLC GAG, GAG/DNA, and collagen type II content compared with controls (although less pronounced than for the soluble factors). Also, canine NCCM-P decreased *VEGF* and increased *KRT19* expression compared with controls, indicating that it inhibited angiogenesis<sup>47</sup> and induced a healthy NP-like phenotype<sup>48</sup>. The bovine CLCs were obtained from relatively healthy/early degenerated IVDs and the canine CLCs from degenerated IVDs, which may explain the difference in response, besides NCCM/CLC species differences.

In the present study, NCCM-P needed to be frozen, since canine NCCM donors were available at unpredictable moments. The effect of freezing EVs is controversial: previous studies demonstrated that EVs were relatively insensitive to freeze/thaw cycles<sup>18, 49</sup>, whereas others showed the opposite<sup>50</sup>. The current study showed that at least 4 days of freezing at -70°C did not influence the biological activity of canine NC-derived pelletable factors compared with non-frozen pelletable factors (kept at 4°C) from the same donor on canine CLC micro-aggregates. Besides long term freezing, also relatively hampered access to the pelletable factors could have accounted for the less pronounced effect of NCCM-P on the canine hydrogels and bovine alginate beads compared with the canine micro-aggregates.

Taken together, the present study demonstrates that the NCCM-P factors (protein aggregates and EVs) exerted a moderate concentration-dependent anabolic effect, but only on canine CLCs. While we cannot exclude that the absence of a biologic effect of EVs present in the NCCM-P may be related to the 100,000g ultracentrifugation<sup>51</sup>, future studies should focus on the effect of different isolation protocols and different populations of purified NC-derived EVs, without interference of protein aggregates present in NCCM-P.

### **Soluble porcine and canine NCCM factors exert anabolic effects on bovine and canine CLCs**

It appeared that most proteins remained in the soluble fraction of canine and porcine NCCM after ultracentrifugation. The effect of porcine NCCM-S on bovine CLCs was similar to that of

NCCM+, suggesting that porcine NCCM exerted its anabolic effect mainly through protein-based mechanisms. Also in the canine species, and the GAG content of NCCM-S-treated hydrogels was rather similar to that of hydrogels treated with NCCM+. However, the hydrogel appeared to have the propensity to bind the GAGs present in NCCM. Correcting for this property indicates that NCCM- may be even more active than NCCM+ or NCCM-S. However, this was not evident from the histological analysis. In our view, the amount of GAGs produced by the CLCs themselves cannot simply be calculated by correcting for the GAG content of empty hydrogels cultured in NCCM, because the incorporated ECM proteins likely changed the micro-environment and consequently affected GAG synthesis<sup>52, 53</sup>.

Generally, notochord/nucleus pulposus specific marker expression was higher after NCCM+ and NCCM-S than after NCCM-P treatment, indicating that NCCM+ and NCCM-S were better able to induce a healthy NP phenotype. Furthermore, *ACAN* and *COL2A1* expression did not differ between NCCM-treated CLCs and controls, while *ADAMTS5* and *MMP13* gene expression levels were generally higher in NCCM+ and/or NCCM-S-treated CLCs compared with other conditions. The latter is most probably related to ECM remodelling rather than catabolism, given that histological analysis points towards a stronger anabolic effect of NCCM+ and NCCM-S than NCCM-P and NCCM-. In NCCM+ and NCCM-S, more pericellular GAGs were observed, suggesting that the CLCs synthesized these GAGs themselves. Also collagen type II deposition was highest after NCCM+ and NCCM-S treatment, again indicating that both porcine and canine NCCM exerted their anabolic effects mainly through proteins. Since no blocking experiment was performed, however, it is difficult to discern if one or combination of factors are responsible for the effects of NCCM.

## Conclusions

The present study demonstrates an anabolic cross-species effect of porcine and canine NCCM+ on bovine and canine CLCs, respectively. Especially on bovine CLCs, a pronounced effect of the soluble NCCM fraction (NCCM-S; peptides, proteins) was found, without an appreciable effect of the pelletable NCCM fraction (NCCM-P; protein aggregates, EVs). However, NCCM-P exerted a moderate anabolic effect on canine CLCs, although the culture system used precludes firm conclusions. Thus, although porcine and canine NCCM exerted their anabolic effects mainly through soluble factors, also the pelletable NCCM factors showed moderate regenerative potential. Although the regenerative potential of NCCM-P should not be overlooked, future studies should focus on unraveling the protein-based regenerative mechanism from NCCM produced from isolated NCs, e.g. by NCCM fractionation and pathway blocking studies.

## Acknowledgements

The authors would like to thank Willem de Jong for help with the execution of experiments and Anita Krouwels for supplying human IVDs.

## References

1. Cheung KM, Karpainen J, Chan D, et al. 2009. Prevalence and pattern of lumbar magnetic resonance imaging changes in a population study of one thousand forty-three individuals. *Spine (Phila Pa 1976)* 34: 934-940.
2. Luoma K, Riihimäki H, Luukkainen R, et al. 2000. Low back pain in relation to lumbar disc degeneration. *Spine (Phila Pa 1976)* 25: 487-492.
3. Bach FC, Willems N, Penning LC, et al. 2014. Potential regenerative treatment strategies for intervertebral disc degeneration in dogs. *BMC Vet Res* 10: 3-6148-10-3.
4. Benneker LM, Andersson G, Iatridis JC, et al. 2014. Cell therapy for intervertebral disc repair: Advancing cell therapy from bench to clinics. *Eur Cell Mater* 27: 5-11.
5. Sakai D, Grad S. 2015. Advancing the cellular and molecular therapy for intervertebral disc disease. *Adv Drug Deliv Rev* 84: 159-171.
6. Sakai D, Andersson GB. 2015. Stem cell therapy for intervertebral disc regeneration: Obstacles and solutions. *Nat Rev Rheumatol* 11: 243-256.
7. Purmessur D, Cornejo MC, Cho SK, Hecht AC, Iatridis JC. 2013. Notochordal cell-derived therapeutic strategies for discogenic back pain. *Global Spine J* 3: 201-218.
8. Abbott RD, Purmessur D, Monsey RD, Iatridis JC. 2012. Regenerative potential of TGFbeta3 + dex and notochordal cell conditioned media on degenerated human intervertebral disc cells. *J Orthop Res* 30: 482-488.
9. Potier E, de Vries S, van Doeselaar M, Ito K. 2014. Potential application of notochordal cells for intervertebral disc regeneration: An in vitro assessment. *Eur Cell Mater* 28: 68-80; discussion 80-1.
10. Korecki CL, Taboas JM, Tuan RS, Iatridis JC. 2010. Notochordal cell conditioned medium stimulates mesenchymal stem cell differentiation toward a young nucleus pulposus phenotype. *Stem Cell Res Ther* 1: 18.
11. Purmessur D, Schek RM, Abbott RD, et al. 2011. Notochordal conditioned media from tissue increases proteoglycan accumulation and promotes a healthy nucleus pulposus phenotype in human mesenchymal stem cells. *Arthritis Res Ther* 13: R81.
12. de Vries SA, Potier E, van Doeselaar M, et al. 2015. Conditioned medium derived from notochordal cell-rich nucleus pulposus tissue stimulates matrix production by canine nucleus pulposus cells and bone marrow-derived stromal cells. *Tissue Eng Part A* 21: 1077-1084.
13. Bach FC, de Vries SA, Krouwels A, et al. 2015. The species-specific regenerative effects of notochordal cell-conditioned medium on chondrocyte-like cells derived from degenerated human intervertebral discs. *Eur Cell Mater* 30: 132-46; discussion 146-7.
14. de Vries SA, van Doeselaar M, Meij BP, Tryfonidou MA, Ito K. 2016. The stimulatory effect of notochordal cell-conditioned medium in a nucleus pulposus explant culture. *Tissue Eng Part A* 22: 103-110.
15. Erwin WM, Ashman K, O'Donnell P, Inman RD. 2006. Nucleus pulposus notochord cells secrete connective tissue growth factor and up-regulate proteoglycan expression by intervertebral disc chondrocytes. *Arthritis Rheum* 54: 3859-3867.
16. Gantenbein B, Calandriello E, Wuertz-Kozak K, et al. 2014. Activation of intervertebral disc cells by co-culture with notochordal cells, conditioned medium and hypoxia. *BMC Musculoskelet Disord* 15: 422-2474-15-422.
17. van der Vlist EJ, Nolte-'t Hoen EN, Stoorvogel W, Arkesteijn GJ, Wauben MH. 2012. Fluorescent labeling of nano-sized vesicles released by cells and subsequent quantitative and qualitative analysis by high-resolution flow cytometry. *Nat Protoc* 7: 1311-1326.
18. Witwer KW, Buzas EI, Bemis LT, et al. 2013. Standardization of sample collection, isolation and analysis methods in extracellular vesicle research. *J Extracell Vesicles* 2: 10.3402/jev.v2i0.20360. eCollection 2013.
19. Anderson HC, Mulhall D, Garimella R. 2010. Role of extracellular membrane vesicles in the pathogenesis of various diseases, including cancer, renal diseases, atherosclerosis, and arthritis. *Lab Invest* 90: 1549-1557.
20. Malda J, Boere J, van de Lest CH, van Weeren PR, Wauben MH. 2016. Extracellular vesicles - new tool for joint repair and regeneration. *Nat Rev Rheumatol* .
21. Arkesteijn ITM. 2013. Maintaining notochordal phenotype. *Global Spine Congress* .
22. Wisniewski JR, Zougman A, Nagaraj N, Mann M. 2009. Universal sample preparation method for proteome analysis. *Nat Methods* 6: 359-362.
23. de Graaf EL, Giansanti P, Altelaar AF, Heck AJ. 2014. Single-step enrichment by Ti4+-IMAC and label-free quantitation enables in-depth monitoring of phosphorylation dynamics with high reproducibility and temporal resolution. *Mol Cell Proteomics* 13: 2426-2434.
24. Marino F, Cristobal A, Binai NA, et al. 2014. Characterization and usage of the EASY-spray technology as part of an online 2D SCX-RP ultra-high pressure system. *Analyst* 139: 6520-6528.
25. R Core Team. 2015. R: A language and environment for statistical computing.
26. Bolstad BM. 2016. Package 'preprocessCore': A collection of pre-processing functions. Version 1.33.0: .
27. Durinck S, Spellman PT, Birney E, Huber W. 2009. Mapping identifiers for the integration of genomic datasets with the R/bioconductor package biomaRt. *Nat Protoc* 4: 1184-1191.
28. Chen H. 2015. Package 'VennDiagram': Generate high-resolution venn and euler plots.
29. Chen J, Bardes EE, Aronow BJ, Jegga AG. 2009. ToppGene suite for gene list enrichment analysis and candidate gene prioritization. *Nucleic Acids Res* 37: W305-11.
30. Carlson M. *GO.db: A set of annotation maps describing the entire gene ontology*. R package version 3.2.2 .

31. Farndale RW, Sayers CA, Barrett AJ. 1982. A direct spectrophotometric microassay for sulfated glycosaminoglycans in cartilage cultures. *Connect Tissue Res* 9: 247-248.
32. Guo JF, Jourdian GW, MacCallum DK. 1989. Culture and growth characteristics of chondrocytes encapsulated in alginate beads. *Connect Tissue Res* 19: 277-297.
33. Arksteijn IT, Smolders LA, Spillekom S, et al. 2015. Effect of coculturing canine notochordal, nucleus pulposus and mesenchymal stromal cells for intervertebral disc regeneration. *Arthritis Res Ther* 17: 60-015-0569-6.
34. Scholz B, Kinzelmann C, Benz K, et al. 2010. Suppression of adverse angiogenesis in an albumin-based hydrogel for articular cartilage and intervertebral disc regeneration. *Eur Cell Mater* 20: 24-36; discussion 36-7.
35. Benz K, Stippich C, Osswald C, et al. 2012. Rheological and biological properties of a hydrogel support for cells intended for intervertebral disc repair. *BMC Musculoskelet Disord* 13: 54-2474-13-54.
36. Binch AL, Cole AA, Breakwell LM, et al. 2015. Class 3 semaphorins expression and association with innervation and angiogenesis within the degenerate human intervertebral disc. *Oncotarget* 6: 18338-18354.
37. Bagnard D, Lohrum M, Uziel D, Puschel AW, Bolz J. 1998. Semaphorins act as attractive and repulsive guidance signals during the development of cortical projections. *Development* 125: 5043-5053.
38. Seghatoleslami MR, Tuan RS. 2002. Cell density dependent regulation of AP-1 activity is important for chondrogenic differentiation of C3H10T1/2 mesenchymal cells. *J Cell Biochem* 84: 237-248.
39. Hiyama A, Gogate SS, Gajghate S, et al. 2010. BMP-2 and TGF-beta stimulate expression of beta1,3-glucuronosyl transferase 1 (GlcAT-1) in nucleus pulposus cells through AP1, TonEBP, and Sp1: Role of MAPKs. *J Bone Miner Res* 25: 1179-1190.
40. Mathiyalagan P, Keating ST, Al-Hasani K, El-Osta A. 2015. Epigenetic-mediated reprogramming of pancreatic endocrine cells. *Antioxid Redox Signal* 22: 1483-1495.
41. Napolitano T, Avolio F, Courtney M, et al. 2015. Pax4 acts as a key player in pancreas development and plasticity. *Semin Cell Dev Biol* 44: 107-114.
42. LeClair EE, Bonfiglio L, Tuan RS. 1999. Expression of the paired-box genes pax-1 and pax-9 in limb skeleton development. *Dev Dyn* 214: 101-115.
43. Barnes GL, Hsu CW, Mariani BD, Tuan RS. 1996. Chicken pax-1 gene: Structure and expression during embryonic somite development. *Differentiation* 61: 13-23.
44. Le LT, Swingler TE, Crowe N, et al. 2015. The microRNA-29 family in cartilage homeostasis and osteoarthritis. *J Mol Med (Berl)*.
45. Luna C, Li G, Qiu J, Epstein DL, Gonzalez P. 2011. Cross-talk between miR-29 and transforming growth factor-betas in trabecular meshwork cells. *Invest Ophthalmol Vis Sci* 52: 3567-3572.
46. He Y, Huang C, Lin X, Li J. 2013. MicroRNA-29 family, a crucial therapeutic target for fibrosis diseases. *Biochimie* 95: 1355-1359.
47. Cornejo MC, Cho SK, Giannarelli C, Iatridis JC, Purmessur D. 2015. Soluble factors from the notochordal-rich intervertebral disc inhibit endothelial cell invasion and vessel formation in the presence and absence of pro-inflammatory cytokines. *Osteoarthritis Cartilage* 23: 487-496.
48. Minogue BM, Richardson SM, Zeef LA, Freemont AJ, Hoyland JA. 2010. Characterization of the human nucleus pulposus cell phenotype and evaluation of novel marker gene expression to define adult stem cell differentiation. *Arthritis Rheum* 62: 3695-3705.
49. Lorincz AM, Timar CI, Marosvari KA, et al. 2014. Effect of storage on physical and functional properties of extracellular vesicles derived from neutrophilic granulocytes. *J Extracell Vesicles* 3: 25465.
50. Dey-Hazra E, Hertel B, Kirsch T, et al. 2010. Detection of circulating microparticles by flow cytometry: Influence of centrifugation, filtration of buffer, and freezing. *Vasc Health Risk Manag* 6: 1125-1133.
51. Nordin JZ, Lee Y, Vader P, et al. 2015. Ultrafiltration with size-exclusion liquid chromatography for high yield isolation of extracellular vesicles preserving intact biophysical and functional properties. *Nanomedicine* 11: 879-883.
52. Gilchrist CL, Darling EM, Chen J, Setton LA. 2011. Extracellular matrix ligand and stiffness modulate immature nucleus pulposus cell-cell interactions. *PLoS One* 6: e27170.
53. Inoue T, Nakamura T, Ikeda T, Takagi K. 2005. Effect of extracellular matrix protein on the rate of proteoglycan synthesis in rabbit intervertebral disc cells. *J Spinal Disord Tech* 18: 52-57.

**Table 1. Proteins identified in canine, porcine, and human NCCM**

Canine	Porcine	Human	Number	Proteins
Yes	Yes	Yes	66	ACAN, FN1, KRT8, COMP, COL6A3, CA3, ALB, VIM, CLU, KRT19, A2M, HSPG2, CHAD, ABI3BP, XYLT1, ENO1, KRT18, CILP, PKM, COL6A1, COL2A1, EFEMP1, LAMB2, HAPLN1, ACTN4, CLEC3A, RNASE4, TP11, ACTN1, ACTC1, EHD2, LMNA, LAMA4, SERPINE2, CILP2, PRELP, LAMC1, CSPG4, COL11A2, HTRA1, CD109, LDHA, ENO3, VCAN, HBB, NID2, QSOX1, PRDX1, ANXA2, LGALS1, FMOD, KRT15, UGP2, PRDX6, PEBP1, YWHAE, YWHAZ, EEF1A1, TUBB4B, RARRES2, THBS4, CHRDL2, ALDOC, PLOD1, MATN2, YWHAG
No	Yes	Yes	26	AEBP1, ANXA1, ANXA5, ACTB, CLEC3B, COL11A1, COL15A1, COL3A1, COL5A1, COL5A2, COL6A2, DPYSL2, EZR, GDI1, FBLN7, MSN, PCOLCE, PFN1, PGAM1, PPIA, PYGL, SERPINB1, SERPINF1, SOD1, TNXB, VCL
Yes	No	Yes	34	TF, APOE, GAPDH, TNC, SERPINA1, SPTAN1, PGK1, GPI, LUM, LYZ, PRG4, DCN, ENO2, ALDOA, SERPINA3, HBA1, GSN, EDIL3, MFGE8, HIST4H4, LGALS3, FBLN1, HSPA8, DES, BGN, SPARC, TGFB1, HSP90AA1, CLSTN1, MDH1, CFH, FRZB, TKT, YWHAB
No	No	Yes	91	COL14A1, COL12A1, THBS1, HBG2, HBG1, PDIA3, IGHG1, THBS3, C4B, PPIB, POTEE, RNASE1, MATN4, CALM1, COL9A1, COL1A1, OGN, SSC5D, IGKC, KRT1, PRDX2, COL1A2, HBD, MATN3, P4HB, CFD, MMP3, EMILIN1, ANG, NUCB1, CAPG, C1S, ACTBL2, IGHG3, SPTBN1, FABP4, ITIH5, COL16A1, APOH, UBC, YWHAQ, IGHG2, C1R, IGHG4, LOXL2, VIT, B2M, CKM, ECM1, SERPINA5, KRT10, TUBA1B, FGF2, FBN1, DBI, PRDX4, TUBB2A, CLEC11A, RCN1, GSTP1, HSPA1B, CA1, FNDC1, KRT7, HNRNPA2B1, HNRNPA1, C3, KRT9, SELENBP1, FSTL1, HAPLN3, PGM1, FGA, FABP5, CALU, SLPI, HSP90B1, IQGAP1, TP53I3, RCN3, FBLN2, FLNA, MXRA5, TMSB4X, S100A10, CAT, HSP90AB1, DSC3, FSCN1, LRP1, CYCS
Yes	Yes	No	21	SEMA3C, ENPP2, CP, CCL16, PCOLCE2, CCDC80, unchar1, APP, THY1, EHD3, KRT75, KRT14, SMOC1, ACTN2, TPM1, LECT2, unchar2, HSPA2, TUBB, TUBB2B, TIMP2
No	Yes	No	36	AHNAK, ANXA8, LOC100157318, CFB, SERPING1, C4A, CAPN2, CHADL, CHI3L1, FLNC, HBQ1, H2BFS, HSPB1, KRT5, LOC100626701, ORM1, HIST2HBE, LOC102164134, LOC100524210, MFI2, MYH9, NME2, NPEPPS, PFKL, PRKCDBP, RDX, LOC100736872, SERPINA3-3, SPARCL1, SPP1, LOC100049693, TPM4, VAT1, SEMA7A, unchar3, H3F3A
Yes	No	No	49	CDH1, SLIT3, OLFML2B, PGAM4, CA2, KRT13, LGALS3BP, SOD3, ANOS1, LOC477441, MB, MRC2, LTF, col11a2, MFAP4, TNFRSF11B, HSPA1A, LOC100855540, LDHB, NCAM1, CHST3, LOC476825, LOXL3, KRT17, LOC100855471, TIMP3, CRYAB, CKB, SEMA3E, CFL1, LOC488254, HSPA5, CCL21, HIST1H2AH, PTRF, CSTB, LECT1, CHST6, PGAM2, TUBA1A, SLC2A1, TUBB4A, CDH2, HIST1H1C, FHL1, SDCBP, KRT78, GSTM3, EFEMP2

3

**Table 2. Gene Ontology analysis of proteins identified in porcine, canine, and human NCCM**

Rank	GO term	Name	q-value FDR B&H	Hit Count in Query List	Hit Count in Genome	Hit in Query List
1	GO:0005539	Glycosaminoglycan binding	7.96E-08	11	216	THBS4,SERPINE2,ANG,FMOD, FN1,COMP,ABI3BP,PRELP,ACAN,VCAN,HAPLN1
2	GO:0005201	Extracellular matrix structural constituent	8.35E-07	7	70	COL2A1,COL11A2,COMP,PRELP,ACAN,LAMA4,LAMC1
3	GO:0005198	Structural molecule activity	4.30E-06	15	748	COL2A1,VIM,TUBB4B,KRT8,COL11A2,KRT15,COMP,LMNA,KRT18,KRT19,PRELP,ACAN,LAMA4,LAMB2,LAMC1
4	GO:0008201	Heparin binding	9.30E-06	8	164	THBS4,SERPINE2,ANG,FMOD, FN1,COMP,ABI3BP,PRELP
5	GO:0005518	Collagen binding	1.23E-05	6	71	NID2,THBS4,FN1,COMP,ABI3BP,CSPG4
6	GO:0032403	Protein complex binding	1.48E-04	15	1053	VIM,NID2,KRT8,THBS4,FN1,COMP,ABI3BP,KRT19,CSPG4,PKM,LAMB2,ACTN4,ACTN1,YWHAE,YWHAZ
7	GO:1901681	Sulfur compound binding	1.48E-04	8	257	THBS4,SERPINE2,ANG,FMOD, FN1,COMP,ABI3BP,PRELP
8	GO:0019899	Enzyme binding	1.48E-04	20	1851	A2M,VIM,HSPG2,FN1,COMP,LMNA,CLU,PEBP1,ANXA2,VCAN,CSPG4,ALB,LDHA,ENO1,YWHA E,YWHAG,YWHAZ,PRDX6,EEF1A1,TPI1
9	GO:0004867	Serine-type endopeptidase inhibitor activity	8.34E-04	5	96	A2M,COL6A3,SERPINE2,PEBP1,CD109
10	GO:0097110	Scaffold protein binding	1.51E-03	4	56	VIM,KRT8,KRT15,KRT18
11	GO:0002020	Protease binding	1.63E-03	5	115	A2M,HSPG2,FN1,COMP,ANXA2
12	GO:0005178	Integrin binding	1.69E-03	5	118	THBS4,FN1,LAMB2,ACTN4,ACTN1
13	GO:0004857	Enzyme inhibitor activity	1.74E-03	8	393	A2M,COL6A3,SERPINE2,PEBP1,ANXA2,CD109,CHAD,YWHAG
14	GO:0004634	Phosphopyruvate hydratase activity	1.74E-03	2	4	ENO1,ENO3
15	GO:0005540	Hyaluronic acid binding	1.79E-03	3	24	ACAN,VCAN,HAPLN1
16	GO:0019838	Growth factor binding	2.28E-03	5	134	COL2A1,A2M,COL6A1,HTRA1,CD109
17	GO:0003723	RNA binding	2.28E-03	16	1608	VIM,TUBB4B,ANG,KRT18,PEBP1,ANXA2,PRDX1,PKM,ACTN4,ACTN1,ENO1,YWHA E,YWHAG,YWHAZ,LGALS1,EEF1A1
18	GO:0061134	Peptidase regulator activity	2.39E-03	6	221	A2M,COL6A3,SERPINE2,FN1,PEBP1,CD109
19	GO:0016209	Antioxidant activity	2.51E-03	4	75	PRDX1,ALB,HBB,PRDX6
20	GO:0005509	Calcium ion binding	2.54E-03	10	694	NID2,THBS4,EFEMP1,COMP,ANXA2,MATN2,VCAN,ACTN4,ACTN1,EHD2

**Table 3. Pathway analysis of proteins identified in porcine and human NCCM**

Rank	ID	Name	q-value FDR B&H	Hit Count in Query List	Hit Count in Genome	Hit in Query List
1	730306	Assembly of collagen fibrils and other multimeric structures	5.9E-09	7	54	COL3A1,COL5A1,COL5A2,COL6A2,COL11A1,COL15A1,PCOLCE
2	645289	Collagen biosynthesis and modifying enzymes	1.1E-08	7	65	COL3A1,COL5A1,COL5A2,COL6A2,COL11A1,COL15A1,PCOLCE
3	645288	Collagen formation	3.5E-08	7	87	COL3A1,COL5A1,COL5A2,COL6A2,COL11A1,COL15A1,PCOLCE
4	576262	Extracellular matrix organization	1.9E-06	8	264	COL3A1,COL5A1,COL5A2,COL6A2,COL11A1,COL15A1,TNXB,PCOLCE
5	161004	Recycling pathway of L1	4.5E-04	3	27	EZR,DPYSL2,MSN
6	106050	Platelet degranulation	5.6E-04	4	85	PFN1,PPIA,VCL,SOD1
7	106048	Response to elevated platelet cytosolic Ca <sup>2+</sup>	6.5E-04	4	90	PFN1,PPIA,VCL,SOD1
8	105688	Axon guidance	3.0E-03	5	262	EZR,COL6A2,DPYSL2,PFN1,MSN
9	161003	L1CAM interactions	1.1E-02	3	94	EZR,DPYSL2,MSN
10	106034	Platelet activation, signaling and aggregation	1.1E-02	4	214	PFN1,PPIA,VCL,SOD1

**Table 4. Pathway analysis of proteins identified in canine and human NCCM**

Rank	ID	Name	q-value FDR B&H	Hit Count in Query List	Hit Count in Genome	Hit in Query List
1	106204	Gluconeogenesis	2.1E-07	6	33	GPI,MDH1,ALDOA,GAPDH, ENO2,PGK1
2	105911	Glycolysis	1.5E-06	5	29	GPI,ALDOA,GAPDH,ENO2,P GK1
3	106196	Metabolism of carbohydrates	3.3E-06	9	266	GPI,LUM,MDH1,DCN,ALDO A,GAPDH,ENO2,PGK1,BGN
4	106199	Glucose metabolism	3.9E-06	6	75	GPI,MDH1,ALDOA,GAPDH, ENO2,PGK1
5	833812	ECM proteoglycans	1.5E-05	5	55	SPARC,LUM,DCN,TNC,BGN
6	366238	Amyloids	1.0E-04	5	85	TGFBI,MFGE8,LYZ,HIST1H4 A,GSN
7	576262	Extracellular matrix organization	2.1E-04	7	264	FBLN1,SPARC,LUM,DCN,TN C,BGN,DDR2
8	771599	Binding and Uptake of Ligands by Scavenger Receptors	4.9E-04	4	61	SPARC,APOE,HBA1,HSP90A A1
9	530764	Disease	3.1E-03	11	1088	TGFBI,MFGE8,APOE,LUM,D CN,LYZ,HIST1H4A,YWHAB, GSN,HSP90AA1,BGN
10	645310	Dermatan sulfate biosynthesis	6.0E-03	2	11	DCN,BGN
11	105679	Caspase-mediated cleavage of cytoskeletal proteins	7.0E-03	2	12	SPTAN1,GSN
12	645311	CS/DS degradation	8.9E-03	2	14	DCN,BGN
13	477135	Metabolism	1.5E-02	12	1575	GPI,APOE,LUM,MDH1,HBA 1,DCN,ALDOA,GAPDH,ENO 2,PGK1,HSP90AA1,BGN
14	645309	Chondroitin sulfate biosynthesis	1.8E-02	2	21	DCN,BGN
15	106050	Platelet degranulation	2.0E-02	3	85	SERPINA1,SPARC,ALDOA
16	106048	Response to elevated platelet cytosolic Ca <sup>2+</sup>	2.3E-02	3	90	SERPINA1,SPARC,ALDOA
17	645305	A tetrasaccharide linker sequence is required for GAG synthesis	2.5E-02	2	26	DCN,BGN
18	685546	MPS VII - Sly syndrome	3.7E-02	3	121	LUM,DCN,BGN
19	685536	Mucopolysaccharidoses	3.7E-02	3	121	LUM,DCN,BGN
20	685547	MPS IX - Natowicz syndrome	3.7E-02	3	121	LUM,DCN,BGN

**Table 5. Pathway analysis of proteins identified in porcine and canine NCCM**

Rank	ID	Name	q-value FDR B&H	Hit Count in Query List	Hit Count in Genome	Hit in Query List
1	106248	Post-chaperonin tubulin folding pathway	2.88E-02	2	19	TUBB2A,TUBB2B
2	106245	Formation of tubulin folding intermediates by CCT/TriC	2.88E-02	2	22	TUBB2A,TUBB2B
3	106244	Prefoldin mediated transfer of substrate to CCT/TriC	2.88E-02	2	28	TUBB2A,TUBB2B
4	106243	Cooperation of Prefoldin and TriC/CCT in actin and tubulin folding	2.88E-02	2	29	TUBB2A,TUBB2B
5	106262	Striated Muscle Contraction	2.88E-02	2	31	TPM1,ACTN2
6	106242	Chaperonin-mediated protein folding	4.66E-02	2	50	TUBB2A,TUBB2B
7	106261	Muscle contraction	4.66E-02	2	51	TPM1,ACTN2
8	106241	Protein folding	4.66E-02	2	55	TUBB2A,TUBB2B

**Table 6. Pathway analysis of proteins identified only in porcine NCCM**

Rank	ID	Name	q-value FDR B&H	Hit Count in Query List	Hit Count in Genome	Hit in Query List
1	106412	Activation of C3 and C5	0.00829	2	5	C4A,CFB
2	576254	Regulation of Complement cascade	0.04694	2	22	C4A,CFB

**Table 7. Pathway analysis of proteins identified only in canine NCCM**

Rank	ID	Name	q-value FDR B&H	Hit Count in Query List	Hit Count in Genome	Hit in Query List
1	576262	Extracellular matrix organization	0.02383	6	264	MFAP4,COL11A2,EFEMP2,NCAM1,LOXL3,CDH1
2	730310	Elastic fibre formation	0.02651	3	41	MFAP4,EFEMP2,LOXL3
3	106248	Post-chaperonin tubulin folding pathway	0.04144	2	19	TUBB4A,TUBA1A
4	105688	Axon guidance	0.04144	5	262	CFL1,SLIT3,NCAM1,SDCBP,SEMA3E
5	106245	Formation of tubulin folding intermediates by CCT/TriC	0.04565	2	22	TUBB4A,TUBA1A

**Table 8. Pathway analysis of proteins identified only in human NCCM**

Rank	ID	Name	q-value FDR B&H	Hit Count in Query List	Hit Count in Genome	Hit in Query List
1	106406	Initial triggering of complement	4.93E-09	9	40	CFD,IGHG1,IGHG2,IGHG3,IGHG4,IGKC,C1R,C1S,C3
2	576262	Extracellular matrix organization	2.82E-08	16	264	THBS1,COL9A1,COL12A1,FBLN2,FBN1,COL16A1,P4HB,LOXL2,MATN3,FGA,COL14A1,MATN4,MMP3,PPIB,COL1A1,COL1A2
3	106405	Complement cascade	6.88E-08	9	58	CFD,IGHG1,IGHG2,IGHG3,IGHG4,IGKC,C1R,C1S,C3
4	645288	Collagen formation	1.23E-07	10	87	COL9A1,COL12A1,COL16A1,P4HB,LOXL2,COL14A1,MMP3,PPIB,COL1A1,COL1A2
5	106409	Classical antibody-mediated complement activation	1.35E-07	7	28	IGHG1,IGHG2,IGHG3,IGHG4,IGKC,C1R,C1S
6	106407	Creation of C4 and C2 activators	5.19E-07	7	34	IGHG1,IGHG2,IGHG3,IGHG4,IGKC,C1R,C1S
7	645289	Collagen biosynthesis and modifying enzymes	2.26E-06	8	65	COL9A1,COL12A1,COL16A1,P4HB,COL14A1,PPIB,COL1A1,COL1A2
8	106050	Platelet degranulation	1.86E-04	7	85	CFD,FLNA,THBS1,CALM2,CALU,FGA,TMSB4X
9	106048	Response to elevated platelet cytosolic Ca <sup>2+</sup>	2.35E-04	7	90	CFD,FLNA,THBS1,CALM2,CALU,FGA,TMSB4X
10	771578	FCGR activation	2.35E-04	5	34	IGHG1,IGHG2,IGHG3,IGHG4,IGKC
11	771599	Binding and Uptake of Ligands by Scavenger Receptors	2.70E-04	6	61	HSP90B1,IGKC,LRP1,HB,D,COL1A1,COL1A2
12	730309	Collagen degradation	3.54E-04	5	38	COL9A1,COL12A1,COL16A1,COL14A1,MMP3
13	771580	Role of phospholipids in phagocytosis	8.80E-04	5	46	IGHG1,IGHG2,IGHG3,IGHG4,IGKC
14	771579	Regulation of actin dynamics for phagocytic cup formation	1.16E-03	6	81	IGHG1,IGHG2,IGHG3,IGHG4,IGKC,HSP90AB1
15	106110	Integrin cell surface interactions	4.22E-03	5	66	THBS1,COL9A1,FBN1,COL16A1,FGA
16	771577	Fcgamma receptor (FCGR) dependent phagocytosis	4.22E-03	6	105	IGHG1,IGHG2,IGHG3,IGHG4,IGKC,HSP90AB1
17	106410	Alternative complement activation	9.39E-03	2	4	CFD,C3
18	833814	Scavenging by Class A Receptors	1.01E-02	3	19	HSP90B1,COL1A1,COL1A2
19	576263	Degradation of the extracellular matrix	1.42E-02	5	89	COL9A1,COL12A1,COL16A1,COL14A1,MMP3
20	730306	Assembly of collagen fibrils and other multimeric structures	1.74E-02	4	54	LOXL2,MMP3,COL1A1,COL1A2

**Table 9. Proteins associated with transcription factor binding sites in porcine, canine and human NCCM**

Venn-group	ID	q-value FDR B&H	Hit Count in Query List	Hit Count in Genome	Hit in Query List
Common	TGANTCA_V\$AP1_C	1.63E-02	15	919	XYLT1,HSPG2,KRT8,KRT15,KRT19,CSPG4,PKM,LAMC1,ACTN4,ENO1,ENO3,YWHAG,YWHAZ,LGALS1,EEF1A1
Common	GGGTGRR_V\$PAX4_03	4.51E-02	15	1068	A2M,VIM,HSPG2,NID2,COL6A3,COL11A2,RARRES2,PRELP,CD109,LAMB2,YWHAZ,YWHAZ,YWHAZ,EEF1A1,HAPLN1
Canine & porcine	TATAAA_V\$TATA_01	2.49E-02	7	1075	CP,LECT2,SEMA3C,ENPP2,KRT14,ACTN2,SMOC1
Canine	V\$ZIC3_01	3.55E-02	6	213	CRYAB,TIMP3,EFEMP2,SLIT3,LOXL3,CHST3
Canine	GGGAGRR_V\$MAZ_Q6	3.55E-02	17	1838	TUBB4A,KRT13,COL11A2,KRT17,MRC2,CFL1,LECT1,EFEMP2,SLIT3,CHST6,NCAM1,PTRF,LOXL3,CDH2,LDHB,SLC2A1,SOD3

**Table 10. Proteins associated with miRNA's in porcine and human NCCM**

	ID	q-value FDR B&H	Hit Count in Query List	Hit Count in Genome	Hit in Query List
Porcine & human	hsa-miR-29b	2.48E-02	7	850	COL3A1,COL5A1,COL5A2,DPYSL2,COL11A1,COL15A1,VCL
Porcine & human	hsa-miR-29a	2.48E-02	7	850	COL3A1,COL5A1,COL5A2,DPYSL2,COL11A1,COL15A1,VCL
Porcine & human	hsa-miR-29c	2.48E-02	7	850	COL3A1,COL5A1,COL5A2,DPYSL2,COL11A1,COL15A1,VCL
Human only	hsa-miR-29c	2.24E-02	4	31	FBN1,FGA,COL1A1,COL1A2

**Supplementary File 1. Primers used for quantitative PCR of canine samples**

Genes	Forward sequence 5' → 3'	Reverse sequence 5' → 3'	Amplicon size	Annealing temp (°C)
<b>Reference genes</b>				
<i>GAPDH</i>	TGTCCCCACCCCAATGTATC	CTCCGATGCCTGCTTCACTACCTT	100	58
<i>HPRT</i>	AGCTTGCTGGTGAAAAGGAC	TTATAGTCAAGGGCATATCC	104	58
<i>RPS19</i>	CCTTCTCAAAAAGTCTGGG	GTTCTCATCGTAGGGAGCAAG	95	61
<i>SDHA</i>	GCCTTGGATCTCTTGATGGA	TTCTTGGCTCTTATGCGATG	92	56.5
<b>Target genes</b>				
<i>ACAN</i>	GGCACTCCTTGCAATTTGAG	GTCATTCCACTCTCCCTTCTC	111	62
<i>ADAMTS5</i>	CTACTGCACAGGGAAGAG	GAACCCATTCCACAAATGTC	149	61
<i>BAX</i>	CCTTTTGCTTCAGGGTTTCA	CTCAGCTTCTTGGTGGATGC	108	58
<i>BCL2</i>	TGGAGAGVGTCAACCGGGAGATGT	AGGTGTGCAGATGCCGGTTCAGGT	87	62
<i>CASP3</i>	ATCACTGAAGATGGATGGGTTGGGTT	TGAAAGGAGCATGTTCTGAAGTAGCACT	139	58
<i>COL1A1</i>	GTGTGTACAGAACGGCCTCA	TCGCAAAATCACGTCATCG	109	61
<i>COL2A1</i>	GCAGCAAGAGCAAGGAC	TTCTGAGAGCCCTCGGT	151	62
<i>COL10A1</i>	CCAACACCAAGACACAG	CAGGAATACCTTGCTCTC	80	61
<i>CCND1</i>	GCCTCGAAGATGAAGGAGAC	CAGTTTGTTCCACCAGGAGCA	117	60
<i>FOXF1</i>	GAGTTCGTCTTCTCCTCAACAC	GCTTGATGCTTGGTAGGTGAC	99	60
<i>KRT8</i>	CCTTAGCGGGTCTCTCGTA	GGGAAGCTGGTGTCTGAGTC	149	63
<i>KRT18</i>	GGACAGCTGACTCCAGGT	AGCTTGGAGAACAGCCTGAG	97	60
<i>KRT19</i>	GCCCAGCTGAGCGATGTGC	TGCTCCAGCCGTGACTTGATGT	86	64
<i>MMP13</i>	CTGAGGAAGACTTCCAGCTT	TTGGACCACTTGAGAGTTCG	250	65
<i>T</i>	AGACAGCCAGCAATCTG	TGGAGGGAAGTGAGAGG	115	53
<i>VEGF</i>	CTTTCTGCTCTCTGGGTGC	GGTTTGTGCTCTCCTCTGTC	101	58

All primers were designed in-house using Perlprimer except for *MMP13*<sup>1</sup> and *BAX*<sup>2</sup>.

Four reference genes (glyceraldehyde 3-phosphate dehydrogenase (*GAPDH*), hypoxanthine-guanine phosphoribosyltransferase (*HPRT*), ribosomal protein S19 (*RPS19*) and succinate dehydrogenase subunit A (*SDHA*), were chosen to normalize gene expression of the target genes: aggrecan (*ACAN*), a disintegrin and metalloproteinase with thrombospondin motifs 5 (*ADAMTS5*), Bcl2-like-protein (*BAX*), B-cell CLL/lymphoma 2 (*BCL2*), caspase-3 (*CASP3*), collagen type I (*COL1A1*), collagen type II (*COL2A1*), collagen type X (*COL10A1*), cyclin D1 (*CCND1*), forkhead box F1 (*FOXF1*), keratin 8 (*KRT8*), keratin 18 (*KRT18*), keratin 19 (*KRT19*), matrix metalloproteinase 13 (*MMP13*), brachyury (*T*), and vascular endothelial growth factor (*VEGF*).

**References**

- Muir P, Danova NA, Argyle DJ, Manley PA, Hao Z. 2005. Collagenolytic protease expression in cranial cruciate ligament and stifle synovial fluid in dogs with cranial cruciate ligament rupture. *Vet Surg* 34: 482-490.
- Mahmoudabady M, Niazmand S, Shafei MN, McEntee K. 2013. Investigation of apoptosis in a canine model of chronic heart failure induced by tachycardia. *Acta Physiol Hung* 100: 435-444.



**Notochordal-cell derived extracellular vesicles exert regenerative effects on canine and human nucleus pulposus cells**

Frances C. Bach<sup>1</sup>, Sten F.W.M. Libregts<sup>2</sup>, Laura B. Creemers<sup>3</sup>, Björn P. Meij<sup>1</sup>, Keita Ito<sup>3,4</sup>, Marca H.M Wauben<sup>2</sup> and Marianna A. Tryfonidou<sup>1</sup>

<sup>1</sup> Department of Clinical Sciences of Companion Animals, Faculty of Veterinary Medicine, Utrecht University, Utrecht, the Netherlands

<sup>2</sup> Department of Biochemistry and Cell Biology, Faculty of Veterinary Medicine, Utrecht University, Utrecht, the Netherlands

<sup>3</sup> Department of Orthopedics, University Medical Centre Utrecht, Utrecht, the Netherlands

<sup>4</sup> Orthopedic Biomechanics, Department of Biomedical Engineering, Eindhoven University of Technology, Eindhoven, the Netherlands

## Abstract

During intervertebral disc ageing, chondrocyte-like cells (CLCs) replace notochordal cells (NCs). NCs have been shown to induce regenerative effects in CLCs. Since vesicles released by NCs may be responsible for these effects, we characterized NC-derived extracellular vesicles (EVs) and determined their effect on CLCs. EVs were purified from porcine NC-conditioned medium (NCCM) through size exclusion chromatography, ultracentrifugation or density gradient centrifugation. Additionally, the EVs were quantitatively analyzed by high-resolution flow cytometry. The effect of NCCM-derived EVs was studied on canine and human CLC micro-aggregates *in vitro* and compared with NCCM-derived proteins and unfractionated NCCM. Porcine NCCM contained a considerable amount of EVs. NCCM-derived EVs induced GAG deposition in canine CLCs to a comparable level as NCCM-derived proteins and unfractionated NCCM, and increased the DNA and glycosaminoglycan (GAG) content of human micro-aggregates, although to a lesser extent than unfractionated NCCM. The biological EV effects were not considerably influenced by ultracentrifugation compared with size exclusion-based purification. Upon ultracentrifugation, interfering GAGs, but not collagens, were lost. Nonetheless, collagen type I or II supplemented to CLCs in a concentration as present in NCCM induced no anabolic effects. Porcine NCCM-derived EVs exerted anabolic effects comparable to NCCM-derived proteins, while unfractionated NCCM was more potent in human CLCs. GAGs and collagens appeared not to mediate the regenerative EV effects. Thus, NC-derived EVs have regenerative potential, and their effects may be influenced by the proteins present in NCCM. The optimal combination of NC-secreted factors needs to be determined to fully exploit the regenerative potential of NC-based technology.

## Introduction

Low back pain, affecting up to 85% of the population and resulting in considerable socioeconomic consequences<sup>1, 2</sup>, has been associated with intervertebral disc (IVD) degeneration<sup>3</sup>. Since dogs experience back pain and IVD degeneration with similar characteristics as humans, they are considered a suitable animal model for human IVD degeneration<sup>4, 5</sup>. The healthy IVD provides stability and flexibility to the spine and consists of a hydrated nucleus pulposus (NP) surrounded by the annulus fibrosus (AF). The NP, composed of glycosaminoglycan (GAG) and collagen type II, is derived from the notochord<sup>6</sup>. GAGs indirectly attract water, and in this way the IVD provides a shock absorption function for the spine. During maturation, notochordal cells (NCs) are replaced by chondrocyte-like cells (CLCs) in the NP. When the IVD degenerates, the CLCs are not able to maintain healthy tissue anymore. The CLCs become depleted, the GAG and water content decreases and collagen type II is replaced by collagen type I, resulting in a more fibrous tissue. The avascular IVD shows inadequate repair, and a vicious circle develops in which the IVD experiences increased vulnerability to damage by physiologic loading<sup>7</sup>.

Current treatments for IVD disease aim at relieving symptoms, but do not address the underlying degeneration. Therefore, regenerative strategies have gained increased attention<sup>8-10</sup>. Successful treatment strategies can be developed by mimicking developmental biology. In this respect, NCs have attracted increasing interest because of their potential regenerative capacity<sup>11</sup>. Large, vacuolated NCs are only present in the NP of young human individuals and disappear around 10 years of age. The replacement of NCs by CLCs precedes the onset of IVD degeneration, implying that NCs may play a role in maintaining IVD health. The regenerative effect of NC-conditioned medium (NCCM) has already been demonstrated on CLCs<sup>12-14</sup>, mesenchymal stromal cells (MSCs)<sup>15-17</sup>, and NP tissue explants<sup>18</sup> *in vitro*, and on rat IVDs *in vivo*<sup>19</sup>. NCCM may exert its effects in several ways: through extracellular matrix (ECM) components such as GAGs<sup>20</sup> and/or through growth factors. Factors that were already found are connective tissue growth factor (CTGF)<sup>19, 21</sup>, transforming growth factor- $\beta_1$  (TGF- $\beta_1$ ), Wnt-induced soluble protein 2, insulin-like growth factor binding protein 7, and angiopoietin-like 7<sup>19</sup> in canine NCCM, and CTGF<sup>22</sup>, alpha-2-macroglobulin, clusterin, and tenascin<sup>16</sup> in porcine NCCM.

Recently, extracellular vesicles (EVs) have gained increased attention. EVs are small, membrane-enclosed particles released by cells that play a role in intercellular signaling<sup>23</sup>, and are involved in tissue regeneration<sup>24, 25</sup>. We previously proposed that EVs may be responsible for regenerative NCCM effects<sup>26</sup>. The anabolic effect of pelletable (theoretically containing EVs and protein aggregates) NCCM factors was, however, less pronounced than that of soluble (peptides, proteins) NCCM factors<sup>26</sup>. This observation could be attributed to the ultracentrifugation (UC) procedure that may negatively affect the biological EV properties<sup>27</sup> or to the interfering protein aggregates present in the pelletable fraction<sup>28</sup>. Therefore, the first aim of the current study was to purify and characterize NC-derived EVs from porcine NCCM. The second aim was to determine the biologic effect of the NCCM-derived EVs on canine and human CLCs from degenerated IVDs *in vitro*.

## Material and Methods

### Sources of porcine NC-rich NP tissue and generation of NCCM

Healthy NP tissue was collected from 7 complete porcine spines (1.5 months of age, Thompson grade I) from the slaughterhouse in accordance with national regulations. To compare NCCM-derived EV and protein fractions with unfractionated NCCM in terms of EV and protein concentration, NCCM generation was slightly modified<sup>12</sup>. Briefly, NP tissue (1 gram/20 mL) was cultured for 4 days in hgDMEM+Glutamax (31966, Invitrogen) with 1% P/S (P11-010, GE Healthcare Life Sciences) at 37°C, 5% CO<sub>2</sub>, 5% O<sub>2</sub>. After 4 days, tissue was removed by 70 µm cell strainer filtration. The filtrate was centrifuged twice at 200g and 500g (ten minutes each, 4°C) to remove cells and to prevent the release of vesicles due to cell damage<sup>29</sup>. Subsequently, the supernatant was centrifuged at 4000g (45 minutes, 4°C) using 3 kDa Amicon Ultra-15 filter tubes (Merck Millipore) to remove small metabolites and waste products due to altered pH<sup>20</sup>. Substances with a molecular weight >3 kDa were suspended in fresh hgDMEM+Glutamax.

### Extracellular vesicle purification from porcine NCCM

EVs present within porcine NCCM were purified by differential UC<sup>29</sup> (Beckman Coulter Optima L-90K ultracentrifuge) and SEC. First, 37 mL of NCCM (previously centrifuged at 200, 500, and 4000g) was centrifuged at 10,000g (SW28 rotor; 4°C; 30 minutes; 8,700 rpm; RCF average 10,016g; RCF max 13,648g;  $\kappa$ -factor 2543.1) to remove cellular debris and apoptotic bodies. The supernatant was aliquoted and stored at -70°C until use. Per donor, 3 mL of 10,000g NCCM supernatant was subjected to qEV SEC-Columns (iZON Science; 1 mL/column) according to the manufacturer's instructions (Figure 1). The qEV columns were calibrated and eluted with either sterile hgDMEM+Glutamax (one column per donor; control, EV<sub>qEV</sub> and P<sub>qEV</sub> conditions, see later) or PBS/0.1% BSA (two columns per donor; EV<sub>UC</sub> and P<sub>UC</sub> conditions, see later) before use. PBS/0.1% BSA was depleted from aggregates by overnight (O/N) UC at 100,000g. Twenty-five fractions of 0.5 mL were collected per qEV column and the respective protein concentration was determined (Nanodrop 2000, A280). Based on expected EV sizes and measured protein content, the three fractions with most EVs (between fraction 6 and 11) and proteins (between fraction 18 and 24) were separately collected and pooled per donor (Supplementary File 1), yielding 4.5 mL enriched with EVs and 4.5 mL enriched with proteins per donor. One and a half mL hgDMEM+Glutamax with NCCM-derived EVs or proteins were directly employed in culture experiments (EV<sub>qEV</sub> and P<sub>qEV</sub>). The remaining 3 mL PBS/0.1% BSA with EVs or proteins was topped up with aggregate-depleted PBS/0.1% BSA in SW40 tubes and ultracentrifuged at 100,000g (SW40 rotor; 4°C; 65 minutes; 23000 rpm; RCF average 10,016g; RCF max 13,648g;  $\kappa$ -factor 2543.1). The 100,000g UC pellets of the pooled EV and protein fractions were separately resuspended in 40 µL aggregate-depleted PBS/0.1% BSA. Thirty-five µL of this 40 µL were employed in culture experiments (EV<sub>UC</sub> and P<sub>UC</sub>). To the remaining 5 µL of the 100,000g UC pellets, 15 µL aggregate-depleted PBS/0.1% BSA was added, yielding 20 µL that were further employed for EV characterization.

### NCCM extracellular vesicle characterization

The EVs present in both 100,000g UC pellets (containing either EVs or proteins) were labelled with PKH67 (MIDI67, Sigma-Aldrich), floated to their buoyant density by O/N sucrose density gradient floatation, and quantitatively analyzed by high-resolution flow

cytometry (BD Influx) as described previously<sup>29</sup>. In brief, 100,000g UC pellets were mixed with 180  $\mu$ L Diluent C (MIDI67, Sigma-Aldrich) and 1.5  $\mu$ L PKH67 and incubated for 3 minutes in SW40 tubes. One hundred  $\mu$ L IMDM (BE12-726F, Lonza) containing 10% EV-depleted Fetal Bovine Serum (generated by O/N UC at 100,000g) was added to stop the labelling process. These suspensions were mixed with 1.5 mL 2.5 M sucrose and overlaid with fifteen 700  $\mu$ L sucrose fractions with decreasing molarity (2.0 until 0.4 M) in SW40 tubes. Sucrose gradients were then subjected to density gradient floatation for 16 hours at 200,000g (SW40 rotor; 4°C; 39,000 rpm; RCF average 192,072g; RCF max 270,519g;  $\kappa$ -factor 144.5). Twelve sucrose gradient fractions of 1 mL were collected from which the density was determined by refractometry. Lastly, density fractions were 20 times diluted in PBS (50  $\mu$ L sample + 950  $\mu$ L PBS) and analyzed for EV content using high-resolution flow cytometry, according to an earlier described method<sup>29</sup>. Detergents (0.1% Triton X-100 and 0.1% SDS) were added to the fraction with the highest number of events to determine whether measured events were truly EVs<sup>30</sup>. Additionally, serial dilution of the fraction with the highest number of measured events was performed to exclude swarm detection<sup>31</sup>. Data were analyzed using FlowJo software.

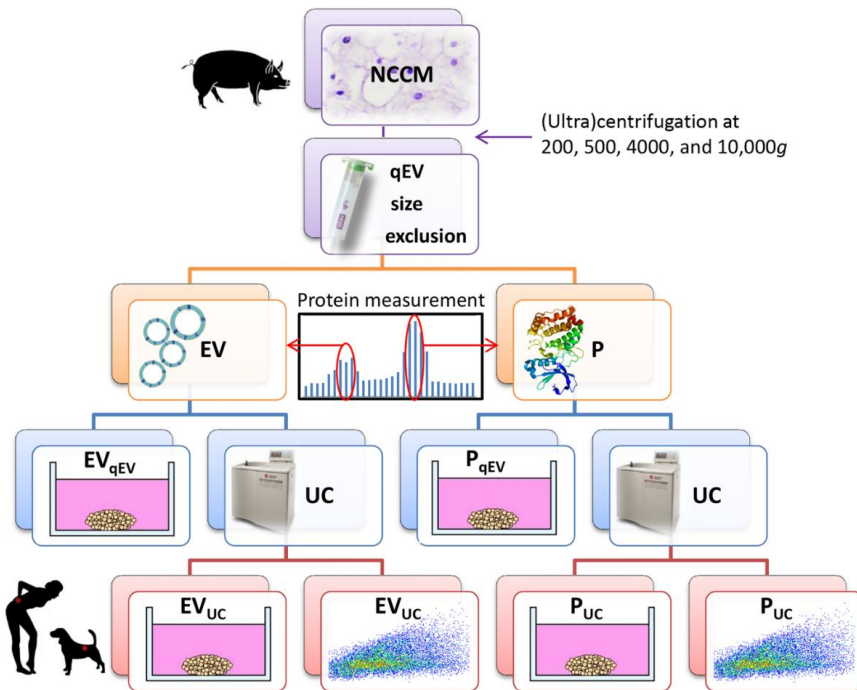


**Figure 1. Schematic representation of the experimental setup.** Notochordal cell-conditioned medium (NCCM) was generated by culturing porcine NC-rich nucleus pulposus tissue for 4 days and (ultra)centrifuged to remove cells and cell debris. For extracellular vesicle (EV) purification, 10,000g NCCM supernatant was subjected to size-exclusion chromatography (SEC). Based on expected EV size and protein measurements, the three fractions with most EVs and proteins (P) were separately collected and pooled (4.5 mL). Part (1.5 mL) was directly used in micro-aggregate culture experiments (EV<sub>qEV</sub> and P<sub>qEV</sub>), and part (3 mL) was subjected to ultracentrifugation (UC) at 100,000g for EV enrichment. The 100,000g UC pellet (40  $\mu$ L) was then partly (35  $\mu$ L) used in culture experiments (EV<sub>UC</sub> and P<sub>UC</sub>), whereas the remainder (5  $\mu$ L) was used for quantitative EV analysis using high-resolution flow cytometric analysis.  $n=7$  porcine NCCM donors, tested on a pool of 4 canine (*in triplo*) and 4 human chondrocyte-like cell donors (*in duplo*) in culture.

## Cell culture

Canine and human CLCs were collected from early degenerated IVDs (Thompson score II-III) as described previously<sup>12</sup>. Briefly, NP tissue was digested with 0.15% pronase (45 minutes) and 0.15% collagenase type II (O/N) at 37°C. Complete canine spines were collected from dogs euthanized in unrelated research studies, approved by the Utrecht University Animal Ethics Committee. Human IVDs (L2-L5, ≤48 hours after death) were obtained in the course of standard postmortem diagnostics, as approved by the scientific committee of the Pathology department of the University Medical Centre Utrecht (UMCU). Anonymous use of redundant tissue for research purposes is part of the standard treatment agreement with UMCU patients (Local Medical Ethical Committee number 12-364). The material was used in line with the code 'Proper Secondary Use of Human Tissue', installed by the Federation of Biomedical Scientific Societies.

CLCs from four canine (2-10 years of age, Beagles) and four human (50-63 years of age) donors were expanded as described previously<sup>12</sup>. At passage 2, the CLCs were pooled per species to assess the effect of donor-specific (EVs/proteins from) porcine NCCM on a representative human and canine CLC population. For micro-aggregate formation, 35,000 CLCs were plated per well in low-adherence cell-repellent surface 96-well plates (650970, CELLSTAR® Greiner Bio-one) in 50 µL basal culture medium (hgDMEM+Glutamax with 1% P/S, 1% ITS+ premix (354352, Corning Life Sciences), 0.04 mg/mL L-proline (P5607, Sigma-Aldrich), 0.1 mM Ascorbic acid 2-phosphate (A8960, Sigma-Aldrich), 1.25 mg/mL Bovine Serum Albumin (A9418, Sigma-Aldrich)) supplemented with 10 ng/mL TGF-β<sub>1</sub> (240-B-010, R&D Systems). The 96-well plates were centrifuged at 50g for 5 minutes to induce micro-aggregate formation. The next day, the culture medium was replaced with (a) hgDMEM+Glutamax that underwent SEC using qEV columns (similarly as 10,000g NCCM supernatant; control), (b) 10,000g NCCM supernatant (NCCM), (c) NCCM-derived EVs obtained by SEC (EV<sub>qEV</sub>), (d) NCCM-derived proteins obtained by SEC (P<sub>qEV</sub>), (e) NCCM-derived EVs obtained by SEC followed by 100,000g UC (EV<sub>UC</sub>), or (f) NCCM-derived proteins obtained by SEC followed by 100,000g UC (P<sub>UC</sub>). All different culture media were supplemented with the factors as present in basal culture medium. EVs and proteins were applied to the CLCs at a similar concentration as present in 10,000g NCCM supernatant. EV<sub>UC</sub> and P<sub>UC</sub> conditions were included to determine whether 100,000g UC affected the biological activity of the NCCM-derived EVs/proteins. The micro-aggregates were cultured for 7 (canine) or 21 (human) days at 37°C, 5% CO<sub>2</sub>, 5% O<sub>2</sub>. Canine CLC micro-aggregates disintegrated after 7 days of culture in NCCM(-derived factors), which prevented a 21-day culture. Culture medium was changed twice weekly.

The micro-aggregates' DNA (dsDNA High Sensitivity Assay Kit, Q32851, Invitrogen) and GAG content (DMMB assay<sup>32</sup>) were determined at day 7 (canine) or 21 (human) as described previously<sup>12</sup> ( $n=7$ , *in duplo* (human) or *triplo* (canine)). Since canine CLC micro-aggregates disintegrated after about 7 days of culture in NCCM(-derived factors), only human CLC micro-aggregates were histologically analyzed. Safranin O/Fast Green staining and collagen type I and II immunohistochemistry were performed as described previously<sup>12</sup>. The collagen and GAG concentration of the different culture media was analyzed using a hydroxyproline<sup>33</sup> and DMMB<sup>32</sup> assay, respectively.

In follow up culture experiments, canine CLCs were cultured for 7 days in basal culture medium, supplemented with or without 0.5, 1 and 2 mg/mL collagen type I (C9791, Sigma-Aldrich) or II (C9301, Sigma-Aldrich) to determine whether collagen (applied at a concentration as present in NCCM, EV<sub>qEV</sub>, EV<sub>UC</sub>, P<sub>qEV</sub> and P<sub>UC</sub>) exerted regenerative effects on CLCs. Lastly, canine CLC micro-aggregates were cultured for 7 days in serial dilutions of 10,000g NCCM supernatant (NCCM), EV<sub>UC</sub>, and P<sub>UC</sub> (1, 1:2, 1:4, 1:8 and 1:16 times concentrated) to determine when NCCM(-derived factors) lost their regenerative potential. The different media were diluted in basal culture medium. The same canine CLC and porcine NCCM donors were used as described earlier. The micro-aggregates' DNA and GAG content were determined as described previously.

### Statistical analysis

Statistical analysis was performed using IBM SPSS (version 24). All data were examined for normal distribution (Shapiro Wilks test). Kruskal Wallis and Mann-Whitney U tests were performed on non-normally distributed data, whereas general linear regression models based on ANOVAs were used for normally distributed data. Benjamini & Hochberg False Discovery Rate *post-hoc* corrections for multiple comparisons were performed. To find correlations between the number of measured events and the micro-aggregates' GAG/(DNA) content, Pearson's correlations were determined. A *p*-value < 0.05 was considered significant.

## Results

### NCCM-derived extracellular vesicle purification and characterization

NCCM-derived EVs were separated from soluble proteins by size-exclusion chromatography (SEC) and separately pelleted by UC at 100,000g. The UC pellets (containing either EVs or proteins) were labelled with PKH67. Thereafter, the EVs were floated in sucrose gradients to their buoyant density. Lastly, the EVs were quantitatively analyzed by high-resolution flow cytometry.

To confirm the presence of true EV within samples upon flow cytometric analysis, detergents can be added to disrupt the EV lipid bilayer<sup>30</sup>. Upon addition of 0.1% SDS or 0.1% Triton X-100 to the samples containing the highest number of EVs (density 1.12 g/mL), the event rate reduced considerably (Supplementary File 1a). This was accompanied by a loss of light scattering events (Supplementary File 1a). Taken together, this confirms that the majority of detected events during flow cytometric analysis were indeed EVs. To demonstrate that during flow cytometric analysis single EVs were measured and not EV swarms (presence of multiple EVs within the measuring spot<sup>31</sup>), the 1.12 g/mL sucrose gradient fractions were serially diluted and analyzed. Upon dilution, the scatter profiles of EVs did not change (Supplementary File 1c). A linear correlation ( $R^2$ : 0.9996) was found between the number of measured events and the dilution (Supplementary File 1b), indicating that single EVs and not swarms of EVs were detected.

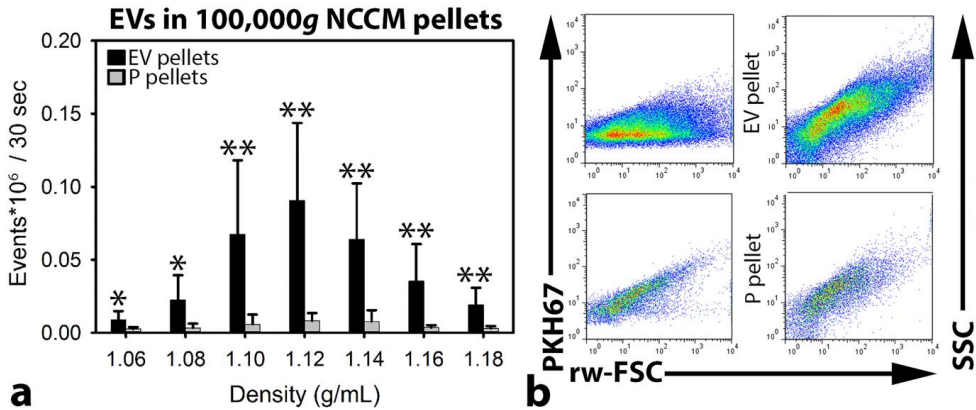


**Figure 2. Quantitative extracellular vesicle (EV) analysis by high-resolution flow cytometry of notochordal cell-conditioned medium (NCCM).** (a) Number of measured events per sucrose gradient fraction (with different densities) (+ SD) from floated porcine NCCM EV 100,000g ultracentrifugation (UC) pellets (black bars) and floated protein (P) 100,000g UC pellets (grey bars). \*, \*\*: significantly more measured events per 30 sec in the sucrose gradient fractions of the EV 100,000g UC pellets than in those of the P 100,000g UC pellets ( $p < 0.05$ ,  $p < 0.01$ , respectively). (b) Dot plots of the sucrose gradient fraction with the highest number of measured events (density 1.12 g/mL) from one representative donor (donor 2). Dot plots represent levels of PKH67 intensity (left) or side scatter (SCC; right) (y-axis) versus reduced wide-angle forward scatter (rw-FSC) (x-axis). Upper dot plots represent the 1.12 g/mL sucrose fraction of the EV 100,000g UC pellet, and lower dot plots represent the 1.12 g/mL sucrose fraction of the P 100,000g UC pellet.  $n = 7$  porcine NCCM donors.

High-resolution flow cytometry of porcine NCCM-derived EV and protein (P) 100,000g UC pellets revealed that the number of EVs differed considerably between donors (Supplementary File 2). The majority of EVs were, however, detected at the same densities. Additionally, the EV scatter profiles were comparable between all donors (Figure 2). In all donors, the highest number of events was measured in the 1.10, 1.12, and 1.14 g/mL sucrose gradient fractions of the EV 100,000g UC pellets. In the P 100,000g UC pellets, most events were also detected in the 1.10-1.14 g/mL sucrose gradient fractions, but the number of events was significantly lower compared to the EV 100,000g UC pellets ( $p < 0.05$ ).

### The effect of porcine NCCM-derived purified extracellular vesicles and proteins on canine and human CLCs

#### *NCCM-derived EVs and proteins induce GAG deposition in canine and human CLC micro-aggregates*

Based on the expected EV sizes and protein measurements, the three NCCM SEC fractions with most EVs and proteins (P) were separately collected (Supplementary File 3). Part was directly used in culture (EV<sub>qEV</sub> and P<sub>qEV</sub>), and part was subjected to 100,000g UC and thereafter used in culture (EV<sub>UC</sub> and P<sub>UC</sub>). After 7 days of culture, no treatment significantly influenced the canine micro-aggregates' DNA content compared with controls (Figure 3a). The GAG and GAG/DNA content of the canine micro-aggregates were, however, significantly increased by 7-day unfractionated NCCM, EV<sub>qEV</sub>, EV<sub>UC</sub>, P<sub>qEV</sub>, and P<sub>UC</sub> treatment ( $p < 0.05$ ), with no differences between these treatments (Figure 3b,c).

The DNA and GAG content of the human micro-aggregates were significantly induced by 21-day unfractionated NCCM, EV<sub>qEV</sub>, EV<sub>UC</sub>, P<sub>qEV</sub>, and P<sub>UC</sub> treatment ( $p < 0.01$ , Figure 3d,e,g). Unfractionated NCCM was most potent in this respect, followed by EV<sub>qEV</sub> and P<sub>qEV</sub>, and lastly EV<sub>UC</sub> and P<sub>UC</sub>. EV<sub>qEV</sub> induced a similar DNA and GAG content in human micro-aggregates as P<sub>qEV</sub> treatment. Also EV<sub>UC</sub> was equally potent in increasing the DNA and GAG content of the human micro-aggregates as P<sub>UC</sub>. Both were, however, less potent than EV<sub>qEV</sub> and P<sub>qEV</sub> in this respect. Only 21-day EV<sub>qEV</sub> and unfractionated NCCM treatment significantly increased the GAG/DNA content of the human micro-aggregates compared with control, P<sub>qEV</sub> and P<sub>UC</sub> treatment ( $p < 0.05$ , Figure 3f). All treatments increased collagen type I deposition compared with controls (Figure 3g). Only in micro-aggregates treated with EV<sub>UC</sub> and P<sub>UC</sub>, limited collagen type II was deposited (Figure 3g).

The total number of EVs in the sucrose fractions (density 1.06-1.18 g/mL) of the porcine NCCM EV 100,000g UC pellets did not correlate with the GAG content of the canine and human micro-aggregates treated with these EVs (Supplementary File 4a-h). Notably, the number of measured EVs and the canine, but not the human, micro-aggregates' GAG/DNA content after 7-day EV<sub>qEV</sub> treatment displayed a moderate correlation ( $r: 0.600$ ,  $p < 0.05$ ; Supplementary File 4c).

#### *Collagen and GAG concentration of the different culture media*

The GAG concentration of unfractionated NCCM, EV<sub>qEV</sub>, EV<sub>UC</sub>, P<sub>qEV</sub>, and P<sub>UC</sub> media was significantly higher than that of control media (in which GAGs were undetectable;  $p < 0.05$ ; Figure 4a). The GAG concentration of unfractionated NCCM was the highest, followed by EV<sub>qEV</sub>, P<sub>qEV</sub>, EV<sub>UC</sub>, and lastly P<sub>UC</sub> ( $p < 0.05$ ). This indicates that with 100,000g UC, GAGs were lost. The collagen concentration of unfractionated NCCM, EV<sub>qEV</sub>, EV<sub>UC</sub>, P<sub>qEV</sub>, and P<sub>UC</sub> media was significantly higher than that of control media (in which collagen was undetectable;  $p < 0.05$ ; Figure 4b). No differences in collagen concentration were detected between NCCM, EV, and P media.

Since in all NCCM-derived culture media collagen was present, it was determined whether collagen alone could exert effects on CLCs when it was applied at a concentration as present in NCCM(-derived EV/P media) (0.5 mg/mL). Interestingly, 0.5 and 1 mg/mL collagen type I or II supplementation did not exert regenerative effects on canine CLCs (Figure 4c,d). Only 2.0 mg/mL collagen type II increased the canine micro-aggregates GAG content compared with controls ( $p < 0.05$ ).

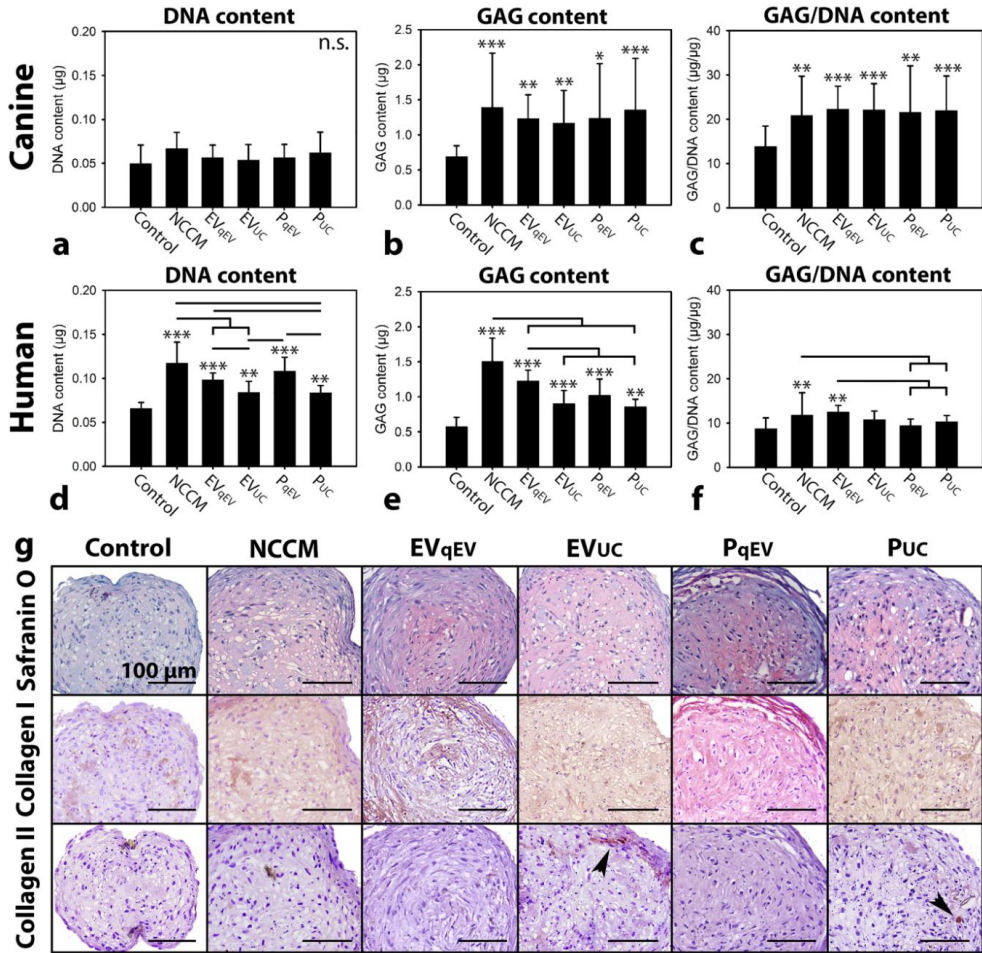


**Figure 3. Notochordal cell-conditioned medium (NCCM)-derived extracellular vesicles (EVs) and proteins (P) induce increased glycosaminoglycan (GAG) deposition in chondrocyte-like cell (CLC) micro-aggregates derived from degenerated discs. (a, d)** DNA content **(b, e)** GAG content, **(c, f)** GAG/DNA content (mean ± SD) of canine and human CLC micro-aggregates, respectively, cultured in control culture medium, unfraktionated porcine NCCM, or porcine NCCM-derived EVs or proteins for 7 (canine) or 21 (human) days. EV<sub>qEV</sub>: NCCM-derived EVs obtained after size exclusion chromatography (SEC), EV<sub>UC</sub>: NCCM-derived EVs obtained after SEC and subsequent 100,000g ultracentrifugation (UC), P<sub>qEV</sub>: NCCM-derived proteins obtained after SEC, P<sub>UC</sub>: NCCM-derived proteins obtained after SEC and subsequent 100,000g UC. Bars indicate significant differences between conditions ( $p < 0.05$ ); \*, \*\*, \*\*\*: significantly different from controls ( $p < 0.05$ ,  $p < 0.01$ ,  $p < 0.001$ , respectively); **(g)** Safranin O/Fast Green staining and collagen type I and II immunohistochemistry of human CLC micro-aggregates after 21 days of culture. Arrowheads indicate collagen type II deposition.  $n = 7$  porcine NCCM donors tested on a pool of 4 canine (*in triplo*) and 4 human CLC donors (*in duplo*). n.s.: not significantly different.

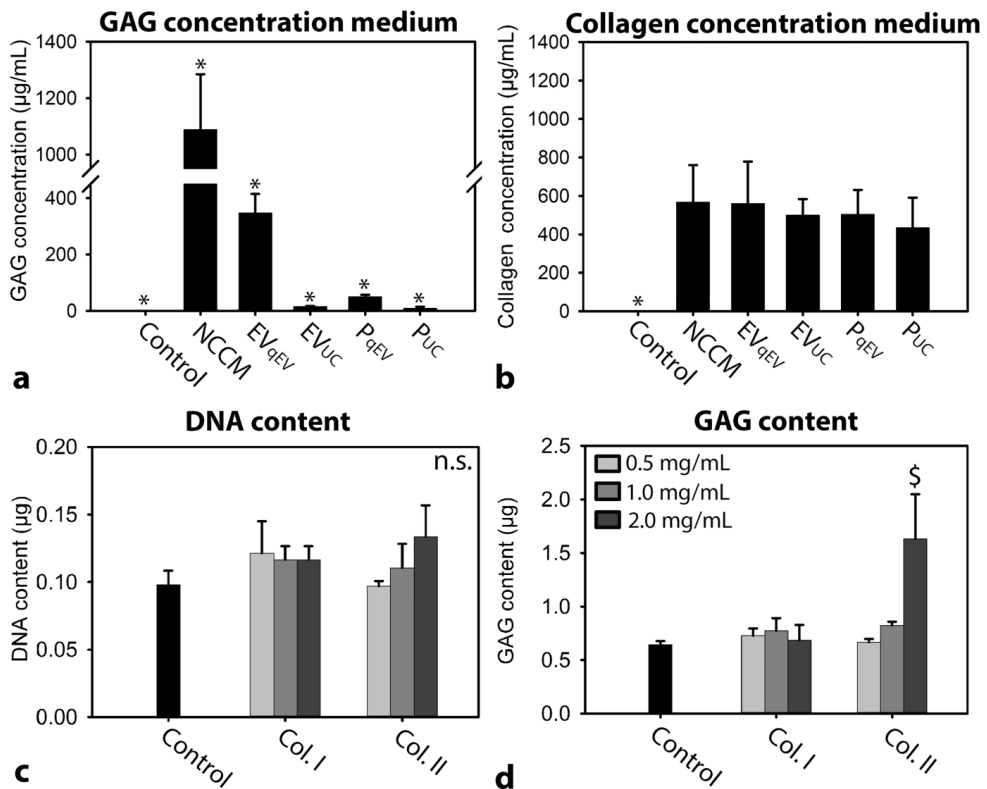


**Figure 4. GAG and collagens are not responsible for the NCCM-mediated anabolic effects.** (a) GAG and (b) collagen concentration of the different culture media.  $n = 7$  porcine NCCM donors. (c) DNA content (d) GAG content (mean + SD) of canine CLC micro-aggregates cultured in basal culture medium (control), supplemented with/without 0.5, 1.0 or 2.0 mg/mL collagen type I or II for 7 days.  $n=6$ , tested on a pool of 4 canine CLC donors. \*: significantly different from all other conditions ( $p<0.05$ ); §: significantly different from control ( $p<0.05$ ); GAG: glycosaminoglycan. n.s.: not significantly different.

#### Serial dilution of NCCM(-derived EVs and proteins)

In follow-up experiments, canine CLC micro-aggregates were cultured for 7 days in serial (1-16 times) dilutions of unfractionated NCCM, EV<sub>UC</sub>, and P<sub>UC</sub> to determine the dose-dependency. A considerable amount of GAGs was present in P<sub>qEV</sub> and especially EV<sub>qEV</sub>, whereas this was almost absent in EV<sub>UC</sub> and P<sub>UC</sub> media. Therefore, P<sub>UC</sub> and EV<sub>UC</sub> were used in this experiment to exclude GAG interference. No treatment significantly influenced the micro-aggregates' DNA content (Figure 5a). The micro-aggregates' GAG content was significantly induced by one until sixteen times diluted unfractionated NCCM ( $p<0.05$ , Figure 5b). NCCM-derived EVs and proteins also induced the micro-aggregates' GAG content, but only until a concentration as present in two (EV<sub>UC</sub>) or four (P<sub>UC</sub>) times diluted NCCM ( $p<0.05$ ). The micro-aggregates' GAG content significantly decreased with serial dilution of unfractionated NCCM, EV<sub>UC</sub>, and P<sub>UC</sub>. The micro-aggregates' GAG/DNA content was only significantly induced by one times concentrated unfractionated NCCM, NCCM-derived EVs and proteins ( $p<0.05$ , Figure 5c).

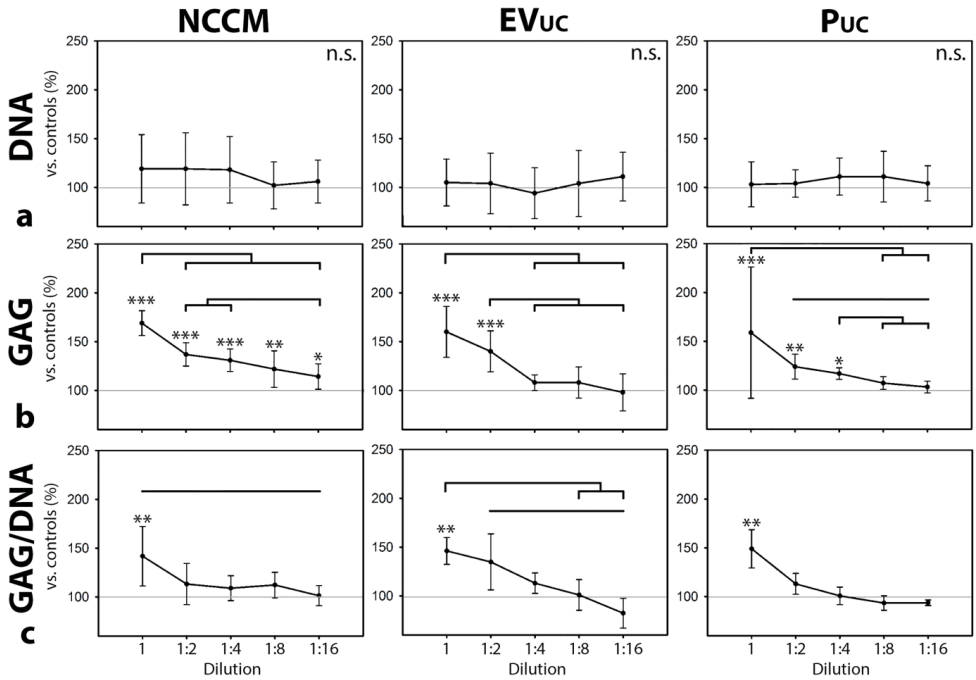


**Figure 5. Serial dilution of notochordal cell-conditioned medium (NCCM), and NCCM-derived extracellular vesicles (EVs) and proteins (P).** (a) DNA content, (b) GAG content, (c) GAG/DNA content (mean  $\pm$  SD) of canine CLC micro-aggregates cultured for 7 days in control culture medium, unfractionated porcine NCCM, or porcine NCCM-derived EVs or proteins. EV<sub>UC</sub>: NCCM-derived EVs obtained after size exclusion chromatography (SEC) and subsequent 100,000g ultracentrifugation (UC), P<sub>UC</sub>: NCCM-derived proteins obtained after SEC and subsequent 100,000g UC. Grey line represents controls (set at 100%). Black bars indicate significant differences between conditions ( $p < 0.05$ ); \*, \*\*, \*\*\*: significantly different from controls ( $p < 0.05$ ,  $p < 0.01$ ,  $p < 0.001$ , respectively).  $n = 6$  porcine NCCM, EV, and P donors tested on a pool of 4 canine CLC donors. GAG: glycosaminoglycan. n.s.: not significantly different.

The micro-aggregates' GAG/DNA content significantly decreased with serial dilution of NCCM-derived EVs, and unfractionated NCCM, but not with serial dilution of NCCM-derived proteins. There was a significant correlation between the total number of EVs in the porcine NCCM 100,000g EV UC pellets and the GAG ( $r: 0.848$ ,  $p < 0.001$ ) and GAG/DNA ( $r: 0.490$ ,  $p < 0.01$ ) content of the canine micro-aggregates treated with these EVs (Figure 6).

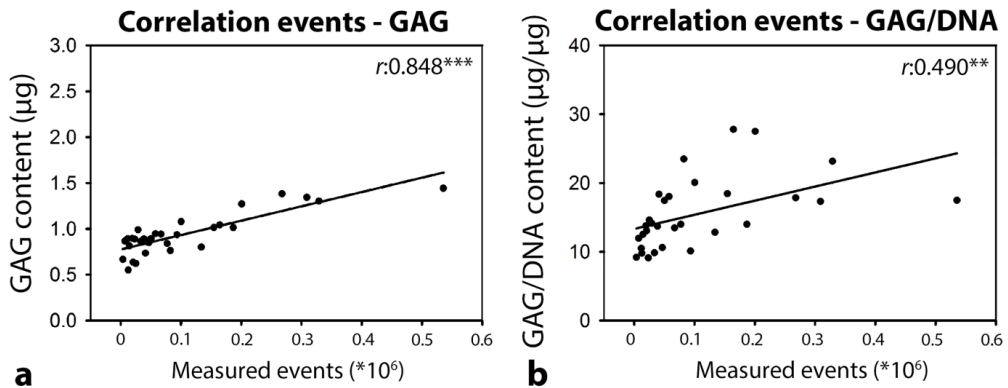


**Figure 6.** Pearson correlation between the total number of EVs (as determined by high-resolution flow cytometry) in the sucrose fractions of the porcine notochordal cell-conditioned medium (NCCM) extracellular vesicle (EV) pellets after size exclusion chromatography (SEC) and 100,000g ultracentrifugation (UC) and the GAG (a) and GAG/DNA (b) content of canine CLC micro-aggregates treated with a serial dilution of EV<sub>UC</sub> (NCCM-derived EVs obtained after SEC and subsequent 100,000g UC).  $n = 6$  porcine NCCM donors tested on a pool of 4 canine CLC donors. \*\*,\*\*\*: significant correlation ( $p < 0.01$ ,  $p < 0.001$ , respectively). GAG: glycosaminoglycan.

## Discussion

### Porcine NCCM contained a considerable amount of EVs which exerted regenerative effects on CLCs

Using SEC, differential UC, density gradient floatation, and quantitative high-resolution flow cytometric analysis, this study is the first to demonstrate that porcine NCs secrete a considerable amount of EVs. We furthermore demonstrate that these EVs have biologic effects across species that suffer from clinical intervertebral disc disease. Notably, NCCM-derived EVs induced GAG deposition in canine CLCs to a comparable level as NCCM-derived soluble proteins and unfractionated NCCM. In contrast, NCCM-derived EVs increased the DNA and GAG content of human CLC micro-aggregates to a similar level as NCCM-derived proteins, but to a lesser extent than unfractionated NCCM. These species-dependent differences could be explained by differences in culture period. Canine micro-aggregate disintegration (in NCCM-derived media, but not in basal culture medium) prohibited a 21-day culture. As such, the 7-day canine CLC culture may be too short to demonstrate the full regenerative potential of NCCM. With serial dilution, NCCM-derived EVs and proteins lost their regenerative effect on canine CLCs earlier than unfractionated NCCM. Taken together, this may indicate that also in canine CLCs, unfractionated NCCM may have a stronger regenerative potential than NCCM-derived EVs or proteins employed at the same concentration. Based on their pronounced loss of biological activity with serial dilution compared with unfractionated NCCM, the EVs may interact with proteins present in NCCM. Notably, there were still some EVs present in the P UC pellets, which are probably smaller in size given the SEC procedure. We cannot exclude that these EVs are another, possibly very potent EV subset. They may, however, also be part of the size continuum of the functional EVs (e.g. not another type, but only smaller EVs).

### **Correlation between the number of EVs and their regenerative effect**

In human CLCs, no linear correlation was found between the number of EVs (when applied at a concentration as present in undiluted NCCM) and their regenerative effect. Previous work could also not find an NCCM dose-dependent effect for neuronal inhibition<sup>20</sup>. In canine CLCs, however, we found a moderate correlation between the number of EVs and the micro-aggregates' GAG/DNA content after 7-day EV<sub>qEV</sub> treatment. These results can possibly be explained by the difference in culture period between the two species. After 7 days, canine CLCs were presumably in a dynamic phase of ECM production. After the 21-day human culture, however, secreted GAGs have already been deposited and only show a cumulative effect over time. Additionally, with serial dilution we found a significant positive correlation between the number of EVs and the GAG content of the canine micro-aggregates treated with these EVs. In conclusion, the results of this study may indicate that EVs induce a dose-dependent regenerative effect. However, a maximal response may be reached at an EV concentration as present in undiluted NCCM and/or after 21-day treatment. It remains to be determined if the EV-mediated anabolic effect can be further maximized with higher EV numbers.

### **Ultracentrifugation mildly affected the biological activity of EVs on human, but not on canine CLCs**

In the current study, the effect of 100,000g UC was compared with SEC-based EV purification, since previous work indicated that UC may not fully preserve the EV biological properties<sup>27, 34</sup>. In canine CLCs, 100,000g UC did not affect the biological activity of NC-derived EVs. In contrast, in human CLCs, UC slightly reduced the biological effect of EVs, since the DNA and GAG content of EV<sub>qEV</sub>-treated micro-aggregates was slightly higher than those of EV<sub>UC</sub>-treated micro-aggregates. Altogether, we have indications that 100,000g UC only mildly affected the biological activity of NCCM-derived EVs on CLCs from degenerated IVDs. Interestingly, collagen type I deposition was similarly induced by all treatments and collagen type II was only mildly deposited in EV<sub>UC</sub>- and P<sub>UC</sub>-treated micro-aggregates. To explain the slight differences in deposited ECM, a comprehensive analysis of the different EV preparations needs to be performed.

### **NC-derived EVs exert regenerative effects in the absence of GAGs**

When EVs were purified with SEC alone, interfering ECM residues (GAGs and collagens) were present. Affirmatively, previous work indicated that preparations obtained by limited processing resulted in ECM-embedded EVs, whereas sequential UC removed this contamination<sup>28</sup>. EVs bind to ECM compartments such as GAGs<sup>35</sup>, collagens<sup>36, 37</sup>, and hyaluronic acid<sup>38</sup> using integrins and other cell surface receptors such as CD44. With UC, interfering GAGs were lost from the preparations. Importantly, EV<sub>UC</sub> and P<sub>UC</sub> devoid of GAGs induced clear regenerative effects, indicating that the regenerative effects of NCCM-derived media were not mediated by GAGs. This finding seems to be in contrast with the notion that the NC-secreted GAG chondroitin sulphate is responsible for NCCM-induced neurite<sup>20</sup> and angiogenesis<sup>39</sup> inhibition. However, it cannot be excluded that neuro- and angiogenesis are differently regulated processes than ECM production.

ECM compartments may provide a favorable micro-environment for CLCs<sup>40</sup>. Unlike GAGs, collagens were not lost with UC. For this reason, we could not determine whether NC-secreted EVs/proteins or collagens were responsible for the regenerative effect induced by

EV<sub>UC</sub> and P<sub>UC</sub>. Collagen type I or II are the most abundant collagen types in the AF and NP, respectively<sup>12, 41</sup>. When collagen type I and II were supplemented at 0.5 mg/mL (a concentration at which collagen is present in NCCM), they did not induce regenerative effects in CLCs. This may suggest that the regenerative effects of EV<sub>UC</sub> and P<sub>UC</sub> were not caused by collagens, but by NC-secreted EVs and other proteins, respectively. Supplementation of 2.0 mg/mL collagen type II, but not collagen type I, induced GAG deposition in canine CLCs. This is in accordance with previous work on human MSCs, in which collagen type II activated MAPK/ERK signalling and was involved in Smad signalling<sup>40, 42</sup>.

## Conclusions

In conclusion, porcine NCCM contained a considerable amount of EVs. These NC-derived EVs exerted comparable anabolic effects as NCCM-derived proteins, while unfractionated NCCM was more potent in human CLCs. The results of this study further imply that NCCM-derived GAGs and collagens were not responsible for the observed EV-mediated effects. Thus, NC-derived EVs have true regenerative potential. Based on their pronounced loss of biological activity with serial dilution compared with unfractionated NCCM, the EVs may interact with proteins present in NCCM. With a clinical directive in mind, the optimal combination of NC-secreted factors and the role of the EV as carrier need to be determined to fully exploit the regenerative potential of NC-derived treatment strategies. The next step would be to identify the bioactive substances which are transported with the EVs and the subsets of EVs that contain them. Thereafter, the (bioactive substances of the) EV subsets of interest could be used in functional *in vivo* studies.

## Acknowledgements

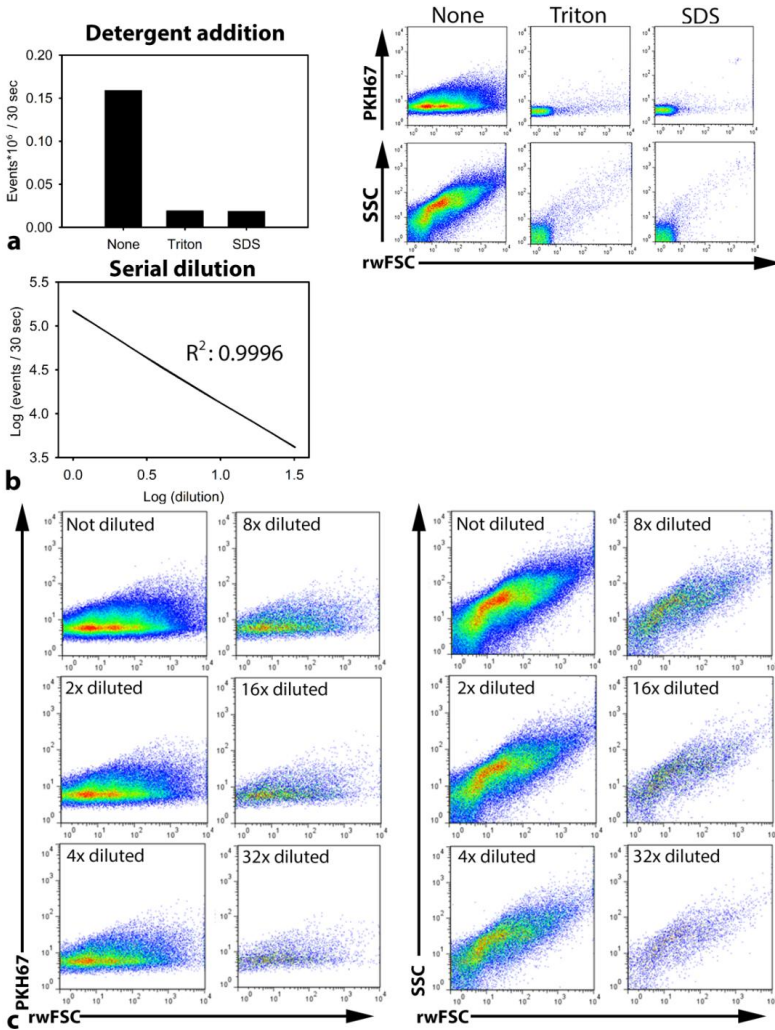
The authors would like to thank Willem de Jong and Stefan Wouters for help with the execution of experiments and Anita Krouwels and Imke Jansen for supplying human CLCs.

## References

1. Katz JN. 2006. Lumbar disc disorders and low-back pain: Socioeconomic factors and consequences. *J Bone Joint Surg Am* 88 Suppl 2: 21-24.
2. Andersson GB. 1999. Epidemiological features of chronic low-back pain. *Lancet* 354: 581-585.
3. Zheng CJ, Chen J. 2015. Disc degeneration implies low back pain. *Theor Biol Med Model* 12: 24-015-0020-3.
4. Bergknut N, Rutges JP, Kranenburg HJ, et al. 2012. The dog as an animal model for intervertebral disc degeneration? *Spine (Phila Pa 1976)* 37: 351-358.
5. Tellegen AR, Willems N, Beukers M, et al. 2017. Intradiscal application of a PCL-PEG-PCL hydrogel loaded with celecoxib for the treatment of back pain in canines: What's in it for humans? *J Tissue Eng Regen Med*.
6. Risbud MV, Schaefer TP, Shapiro IM. 2010. Toward an understanding of the role of notochordal cells in the adult intervertebral disc: From discord to accord. *Dev Dyn* 239: 2141-2148.
7. Bergknut N, Smolders LA, Grinwis GC, et al. 2013. Intervertebral disc degeneration in the dog. part 1: Anatomy and physiology of the intervertebral disc and characteristics of intervertebral disc degeneration. *Vet J* 195: 282-291.
8. Benneker LM, Andersson G, Iatridis JC, et al. 2014. Cell therapy for intervertebral disc repair: Advancing cell therapy from bench to clinics. *Eur Cell Mater* 27: 5-11.
9. Bach FC, Willems N, Penning LC, et al. 2014. Potential regenerative treatment strategies for intervertebral disc degeneration in dogs. *BMC Vet Res* 10: 3-6148-10-3.
10. Sakai D, Grad S. 2015. Advancing the cellular and molecular therapy for intervertebral disc disease. *Adv Drug Deliv Rev* 84: 159-171.
11. Purmessur D, Cornejo MC, Cho SK, Hecht AC, Iatridis JC. 2013. Notochordal cell-derived therapeutic strategies for discogenic back pain. *Global Spine J* 3: 201-218.
12. Bach FC, de Vries SA, Krouwels A, et al. 2015. The species-specific regenerative effects of notochordal cell-conditioned medium on chondrocyte-like cells derived from degenerated human intervertebral discs. *Eur Cell Mater* 30: 132-46; discussion 146-7.
13. Abbott RD, Purmessur D, Monsey RD, Iatridis JC. 2012. Regenerative potential of TGFbeta3 + dex and notochordal cell conditioned media on degenerated human intervertebral disc cells. *J Orthop Res* 30: 482-488.
14. Potier E, de Vries S, van Doeselaar M, Ito K. 2014. Potential application of notochordal cells for intervertebral disc regeneration: An in vitro assessment. *Eur Cell Mater* 28: 68-80; discussion 80-1.
15. Korecki CL, Taboas JM, Tuan RS, Iatridis JC. 2010. Notochordal cell conditioned medium stimulates mesenchymal stem cell differentiation toward a young nucleus pulposus phenotype. *Stem Cell Res Ther* 1: 18.
16. Purmessur D, Schek RM, Abbott RD, et al. 2011. Notochordal conditioned media from tissue increases proteoglycan accumulation and promotes a healthy nucleus pulposus phenotype in human mesenchymal stem cells. *Arthritis Res Ther* 13: R81.
17. de Vries SA, Potier E, van Doeselaar M, et al. 2015. Conditioned medium derived from notochordal cell-rich nucleus pulposus tissue stimulates matrix production by canine nucleus pulposus cells and bone marrow-derived stromal cells. *Tissue Eng Part A* 21: 1077-1084.
18. de Vries SA, van Doeselaar M, Meij BP, Tryfonidou MA, Ito K. 2016. The stimulatory effect of notochordal cell-conditioned medium in a nucleus pulposus explant culture. *Tissue Eng Part A* 22: 103-110.
19. Matta A, Karim MZ, Iseman DE, Erwin WM. 2017. Molecular therapy for degenerative disc disease: Clues from secretome analysis of the notochordal cell-rich nucleus pulposus. *Sci Rep* 7: 45623.
20. Purmessur D, Cornejo MC, Cho SK, et al. 2015. Intact glycosaminoglycans from intervertebral disc-derived notochordal cell-conditioned media inhibit neurite growth while maintaining neuronal cell viability. *Spine J* 15: 1060-1069.
21. Erwin WM, Ashman K, O'Donnell P, Inman RD. 2006. Nucleus pulposus notochord cells secrete connective tissue growth factor and up-regulate proteoglycan expression by intervertebral disc chondrocytes. *Arthritis Rheum* 54: 3859-3867.
22. Gantenbein B, Calandriello E, Wuertz-Kozak K, et al. 2014. Activation of intervertebral disc cells by co-culture with notochordal cells, conditioned medium and hypoxia. *BMC Musculoskelet Disord* 15: 422-2474-15-422.
23. Yanez-Mo M, Siljander PR, Andreu Z, et al. 2015. Biological properties of extracellular vesicles and their physiological functions. *J Extracell Vesicles* 4: 27066.
24. Malda J, Boere J, van de Lest CH, van Weeren PR, Wauben MH. 2016. Extracellular vesicles - new tool for joint repair and regeneration. *Nat Rev Rheumatol*.
25. Silva AM, Teixeira JH, Almeida MI, et al. 2016. Extracellular vesicles: Immunomodulatory messengers in the context of tissue repair/regeneration. *Eur J Pharm Sci*.
26. Bach FC, de Vries SA, Riemers FM, et al. 2016. Soluble and pelletable factors in porcine, canine and human notochordal cell-conditioned medium: Implications for IVD regeneration. *Eur Cell Mater* 32: 163-180.
27. Nordin JZ, Lee Y, Vader P, et al. 2015. Ultrafiltration with size-exclusion liquid chromatography for high yield isolation of extracellular vesicles preserving intact biophysical and functional properties. *Nanomedicine* 11: 879-883.
28. Paolini L, Zendrini A, Di Noto G, et al. 2016. Residual matrix from different separation techniques impacts exosome biological activity. *Sci Rep* 6: 23550.
29. van der Vlist EJ, Nolte-'t Hoen EN, Stoorvogel W, Arksteijn GJ, Wauben MH. 2012. Fluorescent labeling of nano-sized vesicles released by cells and subsequent quantitative and qualitative analysis by high-resolution flow cytometry. *Nat Protoc* 7: 1311-1326.

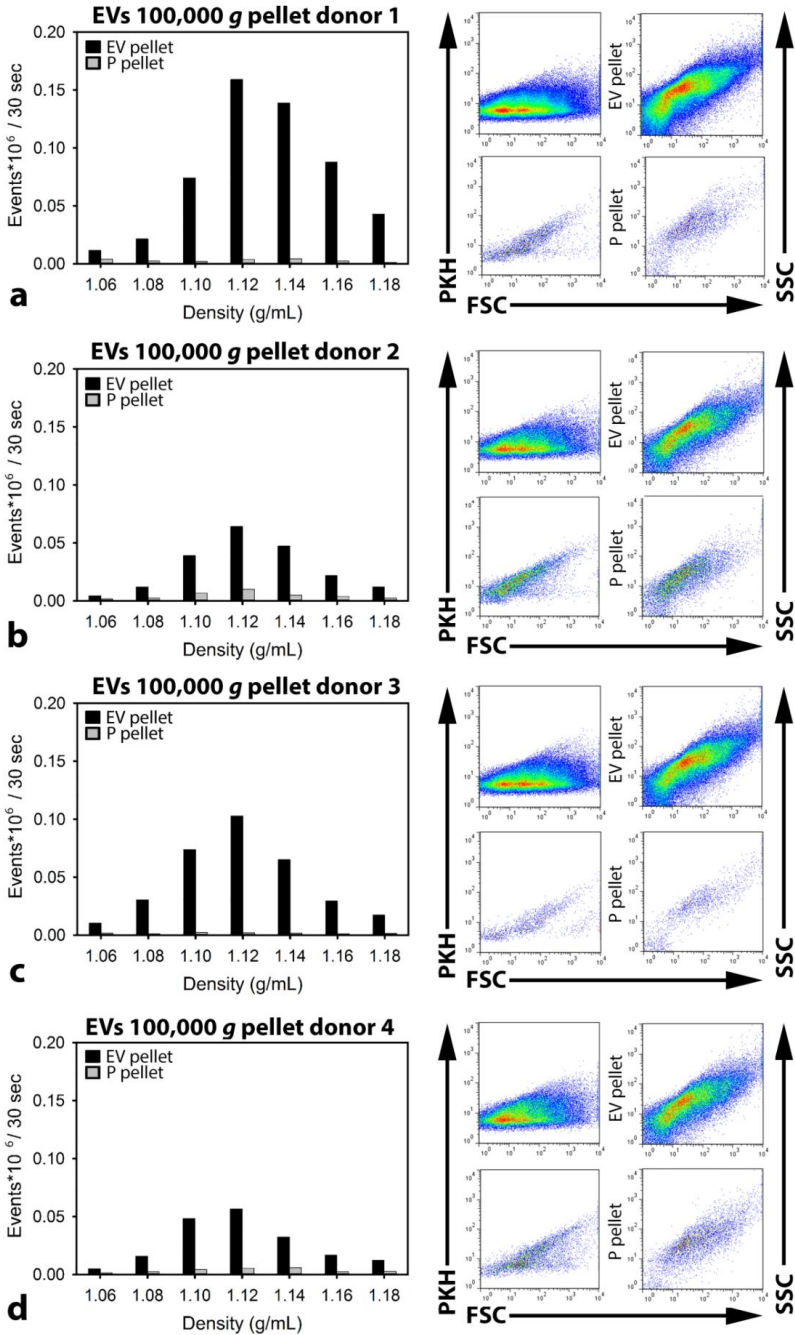
30. Osteikoetxea X, Sodar B, Nemeth A, et al. 2015. Differential detergent sensitivity of extracellular vesicle subpopulations. *Org Biomol Chem* 13: 9775-9782.
31. Groot Kormelink T, Arkesteijn GJ, Nauwelaers FA, et al. 2016. Prerequisites for the analysis and sorting of extracellular vesicle subpopulations by high-resolution flow cytometry. *Cytometry A* 89: 135-147.
32. Farndale RW, Sayers CA, Barrett AJ. 1982. A direct spectrophotometric microassay for sulfated glycosaminoglycans in cartilage cultures. *Connect Tissue Res* 9: 247-248.
33. Neuman RE, Logan MA. 1950. The determination of hydroxyproline. *J Biol Chem* 184: 299-306.
34. Deregibus MC, Figliolini F, D'Antico S, et al. 2016. Charge-based precipitation of extracellular vesicles. *Int J Mol Med* 38: 1359-1366.
35. Christianson HC, Svensson KJ, van Kuppevelt TH, Li JP, Belting M. 2013. Cancer cell exosomes depend on cell-surface heparan sulfate proteoglycans for their internalization and functional activity. *Proc Natl Acad Sci U S A* 110: 17380-17385.
36. Mu W, Rana S, Zoller M. 2013. Host matrix modulation by tumor exosomes promotes motility and invasiveness. *Neoplasia* 15: 875-887.
37. Narayanan R, Huang CC, Ravindran S. 2016. Hijacking the cellular mail: Exosome mediated differentiation of mesenchymal stem cells. *Stem Cells Int* 2016: 3808674.
38. Boere J, van de Lest CH, Libregts SF, et al. 2016. Synovial fluid pretreatment with hyaluronidase facilitates isolation of CD44+ extracellular vesicles. *J Extracell Vesicles* 5: 31751.
39. Cornejo MC, Cho SK, Giannarelli C, Iatridis JC, Purmessur D. 2015. Soluble factors from the notochordal-rich intervertebral disc inhibit endothelial cell invasion and vessel formation in the presence and absence of pro-inflammatory cytokines. *Osteoarthritis Cartilage* 23: 487-496.
40. Lu ZF, Doulabi BZ, Wuisman PI, Bank RA, Helder MN. 2008. Influence of collagen type II and nucleus pulposus cells on aggregation and differentiation of adipose tissue-derived stem cells. *J Cell Mol Med* 12: 2812-2822.
41. Eyre DR, Muir H. 1976. Types I and II collagens in intervertebral disc. interchanging radial distributions in annulus fibrosus. *Biochem J* 157: 267-270.
42. Tao Y, Zhou X, Liu D, et al. 2016. Proportion of collagen type II in the extracellular matrix promotes the differentiation of human adipose-derived mesenchymal stem cells into nucleus pulposus cells. *Biofactors* 42: 212-223.

**Supplementary File 1. Detergent addition to and serial dilution of EV sucrose gradient**

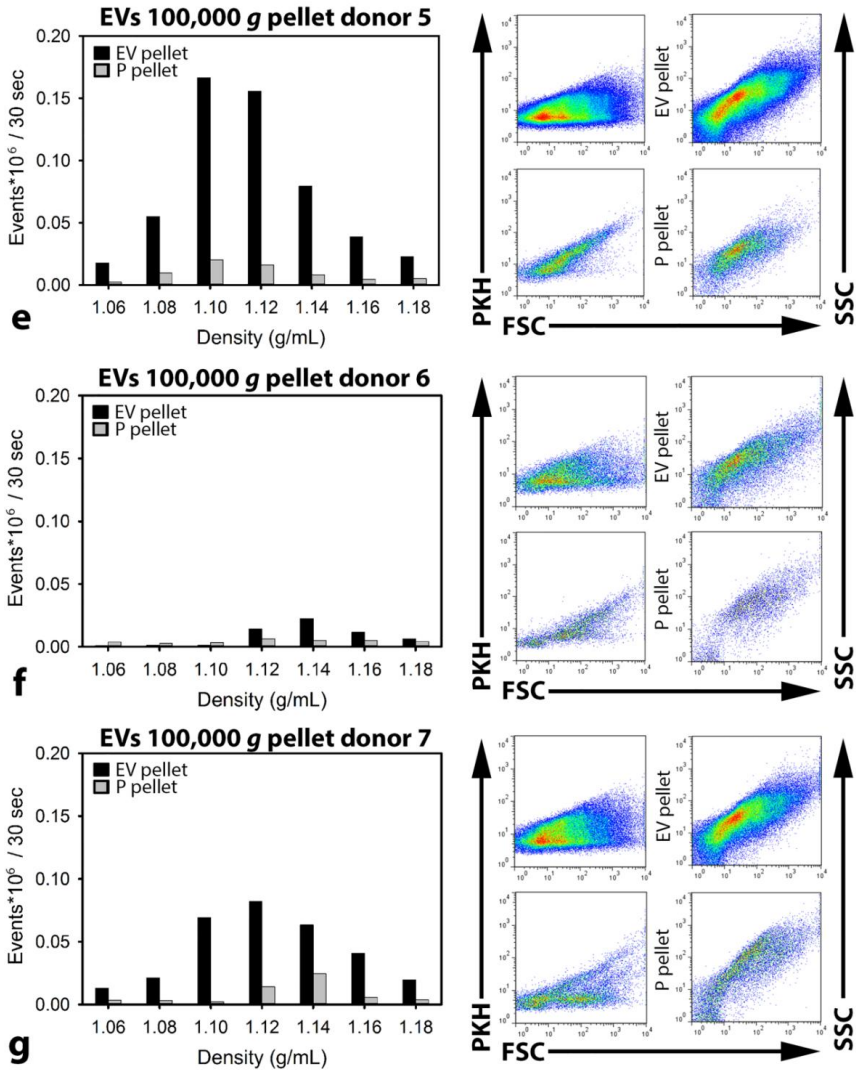


Detergent addition to the sucrose gradient fraction with the highest number of measured events from the porcine NCCM EV 100,000g ultracentrifugation pellet indicates that true EVs were detected with quantitative EV analysis (high resolution flow cytometry). Additionally, serial dilution of this fraction indicates that no swarm (coincident occurrence of multiple particles in the probe volume at the same time) was detected. Graphs and dot plots are depicted from one representative donor. (a) Addition of detergents (0.1% Triton or 0.1% SDS), that disrupt the lipid bilayer of the EVs, to the sucrose gradient fraction with the highest number of events (density 1.12 g/mL) reduced the event rate considerably, indicating that the measured events in this density fraction were indeed EVs. Moreover, light scattering events disappeared in the dot plots of the fraction treated with detergents. Dot plots represent levels of PKH67 intensity of side scatter (SSC) (y-axis) versus reduced wide-angle forward scatter (rwFSC) (x-axis). (b) To demonstrate the absence of swarm, a serial dilution on this sucrose gradient fraction (density 1.12 g/mL) was performed. A linear correlation ( $R^2: 0.9996$ ) was detected between the number of measured events and the dilution of this sucrose gradient fraction, indicating that no swarm was detected. (c) The scatter pattern observed in the dot plots did not change with the serial dilution, further indicating that swarm was absent. Dot plots represent levels of PKH67 intensity (right) or side scatter (SSC; left) (y-axis) versus reduced wide-angle forward scatter (rw-FSC) (x-axis).

**Supplementary File 2. Number of measured events and dot plots of porcine NCCM extracellular vesicle and protein 100,000g ultracentrifugation pellets**

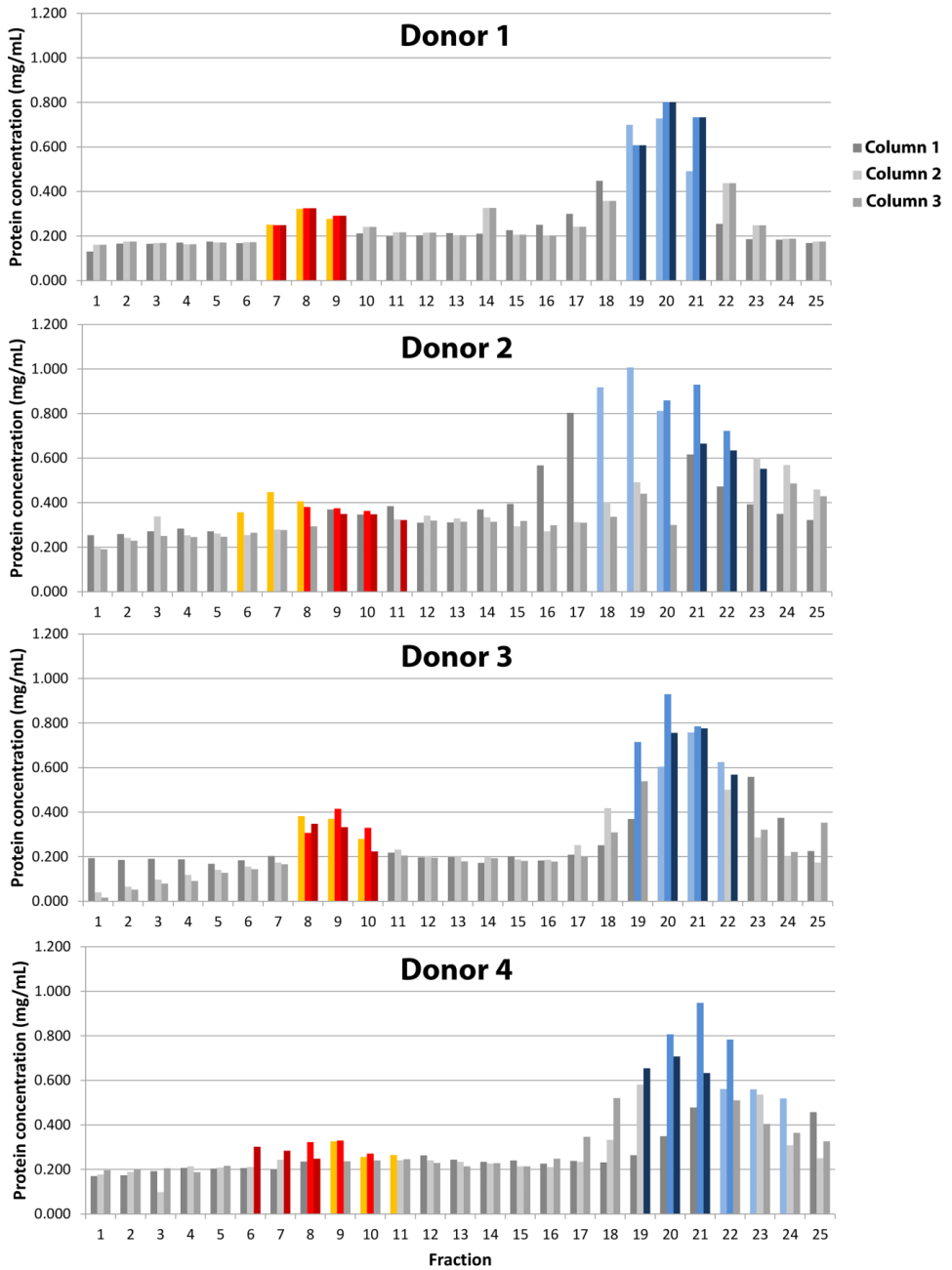


4

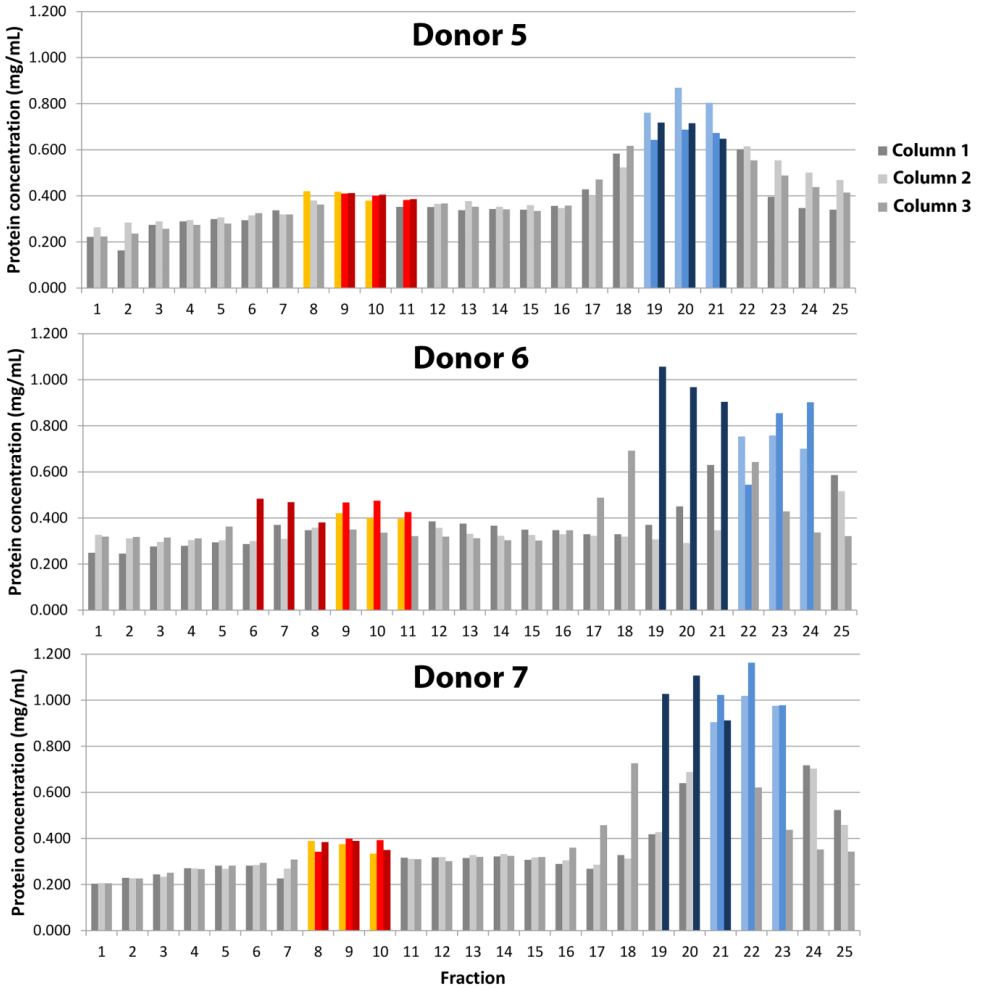


Quantitative flow cytometric extracellular vesicle (EV) analysis of the 100,000g ultracentrifugation pellets from all seven porcine notochordal cell-conditioned medium (NCCM) donors separately. High resolution flow cytometry of the porcine NCCM 100,000g ultracentrifugation pellets indicates that all donors demonstrate a similar pattern in number of measured events (EVs) per sucrose gradient fraction. Considerably more events were measured in the EV than in the protein (P) 100,000g pellet in all donors. In most donors, the highest number of measured events was present in the sucrose fraction with a density of 1.12 g/mL. Only the number of measured events per sucrose fraction differed considerably between donors. (a-g) Left: The number of measured events per sucrose gradient fraction (with different densities) from the porcine NCCM donors. Black bar: number of measured events per 30 sec in the sucrose gradient fractions of the EV 100,000g ultracentrifugation pellet. Grey bar: number of measured events per 30 sec in the sucrose gradient fractions of the P 100,000g ultracentrifugation pellet. Right: Dot plots of the sucrose gradient fraction with the highest number of measured events (density 1.12 g/mL) for most donors. Dot plots represent levels of PKH67 intensity (left) or side scatter (SSC; right) (y-axis) versus reduced wide-angle forward scatter (rw-FSC) (x-axis). Upper plots represent the 1.12 g/mL sucrose fraction of the EV 100,000g ultracentrifugation pellet, and lower plots represent the 1.12 g/mL sucrose fraction of the P 100,000g ultracentrifugation pellet.

**Supplementary File 3. Protein measurements of the different size exclusion columns fractions**

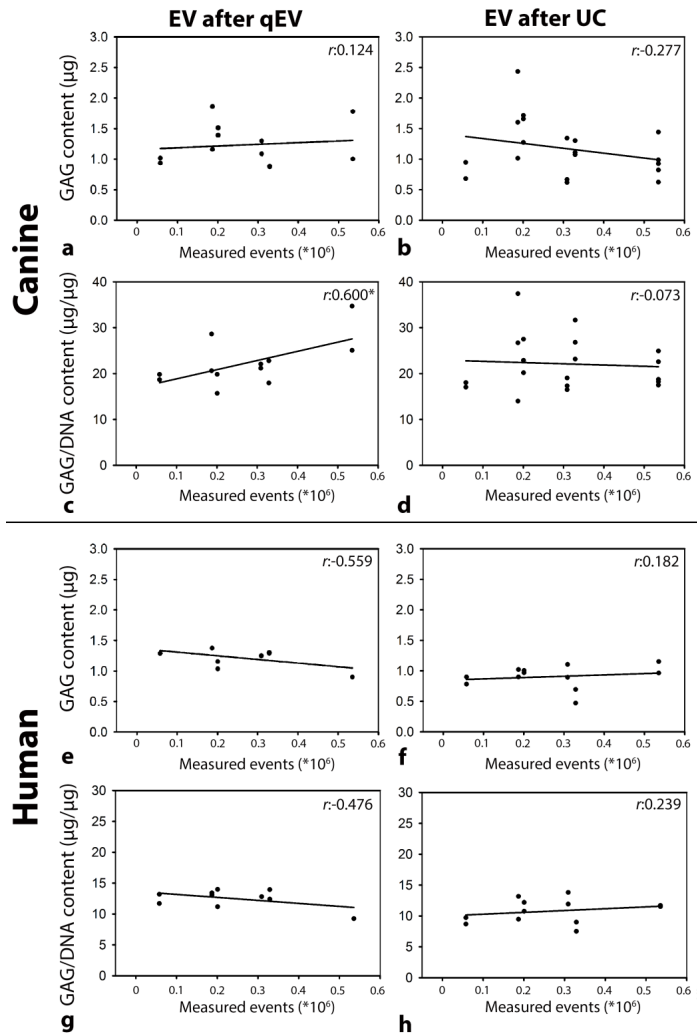


4



Per porcine donor, 3 mL of 10,000g NCCM supernatant was subjected to qEV size exclusion columns (iZON Science; 1 mL/column). Three columns were used per donor (light-dark grey bars). Twenty-five fractions of 0.5 mL were collected per qEV size exclusion column and the respective protein concentration was determined (Nanodrop 2000, A280). Based on expected EV sizes and measured protein content, the three fractions with most EVs (between fraction 6 and 11; orange-red bars) and proteins (between fraction 18 and 24; light-dark blue bars) were separately collected and pooled per donor.

### Supplementary File 4. Correlations between total number of measured events and the GAG content of canine and human CLC micro-aggregates treated with EVs



Pearson correlations between the total number of measured events in the sucrose fractions (1.06-1.18 g/mL) of the extracellular vesicle (EV) gradients and the GAG/(DNA) content of the canine and human chondrocyte-like cell (CLC) micro-aggregates treated with these EVs (after SEC (EV<sub>qEV</sub>) and after SEC plus 100,000g ultracentrifugation (EV<sub>UC</sub>)). Correlation between the total number of measured events and the GAG content of the canine (a) and human (e) CLC micro-aggregates treated with EV<sub>qEV</sub>, the GAG content of the canine (b) and human (f) CLC micro-aggregates treated with EV<sub>UC</sub>, the GAG/DNA content of the canine (c) and human (g) CLC micro-aggregates treated with EV<sub>qEV</sub>, and the GAG/DNA content of the canine (d) and human (h) CLC micro-aggregates treated with EV<sub>UC</sub>. The results indicate that there is no significant correlation between the number of EVs and the GAG content of the canine and human CLC micro-aggregates treated with these EVs, except for the significant positive correlation between the number of events and the GAG/DNA content of canine micro-aggregates treated with EVs after qEV size exclusion.  $n=6$  porcine NCCM donors tested on a pool of 4 canine and 4 human CLC donors. \*: significant correlation ( $p<0.05$ ).



**Biologic intervertebral disc repair by notochordal cell-derived matrix: from bench towards bedside**

Frances C. Bach<sup>1</sup>, Anna R. Tellegen<sup>1</sup>, Martijn Beukers<sup>1</sup>, Alberto Miranda-Bedate<sup>1</sup>, Michelle Teunissen<sup>1</sup>, Willem A.M. de Jong<sup>1</sup>, Stefan A.H. de Vries<sup>2</sup>, Laura B. Creemers<sup>3</sup>, Karin Benz<sup>4</sup>, Björn P. Meij<sup>1</sup>, Keita Ito<sup>2,3</sup>, and Marianna A. Tryfonidou<sup>1,\*</sup>

<sup>1</sup>Department of Clinical Sciences of Companion Animals, Faculty of Veterinary Medicine, Utrecht University, Utrecht, the Netherlands.

<sup>2</sup>Orthopaedic Biomechanics, Department of Biomedical Engineering, Eindhoven University of Technology, Eindhoven, the Netherlands.

<sup>3</sup>Department of Orthopedics, University Medical Centre Utrecht, Utrecht, the Netherlands.

<sup>4</sup>TETEC AG, Reutlingen, Germany.

*Submitted to Science Translational Medicine (under review)*

## Abstract

Because the socioeconomic burden of painful intervertebral disc (IVD) disease is high and current treatments are only symptomatic, minimally invasive strategies that promote biological IVD repair need to be developed. Notochordal cells (NCs) are replaced by chondrocyte-like cells (CLCs) during IVD maturation and degeneration. The regenerative potential of NC-secreted substances on CLCs and mesenchymal stromal cells (MSCs) has already been demonstrated. However, these substances have been elusive to identify. Alternatively, this study exploits the regenerative NC potential by using healthy NC-derived matrix (NCM). The dog serves herein as translational model. NCM (produced from porcine NC-rich tissue) induced anabolic, anti-catabolic, anti-apoptotic, and proliferative effects in human and canine CLCs and facilitated chondrogenic differentiation of canine MSCs *in vitro*. Based on these results, NCM, MSCs and NCM+MSCs were injected in mildly (spontaneously) and moderately (induced) degenerated canine IVDs *in vivo*. Longitudinal quantitative magnetic resonance imaging (MRI) was performed and after six months of treatment, the IVDs were further analyzed. NCM injected in moderately (induced) degenerated canine IVDs exerted beneficial effects at macroscopic and MRI level, induced healthy extracellular matrix production, improved the disc height, and ameliorated local inflammation. MSCs exerted no (additive) effects. In conclusion, NCM induced regenerative effects on degenerated IVDs. NCM may, comparable to demineralized bone matrix in bone regeneration, serve as 'instructive matrix', *e.g.* by locally releasing growth factors and facilitating tissue repair. Therefore, intradiscal NCM injection could be a promising regenerative treatment for IVD disease, circumventing the cumbersome identification of bioactive NC-secreted substances.

## Introduction

Over 80% of the human population experiences low back pain (LBP) at least once in their life, with severe socioeconomic consequences<sup>1</sup>. Degeneration of the intervertebral disc (IVD) is a common cause of chronic LBP<sup>2</sup>. Current treatments for LBP due to IVD degeneration mainly aim at symptom reduction or IVD replacement and are not without their inherent limitations. Therefore, LBP should be addressed at an earlier stage by minimally invasive strategies that induce definitive long-term biological IVD repair.

The IVD transmits loads and provides flexibility to the spine. The healthy IVD consists of a gelatinous nucleus pulposus (NP), surrounded by a fibrous annulus fibrosus (AF) and cartilaginous end plates (EPs). During IVD degeneration, the glycosaminoglycan (GAG) content of the NP decreases and collagen type II is replaced by collagen type I, resulting in more rigid NP tissue not able to sustain compressive loads anymore. Since the IVD cannot adequately repair its matrix, a vicious circle develops in which the IVD weakens and is damaged by physiologic loading<sup>3</sup>. During IVD maturation, a transition in NP cell phenotype takes place from large, vacuolated notochordal cells (NCs) to smaller, non-vacuolated chondrocyte-like cells (CLCs). NC loss in certain species (*e.g.* chondrodystrophic dogs) coincides with the onset of degenerative IVD changes<sup>3</sup>. Moreover, the regenerative potential of NCs has already been demonstrated on CLCs<sup>4-6</sup>, mesenchymal stromal cells (MSCs)<sup>7-9</sup>, and NP tissue explants<sup>10</sup> *in vitro*, and in rat IVDs *in vivo*<sup>11</sup>. Altogether, this indicates that NCs can play a role in maintaining healthy NP tissue. Therefore, NCs are a promising target for regenerative and/or symptom modifying therapies for IVD disease.

Despite the current focus on the NC secretome<sup>11-13</sup>, we here take an alternative approach by using unfractionated NC-derived matrix (NCM) from healthy, NC-rich NP tissue, to facilitate fast translation into the clinics. NCM may act rather comparable to demineralized bone matrix (DBM), which contains ECM and growth factor components native to bone and is currently successfully employed in clinical practice to accelerate bone healing<sup>14</sup>. Therefore, the first aim of this study was to determine the (regenerative) effects of NCM on CLCs from degenerated IVDs *in vitro* and injected NCM in degenerated IVDs *in vivo*. Since cell viability is impaired in the degenerated IVD<sup>15</sup>, NCM alone may not be sufficient. In this respect, intradiscal MSC transplantation is considered a promising regeneration strategy, currently explored in clinical trials<sup>16</sup>. Therefore, the second aim of this study was to determine the effects of NCM combined with MSCs on degenerated canine IVDs *in vivo*. The dog served herein as a translational model, since they experience LBP due to IVD degeneration with similar characteristics as humans<sup>4</sup>.

## Material and Methods

### Overall study design

The first objective of this study was to determine the effect of NCM (produced from porcine NC-rich tissue by lyophilization, pulverization, and resuspension at 10 mg/mL) on human and canine CLCs *in vitro*. Porcine NCM was pooled ( $n=6$ ) to assess the its effect on a representative population of donor-specific (CLCs from) degenerated IVDs. The second aim

was to assess the effect of NCM *in vivo* on degenerated canine IVDs ( $n=6$  Beagles, based on power analysis with power: 85%, alpha: 0.8% and standard deviation 15-30%). Also, the (additive) effect of MSCs was determined. We hypothesized that NCM would exert regenerative effects on canine and human CLCs *in vitro* and degenerated canine IVDs *in vivo* and that MSCs would have an additive effect. For the *in vivo* experiment, NCM, MSCs and NCM+MSCs were intradiscally injected in mildly (spontaneously) and moderately (induced by partial NP removal) degenerated canine IVDs. Treatments were not randomized within each dog to prevent interference of random effects from the spinal segment. After three months, NCM was reinjected in two degenerated IVDs per dog to determine whether multiple injections would exert a more beneficial effect. Longitudinal quantitative MRI was performed and IVDs were macroscopically, histologically, and biochemically analyzed after six months. Outliers were not excluded. The investigators who assessed, measured, or quantified the results were blinded to the intervention.

### Generation of NCM

Thompson score I, healthy IVD tissue was collected from complete spines of six 3-month-old porcine donors from the slaughterhouse in accordance with local regulations (permit 457642.09). To produce NCM, NP tissue was lyophilized overnight, pulverized to fine powder using a microdismembrator (Sartorius) and resuspended at 10 mg/mL in hgDMEM+Glutamax (31966, Invitrogen). For *in vitro* studies, NCM was supplemented with 1% P/S (P11-010, GE Healthcare Life Sciences), 1% ITS+ premix (354352, Corning Life Sciences), 0.04 mg/mL L-proline (P5607, Sigma-Aldrich), 0.1 mM Ascorbic acid 2-phosphate (Asap; A8960, Sigma-Aldrich), and 1.25 mg/mL Bovine Serum Albumin (BSA; A9418, Sigma-Aldrich).

### The effect of NCM on canine and human CLCs and MSCs *in vitro*

IVDs from complete spines were collected from six Beagles (2-7 years of age, 3 male/3 female, Thompson score III) euthanized in unrelated research studies (approved by the Utrecht University Animal Ethics Committee, experimental numbers: 2012.III.07.065, 2013.III.02.017, and 2013.II.12.126). Additionally, IVDs from six human donors (47-72 years of age, 3 male/3 female, Thompson score III) were obtained during standard *postmortem* diagnostics (<48 hours after death). The L2-L5 part of the spine was collected, approved by the scientific committee of the Pathology department of the University Medical Centre Utrecht (UMCU). Anonymous use of redundant tissue for research purposes is a standard agreement with UMCU patients (Local Medical Ethical Committee number 12-364). The IVDs were used according to the code 'Proper Secondary Use of Human Tissue', installed by the Federation of Biomedical Scientific Societies. The NP was collected by precise separation from AF and EPs and digested<sup>4</sup>.

Canine and human CLCs were expanded<sup>4</sup> at 5% O<sub>2</sub>, 5% CO<sub>2</sub>, 37°C until passage 2. Additionally, bone marrow-derived MSCs from three canine donors (two 4-month old Labrador Retrievers, one 3-year old Beagle, male) were isolated, expanded, and characterized<sup>40</sup>. Micro-aggregates of 35,000 CLCs or MSCs were formed<sup>4</sup>. Briefly, CLCs/MSCs were plated in low-adherence cell-repellent surface 96-well plates (650970, CELLSTAR® Greiner Bio-one) in 50 µL basal culture medium (hgDMEM+Glutamax with 1 % P/S, 1% ITS+ premix, 0.04 mg/mL L-proline, 0.1 mM Asap, 1.25 mg/mL BSA). CLC micro-aggregates ( $n=6$ , in duplicates) were cultured in basal medium for (negative) control micro-aggregates,

supplemented with 10 ng/mL human recombinant TGF- $\beta_1$  (240-B, R&D Systems) as positive control, or 10 mg/mL NCM. MSC micro-aggregates ( $n=3$ , in duplicates) were cultured in (a) basal culture medium supplemented with 0.1  $\mu$ M dexamethasone (D8893, Sigma Aldrich) (control), (b) control culture medium supplemented with 10 ng/mL TGF- $\beta_1$ , (c) 10 mg/mL NCM, or (d) 10 mg/mL NCM supplemented with 10 ng/mL TGF- $\beta_1$ . Micro-aggregates were cultured for 28 days at 5% O<sub>2</sub>, 5% CO<sub>2</sub>, 37°C. Culture medium was changed twice weekly.

Gene expression profiling (RT-qPCR) was performed at day 7 (Supplementary File 1a), the DNA (dsDNA High Sensitivity Assay Kit, Invitrogen) and GAG content (DMMB assay<sup>41</sup>) were determined at day 28, and Safranin O/Fast Green staining and immunohistochemistry for collagen type I, II, and X were performed at day 28 ( $n=6$ , in duplicates)<sup>4</sup>. Sulphate incorporation (measure for proteoglycan synthesis rate) was determined during the last 4 hours of a 7-day culture period<sup>42</sup> (Supplementary File 1b).

### Experimental setup of the *in vivo* study

Procedures were approved and conducted in accordance Animal Experiments Committee guidelines (project number: AVD108002015285), required by Dutch regulation. Six intact female Beagles (14 months of age, weight 10-11 kg) were purchased from Marshall BioResources. Bone marrow-derived MSCs were obtained from one 3-year old male canine donor (Beagle, similar donor as used in *in vitro* experiment) to enable tracking of male DNA (MSCs) in female IVDs.

The effect of NCM, MSCs and a combined treatment of NCM+MSCs was tested on mildly and moderately degenerated canine IVDs (Supplementary File 1c). Six weeks before the intradiscal injections (T=-1.5 months), dogs underwent clinical examination. Additionally, more severe (moderate) IVD degeneration was induced in five IVDs per dog by a board-certified veterinary surgeon via partial NP removal (NX) on the left side of the spine. At T=0 months, MRI analysis was performed to determine the degree of IVD degeneration. Thereafter, the IVDs in which no NX was performed (noNX-IVDs; five per dog) and the IVDs in which NX was performed (NX-IVDs; five per dog) were either not injected (control) or injected on the right side of the spine with 50  $\mu$ L of (a)  $1 \times 10^6$  MSCs in a canine albumin-hyaluronan hydrogel<sup>43</sup> (b) 10 mg/mL NCM, or (c)  $1 \times 10^6$  MSCs suspended in 10 mg/mL NCM. At T=3 months, MRI analysis was performed and two IVDs per dog (L6-L7 (noNX-IVD) and L7-S1 (NX-IVD), which previously received 50  $\mu$ L NCM) were reinjected with 50  $\mu$ L of 10 mg/mL NCM, to test whether a better effect could be achieved with multiple injections. At T=6 months, MRI and CT analysis were performed, the dogs were euthanized, and the IVDs were collected. One dog died at T=0 months during the first injection (cause of death unrelated with treatment). This dog was used to determine baseline degree of induced IVD degeneration and confirm the presence of transplanted MSCs.

### Induction of IVD degeneration

Anesthesia and analgesia protocols are described in Supplementary File 1d. IVD degeneration was induced either by a left lateral (T11-T12 until L5-L6) or a dorsal (L6-L7 and L7-S1, assisted by mini-laminectomy) nucleotomy under fluoroscopic guidance. A 2 mm slit was made in the AF with a Beaver knife 65 and NP tissue was collected using a 1 mm ball-tipped probe, and fixed in 4% neutral buffered formaldehyde. Five  $\mu$ m paraffin sections were stained with Hematoxylin (109249, Merck)/Eosin (115935, Merck) and Picrosirius Red

(saturated aqueous picric acid: P6744, Sigma-Aldrich; sirius red: 365548, Sigma-Aldrich)/Alcian Blue (A5268, Sigma-Aldrich)<sup>44</sup>.

### Preparation of MSCs for *in vivo* application

Chondrogenic (Safranin O/Fast Green), adipogenic (Oil-Red-O), osteogenic (Alizarin Red S staining) differentiation and FACS analysis for positive (CD29 (303004, Biolegend), CD90 (12590042, Thermofisher scientific), CD105 (bs-4609R, Bioss antibodies)) and negative (CD34 (559369, BD Pharmingen), CD45 (LS-C127720-100, LifeSpan BioSciences)) MSC markers<sup>45,46</sup> was performed<sup>40</sup>. MSCs from the Beagle donor were expanded until passage 1 and incorporated in (a) albumin-hyaluronan hydrogels (20x10<sup>6</sup> MSCs/mL hydrogel) or (b) 10 mg/mL NCM (20x10<sup>6</sup> MSCs/mL NCM) directly prior to injection. The hydrogels were composed of chemically activated canine albumin (Animal Blood Resources International), bishio-polyethylene glycol, and hyaluronic acid.

### Intradiscal injections

Intradiscal injections of T12-13 until L5-L6 were performed from the right side with 25G needles (Epican, 4502400, B.Braun). The L6-L7 and L7-S1 IVDs were percutaneously approached dorsally with 19G needles (301750, BD Microlance) that guided the 25G needles into the NP under fluoroscopic guidance (Supplementary File 2G-H).

### MRI and CT

Details for the Magnetic Resonance images (MRI) and Computed tomography (CT) analysis are given in Supplementary File 1e. MRI T2 mapping and T1 $\rho$  values were computed by voxelwise fitting. The mean signal intensity in each region of interest was calculated using the Levenberg-Marquardt nonlinear least-squares method<sup>47</sup>. MRI images were blindly evaluated by two independent investigators (FB, MB; Pfirrmann score)<sup>20</sup>. The Pfirrmann, and T1 $\rho$  and T2 mapping inter- and intra-observer reliability was excellent (intra-class correlation>0.95)<sup>48</sup>. Disc height index was calculated on T2W images according to Masuda *et al.*<sup>49</sup>.

### Sample collection, macroscopic and histopathological grading

Details for samples collection are provided in Supplementary File 1f. IVD images were blindly evaluated by two independent investigators (FB, AT; Thompson score)<sup>19</sup>. Inter-observer reliability was excellent (intra-class correlation: 0.85)<sup>48</sup>. Five  $\mu$ m sections were stained with H/E and Picrosirius Red/Alcian Blue and blindly histologically evaluated (Boos score)<sup>21</sup>. Immunohistochemistry for collagen type I, II, and X<sup>4</sup> and COX-2<sup>50</sup> were performed. For COX-2, (positively stained) cell numbers in four randomly selected NP areas per IVD section were manually counted (Adobe Photoshop CC). The mean percentage of immunopositive cells was calculated.

### Gene expression profiling and biochemical analysis

Details on RNA isolation, cDNA synthesis, and RT-qPCR are provided in Supplementary File 1g. To determine the GAG and DNA content, the NP and AF samples were homogenized in complete lysis buffer using TissueLyser II (Qiagen) for 4 minutes at 20 Hz. PGE2 levels were determined in the supernatant using a colorimetric competitive enzyme immunoassay kit (PGE2 high sensitivity EIA kit, ENZO Life Sciences)<sup>50</sup>. The DNA and GAG content were measured in papain-digested supernatant and pellet<sup>47</sup>. A hydroxyproline assay<sup>51</sup> was used to

determine the samples collagen content<sup>47</sup>. MSC fate was determined by *SRY:GAPDH* PCR on genomic DNA isolated from papain-digested sample<sup>52</sup>.

### Statistical analyses

Statistical analyses were performed using IBM SPSS Statistics 24 and R studio. The Shapiro Wilks test was used to examine the data for normal distribution. Non-parametric data were converted to normally distributed data (log transformation) when possible. Two-sided testing was performed. To correct for multiple comparisons, Benjamini & Hochberg False Discovery Rate *post-hoc* tests were performed. For *in vitro* experiments, normally distributed data were examined using general linear regression models based on ANOVAs, whereas non-normally distributed data were subjected to Kruskal Wallis and Mann-Whitney U tests. For *in vivo* experiments, a randomized block design ANOVA was used for normally distributed data (DNA, GAG, collagen, PGE2 content). For DHI, quantitative T1p and T2 mapping, and RT-qPCR data, Cox proportional hazard tests were performed (random effect: donor). For Boos, Thompson, and Pfirrmann data analysis, Mann-Whitney Wilcoxon tests were performed. Because of the small *in vivo* sample size, for all comparisons with  $0.05 \geq p \leq 0.20$ , effect sizes (ES; Hedge's *g* for normally distributed data, Cliff's delta for non-parametric data) were determined and classified<sup>53, 54</sup>. *p*-values <0.05 were considered significant. Medium-very large effect sizes (Hedge's *g*  $\geq 0.5$ , Cliff's delta  $\geq 0.28$ ) were considered relevant.

## Results

### NCM increased DNA content, GAG and collagen deposition in CLC micro-aggregates *in vitro*

NCM increased the canine and human micro-aggregates' DNA content ( $p < 0.05$ , Figure 1a-b), presumably by stimulating cell proliferation and inhibiting apoptosis, since it induced *CCND1* (cell proliferation marker) and reduced *CASP3* (apoptosis marker) mRNA expression in canine CLCs ( $p < 0.05$ ), and tended to do the same in human CLCs ( $p < 0.1$ ) (Supplementary File 3a-d).

NCM increased the GAG and GAG/DNA content of canine and human micro-aggregates after 28 days ( $p < 0.05$ , Figure 1c-f). Since *ACAN* expression was not increased by 7-day NCM treatment (Supplementary File 4a-b), we hypothesized that GAGs were incorporated from GAG-rich NCM. Affirmatively, the <sup>35</sup>SO<sub>4</sub><sup>2-</sup> incorporation assay demonstrated that NCM-treated human CLCs synthesized less proteoglycans ( $p < 0.001$ ; Figure 1h), indicating GAG incorporation from NCM. In contrast, NCM induced proteoglycan synthesis in canine CLCs ( $p < 0.01$ , Figure 1g), indicating that they also synthesized GAGs themselves.

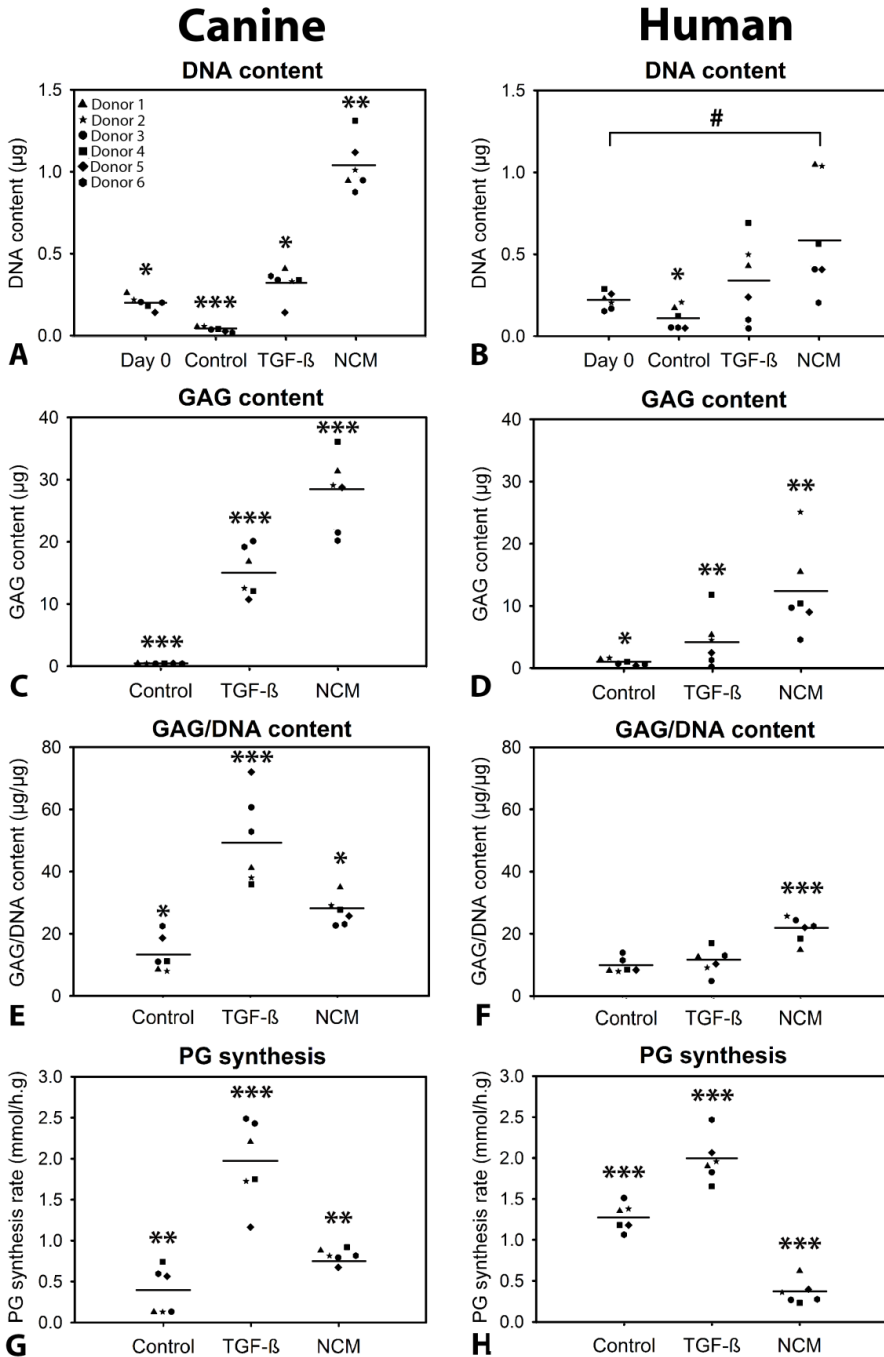


**Figure 1. NCM increases the DNA and glycosaminoglycan (GAG) content of chondrocyte-like cell (CLC) micro-aggregates.** Average of two samples per donor with depicted mean values. CLCs were cultured in basal culture medium (control), supplemented with 10 ng/mL TGF- $\beta_1$ , or 10 mg/mL NCM for 28 days.  $^{35}\text{SO}_4^{2-}$  incorporation (proteoglycan (PG) synthesis rate) was determined at day 7. \*, \*\*, \*\*\*:  $p < 0.05$ ,  $p < 0.01$ , and  $p < 0.001$ , respectively, versus all other conditions; #:  $p < 0.05$  for indicated conditions;  $n = 6$  in duplicates.

Although *COL1A1* and *COL2A1* expression was not increased by 7-day NCM treatment (Supplementary File 4c-f), collagen type I and II deposition appeared increased in 28-day NCM-treated CLC micro-aggregates (Figure 2). Furthermore, NCM decreased *SOX9* (chondrogenic differentiation marker) expression in canine CLCs, but increased this in human CLCs ( $p<0.05$ ) (Supplementary File 4g-h). *MMP13* was not differentially expressed in human CLCs, but was downregulated in canine NCM-treated CLCs ( $p<0.05$ ; Supplementary File 3g-h), suggesting an anti-catabolic effect. Lastly, collagen type X (hypertrophy marker) was not observed (Figure 2). Altogether, NCM induced healthy, GAG and collagen type II-rich matrix deposition in CLCs *in vitro*. Discrepancies between mRNA and protein expression may be due to timing differences (7 versus 28 days).

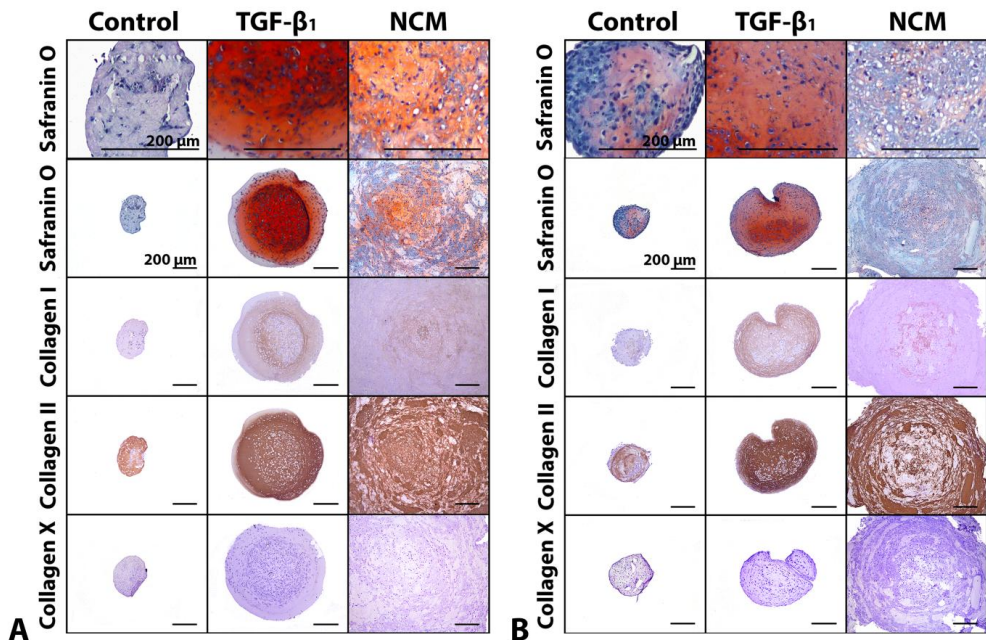


**Figure 2. NCM induces extracellular matrix deposition by chondrocyte-like cells (CLCs).** Safranin O/Fast Green staining and collagen type I, II, and X immunohistochemistry of canine (a) and human (b) CLC micro-aggregates cultured in basal culture medium (control), supplemented with 10 ng/mL TGF- $\beta_1$ , and 10 mg/mL NCM for 28 days.  $n=6$  in duplicates.

### NCM supports MSC chondrogenesis *in vitro*

The effect of NCM was tested on MSCs from three canine donors. Positive control treatment (TGF- $\beta_1$ ) increased the GAG and GAG/DNA content of MSC micro-aggregates versus controls ( $p<0.05$ , Figure 3b-d). The DNA and GAG content of NCM-treated micro-aggregates (with and without TGF- $\beta_1$ ) was higher versus TGF- $\beta_1$ -treated micro-aggregates ( $p<0.05$ ). The GAG/DNA content of micro-aggregates treated with TGF- $\beta_1$ , NCM, and NCM+TGF- $\beta_1$  was increased versus controls ( $p<0.05$ ), with no differences between conditions (Figure 3c). Additionally, TGF- $\beta_1$ , NCM, and NCM+TGF- $\beta_1$  induced collagen type I and II deposition, whereas collagen type X was not deposited (Figure 3d). Lastly, NCM-treated micro-

aggregates contained phenotypically chondrocyte-like cells. Altogether, NCM supported chondrogenesis of canine MSCs *in vitro*.

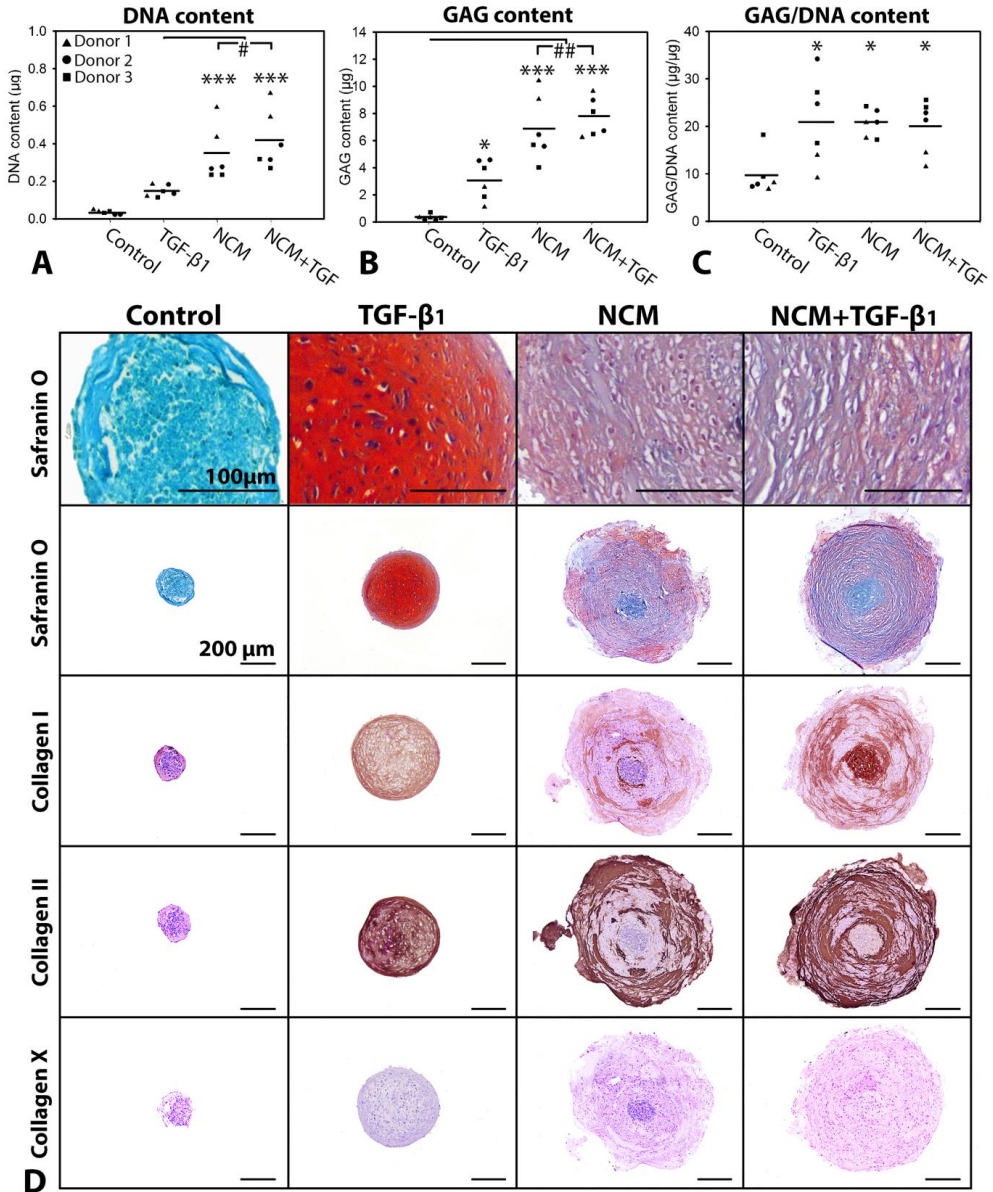


**Figure 3. NCM facilitates chondrogenic differentiation of canine MSCs.** MSCs were cultured in control culture medium, supplemented with 10 ng/mL TGF-β<sub>1</sub>, 10 mg/mL NCM, or NCM + TGF-β<sub>1</sub> for 28 days. **(D)** Safranin O/Fast Green staining and collagen type I, II, and X immunohistochemistry at day 28. \*, \*\*\*, *p*<0.05, *p*<0.001, respectively, versus controls; #, ##: *p*<0.05 and *p*<0.01, respectively, for indicated conditions; *n*=3 in duplicates; mean values are given.

## MSC characterization

To demonstrate that bone marrow-derived stromal cells from the male Beagle donor injected in the female Beagle IVDs met requirements to be defined as MSCs, multilineage differentiation and FACS analysis was performed<sup>17</sup>. Chondrogenic, osteogenic, and adipogenic differentiation were successfully induced, and cells were CD34<sup>-</sup>, CD45<sup>-</sup>, CD29<sup>+</sup> and CD90<sup>+</sup> (Supplementary File 5). Only 4.4% of cells were CD105<sup>+</sup>, possibly explained by low cross-species reactivity of anti-human CD105 used due to unavailability of commercial anti-canine CD105<sup>18</sup>. Altogether, the results confirm the presence of MSCs in the injected cells.

## Induction of IVD degeneration *in vivo*

To enable studying the effect of the treatments on mildly, and also on more severely degenerated IVDs, six weeks before the start of the experiment (T=-1.5 months), moderate IVD degeneration was induced by partial NP removal (NX) in five IVDs per Beagle dog (NX-IVDs; Supplementary File 2a-b). Six weeks later (T=0 months), the noNX-IVDs (IVDs in which no NX was performed) and the NX-IVDs were either not injected (controls) or injected with NCM, MSCs, or NCM+MSCs (Supplementary File 2g-h). At T=3 months, two NCM-treated IVDs per dog received an additional NCM injection. One Beagle died unexpectedly at T=0 (cause of death unrelated to treatment) and the IVDs of this dog were used as baseline values for moderate (induced) IVD degeneration. The AF appeared not affected by induction of moderate IVD degeneration (Supplementary File 2d, i-m). In contrast, NPs of NX-IVDs in comparison with NPs of noNX-IVDs showed macroscopically a brown discoloration (Supplementary File 2d), histologically less intense Alcian blue (GAG) and more intense Picrosirius Red (collagen) staining (Supplementary File 2e-f), and biochemically a decreased GAG and GAG/DNA content ( $p \leq 0.05$ ; Supplementary File 2i, k), indicating that degeneration was successfully modified from mild (spontaneous) to moderate (induced) IVD degeneration.

Lastly, two IVDs of this female dog were injected with male MSCs (Th12-13 (NX) and Th13-L1 (noNX); Supplementary File 2n), and SRY DNA could be detected, indicating that MSCs were properly injected and could be tracked.

## The effect of NCM on degenerated canine IVDs *in vivo*

At T=6 months, the effect of the different treatments (control, 1xNCM, NCM reinjection after three months (2xNCM), MSC, NCM+MSC) on mildly and moderately degenerated canine IVDs was determined using macroscopic, radiologic, histologic and biochemical analysis. First, the IVDs were scored according to macroscopic **Thompson**<sup>19</sup> and MRI-based **Pfirschmann**<sup>20</sup> grading validated for dogs. At T=6 months, control NX-IVDs had a higher Thompson and Pfirschmann score than control noNX-IVDs ( $p=0.08$  with large effect size (ES) and  $p < 0.01$ , respectively; Figure 4a-b), indicating that more severe IVD degeneration was induced with NX. The Thompson and Pfirschmann score of noNX-IVDs did not improve by any treatment. In contrast, 2xNCM-treated NX-IVDs showed a lower Thompson and Pfirschmann score than control NX-IVDs ( $p=0.08$  and  $0.15$ , large ES) and did not differ from control noNX-IVDs. In line with this, all NX-IVD NPs showed a brown discoloration (compatible with IVD degeneration), except 2xNCM-treated IVDs (Figure 4c). Altogether, 2xNCM improved the Thompson and Pfirschmann score of moderately degenerated IVDs.

The **Disc Height Index (DHI)** did not significantly change from T=0 until T=6 months in control-, 1xNCM-, MSC- and NCM+MSC-treated noNX-IVDs, but increased in time by 2xNCM ( $p=0.14$ , large ES; Figure 4d). In control NX-IVDs, the DHI did not considerably change from T=0-6 months. In 1xNCM-, 2xNCM- and NCM+MSC-treated, but not MSC-treated NX-IVDs, the increase in DHI was higher versus control NX- and noNX-IVDs ( $p=0.06-0.09$ , large ES), indicating an NCM specific effect.

**T1 $\rho$  and T2** MRI values were employed for quantitative MRI analysis. T1 $\rho$  values did not significantly change in time, regardless the condition (data not shown). T2 values were not different between T=0 and T=6 months in noNX-IVDs (Figure 4e). In all NX-IVDs, T2 values decreased in time versus control noNX-IVDs ( $p<0.05$ , or  $p=0.05-0.08$  with large ES). Altogether, induction of degeneration reduced T2 values, but no treatment was able to increase T2 values.

Lastly, the presence and progression of **Modic Changes (MCs), periosteal bone formation, ventral spondylosis and EP lysis** was recorded (Supplementary File 6). In noNX-IVDs, no treatment induced MCs or EP lysis. Periosteal bone formation and mild ventral spondylosis was observed in three 1xNCM-treated noNX-IVDs, and two NCM+MSC-treated noNX-IVDs, but not in control, MSC- or 2xNCM-treated noNX-IVDs. Lastly, the NX procedure induced all parameters, while 2xNCM did not induce any of the parameters in NX-IVDs.

For **histological** analysis, all IVDs were scored (Boos grading validated for dogs<sup>21</sup>). At T=6 months, the total Boos score increased in control NX-IVDs versus control noNX-IVDs ( $p<0.05$ ; Figure 5c), indicating that moderate IVD degeneration was induced. Only 2xNCM improved the Boos score compared with control NX-IVDs ( $p=0.18$ , medium ES) and was comparable to control noNX-IVDs. Boos score subcriteria indicated no differences between conditions for AF morphology, CLC morphology and proliferation in the NP, presence of NCs, matrix staining of the NP, and new bone formation (Figure 5a, b, d). The histologic score for chondrocyte metaplasia and tear and cleft formation in the AF (data not shown) and EP morphology (irregularity, thickness; Figure 5e) of control NX-IVDs was increased versus control noNX-IVDs ( $p=0.12-0.16$ , medium-large ES). Additionally, subchondral bone sclerosis was increased in control NX-IVDs versus control noNX-IVDs ( $p<0.05$ ; Figure 5f). In NX-IVDs, 2xNCM improved EP morphology and subchondral bone sclerosis score versus controls ( $p=0.18$ , medium ES). Taken together, EP irregularity and bone sclerosis was induced by NX, while 2xNCM inhibited these pathological processes.

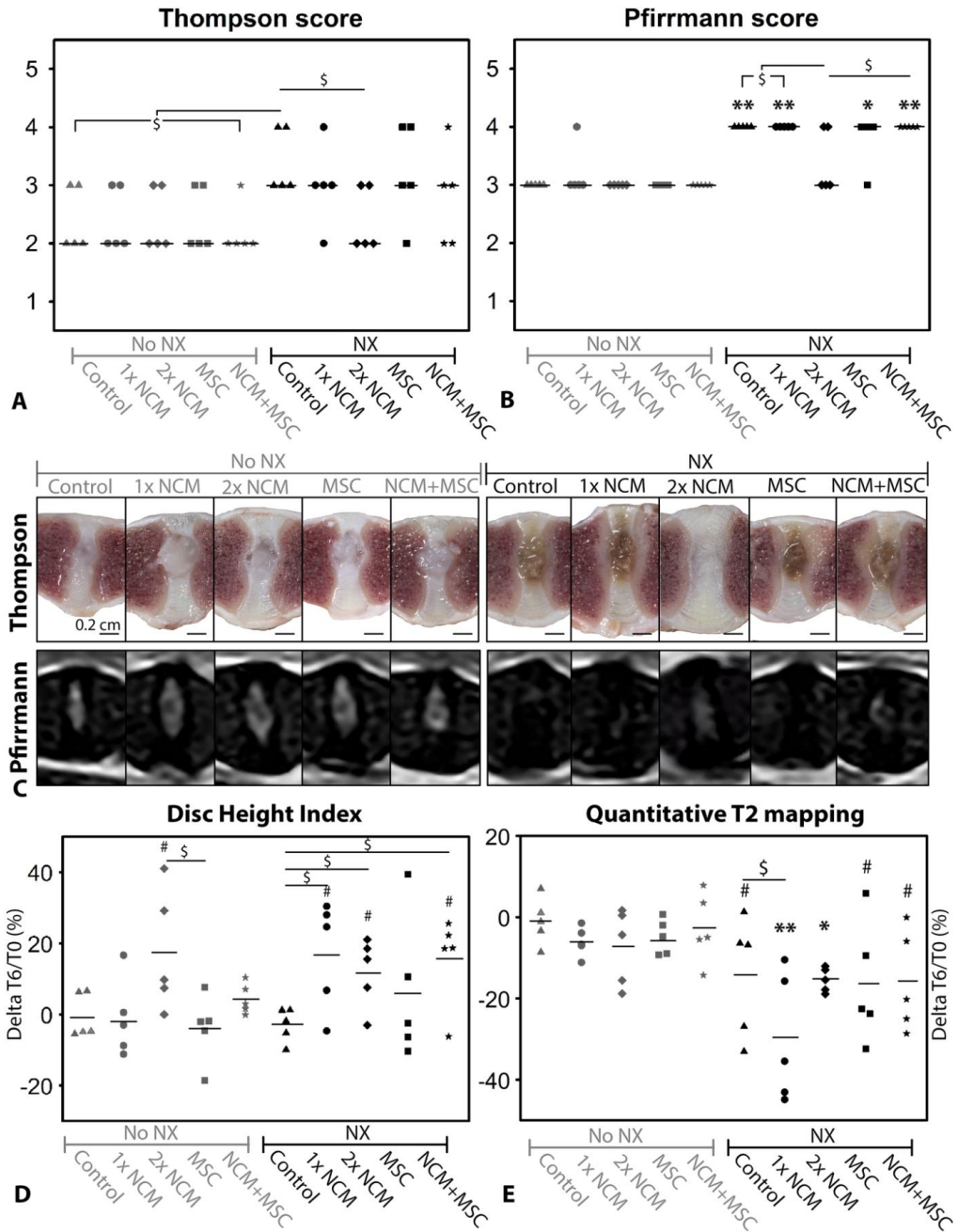


**Figure 4. NCM improves the macroscopic Thompson score and radiologic parameters of degenerated intervertebral discs.** Median (Thompson, Pfirrmann) and mean (Disc Height Index (DHI), T2 values) values are indicated. Change in DHI and T2 mapping values were calculated at individual IVD level. NX: partial NP removal to induce moderate IVD degeneration. \*, \*\*:  $p < 0.05$ ,  $p < 0.01$ , respectively versus control noNX-IVDs; #:  $p = 0.05$ - $0.15$ , large effect size, versus control noNX-IVDs; \$:  $p = 0.05$ - $0.15$ , large effect size, between indicated condition;  $n = 5$ .

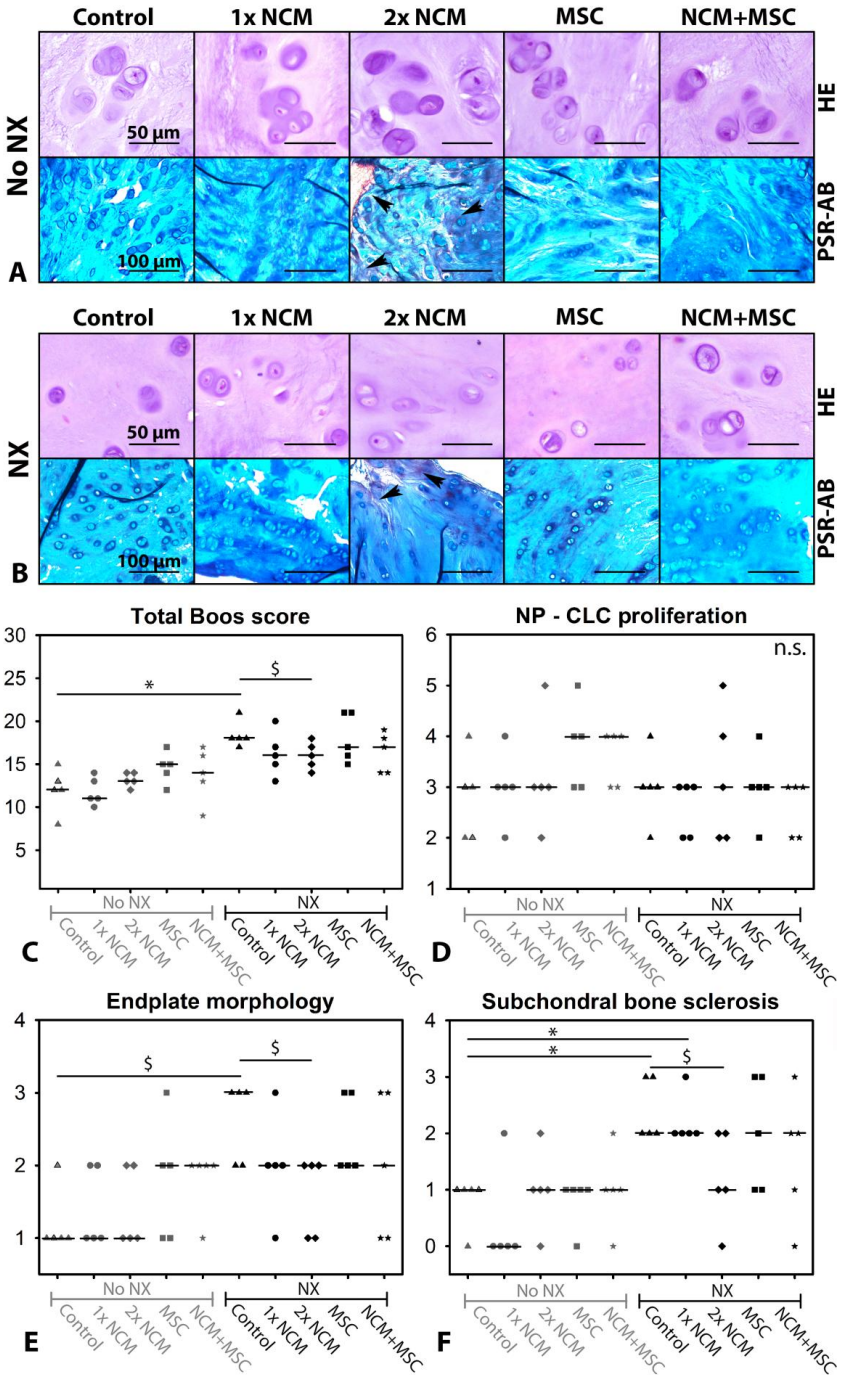


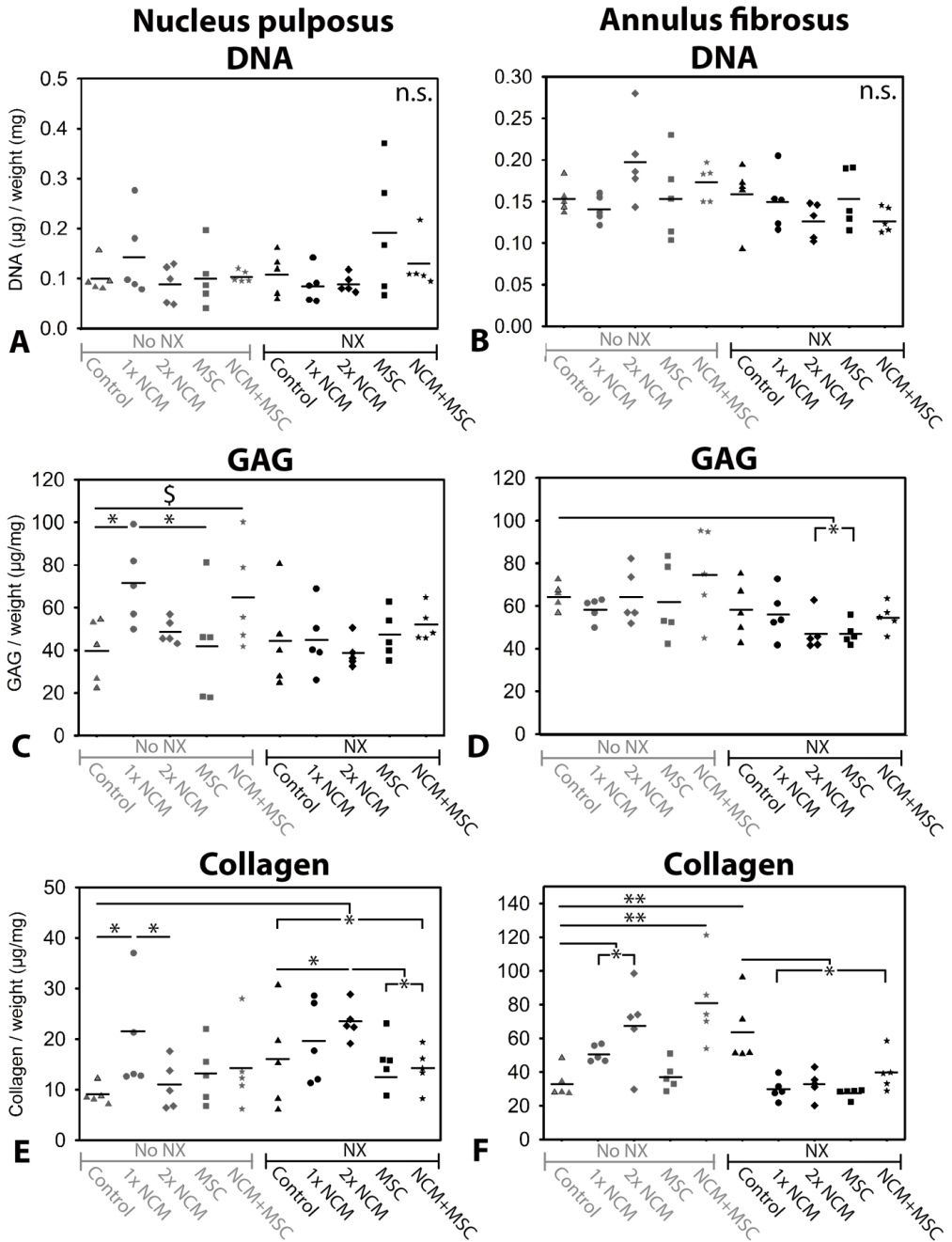
**Figure 5. NCM improves intervertebral disc histology.** H&E and Picosirius Red-Alcian Blue (blue: glycosaminoglycan, red: collagen - arrowheads) staining of canine NP tissue. NX: partial NP removal to induce moderate IVD degeneration. n.s.: not significant; \*:  $p < 0.05$ ;  $\$$ :  $p = 0.05-0.18$  with medium-large effect size;  $n = 5$ . Median values are indicated.

At T=6 months, the **DNA content** of the NP and AF tissue did not significantly differ, regardless the treatment and induction of degeneration (Figure 6a-b). **SRY DNA** was undetectable in the female IVDs in which male MSCs were injected, indicating that the male MSCs had not survived.

The NP and AF **GAG content** was not different between noNX-IVDs and NX-IVDs at T=6 months (Figure 6c-d), but was significantly lower in NPs from NX-IVDs versus NPs from noNX-IVDs ( $p < 0.05$ , Supplementary File 2i, k) at T=0 months (six weeks after NX). Thus, the decreased GAG content of NPs from IVDs in which moderate degeneration was induced (observed at T=0 months) recovered to baseline levels at T=6 months, suggesting an attempt at repair. This repair was further augmented by NCM. At T=6 months, 1xNCM increased the NP GAG content in noNX-IVDs versus control- and MSC-treated noNX-IVDs ( $p < 0.05$ ). Also NCM+MSC treatment increased the NP GAG content versus control noNX-IVDs ( $p = 0.07$  with large ES). Moreover, in NX-IVDs, MSC and 2xNCM treatment significantly decreased the AF GAG content compared with noNX-control IVDs ( $p < 0.05$ ), indicating less degeneration.

The **collagen content** of control NX-IVDs was higher versus control noNX-IVDs (NP:  $p < 0.05$ , AF:  $p < 0.01$ ), indicating that collagen deposition increased with degeneration (Figure 6e-f). In noNX-IVDs, 1xNCM increased the NP collagen content versus control and 2xNCM ( $p < 0.05$ ). Additionally, 1xNCM, 2xNCM, and NCM+MSC increased the AF collagen content versus controls in noNX-IVDs. In NX-IVDs, 2xNCM increased the NP collagen content versus control, MSC, and MSC+NCM ( $p < 0.05$ ). Lastly, the AF collagen content was reduced by all treatments versus controls in NX-IVDs ( $p < 0.05$ ). To determine the types of collagen that were deposited, immunohistochemistry was performed. **Collagen type I** was present in the AF (not differentially expressed), but not in the NP (Figure 7), suggesting the absence of NP fibrosis. **Collagen type II** was present in all NPs (Figure 7). In noNX-IVD NPs, collagen type II was most abundantly present after 1xNCM treatment, while in NX-IVD NPs it was most abundantly deposited by 1xNCM and 2xNCM. **Collagen type X** was undetectable regardless the treatment (Figure 7), indicating absent hypertrophic differentiation.

Altogether, NCM induced healthy, collagen type II-rich matrix *in vivo*. NCM is enriched in collagen and GAGs. Injection of 50  $\mu\text{L}$  of 10 mg/mL NCM (containing both 5 mg/mL GAGs and collagen) would contribute to 0.25 mg GAG and collagen per treated IVD. While 2xNCM increased the NP collagen content, it did not augment the NP GAG content of NX-IVDs. Since GAGs attract water and the biochemical data were corrected for wet weight, we possibly missed the presence of an increased GAG content (per mg dry weight).



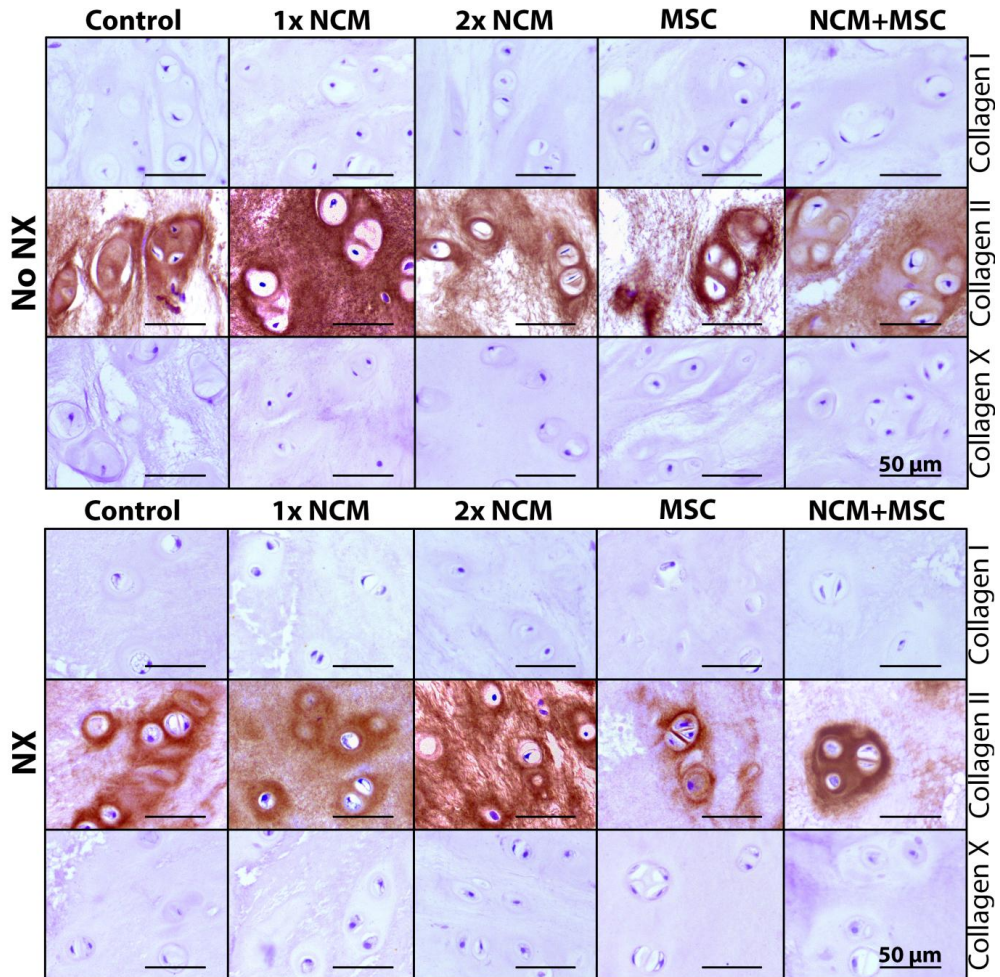


**Figure 7. NCM stimulates healthy collagen type II, but no collagen type I or X deposition in the canine nucleus pulposus *in vivo*.** NX: partial NP removal to induce moderate IVD degeneration.  $n=5$ .

At T=6 months, no differences in NP **mRNA expression** were established between conditions for ECM-related genes *SOX9*, *ACAN*, *COL1A1*, *COLX*, *ADAMTS5* and *MMP13* (data not shown). *COL2A1* mRNA expression was, however, increased in all NX-IVDs versus control noNX-IVDs ( $p<0.05$  or  $p=0.07$  with large ES; Supplementary File 7a). In NX-IVDs, 2xNCM increased *COL2A1* expression versus all other treatments ( $0.05 \geq p \leq 0.17$ , medium ES). *TIMP* expression was increased in NX-IVDs treated with 1xNCM, 2xNCM, MSCs and NCM+MSCs versus control noNX-IVDs ( $p<0.05$ , or  $p=0.14$  with medium ES; Supplementary File 7b). Altogether, NCM induced an anabolic effect by increasing the expression of anti-catabolic gene and by inducing *COL2A1* mRNA. The latter is in line with the augmented collagen type II deposition (IHC). Expression of the cell proliferation- and apoptosis-related genes *CCND1*, *CASP3*, *BCL2*, and *BAX* was not different between conditions (data not shown). Regarding NP-specific markers, 2xNCM induced *KRT18* and *KRT19* expression in mildly degenerated IVDs, and reduced their expression in moderately degenerated IVDs ( $p=0.01-0.10$ , medium-

large ES; Supplementary File 7c-d). *PAI1* expression was induced by 2xNCM in NX-IVDs ( $p < 0.05$ ; Supplementary File 7e), suggesting increased TGF- $\beta$  signaling at mRNA level.

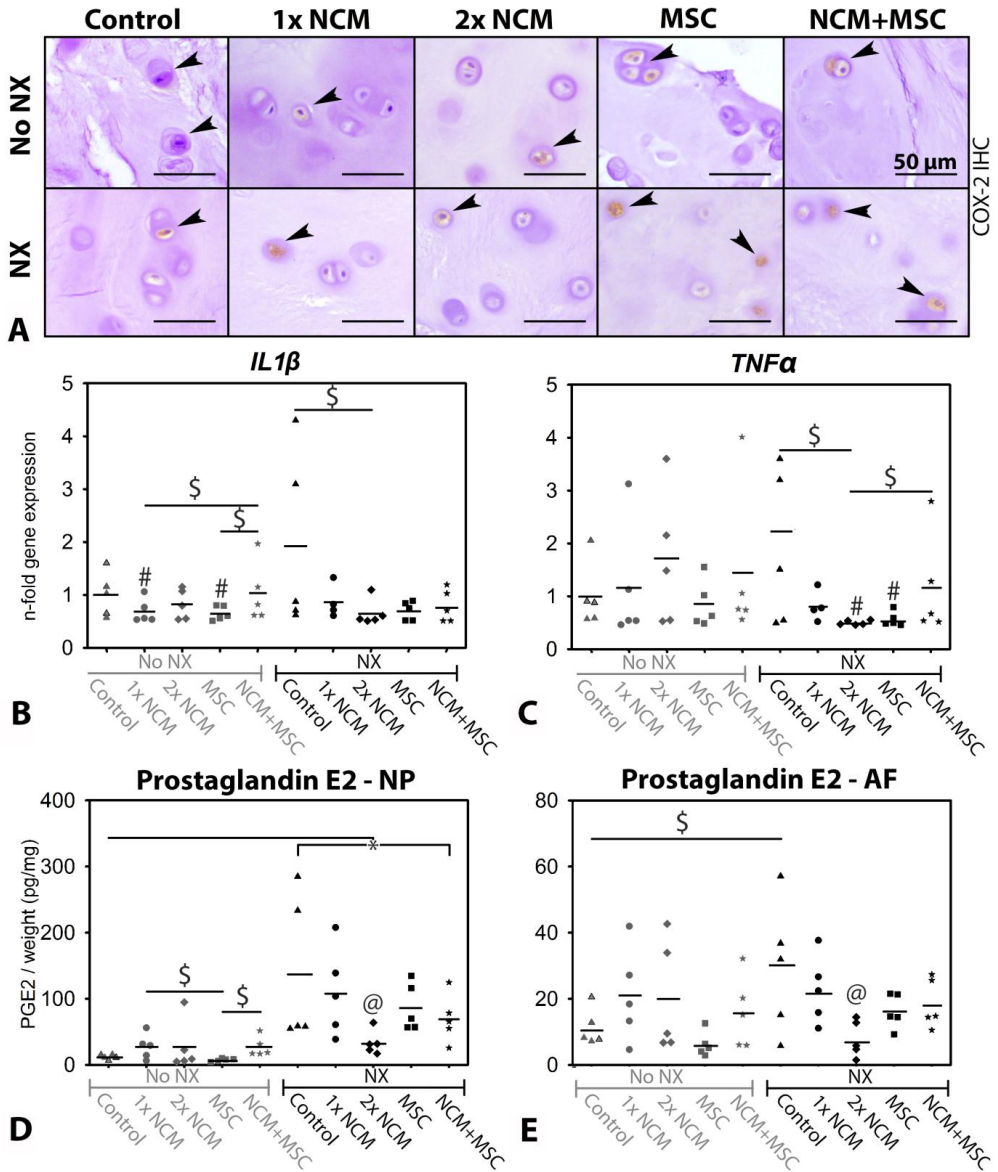


**Figure 8. NCM ameliorates inflammation in canine IVDs *in vivo*.** COX-2 positive CLCs in canine NP tissue are indicated with arrowheads. Relative *IL1 $\beta$*  and *TNF $\alpha$*  expression (control noNX-IVDs were set at 1), and prostaglandin E2 content of canine IVDs at T=6 months are given with indicated mean values. NP: nucleus pulposus. AF: Annulus fibrosus. NX: partial NP removal to induce moderate IVD degeneration. \*:  $p < 0.05$  between indicated conditions; #: different from control noNX-IVDs ( $0.05 \geq p \leq 0.20$ , medium/large ES); \$: difference between indicated conditions with medium/large effect size ( $0.05 \geq p \leq 0.20$ ); @: different from all other conditions in which NX was performed ( $p < 0.05$  or  $p < 0.1$  with large effect size,  $n=5$ ).

To determine the treatment effect on **inflammation**, cyclooxygenase-2 (COX-2) IHC and RT-qPCR were performed, and the prostaglandin E2 (PGE2) content of the IVD tissues was determined. COX-2 immunopositivity was present in every NP and AF (Figure 8a). On average, 7-20% of canine CLCs expressed cytoplasmic COX-2, with no differences between conditions (data not shown). *IL1 $\beta$*  and *TNF $\alpha$*  (pro-inflammatory cytokines) expression was not different between control noNX- and NX-IVDs (Figure 8b-c). In NX-IVDs, however, 2xNCM reduced *IL1 $\beta$*  and *TNF $\alpha$*  expression ( $p=0.09$  and  $0.11$ , medium ES). Control NX-IVDs showed a higher PGE2 content than control noNX-IVDs (NP:  $p<0.05$ , AF:  $p=0.06$ , very large ES; Figure 8d-e), indicating that PGE2 levels (indicative of increased COX-2 activity) increased with degeneration. In line with RT-qPCR results, 2xNCM decreased the NP and AF PGE2 content in NX-IVDs ( $p<0.05$ , large effect size). Altogether, NCM ameliorated inflammation in moderately degenerated IVDs.

## Discussion

The spine field has already demonstrated the regenerative potential of NCs<sup>4-11</sup>. The present study demonstrates that by employing healthy NC-derived NP tissue matrix, we can harness the NC regenerative potential and exploit it for biological IVD repair. As a first step towards bench-to-bedside translation, we demonstrate that NCM exerted regenerative effects on canine and human CLCs from degenerated IVDs *in vitro* and on canine IVDs *in vivo* by inducing anabolic effects and ameliorating inflammation. The question arises how NCM exerts its anabolic effects. It may serve as ‘instructive matrix’, locally increasing growth factor concentrations and promoting their biological activity<sup>22</sup>. In this respect, NCM may be comparable to demineralized bone matrix, which is successfully employed in clinical practice. DBM induces bone regeneration by providing a degradable matrix that facilitates the release and modulates the accessibility of growth factors normally present in bone<sup>14</sup>. Increased *PAI1* (TGF- $\beta$  pathway target gene) expression in 2xNCM-treated IVDs indicate augmented Smad signalling. The exact mechanism of action of NCM remains elusive and is most probably a combination of bioactive factors retained within NCM and ECM molecules modulating their activity<sup>23</sup>.

### MSCs do not exert distinct effects in the degenerated canine IVD *in vivo*

Intradiscal allogeneic MSC delivery is considered a promising IVD regeneration strategy. MSC transplantation was not accompanied by osteophyte formation (a possible complication<sup>24</sup>), most probably because a polymerized hydrogel, which prevents leakage, was used as carrier. Although we detected male DNA (MSCs) in the female IVDs immediately after intradiscal injection, male DNA was undetectable after six months. This result contrasts with previous Beagle studies, in which autologous transplanted MSCs could be traced back up to 12 months and exerted beneficial effects<sup>25-27</sup>. This contradiction, however, needs to be cautiously interpreted since only one quart of IVD tissue was available for SRY analysis, resulting into limited sensitivity (detection limit: 25,000 MSCs/sample). Transplanted MSCs, capable of multilineage differentiation *in vitro*, did not exert beneficial effects *in vivo*, alone or combined with NCM. MSC populations are known to exhibit considerable donor-to-donor and intra-population heterogeneity<sup>28</sup>, and in the harsh environment of the degenerated IVD, this could have contributed to the lack of effect.

### **Intradiscally applied NCM has a regenerative effect on degenerated canine IVDs**

The present study demonstrates that NCM exerted regenerative effects on MSCs and CLCs derived from degenerated IVDs *in vitro*. Although canine CLCs seemed to be more responsive to NCM than human CLCs, NCM exerted an anabolic, anti-apoptotic, and proliferative effect in both species, in line with previous work on decellularized bovine NP ECM<sup>9</sup>.

Based on these promising results, an *in vivo* study was performed. In mildly degenerated IVDs, NCM upregulated mRNA expression of NP-specific markers, augmented the NP GAG and collagen content, and hence seemed to favor IVD health. Notably, in moderately degenerated NX-IVDs, NCM-mediated effects were more pronounced. Mainly 2xNCM exerted beneficial effects on the NPs from NX-IVDs: the macroscopic Thompson, histologic Boos (total, EP morphology, and subchondral bone sclerosis score) and MRI-based Pfirrmann score were improved. Additionally, the DHI of 1xNCM-, 2x NCM- and NCM+MSC-treated NX-IVDs increased during the study. Given that MSC injection alone was not able to increase the DHI, this beneficial effect was presumably NCM-specific. Since 2xNCM induced collagen type II, but no collagen type I and X expression, healthy NP-like ECM, but no fibrotic or hypertrophic ECM<sup>30,31</sup> was deposited. Lastly, 2xNCM was able to exert protective effects on the L7-S1 IVD, a junction that permits the highest range of motion<sup>32</sup> and predisposes this IVD to a high degree of wear and tear. Altogether, these findings imply an NCM-dependent regenerative response, resulting in beneficial quantitative and qualitative ECM changes.

### **Quantitative T1p and T2 mapping did not detect NCM-mediated effects**

In contrast with other readout parameters, T1p and T2 mapping did not detect NCM-mediated regenerative effects. T1p is sensitive for interactions between macromolecules (*e.g.* GAGs) and water<sup>33</sup>, while T2 mapping provides information regarding water content, collagen orientation and ECM structure<sup>34</sup>. Noteworthy, both techniques have been specifically validated for IVD degeneration, but not for regeneration, which does not necessarily follow an identical reverse process. For example, the NP collagen content was increased in 2xNCM-treated NX-IVDs versus control NX-IVDs, but T2 values were not different between those conditions. Furthermore, while the collagen and GAG content was not different between control noNX-IVD and NX-IVD NPs, T2 values were lower in the latter, probably due to structural changes related to degeneration<sup>35</sup>.

### **NCM exerts anti-inflammatory effects in degenerated canine IVDs**

Besides beneficial effects on macroscopic, radiologic, biochemical, and histological level, NCM also exerted anti-inflammatory effects on degenerated IVDs *in vivo*. The PGE2-producing enzyme COX-2 was uniformly present in NPs, implying local PGE2 synthesis. PGE2 levels were, however, decreased by 2xNCM in NX-IVD NPs, indicating that 2xNCM decreased COX-2 activity and inhibited inflammation. In line with this, all NX-IVD NPs, except 2xNCM-treated NPs, showed a brown discoloration. This brown color was presumably caused by accumulation of advanced glycation end products (AGEs). AGEs are formed through non-enzymatic glycation of amino residues and oxidation of fatty acids during IVD degeneration<sup>36,37</sup> and can act as pro-inflammatory mediator<sup>38</sup>. Altogether, 2xNCM may prevent AGE accumulation in degenerated IVDs, thereby exerting an anti-inflammatory effect. This hypothesis is confirmed by the decreased PGE2 content and downregulated *IL16*

and *TNF $\alpha$*  expression in 2xNCM-treated NX-IVDs. These anti-inflammatory NC properties have already been demonstrated previously<sup>39</sup>.

### Limitations and future directions

The present study demonstrates that 10 mg/mL NCM exerted beneficial effects on canine and human CLCs from degenerated IVDs *in vitro* and degenerated Beagle IVDs *in vivo*. Given that 0.5 mg NCM/IVD exerted beneficial effects, it is tempting to hypothesize that higher NCM dosages may further improve the regenerative and anti-inflammatory effects. After fine-tuning the dose-dependent efficacy of NCM, follow-up studies should look into the application of NCM in hydrogel form, which reduces the risk of leakage after intradiscal injection. Furthermore, for safe (veterinary and human) clinical application, removal of nucleic acid from NCM should be achieved with preservation of bioactivity<sup>29</sup>.

## Conclusions

The present study demonstrates that NCM exerted regenerative effects on canine MSCs and canine and human CLCs from degenerated IVDs *in vitro* as well as canine IVDs *in vivo*. *In vivo*, NCM mainly exerted pronounced effects on moderately degenerated IVDs; a repeated intradiscal NCM injection exerted beneficial effects on macroscopic, radiologic, biochemical, and histological level and inhibited inflammation. This study shows that intradiscally injected NCM could be a promising treatment for human and canine IVD disease, by harnessing the NC regenerative and anti-inflammatory potential, and circumventing the challenging identification of bioactive NC-secreted factors. Future studies should focus on removal of nucleic acid from NCM and the mechanism of NCM-mediated regeneration.

## Acknowledgements

The authors would like to thank Simon Mastbergen and Katja Coeleveld for help with the <sup>35</sup>SO<sub>4</sub><sup>2-</sup> incorporation assay, Saskia Plomp, Amber van Heezen, and Pascal Kamphuis for the help with execution of experiments, Anita Krouwels and Imke Janssen for supplying human CLCs, and Nico Attevelt, Jeroen van Ark and Helma Aeverzaat (Animal Facilities of Utrecht University) for support during this study.

## References

1. Katz JN. 2006. Lumbar disc disorders and low-back pain: Socioeconomic factors and consequences. *J Bone Joint Surg Am* 88: 21-24.
2. Freemont AJ. 2009. The cellular pathobiology of the degenerate intervertebral disc and discogenic back pain. *Rheumatology (Oxford)* 48: 5-10.
3. Bergknut N, Smolders LA, Grinwis GC, et al. 2013. Intervertebral disc degeneration in the dog. part 1: Anatomy and physiology of the intervertebral disc and characteristics of intervertebral disc degeneration. *Vet J* 195: 282-291.
4. Bach FC, de Vries SA, Krouwels A, et al. 2015. The species-specific regenerative effects of notochordal cell-conditioned medium on chondrocyte-like cells derived from degenerated human intervertebral discs. *Eur Cell Mater* 30: 132-47.
5. Abbott RD, Purmessur D, Monsey RD, Iatridis JC. 2012. Regenerative potential of TGFbeta3 + dex and notochordal cell conditioned media on degenerated human intervertebral disc cells. *J Orthop Res* 30: 482-488.
6. Potier E, de Vries S, van Doeselaar M, Ito K. 2014. Potential application of notochordal cells for intervertebral disc regeneration: An in vitro assessment. *Eur Cell Mater* 28: 68-81.
7. Korecki CL, Taboas JM, Tuan RS, Iatridis JC. 2010. Notochordal cell conditioned medium stimulates mesenchymal stem cell differentiation toward a young nucleus pulposus phenotype. *Stem Cell Res Ther* 1: 18.
8. Purmessur D, Schek RM, Abbott RD, et al. 2011. Notochordal conditioned media from tissue increases proteoglycan accumulation and promotes a healthy nucleus pulposus phenotype in human mesenchymal stem cells. *Arthritis Res Ther* 13: R81.
9. de Vries SA, Potier E, van Doeselaar M, et al. 2015. Conditioned medium derived from notochordal cell-rich nucleus pulposus tissue stimulates matrix production by canine nucleus pulposus cells and bone marrow-derived stromal cells. *Tissue Eng Part A* 21: 1077-1084.
10. de Vries SA, van Doeselaar M, Meij BP, Tryfonidou MA, Ito K. 2016. The stimulatory effect of notochordal cell-conditioned medium in a nucleus pulposus explant culture. *Tissue Eng Part A* 22: 103-110.
11. Matta A, Karim MZ, Isenman DE, Erwin WM. 2017. Molecular therapy for degenerative disc disease: Clues from secretome analysis of the notochordal cell-rich nucleus pulposus. *Sci Rep* 7: 45623.
12. Bach FC, de Vries SA, Riemers FM, et al. 2016. Soluble and pelletable factors in porcine, canine and human notochordal cell-conditioned medium: Implications for IVD regeneration. *Eur Cell Mater* 32: 163-180.
13. F.C. Bach, S.F.W.M. Libregts, L.B. Creemers, B.P. Meij, K. Ito, M.H.M. Wauben, M.A. Tryfonidou. 2017. Notochordal-cell derived extracellular vesicles exert regenerative effects on canine and human nucleus pulposus cells. *Oncotarget* 8: 88845-88856.
14. Gruskin E, Doll BA, Futrell FW, Schmitz JP, Hollinger JO. 2012. Demineralized bone matrix in bone repair: History and use. *Adv Drug Deliv Rev* 64: 1063-1077.
15. Sakai D, Nakai T, Mochida J, Alini M, Grad S. 2009. Differential phenotype of intervertebral disc cells: Microarray and immunohistochemical analysis of canine nucleus pulposus and annulus fibrosus. *Spine (Phila Pa 1976)* 34: 1448-1456.
16. Wu T, Song HX, Dong Y, Li JH. 2016. Cell-based therapies for lumbar discogenic low back pain - systematic review and single arm meta-analysis. *Spine (Phila Pa 1976)* *Epub ahead of print*.
17. Dominici M, Le Blanc K, Mueller I, et al. 2006. Minimal criteria for defining multipotent mesenchymal stromal cells. the international society for cellular therapy position statement. *Cytotherapy* 8: 315-317.
18. Screven R, Kenyon E, Myers MJ, et al. 2014. Immunophenotype and gene expression profile of mesenchymal stem cells derived from canine adipose tissue and bone marrow. *Vet Immunol Immunopathol* 161: 21-31.
19. Bergknut N, Grinwis G, Pickee E, et al. 2011. Reliability of macroscopic grading of intervertebral disk degeneration in dogs by use of the thompson system and comparison with low-field magnetic resonance imaging findings. *Am J Vet Res* 72: 899-904.
20. Bergknut N, Auriemma E, Wijsman S, et al. 2011. Evaluation of intervertebral disk degeneration in chondrodystrophic and nonchondrodystrophic dogs by use of pfirrmann grading of images obtained with low-field magnetic resonance imaging. *Am J Vet Res* 72: 893-898.
21. Bergknut N, Meij BP, Hagman R, et al. 2013. Intervertebral disc disease in dogs - part 1: A new histological grading scheme for classification of intervertebral disc degeneration in dogs. *Vet J* 195: 156-163.
22. Ishida K, Acharya C, Christiansen BA, et al. 2013. Cartilage oligomeric matrix protein enhances osteogenesis by directly binding and activating bone morphogenetic protein-2. *Bone* 55: 23-35.
23. Ayerst BI, Merry CLR, Day AJ. 2017. The good the bad and the ugly of glycosaminoglycans in tissue engineering applications. *Pharmaceuticals (Basel)* 10: 10.3390/ph10020054.
24. Vadala G, Sowa G, Hubert M, et al. 2012. Mesenchymal stem cells injection in degenerated intervertebral disc: Cell leakage may induce osteophyte formation. *J Tissue Eng Regen Med* 6: 348-355.
25. Ganey T, Hutton WC, Moseley T, Hedrick M, Meisel HJ. 2009. Intervertebral disc repair using adipose tissue-derived stem and regenerative cells: Experiments in a canine model. *Spine (Phila Pa 1976)* 34: 2297-2304.
26. Hiyama A, Mochida J, Iwashina T, et al. 2008. Transplantation of mesenchymal stem cells in a canine disc degeneration model. *J Orthop Res* 26: 589-600.
27. Serigano K, Sakai D, Hiyama A, et al. 2010. Effect of cell number on mesenchymal stem cell transplantation in a canine disc degeneration model. *J Orthop Res* 28: 1267-1275.

28. Phinney DG. 2012. Functional heterogeneity of mesenchymal stem cells: Implications for cell therapy. *J Cell Biochem* 113: 2806-2812.
29. Illien-Junger S, Sedaghatpour DD, Laudier DM, et al. 2016. Development of a bovine decellularized extracellular matrix-biomaterial for nucleus pulposus regeneration. *J Orthop Res* 34: 876-888.
30. Rutges JP, Duit RA, Kummer JA, et al. 2010. Hypertrophic differentiation and calcification during intervertebral disc degeneration. *Osteoarthritis Cartilage* 18: 1487-1495.
31. Eyre DR, Muir H. 1977. Quantitative analysis of types I and II collagens in human intervertebral discs at various ages. *Biochim Biophys Acta* 492: 29-42.
32. Smolders LA, Kingma I, Bergknut N, et al. 2012. Biomechanical assessment of the effects of decompressive surgery in non-chondrodystrophic and chondrodystrophic canine multisegmented lumbar spines. *Eur Spine J* 21: 1692-1699.
33. Johannessen W, Auerbach JD, Wheaton AJ, et al. 2006. Assessment of human disc degeneration and proteoglycan content using T1rho-weighted magnetic resonance imaging. *Spine (Phila Pa 1976)* 31: 1253-1257.
34. Link TM, Stahl R, Woertler K. 2007. Cartilage imaging: Motivation, techniques, current and future significance. *Eur Radiol* 17: 1135-1146.
35. Johnstone B, Bayliss MT. 1995. The large proteoglycans of the human intervertebral disc. changes in their biosynthesis and structure with age, topography, and pathology. *Spine (Phila Pa 1976)* 20: 674-684.
36. Sivan SS, Tsitron E, Wachtel E, et al. 2006. Age-related accumulation of pentosidine in aggrecan and collagen from normal and degenerate human intervertebral discs. *Biochem J* 399: 29-35.
37. J. Urban, S. Roberts, J. Ralphs. 2000. The nucleus of the intervertebral disc from development to degeneration. *Amer Zool* 40: 53-61.
38. Illien-Junger S, Grosjean F, Laudier DM, et al. 2013. Combined anti-inflammatory and anti-AGE drug treatments have a protective effect on intervertebral discs in mice with diabetes. *PLoS One* 8: e64302.
39. Kim JH, Moon HJ, Lee JH, et al. 2012. Rabbit notochordal cells modulate the expression of inflammatory mediators by human annulus fibrosus cells cocultured with activated macrophage-like THP-1 cells. *Spine (Phila Pa 1976)* 37: 1856-1864.
40. Malagola E, Teunissen M, van der Laan LJ, et al. 2016. Characterization and comparison of canine multipotent stromal cells derived from liver and bone marrow. *Stem Cells Dev* 25: 139-150.
41. Farndale RW, Sayers CA, Barrett AJ. 1982. A direct spectrophotometric microassay for sulfated glycosaminoglycans in cartilage cultures. *Connect Tissue Res* 9: 247-248.
42. Lafeber FP, Vander Kraan PM, Van Roy JL, Huber-Bruning O, Bijlsma JW. 1993. Articular cartilage explant culture; an appropriate in vitro system to compare osteoarthritic and normal human cartilage. *Connect Tissue Res* 29: 287-299.
43. Benz K, Stippich C, Osswald C, et al. 2012. Rheological and biological properties of a hydrogel support for cells intended for intervertebral disc repair. *BMC Musculoskelet Disord* 13: 54-2474-13-54.
44. Gruber HE, Ingram J, Hanley EN, Jr. 2002. An improved staining method for intervertebral disc tissue. *Biotech Histochem* 77: 81-83.
45. Lv FJ, Tuan RS, Cheung KM, Leung VY. 2014. Concise review: The surface markers and identity of human mesenchymal stem cells. *Stem Cells* 32: 1408-1419.
46. Robey P. 2017. "Mesenchymal stem cells": Fact or fiction, and implications in their therapeutic use. *F1000Res* 6: 10.12688/f1000research.10955.1. eCollection 2017.
47. Willems N, Bach FC, Plomp SG, et al. 2015. Intradiscal application of rhBMP-7 does not induce regeneration in a canine model of spontaneous intervertebral disc degeneration. *Arthritis Res Ther* 17: 137-015-0625-2.
48. Landis JR, Koch GG. 1977. The measurement of observer agreement for categorical data. *Biometrics* 33: 159-174.
49. Masuda K, Imai Y, Okuma M, et al. 2006. Osteogenic protein-1 injection into a degenerated disc induces the restoration of disc height and structural changes in the rabbit anular puncture model. *Spine (Phila Pa 1976)* 31: 742-754.
50. Willems N, Tellegen AR, Bergknut N, et al. 2016. Inflammatory profiles in canine intervertebral disc degeneration. *BMC Vet Res* 12: 10-016-0635-6.
51. Neuman RE, Logan MA. 1950. The determination of hydroxyproline. *J Biol Chem* 184: 299-306.
52. Bach FC, Miranda-Bedate A, van Heel FW, et al. 2017. Bone morphogenetic protein-2, but not mesenchymal stromal cells, exert regenerative effects on canine and human nucleus pulposus cells. *Tissue Eng Part A* 23: 233-242.
53. Sawilowsky S. 2009. New effect size rules of thumb. *Journal of Modern Applied Statistical Methods* 8: 597-599.
54. Cliff N. 1993. Dominance statistics: Ordinal analyses to answer ordinal questions. *Psychological Bulletin* 114: 494-509.

## Supplementary File 1. Detailed information on Materials and Methods

I. *In vitro* studies

## a. Real time qPCR

## Primers used for quantitative PCR of canine samples

Genes	Forward sequence 5' → 3'	Reverse sequence 5' → 3'	Amplicon size	Annealing temp (°C)
<b>Reference genes</b>				
<i>GAPDH</i>	TGTCCCCACCCCAATGTATC	CTCCGATGCCTGCTTCACTACCTT	100	58
<i>HPRT</i>	AGCTTGCTGGTGAAAAGGAC	TTATAGTCAAGGGCATATCC	104	58
<i>RPS19</i>	CCTTCTCAAAAAGTCTGGG	GTTCTCATCGTAGGGAGCAAG	95	61
<i>SDHA</i>	GCCTTGGATCTCTTGATGGA	TTCTTGGCTCTTATGCGATG	92	56.5
<b>Target genes</b>				
<i>ACAN</i>	GGACACTCCTTGCAATTTGAG	GTCATTCCACTCTCCCTTCTC	111	62
<i>ADAMTS5</i>	CTACTGCACAGGGAAGAG	GAACCCATTCCACAAATGTC	149	61
<i>CASP3</i>	CGGACTTCTTGATGCTTACTC	CACAAAGTGACTGGATGAACC	89	61
<i>CCND1</i>	GCCTCGAAGATGAAGGAGAC	CAGTTTGTTCACCAGGAGCA	117	60
<i>COL1A1</i>	GTGTGTACAGAACGGCCTCA	TCGCAAATCAGTCATCG	109	61
<i>COL2A1</i>	GCAGCAAGAGCAAGGAC	TTCTGAGAGCCCTCGGT	151	62
<i>COL10A1</i>	CCAACACCAAGACACAG	CAGGAATACCTTGTCTC	80	61
<i>IL-1β</i>	TGCTGCCAAGACCTGAACCAC	TCCAAAGCTACAATGACTGACACG	115	68
<i>KRT18</i>	GGACAGCTCTGACTCCAGGT	AGCTTGAGAAACAGCCTGAG	97	60
<i>KRT19</i>	GCCAGCTGAGCGATGTGC	TGCTCCAGCCGTGACTTGATGT	86	64
<i>MMP13</i>	CTGAGGAAGACTTCCAGCTT	TTGGACCACTTGAGAGTTCG	250	65
<i>PAI1</i>	AAACTGGCGGACTTCTC	ACTGTGCCACTCTCATTAC	98	61.5
<i>SOX9</i>	CGCTCGCAGTACGACTACAC	GGGGTTCATGTAGGTGAAGG	105	62
<i>TIMP1</i>	GGCGTTATGAGATCAAGATGAC	ACCTGTGCAAGTATCCGC	120	66
<i>TNFα</i>	CCCCGGGCTCCAGAAGGTG	GCAGCAGGCAGAAGAGTGTGGTG	99	65

## Primers used for quantitative PCR of human samples

Genes	Forward sequence 5' → 3'	Reverse sequence 5' → 3'	Amplicon size	Annealing temp (°C)
<b>Reference genes</b>				
<i>HPRT</i>	TATTGTAATGACCAGTCAACAG	GGTCTTTTTCAACAGCAAG	192	60
<i>SDHA</i>	TGGGAACAAGAGGGCATCTG	CCACCACTGCATCAAATTCATG	86	58
<i>TBP</i>	TGCACAGGAGCCAAGAGTGAA	CACATCACAGTCCCCACCA	132	63.5
<i>YWHAZ</i>	ACTTTTGGTACATTTGGCTTCAA	CCGCCAGGACAAACCAGTAT	94	64
<b>Target genes</b>				
<i>ACAN</i>	CAACTACCCGGCCATCC	GATGGCTCTGTAATGGAACAC	160	63.5
<i>ADAMTS5</i>	GCCAGCGGATGTGCAAGC	ACACTTCCCCGGAGCAGAGA	130	62.5
<i>CASP3</i>	CAGTGGAGGCCGACTTCTTG	TGGCACAAGCGACTGGAT	102	58
<i>CCND1</i>	AGTCCTGTGCTGCGAAGTGAAAC	AGTGTTCAATGAAATCGTGCGGGT	480	65
<i>COL1A1</i>	TCCAACGAGATCGAGATCC	AAGCCGAATTCCTGGTCT	191	61
<i>COL2A1</i>	AGGGCCAGGATGTCGGCA	GGGTCCAGGTTCTCCATCT	195	63.5
<i>COL10A1</i>	CACTACCCAACCAAGACA	CTGGTTTCCTACAGCTGAT	225	61
<i>KRT18</i>	CGGGCATTGTCCACAGTATT	GGGAGCACTTGAGAAAGAAG	108	65
<i>KRT19</i>	CTTCCGAACCAAGTTTGAGAC	AGCGTACTGATTTCTCTCTC	183	64
<i>MMP13</i>	TCCCAGGAATTGGTGATAAAGTAGA	CTGGCATGACGCGAACAATA	123	64
<i>PAI1</i>	GCTGGTGAATGCCCTCTAC	GGCAGCCTGGTCATGTTG	318	65
<i>SOX9</i>	CCCAACGCCATCTTCAAGG	CTGCTCAGTCCCGATGT	242	65.5
<i>TIMP1</i>	CTTCTGGCATCTGTTGTTG	GGTATAAGGTGGTCTGGTTG	153	64

Reference genes: *HPRT*: Hypoxanthine-guanine phosphoribosyltransferase, *SDHA*: Succinate dehydrogenase complex subunit A, *TBP*: TATA-Box binding protein, *YWHAZ*: tyrosine 3-monooxygenase/tryptophan 5-monooxygenase activation protein zeta, *RPS19*: 40S ribosomal protein S19.

Target genes: *ACAN*: aggrecan, *ADAMTS5*: A disintegrin and metalloproteinase with thrombospondin motifs 5, *CASP3*: caspase 3, *CCND1*: cyclin D1, *COL1A1*: collagen type I, *COL2A1*: collagen type II, *COL10A1*: collagen type X, *IL-1β*: interleukin-1β, *KRT18*: cytokeratin 18, *KRT19*: cytokeratin 19, *MMP13*: matrix metalloproteinase 13, *PAI1*: Plasminogen activator inhibitor type 1, *SOX9*: sex determining region Y-box 9, *TIMP1*: tissue inhibitor of metalloproteinases, *TNFα*: Tumor Necrosis Factor alpha.

**b. Sulphate incorporation assay**

Shortly, CLCs from the six canine and human donors were cultured in micro-aggregates in duplicates in basal culture medium, basal culture medium supplemented with 10 ng/mL TGF-β<sub>1</sub> or 10 mg/mL NCM. After 7 days, the micro-aggregates were pulsed with 20 μCi <sup>35</sup>SO<sub>4</sub><sup>2-</sup>. Four hours later, the micro-aggregates were washed twice with 500 μL PBS and frozen at -20°C. After one day, the micro-aggregates were digested for two hours in papain buffer. The next day, the amount of <sup>35</sup>SO<sub>4</sub><sup>2-</sup>-labelled GAGs in the papain digest was measured by liquid scintillation analysis and normalized for the micro-aggregates’ DNA content.

**II. In vivo studies**

**c. Overview of the treatment per canine IVD**

	T11	T12	T13	L1	L2	L3	L4	L5	L6	L7	S1
Level	T11-12	T12-13	T13-L1	L1-L2	L2-L3	L3-L4	L4-L5	L5-L6	L6-L7	L7-S1	
NX/-	-	NX	-	NX	-	NX	-	NX	-	NX	
Treatment (T= 0 m)	-	MSC	MSC	-	NCM	NCM	NCM+ MSC	NCM+ MSC	NCM	NCM	
Treatment (T= 3 m)	-	-	-	-	-	-	-	-	NCM	NCM	

Six weeks before the start of the experiment (T=-1.5 months), more severe (moderate) IVD degeneration was induced in five IVDs per dog by partial NP removal (NX; T12-T13, L1-L2, L3-L4, L5-L6, and L7-S1) on the left side of the spine. At the start of the experiment (T=0 months), the mildly and moderately degenerated canine IVDs were injected on the right side of the spine with 50 μL of (a) 1\*10<sup>6</sup> canine mesenchymal stromal cells (MSCs) incorporated in an albumin-based hydrogel, (b) 10 mg/mL notochordal cell-derived matrix (NCM), or (c) 1\*10<sup>6</sup> canine MSCs suspended in 10 mg/mL NCM. Three months after the first injections (T=3 months), two IVDs per dog (L6-L7 and L7-S1) were again injected with 50 μL of 10 mg/mL NCM. Every dog received a similar treatment per spinal location. -: no NX/no treatment.

#### d. Anesthesia and analgesia protocols Beagles *in vivo*

For the induction of degeneration and intradiscal injections anesthesia was provided by intravenous buprenorphine (20 µg/kg) and dexmedetomidine (10 µg/kg), induced by intravenous propofol (1-2 mg/kg) and maintained by intravenous propofol (100 mg/kg/hr) and inhalation of 1-1.5% isoflurane. Peri- and postoperative analgesia was provided by intramuscular buprenorphine (20 µg/kg, one day, three times a day) and subcutaneous carprofen (4 mg/kg, five days, once a day). Additionally, the dogs received preoperative intravenous cefazolin (20 mg/kg) once. For MRI and CT, anesthesia was provided by intravenous butorphanol (0.2 mg/kg) and dexmedetomidine (10 µg/kg), induced by intravenous propofol (1-2 mg/kg) and maintained by inhalation of 1-1.5% isoflurane. At T=6 months, the Beagles were euthanized after the MRI by intravenous pentobarbital (200 mg/kg).

#### e. MRI and CT

Magnetic resonance images (MRI) were obtained at T=0, 3, and 6 months using a 1.5T high field MRI unit (Ingenia, Philips). Sagittal T1-weighted Turbo Spin Echo (repetition time (TR): 400 ms, echo time (TE): 8 ms), and T2-weighted Turbo Spin Echo (TR: 3000 ms, TE: 110 ms) images were acquired using a field of view (FOV) of 75 x 220 mm and acquisition matrix of 124 x 313 and 124 x 261. Thirteen 2 mm-thick slices covered the spine from T10 to S1. For T2 mapping, a quantitative multiple spin-echo T2-mapping sequence was used with the following parameters; FOV: 75 x 219 mm, acquisition matrix: 96 x 273, slice thickness: 3 mm, TR: 2000 ms. Eight echoes were acquired with TE: 13-104 ms with 13 ms echo spacing. Sagittal T1 $\rho$ -weighted imaging was performed using a spinlock-prepared sequence with 3D multi-shot gradient echo (T1-TFE) readout with FOV: 76 x 220 mm, acquisition matrix: 76 x 220, slice thickness: 2 mm, TR/TE: 4.6s/2.3s, TR: 5ms, TE: 2.5ms, TFE factor: 50, flip angle: 45°, shot interval: 3000 ms. For quantitative T1 $\rho$  mapping, data were acquired with spinlock times: 0, 10, 20, 30 and 40 ms, spinlock pulse amplitude: 500 Hz. An oval region of interest (ROI) was manually segmented on the NP of all spinal segments.

Computed tomography (CT) images were obtained *postmortem* with dogs positioned in dorsal recumbency to monitor extradiscal calcification and EP pathology. The CT scans were made using a 64 slice CT scanner (Siemens Somatom Definition AS, Siemens Healthcare) with the following parameters: 120 kV, 350 mas, 1000 ms tube rotation time, 0.6 mm slice thickness, 0.35 spiral pitch factor, 512 x 512 pixel matrix and 93 mm fixed field view. Reconstructions were made in transverse and sagittal planes using soft tissue and bone reconstruction kernels and images were reviewed in soft tissue/bone settings (window length 50, width 300, and window length 600, width 3000, respectively).

#### f. Sample collection

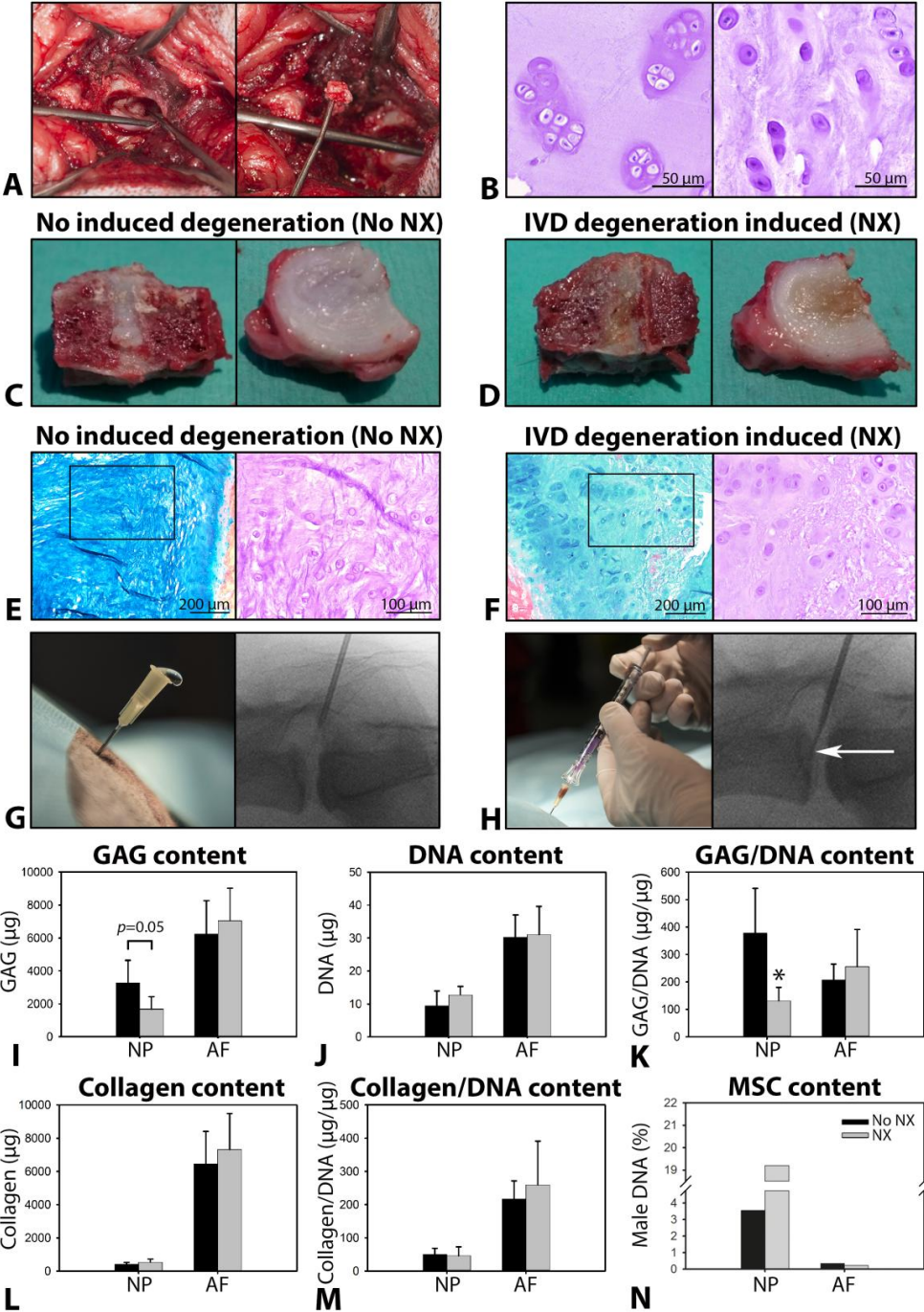
The vertebral column (T11-S1) was harvested using an electric multipurpose saw (Bosch). The muscles were removed and the vertebrae were transversely transected using a band saw (EXAKT tape saw). The ten spinal units (½ vertebra – endplate - IVD - endplate - ½ vertebra) were sagittally transected into two identical parts using a diamond band saw (EXAKT 312). In one part the bisected IVD tissue was isolated from the endplate and vertebra with a surgical knife and was snap frozen in liquid nitrogen and stored at -70°C for biochemical analyses. The other part was used to photograph (Olympus VR-340) the other half of the IVD for macroscopic Thompson score evaluation. The samples were fixed in 4%

buffered formaldehyde for 14 days, decalcified in PBS with 0.5M EDTA for two months and embedded in paraffin.

**g. RNA isolation, cDNA synthesis, and RT-qPCR**

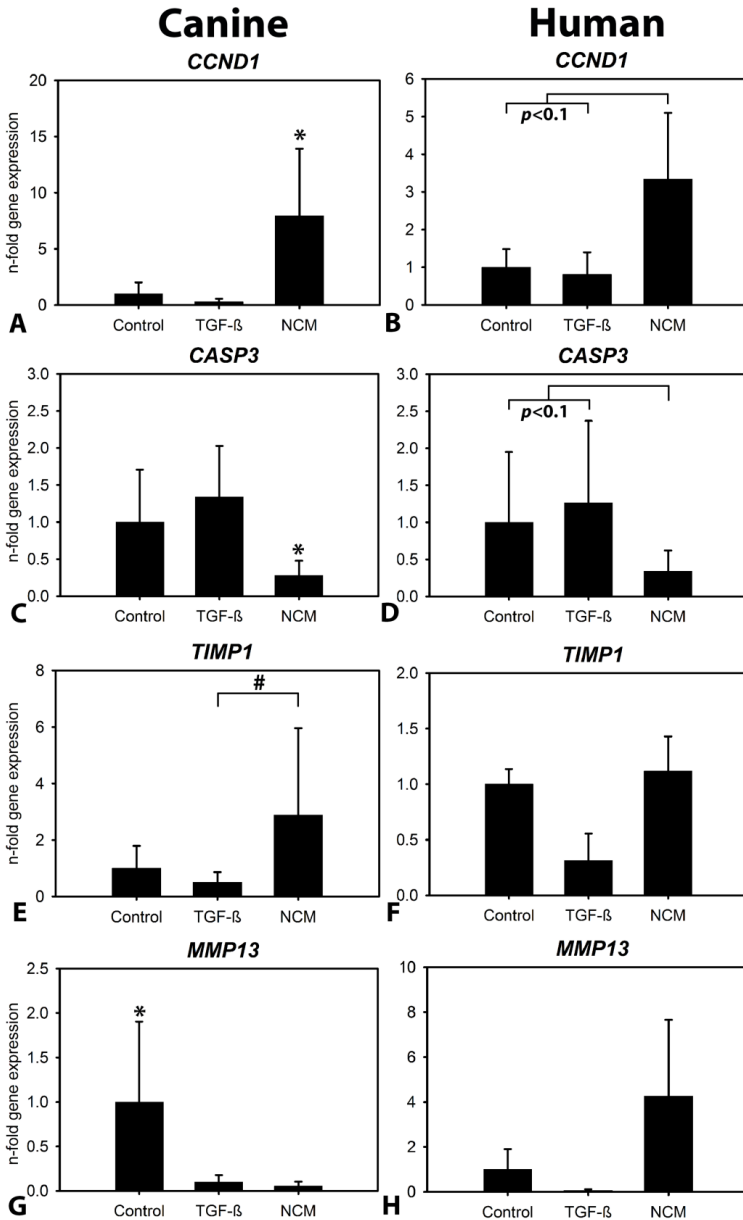
For RT-qPCR, the NP and AF were carefully separated and cut into small pieces. Half of the NP/AF tissues was collected in 400 and 750  $\mu$ L complete lysis buffer (04719956001, Roche Diagnostics), respectively, and stored at  $-70^{\circ}\text{C}$  until biochemical analysis. The other tissue halves were separately collected in 300  $\mu$ L Exiqon Kit RNA buffer and stored at  $-70^{\circ}\text{C}$  until biomolecular analysis. The RNA samples were homogenized using the TissueLyser II (Qiagen) for 4 minutes at 20 Hz. Thereafter, RNA was isolated (miRCURY RNA Isolation Kit (300110, Exiqon)) and cDNA was synthesized (iScript<sup>TM</sup> cDNA Synthesis Kit (170-8891, Bio-Rad)) and amplified (Sso Advanced<sup>TM</sup> PreAmp Supermix (1725160, Bio-Rad)) according to the manufacturer's instructions. RT-qPCR was performed as described with the *in vitro* studies. For primer sequences, see Sup. File 7a.

Supplementary File 2. Induction of intervertebral disc (IVD) degeneration by partial NP removal



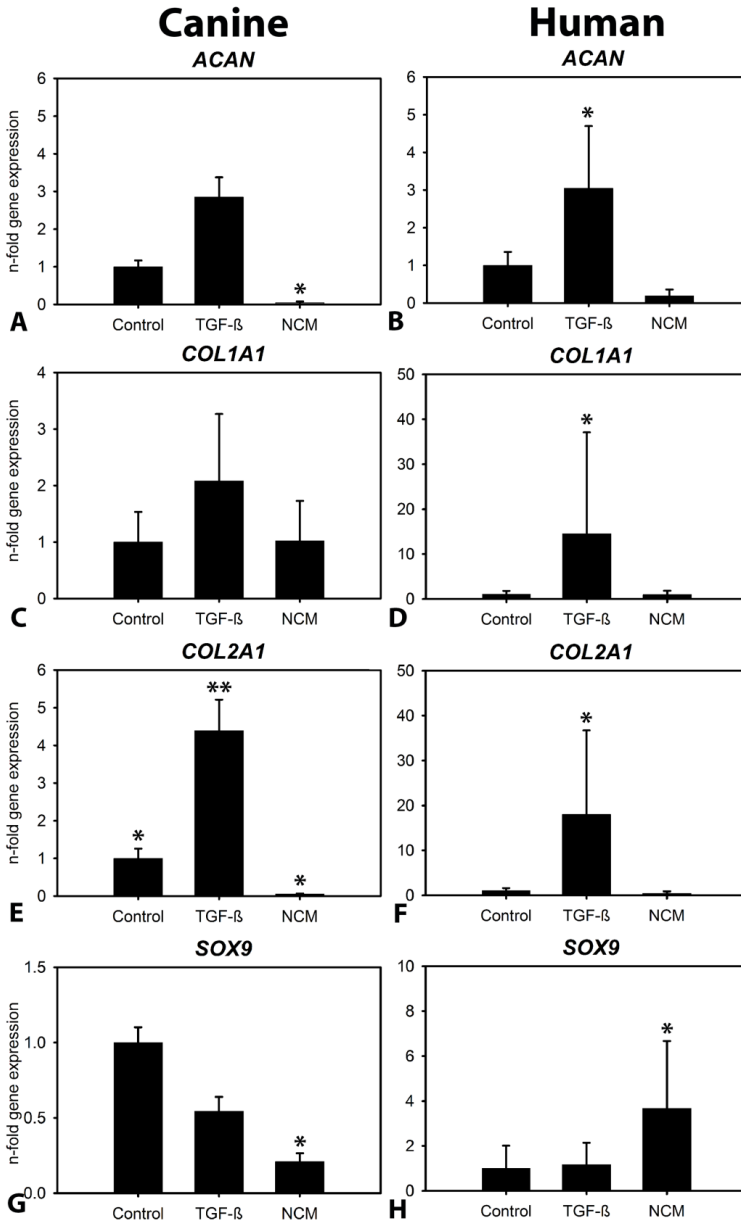
Six weeks before the start of the experiment (T=-1.5 months), moderate IVD degeneration was induced in five IVDs per dog by partial removal of the NP (NX; T12-T13, L1-L2, L3-L4, L5-L6, and L7-S1) (**a**). The removed NP tissue showed CLC clusters and single cells (H&E staining) (**b**). At the start of the experiment (T=0 months), the IVDs of the dog that died unexpectedly were used for baseline analysis and were examined macroscopically (**c**, **d**), histologically (Alcian Blue-Picrosirius Red (left) and H&E staining (right) (**e,f**)) and biochemically for GAG (**i**), DNA (**j**), GAG/DNA (**k**), collagen (**l**) and collagen/DNA (**m**) content. The NPs of the IVDs in which moderate degeneration was induced by NX showed macroscopically a brown discoloration, histologically less blue (GAG) and more red (collagen) in their NP tissue, and biochemically a decreased GAG and GAG/DNA content. Pictures of the (fluoroscopic) through the needle injections with NCM/MSCs are shown in **g** (positioning of the 19G needle) and **h** (through the needle injection with a 25G needle, arrow). The fate of the MSCs (at T=0 months, directly after injection) was determined by *SRY:GAPDH* PCR on genomic DNA of the deceased dog IVDs (**n**). The male DNA percentage in the female IVD indicates the percentage of MSCs present in the IVD.  $n=5$  IVDs per condition (DNA, GAG, collagen content) and  $n=1$  IVD per condition (MSC content, male DNA percentage).

**Supplementary File 3. Effect of notochordal cell-derived matrix (NCM) on canine and human CLC gene expression**



Target gene expression levels of canine and human chondrocyte-like cells (CLCs) cultured in micro-aggregates in basal culture medium (control), basal culture medium supplemented with 10 ng/mL TGF-β<sub>1</sub>, and 10 mg/mL NCM. Relative *CCND1* (a, b), *CASP3* (c, d), *TIMP1* (e, f), and *MMP13* (g, h) gene expression (mean+SD) of the micro-aggregates at day 7. The control micro-aggregates were set at 1. #: significant difference ( $p < 0.05$ ). \*, \*\*: significant difference between this condition and all other conditions ( $p < 0.05$  and  $p < 0.01$ , respectively).  $n = 6$ .

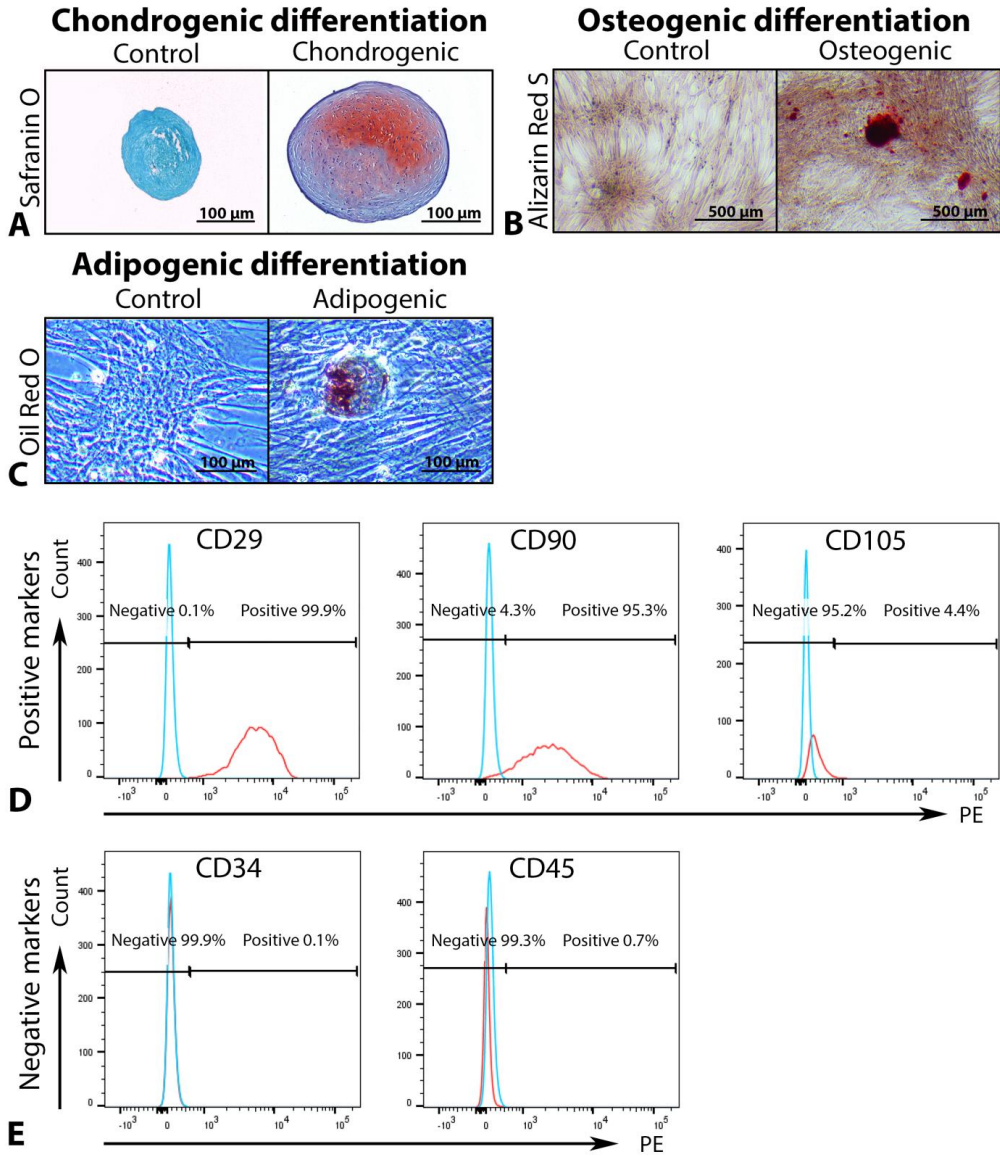
**Supplementary File 4. Effect of notochordal cell-derived matrix (NCM) on canine and human CLC anabolism gene expression**



Target gene expression levels of canine and human chondrocyte-like cells (CLCs) cultured in micro-aggregates in basal culture medium (control), basal culture medium supplemented with 10 ng/mL TGF-β<sub>1</sub>, and 10 mg/mL NCM. Relative *ACAN* (a, b), *COL1A1* (c, d), *COL2A1* (e, f), and *SOX9* (g, h) gene expression (mean+SD) of the micro-aggregates at day 7. Control micro-aggregates were set at 1. \*, \*\*: significant difference between this condition and all other conditions ( $p < 0.05$  and  $p < 0.01$ , respectively);  $n = 6$ .

5

Supplementary File 5. Mesenchymal stromal cell (MSC) characterisation



Characterisation of bone marrow-derived MSCs of the male Beagle donor used in the *in vivo* experiment. (a) Chondrogenic (Safranin O/Fast Green staining), (b) osteogenic (Alizarin Red S staining), and (c) adipogenic (Oil-Red-O staining) differentiation and (d) FACS analysis for positive (CD29, CD90, CD105) and (e) negative (CD34, CD45) MSC markers. Chondrogenic, osteogenic, and adipogenic differentiation was successfully achieved. The cells were found to be CD34<sup>-</sup>, CD45<sup>-</sup>, CD29<sup>+</sup> and CD90<sup>+</sup>. However, only 4.4% of cells was CD105<sup>+</sup>, this could be explained by a low cross-species reactivity of the anti-human CD105, which was used due to unavailability of commercial anti-canine CD105. Altogether, the results confirm the presence of MSCs in the injected cells. PE: Phycoerythrin fluorescent dye.

**Supplementary File 6. Modic changes, periosteal bone formation, spondylosis and EP lysis**

The development of **Modic Changes** (MC) was recorded during the study. In noNX-IVDs, only one MC type 3 was observed at T=0, 3, and 6 months. In NX-IVDs, one and a half month after NX, and before the different treatments were applied (T=0 months), several MCs were already present. During the study, *i.e.* after the first intradiscal injections, control NX-IVDs developed two type 1 MCs, while 1xNCM-treated NX-IVDs developed one additional type 1 MC and one type 1 MC progressed towards a type 3 MC, MSC-treated NX-IVDs developed one type 1 MC, and NCM+MSC-treated NX-IVDs developed four type 1 and two type 3 MCs. In contrast, 2xNCM-treated NX-IVDs did not develop any additional MCs, presumably (also) due to the less invasive percutaneous approach of the L7-S1 IVD.

**Modic changes at T=0 months**

Dog	No NX					NX				
	Control	1xNCM	2xNCM	MSC	NCM+MSC	Control	1xNCM	2xNCM	MSC	NCM+MSC
1	-	-	3	-	-	-	-	-	-	-
2	-	-	-	-	-	-	-	-	-	-
3	-	-	-	-	-	1	1	-	-	-
4	-	-	-	-	-	-	1	2+3	-	-
5	-	-	-	-	-	-	-	1+3	1	-

**Modic changes at T=3 months**

Dog	No NX					NX				
	Control	1xNCM	2xNCM	MSC	NCM+MSC	Control	1xNCM	2xNCM	MSC	NCM+MSC
1	-	-	3	-	-	-	-	-	-	-
2	-	-	-	-	-	-	-	-	1	-
3	-	-	-	-	-	1	1	-	-	1
4	-	-	-	-	-	1	1	2+3	-	1
5	-	-	-	-	-	-	1	3	1	1

**Modic changes at T=6 months**

Dog	No NX					NX				
	Control	1xNCM	2xNCM	MSC	NCM+MSC	Control	1xNCM	2xNCM	MSC	NCM+MSC
1	-	-	3	-	-	-	-	-	-	1
2	-	-	-	-	-	-	-	-	1	3
3	-	-	-	-	-	1	1	-	-	1
4	-	-	-	-	-	-	3	2+3	-	3
5	-	-	-	-	-	1	-	1+3	1	-

Overview of the type of Modic changes observed by MRI analysis. - : no Modic changes observed. Grey depicted Modic changes are different from T=0 months (1.5 month after moderate degeneration was induced by partial NP removal (NX)). *n*=5

The development of **periosteal bone formation** and **ventral spondylosis** was determined at T=6 months using CT. When these features were present, they were located at the left side of the spinal column, the side employed to induce IVD degeneration. No periosteal bone formation or ventral spondylosis was detected in control, 2xNCM and MSC-treated noNX-IVDs. In contrast, mild ventral spondylosis was observed in 1xNCM-treated (3/5) and NCM+MSC-treated (1/5) noNX-IVDs. Additionally, minimal (1/5) and distinct (1/5) periosteal bone formation was observed in NCM+MSC-treated noNX-IVDs. In NX-IVDs, more pathological features were detected. In 4/5 control NX-IVDs, distinct periosteal bone formation was detected. Furthermore, 1xNCM-treated NX-IVDs showed mild-distinct bone formation (5/5) and mild spondylosis (3/5), and MSC- and MSC+NCM-treated NX-IVDs showed distinct bone formation (2/5 and 4/5, respectively). 2xNCM-treated NX-IVDs showed none of these pathological processes on CT analysis, again presumably due to the less invasive approach of the L7-S1 IVD.

5

Dog	No NX					NX				
	Control	1xNCM	2xNCM	MSC	NCM+MSC	Control	1xNCM	2xNCM	MSC	NCM+MSC
1	-	- <sup>a</sup>	-	-	-	-	+	-	+	+
2	-	-	-	-	-	+	+/- <sup>a</sup>	-	-	-
3	-	- <sup>a</sup>	-	-	+/- <sup>a</sup>	+	+	-	-	+
4	-	- <sup>a</sup>	-	-	-	+	+ <sup>a</sup>	-	+	+
5	-	-	-	-	+	+	+ <sup>a</sup>	-	-	+

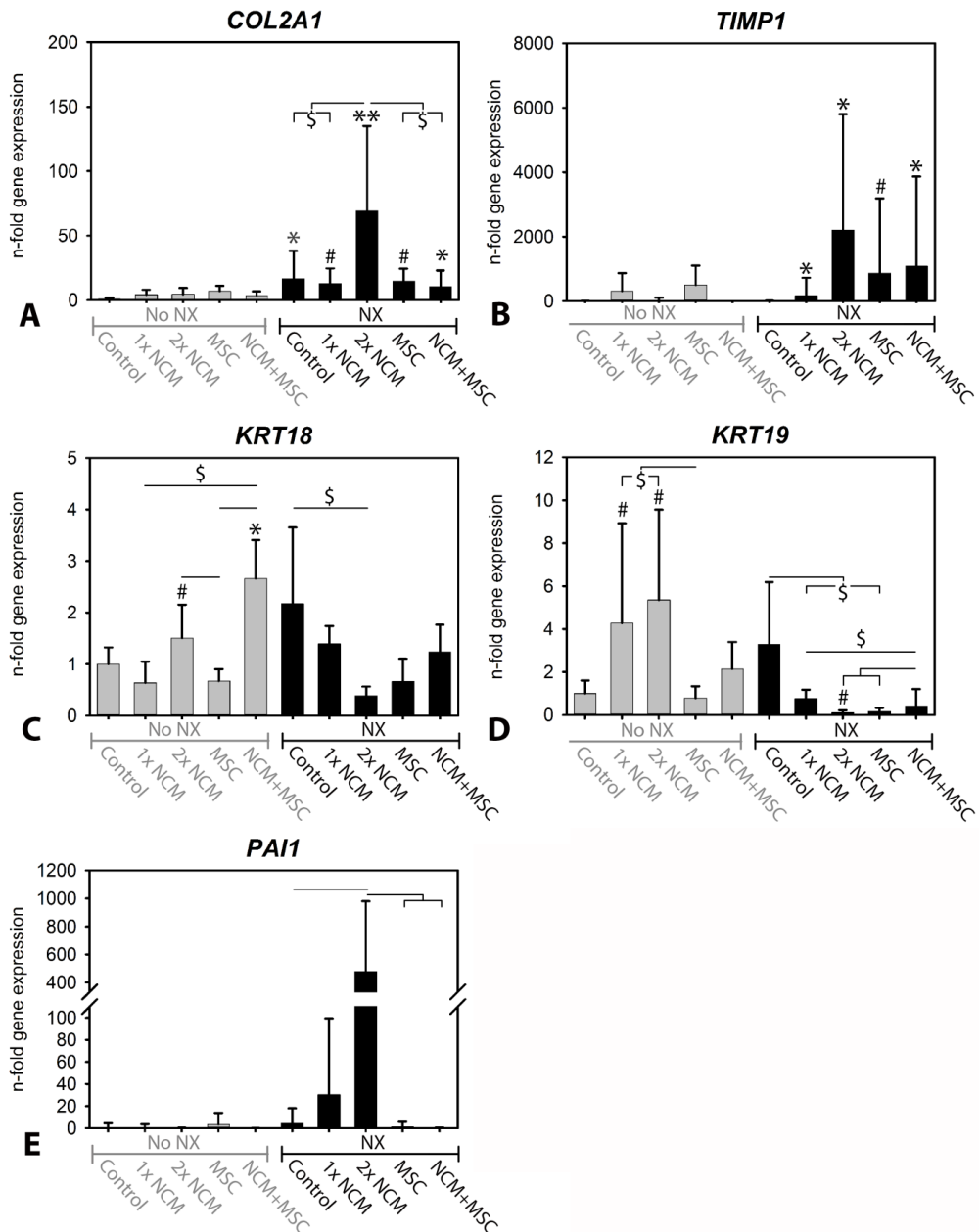
- =: no periosteal bone formation, +/-: minimal periosteal bone formation, +: distinct periosteal bone formation. a: mild spondylosis. Bone formation was only detected at the left side (induction of degeneration side). n=5

**EP lysis** (determined by CT analysis at T=6 months) was only present in NX-IVDs, most probably due to the NX procedure.

Dog	No NX					NX				
	Control	1xNCM	2xNCM	MSC	NCM+MSC	Control	1xNCM	2xNCM	MSC	NCM+MSC
1	-	-	-	-	-	-	-	-	+	-
2	-	-	-	-	-	-	+	-	-	+
3	-	-	-	-	-	-	-	-	-	+
4	-	-	-	-	-	-	+	-	+	+
5	-	-	-	-	-	-	-	-	-	+

- =: no EP lysis, +: EP lysis. n=5

**Supplementary File 7. mRNA expression of the degenerated canine IVDs *in vivo***



Relative target gene expression (mean±SD) of (a) *COL2A1*, (b) *TIMP1*, (c) *KRT18*, (d) *KRT19*, and (e) *PAI1* at T=6 months. The control noNX-IVDs were set at 1. NX: partial NP removal was performed to induce moderate IVD degeneration. Bars represent significant differences between conditions ( $p < 0.05$ ); n.s.: not significantly affected; \*, \*\*: significantly different from control noNX-IVDs ( $p < 0.05$ ,  $p < 0.01$ , respectively); #: different from control noNX-IVDs ( $0.05 \leq p \leq 0.20$ , medium/large effect size); \$: difference between conditions with medium/large effect size ( $0.05 \leq p \leq 0.20$ );  $n = 5$ .

5



## Part II – Growth factor-based therapies



**Intradiscal application of rhBMP7 does not induce regeneration in a canine model of spontaneous intervertebral disc degeneration**

Nicole Willems<sup>1</sup>, Frances C. Bach<sup>1</sup>, Saskia G.M. Plomp<sup>2</sup>, Mattie H.P. van Rijen<sup>2</sup>, Jeannette Wolfswinkel<sup>1</sup>, Guy C.M. Grinwis<sup>3</sup>, Clemens Bos<sup>4</sup>, Gustav J. Strijkers<sup>5</sup>, Wouter J.A. Dhert<sup>1,2</sup>, Björn P. Meij<sup>1</sup>, Laura B. Creemers<sup>2</sup>, Marianna A. Tryfonidou<sup>1</sup>

<sup>1</sup> Department of Clinical Sciences of Companion Animals, Faculty of Veterinary Medicine, Utrecht University, Utrecht, the Netherlands

<sup>2</sup> Department of Orthopedics, University Medical Center Utrecht, Utrecht, the Netherlands

<sup>3</sup> Department of Pathobiology, Faculty of Veterinary Medicine, The Netherlands

<sup>4</sup> Department of Radiotherapy, University Medical Center, Utrecht, The Netherlands

<sup>5</sup> Department of Biomedical Engineering, Eindhoven University of Technology, Eindhoven, the Netherlands

## Abstract

Strategies for biological repair and regeneration of the intervertebral disc (IVD) by cell and tissue engineering are promising, but few have made it into the clinic. Recombinant human bone morphogenetic protein 7 (rhBMP7) has been shown to stimulate matrix production by IVD cells *in vitro*, and *in vivo* in animal models of induced IVD degeneration. The aim of this study was to determine the most effective dose of intradiscally injected rhBMP7 in a spontaneous canine IVD degeneration model for translation into a clinical application for patients with low back pain. Canine nucleus pulposus derived chondrocyte-like cells (CLCs) were cultured with rhBMP7 to assess the anabolic effect of rhBMP7 *in vitro*, and samples were evaluated for glycosaminoglycan (GAG) and DNA content, histology, and matrix-related gene expression. Three different dosages of rhBMP7 (2.5  $\mu\text{g}$ , 25  $\mu\text{g}$ , and 250  $\mu\text{g}$ ) were injected *in vivo* into early degenerated IVDs of canines, which were followed up for 6 months by magnetic resonance imaging (T2-weighted images, T1 $\rho$  and T2 maps). *Postmortem*, the effects of rhBMP7 were determined by radiography, computed tomography and macroscopy, and by histological, biochemical (GAG, DNA, collagen), and biomolecular analyses of IVD tissue. *In vitro*, rhBMP7 stimulated matrix production in canine CLCs as GAG deposition was enhanced, DNA content was maintained and gene expression levels of *ACAN* and *COL2A1* were significantly upregulated. Despite the wide dose range of rhBMP7 (2.5 – 250  $\mu\text{g}$ ) administered *in vivo*, no regenerative effects were observed at the IVD level. Instead, extensive extradiscal bone formation was noticed after intradiscal injection of 25  $\mu\text{g}$  and 250  $\mu\text{g}$  of rhBMP7. In conclusion, intradiscal bolus injection of 2.5, 25, and 250  $\mu\text{g}$  rhBMP7 showed no regenerative effects in a spontaneous canine IVD degeneration model. In contrast, intradiscal injection of 250  $\mu\text{g}$  rhBMP7, and to a lesser extent 25  $\mu\text{g}$  rhBMP7, resulted in extensive extradiscal bone formation, indicating that a bolus injection of rhBMP7 alone cannot be used for treatment of IVD degeneration in human or canine patients.

## Introduction

Low back pain is one of the major sources of disability in humans<sup>1</sup>. Several studies have provided evidence for its association with intervertebral disc (IVD) degeneration<sup>2,3</sup>. Current therapies, such as physiotherapy, anti-inflammatory medications, and surgery alleviate symptoms, but do not restore the physiological function of the degenerated IVD. Prevention of further degeneration or regeneration of the IVD requires intervention at an early stage. Strategies for biological repair and regeneration of the IVD by cell and tissue engineering are promising, but are not widely clinically applicable thus far. A number of studies have been performed on bone morphogenetic proteins (BMPs) given their potential regenerative role in degenerative IVD disease<sup>4</sup>. BMPs belong to the transforming growth factor- $\beta$  (TGF- $\beta$ ) superfamily, and are involved in many developmental processes<sup>4,5</sup>. Recombinant human bone morphogenetic protein 7 (rhBMP7) has been tested extensively and appears to be a promising BMP for IVD regeneration<sup>6-8</sup>, as it has been shown to have beneficial effects on extracellular matrix production of rabbit, bovine, and human IVD cells *in vitro*<sup>7,9-13</sup>. Several animal models with experimental IVD degeneration were used to study the efficacy and translational aspects of BMP7 towards a clinical application in humans<sup>14</sup>. In rabbits with experimentally induced IVD degeneration, rhBMP7 restored disc height and improved the IVD viscoelastic properties by increasing the proteoglycan content<sup>15,16</sup>. An anti-catabolic effect of rhBMP7 was shown in a rat model with induced IVD degeneration<sup>17</sup>. Also in a canine model of allogenic IVD transplantation, nucleus pulposus derived chondrocyte-like cells (CLCs) expressing rhBMP7 prevented degeneration of the transplanted IVD at 6 months follow-up<sup>18</sup>. Thus far, novel regenerative therapies deploying rhBMP7 intradiscally have been tested in animal models with induced IVD degeneration, but not in an animal model with spontaneous IVD degeneration that more closely resembles the biological condition in humans. Furthermore, dose response studies evaluating intradiscal injection of rhBMP7 and possible adverse effects are not available<sup>4,19</sup>.

The goal of this study was to assess the effect of a wide range of intradiscally injected dosages of rhBMP7 (2.5 – 250  $\mu$ g) in a canine model with spontaneous IVD degeneration that closely resembles IVD degeneration and disease in man<sup>20,21</sup>. For this, we first investigated the anabolic effect of two dosages of rhBMP7 on canine CLCs from early degenerated IVDs *in vitro*. Potential regenerative effects of rhBMP7 *in vivo* were studied by obtaining conventional T2-weighted images and T2 and T1 $\rho$  maps in a longitudinal manner. Both T1 $\rho$  and T2 relaxation times are correlated with IVD degeneration since T2 relaxation times correlate strongly with water content, while T1 $\rho$  relaxation times are particularly sensitive to a decrease in glycosaminoglycan (GAG) content in the NP<sup>22,23</sup>. At 6 months follow up, the effects of rhBMP7 were determined *postmortem* by radiography and computed tomography, macroscopy, and by histological, biochemical, and biomolecular analyses.

## Materials and methods

### Ethics statement

All procedures involving animals were approved and conducted in accordance with the guidelines set by the Animal Experiments Committee (DEC) of Utrecht University (Experimental numbers: 2012.III.07.065, 2013.III.02.017, and 2013.II.12.126), as required by Dutch regulation.

### Isolation and culture of chondrocyte-like cells

Nucleus pulposus tissue was separated from early degenerated IVDs (Pfirrmann grade 2) of twelve laboratory beagle dogs; care was taken to avoid the transitional zone. Tissue was washed with hgDMEM + Glutamax + pyruvate (31966, Invitrogen, Paisley, UK) + 1% penicillin/streptomycin (P/S) (P11-010, PAA Laboratories GmbH, Piscataway, NJ, USA) and digested with 0.15% pronase (11459643001, Roche Diagnostics, Indianapolis, USA) for 45 minutes at 37°C and subsequently digested overnight with 0.15% collagenase II (4176, Worthington, Lakewood, NJ, USA) at 37°C. CLCs were filtered over a 70 µm filter, centrifuged (5 min at 500g), and cryopreserved at passage 0 (hgDMEM + Glutamax + 10% DMSO + 10% FBS (High performance 16000-044, Gibco, Bleiswijk, The Netherlands)) until further use. CLCs were expanded in expansion medium (hgDMEM + Glutamax + pyruvate (Invitrogen), 10% FBS, 1% p/s, 0.1 mM ascorbate-2-phosphate (A8960, Sigma-Aldrich, Saint Louis, MO, USA), 10<sup>-9</sup> M dexamethasone (D1756, Sigma-Aldrich), 1 ng/mL bFGF (PHP105, AbD Serotec, Oxford, UK), 0.5% Fungizone (15290-018, Invitrogen) in 175 cm<sup>2</sup> cell culture flasks (660175, Greiner bio-one, Cellstar, Alphen aan den Rijn, The Netherlands) until passage 2. Cells (P2) were pooled to yield 5 different CLC donor groups and pelleted in ultra-low attachment 96 wells plates (Corning Costar 7007, Sigma-Aldrich) by centrifugation at 185g for 8 minutes. Each pellet contained 200,000 CLCs and was cultured in 200 µL chondrogenic culture medium for 28 days (5% CO<sub>2</sub>, 20% O<sub>2</sub>). Standard chondrogenic medium (hgDMEM+Glutamax (Invitrogen), was supplemented 1% ITS + premix (354352 Corning, Tewksbury, MA, USA), 0.04 mg/mL proline (P5607 Sigma-Aldrich), 1% P/S, 0.5% Fungizone, 0.1 mM ascorbate-2-phosphate) and remained untreated (negative control) or was supplemented with 10 or 100 ng/mL rhBMP7 (mammalian cell derived; 354-BP-010 R&D Systems Europe Ltd, Oxon, UK). Media were renewed twice weekly, collected per week, and stored at -80°C for analysis of GAG content.

### GAG and DNA content of CLC pellets and GAG content of culture media

At days 7 and 28, two CLC pellets per donor and condition were digested overnight at 60°C in papain (250 µg/mL papain (P3125-100 mg, Sigma-Aldrich) + 1.57 mg cysteine HCL (C7880, Sigma-Aldrich)). The 1,9-dimethylmethylene blue (DMMB) assay was used to quantify GAG content<sup>24</sup> of the pellets and media. GAG concentrations were calculated by using chondroitin sulfate from shark cartilage (C4384, Sigma-Aldrich) as a standard and the absorbance was read at 540/595nm. The Quant-iT<sup>TM</sup> dsDNA Broad-Range assay kit in combination with a Qubit<sup>TM</sup> fluorometer (Invitrogen) was used in accordance with the manufacturer's instructions to determine the DNA content of the CLC pellets.

### RNA isolation and quantitative RT-PCR (qPCR) of CLC pellets

At days 7 and 28, RNA was isolated from two pellets per donor and condition and pooled. After crushing the pellets with a pellet pestle (9951-901, Argos Technologies, Elgin, IL, USA),

total RNA was isolated by using the RNeasy microkit according to the manufacturer's instructions. After on-column DNase-I digestion (Qiagen RNase-free DNase kit), RNA was quantified by using a NanoDrop 1000 spectrophotometer (Isogen Life Science, IJsselstein, The Netherlands). The iScript<sup>TM</sup> cDNA Synthesis Kit (Bio-Rad, Veenendaal, The Netherlands) was used to synthesize cDNA. qPCR was performed using an iCycler CFX384 Touch thermal cycler, and IQ SYBRGreen Super mix (Bio-Rad). Quantitative PCR (qPCR) was performed to assess the effects of rhBMP7 at gene expression levels on: 1) extracellular matrix (ECM) anabolism; *aggrecan (ACAN)*, *collagen type 2 alpha 1 (COL2A1)*, *collagen type 1 alpha 1 (COL1A1)*; 2) proliferation; *cyclin-D1 (CCND1)*; 3) ECM catabolism (*a disintegrin and metalloproteinase with thrombospondin motifs (ADAMTS5)*, *matrix metalloproteinase 13 (MMP13)*, *tissue inhibitor of metalloproteinase 1 (TIMP1)*); 4) apoptotic markers: *B-cell lymphoma 2-associated X (BAX)*, *B-cell lymphoma 2 (BCL2)* and *caspase 3 (CASP3)*; and 5) BMP signaling: *BMP receptor 1A (BMPR1A)*, *BMP receptor 1B (BMPR1B)*, *BMP receptor 2 (BMPR2)*, *inhibitor of DNA binding 1 (ID1)*, *noggin (NOG)* (Supplementary File 1). All dog-specific primers were designed in-house using Perlprimer<sup>25</sup> except for *MMP13*<sup>26</sup>. Primer specificity was evaluated with BLAST, and the designed amplicon was tested for secondary structures using MFold<sup>27</sup>. Primers were purchased from Eurogentec, Maastricht, The Netherlands. Amplification efficiencies ranged from 86% to 119%. Relative expression levels were determined by the efficiency-corrected delta-delta CT ( $\Delta\Delta CT$ ) method. CT values of each target gene were normalized by the mean CT value of 4 reference genes ( $\Delta CT$ ), i.e. *glyceraldehyde 3-phosphate dehydrogenase (GAPDH)*, *ribosomal protein S19 (RPS19)*, *succinate dehydrogenase complex, subunit A, flavoprotein variant (SDHA)*, and *hypoxanthine-guanine phosphoribosyltransferase (HPRT)*, whereas the mean CT of all conditions for each target gene was used as a calibrator ( $\Delta\Delta CT$ ).

### Histopathological evaluation of CLC pellets

Safranin O/Fast Green staining was performed to evaluate the presence of GAG deposition at a histopathological level. Two pellets per donor and condition were fixed overnight in neutral buffered formaldehyde 4% (Boom B.V., Meppel, The Netherlands) supplemented with 1% eosin (115935, Merck, Schiphol-Rijk, The Netherlands). Subsequently, the pellets were first embedded in alginate and thereafter in paraffin. Sections (5  $\mu m$ ) were stained with Mayer's hematoxylin (3870, Avantor Performance Materials, Center Valley, PA), Safranin-O (58884, Sigma-Aldrich) and, as a counterstaining, Fast Green (F7252, Sigma-Aldrich).

### Experimental animals

Seven intact male beagle dogs with a median age of 1.3 years (range 1.1 – 1.8) and a median weight of 11.7 kg (range 10.2 – 12.8) were purchased from Harlan (Gannat, France). All dogs underwent a general, orthopedic, and neurologic examination by a board-certified veterinary surgeon (BM). The study was set up following a randomized block design. Single bolus injections of 2.5, 25, 250  $\mu g$  rhBMP7 (mammalian cell derived, CYT-276, ProSpec-Tany TechnoGene Ltd, Ness-Ziona, Israel), and a sucrose buffer (sham) were injected into the NPs in the T13-S1 spinal segments in a balanced Latin square design. IVDs adjacent to those injected with 250  $\mu g$  of rhBMP7 remained untreated. Preliminary studies in cadaveric spines showed that a volume of 40  $\mu L$  could be injected into the NP without considerable resistance (unpublished data). The highest dosage of rhBMP7 was constrained by the highest possible concentration that could be accomplished via dialysis, i.e. 250  $\mu g$  in 40  $\mu L$ .

### Preparation of rhBMP7 for *in vivo* application

Prior to the *in vivo* studies, the biological activity of rhBMP7 from different manufacturers was determined in an ALP activity assay in ATDC5 cells, amongst them rhBMP7 from R&D and ProSpec-Tany. rhBMP7 from ProSpec-Tany showed highest biological activity and was further chosen to be employed in the *in vivo* studies (Supplementary File 2).

RhBMP7 (CYT-276, ProSpec-Tany TechnoGene Ltd) was reconstituted in 60  $\mu\text{L}$  sterile water. This solution was dialyzed against a buffer solution containing 17% sucrose, 20% mannitol, 332 mM glycine and 0.8% Tween 20, using a slide-A-Lyzer dialysis cassette (66454, Thermo Fisher Scientific Inc., Rockford, IL, USA) with a molecular weight cutoff of 10 kDa overnight with 4 buffer changes. The final solution containing 300  $\mu\text{g}$  of rhBMP7 (calculated amount) was freeze-dried overnight and reconstituted in sterile water, to achieve a final concentration of 250  $\mu\text{g}$  rhBMP7 in 40  $\mu\text{L}$  buffer solution containing 1% sucrose, 1.2% mannitol, 20 mM glycine, and 0.05% Tween 20. Activity of the dialysate was shown to be retained *in vitro* through its capacity to induce ALP production in murine ATDC5 cells (Supplementary File 2).

### Magnetic resonance (MR) imaging

MR images of the lumbar vertebral column were obtained in fully anesthetized dogs prior to surgery ( $t_0$ ) and at 6 ( $t_6$ ), 12 ( $t_{12}$ ), and 24 ( $t_{24}$ ) weeks after surgery. Dogs were pre-medicated with dexmedetomidine 10  $\mu\text{g}/\text{kg}$  intravenously (i.v.) and butorphanol 0.1 mg/kg i.v., and anesthesia was induced with propofol (3-4 mg/kg) continuous rate infusion (c.r.i.) and dexmedetomidine 1  $\mu\text{g}/\text{kg}$  c.r.i. A laryngeal mask was inserted, and anesthesia was maintained with isoflurane (2-3%) in a 1:1 oxygen/air mixture. Prior to the first MRI, a blood sample was drawn from the jugular vein to assess white blood cell count and differentiation, to exclude systemic inflammation. MRI was performed with a 1.5 Tesla scanner using a Spine array coil (Philips Healthcare, Best, The Netherlands). Sagittal T2-weighted (T2W) images were acquired using a turbo-spin echo (TSE) pulse sequence with the following parameters: repetition time (TR) = 2557 ms, echo time (TE) = 100 ms, field of view (FOV) = 200 mm, acquisition matrix = 332 x 306, slice thickness = 2 mm, number of slices = 13. For T2 mapping acquisition parameters were as follows: TR = range 2000 – 4000 ms, TE = 12.5 ms to 100 ms in 12.5 ms increments, FOV = 250 mm, acquisition matrix = 416 x 200, slice thickness = 2 mm, number of slices = 11. Sagittal T1 $\rho$  weighted imaging was performed using a spin-lock-prepared sequence with a 3D multi-shot ultrafast gradient echo (T1-TFE) readout with the following parameters: TR = 8.3 ms, TE = 4.3 ms, FOV = 250 mm, acquisition matrix = 416 x 378, slice thickness = 2 mm, number of slices = 25, TFE factor = 64, flip angle = 10°, shot interval = 2000 ms. To allow quantitative T1 $\rho$  mapping, data were acquired five times, each with a different spin-lock time (TSL); 1, 10, 20, 40 and 80 ms. Spin-lock amplitude was set to 500 Hz.

### T2 and T1 $\rho$ quantification

Mid-sagittal slices of T2W images were used to evaluate the grade of degeneration at all time points. Lumbar IVDs were assessed by a veterinary radiologist that was blinded to treatment allocation, according to the Pfirrmann classification validated for dogs by Bergknut *et al*<sup>28</sup>. Only lumbar IVDs with a Pfirrmann score II at  $t_0$  were included for injection. Disc height index (DHI) was calculated at all time points on T2W images for each IVD according to the method described by Masuda *et al*<sup>15</sup>. In short, DHI was calculated by

averaging widths of the dorsal, middle, and ventral parts of the vertebral disc and dividing that by the average of dorsal, middle, and ventral body heights of the adjacent cranial and caudal vertebrae. To calculate the DHI of L7 – S1, the average body height of only the cranial vertebra (L7) was used, as S1 has a different shape than the lumbar vertebrae. For the analysis of T2 and T1 $\rho$  values, an oval shaped region of interest (ROI) was manually segmented on mid-sagittal sections, to select NP tissue in each IVD in the free open-source DICOM viewer Osirix (Pixmeo, Geneva, Switzerland). ROIs were exported to and analyzed with Wolfram Mathematica 10.0 (Wolfram Research, Champaign, IL, USA). T2 and T1 $\rho$  values were computed by calculating the mean signal intensity (S) in each ROI, and by fitting these intensity data into equations:

$$1) S(\text{TSL}) = S_0 e^{-\text{TSL}/\text{T1}\rho}$$

or

$$2) S(\text{TE}) = S_0 e^{-\text{TE}/\text{T2}}$$

respectively, using the Levenberg-Marquardt nonlinear least-squares method implemented in Mathematica.  $S_0$  denotes the equilibrium magnetization, whereas S(TSL) and S(TE) indicate the T1 $\rho$ - and T2-prepared signals, respectively.

### Surgical procedure

The anesthesia protocol for MR imaging and surgery was identical. Analgesia was provided pre-operatively by methadone 0.5 mg/kg i.v. and carprofen 4 mg/kg i.v., and peri-operatively by a combination of fentanyl (loading dose 10  $\mu\text{g}/\text{kg}$ , 15-20  $\mu\text{g}/\text{kg}/\text{hr}$  continuous rate infusion, c.r.i.) and ketamine (0.5 mg/kg loading dose, 10  $\mu\text{g}/\text{kg}/\text{min}$  c.r.i.). Dogs were positioned in right recumbence to expose and inject T13-L6 via a left lateral approach, and subsequently in ventral recumbence to expose and inject L6-S1 via a dorsal approach. A 100  $\mu\text{L}$  gastight syringe (7656-01 Model 1710 RN) with a 27G needle (25 mm, 12° beveled point; Hamilton Company USA, Reno, Nevada, USA) was used to inject 40  $\mu\text{L}$  of the BMP7 containing solutions or control into the NP under magnified vision (3.3x). Location of the tip of the needle in the NP was estimated by the distance of passage through the annulus fibrosus (AF) (1 cm), while encountering steady resistance. When the NP was reached, the resistance decreased and the volume of 40  $\mu\text{L}$  could be easily injected. The needle was retracted slowly to allow the AF puncture site to close, and the site was inspected for extrusion of the administered compound and rinsed with 0.9% NaCl. Postoperative pain management in all dogs consisted of methadone 0.3 mg/kg intramuscular (i.m.) every (q).6.h. and carprofen 4 mg/kg subcutaneously (s.c.) once a day during the first 24 hours, and tramadol 2-5 mg/kg per os (p.o.) four times a day, and carprofen 4 mg/kg p.o. the following 7 and 10 days, respectively. All dogs were treated postoperatively with antibiotics (amoxicillin/clavulanic acid 12.5 mg/kg twice a day) during 5 days. Dogs were monitored daily throughout the study to assess pain symptoms according to the short form of the Glasgow composite pain scale<sup>29</sup>. Dogs that showed signs of pain, received carprofen and/or tramadol.

### Radiographic imaging and computed tomography (CT)

Radiographs and CT-scans of the T11 – S3 segment were obtained postmortem ( $t_{24}$ ) and were evaluated by an independent veterinary radiologist for new bone formation, end plate sclerosis and disc protrusion (only CT). Lateral and dorsoventral radiographs were obtained with a digital radiography system (Philips digital Rad TH, Eindhoven, The Netherlands) using 50 kVp and 5 mA. Transverse CT images were acquired with a third-generation single-slice helical CT-scanner (Philips Secura, Eindhoven, The Netherlands). Contiguous 2 mm thick slices with 1 mm overlap were obtained from T11 – S3 with exposure settings of 120 kV and 260 mA.

### Sample collection, macroscopic grading, and histopathological grading

Dogs were euthanized 24 weeks post-injection by way of sedation with dexmedetomidine 0.04 mg/kg i.v., followed by pentobarbital 200 mg/kg i.v.. Subsequently, the vertebral column (T12 – S1) was harvested by using an electric multipurpose saw (Bosch, Stuttgart, Germany). All muscles were removed and the lumbar vertebrae were transected transversely with a band saw (EXAKT tape saw, EXAKT Advanced Technologies GmbH, Norderstedt, Germany) resulting in nine spinal units ( $\frac{1}{2}$  vertebra – endplate – IVD – endplate –  $\frac{1}{2}$  vertebra). A diamond band pathology saw (EXAKT 312 saw; EXAKT diamond cutting band 0.1 mm D64; EXAKT Advanced Technologies GmbH, Norderstedt, Germany), was used to transect these units sagittally into two identical parts. From one part, the endplate and vertebra were removed with a surgical knife and the remaining IVD tissue, containing NP and AF, was snap frozen in liquid nitrogen and stored at  $-80^{\circ}\text{C}$  for biochemical and biomolecular analyses. The other part was photographed (Olympus VR-340, Hamburg, Germany) for macroscopic evaluation (Thompson score) and fixed in 50 mL of 4% buffered formaldehyde (Klinipath) at  $4^{\circ}\text{C}$  for 14 days. Images of the IVD segments were evaluated blinded and in random order by two independent blinded investigators according to the Thompson grading scheme, which has been validated in dogs<sup>30</sup>.

Samples were decalcified in 35% formic acid and 6.8% sodium formate in a microwave oven (Milestone Microwave Laboratory Systems, Italy) overnight at  $37^{\circ}\text{C}$ , during 7 nights and embedded in paraffin<sup>31</sup>. Sections ( $5\ \mu\text{m}$ ) were stained with hematoxylin (109249, Merck) and eosin (115935, Merck) and with picosirius red (saturated aqueous picric acid: 36011, Sigma-Aldrich, sirius red: 80115, Klinipath)/alcian blue (alcian blue: 05500, Sigma-Aldrich; glacial acetic acid: 100063, Merck) and evaluated according to a grading scheme according to Bergknut *et al.*<sup>21</sup> Histological sections were scored blinded and in random order by two independent investigators (NW, SP) using an Olympus BX41 microscope. In case of disagreement, samples were also scored by a board-certified veterinary pathologist (GG).

### RNA isolation and qPCR of NP and AF

Cryosections ( $60\ \mu\text{m}$ ) of the IVD of the remaining spinal unit (endplate – IVD) were cut with a cryostat (Leica CM1800 cryostat, Leica Microsystems Inc., Bannockburn, USA) and collected on RNA-se free glass slides. The NP and AF tissues were separated and half of the tissues were collected in  $400\ \mu\text{L}$  and  $750\ \mu\text{L}$  complete lysis M EDTA-free buffer (Roche Diagnostics Nederland B.V., Almere, The Netherlands) respectively, and stored at  $-80^{\circ}\text{C}$  until biochemical analysis. The other halves were collected in  $300\ \mu\text{L}$  RLT buffer containing 1%  $\beta$ -mercapto-ethanol (Qiagen, Venlo, The Netherlands) and stored at  $-80^{\circ}\text{C}$  until biomolecular analysis.

Total RNA was isolated by using the RNeasy Fibrous Tissue Mini Kit (Qiagen, Venlo, The Netherlands). The incubation period with proteinase K was reduced to five minutes to increase RNA yield. RNA quantification and cDNA synthesis were performed in a similar way as described for the CLC pellets *in vitro*. Reference genes and the subset of target genes were similar to those determined *in vitro*.

### GAG, DNA and collagen assays of NP and AF

To measure GAG and DNA content, the NP and AF samples were homogenized in complete lysis M EDTA-free buffer in a TissueLyser II (Qiagen) for 2x 30 s at 20 Hz. The supernatant and pellet of each NP and AF were digested overnight in papain and measurements were performed as described *in vitro*. Collagen was quantified in the pellets of the NP and AF by using a hydroxyproline assay<sup>32</sup>. Samples were freeze-dried overnight, hydrolyzed at 108 °C overnight in 4M NaOH, centrifuged (15 s, 14000 g) and stored at -20 °C. Prior to measurements, samples were centrifuged (15 s, 14000 g) once more, chloramine T reagent (2426, Merck) was added and samples were allowed to shake for 20 min at 170 rpm. Freshly prepared dimethylaminobenzaldehyde (3058 Merck) was added, and samples were incubated for 20 minutes at 60°C. The absorbance was read at 570nm and collagen content was calculated from the hydroxyproline content by multiplying with a factor 7.5<sup>32</sup>. DNA and collagen content in the supernatants were negligible and therefore not included in the calculations. Total GAG and collagen content were normalized to DNA content in the sample.

### Statistical analyses

All data were analyzed by using R statistical software, package 3.0.2<sup>33</sup>. Residual plots and quantile-quantile (Q-Q)-plots were used to check normality of the data. In case of violation, data were logarithmically transformed. If non-normality remained after transformation, nonparametric tests were employed. *In vitro*, cumulative GAG release, GAG and DNA content, the GAG/DNA ratio and  $\Delta$ CT values for the investigated target genes, were statistically evaluated by using the nonparametric Kruskal-Wallis test, followed by a Mann-Whitney U-test. The effect of the injected treatments *in vivo* on GAG, DNA and collagen content, DHI, and T1p and T2 values was analyzed with a linear mixed effect model. A random effect 'dog' (dog 1-7), was incorporated to capture the correlation between multiple measurements within one dog. For GAG, DNA and collagen analysis, factors incorporated into the model as a fixed effect were 'treatment' (2.5  $\mu$ g rhBMP7, 25  $\mu$ g rhBMP7, 250  $\mu$ g rhBMP7, and sham), 'tissue' (NP and AF), and their interaction. For DHI analysis 'treatment', 'time' ( $t_0$ ,  $t_6$ ,  $t_{12}$ , and  $t_{24}$ ), and their interaction served as fixed effect factors. The Cox proportional hazards regression model was used to estimate the effect of the injected treatments on gene expression levels *in vivo*. Calculations were performed on the ratio of the CT values for each target gene to the mean CT value of the reference genes. CT values  $\geq 40$  were right censored. Regression coefficients were estimated by the maximum likelihood method. Model selection was based on the lowest Akaike Information Criteria (AIC). Differences between treatments were considered significant if the confidence interval did not include 0, whereas hazard ratios were considered significant if the confidence interval did not include 1. For *in vitro* and *in vivo* analyses, confidence intervals were calculated and stated at the 99% confidence level to correct for multiple comparisons. Significant differences and the corresponding confidence intervals are represented in Supplementary File 3.

## Results

### Effect of rhBMP7 on early degenerated canine CLC pellets *in vitro*

#### Cell maintenance and increased GAG release and content by rhBMP7

CLC pellets treated with 10 and 100 ng/mL rhBMP7 showed a dose-dependent significant increase in cumulative GAG release into the medium compared with the negative control (Figure 1a). Regardless of the culture condition, DNA content of the CLC pellets was significantly lower compared with DNA content at day 0. Treatment with 100 ng/mL rhBMP7 resulted in a significantly higher DNA content at day 28 compared with the negative control and the 10 ng/mL rhBMP7 treated CLC pellets (Figure 1b). A significant increase in GAG content and GAG/DNA at day 28 was shown in the rhBMP7 100 ng/mL treated CLC pellets compared with the negative control and the 10 ng/mL rhBMP7 treated CLC pellets. Safranin-O/Fast green staining of the CLC pellets at day 28 showed a higher GAG deposition in the matrix of the pellets treated with 100 ng/mL rhBMP7 compared with the negative control and the 10 ng/mL rhBMP7 treated pellets (Figure 2).

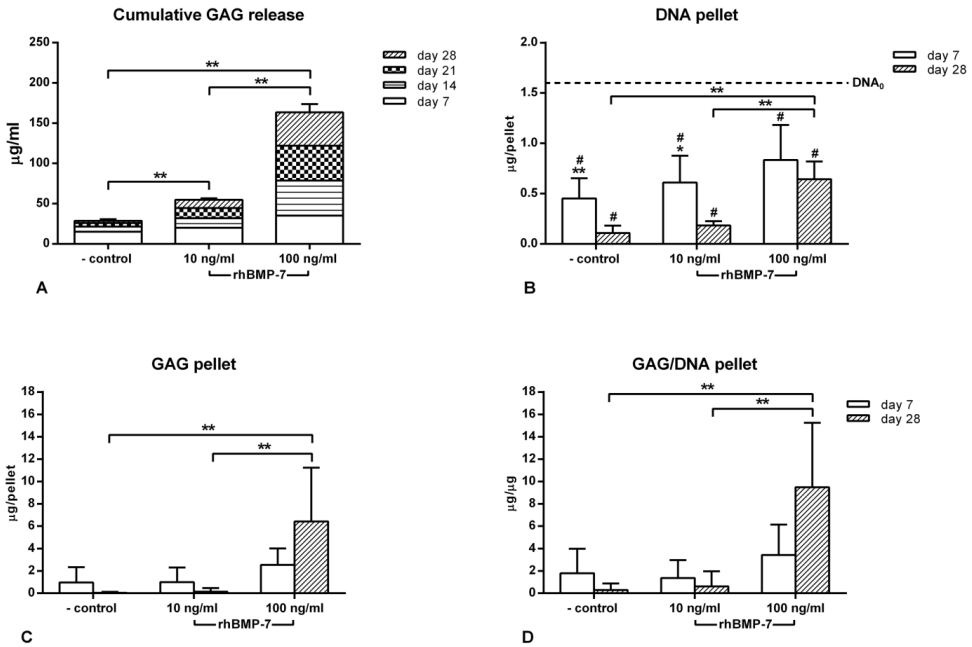


**Figure 1. GAG release, GAG, DNA and GAG/DNA content in cultured nucleus pulposus cells (CLCs) treated with 10 or 100 ng/mL rhBMP7.** (a) CLC pellets treated with rhBMP7 show a significant dose-dependent increase in cumulative GAG release into the medium compared with the negative control. (b) Regardless of the culture condition, DNA content of the CLC pellets was significantly lower compared with DNA content at day 0 ( $DNA_0$ ; dashed line), indicated by #. CLC pellets treated with 100 ng/mL rhBMP7 showed a significantly higher DNA content at day 28 compared with the negative control and the 10 ng/mL rhBMP7 treated CLC pellets. (c, d) A significant increase in GAG content and GAG/DNA at day 28 was shown in the rhBMP7 100 ng/mL treated CLC pellets compared with the negative control and the 10 ng/mL rhBMP7 treated CLC pellets. Data are expressed as mean + SD. \*\*: significant difference at a 99% confidence interval (CI); #: significant difference at a 98% CI

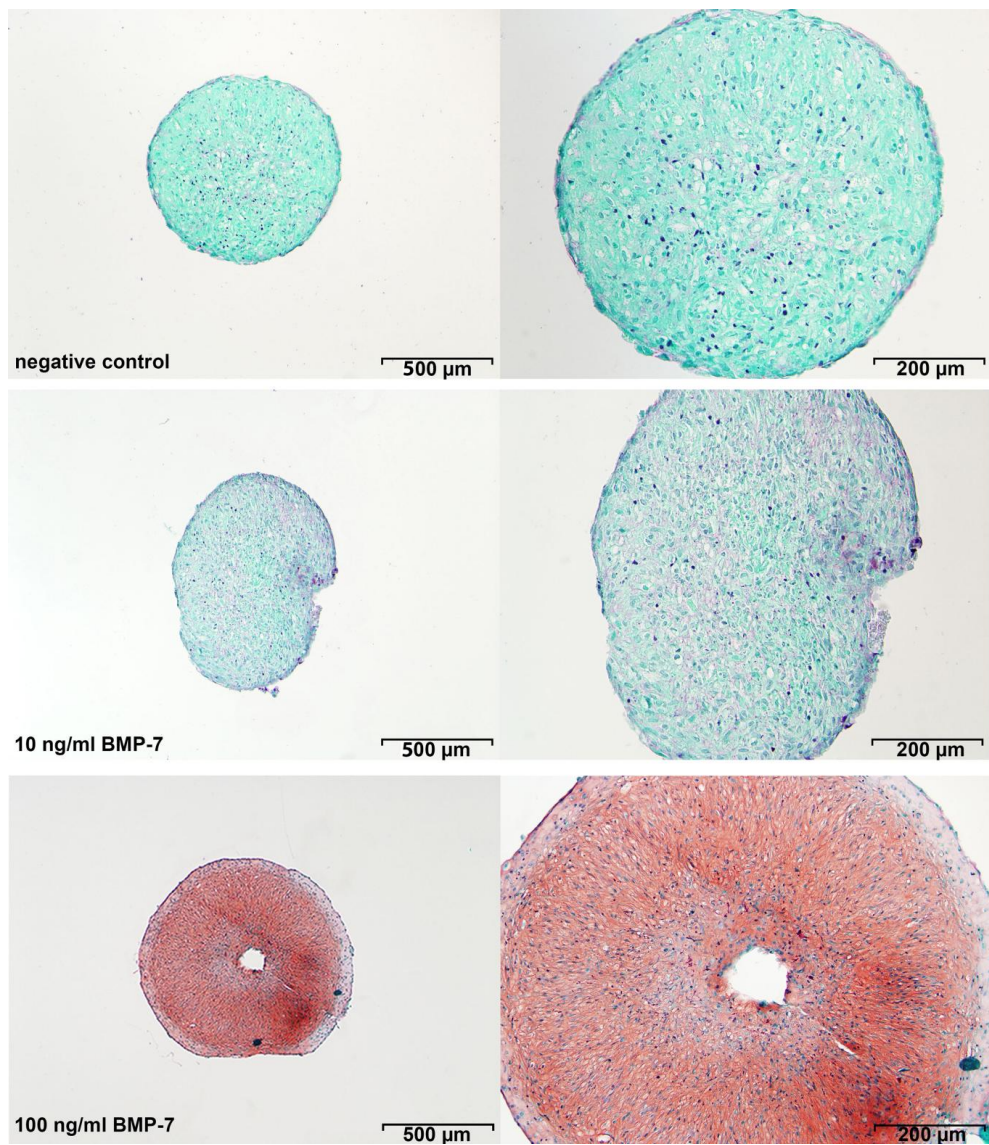


**Figure 2. Representative histological images of nucleus pulposus cells (CLCs) cultured in pellets for 28 days stained with Safranin O/Fast Green.** CLC pellets treated with 100 ng/mL rhBMP7 showed a positive Safranin-O/Fast green staining for GAGs and an increased size compared with the negative control and the 10 ng/mL rhBMP7-treated pellets.

*Pro-anabolic and anti-apoptotic effect of rhBMP7*

Expression of ECM genes *ACAN* and *COL2A1* was significantly upregulated at day 7 in the 100 ng/mL rhBMP7-treated CLC pellets compared with the negative control and the 10 ng/mL rhBMP7 treated CLC pellets (Figure 3a). *COL2A1* expression was significantly upregulated in the 100 ng/mL rhBMP7 treated CLC pellets compared with the negative control at day 28. Expression of *COL1A1* did not differ between conditions at any of the time points. Relative expression of the proliferative marker *CCND1* was significantly upregulated in all conditions at day 28 compared with day 7, while it was also significantly higher in the 100 ng/mL rhBMP7 treated CLC pellets at day 7 compared with the negative control. Furthermore, *CCND1* expression levels were significantly higher in the CLC pellets treated with 10 ng/mL rhBMP7 at day 28 compared with the negative control.

Gene expression of the catabolic gene *ADAMTS5* was significantly lower in the 100 ng/mL rhBMP7 treated CLC pellets compared with the 10 ng/mL rhBMP7 treated CLC pellets at day 28 (Figure 3b). In the CLC pellets treated with 10 and 100 ng/mL rhBMP7, gene expression of the catabolic gene *MMP13* was significantly lower at day 28 compared with day 7. The relative gene expression of the anti-catabolic gene *TIMP1* was significantly higher in the negative control and 10 ng/mL rhBMP7 treated CLC pellets at day 7 compared with day 28. The *BAX/BCL2* ratio in the 100 ng/mL rhBMP7 treated CLC pellets was significantly higher at day 28 compared with day 7 (Figure 3c). Relative expression of the apoptotic marker *CASP3* was significantly downregulated at day 28 in the 10 and 100 ng/mL rhBMP7 treated CLC pellets. Altogether, these results show a stimulatory effect of 100 ng/mL rhBMP7 on matrix anabolism, that seemed most profound at day 7, and an anti-apoptotic effect, most profound at day 28.

**Intradiscal application of rhBMP7 in laboratory Beagle dogs***No regenerative changes of rhBMP7 at IVD level on macroscopy and T2W MR images*

All dogs recovered uneventfully from surgery and were ambulant the next day. During follow-up all dogs were treated with analgesics and antibiotics in accordance with the protocol described under 'surgical procedure', and none of the dogs required additional medication. Before surgery a total of 63 IVDs were graded on T2W MR images ( $t_0$ ). 62/63 IVDs were assigned a grade II according to the Pfirrmann system, whereas 1 IVD was assigned a grade III. A total of 42 grade II IVDs were injected. In 61/63 IVDs, the Pfirrmann scores remained unchanged over time. The IVD that was assigned a grade III at  $t_0$ , was assigned a grade II at all subsequent time points, and 1 IVD, treated with the sucrose buffer, that was scored a grade II at  $t_0$ , was re-graded a Pfirrmann score III. *Postmortem*, 62/63 IVDs were assigned a Thompson score grade II, consistent with early IVD degeneration, whereas 1 IVD, treated with 250  $\mu$ g rhBMP7, was assigned a grade IV.

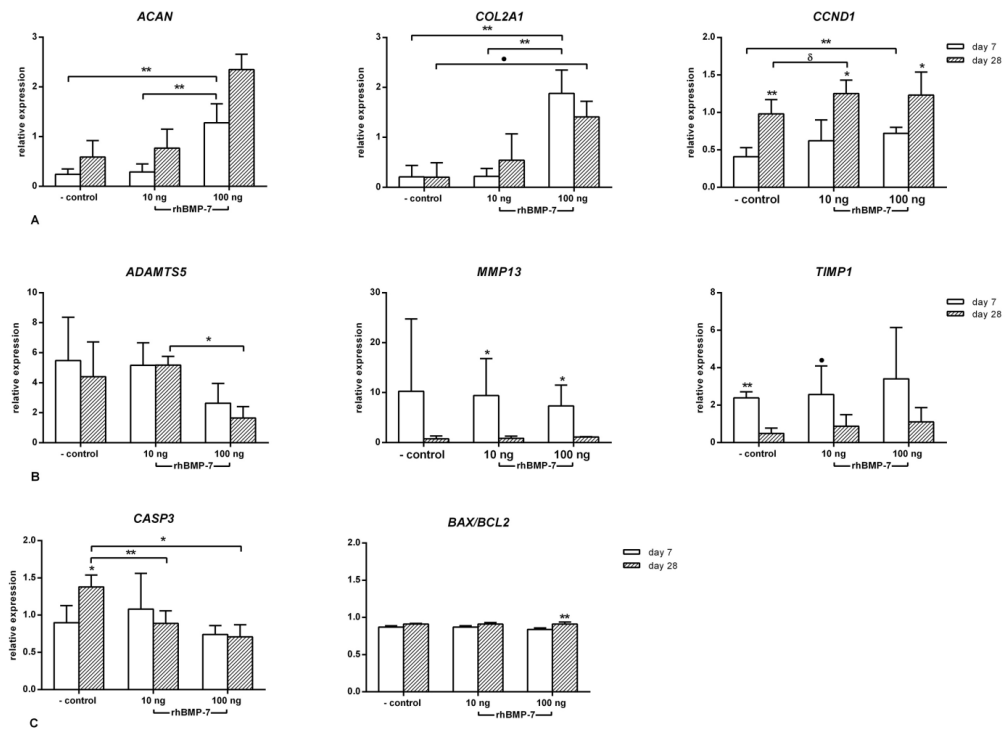


**Figure 3. Relative gene expression of relevant target genes in nucleus pulposus cells (CLCs) cultured in pellets at day 7 and 28.** (a) Anabolic markers: aggrecan (*ACAN*), collagen type 2 alpha 1 (*COL2A1*), cyclin-D1 (*CCND1*); (b) Catabolic markers: a disintegrin and metalloproteinase with thrombospondin motifs 5 (*ADAMTS5*), matrix metalloproteinase 13 (*MMP13*), tissue inhibitor of metalloproteinase 1 (*TIMP1*); (c) apoptotic markers: caspase 3 (*CASP3*), B-cell lymphoma 2-associated X (*BAX*), and B-cell lymphoma 2 (*BCL2*) in non-treated (negative control) and 10 and 100 ng/mL rhBMP7 treated CLC pellets. Data are expressed as relative expression + SD, except for the *BAX/BCL2* ratio. \*\*: significant difference at a 99% confidence interval (CI); \*: significant difference at a 98% CI;  $\delta$ : significant difference at a 97% CI;  $\bullet$ : significant difference at a 96% CI.

#### *Extradiscal new bone formation after intradiscal injection of 25 and 250 $\mu$ g rhBMP7*

In 1/63 IVDs, extensive new bone formation was noted on the ventral aspect on MRI at 6, 12 and 24 weeks post-surgery ( $t_6$ ,  $t_{12}$ , and  $t_{24}$ ). Ventral bone formation was noted on macroscopy *postmortem* in this particular IVD and in another (2/63 IVDs). The IVD that was scored a Thompson grade IV showed rupturing of the dorsal AF, with NP material extending into the spinal canal, irregularity of the endplates, and focal sclerosis in the subchondral bone (Figure 4). CT images of this dog showed symmetric extensive bulging of the L7-S1 IVD (lumbosacral junction) that had been injected. In 4/63 IVDs, radiographs and CT images revealed marginated extradiscal new bone formation ventrally, laterally (left) and ventrolaterally (right side) in combination with mild sclerosis of the underlying bone *postmortem* (Figure 4). In 3/42 IVDs these findings were associated with treatment with 250  $\mu$ g rhBMP7, in 1/42 with 25  $\mu$ g rhBMP7. In 2/63 IVDs mineralization was shown on CT images; one of these IVDs had been injected with 2.5  $\mu$ g rhBMP7, whereas the other one had not been injected. DHI, T2-values, as well as T1 $\rho$ -values did not show significant differences between treatments over time.

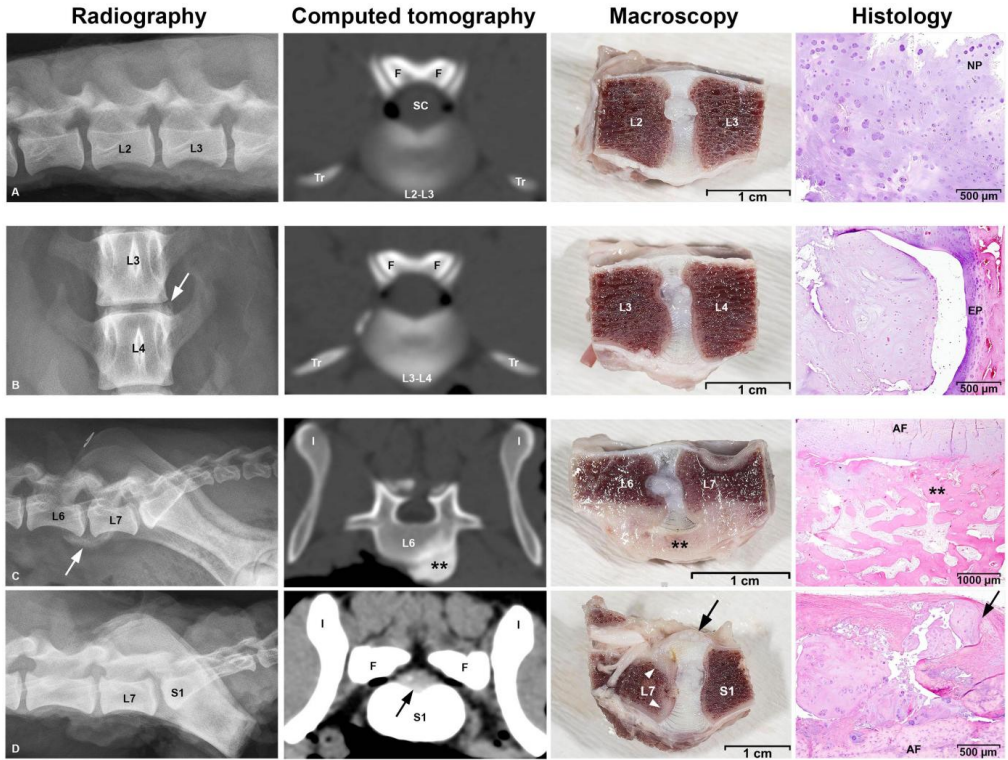


**Figure 4. Extradiscal bone formation after intradiscal injection of rhBMP7.** Radiography, computed tomography (CT), macroscopy, and histology of intervertebral discs (IVDs) injected with 2.5 µg (a), 25 µg (b), and 250 µg (c, d) rhBMP7. (a) Unremarkable findings after injecting 2.5 µg rhBMP7 into the intervertebral disc (IVD). The histological image shows a typical example of an early degenerated NP, consisting of clusters of chondrocyte-like cells. (b) On the left lateral site of the vertebral column extradiscal new bone formation is shown on the radiograph and CT image (*white arrow*) next to the IVD injected with 25 µg rhBMP7. Histology was consistent with early degenerative changes in the IVD as shown in A. (c) Extradiscal new bone formation ventrally of the vertebral column and sclerosis of the ventral vertebral cortex is shown on radiography (*white arrow*), CT, macroscopy and histology (*double asterisk*) after injecting 250 µg rhBMP7 into the IVD. (d) Rupturing of the dorsal AF, and protrusion of NP material into the spinal canal (*black arrow*) on CT, macroscopy and histology image of an IVD injected with 250 µg rhBMP7. Irregularity of the endplates, and focal sclerosis in the subchondral bone (*white arrowheads*) was seen on macroscopy and confirmed on histology (*not shown in this image*). L=lumbar vertebra, F=facet joint, SC=spinal cord, Tr=transverse process, I=ilium, NP=nucleus pulposus, EP=endplate, AF=annulus fibrosus, S=sacral vertebra

### Anti-apoptotic effect of 250 $\mu$ g rhBMP7

All IVDs were evaluated histopathologically according to the grading scheme according to Bergknut *et al*<sup>21</sup>. The median histological grade was 13 (range: 8 – 20) and there were no significant differences between the treatments. In the IVD treated with 250  $\mu$ g rhBMP7 that was scored a Thompson grade IV, NP material and fibroblasts were present in the outer AF. Furthermore, in two IVDs treated with 250  $\mu$ g rhBMP7, bone formation was confirmed. The *BAX/BCL2* ratio in the IVDs (NP and AF) treated with 250  $\mu$ g rhBMP7 were significantly upregulated compared with the IVDs (NP and AF) treated with the sham and 25  $\mu$ g rhBMP7, suggestive of an anti-apoptotic effect of 250  $\mu$ g rhBMP7. Relative gene expression of *CASP3* in the NP was significantly higher than in the AF in all treatments, indicative of a higher apoptotic rate in the NP (Figure 5).

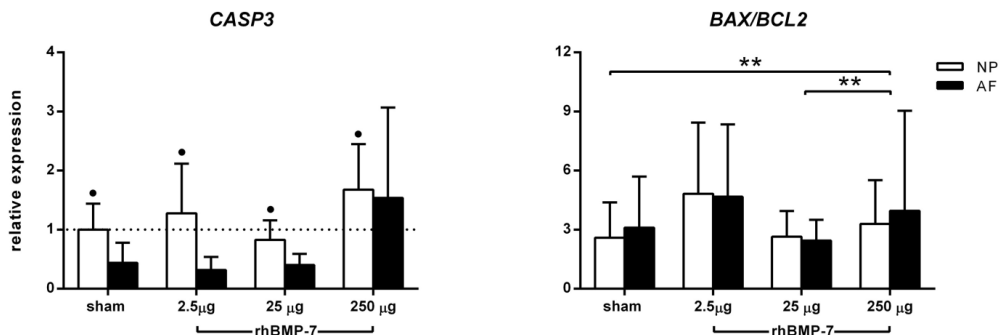


**Figure 5. Relative gene expression of genes associated with apoptosis.** Relative gene expression of caspase 3 (*CASP3*), B-cell lymphoma 2-associated X (*BAX*)/B-cell lymphoma 2 (*BAX/BCL2*) ratio in the nucleus pulposus (NP) (open bars) and the annulus fibrosus (AF) (filled bars) injected with a sucrose buffer (sham), 2.5, 25, or 250  $\mu$ g rhBMP7, were indicative of an anti-apoptotic effect of 250  $\mu$ g rhBMP7. The sham treated NP was used as a reference, and was set at 1 (dashed line). Data are expressed as n-fold change + SD. \*\*: significant difference at a 99% confidence interval (CI); •: significant difference at a 96% CI.

### No anabolic effects of rhBMP7 on extracellular matrix

No significant differences in GAG corrected for DNA, nor in collagen corrected for DNA were found between the treatments in the NP or the AF (Figure 6a). Regardless of the treatment, GAG/DNA in the NP was significantly higher than in the AF, consistent with the known physiological differences in matrix composition at protein level between the NP and the AF. These physiological differences were also reflected by relative gene expression, as gene expression levels of *COL2A1* were significantly higher in the NP than in the AF, and the expression levels of *COL1A1* were significantly lower in the NP than in the AF (Figure 6b). Relative gene expression of anabolic (*ACAN*, *COL2A1*, *COL1A1*), catabolic (*MMP13*) and anti-catabolic (*TIMP1*) genes did not significantly differ between treatments. Gene expression of *ADAMT5*, and BMP receptors *BMPR1A*, and *BMPR1B* were below the detection level in both the NP and the AF, independent of treatment. BMP7 receptor *BMPR2*, and the downstream target of the BMP7 signaling pathway gene *ID1*, did not significantly differ between the treatments. Relative gene expression of BMP signaling inhibitor *NOG* varied a lot regardless of the groups and was significantly higher in IVDs treated with 25  $\mu$ g compared with 2.5  $\mu$ g and sham treated IVDs (Supplementary File 4).

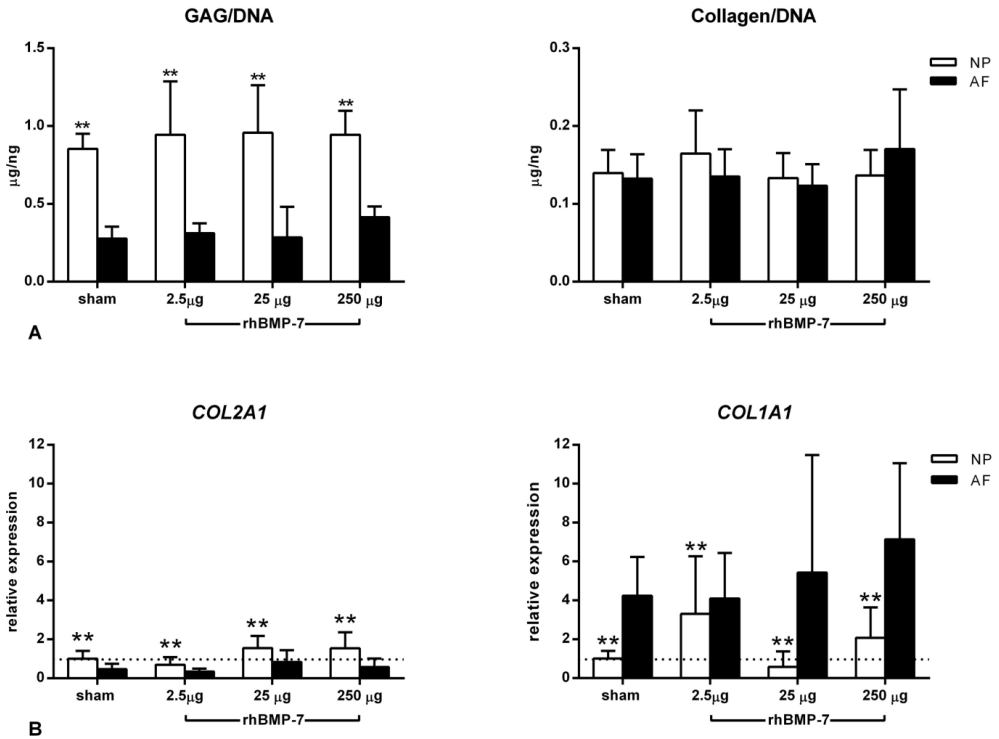


**Figure 6. Relative gene expression of matrix-related target genes and DNA, GAG, and collagen content in IVDs injected with rhBMP7.** (a) GAG/DNA and collagen/DNA did not significantly differ between the treatments. GAG/DNA in the nucleus pulposus (NP) (open bars) was significantly higher than in the annulus fibrosus (AF) (filled bars). (b) Relative gene expression of *collagen type 2 alpha 1 (COL2A1)* and collagen type 1 alpha 1 (*COL1A1*) did not significantly differ between treatments. Gene expression levels of *COL2A1* were significantly higher in the NP than in the AF, whereas the expression levels of *COL1A1* were significantly lower in the NP than in the AF. GAG/DNA and collagen/DNA are expressed as mean + SD, and *COL2A1* and *COL1A1* as relative expression + SD. \*\*: significant difference at a 99% confidence interval (CI).

## Discussion

In this study we first showed that 100 ng/mL rhBMP7 was biologically active in canine CLCs from mildly, spontaneously degenerated IVDs *in vitro*. Treatment with 100 ng/mL rhBMP7 stimulated matrix production by canine CLC pellets isolated from degenerated discs, reflected by a significant higher expression of *ACAN* and *COL2A1* seen at day 7 and a significant increase in GAG release and deposition mainly seen at day 28 of culture. Treatment with 10 ng/mL rhBMP7 showed a significant increase in GAG release compared with the negative control, but did not result in increased GAG deposition. This is most likely due to a suboptimal balance in GAG and collagen synthesis and breakdown, resulting in the inability to deposit GAGs in a newly formed collagen network. During pellet culture, in the absence of rhBMP7, DNA content decreased significantly over time. CLC pellets treated with rhBMP7 showed preservation of the DNA content at initial levels, with a significant upregulation of the biomolecular proliferative marker *CCND1* limited to day 7, and a significant downregulation of the pro-apoptotic marker *CASP3* and an increase of the

*BAX/BCL2* ratio at day 28. Our findings are consistent with the pro-anabolic and anti-apoptotic properties of rhBMP7 that have been shown *in vitro* in NP cells of different species, *i.e.* bovine, rabbit, human<sup>8, 12, 13, 34, 35</sup>.

Next, we aimed at determining the safe and optimal regenerative dose of rhBMP7 for intradiscal application in a spontaneous canine disc degeneration model. However, intradiscal injection of a wide dose range of rhBMP7 (2.5 – 250 µg) did not result in regeneration of the canine IVD. In contrast to what has been described in rabbit models, extracellular matrix production in the NP and the AF did not differ between treatments. It should be noted that our data analysis is limited by the absence of wet weight data of the samples and that the necessary correction for DNA content might have leveled out the effects between treatments. However, disc height index, T2, and T1p maps and histological grading did not differ between treatments confirming the biochemical data and hence corroborating the absence of a regenerative effect after intradiscal application of a wide range of dosages of rhBMP7.

Contrasting findings between the current canine model based on spontaneous degeneration and the healthy or rabbit models of induced IVD degeneration, are most likely related to differences in disc size and cell types that populate the NP. Cell type variation related to differences in genetic background may play a role, with a concomitant difference in degenerative, as well as regenerative pathways. Notochordal cells (NCs) are thought to play a key role in regeneration<sup>36</sup>. In rabbits, NCs are retained in the NP at least until 12 months of age, while in humans NCs are lost before 4-10 years of age, and in chondrodystrophic dogs, *e.g.* Beagles, before 1 year of age<sup>37</sup>. Although induction of rabbit IVD degeneration by trauma is accompanied by an inflammatory response, and ultimately results in decreased amounts of extracellular matrix, a clear loss in disc height, and replacement of notochordal cells by chondrocyte-like and fibroblast-like cells, persistence of notochordal cells cannot be ruled out.

Nevertheless, early degenerated canine CLCs in culture respond in a similar way to rhBMP7 as rabbit NP cells, also suggestive of differences in rhBMP7 activity *in vitro* and *in vivo* in the canine model. The anabolic and anti-apoptotic effect of rhBMP7 on the tissue cells is mediated via specific BMP receptors that activate the intracellular signaling protein Smad1/5/8. The latter then forms a complex with Smad4, and the complex translocates into the nucleus and regulates transcription of target genes. BMP7 in addition, upregulates natural BMP antagonists, *e.g.* *NOG*, that block the binding sites of the BMP receptors, thereby bringing rhBMP7 in an inactive state<sup>38</sup>. Relative gene expression of *NOG* was significantly upregulated in IVDs treated with 25 µg vs 2.5 µg and sham treated IVDs, indicating that BMP antagonists may indeed play a role in the regulation of *in vivo* BMP7 signaling. Given that the BMP signaling pathway is complicated, we can only speculate on the possible confounding effects limiting the biological effect of rhBMP7 *in vivo* after 6 months follow-up, including availability of BMP receptors, activity of *NOG*, and the presence and ability of proteases in the degenerated IVD to degrade rhBMP7. Another explanation for the differences *in vitro* and *in vivo*, was the addition of rhBMP7 biweekly *in vitro*, while a single dose was applied intradiscally *in vivo*. Protein activity *in vivo* is likely to be lost quickly, due to a short biological half-life and by diffusion out of the tissue<sup>39</sup>. The bioavailability of rhBMP7 *in vivo* could be increased by using controlled-release systems, *e.g.* hydrogels or

microspheres, that allow a sustained release of rhBMP7 over a prolonged period of time, or by vector-mediated introduction of BMP7 encoding genes.

Strikingly, mild to severe extradiscal new bone formation was seen after intradiscal administration of 25 µg and 250 µg rhBMP7 in our canine model. Induction of bone formation requires three essential components: an osteo-inductive signal, a substratum and interactive host cells. The surgical procedure, associated with tissue injury, might have provided the chemotactic stimulus for the recruitment of required mesenchymal precursor cells. The application of rhBMP7 might have provided the osteo-inductive stimulus for chondro-osteogenic differentiation, resulting in ectopic bone formation. Although suboptimal delivery of BMP7 by our injection technique might have played a role, the rhBMP7 might also have diffused out of the NP. This phenomenon was also described previously in a rabbit model in which osteophyte formation was induced by intradiscal injection of labelled mesenchymal stem cells<sup>40</sup>. Diffusion of rhBMP7 out of the IVD may have been enhanced by biomechanical forces and/or disorganization of the lamellar structure of the AF that are part of the early IVD degeneration process<sup>2</sup>. Various dosages of rhBMP7, ranging from 0.005 µg – 2 mg, with or without a carrier, have been reported to induce endochondral bone formation in extraskeletal sites (muscle, subcutis, tendon, thyroid cartilage, and subdural space) and in several species, *e.g.* baboons, rats, and dogs<sup>6, 41-44</sup>. In all these studies, the microenvironment appeared to be an essential component in tissue regeneration. Indeed, in humans rhBMP7 is approved for the treatment of non-unions of long bones and the pelvis, and posterior lumbar fusion<sup>45</sup>. rhBMP7 is frequently used in man, however, adverse effects, such as ectopic bone formation, are only occasionally reported<sup>45-47</sup>. Based on statements of researchers in reviews from 2008 and 2011, a multicenter clinical trial in the U.S. was started, in which BMP7 was intradiscally injected into human patients with degenerative disc disease<sup>48, 49</sup>. However, thus far, results have not been published.

## Conclusions

An anabolic effect of rhBMP7 on extracellular matrix production of canine CLCs isolated from early degenerated IVDs was shown *in vitro*. Despite intradiscal administration of a wide dose range of rhBMP7 (2.5 – 250µg) in spontaneously early degenerated canine IVDs, we did not observe regenerative effects at the IVD level. In fact, injection of 250 µg rhBMP7, and to a lesser extent 25 µg rhBMP7, resulted in extensive extradiscal bone formation. Altogether, this study indicates that additional issues need to be addressed before intradiscally applied rhBMP7 can be translated into a clinical application to treat low back pain in human and canine patients.

## Acknowledgements

The authors would like to acknowledge the help of Greet Bouwman with obtaining the MR images, Hans Vernooij with the statistical analyses, and the assistance of Lucy Verdonschot and Bianca Kuster in cell culture studies.

## References

1. Freburger JK, Holmes GM, Agans RP, et al. 2009. The rising prevalence of chronic low back pain. *Arch Intern Med* 169: 251-258.
2. Adams MA, Roughley PJ. 2006. What is intervertebral disc degeneration, and what causes it? *Spine (Phila Pa 1976)* 31: 2151-2161.
3. Luoma K, Riihimäki H, Luukkonen R, et al. 2000. Low back pain in relation to lumbar disc degeneration. *Spine (Phila Pa 1976)* 25: 487-492.
4. Than KD, Rahman SU, Vanaman MJ, et al. 2012. Bone morphogenetic proteins and degenerative disk disease. *Neurosurgery* 70: 996-1002; discussion 1002.
5. Reddi AH. 1994. Bone and cartilage differentiation. *Curr Opin Genet Dev* 4: 737-744.
6. Katic V, Majstorovic L, Maticic D, et al. 2000. Biological repair of thyroid cartilage defects by osteogenic protein-1 (bone morphogenetic protein-7) in dog. *Growth Factors* 17: 221-232.
7. Kawakami M, Matsumoto T, Hashizume H, et al. 2005. Osteogenic protein-1 (osteogenic protein-1/bone morphogenetic protein-7) inhibits degeneration and pain-related behavior induced by chronically compressed nucleus pulposus in the rat. *Spine (Phila Pa 1976)* 30: 1933-1939.
8. Masuda K, Takegami K, An H, et al. 2003. Recombinant osteogenic protein-1 upregulates extracellular matrix metabolism by rabbit annulus fibrosus and nucleus pulposus cells cultured in alginate beads. *J Orthop Res* 21: 922-930.
9. Chen P, Vukicevic S, Sampath TK, Luyten FP. 1993. Bovine articular chondrocytes do not undergo hypertrophy when cultured in the presence of serum and osteogenic protein-1. *Biochem Biophys Res Commun* 197: 1253-1259.
10. Chubinskaya S, Kuettner KE. 2003. Regulation of osteogenic proteins by chondrocytes. *Int J Biochem Cell Biol* 35: 1323-1340.
11. Flechtenmacher J, Huch K, Thonar EJ, et al. 1996. Recombinant human osteogenic protein 1 is a potent stimulator of the synthesis of cartilage proteoglycans and collagens by human articular chondrocytes. *Arthritis Rheum* 39: 1896-1904.
12. Imai Y, Miyamoto K, An HS, et al. 2007. Recombinant human osteogenic protein-1 upregulates proteoglycan metabolism of human anulus fibrosus and nucleus pulposus cells. *Spine (Phila Pa 1976)* 32: 1303-9; discussion 1310.
13. Wei A, Brisby H, Chung SA, Diwan AD. 2008. Bone morphogenetic protein-7 protects human intervertebral disc cells in vitro from apoptosis. *Spine J* 8: 466-474.
14. Alini M, Eisenstein SM, Ito K, et al. 2008. Are animal models useful for studying human disc disorders/degeneration? *Eur Spine J* 17: 2-19.
15. Masuda K, Imai Y, Okuma M, et al. 2006. Osteogenic protein-1 injection into a degenerated disc induces the restoration of disc height and structural changes in the rabbit anular puncture model. *Spine (Phila Pa 1976)* 31: 742-754.
16. An HS, Takegami K, Kamada H, et al. 2005. Intradiscal administration of osteogenic protein-1 increases intervertebral disc height and proteoglycan content in the nucleus pulposus in normal adolescent rabbits. *Spine (Phila Pa 1976)* 30: 25-31; discussion 31-2.
17. Chubinskaya S, Kawakami M, Rappoport L, et al. 2007. Anti-catabolic effect of OP-1 in chronically compressed intervertebral discs. *J Orthop Res* 25: 517-530.
18. Chaofeng W, Chao Z, Deli W, et al. 2013. Nucleus pulposus cells expressing hBMP7 can prevent the degeneration of allogenic IVD in a canine transplantation model. *J Orthop Res* 31: 1366-1373.
19. Harwood PJ, Giannoudis PV. 2005. Application of bone morphogenetic proteins in orthopedic practice: Their efficacy and side effects. *Expert Opin Drug Saf* 4: 75-89.
20. Bergknut N, Rutges JP, Kranenburg HC, et al. 2012. The dog as an animal model for intervertebral disc degeneration? *Spine (Phila Pa 1976)* 37: 351-358.
21. Bergknut N, Meij BP, Hagman R, et al. 2013. Intervertebral disc disease in dogs - part 1: A new histological grading scheme for classification of intervertebral disc degeneration in dogs. *Vet J* 195: 156-163.
22. Johannessen W, Auerbach JD, Wheaton AJ, et al. 2006. Assessment of human disc degeneration and proteoglycan content using T1rho-weighted magnetic resonance imaging. *Spine (Phila Pa 1976)* 31: 1253-1257.
23. Marinelli NL, Houghton VM, Munoz A, Anderson PA. 2009. T2 relaxation times of intervertebral disc tissue correlated with water content and proteoglycan content. *Spine (Phila Pa 1976)* 34: 520-524.
24. Farndale RW, Sayers CA, Barrett AJ. 1982. A direct spectrophotometric microassay for sulfated glycosaminoglycans in cartilage cultures. *Connect Tissue Res* 9: 247-248.
25. Marshall OJ. 2004. PerlPrimer: Cross-platform, graphical primer design for standard, bisulphite and real-time PCR. *Bioinformatics* 20: 2471-2472.
26. Muir P, Danova NA, Argyle DJ, Manley PA, Hao Z. 2005. Collagenolytic protease expression in cranial cruciate ligament and stifle synovial fluid in dogs with cranial cruciate ligament rupture. *Vet Surg* 34: 482-490.
27. Zuker M. 2003. Mfold web server for nucleic acid folding and hybridization prediction. *Nucleic Acids Res* 31: 3406-3415.
28. Bergknut N, Auriemma E, Wijsman S, et al. 2011. Evaluation of intervertebral disk degeneration in chondrodystrophic and nonchondrodystrophic dogs by use of pfirrmann grading of images obtained with low-field magnetic resonance imaging. *Am J Vet Res* 72: 893-898.
29. Murrell JC, Psatha EP, Scott EM, Reid J, Hellebrekers LJ. 2008. Application of a modified form of the glasgow pain scale in a veterinary teaching centre in the netherlands. *Vet Rec* 162: 403-408.

30. Bergknut N, Grinwis G, Pickee E, et al. 2011. Reliability of macroscopic grading of intervertebral disk degeneration in dogs by use of the thompson system and comparison with low-field magnetic resonance imaging findings. *Am J Vet Res* 72: 899-904.
31. Kristensen HK. 1948. An improved method of decalcification. *Stain Technol* 23: 151-154.
32. Neuman RE, Logan MA. 1950. The determination of hydroxyproline. *J Biol Chem* 184: 299-306.
33. The R Project for Statistical Computing. Vienna, Austria: The R Foundation for Statistical Computing.
34. Zhang Y, Phillips FM, Thonar EJ, et al. 2008. Cell therapy using articular chondrocytes overexpressing BMP7 or BMP-10 in a rabbit disc organ culture model. *Spine (Phila Pa 1976)* 33: 831-838.
35. Zhang Y, An HS, Toofanfard M, et al. 2005. Low-dose interleukin-1 partially counteracts osteogenic protein-1-induced proteoglycan synthesis by adult bovine intervertebral disk cells. *Am J Phys Med Rehabil* 84: 322-329.
36. Erwin WM, Islam D, Inman RD, Fehlings MG, Tsui FW. 2011. Notochordal cells protect nucleus pulposus cells from degradation and apoptosis: Implications for the mechanisms of intervertebral disc degeneration. *Arthritis Res Ther* 13: R215.
37. Hunter CJ, Matyas JR, Duncan NA. 2004. Cytomorphology of notochordal and chondrocytic cells from the nucleus pulposus: A species comparison. *J Anat* 205: 357-362.
38. Groppa J, Greenwald J, Wiater E, et al. 2003. Structural basis of BMP signaling inhibition by noggin, a novel twelve-membered cysteine knot protein. *J Bone Joint Surg Am* 85-A Suppl 3: 52-58.
39. Luginbuehl V, Meinel L, Merkle HP, Gander B. 2004. Localized delivery of growth factors for bone repair. *Eur J Pharm Biopharm* 58: 197-208.
40. Vadala G, Sowa G, Hubert M, et al. 2012. Mesenchymal stem cells injection in degenerated intervertebral disc: Cell leakage may induce osteophyte formation. *J Tissue Eng Regen Med* 6: 348-355.
41. Ripamonti U, Ramoshebi LN, Matsaba T, et al. 2001. Bone induction by BMPs/OPs and related family members in primates. *J Bone Joint Surg Am* 83-A Suppl 1: S116-27.
42. Sampath TK, Maliakal JC, Hauschka PV, et al. 1992. Recombinant human osteogenic protein-1 (hOP-1) induces new bone formation in vivo with a specific activity comparable with natural bovine osteogenic protein and stimulates osteoblast proliferation and differentiation in vitro. *J Biol Chem* 267: 20352-20362.
43. Forslund C, Aspenberg P. 1998. OP-1 has more effect than mechanical signals in the control of tissue differentiation in healing rat tendons. *Acta Orthop Scand* 69: 622-626.
44. Paramore CG, Laurysen C, Rauzzino MJ, et al. 1999. The safety of OP-1 for lumbar fusion with decompression-- a canine study. *Neurosurgery* 44: 1151-5; discussion 1155-6.
45. Dimitriou R, Dahabreh Z, Katsoulis E, et al. 2005. Application of recombinant BMP7 on persistent upper and lower limb non-unions. *Injury* 36 Suppl 4: S51-9.
46. Axelrad TW, Steen B, Lowenberg DW, Creevy WR, Einhorn TA. 2008. Heterotopic ossification after the use of commercially available recombinant human bone morphogenetic proteins in four patients. *J Bone Joint Surg Br* 90: 1617-1622.
47. Kim PD, Ludwig S, Poelstra K, et al. 2010. Ectopic bone formation in the pelvis after combined anterior and posterior fusion of the spine with osteogenic protein-1 use: A case report. *J Spinal Disord Tech* 23: 215-220.
48. Zhang Y, Chee A, Thonar EJ, An HS. 2011. Intervertebral disk repair by protein, gene, or cell injection: A framework for rehabilitation-focused biologics in the spine. *PM R* 3: S88-94.
49. Masuda K. 2008. Biological repair of the degenerated intervertebral disc by the injection of growth factors. *Eur Spine J* 17 Suppl 4: 441-451.

## Supplementary file 1. Primers used for quantitative PCR

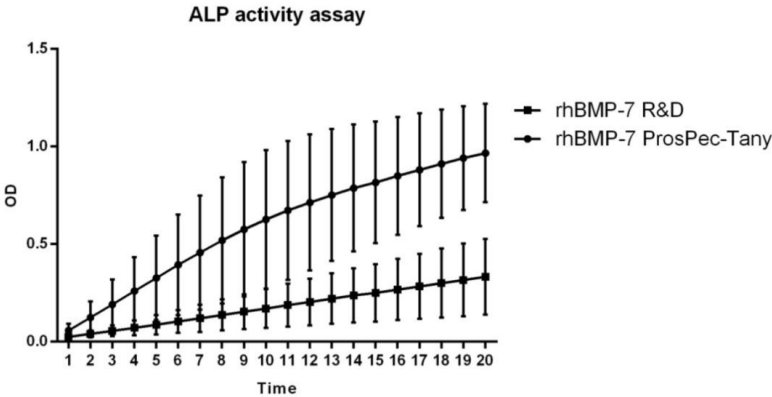
Gene	Forward sequence 5' -> 3'	Reverse sequence 5' -> 3'	Amplicon size	Annealing temp (°C)
<b>Reference genes</b>				
<i>GAPDH</i>	TGTCCCACCCCAATGTATC	CTCCGATGCCTGCTTCACTACCTT	100	58
<i>RPS19</i>	CCTTCCTCAAAAAGTCTGGG	GTTCTCATCGTAGGGAGCAAG	95	61
<i>SDHA</i>	GCCTTGGATCTCTTGATGGA	TTCTTGGCTCTTATGCGATG	92	61
<i>HPRT</i>	AGCTTGCTGGTGAAAAGGAC	TTATAGTCAAGGGCATATCC	104	58
<b>Target genes</b>				
<i>ACAN</i>	GGACACTCCTTGAATTTGAG	GTCATTCCACTCTCCCTTCTC	111	62
<i>COL2A1</i>	GCAGCAAGAGCAAGGAC	TTCTGAGAGCCCTCGGT	151	62
<i>COL1A1</i>	GTGTGTACAGAACGGCCTCA	TCGCAAATCACGTCATCG	109	61
<i>ADAMTS5</i>	CTACTGCACAGGGAAGAG	GAACCCATTCCACAAATGTC	149	61
<i>MMP13</i>	CTGAGGAAGACTTCCAGCTT	TTGGACCACTTGAGAGTTTCG	250	65
<i>TIMP1</i>	GGCGTTATGAGATCAAGATGAC	ACCTGTGCAAGTATCCGC	120	66
<i>CCND1</i>	GCCTCGAAGATGAAGGAGAC	CAGTTTGTTACCAGGAGCA	151	60
<i>BAX</i>	CCTTTTGCTTCAGGGTTTCA	CTCAGCTTCTGGTGGATGC	108	59
<i>BCL2</i>	TGGAGAGVGTCAACCGGGAGATGT	AGGTGTGCAGATGCCGGTTCAGGT	87	62
<i>CASP3</i>	ATCACTGAAGATGGATGGGTTGGGT	TGAAAGGAGCATGTTCTGAAGTAGCACT	139	58

Primers used for qPCR analysis of reference genes glyceraldehyde 3-phosphate dehydrogenase (*GAPDH*), ribosomal protein S19 (*RPS19*), succinate dehydrogenase complex, subunit A, flavoprotein variant (*SDHA*), and hypoxanthine-guanine phosphoribosyltransferase (*HPRT*), and target genes aggrecan (*ACAN*), collagen type II (*COL2A1*), collagen type I (*COL1A1*), a disintegrin and metalloproteinase with thrombospondin motifs (*ADAMTS5*), matrix metalloproteinase 13 (*MMP13*), tissue inhibitor of metalloproteinase 1 (*TIMP1*), cyclin-D1 (*CCND1*), B-cell lymphoma 2-associated X (*BAX*), B-cell lymphoma 2 (*BCL2*) and caspase 3 (*CASP3*).

**Supplementary file 2. ALP activity rhBMP7**

*Induction of ALP activity by rhBMP7 from two different manufacturers in vitro*

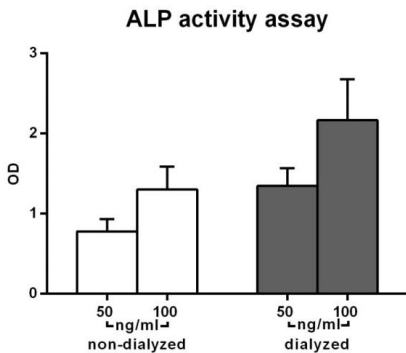
rhBMP7 of manufacturers R&D and ProsPec-Tany were evaluated for their activity to induce ALP activity in mice ATDC5 cells. Cells were plated on 24-well plates (Greiner Cellstar, Alphen a/d Rijn, The Netherlands) at a density of  $4 \times 10^4$  cells/plate. After 24 hours, standard differentiation culture medium with 100 ng/mL BMP7 was added, and cells were cultured for another 72 hours and total ALP activity was measured kinetically in the cell lysate in a kinetic microplate reader at 405 nm (Bio-Rad Benchmark, Veenendaal, The Netherlands). A volume of 50  $\mu$ L of the cell lysate incubated with 50  $\mu$ L p-nitrophenyl phosphate for 20 minutes. rhBMP7 of ProsPec-Tany induces a higher ALP activity compared with rhBMP7 of R&D at the same concentration:



rhBMP7 of ProsPec-Tany induces a higher ALP activity compared with rhBMP7 of R&D at the same concentration in ATDC5 cells undergoing differentiation.

*Induction of ALP activity by rhBMP7 dialysate in vitro*

After dialysis of the rhBMP7 (ProsPec-Tany) biologic activity of the dialysate was determined by induction of ALP activity in mice ATDC5 cells (ProsPec-Tany) and compared to pre-dialyzed BMP7 at the same concentration. The dialysate of ProsPec-Tany retained its biological activity:



Dialyzed rhBMP7 retained its biological activity at similar levels as the non-dialyzed product.



## Supplementary file 3. Significant differences and the corresponding confidence intervals

Table 1. Statistical analyses performed on data of the *in vitro* experiment

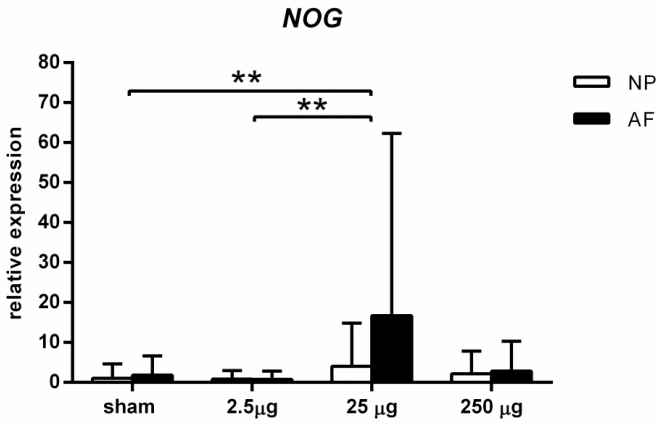
Condition	vs	Condition	Difference in location*	Confidence interval (CI)	CI (%)	p-value
<b>Figure 1. DNA, GAG and GAG/DNA content in pellets containing nucleus pulposus cells</b>						
<b>GAG release</b>						
control		10 ng/mL rhBMP7	-25.40	-44.51 – -3.93	99	0.008
control		100 ng/mL rhBMP7	-125.26	-165.73 – -88.63	99	0.008
10 ng/mL rhBMP7		100 ng/mL rhBMP7	-101.49	-143.78 – -63.23	99	0.008
<b>DNA content</b>						
control at day 7		day 0	1.09	0.36 – 1.73	99	0.008
10 ng/mL rhBMP7 at day 7		day 0	1.07	0.23 – 1.76	99	0.008
100 ng/mL rhBMP7 at day 7		day 0	0.65	0.16 – 1.45	96	0.03
control at day 28		day 0	1.41	0.91 – 2.00	99	0.009
10 ng/mL rhBMP7 at day 28		day 0	1.33	0.85 – 1.88	99	0.009
100 ng/mL rhBMP7 at day 7		day 0	0.93	0.21 – 1.52	99	0.008
control at day 7		control at day 28	0.27	0.09 – 0.73	99	0.009
10 ng/mL rhBMP7 at day 7		10 ng/mL rhBMP7 at day 28	0.54	0.04 – 0.74	98	0.01
10 ng/mL rhBMP7 at day 28		100 ng/mL rhBMP7 at day 28	-0.40	-0.76 – -0.24	99	0.009
control at day 28		100 ng/mL rhBMP7 at day 28	-0.30	-0.88 – -0.30	99	0.009
<b>GAG content</b>						
10 ng/mL rhBMP7 at day 28		100 ng/mL rhBMP7 at day 28	-6.41	-13.74 – -1.27	99	0.008
control at day 28		100 ng/mL rhBMP7 at day 28	-6.42	-13.74 – -1.80	99	0.007
<b>GAG content/DNA content</b>						
10 ng/mL rhBMP7 at day 28		100 ng/mL rhBMP7 at day 28	-8.2	-15.49 – -0.39	99	0.008
control at day 28		100 ng/mL rhBMP7 at day 28	-8.2	-15.49 – -2.48	99	0.007

\*Difference in location estimates the median of the difference between condition x and condition y.

Table 2. Statistical analyses performed on data of the *in vivo* experiment

Protein	Condition	vs	Condition	Hazard ratio (HR)	Confidence interval (CI)	CI (%)	p-value
<b>Figure 5. Relative gene expression of genes associated with apoptosis</b>							
CASP3	NP		AF	2.13	1.02 – 4.44	96	0.03
BAX/BCL2	250 µg rhBMP7		Sham	7.05	1.07 – 12.52	98	0.02
	25 µg rhBMP7		250 µg rhBMP7	0.26	0.08 – 0.89	99	0.005
<b>Figure 6. Relative gene expression of matrix-related target genes and DNA, GAG, and collagen content in IVDs</b>							
COL1A1	NP		AF	0.22	0.08 – 0.61	99	0.0001
COL2A1	NP		AF	2.46	1.07 – 5.65	99	0.006
GAG/DNA	NP		AF	1.13	0.99 – 1.26	99	<0.0001
<b>Supplementary file 4. Relative gene expression of BMP antagonist noggin (NOG) in IVDs injected with rhBMP7</b>							
NOG	25 µg rhBMP7		2.5 µg rhBMP7	0.12	0.02 – 0.63	99	0.0009
	25 µg rhBMP7		sham	0.15	0.03 – 0.73	99	0.002

Supplementary file 4. Relative gene expression of noggin in IVDs injected with rhBMP7



Relative gene expression of BMP antagonist noggin (*NOG*) in canine IVDs injected with rhBMP7.  
\*\* : significant difference at a 99% confidence interval (CI)

**Bone morphogenetic protein-2, but not mesenchymal stromal cells, exert regenerative effects on canine and human nucleus pulposus cells**

Frances C. Bach<sup>1</sup>, Alberto Miranda-Bedate<sup>1</sup>, Ferdi W.M. van Heel<sup>1</sup>, Frank M. Riemers<sup>1</sup>, Margot C.M.E. Müller<sup>1</sup>, Laura B. Creemers<sup>2</sup>, Keita Ito<sup>2,3</sup>, Karin Benz<sup>4</sup>, Björn P. Meij<sup>1</sup>, Marianna A. Tryfonidou<sup>1</sup>

<sup>1</sup> Department of Clinical Sciences of Companion Animals, Faculty of Veterinary Medicine, Utrecht University, Utrecht, the Netherlands

<sup>2</sup> Department of Biomedical Engineering, Eindhoven University of Technology, Eindhoven, the Netherlands

<sup>3</sup> Department of Orthopedics, University Medical Center Utrecht, Utrecht, the Netherlands

<sup>4</sup> TETEC AG, Reutlingen, Germany

*Published in Tissue Engineering Part A (2017); 23 (5-6)*

## Abstract

Chronic back pain is related to intervertebral disc (IVD) degeneration and dogs are employed as animal models to develop growth factor- and cell-based regenerative treatments. In this respect, the differential effects of transforming growth factor beta-1 (TGF- $\beta_1$ ) and bone morphogenetic protein-2 (BMP2) on canine and human chondrocyte-like cells (CLCs) derived from the nucleus pulposus of degenerated IVDs were studied. Human and canine CLCs were cultured in 3D micro-aggregates in basal culture medium supplemented with/without TGF- $\beta_1$  (10 ng/mL) or BMP2 (100 or 250 ng/mL). Both TGF- $\beta_1$  and BMP2 increased proliferation and GAG deposition of human and canine CLCs. TGF- $\beta_1$  induced collagen type I deposition and fibrotic (re)differentiation, whereas BMP2 induced more collagen type II deposition. In dogs, TGF- $\beta_1$  induced Smad1 and Smad2 signaling, whereas in humans, it only tended to induce Smad2 signaling. BMP2 supplementation increased Smad1 signaling in both species. This altogether indicates that Smad1 signaling was associated with collagen type II production, whereas Smad2 signaling was associated with fibrotic CLC (re)differentiation. As a step towards preclinical translation, treatment with BMP2 alone and combined with mesenchymal stromal cells (MSCs) was further investigated. Canine male CLCs were seeded in albumin-based hydrogels with/without female bone marrow-derived MSCs (50:50) in basal or 250 ng/mL BMP2-supplemented culture medium. Although the results indicate that a sufficient amount of MSCs survived the culture period, total GAG production was not increased and GAG production per cell was even decreased by the addition of MSCs, implying that MSCs did not exert additive regenerative effects on the CLCs.

## Introduction

Low back pain is a major cause of disability<sup>1</sup> and has been associated with intervertebral disc (IVD) degeneration<sup>2</sup>. The IVD consists of an outer annulus fibrosus and inner nucleus pulposus (NP), and provides flexibility to the spine. The NP cell phenotype changes during maturation of the IVD: a shift from typical large, vacuolated notochordal cells (NCs) towards smaller chondrocyte-like cells (CLCs). During IVD degeneration, the glycosaminoglycan (GAG) and water content of the NP decreases. IVD disease is currently treated by physiotherapy, medication, and surgery to reduce pain, but these therapies only relieve symptoms and do not achieve IVD repair. Therefore, there is increasing interest in regenerative strategies stimulating functional IVD restoration, including growth factor supplementation and/or cell transplantation<sup>3</sup>.

Extracellular matrix (ECM) synthesis and cell proliferation can be stimulated with growth factors, such as members of the transforming growth factor beta (TGF- $\beta$ ) superfamily, e.g. TGF- $\beta_1$  and bone morphogenetic protein-2 (BMP2). Members of this family transduce their signals by phosphorylation of the type I receptor by the type II receptor. Generally, type I receptors ALK1, ALK2, ALK3, and ALK6 are activated by BMPs and phosphorylate Smad1/5/8, whereas ALK4, ALK5, and ALK7 are activated by TGF- $\beta$  and phosphorylate Smad2/3<sup>4</sup>. After phosphorylation, Smad2/3 and 1/5/8 form complexes with Smad4, translocate to the nucleus, and assemble target gene transcription. Subsequently, Smad2/3 and 1/5/8 target distinctive genes, resulting into differential effects<sup>4,5</sup>. TGF- $\beta$  and BMP2 have already been tested *in vitro*<sup>6-8</sup> and *in vivo* in animal models with experimentally induced IVD degeneration<sup>9-11</sup>.

Growth factor stimulation alone may, however, be insufficient for IVD repair, since cell viability is impaired in degenerated IVDs<sup>12</sup>. Combined cell- and growth factor-based therapy may solve this problem<sup>13-15</sup>. Mesenchymal stromal cells (MSCs) are an emerging cell source for regenerative treatments. They can be isolated from various tissues, e.g. bone marrow and adipose tissue, and can differentiate into different cell types, e.g. osteoblasts, adipocytes and chondrocytes<sup>16,17</sup>. Tissue regeneration can be supported by MSCs because of their immunosuppressive properties and the trophic factors they secrete<sup>18</sup>. Affirmatively, MSC transplantation increased ECM synthesis in animal models with experimentally induced IVD degeneration<sup>19-25</sup>.

While the aforementioned growth factors have been studied separately, their differential effects on the IVD have not been addressed. Therefore, in this study the effect of TGF- $\beta_1$  and BMP2 was determined on canine and human CLCs derived from degenerated IVDs. Since dogs suffer from spontaneous IVD degeneration with similar characteristics as observed in humans, they are considered a valid *in vivo* animal model for human IVD degeneration<sup>26</sup>. Based on physical appearance, dog breeds can be divided into chondrodystrophic (CD) and non-chondrodystrophic (NCD)<sup>27</sup>. CD dogs have short bowlegs due to disrupted endochondral ossification. This polygenetic trait has strongly been linked with IVD degeneration. In CD dogs, replacement of NCs by CLCs in the NP starts already before one year of age. IVD disease occurs frequently and develops around 3–7 years of age, usually in the cervical or thoracolumbar spine<sup>27</sup>. In contrast, in NCD dogs, NCs remain the predominant cell type until later in life. If IVD disease develops, it usually occurs around 6–8

years of age due to wear-and tear, in the caudal cervical or lumbosacral spine<sup>27</sup>. Since CD and NCD dogs show differences in cause, prevalence, and age of onset of IVD degeneration, the regenerative potential of their CLCs could differ from each other, but also from human CLCs. Therefore, we aimed to define whether CD and/or NCD dogs were, besides a valid *in vivo*, also a suitable *in vitro* animal model for growth factor-based treatment of human IVD degeneration. Lastly, as a step towards preclinical translation, the additive regenerative effect of MSCs on growth factor-based treatment of IVD disease was studied in an albumin-based hydrogel that has already been employed *in vivo* for intradiscal cell delivery<sup>28</sup>.

## Material and Methods

### The effect of TGF- $\beta_1$ and BMP2 on canine and human CLC micro-aggregates

#### *IVD tissue sources*

CLCs of 3 human (2 females, 1 male, 47-63 years), 4 chondrodystrophic (CD; Beagles, male, 3-10 years) and 4 non-chondrodystrophic (NCD; 2 mixed breed dogs, 1 Jack Russell terrier, 1 German Shepherd dog, 3 females, 1 male, 2-11 years) canine donors were obtained from Thompson grade III IVDs. The NPs from all human and canine donors contained approximately 100% CLCs. During standard *postmortem* diagnostic procedures at the University Medical Centre (UMC) Utrecht, the L2-L5 part of the human spine was collected. Anonymous use of redundant tissue for research purposes is a standard treatment agreement with patients in the UMC Utrecht (Local Medical Ethical Committee number 12-364). The material was used in line with the 'Proper Secondary Use of Human Tissue' code installed by the Federation of Biomedical Scientific Societies. Canine spines were collected from dogs euthanized in unrelated research studies (University 3R-policy, approved by the Utrecht University Animal Ethics Committee) and client-owned dogs submitted for necropsy to the Department of Pathobiology (Faculty of Veterinary Medicine, Utrecht University). Briefly, NPs were digested by 0.15% pronase (45 min) and 0.15% collagenase (overnight) treatment. The CLCs were stored in hgDMEM+Glutamax (1966, Invitrogen) with 10% Fetal Bovine Serum and 10% DMSO (-196°C) until use.

#### *Cell culture*

First, the CLCs were expanded at 21% O<sub>2</sub>, 5% CO<sub>2</sub>, 37°C<sup>29</sup>. The CLCs were pooled at passage 2 in order to have biological representative samples of the respective populations. Human, NCD, and CD canine micro-aggregates of 35,000 CLCs were formed in low-adherence cell-repellent surface 96-well plates (650970, CELLSTAR® Greiner Bio-one) in 50  $\mu$ L basal culture medium/well: hgDMEM+Glutamax, 1% P/S (P11-010, GE Healthcare Life Sciences), 1% ITS+ premix (354352, Corning Life Sciences), 0.04 mg/mL L-proline (P5607, Sigma-Aldrich), 0.1 mM Ascorbic acid 2-phosphate (A8960, Sigma-Aldrich), and 1.25 mg/mL Bovine Serum Albumin (A9418, Sigma-Aldrich). The 96-well plates were centrifuged for 5 min at 50 *g* to stimulate micro-aggregate formation. The next day, basal culture medium was replaced with basal culture medium either or not supplemented with growth factors at a concentration well-known to be biologically active<sup>6, 29-31</sup>: 10 ng/mL human recombinant TGF- $\beta_1$  (240-B, R&D Systems), 100 ng/mL (BMP2<sub>100</sub>) or 250 ng/mL (BMP2<sub>250</sub>) human recombinant BMP2 (pharmaceutical quality, gift from TETEC AG). The micro-aggregates were cultured at 21% O<sub>2</sub>, 5% CO<sub>2</sub>, 37°C for 28 days.

### *Gene expression profiling*

Micro-aggregates were collected at day 7 ( $n=7$ ). RNA isolation, cDNA synthesis, and RT-qPCR were performed as described previously<sup>29</sup>. Primer specifications for all canine and human reference and target genes are given in Supplementary File 1.

### *DNA and GAG content and release*

Micro-aggregates were collected at day 28 ( $n=7$ ). DNA and GAG sample preparation was performed as described previously<sup>29</sup>. The GAG content of the micro-aggregates was determined using a dimethyl methylene blue (DMMB) assay<sup>32</sup>. The DNA content was measured using the Qubit® dsDNA High Sensitivity Assay Kit (Q32851, Invitrogen) according to the manufacturer's instructions.

### *Histology*

At day 28, the micro-aggregates were fixed in 4% neutral buffered formaldehyde (4286, Klinipath B.V.) with 1% eosin (115935, Merck Millipore) and embedded in 2.4% alginate and paraffin. Five  $\mu\text{m}$  sections were mounted on Microscope KP+ slides (KP-3056, Klinipath B.V.). Alizarin Red S<sup>16</sup>, Safranin O/Fast Green staining and Collagen type I, II, and X immunohistochemistry<sup>29</sup> was performed as described previously using collagen I mouse monoclonal antibody (0.07  $\mu\text{g}/\text{mL}$  (canine) and 0.1  $\mu\text{g}/\text{mL}$  (human), ab6308, Abcam), collagen II mouse monoclonal antibody (0.02  $\mu\text{g}/\text{mL}$  (canine) and 0.4  $\mu\text{g}/\text{mL}$  (human), II-I6B3, DSHB) and collagen X mouse monoclonal antibody (2031501005, Quartett). In isotype controls, normal mouse IgG (3877, Santa Cruz Biotechnology) showed no aspecific staining. The positive control for collagen type X (growth plate) showed specific staining.

### *pSmad1 and pSmad2 ELISA*

200,000 human, CD, and NCD canine CLCs ( $n=4$ ) were plated per well (12-wells plate, 665180, Greiner CELLSTAR®) in expansion medium. After 2 days, the expansion medium was replaced with basal culture medium with/without 10 ng/mL TGF- $\beta_1$  or 250 ng/mL BMP2. After 24 hours of growth factor treatment, cells were homogenized in RIPA buffer containing 0.6 mM phenylmethylsulphonyl fluoride, 17  $\mu\text{g}/\text{mL}$  aprotinin and 1 mM sodium orthovanadate (Sigma-Aldrich). Protein concentrations were measured using the Qubit® Protein Assay Kit (Q32851, Invitrogen) and ELISAs for pSmad1 (SER463/465, PEL-SMAD1-S463, RayBiotech) and pSmad2 (S245/250/255, PEL-SMAD2-S245, RayBiotech) were performed according to the manufacturer's instructions.

### **The effect of BMP2 on canine CLCs and MSCs in a hydrogel**

The same CD and NCD canine CLC donor pools were used as described for the micro-aggregate experiments. Bone marrow-derived MSCs were obtained from a Beagle (CD) and a mixed breed dog (NCD) (both female, 2-years-old), which were euthanized in unrelated research studies. The MSCs were isolated, expanded, and characterized<sup>16</sup>. Thereafter, CLCs and MSCs were incorporated in 40  $\mu\text{L}$  hydrogels composed of albumin crosslinked by polyethylene glycol spacers to hyaluronic acid<sup>33</sup> ( $3 \cdot 10^6$  CLCs/mL hydrogel (CLC),  $1.5 \cdot 10^6$  CLCs/mL hydrogel +  $1.5 \cdot 10^6$  MSCs/mL hydrogel (CLC:MSC) and  $1.5 \cdot 10^6$  CLCs/mL hydrogel ( $\frac{1}{2}$  CLC)) and cultured in basal culture medium with/without 250 ng/mL BMP2 at 21%  $\text{O}_2$ , 5%  $\text{CO}_2$ , 37°C for 28 days. Since the differentiation potential of canine MSCs differs between breeds<sup>34</sup>, it was decided to only combine CLCs and MSCs of one breed: CD (Beagle) CLCs + CD (Beagle) MSCs and NCD (mixed breed) CLCs + NCD (mixed breed) MSCs.

DNA and GAG content measurements ( $n=8$ ), Safranin O/Fast Green staining and collagen type I and II immunohistochemistry ( $n=3$ ) was performed as described above, with adjustment of the pH of the papain and DMMB solution to 6.8 and addition of 2.16 M guanidinium chloride to mask the hyaluronic acid. To determine the fate of the MSCs after 28 days, the CLC (male): MSC (female) ratio was determined by *SRY:GAPDH* PCR on genomic DNA isolated from 20  $\mu$ L papain digested sample using the DNEasy Blood and tissue kit (69581, Qiagen). The DNA was diluted 10x and used for *SRY* or *GAPDH* qPCR (Supplementary File 1). To determine the samples male DNA percentage, a standard series with known female:male genomic DNA amounts was used.  $C_q$  *SRY*: $C_q$  *GAPDH* was used to interpolate the amount of male DNA in the samples from that of the known standard series.

### Statistical analysis

Statistical analyses were performed using IBM SPSS statistics 22. Data were examined for normal distribution using a Shapiro Wilks test. General linear regression models based on ANOVAs were used for normally distributed data and Kruskal Wallis and Mann-Whitney U tests for non-normally distributed data. To correct for multiple comparisons, a Benjamini & Hochberg False Discovery Rate *post-hoc* test was performed.  $p$ -values < 0.05 were considered significant.

## Results

### The effect of TGF- $\beta_1$ and BMP2 on CLC proliferation and apoptosis

The effects of 100 and 250 ng/mL BMP2 (BMP2<sub>100</sub> and BMP2<sub>250</sub>, respectively) and 10 ng/mL TGF- $\beta_1$  were determined on micro-aggregate cultures of CD and NCD canine and human CLCs from degenerated IVDs. The DNA content of the human, CD and NCD canine micro-aggregates was significantly increased by TGF- $\beta_1$ , BMP2<sub>100</sub> and BMP2<sub>250</sub> treatment compared with controls, with the lowest increase in BMP2<sub>100</sub>-treated micro-aggregates (Figure 1a,  $p<0.01$ ). TGF- $\beta_1$  induced the highest DNA content in human ( $p<0.01$ ) and CD canine ( $p<0.001$ ) micro-aggregates, whereas in NCD canine micro-aggregates, TGF- $\beta_1$  and BMP2<sub>250</sub> were equally potent in this respect. At day 7, expression of proliferation marker *CCND1* was not increased by TGF- $\beta_1$  in human nor canine CLCs, while both BMP2 concentrations induced *CCND1* expression compared with controls in CD canine and human CLCs ( $p<0.05$ , Supplementary File 2).

In BMP2<sub>100</sub>-treated CD and NCD canine and in BMP2<sub>250</sub>-treated CD canine micro-aggregates, a central area containing cells with karyorrhexis and pyknosis was observed, while there were no signs of apoptosis in the human micro-aggregates (Figure 2). BMP2<sub>250</sub>, however, significantly reduced apoptosis marker *BAX* expression in NCD canine CLCs ( $p<0.05$ , Supplementary File 2) and tended to decrease *BAX* expression compared with controls in human and CD canine CLCs ( $p<0.1$ ). Expression of *BAX* was significantly decreased by TGF- $\beta_1$  in CD and NCD canine CLCs compared with controls ( $p<0.05$ ).

### The effect of TGF- $\beta_1$ and BMP2 on CLC matrix production and remodeling

*ACAN* expression was significantly increased by BMP2<sub>250</sub> treatment in CD canine and human CLCs compared with control- and TGF- $\beta_1$ -treated CLCs ( $p<0.05$ ), but not in NCD CLCs

(Supplementary File 2). Nevertheless, GAG deposition was significantly increased by BMP2<sub>100</sub>, BMP2<sub>250</sub>, and TGF- $\beta_1$  treatment in human and canine CLCs compared with controls ( $p < 0.05$ , Figure 1b and Figure 2). BMP2 concentration-dependently increased GAG deposition in human and canine CLCs ( $p < 0.05$ ). In CD canine CLCs, TGF- $\beta_1$  was significantly more potent than BMP2 in inducing GAG deposition ( $p < 0.05$ ). In contrast, NCD canine micro-aggregates treated with BMP2<sub>250</sub> had a significantly higher GAG content than those treated with TGF- $\beta_1$  ( $p < 0.001$ ), whereas TGF- $\beta_1$  and BMP2<sub>250</sub> were equally potent in increasing GAG deposition by human CLCs. The GAG/DNA content of the BMP2<sub>250</sub>-treated human and canine micro-aggregates was significantly increased compared with all other conditions ( $p < 0.05$ , Figure 1c). In human and CD canine CLC micro-aggregates, the GAG/DNA content was significantly more increased by TGF- $\beta_1$  than by BMP2<sub>100</sub> treatment, whereas in NCD dogs, the opposite occurred.

TGF- $\beta_1$  and BMP2<sub>250</sub> were equally potent in inducing *COL2A1* expression in canine and human CLCs (Supplementary File 2), while collagen type II protein deposition was induced by both TGF- $\beta_1$  and BMP2 in canine CLCs, but only by BMP2<sub>250</sub> in human CLCs (Figure 2). *COL10A1* expression was only detected in TGF- $\beta_1$ -treated human CLCs (data not shown), but collagen type X protein was not detected in canine nor human micro-aggregates regardless the treatment (Supplementary File 3). Additionally, mRNA of the osteogenic marker *OSX* was not detected in any culture condition, and *RUNX2* and *BGLAP* gene expression was very low ( $C_q$ -values  $> 37$ ) and not significantly different between conditions (data not shown). Moreover, Alizarin Red S staining showed no calcium deposition regardless the treatment (Supplementary File 3).

In all species, TGF- $\beta_1$ -treated micro-aggregates showed signs of fibrotic (re)differentiation. Expression of collagen type I gene (Supplementary File 2) and protein (Figure 2) was increased by TGF- $\beta_1$  compared with control and BMP2 treatment in both species, except for *COL1A1* expression in CD canine CLCs. Morphologically, a GAG-depleted, collagen type I-rich outer rim was formed after TGF- $\beta_1$  treatment, which contained almost no cells in canine, and fibroblast-like cells in human micro-aggregates (Figure 2).

Expression of the matrix remodeling gene *MMP13* was significantly induced by BMP2 in canine CLCs, but only induced by TGF- $\beta_1$  treatment in human CLCs ( $p < 0.05$ , Supplementary File 2). *ADAMTSS5* expression was not significantly affected by the different growth factors in human CLCs (data not shown). In contrast, TGF- $\beta_1$  decreased CD canine CLC *ADAMTSS5* expression 10-fold, whereas BMP2<sub>250</sub> decreased NCD canine CLC *ADAMTSS5* expression 7-fold compared with controls ( $p < 0.05$ , data not shown). *TIMP1* (inhibitor of matrix metalloproteinase) expression was decreased in TGF- $\beta_1$ - and BMP2<sub>250</sub>-treated human CLCs (2-fold and 1.5-fold, respectively) compared with controls ( $p < 0.05$ ), whereas it was 30-fold decreased by BMP2<sub>250</sub> in NCD canine CLCs ( $p < 0.05$ ), and not affected by growth factor treatment in CD canine CLCs (data not shown).

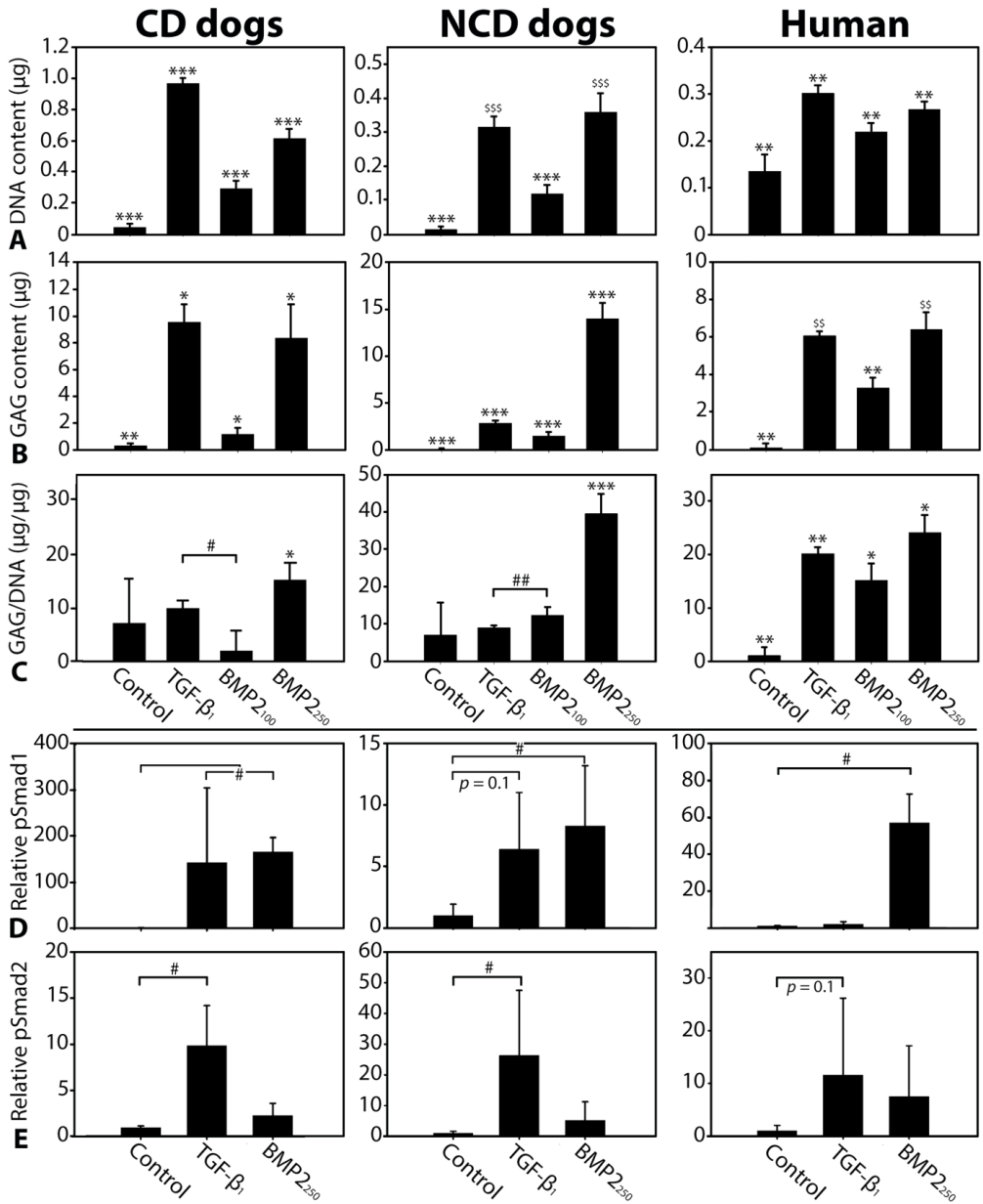


**Figure 1. The effect of TGF- $\beta_1$  and BMP2 on human and canine chondrocyte-like cell proliferation, matrix production and Smad signaling.** Micro-aggregates of chondrocyte-like cells derived from degenerated human/canine intervertebral discs were cultured for 28 days (DNA and GAG content) or 24 hours (phosphorylated (p)Smad1, pSmad2 signaling). (a) DNA content, (b) GAG content, (c) GAG/DNA content, (d) and (e) Relative pSmad1 and pSmad2 expression (controls set at 1),  $n=4$  (pSmad) - 7 (DNA and GAG content). GAG: glycosaminoglycan, CD: chondro dystrophic, NCD: non-chondro dystrophic. \*, \*\*, \*\*\*: significantly different from all other conditions ( $p < 0.05$ ,  $p < 0.01$ ,  $p < 0.001$ , respectively); \$, \$\$\$: significantly different from all other conditions except the one with the same mark type ( $p < 0.01$ ,  $p < 0.001$ , respectively); #:  $p < 0.05$ , ##:  $p < 0.01$ .

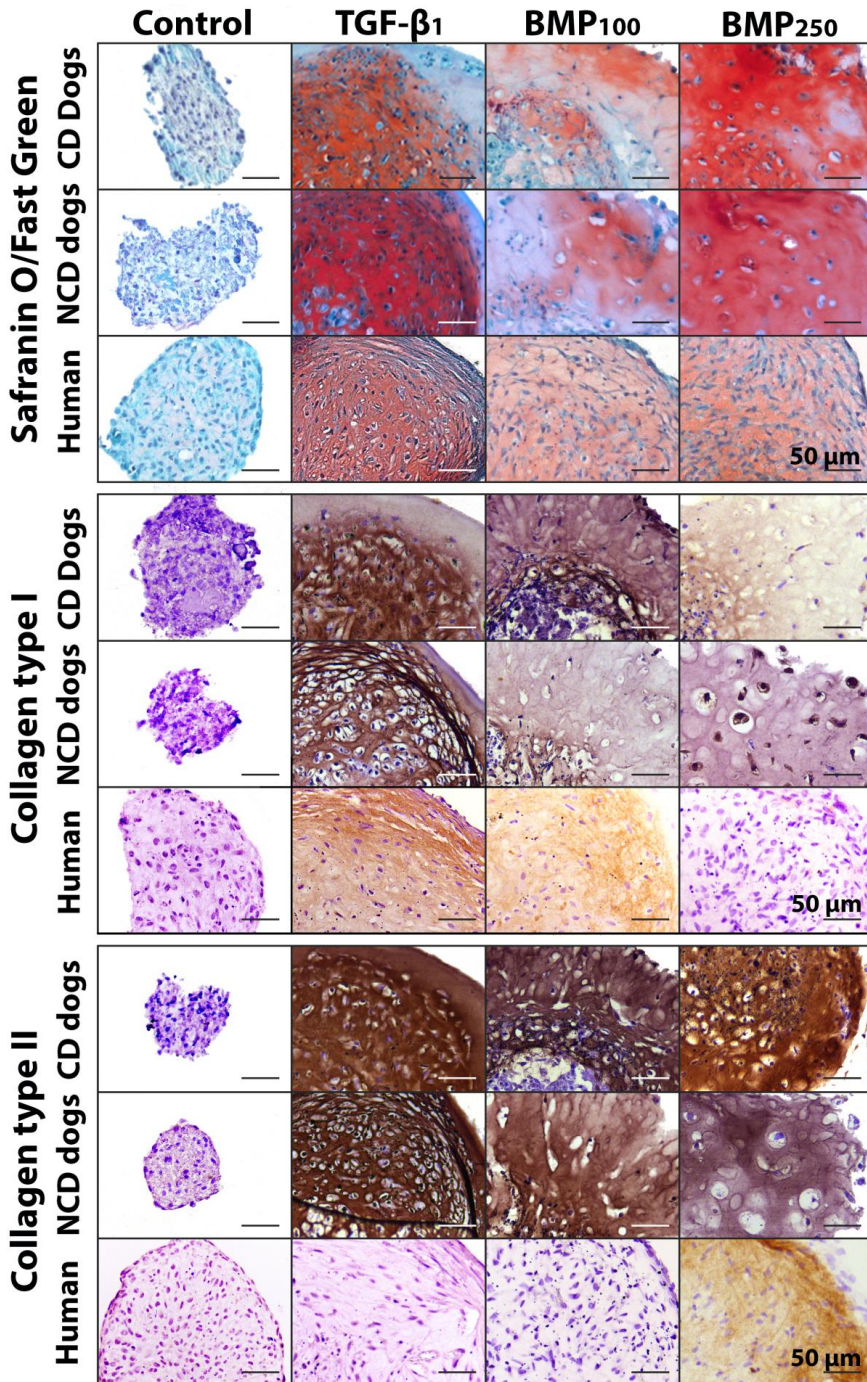


**Figure 2.** The effect of TGF- $\beta_1$  and BMP2 on glycosaminoglycan, collagen type I and II deposition of human and canine chondrocyte-like cell (CLC) micro-aggregates. Micro-aggregates of CLCs derived from degenerated human/canine intervertebral discs were cultured for 28 days. Red staining in Safranin O/Fast Green indicates glycosaminoglycan deposition. CD: chondrodystrophic, NCD: non-chondrodystrophic.  $n=7$ .

### The effect of TGF- $\beta_1$ and BMP2 on Smad signaling

To determine the effect of TGF- $\beta_1$  and BMP2<sub>250</sub> on Smad signaling, ELISAs for phosphorylated (p) Smad1 and Smad2 were performed. In CD canine CLCs, TGF- $\beta_1$  significantly induced Smad1 and Smad2 signaling, whereas BMP2<sub>250</sub> only induced pSmad1 levels ( $p < 0.05$ , Figure 1d-e). In NCD canine CLCs, TGF- $\beta_1$  significantly increased pSmad2 ( $p < 0.05$ ) and tended to increase pSmad1 levels ( $p = 0.1$ ), whereas BMP2<sub>250</sub> significantly increased pSmad1 levels ( $p < 0.05$ ). TGF- $\beta_1$ -treated human CLCs showed a tendency towards increased pSmad2 levels ( $p = 0.1$ ), whereas BMP2<sub>250</sub>-treated human CLCs showed significantly increased Smad1 signaling ( $p < 0.05$ ).

### The effect of BMP2 on canine CLCs and MSCs in 3D hydrogel cultures

The best growth factor was considered the one that induced GAG and collagen type II production and cell proliferation, and inhibited apoptosis and fibrotic (collagen type I-rich) and osteogenic (collagen type X- and calcium-rich) ECM deposition. In this respect, human and canine CLC micro-aggregates responded best to 250 ng/mL BMP2. Therefore, the effect of 250 ng/mL BMP2 alone or in combination with MSCs was determined on canine CLCs using hydrogels employed for intradiscal cell transplantation<sup>28</sup>. Canine CLCs and MSCs from CD and NCD breeds were incorporated at different concentrations:  $3 \times 10^6$  CLCs/mL (CLC),  $1.5 \times 10^6$  CLCs/mL +  $1.5 \times 10^6$  MSCs/mL (CLC:MSC) and  $1.5 \times 10^6$  CLCs/mL (½ CLC).

In hydrogels containing CD (Figure 3) and NCD (Supplementary File 4) canine ½ CLC, CLC and CLC:MSC, BMP2 treatment significantly increased the DNA content, GAG release, GAG deposition, and collagen type I and II deposition compared with controls ( $p < 0.05$ ). Generally, BMP2 treatment also significantly increased the GAG/DNA content of NCD (Supplementary File 4) and CD (Figure 3d) canine cell containing hydrogels ( $p < 0.01$ ), only not the GAG/DNA content of CD CLC:MSC containing hydrogels.

Although at day 0, the DNA content of CLC and CLC:MSC containing hydrogels was comparable, after 28 days, the DNA content of NCD CLC:MSC containing control hydrogels was higher than that of NCD CLC containing control hydrogels ( $p < 0.01$ , Supplementary File 4). The DNA content of the BMP2-treated CLC:MSC containing hydrogels was higher than that of the BMP2-treated CLC containing hydrogels in both CD and NCD dogs ( $p < 0.05$ , Figure 3a and Supplementary File 4). At day 0, the CLC (male)-derived DNA content of CD CLC:MSC containing hydrogels was 50% (0.45  $\mu\text{g}$ ) of the total DNA content. After 28 days of culture, 57% (0.30  $\mu\text{g}$ ) of cells in CD CLC:MSC containing control hydrogels appeared female (MSC)-derived, whereas this was 27% (0.34  $\mu\text{g}$ ) in CD BMP2-treated CLC:MSC containing hydrogels (Figure 3a), indicating that in absolute terms, the MSC-derived DNA content remained relatively unchanged throughout culture. At day 28, the CLC (male)-derived DNA content of CD CLC:MSC containing hydrogels was comparable with the total DNA content of CD CLC containing hydrogels, both in the presence and absence of BMP2 (Figure 3a).

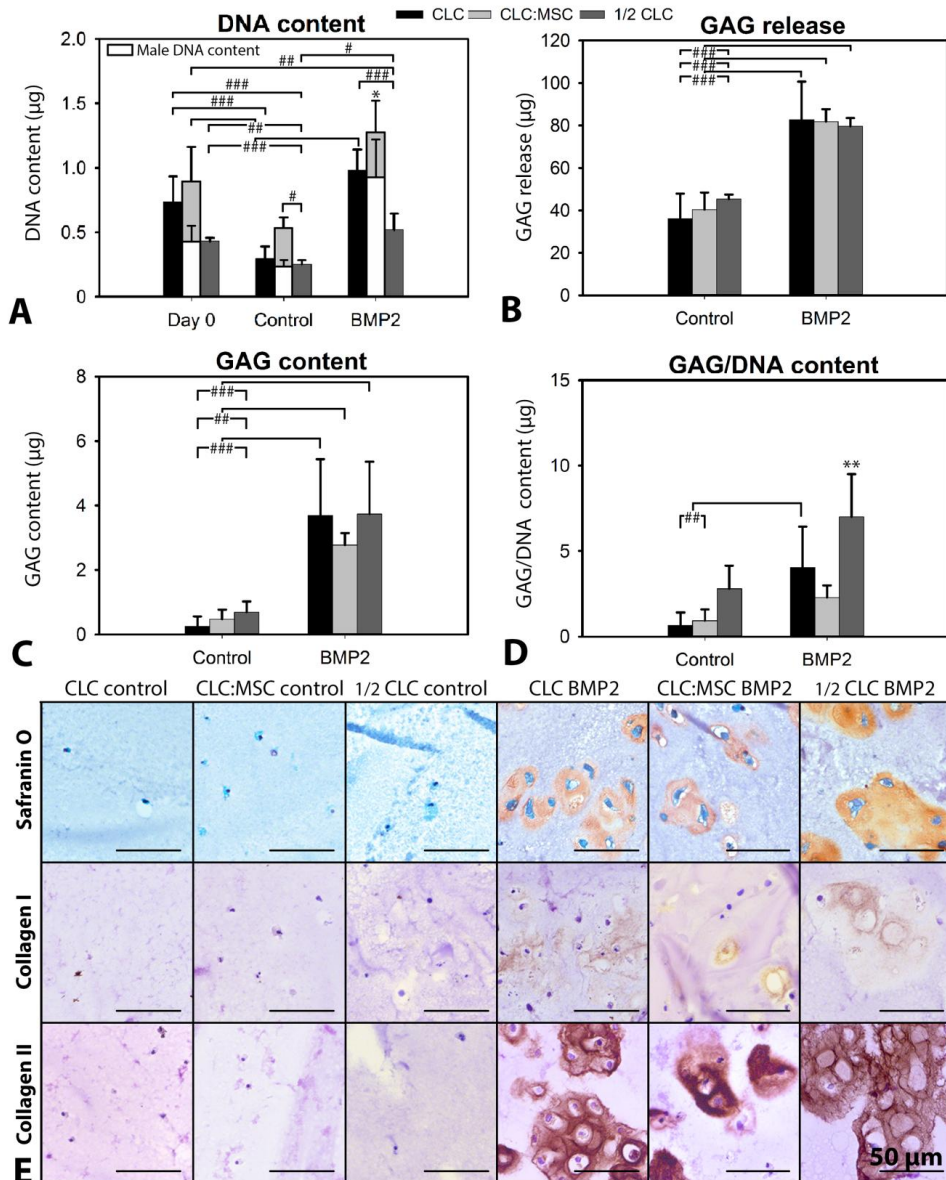


**Figure 3.** The effect of BMP2 on matrix production and cell proliferation of chondrocyte-like cells (CLCs) and mesenchymal stromal cells (MSCs). CLC ( $3 \times 10^6$ /mL hydrogel),  $\frac{1}{2}$  CLC ( $1.5 \times 10^6$ /mL) or CLC:MSC (1:1, both  $1.5 \times 10^6$ /mL) hydrogels were cultured for 28 days with or without 250 ng/mL BMP2. (a) Total and male (CLC-derived) DNA content, (b) GAG release, (c) GAG content, (d) GAG/DNA content, (e) Safranin O/Fast green staining and collagen type I and II immunohistochemistry. Red staining in Safranin O/Fast Green indicates glycosaminoglycan (GAG) deposition.  $n=8$ . #, ##, ###:  $p < 0.05$ ,  $p < 0.01$  and  $p < 0.001$ , respectively; \*, \*\*: significantly different from all other conditions ( $p < 0.05$ ,  $p < 0.01$ , respectively).

GAG release and deposition was comparable in all BMP2-treated cell-hydrogel combinations. The GAG/DNA content was highest in the hydrogels containing BMP2-treated ½ CLC, followed by BMP2-treated CLC hydrogels (Figure 3d, Supplementary File 4). The GAG/DNA content of NCD and CD BMP2-treated CLC:MSC containing hydrogels was significantly lower than that of BMP-treated ½ CLC and CLC containing hydrogels ( $p < 0.01$ ). A schematic overview of the observed effects of TGF- $\beta_1$  and BMP2 on CD and NCD canine and human CLCs is given in Supplementary File 5.

## Discussion

Both humans and dogs experience chronic back pain related to IVD degeneration. As current treatments do not achieve IVD repair, there is need for cell- and growth factor-based regenerative treatments leading to functional IVD restoration. This study demonstrates that both growth factors BMP2 and TGF- $\beta_1$  increased proliferation and matrix production of human and canine CLCs, but that TGF- $\beta_1$  induced a fibrotic phenotype, whereas BMP2 did not. To determine whether MSCs exerted additional regenerative effects, canine CLCs and MSCs were cultured in a hydrogel that has already been shown to facilitate IVD repair<sup>28</sup>. Although the results indicate that a considerable amount of MSCs survived the culture period, they did not exert additive regenerative effects on the CLCs.

### The effect of TGF- $\beta_1$ and BMP2 on human and canine CLCs

It has already been shown that BMP2<sup>6,7</sup> and TGF- $\beta$ <sup>8,29</sup> are able to induce GAG deposition in CLCs. In the current study, the response of CD and NCD canine CLCs to these growth factors was in a similar direction as observed in human CLCs, but sometimes with a different intensity. Both BMP2 and TGF- $\beta$  increased cell proliferation and ECM production, while they decreased the expression of apoptotic-related genes in human and canine CLCs. These effects were reflected in a high DNA and GAG content of the CLC micro-aggregates at the end of the study. TGF- $\beta_1$  stimulated Smad1 and Smad2 signaling in canine CLCs (as also shown in chondrocytes<sup>35</sup>), and induced GAG, collagen type I and II deposition and a cell/GAG-depleted fibrotic rim. In contrast, BMP2 only stimulated Smad1 signaling in canine CLCs, and induced GAG and collagen type II deposition, but no collagen type I deposition or fibrotic phenotype. In human CLCs, TGF- $\beta_1$  tended to stimulate only Smad2 signaling, and induced a fibroblast-rich construct, GAG and collagen type I, but no collagen type II deposition. Moreover, BMP2 only stimulated Smad1 signaling in human CLCs, and induced GAG and collagen type II but no collagen type I deposition. Altogether, these results suggest that Smad1 signaling was associated with collagen type II production, whereas Smad2 signaling accompanied fibrotic (re)differentiation in human and canine CLCs. In line with our results, TGF- $\beta$  is a well-known, collagen type I-inducing, fibrotic agent<sup>36</sup>, whereas BMP2 did not increase *COL1A1* expression in human CLCs<sup>37</sup>. In chondrocytes, however, TGF- $\beta_1$ -mediated Smad2/3 signaling results in protective, and Smad1/5/8 signaling in deleterious responses<sup>35</sup>, indicating that CLCs respond distinctively different to (TGF- $\beta_1$ -mediated) Smad2/3 signaling than chondrocytes.

Hypertrophic differentiation is known to precede BMP (Smad1/5/8)-induced bone formation in articular chondrocytes<sup>35,38</sup>. In the current study, however, no signs for

hypertrophic differentiation or osteogenic matrix production were detected in BMP2-treated canine or human CLCs. In line with our results, others showed only chondrogenic, but no osteogenic effects of BMP2 on rabbit NCs<sup>30</sup>, human CLCs<sup>7,37</sup> and degenerated goat IVDs<sup>11</sup>, indicating that CLCs may also respond rather different to BMP2 (Smad1/5/8 signaling) than chondrocytes.

Altogether, the results of this study suggest that BMP2 can be a valuable candidate for IVD regeneration, since it induced chondrogenic, but no osteogenic or fibrotic ECM production in canine and human CLCs. Future studies should, however, investigate long-term exposure to BMP2. Lastly, CD and NCD canine CLCs responded rather comparably to growth factor treatment as human CLCs, indicating that CLCs from both CD and NCD dogs can be used as *in vitro* animal model for human IVD degeneration.

### The effect of MSCs on canine CLCs

Hydrogels that are already applied in clinical studies for intradiscal cell transplantation<sup>28</sup> were used to determine the possible additive regenerative effect of MSCs on BMP2-treated CLCs. The results of the current study indicate that a considerable amount of MSCs survived the 28-day CLC:MSC co-culture period. Also *in vivo*, injected MSCs maintain their viability for at least 28 days within rat IVDs<sup>39</sup>. In co-cultures, MSCs have been shown to stimulate chondrocyte proliferation and ECM production<sup>40</sup>. Although previous work on human CLC:MSC co-cultures also showed (modest) trophic effects of MSCs<sup>41,42</sup>, the present study on canine CLC:MSC co-cultures did not. Comparable results as observed in this canine co-culture study have been demonstrated for human chondrocyte:MSC co-cultures<sup>43</sup>, stressing the importance of using proper controls. Cells should be seeded at comparable densities, but also at lower densities to account for possible differences in available nutrition or cells producing factors inhibiting their own proliferation.

Taken together, MSCs did not exert regenerative effects on CD or NCD canine CLCs *in vitro*. The discrepancy between these results and the results of previous work<sup>41,42</sup> could be due to species differences. Additionally, our experiments were performed in normoxia, whereas the NP is an hypoxic tissue<sup>44</sup>. Hypoxia produces a favorable microenvironment that improves MSC cell viability, as well as differentiation into NP-like cells and ECM synthesis<sup>45</sup>. Furthermore, previous work indicated that the optimal CLC:MSC ratio for MSC differentiation appeared 75:25<sup>42,46</sup>. Therefore, future studies should test different CLC:MSC ratios under hypoxic culture conditions. The results of the current study do not directly imply that MSCs will not have regenerative effects on degenerated IVDs *in vivo*. Given that regenerative effects of MSCs were encountered in different animal models with experimentally induced IVD degeneration<sup>19-25</sup>, future studies should investigate whether MSCs also have beneficial effects in dogs with spontaneously degenerated IVDs, a valid *in vivo* animal model for human IVD degeneration<sup>26</sup>.

## Conclusions

This study demonstrates that while both TGF- $\beta_1$  and BMP2 exerted regenerative effects on human and canine CLCs, BMP2 induced a more healthy NP matrix than TGF- $\beta_1$ . (BMP2-mediated) Smad1 signaling increased collagen type II production, whereas (TGF- $\beta_1$ -mediated) Smad2 signaling induced fibrotic CLC (re)differentiation. MSCs did not exert additive regenerative effects on control- or BMP2-treated canine CLCs. Since CD and NCD canine CLCs responded rather comparable to TGF- $\beta_1$  and BMP2 as human CLCs, support for the dog as a valid *in vitro* model for human IVD degeneration was provided.

## Acknowledgments

The authors would like to thank Anita Krouwels for supplying the human CLCs and Willem de Jong and Sanne Loos for assistance during the execution of experiments.

## References

1. Freburger JK, Holmes GM, Agans RP, et al. 2009. The rising prevalence of chronic low back pain. *Arch Intern Med* 169: 251-258.
2. Mok FP, Samartzis D, Karppinen J, et al. 2016. Modic changes of the lumbar spine: Prevalence, risk factors, and association with disc degeneration and low back pain in a large-scale population-based cohort. *Spine J* 16: 32-41.
3. Benneker LM, Andersson G, Iatridis JC, et al. 2014. Cell therapy for intervertebral disc repair: Advancing cell therapy from bench to clinics. *Eur Cell Mater* 27: 5-11.
4. Mahlawat P, Ilangovan U, Biswas T, Sun LZ, Hinck AP. 2012. Structure of the Alk1 extracellular domain and characterization of its bone morphogenetic protein (BMP) binding properties. *Biochemistry* 51: 6328-6341.
5. Jain AP, Pundir S, Sharma A. 2013. Bone morphogenetic proteins: The anomalous molecules. *J Indian Soc Periodontol* 17: 583-586.
6. Gilbertson L, Ahn SH, Teng PN, et al. 2008. The effects of recombinant human bone morphogenetic protein-2, recombinant human bone morphogenetic protein-12, and adenoviral bone morphogenetic protein-12 on matrix synthesis in human annulus fibrosus and nucleus pulposus cells. *Spine J* 8: 449-456.
7. Kim DJ, Moon SH, Kim H, et al. 2003. Bone morphogenetic protein-2 facilitates expression of chondrogenic, not osteogenic, phenotype of human intervertebral disc cells. *Spine (Phila Pa 1976)* 28: 2679-2684.
8. Moon SH, Nishida K, Gilbertson LG, et al. 2008. Biologic response of human intervertebral disc cells to gene therapy cocktail. *Spine (Phila Pa 1976)* 33: 1850-1855.
9. Walsh AJ, Bradford DS, Lotz JC. 2004. In vivo growth factor treatment of degenerated intervertebral discs. *Spine (Phila Pa 1976)* 29: 156-163.
10. Huang KY, Yan JJ, Hsieh CC, Chang MS, Lin RM. 2007. The in vivo biological effects of intradiscal recombinant human bone morphogenetic protein-2 on the injured intervertebral disc: An animal experiment. *Spine (Phila Pa 1976)* 32: 1174-1180.
11. Peeters M, Detiger SE, Karfeld-Sulzer LS, et al. 2015. BMP-2 and BMP-2/7 heterodimers conjugated to a fibrin/hyaluronic acid hydrogel in a large animal model of mild intervertebral disc degeneration. *Biores Open Access* 4: 398-406.
12. Sakai D, Nakai T, Mochida J, Alini M, Grad S. 2009. Differential phenotype of intervertebral disc cells: Microarray and immunohistochemical analysis of canine nucleus pulposus and annulus fibrosus. *Spine (Phila Pa 1976)* 34: 1448-1456.
13. Mwale F, Wang HT, Roughley P, Antoniou J, Haglund L. 2014. Link N and mesenchymal stem cells can induce regeneration of the early degenerate intervertebral disc. *Tissue Eng Part A* 20: 2942-2949.
14. Chen WH, Liu HY, Lo WC, et al. 2009. Intervertebral disc regeneration in an ex vivo culture system using mesenchymal stem cells and platelet-rich plasma. *Biomaterials* 30: 5523-5533.
15. Bucher C, Gazdhar A, Benneker LM, Geiser T, Gantenbein-Ritter B. 2013. Nonviral gene delivery of growth and differentiation factor 5 to human mesenchymal stem cells injected into a 3D bovine intervertebral disc organ culture system. *Stem Cells Int* 2013: 326828.
16. Malagola E, Teunissen M, van der Laan LJ, et al. 2015. Characterization and comparison of canine multipotent stromal cells derived from liver and bone marrow. *Stem Cells Dev* 25(2): 139-150.
17. Mo M, Wang S, Zhou Y, Li H, Wu Y. 2016. Mesenchymal stem cell subpopulations: Phenotype, property and therapeutic potential. *Cell Mol Life Sci* 73: 3311-3321.
18. Meirelles Lda S, Fontes AM, Covas DT, Caplan AI. 2009. Mechanisms involved in the therapeutic properties of mesenchymal stem cells. *Cytokine Growth Factor Rev* 20: 419-427.
19. Sakai D, Mochida J, Iwashina T, et al. 2006. Regenerative effects of transplanting mesenchymal stem cells embedded in atelocollagen to the degenerated intervertebral disc. *Biomaterials* 27: 335-345.
20. Yang F, Leung VY, Luk KD, Chan D, Cheung KM. 2009. Mesenchymal stem cells arrest intervertebral disc degeneration through chondrocytic differentiation and stimulation of endogenous cells. *Mol Ther* 17: 1959-1966.
21. Sakai D, Mochida J, Iwashina T, et al. 2005. Differentiation of mesenchymal stem cells transplanted to a rabbit degenerative disc model: Potential and limitations for stem cell therapy in disc regeneration. *Spine (Phila Pa 1976)* 30: 2379-2387.
22. Chun HJ, Kim YS, Kim BK, et al. 2012. Transplantation of human adipose-derived stem cells in a rabbit model of traumatic degeneration of lumbar discs. *World Neurosurg* 78: 364-371.
23. Ganey T, Hutton WC, Moseley T, Hedrick M, Meisel HJ. 2009. Intervertebral disc repair using adipose tissue-derived stem and regenerative cells: Experiments in a canine model. *Spine (Phila Pa 1976)* 34: 2297-2304.
24. Hiyama A, Mochida J, Iwashina T, et al. 2008. Transplantation of mesenchymal stem cells in a canine disc degeneration model. *J Orthop Res* 26: 589-600.
25. Serigano K, Sakai D, Hiyama A, et al. 2010. Effect of cell number on mesenchymal stem cell transplantation in a canine disc degeneration model. *J Orthop Res* 28: 1267-1275.
26. Bergknot N, Rutges JP, Kranenburg HJ, et al. 2012. The dog as an animal model for intervertebral disc degeneration? *Spine (Phila Pa 1976)* 37: 351-358.
27. Smolders LA, Bergknot N, Grinwis GC, et al. 2013. Intervertebral disc degeneration in the dog. part 2: Chondrodystrophic and non-chondrodystrophic breeds. *Vet J* 195: 292-299.

28. Benz K, Stippich C, Fischer L, et al. 2012. Intervertebral disc cell- and hydrogel-supported and spontaneous intervertebral disc repair in nucleotomized sheep. *Eur Spine J* 21: 1758-1768.
29. Bach FC, de Vries SA, Krouwels A, et al. 2015. The species-specific regenerative effects of notochordal cell-conditioned medium on chondrocyte-like cells derived from degenerated human intervertebral discs. *Eur Cell Mater* 30: 132-47.
30. Lee KI, Moon SH, Kim H, et al. 2012. Tissue engineering of the intervertebral disc with cultured nucleus pulposus cells using atelocollagen scaffold and growth factors. *Spine (Phila Pa 1976)* 37: 452-458.
31. Noth U, Rackwitz L, Heymer A, et al. 2007. Chondrogenic differentiation of human mesenchymal stem cells in collagen type I hydrogels. *J Biomed Mater Res A* 83: 626-635.
32. Farndale RW, Sayers CA, Barrett AJ. 1982. A direct spectrophotometric microassay for sulfated glycosaminoglycans in cartilage cultures. *Connect Tissue Res* 9: 247-248.
33. Benz K, Stippich C, Osswald C, et al. 2012. Rheological and biological properties of a hydrogel support for cells intended for intervertebral disc repair. *BMC Musculoskelet Disord* 13: 54-2474-13-54.
34. Bertolo A, Steffen F, Malonzo-Marty C, Stoyanov J. 2015. Canine mesenchymal stem cell potential and the importance of dog breed: Implication for cell-based therapies. *Cell Transplant* 24: 1969-1980.
35. Blaney Davidson EN, Remst DF, Vitters EL, et al. 2009. Increase in ALK1/ALK5 ratio as a cause for elevated MMP-13 expression in osteoarthritis in humans and mice. *J Immunol* 182: 7937-7945.
36. Munoz-Felix JM, Gonzalez-Nunez M, Lopez-Novoa JM. 2013. ALK1-Smad1/5 signaling pathway in fibrosis development: Friend or foe? *Cytokine Growth Factor Rev* 24: 523-537.
37. Kim H, Lee JU, Moon SH, et al. 2009. Zonal responsiveness of the human intervertebral disc to bone morphogenetic protein-2. *Spine (Phila Pa 1976)* 34: 1834-1838.
38. van Caam A, Blaney Davidson E, Garcia de Vinuesa A, et al. 2015. The high affinity ALK1-ligand BMP9 induces a hypertrophy-like state in chondrocytes that is antagonized by TGFbeta1. *Osteoarthritis Cartilage* 23: 985-995.
39. Crevensten G, Walsh AJ, Ananthakrishnan D, et al. 2004. Intervertebral disc cell therapy for regeneration: Mesenchymal stem cell implantation in rat intervertebral discs. *Ann Biomed Eng* 32: 430-434.
40. Wu L, Prins HJ, Helder MN, van Blitterswijk CA, Karperien M. 2012. Trophic effects of mesenchymal stem cells in chondrocyte co-cultures are independent of culture conditions and cell sources. *Tissue Eng Part A* 18: 1542-1551.
41. Vadala G, Studer RK, Sowa G, et al. 2008. Coculture of bone marrow mesenchymal stem cells and nucleus pulposus cells modulate gene expression profile without cell fusion. *Spine (Phila Pa 1976)* 33: 870-876.
42. Sobajima S, Vadala G, Shimer A, et al. 2008. Feasibility of a stem cell therapy for intervertebral disc degeneration. *Spine J* 8: 888-896.
43. Bekkers JEJ, Saris, DBF, Tsuchida AI, et al. 2010. Co-culturing of human bone marrow mononuclear cells and primary chondrocytes to improve cartilage formation. *ICRS Congress, Barcelona*.
44. Risbud MV, Schipani E, Shapiro IM. 2010. Hypoxic regulation of nucleus pulposus cell survival: From niche to notch. *Am J Pathol* 176: 1577-1583.
45. Wang F, Shi R, Cai F, Wang YT, Wu XT. 2015. Stem cell approaches to intervertebral disc regeneration: Obstacles from the disc microenvironment. *Stem Cells Dev* 24: 2479-2495.
46. Richardson SM, Walker RV, Parker S, et al. 2006. Intervertebral disc cell-mediated mesenchymal stem cell differentiation. *Stem Cells* 24: 707-716.

## Supplementary File 1. Primers used for quantitative PCR

## Primers used for quantitative PCR of canine samples

Genes	Forward sequence 5' → 3'	Reverse sequence 5' → 3'	Amplicon size	Annealing temp (°C)
<b>Reference genes</b>				
<i>GAPDH</i>	TGTC CCCACCCCAATGTATC	CTCCGATGCCTGCTTCACTACCTT	100	58
<i>HPRT</i>	AGCTTGCTGGTGAAAAGGAC	TTATAGTCAAGGGCATATCC	104	58
<i>RPS19</i>	CCTTCTCAAAAAGTCTGGG	GTTCTCATCGTAGGGAGCAAG	95	61
<i>SDHA</i>	GCCTTGATCTCTTGATGGA	TTCTTGGCTCTTATGCGATG	92	56.5
<b>Target genes</b>				
<i>ACAN</i>	GGACTCTCTTGCAATTTGAG	GTCATTCCACTCTCCCTTCTC	111	62
<i>ADAMTS5</i>	CTACTGCACAGGGAAGAG	GAACCCATTCCACAAATGTC	149	61
<i>BAX</i>	CCTTTTGCTTCAGGGTTTCA	CTCAGCTTCTTGGTGGATGC	108	58
<i>BGLAP</i>	CTGATGGTCCTTGCCCT	CTTGGACACGAAGGTTGC	116	61
<i>CCND1</i>	GCCTCGAAGATGAAGGAGAC	CAGTTTGTTCACCAGGAGCA	117	60
<i>COL1A1</i>	GTGTGTACAGAACGGCCTCA	TCGCAAATCACGTCATCG	109	61
<i>COL2A1</i>	GCAGCAAGAGCAAGGAC	TTCTGAGAGCCCTCGGT	151	62
<i>COL10A1</i>	CCAACACCAAGACACAG	CAGGAATACCTTGCTCTC	80	61
<i>MMP13</i>	CTGAGGAAGACTTCCAGCTT	TTGGACCACTTGAGAGTTTCG	250	65
<i>OSX</i>	GAGGAGGAAGCTCACTATGG	CTGAAAGGTCACTGCCCA	147	59
<i>RUNX2</i>	AACGATCTGAGATTTGTGGGC	TGTGATAGGTGGCTACTTGGG	97	64
<i>SRY</i>	TGAAAGCGGAGGAAACGGTA	TGCTGATCTCTGAGTTTTGCATT	130	55.5
<i>TIMP1</i>	GGCGTTATGAGATCAAGATGAC	ACCTGTGCAAGTATCCGC	120	66

All primers were designed in-house using Perlprimer except for MMP13<sup>1</sup> and BAX<sup>2</sup>.

Stably expressed reference genes (TATAA-box binding protein (*TBP*), hypoxanthine-guanine phosphoribosyltransferase (*HPRT*), succinate dehydrogenase subunit A (*SDHA*) and tyrosine 3-monooxygenase/tryptophan 5-monooxygenase activation protein and zeta polypeptide (*YWHAZ*) for the human samples and glyceraldehyde 3-phosphate dehydrogenase (*GAPDH*), ribosomal protein S19 (*RPS19*), *SDHA* and *HPRT* for the canine samples) were chosen to normalize gene expression of the target genes: aggrecan (*ACAN*), a disintegrin and metalloproteinase with thrombospondin motifs 5 (*ADAMTS5*), Bcl2-like-protein (*BAX*), bone gamma-carboxylglutamate protein/osteocalcin (*BGLAP*), cyclin D1 (*CCND1*), collagen type I (*COL1A1*), collagen type II (*COL2A1*), collagen type X (*COL10A1*), matrix metalloproteinase 13 (*MMP13*), osterix (*OSX*), runt-related transcription factor 2 (*RUNX2*), sex determining region Y (*SRY*), and a tissue inhibitor of metalloproteinases (*TIMP1*).

## Primers used for quantitative PCR of human samples

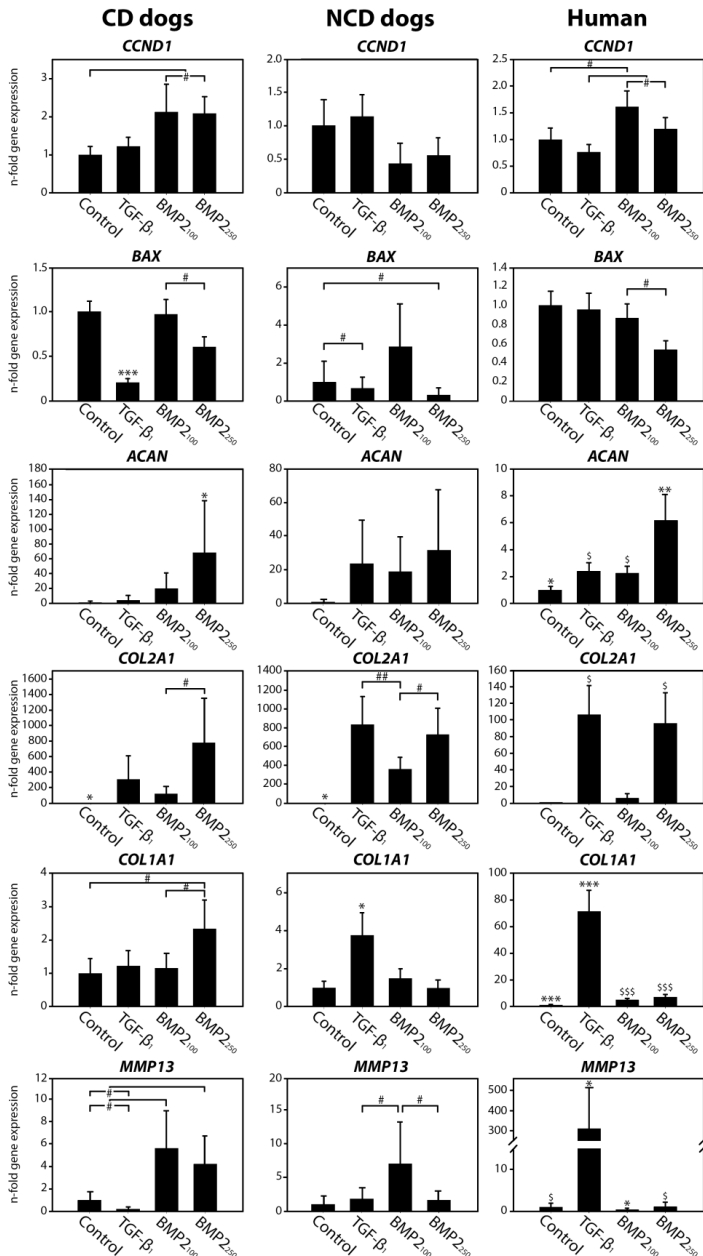
Genes	Forward sequence 5' → 3'	Reverse sequence 5' → 3'	Amplicon size	Annealing temp (°C)
<b>Reference genes</b>				
<i>HPRT</i>	TATTGTAATGACCAGTCAACAG	GGTCCTTTTCACCAGCAAG	192	60
<i>SDHA</i>	TGGGAACAAGAGGGCATCTG	CCACCACTGCATCAAATTCATG	86	58
<i>TBP</i>	TGCACAGGAGCCAAGAGTGAA	CACATCACAGCTCCCCACCA	132	63.5
<i>YWHAZ</i>	ACTTTTGGTACATTGTGGCTTCAA	CCGCCAGGACAAACCAGTAT	94	64
<b>Target genes</b>				
<i>ACAN</i>	CAACTACCCGGCCATCC	GATGGCTCTGTAATGGAACAC	160	63.5
<i>ADAMT55</i>	GCCAGCGGATGTGCAAGC	ACACTTCCCCCGACGCAGA	130	62.5
<i>BAX</i>	GGACGAACTGGACAGTAACATGG	GCAAAGTAGAAAAGGGCGACAAC	150	60
<i>CCND1</i>	AGCTCCTGTGCTCGAAGTGGAAC	AGTGTTC AATGAAATCGTGC GGGGT	480	65
<i>COL1A1</i>	TCCAACGAGATCGAGATCC	AAGCCGAATTCCTGGTCT	191	61
<i>COL2A1</i>	AGGGCCAGGATGTCCGGCA	GGGTCCCAGGTTCTCCATCT	195	63.5
<i>COL10A1</i>	CACTACCCAACCCAAGACA	CTGGTTTCCCTACAGCTGAT	225	61
<i>MMP13</i>	TCCCAGGAATTGGTGATAAAGTAGA	CTGGCATGACGCGAACAATA	123	64
<i>TIMP1</i>	CTTCTGGCATCTGTTGTTG	GGTATAAGGTGGTCTGGTTG	153	64

All reference gene primers were designed in-house using Perlprimer. Primers for the target genes *ACAN*, *ADAMT55*, *COL1A1*, and *COL2A1* were kindly provided by UMC Utrecht, the Netherlands. Primers for *BAX*<sup>3</sup>, *CCND1*<sup>4</sup>, and *MMP13*<sup>5</sup> were obtained from the literature.

### References

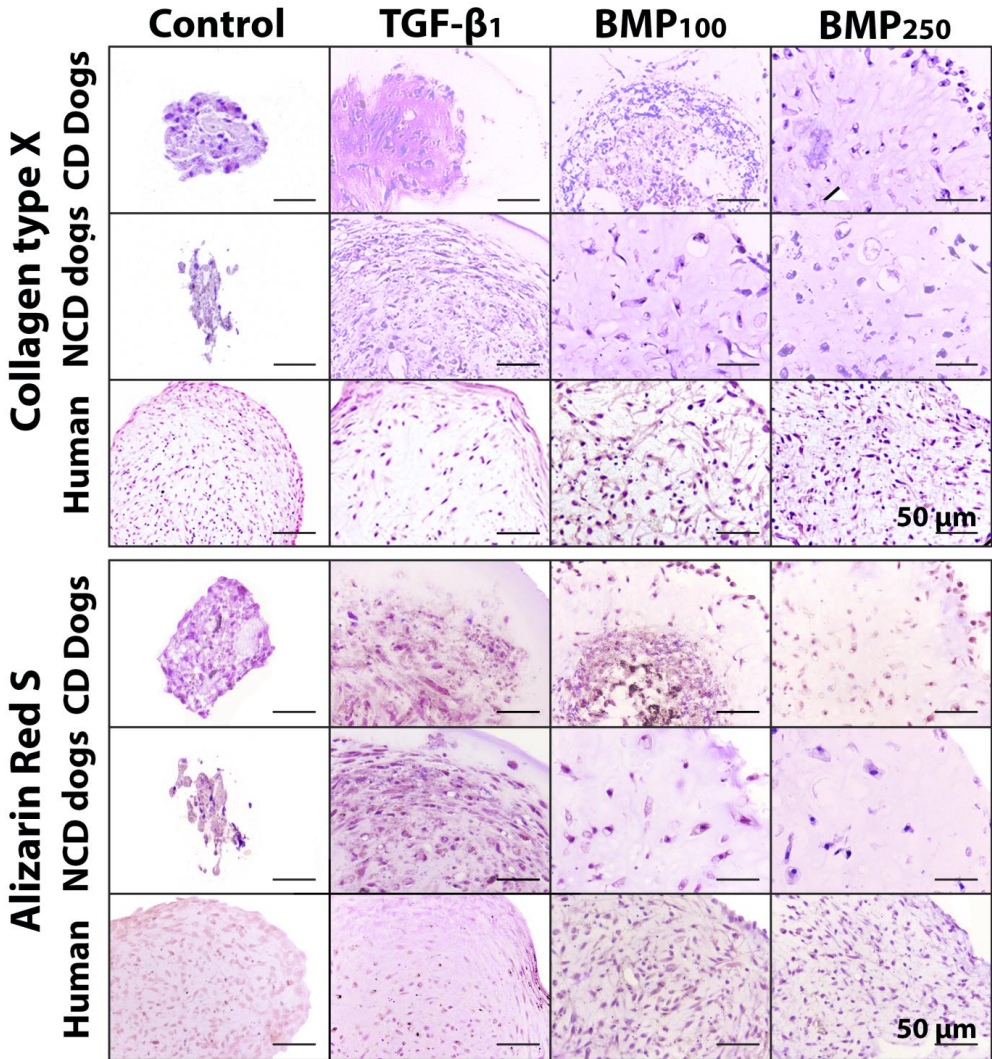
1. Muir P, Danova NA, Argyle DJ, Manley PA, Hao Z. 2005. Collagenolytic protease expression in cranial cruciate ligament and stifle synovial fluid in dogs with cranial cruciate ligament rupture. *Vet Surg* 34: 482-490.
2. Mahmoudabady M, Niazmand S, Shafei MN, McEntee K. 2013. Investigation of apoptosis in a canine model of chronic heart failure induced by tachycardia. *Acta Physiol Hung* 100: 435-444.
3. Porichi O, Nikolaidou ME, Apostolaki A, et al. 2009. BCL-2, BAX and P53 expression profiles in endometrial carcinoma as studied by real-time PCR and immunohistochemistry. *Anticancer Res* 29: 3977-3982.
4. Wen W, Ding J, Sun W, et al. 2010. Suppression of cyclin D1 by hypoxia-inducible factor-1 via direct mechanism inhibits the proliferation and 5-fluorouracil-induced apoptosis of A549 cells. *Cancer Res* 70: 2010-2019.
5. Ito TK, Ishii G, Chiba H, Ochiai A. 2007. The VEGF angiogenic switch of fibroblasts is regulated by MMP-7 from cancer cells. *Oncogene* 26: 7194-7203.

**Supplementary File 2. The effect of TGF- $\beta_1$  and BMP2 on gene expression of human and canine chondrocyte-like cells (CLCs) derived from degenerated intervertebral discs (IVDs)**



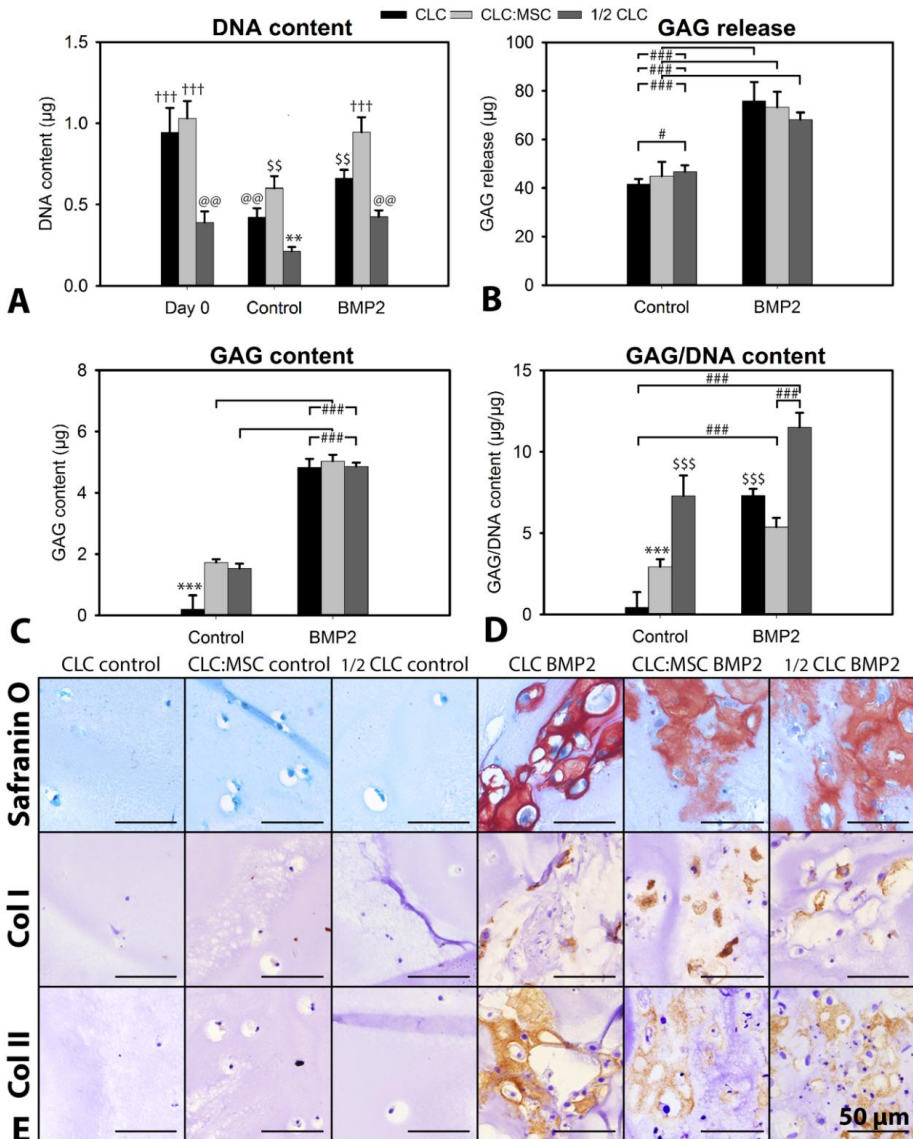
Relative *CCND1*, *BAX*, *ACAN*, *COL2A1*, *COL1A1* and *MMP13* gene expression (mean+SD) of the CLC micro-aggregates at day 7. The control micro-aggregates were set at 1.  $n=7$ . CD: chondrodystrophic, NCD: non-chondrodystrophic. \*, \*\*, \*\*\*: significantly different from all other conditions ( $p<0.05$ ,  $p<0.01$ ,  $p<0.001$ , respectively); \$, \$\$, \$\$\$: significantly different from all other conditions except the one with the other \$, \$\$, or \$\$\$ mark ( $p<0.05$ ,  $p<0.01$ ,  $p<0.001$ , respectively); #:  $p<0.05$ , ##:  $p<0.01$ .

**Supplementary File 3. TGF-β<sub>1</sub> and BMP2 do not induce collagen type X and calcium (identified by Alizarin Red S staining) deposition in human and canine chondrocyte-like cell (CLC) micro-aggregates**



Micro-aggregates of CLCs derived from degenerated human/canine intervertebral discs (IVDs) were cultured for 28 days. *n*=7 per condition. CD: chondrodystrophic, NCD: non-chondrodystrophic.

**Supplementary File 4. The effect of BMP2 on matrix production and cell proliferation of non-chondrodystrophic (NCD) canine chondrocyte-like cells (CLCs) and mesenchymal stromal cells (MSCs)**



CLC ( $3 \times 10^6/\text{mL}$  hydrogel),  $1/2$  CLC ( $1.5 \times 10^6/\text{mL}$ ) or CLC:MSC (1:1, both  $1.5 \times 10^6/\text{mL}$ ) hydrogels were cultured for 28 days with or without 250 ng/mL BMP2. (a) DNA content, (b) GAG release, (c) GAG content, (d) GAG/DNA content, (e) Safranin O/Fast green staining and collagen type I and II immunohistochemistry.  $n=8$ . #, ###:  $p < 0.05$  and  $p < 0.001$ , respectively; \*\*, \*\*\*: significantly different from all other conditions ( $p < 0.01$ ,  $p < 0.001$ , respectively); †††: significantly different from all other conditions except for the one with the same ††† mark ( $p < 0.001$ ); @@: significantly different from all other conditions except for the one with the same @@ mark ( $p < 0.01$ ); \$\$, \$\$\$: significantly different from all other conditions except for the one with the same \$\$ or \$\$\$ mark ( $p < 0.01$ ,  $p < 0.001$ , respectively).

**Supplementary File 5. Schematic overview of the observed effects of TGF- $\beta_1$  and BMP2 on chondrodystrophic (CD) and non-chondrodystrophic (NCD) canine and human chondrocyte-like cells (CLCs) derived from degenerated intervertebral discs**

Species, protein	10 ng/mL TGF- $\beta_1$			250 ng/mL BMP2		
	CD canine	NCD canine	Human	CD canine	NCD canine	Human
pSmad1	+	+/- (trend; $\rho = 0.1$ )	-	+	+	+
pSmad2	+	+	+/- (trend; $\rho = 0.1$ )	-	-	-
DNA content	++	+	++	+	+	+
GAG content	++	+	+	+	++	+
Collagen I	+	+	+	+/-	+/-	-
Collagen II	+	+	-	+	+	+
Collagen X	-	-	-	-	-	-

++: more increased compared with controls than under influence of the other growth factor (TGF- $\beta_1$ /BMP2); +: increased compared with controls; +/- moderately/mildly increased compared with controls; - not increased compared with controls.

**Link-N: the missing link towards intervertebral disc repair is species-specific**

Frances C. Bach<sup>1</sup>, Lisanne T. Laagland<sup>1</sup>, Michael P. Grant<sup>2,3</sup>, Laura B. Creemers<sup>4</sup>, Keita Ito<sup>4,5</sup>, Björn P. Meij<sup>1</sup>, Fackson Mwale<sup>2</sup>, Marianna A. Tryfonidou<sup>1,\*</sup>

<sup>1</sup> Department of Clinical Sciences of Companion Animals, Faculty of Veterinary Medicine, Utrecht University, Utrecht, the Netherlands

<sup>2</sup> Department of Surgery, McGill University, Montreal, Canada

<sup>3</sup> Orthopedic Research Laboratory, Lady Davis Institute for Medical Research, SMBD-Jewish General Hospital, Montreal, Canada

<sup>4</sup> Department of Orthopedics, University Medical Center Utrecht, Utrecht, the Netherlands

<sup>5</sup> Orthopedic Biomechanics, Department of Biomedical Engineering, Eindhoven University of Technology, Eindhoven, the Netherlands

## Abstract

Degeneration of the intervertebral disc (IVD) is a frequent cause for back pain in humans and dogs. Link-N stabilizes proteoglycan aggregates in cartilaginous tissues and exerts growth factor-like effects. The human variant of Link-N facilitates IVD regeneration in several species *in vitro* by inducing Smad1 signaling, but it is not clear whether this is species specific. Dogs with IVD disease could possibly benefit from Link-N treatment, but Link-N has not been tested on canine IVD cells. If Link-N appears to be effective in canines, this would facilitate translation of Link-N into the clinic using the dog as an *in vivo* large animal model for human IVD degeneration. This study's objective was to determine the effect of the human and canine variant of Link-N and short (s) Link-N on canine chondrocyte-like cells (CLCs) and compare this to those on already studied species, *i.e.* human and bovine CLCs. Extracellular matrix (ECM) production was determined by measuring glycosaminoglycan (GAG) content and histological evaluation. Additionally, the micro-aggregates' DNA content was measured. Phosphorylated (p) Smad1 and -2 levels were determined using ELISA. Human (s)Link-N induced GAG deposition in human and bovine CLCs, as expected. In contrast, canine (s)Link-N did not affect ECM production in human CLCs, while it mainly induced collagen type I and II deposition in bovine CLCs. In canine CLCs, both canine and human (s)Link-N induced negligible GAG deposition. Surprisingly, human and canine (s)Link-N did not induce Smad signaling in human and bovine CLCs. Human and canine (s)Link-N only mildly increased pSmad1 and Smad2 levels in canine CLCs. In conclusion, human and canine (s)Link-N exerted species-specific effects on CLCs from early degenerated IVDs. Both variants, however, lacked the potency as canine IVD regeneration agent. While these studies demonstrate the challenges of translational studies in large animal models, (s)Link-N still holds a regenerative potential for humans.

## Introduction

Low back pain affects up to 85% of the human population at some point during their lives, and this results in major socioeconomic consequences<sup>1,2</sup>. Degeneration of the intervertebral disc (IVD) is frequently associated with low back pain<sup>3</sup>. The healthy IVD consists of a central, gelatinous nucleus pulposus (NP), fibrous annulus fibrosus, and cartilaginous endplates. During IVD maturation, the vacuolated notochordal cells (NCs) are gradually replaced by smaller chondrocyte-like cells (CLCs). When the IVD degenerates, the CLCs are not able to maintain healthy NP tissue anymore: CLCs become senescent, the glycosaminoglycan (GAG) content decreases and collagen type II is replaced by collagen type I, resulting in a more fibrous NP tissue with decreased swelling pressure. The avascular IVD exhibits inadequate matrix repair, and a vicious circle develops in which the IVD experiences increased vulnerability to damage by physiologic loading<sup>4</sup>.

Current treatments for low back pain aim at relieving symptoms rather than restoring IVD function. Therefore, regenerative agents stimulating biological repair of the IVD (e.g. cell transplantation and growth factors) have gained interest<sup>5,6</sup>. Several regenerative agents have been shown to successfully decrease cell apoptosis, stimulate chondrogenic extracellular matrix (ECM) production, and/or enhance mesenchymal stromal cell (MSC) differentiation to an NP-like phenotype, but disadvantages are high costs and potential side-effects<sup>7,8</sup>. Several of these regenerative strategies, e.g. mesenchymal precursor cell (NCT01290367)/disc chondrocyte (NCT01640457) transplantation and growth factor application (NCT00813813) have entered the clinical trial phase, but no effective regenerative therapy for IVD degeneration is clinically available yet. Therefore, there is need for identifying new therapeutic agents that can induce IVD regeneration.

A promising alternative agent that can be produced synthetically, and is therefore relatively cheap, is Link-N peptide. Link-N (DHLSDNYTLHDRAIH) is the N-terminal peptide of the link protein that stabilizes proteoglycan aggregates in the IVD and cartilage. It is generated *in vivo* by proteolytic degradation during tissue turnover<sup>8-11</sup>. The human variant of Link-N peptide has been demonstrated to stimulate GAG and/or collagen production *in vitro* in rabbit<sup>12</sup>, human<sup>7,11,13</sup>, and bovine<sup>7,9,13</sup> IVD cells, and degenerated bovine IVDs<sup>14</sup>. Furthermore, it exerted regenerative effects on experimentally induced degenerated rabbit IVDs<sup>8</sup>, but has not yet been tested *in vivo* on large animal models. It is known that Link-N exerts its growth factor-like effects on rabbit NCs via the bone morphogenetic protein receptor type II (BMPRII), inducing a complex, positive Smad1/5/8 feedback loop<sup>12</sup>, but this has not been investigated in other species yet. Previous work indicated that Link-N is cleaved by AF cells, creating a peptide consisting of only the first eight amino acids of full-length Link-N (DHLSDNYT)<sup>13</sup>. This small peptide, named short Link-N (sLink-N), induced GAG synthesis in both human and bovine IVD cells to a similar extent as full-length Link-N<sup>13</sup> and repaired bovine IVDs in which degeneration was induced in a whole organ culture model<sup>15</sup>.

Altogether, Link-N and sLink-N may be promising candidates for the treatment of patients with IVD disease. Since dogs also experience back pain related to IVD degeneration, the dog is a particularly clinically relevant animal model<sup>16</sup>. Given that both species show similar pathophysiologic mechanisms of IVD degeneration, treatment strategies can be approached by the “One Medicine” concept: advances in the biomedical field of IVD regeneration hold a

future, also for the veterinary patient. However, thus far, the effect of (short) Link-N on canine IVDs has not been delineated yet. Therefore, the objective of this study was to determine the effect of (short) Link-N on canine CLCs and compare the effects to those on already studied species, *i.e.* human and bovine CLCs. Our hypothesis was that human, and especially canine (short) Link-N would induce ECM production in canine CLCs. If human/canine (short) Link-N indeed appears to be effective in canine CLCs, this would facilitate the translation of (short) Link-N into the clinic using the dog as an *in vivo* large animal model for human IVD degeneration. Additionally, it would pave the way to an effective and affordable regenerative treatment for both human and canine patients with IVD disease.

## Materials and methods

### IVD collection and CLC isolation

CLCs from human (Thompson score III), bovine (Thompson score II), and chondrodystrophic (CD) and non-chondrodystrophic (NCD) canine (Thompson score II-III) donors were collected from early degenerated IVDs as described previously<sup>17</sup>. Briefly, NP tissue was enzymatically digested with 0.15% pronase (11459643001, Roche Diagnostics) for 45 minutes and 0.15% collagenase type II (4176, Worthington) for 15 hours at 37°C. After digestion, 100% CLCs, and no NCs were present in all species. Human IVDs were obtained during standard postmortem diagnostics. The L2-L5 part of the spine was collected ( $\leq 48$  hours after death), as approved by the scientific committee of the Pathology department of the University Medical Centre Utrecht (UMCU). Anonymous use of redundant tissue for research purposes is a standard treatment agreement with UMCU patients (Local Medical Ethical Committee number 12-364). The material was used in line with the code 'Proper Secondary Use of Human Tissue', installed by the Federation of Biomedical Scientific Societies. Bovine tails were collected from the slaughterhouse (Nederlandse Voedsel- en Warenautoriteit, Utrecht, the Netherlands, permit number 457642.09) and IVDs from complete canine spines were collected from dogs euthanized in unrelated research studies<sup>18</sup>, approved by the Utrecht University Animal Ethics Committee (experimental numbers: 2012.III.07.065, 2013.III.02.017, and 2013.II.12.126).

### Cell culture

Since culturing IVD cells in a 3D environment maintains their disc phenotype better than 2D culture<sup>19, 20</sup> and canine cells do not thrive in alginate beads<sup>21</sup>, CLC micro-aggregates were used to determine the effect of (s)Link-N. Previous *in vitro* studies demonstrating regenerative effects of (s)Link-N were performed in human or bovine monolayer<sup>11, 22</sup> or alginate bead<sup>7, 13</sup> cultures. To allow inter-species comparison in this study, canine, human, and bovine CLC micro-aggregate cultures were used.

One million CLCs from three human (47, 63, and 67 years of age), six bovine (2 years of age), six CD canine (2-6 years of age, Beagles) and six NCD canine (4-11 years of age, 3 German shepherds, 1 Cocker Spaniël, 1 Greyhound, and 1 Irish Setter) donors were expanded as described previously<sup>17</sup> in expansion medium containing hgDMEM+Glutamax (31966, Invitrogen) with 10% FBS (16000-044, Life Technologies), 1% penicillin/streptomycin (P/S, P11-010, PAA Laboratories), 0.1 mM Ascorbic acid 2-phosphate (Asap, A8960, Sigma-

Aldrich),  $10^{-8}$  M dexamethasone (AD1756, Sigma-Aldrich) and 1 ng/mL bFGF (PHP105, AbD Serotec). After expansion for two (bovine, canine) or three (human) passages, 35,000 CLCs were plated per well in low-adherence cell-repellent surface 96-well plates (650970, CELLSTAR® Greiner Bio-one) in 50  $\mu$ L basal culture medium: hgDMEM+Glutamax, 1% P/S, 1% ITS+ premix (354352, Corning Life Sciences), 0.04 mg/mL L-proline (P5607, Sigma-Aldrich), 0.1 mM Asap, and 1.25 mg/mL Bovine Serum Albumin (A9418, Sigma-Aldrich). The 96-well plates were centrifuged at 50g for 5 minutes to induce micro-aggregate formation. The next day, basal culture medium was replaced with basal culture medium (negative controls) or supplemented with (a) 10 ng/mL human recombinant TGF- $\beta_1$  (240-B, R&D Systems), (b) 1  $\mu$ g/mL or 10 ng/mL human Link-N (DHLSDNYT-LDHDRAIH, CanPeptide), (c) 0.5  $\mu$ g/mL or 5 ng/mL human sLink-N (DHLSDNYT, CanPeptide), (d) 1  $\mu$ g/mL or 10 ng/mL canine Link-N (DHHSDNYT-LNYDVIH, CanPeptide), or (e) 0.5  $\mu$ g/mL or 5 ng/mL canine sLink-N (DHHSDNYT, CanPeptide). Culture medium was replaced twice weekly and (s)Link-N was supplemented with every medium change. (s)Link-N concentrations were chosen based upon previous work<sup>9, 13, 14</sup> and on a monolayer pilot study with CD canine CLCs (Supplementary File 1). Since canine CLCs do not produce a considerable amount of GAGs if no growth factor is supplied, TGF- $\beta_1$  was used to show that the canine CLCs were able to produce GAGs if a proper stimulus was provided. Initially, the micro-aggregates were cultured for 28 days at 21% O<sub>2</sub>, 5% CO<sub>2</sub>, 37°C to determine the effects of human (s)Link-N. Follow-up culture experiments (*i.e.* using canine (s)Link-N) were performed at 5% O<sub>2</sub>, 5% CO<sub>2</sub>, 37°C, to improve the chondrogenic response of the CLCs<sup>23, 24</sup>.

#### **Read out parameters for the biologic effect of (s)Link-N at the matrix level**

At day 28, micro-aggregates were collected for determining the GAG and DNA content (in duplicates). Sample preparation was performed as described previously<sup>17</sup>. Papain digestion solution (pH 6, 200 mM H<sub>2</sub>NaPO<sub>4</sub>\*2 H<sub>2</sub>O (21254, Boom B.V.), 10 mM EDTA (100944, Merck Millipore), 10 mM cysteine HCl (C7880, Sigma-Aldrich), and 10 mM papain (P3125, Sigma-Aldrich) was added to each micro-aggregate, followed by overnight incubation at 60°C. The micro-aggregates' GAG content and release in the culture medium (cumulative GAG release over the 28 day period) was measured using a dimethyl methylene blue (DMMB) assay<sup>25</sup>. Immediately after DMMB (341088, Sigma-Aldrich) was added, the absorbance (540/595 nm) was measured using a microplate reader. The GAG content was calculated using a chondroitin sulphate (C4384, Sigma-Aldrich) standard line with polynomial properties. DNA content was measured using the Qubit® dsDNA High Sensitivity Assay Kit (Q32851, Invitrogen) according to the manufacturer's instructions.

Also at day 28, micro-aggregates were fixed in 4% neutral buffered formaldehyde for 24 hours and embedded in alginate and paraffin (in duplicates). Five  $\mu$ m sections were mounted and Safranin O/Fast Green staining, and collagen type I and II immunohistochemistry were performed as described previously<sup>17</sup>. The primary antibodies for collagen type I (human and bovine: 0.1  $\mu$ g/mL, canine: 0.07  $\mu$ g/mL; ab6308, Abcam) and II (human and bovine: 0.4  $\mu$ g/mL, canine: 0.02  $\mu$ g/mL; II-II6B3, DSHB) were applied with adjusted concentrations per species. In isotype controls, normal mouse IgG (3877, Santa Cruz) employed at the same concentration as the primary antibody showed no staining.

### BMP receptor expression and activation of Smad signaling by (s)Link-N

At day 7, *BMPRIa*, *BMPRIb*, and *BMPRII* gene expression was determined in CD canine CLC micro-aggregates treated with control culture medium supplemented with/without 10 ng/mL TGF- $\beta_1$ , 1  $\mu$ g/mL or 10 ng/mL canine Link-N, or 0.5  $\mu$ g/mL or 5 ng/mL canine sLink-N. The micro-aggregates were frozen in liquid nitrogen and crushed using pestles (P9951-901, Argos Technologies). RNA was extracted with the RNeasy<sup>®</sup> Micro kit (74004, Qiagen) according to the manufacturer's instructions. A DNase (RNase-Free DNase Set, 79254, Qiagen) step was included to ensure DNA removal. The quality of the isolated RNA was assessed with an Agilent 2100 Bioanalyzer and RNA Nanochip kit (5067-1511, Agilent Technologies). cDNA was synthesized using the iScript<sup>™</sup> cDNA Synthesis Kit (170-8891, Bio-Rad) according to the manufacturer's instructions. Primer sequences were designed using PerlPrimer (<http://perlprimer.sourceforge.net>). M-fold was used to check for secondary structure formation<sup>26</sup>. Primer uniqueness and specificity was determined using BLAST<sup>27</sup>. Annealing temperatures were established by performing a temperature gradient PCR on a 16-fold dilution series. The four most stably expressed reference genes were chosen to normalize gene expression of the target genes (Table 1).

**Table 1. Primers used for quantitative PCR**

Genes	Forward sequence 5' → 3'	Reverse sequence 5' → 3'	Amplicon size	Annealing temp (°C)
<b>Reference genes</b>				
<i>GAPDH</i>	TGCCCCACCCCAATGTATC	CTCCGATGCCTGCTTCACTACCTT	100	58
<i>HPRT</i>	AGCTTGCTGGTGAAAAGGAC	TTATAGTCAAGGGCATATCC	104	58
<i>RPS19</i>	CCTTCTCAAAAAGTCTGGG	GTTCTCATCGTAGGGAGCAAG	95	61
<i>SDHA</i>	GCCTTGATCTCTTGATGGA	TTCTTGGCTCTTATGCGATG	92	56.5
<b>Target genes</b>				
<i>BMPRIa</i>	TTTGGGAAATGGCTCGTC	CGTATGATGGATCGTTGGG		60
<i>BMPRIb</i>	CCCTATCATGACCTAGTGCC	TGCCTCAGACTCATCAC		63
<i>BMPRII</i>	GTCTTACAGTATGAACATGATGG	AACACTTTCACAGCAACTGG	150	64
<i>GAPDH</i> :	glyceraldehyde	3-phosphate	dehydrogenase,	<i>HPRT</i> :
			phosphoribosyltransferase,	hypoxanthine-guanine
			<i>RPS19</i> :	phosphoribosyltransferase,
			ribosomal protein S19,	
			<i>SDHA</i> :	succinate dehydrogenase subunit A.

RT-qPCR was performed using the iQTTM SYBR Green Supermix Kit (Bio-Rad) and the CFX384 Touch<sup>™</sup> Real-Time PCR Detection System (Bio-Rad) (40 cycles; denaturation 95°C, annealing temp (Table 1), extension 65°C). For determination of relative quantitative gene expression, the Normfirst ( $E^{\Delta\Delta Cq}$ ) method was used. For each target gene, the Cq-value of the test sample and the calibrator sample was normalized to the mean Cq-value of the reference genes:  $\Delta Cq = Cq_{\text{mean ref}} - Cq_{\text{target}}$ . Cq-values of the negative control micro-aggregates were used as calibrator. Secondly, the  $E^{\Delta Cq}$ -value for the test and calibrator sample was calculated. In this formula, E indicates the amplification efficiency of the target/reference gene.  $E^{\Delta\Delta Cq}$  was calculated by normalizing the  $E^{\Delta Cq}$ -value of the test sample to the one of the calibrator:  $E^{\Delta\Delta Cq} = E^{\Delta Cq}_{\text{test}} - E^{\Delta Cq}_{\text{calibrator}}$ . For each target gene, the mean n-fold changes and standard deviations in gene expression were calculated.

ELISAs for phosphorylated (p) Smad1 (SER463/465, PEL-SMAD1-S463, RayBiotech) and pSmad2 (S245/250/255, PEL-SMAD2-S245, RayBiotech) were used to determine activation of the BMP and TGF- $\beta$  Smad signaling pathway. For this purpose, 200,000 CLCs from five human (44, 47, 47, 63, and 67 years of age), five bovine (2 years of age), and five canine (Beagles, 2-6 years of age) donors were plated per well (12-wells plate, 665180, Greiner CELLSTAR®) in expansion medium, which was replaced after 2 days with basal culture medium alone or supplemented with 10 ng/mL TGF- $\beta_1$ , 250 ng/mL BMP2 (TETEC AG), 1  $\mu$ g/mL human Link-N, 1  $\mu$ g/mL canine Link-N, 0.5  $\mu$ g/mL human sLink-N or 0.5  $\mu$ g/mL canine sLink-N. TGF- $\beta_1$  and BMP2 served here as positive controls. After 24 hours (time point based on Wang *et al.*, 2013<sup>12</sup>), cells were homogenized in cell lysis buffer containing 0.6 mM phenylmethylsulphonyl fluoride, 17  $\mu$ g/mL aprotinin and 1 mM sodium orthovanadate (Sigma-Aldrich). The data were corrected for the samples protein concentration, measured using the Qubit® Protein Assay Kit (Q32851, Invitrogen).

### **(Short) Link-N peptide structure prediction and docking**

The human, canine and bovine models of (s)Link-N were generated using the PEP-FOLD3 server<sup>28</sup>. The first eight residues of human and canine/bovine Link protein were inputted and the best predicted model was used for docking. Human, canine, and bovine (s)Link-N molecular structures were viewed and aligned using PyMOL (The PyMOL Molecular Graphics System, Version 1.8, Schrödinger, Germany). Docking of (s)Link-N to BMPRII was performed using the CABS-dock server ([www.biocomp.chem.uw.edu.pl/CABSdock/](http://www.biocomp.chem.uw.edu.pl/CABSdock/)) and the crystal structure of the extracellular domain of BMPRII (PDB ID: 2HLR)<sup>29</sup> downloaded from the Protein Data Bank ([www.rcsb.org](http://www.rcsb.org)). The original crystal structure of the BMPRII extracellular domain was from sheep, since there are no entries for the crystal structures of human, bovine, or canine BMPRII extracellular domains. The best-fit model with the lowest root-mean-square deviation (RMSD) was used for imaging with PyMOL.

### **Statistical analysis**

Statistical analyses were performed using IBM SPSS statistics 22. Data were examined for normal distribution with the Shapiro Wilks test. General linear regression models based on ANOVAs were used for normally distributed data, whereas Kruskal Wallis and Mann-Whitney U tests were used for non-normally distributed data. Benjamini & Hochberg False Discovery Rate *post-hoc* tests were performed to correct for multiple comparisons. *p*-values < 0.05 were considered significant.

## Results

### Human (s)Link-N induced GAG and collagen type I deposition by human CLCs

The first objective of this study was to determine the effects of human (s)Link-N on canine CLCs and to compare those to already studied species. Therefore, the effects of human (s)Link-N were initially determined on human and bovine CLC micro-aggregates.

TGF- $\beta_1$  treatment resulted in the highest GAG content of the human CLC micro-aggregates after 28 days ( $p < 0.05$ ; Figure 1a). Treatment with 1  $\mu\text{g}/\text{mL}$  human Link-N also resulted in a significantly increased GAG content of the micro-aggregates compared with control and 10 ng/mL human Link-N treatment ( $p < 0.05$ ), indicating a concentration-dependent effect. This was confirmed by Safranin O/Fast Green staining (Figure 1e). No treatment affected the DNA content of the micro-aggregates (Figure 1b). Only TGF- $\beta_1$  upregulated the GAG/DNA content (indication of GAG incorporation in the micro-aggregate per cell) compared with controls ( $p < 0.05$ ; Figure 1c). GAG release into the culture medium was significantly increased by TGF- $\beta_1$ , 1  $\mu\text{g}/\text{mL}$  human Link-N and 0.5  $\mu\text{g}/\text{mL}$  human sLink-N treatment compared with control, 10 ng/mL human Link-N, and 5 ng/mL human sLink-N treatment ( $p < 0.05$ ; Figure 1d). GAG incorporation (GAG content micro-aggregate divided by total GAG production micro-aggregate) was, however, not significantly different between control, TGF- $\beta_1$ , 1  $\mu\text{g}/\text{mL}$  human Link-N and 0.5  $\mu\text{g}/\text{mL}$  human sLink-N treatment (Supplementary File 2a). Both TGF- $\beta_1$  and human (s)Link-N induced collagen type I deposition, whereas only TGF- $\beta_1$  increased collagen type II deposition compared with controls (Figure 1e).

### Human (s)Link-N induced GAG and collagen type I deposition by bovine CLCs

Treatment with TGF- $\beta_1$ , 1  $\mu\text{g}/\text{mL}$  human Link-N, and 0.5  $\mu\text{g}/\text{mL}$  human sLink-N resulted in a significantly higher GAG, DNA, and GAG/DNA content, GAG incorporation percentage and GAG release of the bovine CLC micro-aggregates compared with control, 10 ng/mL human Link-N, and 5 ng/mL human sLink-N treatment ( $p < 0.05$ ; Figure 2a-d and Supplementary File 2c), indicating a concentration-dependent effect. This was confirmed by Safranin O/Fast Green staining (Figure 2e). A rim of collagen type I was detected around the micro-aggregates treated with 10 ng/mL human Link-N and 5 ng/mL human sLink-N, while 1  $\mu\text{g}/\text{mL}$  human Link-N and 0.5  $\mu\text{g}/\text{mL}$  human sLink-N treatment induced collagen type I deposition in the center of the micro-aggregates (Figure 2e). Deposition of collagen type II was not observed with TGF- $\beta_1$  or human Link-N treatment (Figure 2e).

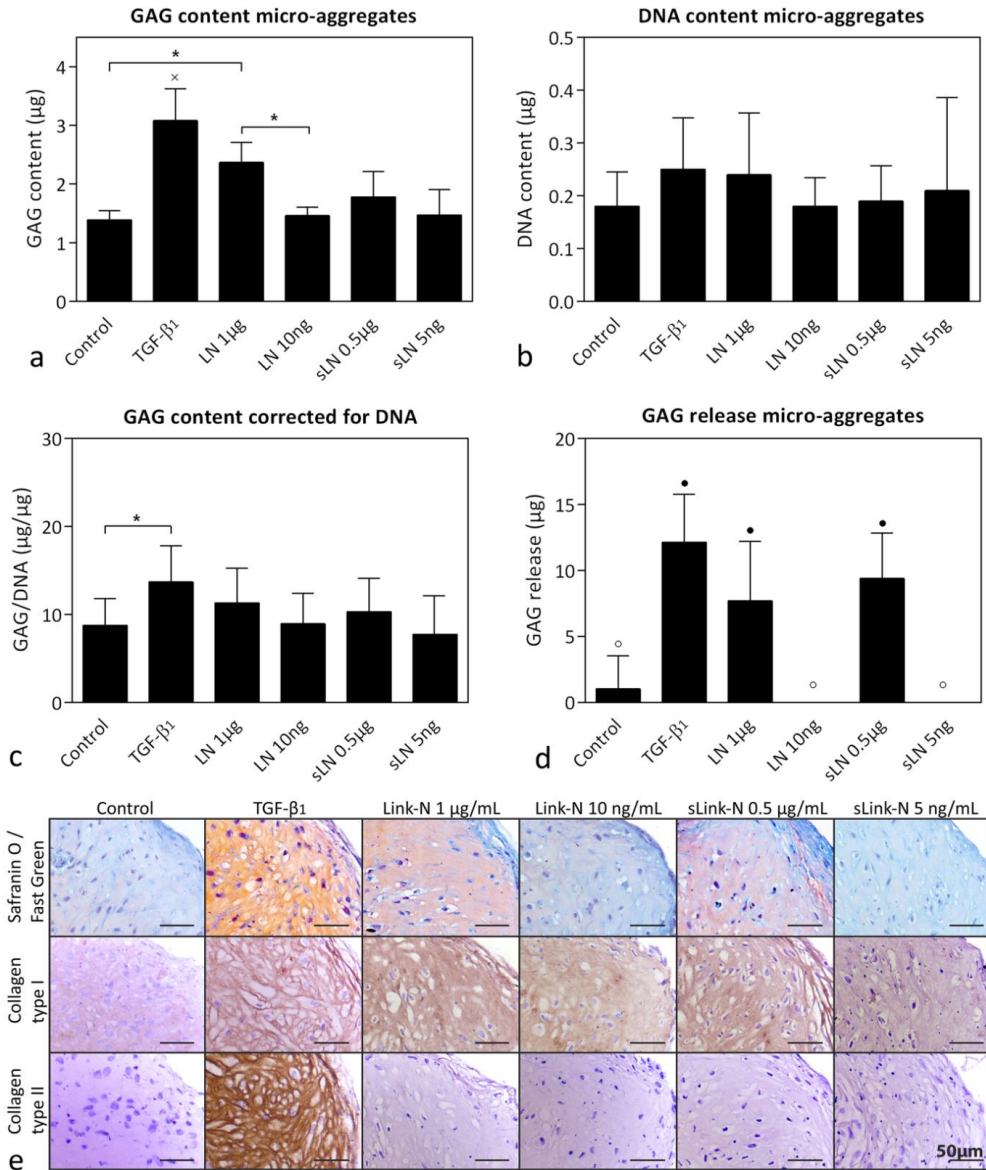


**Figure 1. Effect of human (short) Link-N on human chondrocyte-like cells (CLCs).** GAG and DNA content (mean + SD) and histological evaluation of human CLC micro-aggregates treated with basal culture medium (control), supplemented with 10 ng/mL TGF- $\beta_1$  (positive control), 1  $\mu\text{g}/\text{mL}$  or 10 ng/mL human Link-N (LN), or 0.5  $\mu\text{g}/\text{mL}$  or 5 ng/mL human short Link-N (sLN) for 28 days in normoxia (21%  $\text{O}_2$ ). (a) GAG content, (b) DNA content, (c) GAG content (incorporation in the micro-aggregate) corrected for DNA content, (d) total amount of GAGs released in the culture medium, (e) representative histological images of the Safranin O/Fast Green staining and collagen type I and II immunohistochemistry. \*:  $p < 0.05$ ; • and ○ : significantly different ( $p < 0.05$ ) from all other conditions except for the bars with the same symbol; x: significantly different ( $p < 0.05$ ) from all other conditions.  $n = 3$  (in duplicates).

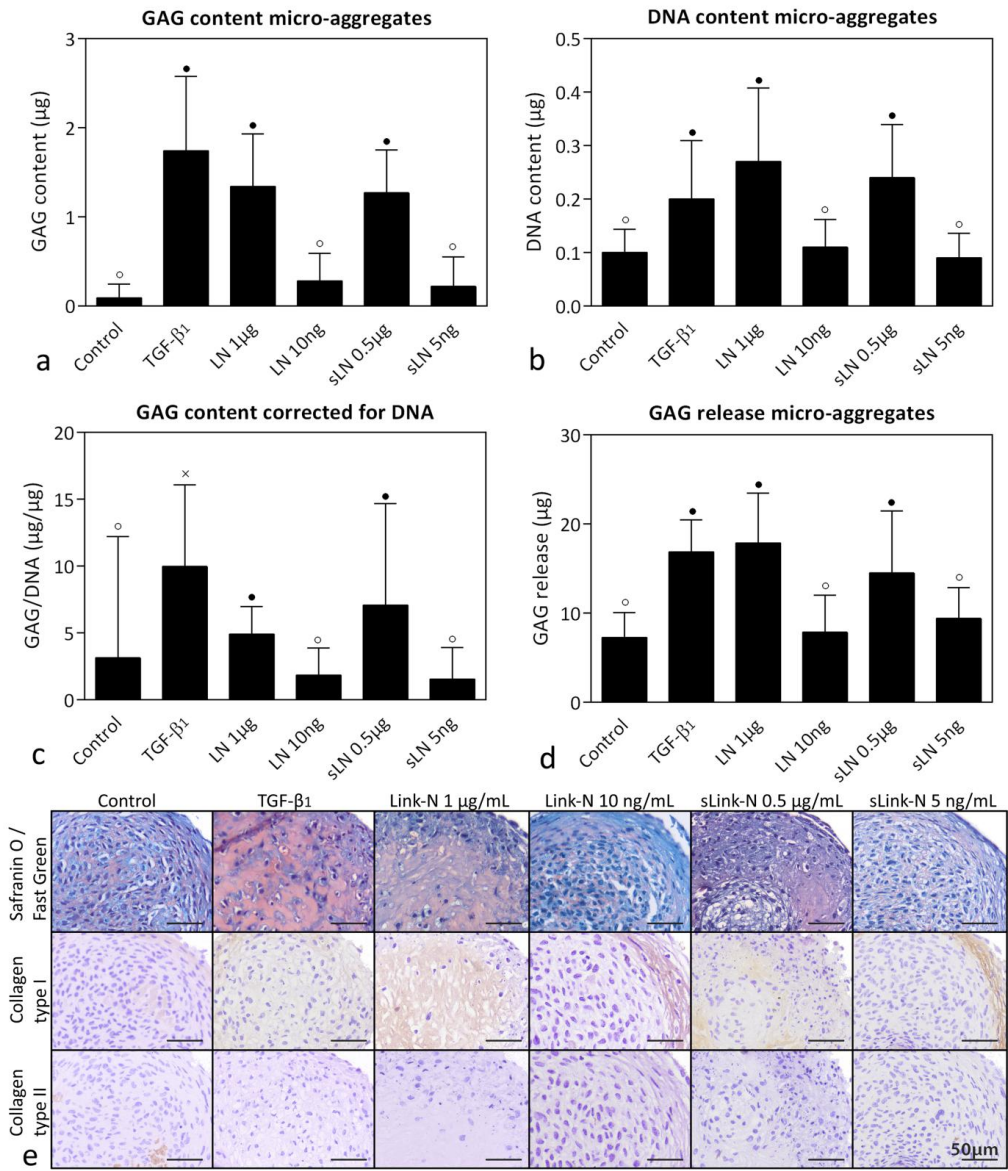


**Figure 2. Effect of human (short) Link-N on bovine chondrocyte-like cells (CLCs).** GAG and DNA content (mean + SD) and histological evaluation of bovine CLC micro-aggregates treated with basal culture medium (control), supplemented with 10 ng/mL TGF-β<sub>1</sub>, 1 µg/mL or 10 ng/mL human Link-N (LN), or 0.5 µg/mL or 5 ng/mL human short Link-N (sLN) for 28 days in normoxia (21% O<sub>2</sub>). (a) GAG content, (b) DNA content, (c) GAG content (incorporation in the micro-aggregate) corrected for DNA content, (d) total amount of GAGs released in the culture medium, (e) representative histological images of the Safranin O/Fast Green staining and collagen type I and II immunohistochemistry. ● and ○ : significantly different ( $p < 0.05$ ) from all other conditions except for the bars with the same symbol; x: significantly different ( $p < 0.05$ ) from all other conditions.  $n = 6$  (in duplicates).

### Human (s)Link-N induced negligible GAG deposition by CD canine CLCs

Although far less potent as TGF- $\beta_1$ , human (s)Link-N treatment at all concentrations significantly increased the GAG content of the CD canine CLC micro-aggregates compared with controls, both corrected ( $p < 0.001$ ) and not corrected ( $p < 0.01$ ) for the DNA content (Figure 3a,c). Additionally, human (s)Link-N at all concentrations also significantly increased GAG incorporation compared with controls ( $p < 0.05$ ; Supplementary File 2e). TGF- $\beta_1$  induced the highest DNA content, GAG release and GAG incorporation compared with all the other conditions ( $p < 0.01$ ), whereas human (s)Link-N did not affect the DNA content and GAG release compared with controls (Figure 3b,d).

In line with the biochemical data, Safranin O/Fast Green staining demonstrated limited GAG deposition in the human (s)Link-N-treated micro-aggregates (Figure 3e). Addition of TGF- $\beta_1$  resulted in most GAG deposition and a cell-depleted rim around the micro-aggregates. Collagen type I deposition was slightly induced by TGF- $\beta_1$  and human (s)Link-N, while no differences in collagen type II deposition were detected between conditions (Figure 3e).

Given that a lower O<sub>2</sub> tension has been shown to facilitate ECM deposition<sup>23</sup>, the effect of human (s)Link-N on CD canine CLCs was also studied under hypoxia (Supplementary File 3). It appeared that the effects of human (s)Link-N were not affected by the O<sub>2</sub> tension: in both conditions, human (s)Link-N exerted a limited anabolic effect compared with controls. Nevertheless, since the IVD is an avascular structure, hypoxia better mimics the *in vivo* situation and has been shown to better preserve the regenerative potential of CLCs<sup>23, 24</sup>, follow-up experiments (*e.g.* using canine (s)Link-N) were continued in hypoxia.

### Species differences in amino acid sequence of (short) Link-N

A possible explanation for the limited response of the canine CLCs to human (s)Link-N could be differences in amino acid sequence between human and canine (s)Link-N. Indeed, alignment of human, bovine, and canine Link-N revealed that the amino acid sequence of canine Link-N differed by five residues and bovine Link-N by three residues when compared to human Link-N (Table 2). Furthermore, the predicted molecular structures of bovine Link-N and canine Link-N also revealed differences when aligned with human Link-N (Figure 4a,b). The amino acid sequences of canine and bovine sLink-N are similar and differ by only one amino-acid from human sLink-N (Table 2). A schematic of the predicted molecular structures of human and canine/bovine sLink-N show that these amino acid substitutions influence the conformation of the peptide (Figure 4c). Interestingly, when we prepared docking simulations of all three Link-N species to the extracellular domain of BMPRII, bovine, canine, and human Link-N docked differently (Figure 4d). Docking differences were also observed for human and canine/bovine sLink-N variants (Figure 4e).

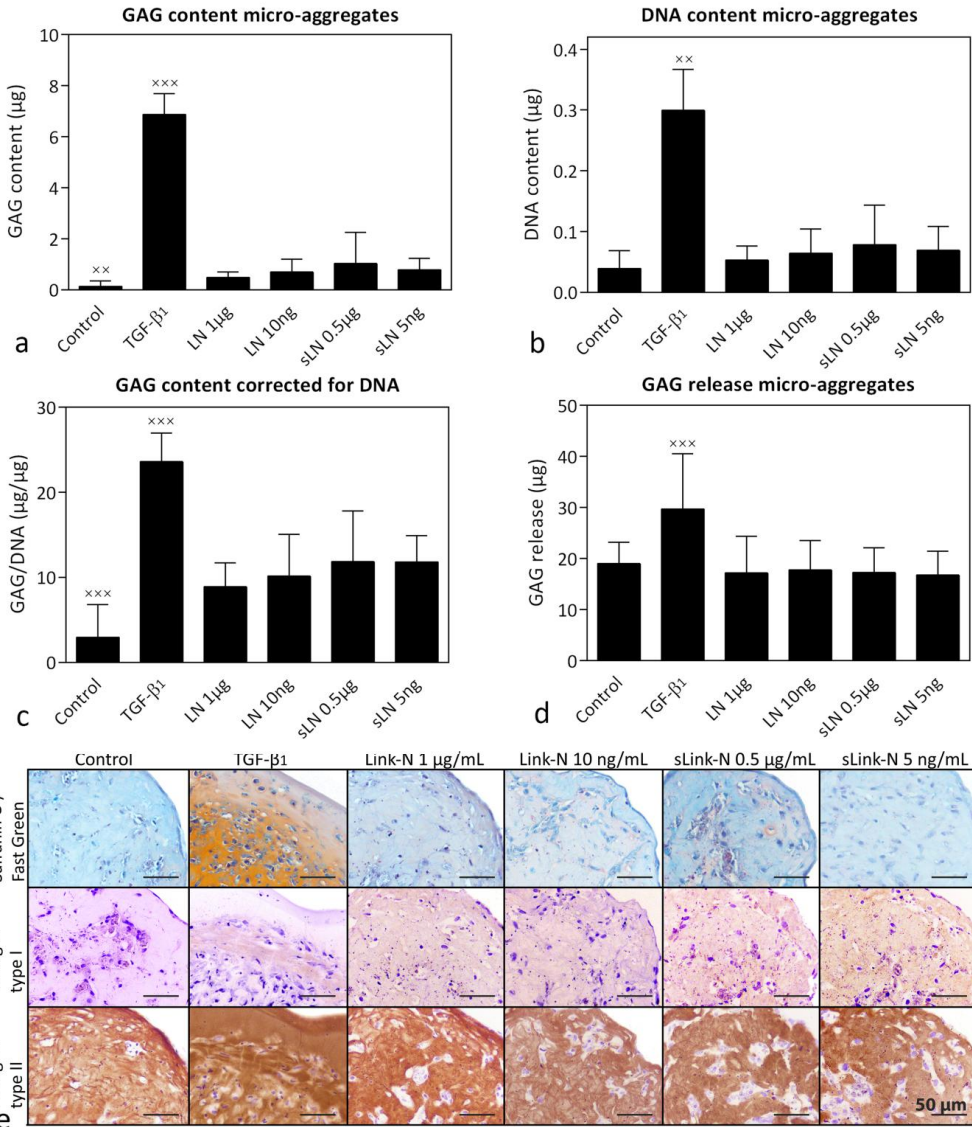


**Figure 3. Effect of human (short) Link-N on CD canine chondrocyte-like cells (CLCs).** GAG and DNA content (mean + SD) and histological evaluation of CD canine CLC micro-aggregates treated with basal culture medium (control), supplemented with 10 ng/mL TGF-β<sub>1</sub>, 1 µg/mL or 10 ng/mL human Link-N (LN), or 0.5 µg/mL or 5 ng/mL human short Link-N (sLN) for 28 days in normoxia (21% O<sub>2</sub>). (a) GAG content, (b) DNA content, (c) GAG content (incorporation in the micro-aggregate) corrected for DNA content, (d) total amount of GAGs released in the culture medium, (e) representative histological images of the Safranin O/Fast Green staining and collagen type I and II immunohistochemistry. xx, xxx: significantly different ( $p < 0.01$  and  $p < 0.001$ , respectively) from all other conditions.  $n = 6$  (in duplicates).

**Table 2. Alignment of human, bovine, and canine (short) Link-N peptides.**

Residue	1	2	3	4	5	6	7	8	-	9	10	11	12	13	14	15	16
<b>Human</b>	D	H	L	S	D	N	Y	T	-	L	D	H	D	R	A	I	H
<b>Bovine</b>	D	H	H	S	D	N	Y	T	-	V	D	H	D	R	V	I	H
<b>Canine</b>	D	H	H	S	D	N	Y	T	-	V	N	Y	D	R	V	I	H

Short Link-N represents residues 1-8. Bovine and canine short Link-N share similarity.

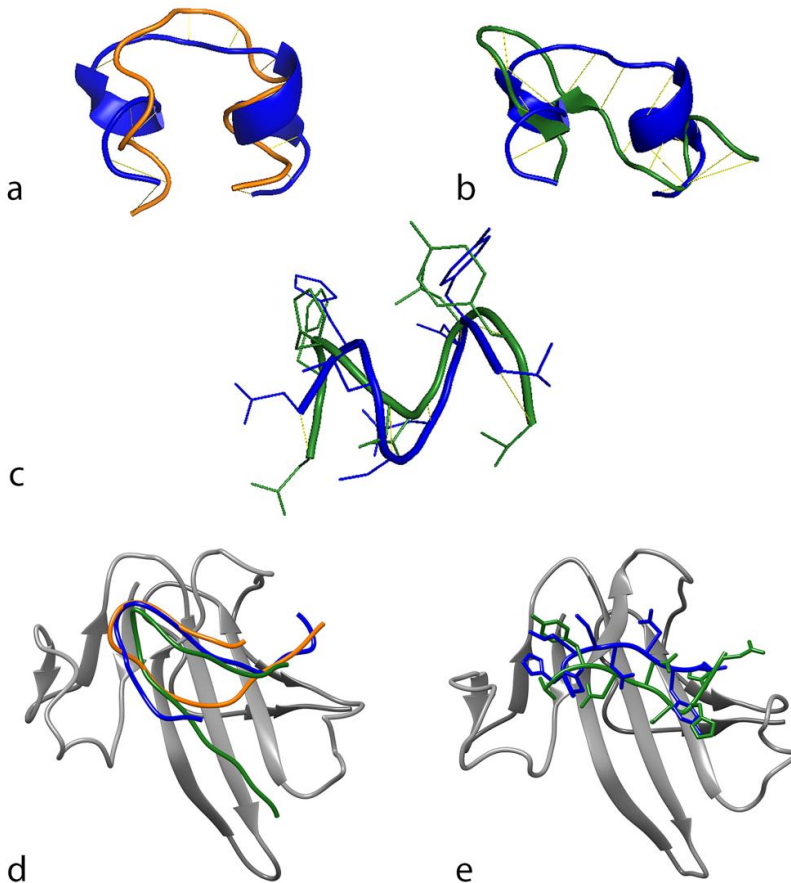


**Figure 4. Alignment and docking of human, bovine, and canine (short) Link-N variants.** Schematic of the predicted molecular model and alignment of human (blue) and bovine (orange) Link-N (a) and human (blue) and canine (green) Link-N (b). (c) Schematic of the predicted molecular model and alignment of human (blue) and canine/bovine (green) short Link-N. (d) Docking of human (blue), bovine (orange) and canine (green) Link-N to the extracellular domain of BMPRII. (e) Docking of human (blue) and canine/bovine (green) short Link-N to the extracellular domain of BMPRII. Models represent best-fit predictions for their interaction.

### Canine (s)Link-N did not affect ECM production by human CLCs

Since we detected species differences in amino acid sequence and receptor docking of human and canine (s)Link-N which could possibly explain the limited response of canine CLCs to human (s)Link-N, the effect of canine (s)Link-N was determined on human, bovine and canine CLCs. As under normoxic culture conditions, TGF- $\beta_1$  induced the GAG content of human CLC micro-aggregates cultured under hypoxic conditions ( $p < 0.05$ ; Figure 5a), which was confirmed by Safranin O/Fast Green staining (Figure 5e). In contrast, canine (s)Link-N treatment did not augment GAG deposition compared with controls (Figure 5a). No treatment affected the DNA content of the micro-aggregates (Figure 5b). The GAG/DNA content of the micro-aggregates treated with 5 ng/mL canine sLink-N was significantly higher than those treated with 10 ng/mL canine Link-N ( $p < 0.05$ ), but no treatment affected the GAG/DNA content compared with controls (Figure 5c). There were no significant effects of canine (s)Link-N or TGF- $\beta_1$  on GAG release compared with controls (Figure 5d). Also, GAG incorporation percentages were not significantly different between the conditions (Supplementary File 2b). The deposition of collagen type I was prominently increased by TGF- $\beta_1$  and slightly increased by 10 ng/mL canine Link-N and 5 ng/mL canine sLink-N compared with controls (Figure 5e). TGF- $\beta_1$  increased collagen type II deposition, whereas this was not affected by canine (s)Link-N (Figure 5e).

### Canine (s)Link-N mainly induced collagen type I and II deposition by bovine CLCs

The bovine CLC micro-aggregates' GAG content was slightly increased by 1  $\mu\text{g/mL}$  canine Link-N and 0.5  $\mu\text{g/mL}$  canine sLink-N treatment compared with controls ( $p < 0.05$ ; Figure 6a). The GAG content of micro-aggregates treated with 1  $\mu\text{g/mL}$  canine Link-N and 0.5  $\mu\text{g/mL}$  canine sLink-N was significantly higher than that of the micro-aggregates treated with 10 ng/mL canine Link-N and 5 ng/mL canine sLink-N, indicating a concentration-dependent effect ( $p < 0.05$ ). TGF- $\beta_1$ , however, induced the most potent increase in GAG content ( $p < 0.01$ ). GAG incorporation percentages were not significantly different between conditions (Supplementary File 2D). Safranin O/Fast Green staining showed the presence of GAGs in all conditions, but most prominently in the TGF- $\beta_1$ -treated micro-aggregates (Figure 6e). Treatment with canine (s)Link-N did not increase the micro-aggregates' DNA content compared with controls, whereas TGF- $\beta_1$  significantly increased the DNA content compared with all other conditions ( $p < 0.01$ ; Figure 6b). The GAG/DNA content was not different between conditions (Figure 6c). TGF- $\beta_1$  induced the highest GAG release compared with all other conditions ( $p < 0.01$ ), whereas the GAG release was decreased with 10 ng/mL canine Link-N compared with controls and compared with 5 ng/mL sLink-N treatment ( $p < 0.05$ ; Figure 6d). Collagen type I was present in all micro-aggregates, but most prominent in the canine (s)Link-N-treated ones (Figure 6e). Treatment with canine (s)Link-N prominently increased collagen type II deposition compared with controls and TGF- $\beta_1$ -treated micro-aggregates (Figure 6e).

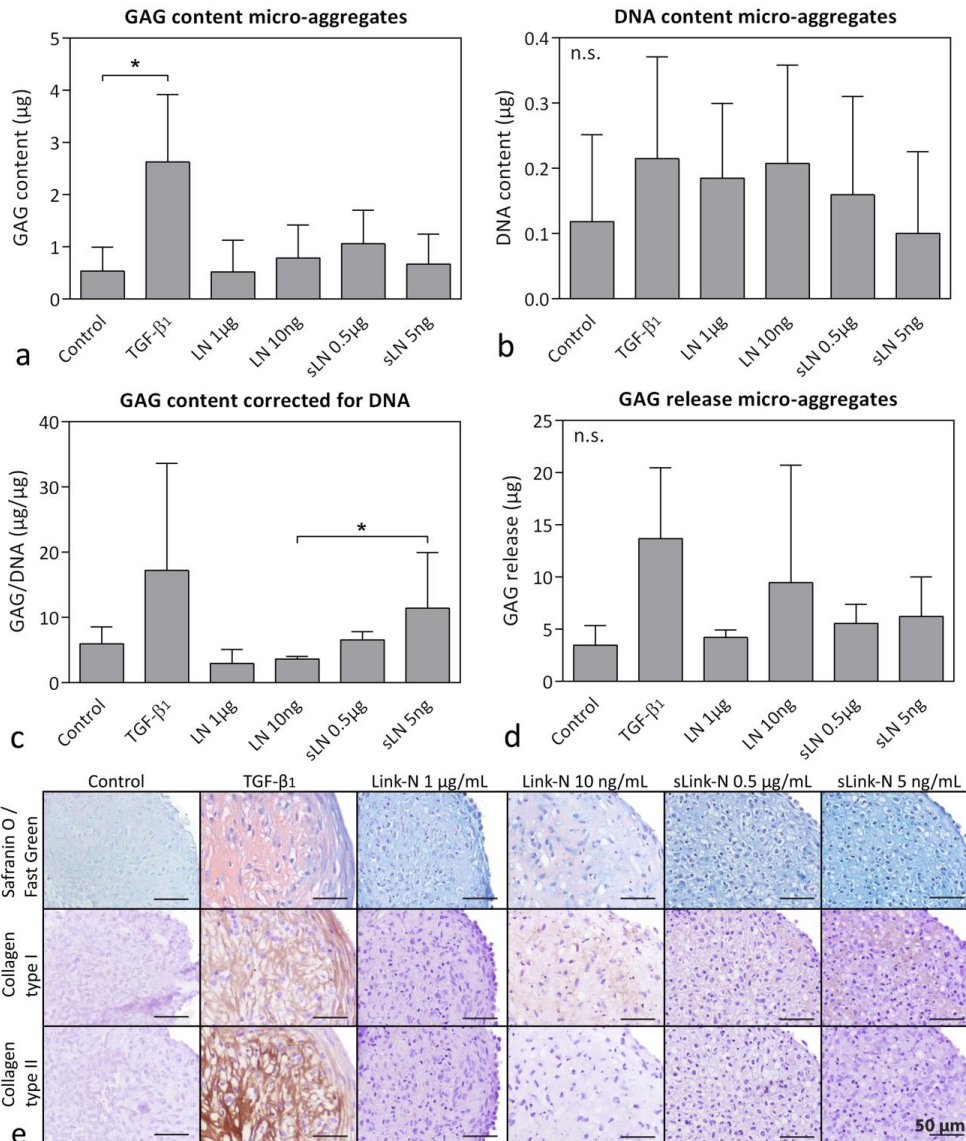


**Figure 5. Effect of canine (short) Link-N on human chondrocyte-like cells (CLCs).** GAG and DNA content (mean + SD) and histological evaluation of human CLC micro-aggregates treated with basal culture medium (control), supplemented with 10 ng/mL TGF- $\beta_1$ , 1  $\mu\text{g}/\text{mL}$  or 10 ng/mL canine Link-N (LN), or 0.5  $\mu\text{g}/\text{mL}$  or 5 ng/mL canine short Link-N (sLN) for 28 days in hypoxia (5%  $\text{O}_2$ ). (a) GAG content, (b) DNA content, (c) GAG content (incorporation in the micro-aggregate) corrected for DNA content, (d) total amount of GAGs released in the culture medium, (e) representative histological images of the Safranin O/Fast Green staining and collagen type I and II immunohistochemistry. \*:  $p < 0.05$ .  $n = 3$  (in duplicates).

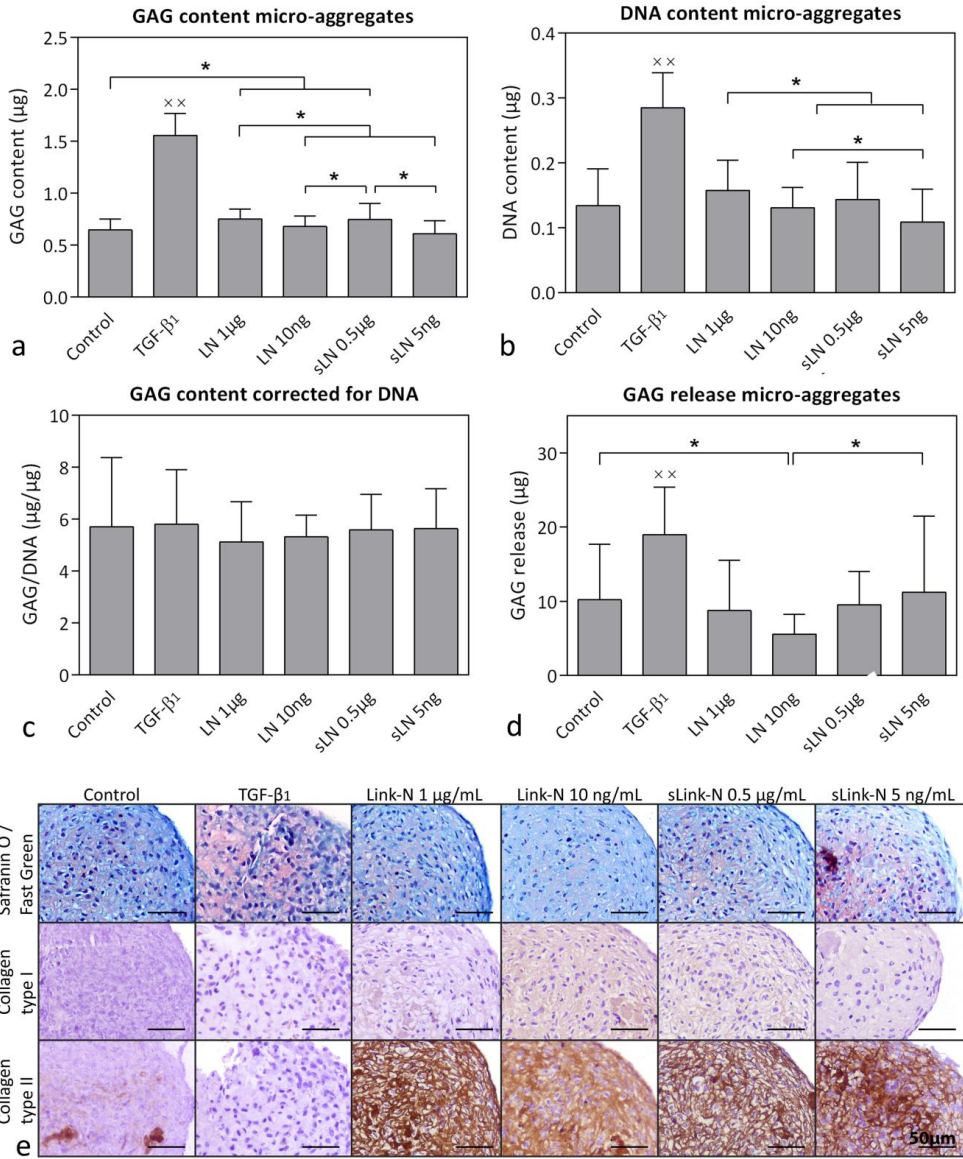


**Figure 6.** Effect of canine (short) Link-N on bovine chondrocyte-like cells (CLCs). GAG and DNA content (mean + SD) and histological evaluation of bovine CLC micro-aggregates treated with basal culture medium (control), supplemented with 10 ng/mL TGF-β<sub>1</sub>, 1 µg/mL or 10 ng/mL canine Link-N (LN), or 0.5 µg/mL or 5 ng/mL canine short Link-N (sLN) for 28 days in hypoxia (5% O<sub>2</sub>). (a) GAG content, (b) DNA content, (c) GAG content (incorporation in the micro-aggregate) corrected for DNA content, (d) total amount of GAGs released in the culture medium, (e) representative histological images of the Safranin O/Fast Green staining and collagen type I and II immunohistochemistry. \*:*p*<0.05; xx: significantly different (*p*<0.01) from all other conditions. *n*=6 (in duplicates).

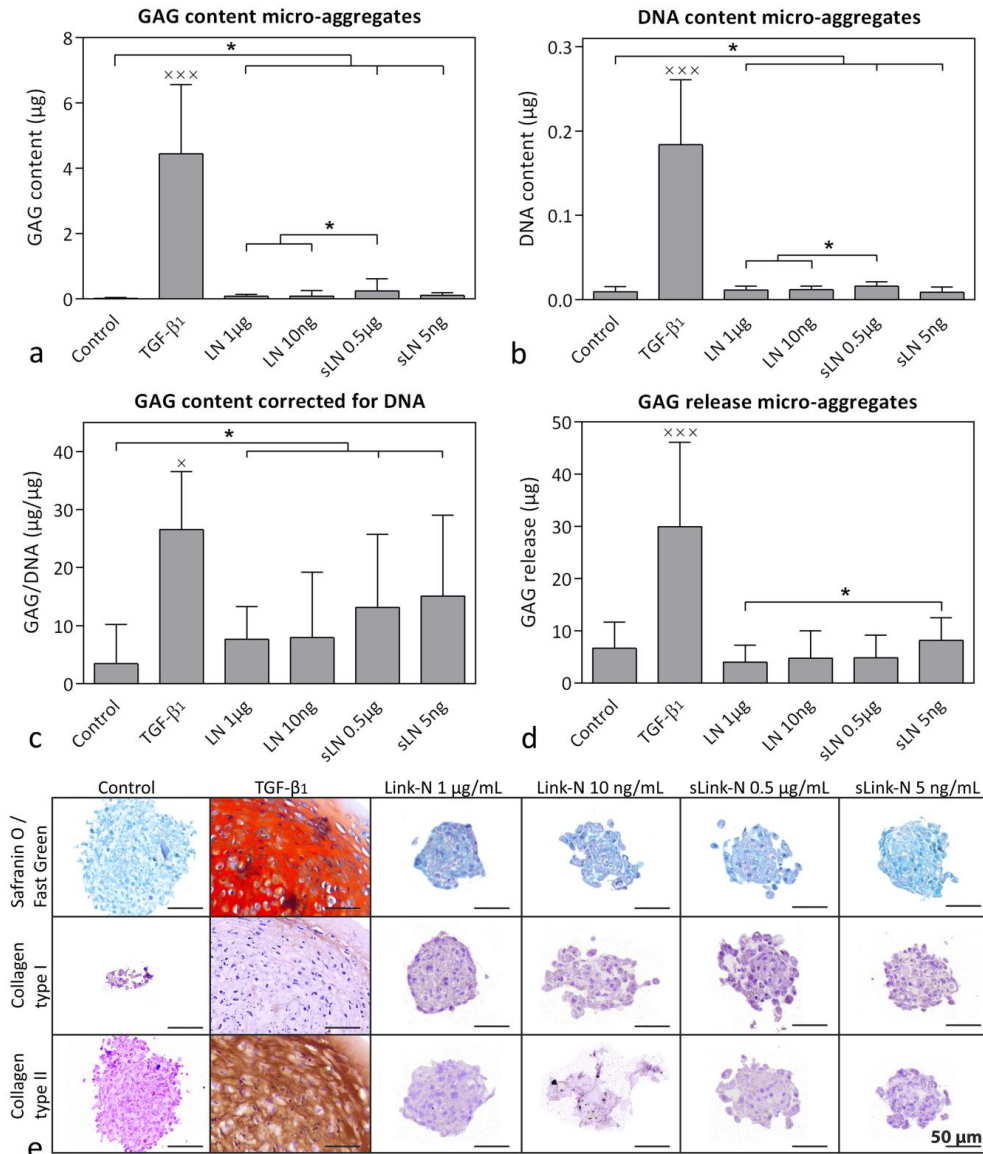


**Figure 7. Effect of canine (short) Link-N on CD canine chondrocyte-like cells (CLCs).** GAG and DNA content (mean + SD) and histological evaluation of CD canine CLC micro-aggregates treated with basal culture medium (control), supplemented with 10 ng/mL TGF-β<sub>1</sub>, 1 µg/mL or 10 ng/mL canine Link-N (LN), or 0.5 µg/mL or 5 ng/mL canine short Link-N (sLN) for 28 days in hypoxia (5% O<sub>2</sub>). (a) GAG content, (b) DNA content, (c) GAG content (incorporation in the micro-aggregate) corrected for DNA content, (d) total amount of GAGs released in the culture medium, (e) representative histological images of the Safranin O/ Fast Green staining and collagen type I and II immunohistochemistry. \*:  $p < 0.05$ ; x, xxx: significantly different ( $p < 0.05$  and  $p < 0.001$  respectively) from all other conditions.  $n = 6$  (in duplicates).

### Canine (s)Link-N induced negligible GAG deposition by CD canine CLCs

CD canine CLC micro-aggregates treated with 1 µg/mL canine Link-N and 5 ng/mL and 0.5 µg/mL canine sLink-N showed a slight, but significantly higher GAG, DNA, and GAG/DNA content compared with controls ( $p < 0.05$ ; Figure 7a-c). TGF- $\beta_1$ , however, induced by far the highest GAG, DNA, and GAG/DNA content ( $p < 0.05$ ; Figure 7a-c), which was confirmed by Safranin O/Fast Green staining (Figure 7e). TGF- $\beta_1$  also induced the highest GAG incorporation in the micro-aggregates ( $p < 0.05$ ), whereas canine (s)Link-N did not significantly increase GAG incorporation compared with controls (Supplementary File 2f). Histological analysis indicated that canine (s)Link-N decreased the micro-aggregates size compared with controls (Figure 7e). Canine (s)Link-N did not affect GAG release compared with controls, whereas TGF- $\beta_1$  significantly increased release compared with all other conditions ( $p < 0.001$ ; Figure 7d). Collagen type I and II deposition was not influenced by canine (s)Link-N treatment, whereas TGF- $\beta_1$  induced a collagen type I-rich rim and prominently increased collagen type II deposition (Figure 7e).

### Human and canine (s)Link-N do not induce GAG deposition by NCD canine CLCs

Based on physical appearance, dog breeds can be divided into chondrodystrophic (CD) and non-chondrodystrophic (NCD). CD dogs have short bowlegs due to disrupted endochondral ossification. This polygenetic trait has strongly been linked with IVD degeneration. In CD dogs, replacement of NCs by CLCs in the NP starts already before one year of age and IVD disease occurs frequently. In contrast, in NCD dogs, NCs remain the predominant cell type until later in life. If IVD disease develops, it usually occurs later in life due to wear-and-tear<sup>30</sup>. Since CD and NCD dogs differ in their genetic background and show differences in cause, prevalence, and age of onset of IVD degeneration, the regenerative potential of their CLCs could in the presence of (s)Link-N differ from each other. Therefore, we also tested the effect of (s)Link-N on NCD canine CLCs. However, both human and canine (s)Link-N did not induce any substantial effect on the GAG, DNA or GAG/DNA content or GAG release of NCD canine CLCs (Supplementary File 4).

### Human and canine (s)Link-N do not affect Smad signaling in human and bovine CLCs and only mildly induce Smad signaling in canine CLCs

A possible reason for the limited response of canine CLCs to (s)Link-N could be that canine CLCs do not express BMPRII or that Smad signaling was not properly induced. Gene expression analysis, however, indicated that CD canine CLCs expressed *BMPRII* and *BMPRIa*, whereas no *BMPRIb* mRNA was detected (Figure 8a,b). *BMPRII* and *BMPRIa* gene expression was not significantly affected by canine (s)Link-N treatment.

Surprisingly, canine and human (s)Link-N did not significantly increase pSmad1 or pSmad2 protein levels in human and bovine CLCs after 24 hours of treatment (Figure 8c-f). Both human and canine (s)Link-N, however, induced a mild, but significant increase in pSmad1 levels in canine CLCs ( $p < 0.05$ ; Figure 8g). Only 1 µg/mL canine Link-N mildly induced pSmad2 levels in canine CLCs ( $p < 0.05$ ; Figure 8h).

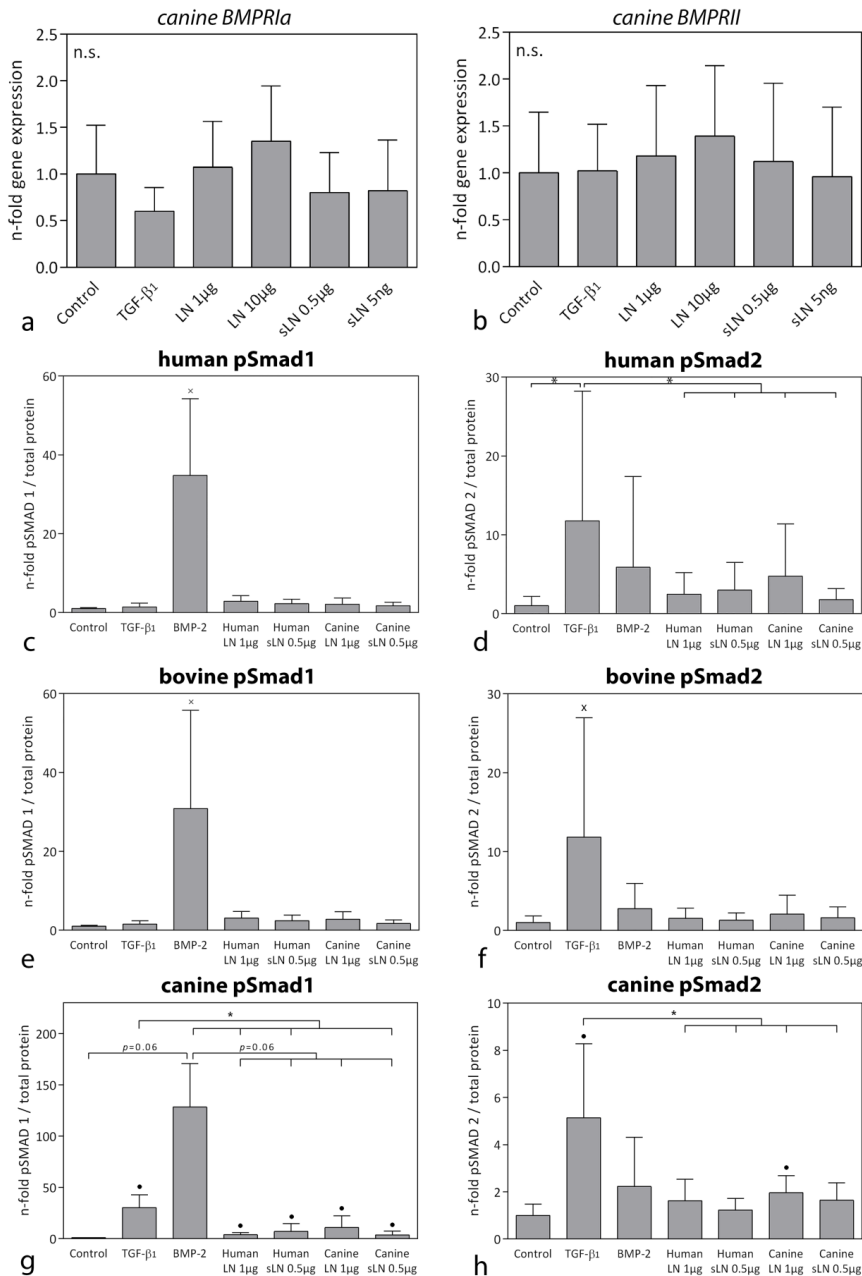


**Figure 8. BMP receptor expression and activation of Smad signaling by (s)Link-N in human, bovine, and CD canine chondrocyte-like cells (CLCs).** Relative *BMPRIa* (a) and *BMPRII* (b) gene expression (mean + SD) in CD canine CLC micro-aggregates treated with basal culture medium (control), supplemented with 10 ng/mL TGF- $\beta$ 1, 1  $\mu$ g/mL or 10 ng/mL canine Link-N (LN), or 0.5  $\mu$ g/mL or 5 ng/mL canine short Link-N (sLN) for 7 days in hypoxia (5% O<sub>2</sub>). Controls were set at 1.  $n=6$ . Phosphorylated (p)Smad 1 and 2 levels in human (c, d), bovine (e, f), and canine (g, h) CLCs cultured in monolayers stimulated with 1  $\mu$ g/mL human and canine Link-N (LN) and 0.5  $\mu$ g/mL human and canine short Link-N (sLN) in hypoxia (5% O<sub>2</sub>) for 24 hours. \*:  $p<0.05$ ; •: significantly different ( $p<0.05$ ) from controls; x: significantly different ( $p<0.05$ ) from all other conditions.  $n=5$ .

## Discussion

### Full length and short Link-N exerted comparable potent effects on CLCs

The current study confirms the results of previous work<sup>13</sup>, since in all three tested species, sLink-N exerted comparable (regenerative) effects as full length Link-N. This confirms that the biological active part is maintained in the first eight amino acids of Link-N peptide. These results support the advantage of sLink-N compared to Link-N: the production costs of sLink-N are lower than that of Link-N and a smaller peptide is more amenable for optimization of the biological stability<sup>13</sup>.

### Human (s)Link-N induced GAG deposition by human and bovine CLCs, but exerted limited effects on canine CLCs

Human (s)Link-N induced no effect on NCD canine CLC micro-aggregates. Additionally, it induced a significant, but very mild, concentration-independent increase in GAG content of CD canine CLC micro-aggregates. This increase was, however, considered negligible compared with the anabolic effect of TGF- $\beta_1$ . In the current study, human and bovine CLC micro-aggregates served as comparators for the 3D culture system employed. CLCs from these species have already been demonstrated to respond to Link-N in monolayers<sup>11</sup> and alginate beads<sup>7, 13</sup> with increased GAG<sup>7</sup> and collagen type I deposition<sup>13</sup>, in line with the present study. Differences in culture conditions may explain our observation that human (s)Link-N did not induce collagen type II deposition in human and bovine CLCs, in contrast with previous reports<sup>9, 11</sup>, while it increased the DNA content of bovine CLC micro-aggregates. The anabolic, concentration-dependent effect of human (s)Link-N on human and bovine CLCs suggests that the culture system allowed GAG deposition by (s)Link-N treatment, the (s)Link-N batch was active and that the limited response of canine CLCs could not be ascribed to inactive peptide.

### Interspecies differences in CLC response to canine (s)Link-N treatment

A potential reason for the mild response of canine CLCs to human (s)Link-N could be species differences in the (s)Link-N amino acid sequence. Indeed, the amino acid sequences of canine and bovine Link-N differ by five and three residues, respectively, when compared to human Link-N. Additionally, the amino acid sequences of canine and bovine sLink-N are similar and vary by only one residue from human sLink-N. Each amino acid substitution potentially affects the function of a protein<sup>31</sup>. Particularly the substitution of the third amino acid of human (s)Link-N (histidine) by leucine in bovine/canine (s)Link-N likely influences the 3D structure, and subsequently, receptor-docking of the peptide due to polarity differences. Therefore, we decided to also study the effects of canine (s)Link-N on human, bovine, and especially canine CLCs.

In line with previous work, in our study, human (s)Link-N exerted an anabolic effect on human CLCs<sup>7, 11, 13</sup>, whereas canine (s)Link-N exerted no anabolic effects on human CLCs. Although suggesting a species-specific requirement, bovine CLCs were able to respond to human (s)Link in our and previous studies by increasing the production of GAG<sup>7, 9, 13</sup>, despite the difference in amino acid sequence and polarity between human and bovine (s)Link-N. Since bovine and canine Link-N do not differ in polarity and the sLink-N sequence is similar, we hypothesized that canine (s)Link-N would exert an even more potent regenerative effect on bovine CLCs than human (s)Link-N. The present study, however, showed that canine

(s)Link-N only slightly increased GAG deposition, whereas it mainly induced collagen type I and II deposition in bovine CLCs, in contrast to the response to human (s)Link-N. Thus, canine (s)Link-N may activate other pathways than human (s)Link-N in bovine CLCs. Altogether, abovementioned findings imply that species differences in amino acid sequence cannot only determine whether CLCs of a specific species respond to (s)Link-N or not, but can also determine the direction of the CLC response to (s)Link-N. To confirm or reject this hypothesis, future studies should look into the (difference in) specific pathways that are influenced by species-specific (s)Link-N in CLCs from different species.

Since human (s)Link-N exerted only a limited anabolic effect on canine CLCs, we envisioned to optimize the potency of this treatment by using canine (s)Link-N. The species-specific (s)Link-N, however, also only exerted a minor anabolic effect on CD canine CLCs and no effect on NCD canine CLCs. Thus, the results of this study indicate that both canine and human (s)Link-N do not have the potency to be used as a regenerative therapy for canines with IVD disease. Moreover, this implies that the dog cannot serve as a valid large animal model for (s)Link-N treatment of human IVD degeneration.

### **Human and canine (s)Link-N slightly increased Smad signaling in canine CLCs**

As human Link-N was shown to exert its effects on rabbit NCs via BMPRII by increased Smad1/5/8 signaling<sup>12</sup>, possible reasons for the limited response of canine CLCs to (s)Link-N are insufficient expression of BMPRII and/or not properly induced Smad signaling. In the present study, canine CLCs expressed *BMPRII* mRNA, although this does not necessarily indicate that the protein is expressed at the cell surface. Nonetheless, (s)Link-N mildly induced Smad signaling in canine CLCs, indicating that the canine CLCs showed a receptor-mediated effect. In contrast to rabbit NCs and canine CLCs, human and bovine CLCs did not demonstrate increased pSmad1 or -2 levels after 24 hours of human or canine (s)Link-N treatment. This discrepancy can possibly be explained by species differences and/or different cell types present in the NP (rabbit – NCs, human/bovine - CLCs). It remains to be determined through which signaling pathways human (s)Link-N induces its effects, other than via Smad signaling in human and bovine CLCs. Notably, while human/canine (s)Link-N mildly induced Smad signaling in canine CLCs, it did not induce regenerative effects. Taken together, the results of this study indicate that (s)Link-N signaling is species-specific. Additionally, it appears that (s)Link-N can act via a yet unknown receptor besides BMPRII in human and bovine CLCs, which is not or hardly present in canine CLCs. Therefore, future studies should look into the efficacy of binding of (s)Link-N to different receptors in the different species.

## **Conclusions**

The current study demonstrates that human and canine (s)Link-N exerted species-specific effects on CLCs from early degenerated IVDs. Although human (s)Link-N induced GAG deposition in human and bovine CLCs, canine (s)Link-N did not affect ECM production in human CLCs and mainly induced collagen deposition in bovine CLCs. Both canine and human (s)Link-N, however, did not have the potency to be used as a regenerative therapy for canines with IVD disease. This implies that the dog cannot serve as a large animal model for (s)Link-N treatment of human IVD degeneration. From a clinical perspective, the present

study underscores the importance of testing the validity of animals that serve as a model for human IVD degeneration.

## **Acknowledgements**

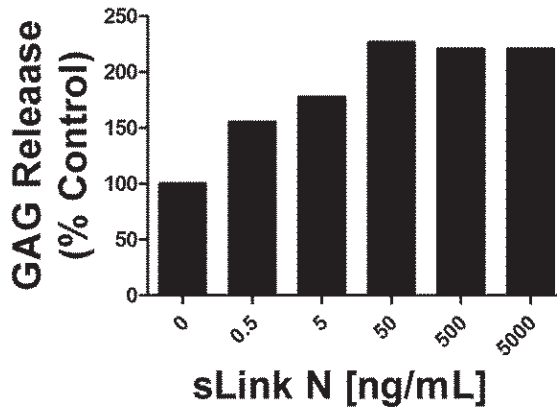
The authors would like to thank Anita Krouwels for supplying human CLCs, Stefan de Vries for supplying bovine CLCs and Lisa Hol and Janneke Oskam for help with the execution of experiments. BMP-2 was generously provided by TETEC AG.

## References

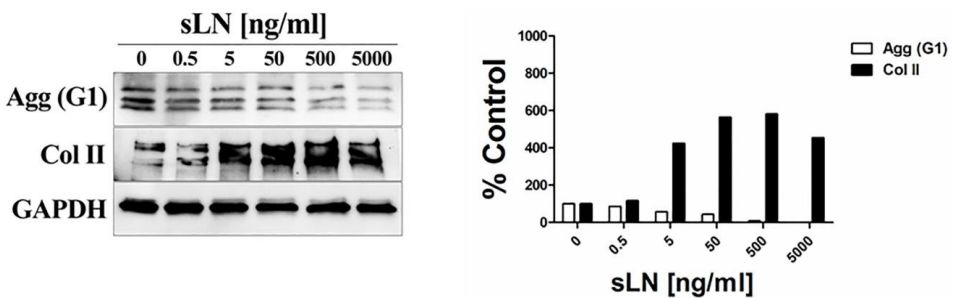
1. Katz JN. 2006. Lumbar disc disorders and low-back pain: Socioeconomic factors and consequences. *J Bone Joint Surg Am* 88: 21-24.
2. Andersson GB. 1999. Epidemiological features of chronic low-back pain. *Lancet* 354: 581-585.
3. Freemont AJ. 2009. The cellular pathobiology of the degenerate intervertebral disc and discogenic back pain. *Rheumatology (Oxford)* 48: 5-10.
4. Bergknut N, Smolders LA, Grinwis GC, et al. 2013. Intervertebral disc degeneration in the dog. part 1: Anatomy and physiology of the intervertebral disc and characteristics of intervertebral disc degeneration. *Vet J* 195: 282-291.
5. Bach FC, Willems N, Penning LC, et al. 2014. Potential regenerative treatment strategies for intervertebral disc degeneration in dogs. *BMC Vet Res* 10: 3-6148-10-3.
6. Benneker LM, Andersson G, Iatridis JC, et al. 2014. Cell therapy for intervertebral disc repair: Advancing cell therapy from bench to clinics. *Eur Cell Mater* 27: 5-11.
7. Gawri R, Antoniou J, Ouellet J, et al. 2013. Best paper NASS 2013: Link-N can stimulate proteoglycan synthesis in the degenerated human intervertebral discs. *Eur Cell Mater* 26: 107-19.
8. Mwale F, Masuda K, Pichika R, et al. 2011. The efficacy of link N as a mediator of repair in a rabbit model of intervertebral disc degeneration. *Arthritis Res Ther* 13: R120.
9. Mwale F, Demers CN, Petit A, et al. 2003. A synthetic peptide of link protein stimulates the biosynthesis of collagens II, IX and proteoglycan by cells of the intervertebral disc. *J Cell Biochem* 88: 1202-1213.
10. Nguyen Q, Murphy G, Hughes CE, Mort JS, Roughley PJ. 1993. Matrix metalloproteinases cleave at two distinct sites on human cartilage link protein. *Biochem J* 295 ( Pt 2): 595-598.
11. Petit A, Yao G, Rowas SA, et al. 2011. Effect of synthetic link N peptide on the expression of type I and type II collagens in human intervertebral disc cells. *Tissue Eng Part A* 17: 899-904.
12. Wang Z, Weitzmann MN, Sangadala S, Hutton WC, Yoon ST. 2013. Link protein N-terminal peptide binds to bone morphogenetic protein (BMP) type II receptor and drives matrix protein expression in rabbit intervertebral disc cells. *J Biol Chem* 288: 28243-28253.
13. Gawri R, Ouellet J, Onnerfjord P, et al. 2014. Link N is cleaved by human annulus fibrosus cells generating a fragment with retained biological activity. *J Orthop Res* 32: 1189-1197.
14. Mwale F, Wang HT, Roughley P, Antoniou J, Haglund L. 2014. Link N and mesenchymal stem cells can induce regeneration of the early degenerate intervertebral disc. *Tissue Eng Part A* 20: 2942-2949.
15. AlGarni N, Grant MP, Epure LM, et al. 2016. Short link N stimulates intervertebral disc repair in a novel long-term organ culture model that includes the bony vertebrae. *Tissue Eng Part A* 22: 1252-1257.
16. Bergknut N, Rutges JP, Kranenburg HJ, et al. 2012. The dog as an animal model for intervertebral disc degeneration? *Spine (Phila Pa 1976)* 37: 351-358.
17. Bach FC, de Vries SA, Krouwels A, et al. 2015. The species-specific regenerative effects of notochordal cell-conditioned medium on chondrocyte-like cells derived from degenerated human intervertebral discs. *Eur Cell Mater* 30: 132-47.
18. Willems N, Bach FC, Plomp SG, et al. 2015. Intradiscal application of rhBMP-7 does not induce regeneration in a canine model of spontaneous intervertebral disc degeneration. *Arthritis Res Ther* 17: 137-015-0625-2.
19. Maldonado BA, Oegema TR, Jr. 1992. Initial characterization of the metabolism of intervertebral disc cells encapsulated in microspheres. *J Orthop Res* 10: 677-690.
20. Lee JY, Hall R, Pelinkovic D, et al. 2001. New use of a three-dimensional pellet culture system for human intervertebral disc cells: Initial characterization and potential use for tissue engineering. *Spine (Phila Pa 1976)* 26: 2316-2322.
21. Arkesteijn IT, Smolders LA, Spillekom S, et al. 2015. Effect of coculturing canine notochordal, nucleus pulposus and mesenchymal stromal cells for intervertebral disc regeneration. *Arthritis Res Ther* 17: 60-015-0569-6.
22. Antoniou J, Wang HT, Alaseem AM, et al. 2012. The effect of link N on differentiation of human bone marrow-derived mesenchymal stem cells. *Arthritis Res Ther* 14: R267.
23. Yang SH, Hu MH, Sun YH, Lin FH. 2013. Differential phenotypic behaviors of human degenerative nucleus pulposus cells under normoxic and hypoxic conditions: Influence of oxygen concentration during isolation and cultivation. *Spine J* 13.
24. Feng G, Li L, Liu H, et al. 2013. Hypoxia differentially regulates human nucleus pulposus and annulus fibrosus cell extracellular matrix production in 3D scaffolds. *Osteoarthritis Cartilage* 21: 582-588.
25. Farndale RW, Sayers CA, Barrett AJ. 1982. A direct spectrophotometric microassay for sulfated glycosaminoglycans in cartilage cultures. *Connect Tissue Res* 9: 247-248.
26. Zuker M. 2003. Mfold web server for nucleic acid folding and hybridization prediction. *Nucleic Acids Res* 31: 3406-3415.
27. Altschul SF, Madden TL, Schaffer AA, et al. 1997. Gapped BLAST and PSI-BLAST: A new generation of protein database search programs. *Nucleic Acids Res* 25: 3389-3402.
28. Shen Y, Maupetit J, Derreumaux P, Tuffery P. 2014. Improved PEP-FOLD approach for peptide and miniprotein structure prediction. *J Chem Theory Comput* 10: 4745-4758.
29. Mace PD, Cutfield JF, Cutfield SM. 2006. High resolution structures of the bone morphogenetic protein type II receptor in two crystal forms: Implications for ligand binding. *Biochem Biophys Res Commun* 351: 831-838.
30. Smolders LA, Bergknut N, Grinwis GC, et al. 2013. Intervertebral disc degeneration in the dog. part 2: Chondrodystrophic and non-chondrodystrophic breeds. *Vet J* 195: 292-299.
31. Ng PC, Henikoff S. 2001. Predicting deleterious amino acid substitutions. *Genome Res* 11: 863-874.

**Supplementary File 1. Concentration range human sLink-N on CD canine CLCs**

Before the start of the current study, a concentration range of human (s)Link-N was tested on one CD canine CLC donor (Beagle, 2 years of age). One hundred fifty thousand CLCs were seeded in 6-well plates and treated with the indicated concentrations of sLink-N for 24 hours. Conditioned media was collected and quantified for GAG content. 0.5-5000 ng/mL sLink-N increased GAG release in the culture medium. An optimal GAG release was established at 50-5000 ng/mL sLink-N:

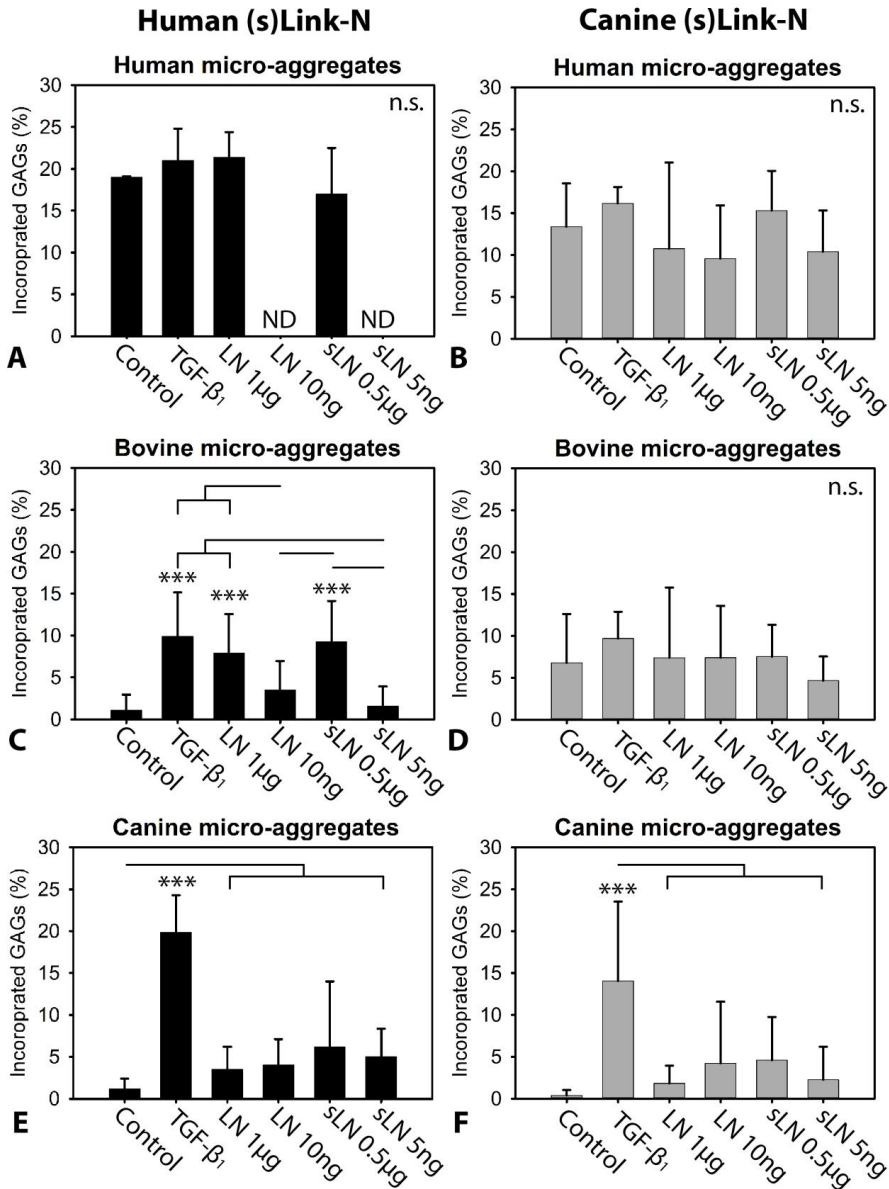


Additionally, 150.000 CLCs were seeded in 6-well plates and treated with the indicated concentrations of sLink N for 7 days. Protein was extracted in RIPA buffer and processed for Western blotting. Decreased G1 fragment indicates less aggrecan degradation.



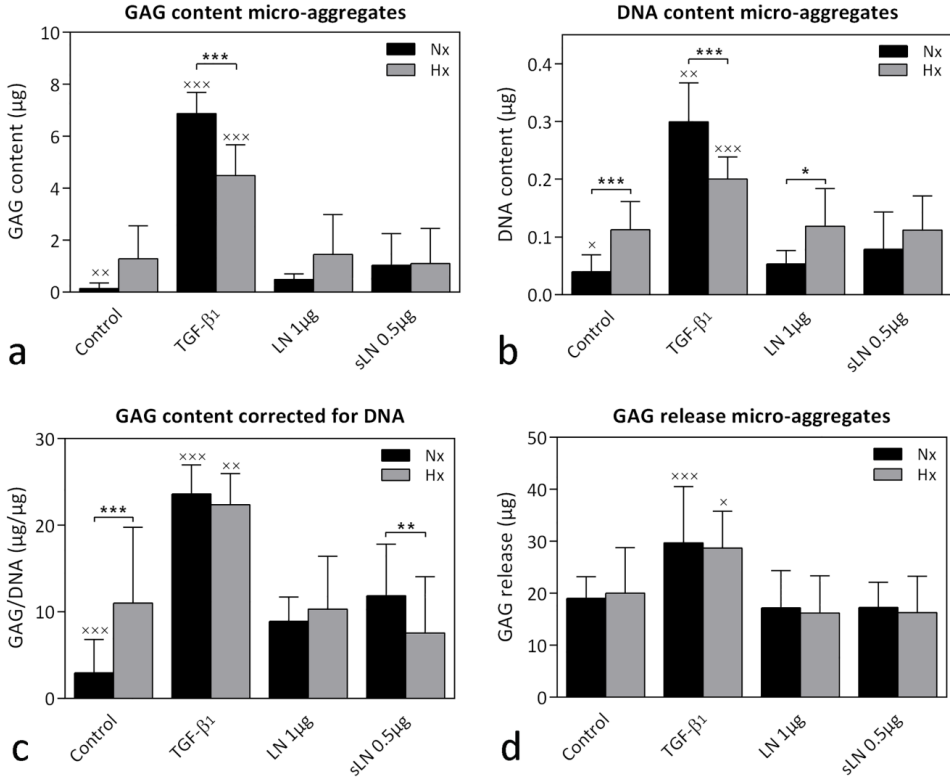
Collagen type II deposition was increased from 5 ng/mL sLink-N onwards. However, 50-5000 ng/mL did not seem to further increase collagen type II deposition. Aggrecan degradation was concentration-dependently decreased with 5 ng/mL sLink-N onwards. For these reasons, we chose to apply 5 and 500 ng/mL sLink-N and corresponding Link-N concentrations (10 and 1000 ng/mL) in the 3D micro-aggregates in the manuscript. Since culturing CLCs in a 3D environment maintains their disc phenotype better than 2D culture, 3D micro-aggregates were used to determine the effect of (s)Link-N in the current study.

## Supplementary File 2. The effect of human and canine (s)Link-N on GAG incorporation



GAG incorporation ratio (mean + SD) of human, bovine, and CD canine CLC micro-aggregates treated with basal culture medium (control), supplemented with 10 ng/mL TGF- $\beta_1$  (positive control), 1  $\mu$ g/mL or 10 ng/mL human or canine Link-N (LN) or 0.5  $\mu$ g/mL or 5 ng/mL human or canine sLink-N (sLN). The CLC micro-aggregates were cultured for 28 days. GAG incorporation percentages were calculated as the GAG content of the micro-aggregate divided by the total amount of GAGs produced by that micro-aggregate (GAGs released in the culture medium + GAG content of the micro-aggregate). \*\*\*: significantly different from controls. Bars indicate significant differences between conditions ( $p < 0.05$ ).  $n = 3$ , (human) or 6 (bovine and canine), all in duplicates. ND: not determined, since GAG release was below the detection limit.

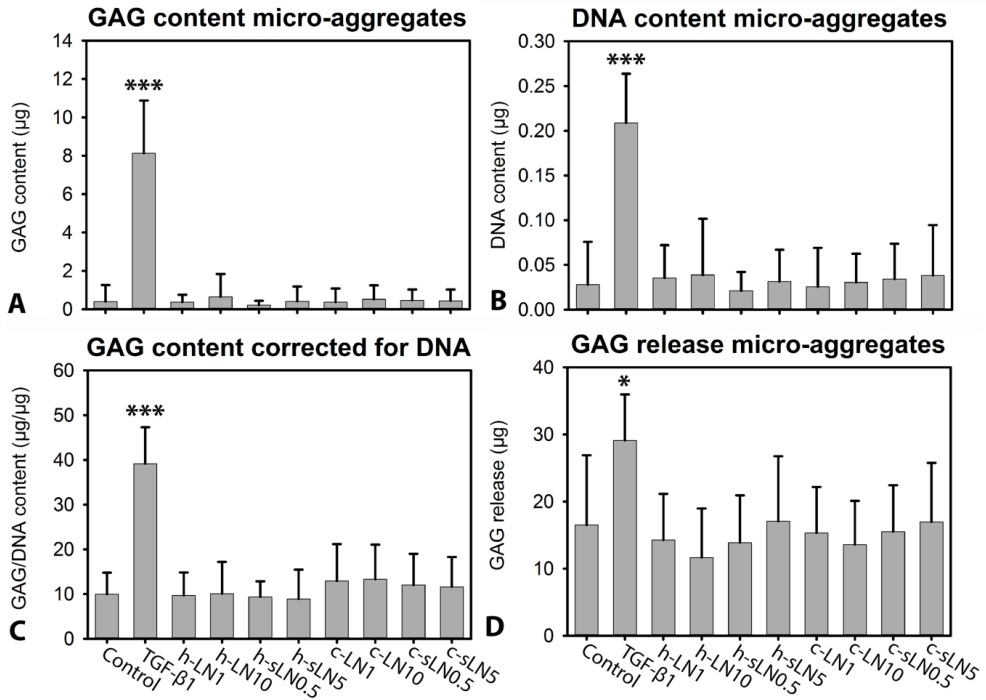
**Supplementary File 3. The effect of human (s)Link-N on canine CLCs in hypoxia vs. normoxia**



GAG and DNA content (mean + SD) of CD canine CLC micro-aggregates treated with basal culture medium (control), supplemented with 10 ng/mL TGF-β<sub>1</sub> (positive control), 1 µg/mL human Link-N (LN) or 0.5 µg/mL human sLink-N (sLN). The CLC micro-aggregates were cultured for 28 days in normoxia (Nx, 21% O<sub>2</sub>) or hypoxia (Hx, 5% O<sub>2</sub>). (a) GAG content (b) DNA content (c) GAG content corrected for DNA content (d) Total amount of GAGs released in the culture medium. \*:p<0.05, \*\*:p<0.01, \*\*\*:p<0.001. x, xx, xxx: significantly different (p<0.05, p<0.01, p<0.001, respectively) from all other conditions (growth factor treatment) in either Hx or Nx. n=6 (in duplicates).



**Supplementary File 4. The effect of human and canine (s)Link-N on non-chondrodystrophic canine CLCs**



Effect of human and canine (short) Link-N on non-chondrodystrophic (NCD) canine chondrocyte-like cells (CLCs). The NCD canine CLC micro-aggregates were treated with basal culture medium (control), supplemented with 10 ng/mL TGF-β1, 1 µg/mL or 10 ng/mL canine or human Link-N (LN), or 0.5 µg/mL or 5 ng/mL human or canine short Link-N (sLN) for 28 days in hypoxia (5% O<sub>2</sub>). (a) GAG content, (b) DNA content, (c) GAG content corrected for DNA content, (d) total amount of GAGs released in the culture medium. \*, \*\*\*: significantly different from all other conditions ( $p < 0.05$ ,  $p < 0.001$ , respectively).  $n = 6$  (in duplicates).



**Increased caveolin-1 in intervertebral disc degeneration facilitates repair**

Frances C. Bach, Ying Zhang<sup>2</sup>, Alberto Miranda Bedate<sup>1</sup>, Lucy C. Verdonschot<sup>1</sup>, Niklas Bergknut<sup>1</sup>, Laura B. Creemers<sup>3</sup>, Keita Ito<sup>3,4</sup>, Daisuke Sakai<sup>5</sup>, Danny Chan<sup>2</sup>, Björn P. Meij<sup>1</sup>, Marianna A. Tryfonidou<sup>1</sup>

<sup>1</sup> Department of Clinical Sciences of Companion Animals, Faculty of Veterinary Medicine, Utrecht University, the Netherlands

<sup>2</sup> Department of Biochemistry, The University of Hong Kong, Hong Kong, China

<sup>3</sup> Department of Orthopedics, University Medical Center Utrecht, the Netherlands

<sup>4</sup> Orthopedic Biomechanics, Department of Biomedical Engineering, Eindhoven University of Technology, the Netherlands

<sup>5</sup> Department of Orthopedic Surgery, Tokai University School of Medicine, Isehara, Japan

## Abstract

Preceding intervertebral disc (IVD) degeneration, the cell phenotype in the nucleus pulposus (NP) shifts from notochordal cells (NCs) to chondrocyte-like cells (CLCs). Microarray analysis showed a correlation between caveolin-1 expression and the phenotypic transition of NCs to CLCs. With a clinical directive in mind, the aim of this study was to determine the role of caveolin-1 in IVD degeneration. As a scaffolding protein, caveolin-1 influences several signaling pathways and TGF- $\beta$  receptors have been demonstrated to colocalize with caveolin-1. Therefore, the hypothesis of this study was that caveolin-1 facilitates repair by enhancing TGF- $\beta$  signaling in the IVD. Protein expression (caveolin-1, apoptosis, progenitor cell markers, extracellular matrix and phosphorylated Smad2 (pSmad2)) was determined in IVDs of wild type (WT) and caveolin-1 null mice and canine IVDs of different degeneration grades (immunofluorescence, immunohistochemistry, TUNEL assay). Canine/human CLC micro-aggregates were treated with chondrogenic medium alone or in combination with caveolin-1 scaffolding domain (CSD) peptide and/or caveolin-1 siRNA. After 28 days, gene and protein expression profiles were determined. The NP of WT mice was rich in viable NCs, whereas the NP of caveolin-1 null mice contained more collagen-rich extracellular matrix and less cells together with increased progenitor cell marker expression, pSmad2 TGF- $\beta$  signaling and a high apoptotic activity. During canine IVD degeneration, caveolin-1 expression and apoptotic activity increased. *In vitro* caveolin-1 silencing decreased the CLC micro-aggregates glycosaminoglycan (GAG) content, which could be rescued by CSD treatment. Furthermore, CSD increased TGF- $\beta$ /pSmad2 signaling at gene and protein expression level and enhanced the anabolic effects of TGF- $\beta_1$  reflected in increased extracellular matrix deposition by the CLCs. Caveolin-1 plays a role in preservation of the NC phenotype. Additionally, it may be related with CLC apoptosis given its increased expression in degenerated IVDs. Nevertheless, CSD enhanced CLC GAG deposition *in vitro*, and hence the increased caveolin-1 expression during IVD degeneration may also facilitate an ultimate attempt of repair. Further studies are needed to investigate how caveolin-1 modifies other signaling pathways and facilitates IVD repair.

## Introduction

Low back pain has been identified as one of the highest burden conditions by the World Health Organization and is the most common type of pain restricting daily activity<sup>1</sup>. Low back pain is strongly related to intervertebral disc (IVD) degeneration<sup>2</sup>. The IVD consists of a central nucleus pulposus (NP) and outer annulus fibrosus (AF). During IVD degeneration, the glycosaminoglycan (GAG) and water content of the NP decreases. Like humans, dogs suffer from spontaneous IVD degeneration with similar characteristics<sup>3</sup>. In both species, notochordal cells (NCs) are replaced by chondrocyte-like cells (CLCs) in the NP during maturation and early IVD degeneration. Therefore, the dog is considered to be a suitable animal model for human IVD degeneration<sup>3</sup>. Dogs can be divided into chondrodystrophic (CD) and non-chondrodystrophic (NCD) breeds based on their physical appearance. In CD dogs, replacement of NCs by CLCs starts around one year of age and IVD disease typically develops around 3–7 years of age, whereas in NCD dogs, NCs remain the predominant cell type until middle/old age and if IVD disease develops it occurs around 6–8 years of age<sup>4</sup>. Current treatments for IVD disease (physiotherapy, medication and surgery) focus on reducing pain and spinal cord/nerve decompression, but do not induce IVD repair. Therefore, there is substantial interest in agents stimulating biological repair of the degenerated IVD resulting in functional restoration<sup>5</sup>. Caveolin-1 could be such an agent, as its advantageous effects have been demonstrated in several tissue types<sup>6–9</sup>.

The mammalian caveolin family consists of three proteins (caveolin-1, -2, and -3), which are integral membrane proteins essential for the structural integrity and function of caveolae (flask-shaped invaginations of the plasma membrane) of many differentiated cell types<sup>10–12</sup>. Caveolin-1 is involved in endocytosis, the formation and transport of caveolae, cell adhesion and migration<sup>13</sup>. Moreover, caveolin-1 is implicated in cell cycle regulation, senescence (cell cycle arrest due to resistance to external stimuli<sup>10</sup>) and apoptosis<sup>14</sup>. As a scaffolding protein, it regulates signal transduction<sup>12</sup> and caveolin binding motifs have been identified in several target proteins<sup>7</sup>. The effect of caveolin-1 on signaling pathways is usually inhibitory due to sequestration and inactivation of molecules in caveolar membranes, but signaling can also be enhanced by bringing molecules together<sup>7</sup>. Altogether, caveolin-1 has been shown to exert context-dependent effects, *i.e.* differing per tissue/cell type, age, and stage of degeneration<sup>11</sup>.

Caveolin-1 is differentially expressed in the IVD: the NP of early degenerated canine IVDs expresses lower caveolin-1 levels than healthy canine NC-rich NPs<sup>15</sup>. In addition, the NP of wild type (WT) mice is rich in viable NCs, whereas the NP of caveolin-1 null mice mainly contains CLCs<sup>15</sup>. In humans, CLCs derived from degenerated IVDs express higher caveolin-1 levels than CLCs from non-degenerated IVDs<sup>16</sup>. During IVD degeneration, accelerated cell senescence takes place<sup>16,17</sup> and a positive relationship between caveolin-1 expression and premature stress-induced senescence has been reported in articular cartilage<sup>18</sup> and the IVD<sup>16</sup>. Altogether, this implies that caveolin-1 could play an important role in IVD degeneration.

The aim of this study was to determine the role of caveolin-1 in IVD degeneration. TGF- $\beta$  signaling is known to play a role in the degenerative/regenerative processes of cartilaginous tissues<sup>19</sup> and TGF- $\beta$  receptors have been demonstrated to colocalize with caveolin-1<sup>20</sup>.

Therefore, we hypothesized that caveolin-1 modifies TGF- $\beta$  signaling in the IVD and thereby facilitates repair. To assess the effect of *in vivo* caveolin-1 depletion we studied murine caveolin-1 null IVDs. With a clinical directive in mind, functional studies focused on the effect of caveolin-1 on CLCs, since degenerated canine and human IVDs contain almost 100% CLCs. Caveolin-1 expression and apoptosis levels were determined in canine IVDs of different degeneration grades and human and canine CLCs were silenced for caveolin-1 and/or supplemented with caveolin-1 scaffolding domain (CSD) peptide *in vitro* to determine the (regenerative) effect of caveolin-1 on CLCs. In the present study we show that, while caveolin-1 preserved the NC phenotype, its expression increased in degenerated IVDs. Given that CSD supplementation enhanced the anabolic effects of TGF- $\beta_1$  on CLCs in terms of increased GAG deposition *in vitro*, the increased caveolin-1 expression during IVD degeneration may facilitate an ultimate attempt of repair by lowering the loss of GAGs.

## Material and methods

### Caveolin-1 null mice

#### *Study population*

Thoracic and lumbar spines were collected from 1.5-, 3-, and 6-month-old caveolin-1 null (*Cav<sup>tm1Ms</sup>*, JAX<sup>®</sup>, the Jackson Laboratory) and wild type (WT) mice (B6129SF2, JAX<sup>®</sup>) of the same genetic background. Experimental procedures were performed according to the guidelines of the Utrecht University Ethics Committee (DEC 2008.III.01.001).

#### *Histology on paraffin embedded tissues*

Murine lumbar spines were fixed in 4% neutral buffered formaldehyde (Klinipath), decalcified (7 days in 10% EDTA) and embedded in paraffin. Mid-sagittal sections of 5  $\mu$ m were mounted on Microscope KP+ slides (KP-3056, Klinipath), stained with H&E and Alcian Blue/Picosirius Red<sup>21</sup> and immunohistochemically stained for Ki-67 and collagen type II (Table 1). An Apoptag<sup>®</sup> Plus Peroxidase In Situ Apoptosis Detection Kit (TUNEL assay, S7101, Merck Millipore) was used to detect apoptotic cells on lumbar midsagittal sections. All lumbar IVDs were evaluated (approximately four IVDs per lumbar spine). Raw images of the sections were made using a Leica DFC420C digital camera (Leica Microsystems) mounted to a BX60 microscope (Olympus) and the Leica Application Suite (V4.2) software package. Adobe Photoshop CS6 was used to manually count (positively stained) cell numbers in each NP. The percentage of nuclei that stained positive for TUNEL over the total number of nuclei present was determined for every murine NP in conjunction with morphology to avoid false positive results.

**Table 1. Details of the immunohistochemistry protocol**

Target protein	Manufacturer	Origin	Antigen retrieval	Block	Concentration 1 <sup>st</sup> Ab	2 <sup>nd</sup> Ab
Caveolin-1	Clone 2297, 610406, BD Biosciences	Mouse	Citrate (10mM) 70°C, 60 min	0.3% H <sub>2</sub> O <sub>2</sub> + 10% goat serum	5µg/mL in PBS	Goat Anti-Mouse, (K4001, Dako)
Ki-67	Clone SP6, RM-9106-S, Thermo Scientific™	Rabbit	Citrate (10mM) 80°C, 90 min	0.3% H <sub>2</sub> O <sub>2</sub> + 10% goat serum	4µg/mL in PBS	Goat Anti-Rabbit, (K4003, Dako)
Collagen type II	II-II6B3, DSHB	Mouse	1 mg/mL pronase + 10 mg/mL hyaluronidase 37°C, 30 min	0.3% H <sub>2</sub> O <sub>2</sub> + 5% BSA/PBS	0.02µg/mL (murine, canine) or 0.4µg/mL (human) in 5% BSA/PBS	Goat Anti-Mouse, (K4001, Dako)
Collagen type I	ab6308, Abcam	Mouse	1 mg/mL pronase + 10 mg/mL hyaluronidase 37°C, 30 min	0.3% H <sub>2</sub> O <sub>2</sub> + 5% BSA/PBS	0.1µg/mL (human) or 0.07µg/mL (canine) in 5% BSA/PBS	Goat Anti-Mouse, (K4001, Dako)

Midsagittal IVD sections were deparaffinized with xylene and graded ethanol. The primary antibody was applied at 4°C overnight. In control experiments, the primary antibody was substituted with mouse IgG<sub>1</sub> (3877, Santa Cruz Biotechnology); no false positive-staining was observed. The secondary antibody was applied for 60 minutes and the sections were incubated with the liquid DAB substrate chromogen system (K3468, Dako) for 10 minutes. The slides were stained with Hematoxylin QS solution (H3404, Vector Laboratories) for 10 seconds, dehydrated and mounted (H5000, Vector Laboratories). BSA: bovine serum albumin. PBS: phosphate buffered saline.

### *Immunofluorescent staining*

Thoracic IVDs were snap frozen and stored at -70°C until analysis. Ten µm transverse cryosections were stained for caveolin-1, phosphorylated Smad2 (pSmad2 indicating activated TGF-β signaling), and NP progenitor cell (NPPC) markers tyrosine-like receptor Tie2 and disialoganglioside 2 (GD2) (Table 2). Within 48 hours, confocal images were obtained with a Zeiss LSM Upright Confocal Laser Scanning Microscope and the sections were analyzed with Zen software 2011 (Zeiss Microscopy) in 2-3 transverse thoracic NP sections per animal. Based on the observed expression pattern, caveolin-1, Tie2 and GD2 were scored as being present or not present. The percentage of nuclei that stained positive for pSmad2 over the total number of nuclei present (pSmad2 ratio) was manually counted and calculated per murine NP and the mean pSmad2 ratio was determined per age group.

**Table 2. Details of the immunofluorescence protocol**

Antibody	Specifications	Host	Dilution	Secondary antibody
Tie-2	324, Santa Cruz	Rabbit	4µg/mL	Alexa Fluor® 594 AffiniPure Donkey Anti-Rabbit IgG (711-165-152, Jackson ImmunoResearch)
GD2	554272, BD Biosciences	Mouse	10µg/mL	<b>Alexa Fluor™ 488 Donkey Anti-Mouse IgG (A21202, Invitrogen)</b>
Caveolin-1	2910, Abcam	Rabbit	5µg/mL	Alexa Fluor® 594 AffiniPure Donkey Anti-Rabbit IgG (711-165-152, Jackson ImmunoResearch)
pSMAD2	3101s, Cell Signaling	Rabbit	5µg/mL	Alexa Fluor™ 488 Donkey Anti-Rabbit IgG (A21206, Invitrogen)
Negative control	Primary antibody omitted	-	-	Alexa Fluor™ 488 Donkey Anti-Mouse IgG (A21202, Invitrogen) + Alexa Fluor® 594 AffiniPure Donkey Anti-Rabbit IgG (711-165-152, Jackson ImmunoResearch)

The thoracic IVDs were embedded in OCT (14020108926, Leica Microsystems), transverse 10 µm cryosections were mounted on Superfrost Plus slides (4951PLUS4, Thermo Scientific) and treated with 1:1 in PBS diluted TrypLE™ Express Enzyme (12605, Life Technologies) for 10 minutes at 37°C. They were blocked with 3% BSA and 0.25% TritonX-100 (T8787, Sigma-Aldrich) for 30 minutes and incubated overnight at 4°C with the primary antibodies diluted in 1% BSA in PBS. The secondary antibody was 1:250 diluted in 1% BSA and 0.1% TritonX-100 in PBS and applied for 45 minutes at RT. The sections were mounted with Vectashield mounting medium with DAPI (H-1200, Vector Laboratories).

### Caveolin-1 expression in canine IVD degeneration

37 thoracolumbar or lumbosacral IVD samples from 16 canine cadavers were studied. The dogs were of various breeds (5 CD, 11 NCD), age (1-16 years) and gender (11 female, 5 male). The samples were divided into 5 different grades of degeneration based on gross morphology of midsagittal sections (Thompson grading): score I is healthy and score V represents end stage degeneration<sup>22, 23</sup>. The IVD donors were chosen based on equal representation of all IVD degeneration grades ( $n=8-7-8-7-7$  for grade I-V, respectively). All dogs had been euthanized in unrelated research projects or were client-owned dogs that were submitted for necropsy to the Pathobiology Department (Faculty of Veterinary Medicine, Utrecht University). Five µm thick midsagittal consecutive IVD sections were mounted on Microscope KP+ slides and processed for caveolin-1 immunohistochemistry (Table 1) and a TUNEL assay. Thereafter, raw images of the sections were made using a Leica DFC420C digital camera (Leica Microsystems) mounted to a BX60 microscope (Olympus) and the Leica Application Suite (V4.2) software package. Adobe Photoshop CS6 was used to manually count (positively stained) TUNEL cell numbers and the integrated option 'color range' was used to determine the area within the NP that stained positive for caveolin-1 (caveolin-1 ratio) in four randomly selected NP areas per IVD section. The mean percentage of nuclei that stained positive for TUNEL over the total number of nuclei present in the four randomly selected NP areas was determined in conjunction with morphology to avoid false positive results.

## ***In vitro* effects of caveolin-1 peptide on human and canine CLCs derived from degenerated IVDs**

### *CLC collection*

In total, IVD tissue from 16 canine (11 CD, 5 NCD) and 3 human donors was collected. Complete spines (2-11 years of age, Thompson score II-III) were collected from dogs that had been euthanized in unrelated research studies (approved by the Utrecht University Animal Ethics Committee). IVD tissue of three human donors (one male, two females, 47-63 years of age, Thompson score III) derived from the L2-L5 spinal region were obtained at autopsy. Anonymous use of redundant tissue for research purposes is a standard treatment agreement with patients in University Medical Centre Utrecht (Local Medical Ethical Committee number 12-364). Thus, all necessary consent from patients involved in the study was present. The material was collected as part of the tissue bank of the Department of Pathology/UMCU Biobank UMC Utrecht. The scientific committee from the Department of Pathology of UMC Utrecht (Wetenschappelijke Adviesraad Biobank) approved the study. All tissue was used in line with the code Proper Secondary Use of Human Tissue, as installed by the Federation of Biomedical Scientific Societies<sup>24</sup>.

### *Cell culture and experimental design*

CLCs were collected from the canine and human NPs<sup>25</sup> and thereafter expanded in expansion medium<sup>26</sup>. NCD canine donors that only contained CLCs in their NP were selected using cytopspins (Supplementary File 1). After the CLCs reached 80% confluence in P2, they were plated in a 96-well plate (CLS7007, Costar®) at a density of 35,000 cells/well in 50 µl chondrogenic culture medium: hgDMEM+Glutamax (31966, Invitrogen) with 1% P/S (P11-010, GE Healthcare Life Sciences), 1% ITS+ premix (354352, Corning Life Sciences), 0.04 mg/mL L-proline (P5607, Sigma-Aldrich), 0.1 mM Ascorbic acid 2-phosphate (A8960, Sigma-Aldrich), 1.25 mg/mL Human Serum Albumin (human CLCs, Sanquin Research) or Bovine Serum Albumin (canine CLCs, A9418, Sigma-Aldrich) and 10 ng/mL TGF-β<sub>1</sub> (240-B, R&D Systems). The micro-aggregates were cultured for 14 days (21% O<sub>2</sub>, 5% CO<sub>2</sub>, 37°C).

Caveolin-1 expression was silenced in CLCs from 6 CD canine donors and the following conditions were tested: mock (100 nM Stealth™ RNAi Negative Control Duplex), siRNA (100 nM caveolin-1 Stealth™ RNAi siRNA Duplex) and siRNA + caveolin-1 scaffolding domain peptide (CSD) (100 nM caveolin-1 siRNA oligo and 10 µM CSD (ALX-153-064, Enzo Life Sciences)). The canine CLCs were transfected with 3 µL/mL Lipofectamine™ RNAiMAX (13778-075, Invitrogen) at the moment of plating. Six hours after plating, the 96-well plates were centrifuged at 50g for 5 minutes to induce micro-aggregate formation. Stealth™ RNAi siRNA Duplex (10620312, Invitrogen) was used to silence caveolin-1 (NM\_001003296): 5' CACACCAAGGAAAUCGACCUGGUCA 3' (GC percentage 52%). Stealth™ RNAi Negative Control Duplex (GC percentage 48%, 12935-300, Invitrogen) was used to determine the effect of Stealth™ RNAi siRNA Duplex versus background (mock).

To determine the optimal conditions for CSD to exert its effects, CLCs from three human donors, five CD and five NCD canine donors with the following conditions were studied: T<sub>2</sub> (chondrogenic culture medium with 2 ng/mL TGF-β<sub>1</sub>), T<sub>2</sub>C<sub>10</sub> (2 ng/mL TGF-β<sub>1</sub> and 10 µM CSD), T<sub>2</sub>C<sub>25</sub> (2 ng/mL TGF-β<sub>1</sub> and 25 µM CSD), T<sub>10</sub> (10 ng/mL TGF-β<sub>1</sub>), T<sub>10</sub>C<sub>10</sub> (10 ng/mL TGF-β<sub>1</sub> and 10 µM CSD) and T<sub>10</sub>C<sub>25</sub> (10 ng/mL TGF-β<sub>1</sub> and 25 µM CSD).

### Read out parameters

Two micro-aggregates per donor and condition were snap frozen at day 4 and RNA was extracted, cDNA was made and RT-qPCR was performed for the target genes aggrecan (*ACAN*), a disintegrin and metalloproteinase with thrombospondin motifs 5 (*ADAMTS5*), activin receptor-like kinase 1 (*ALK1*), activin receptor-like kinase 5 (*ALK5*), BCL2-associated protein (*BAX*), B-cell CLL/lymphoma 2 (*BCL2*), caspase 3 (*CASP3*), caveolin-1 (*CAV1*), cyclin D1 (*CCND1*), collagen type 1A1 (*COL1A1*), collagen type 2A1 (*COL2A1*), inhibitor of DNA binding 1 (*ID1*), matrix metalloproteinase 13 (*MMP13*), plasminogen activator inhibitor-1 (*PAI1*, a read out for activated Smad2/3 signaling<sup>27-29</sup>), sex determining region Y-box 9 (*SOX9*), and tissue inhibitor of metalloproteinases (*TIMP1*) and the reference genes glyceraldehyde 3-phosphate dehydrogenase (*GAPDH*), ribosomal protein S19 (*RPS19*), hypoxanthine-guanine phosphoribosyltransferase (*HPRT*) and succinate dehydrogenase subunit A (*SDHA*) as previously described<sup>26</sup>. An overview of the primer pairs is given in Supplementary File 2. In addition, two micro-aggregates per condition per donor were collected at day 7 and 14 and the GAG and DNA content of the CLC micro-aggregates and GAG release into the culture medium was determined as previously described<sup>26</sup>. To determine caveolin-1 protein silencing efficiency, two snap frozen micro-aggregates per condition per donor were pooled, crushed and dissolved in RIPA buffer at day 7 and 14. Caveolin-1 protein was measured using an ELISA (SEA214Ca, Cloud-Clone Corp.). Histopathological evaluation of the micro-aggregates was performed with Safranin O/Fast Green staining<sup>26</sup> and collagen type I and II immunohistochemistry (Table 1). Western blot analysis was performed as described previously for pSmad2 (Ser 465/467, 60 kDa, 3101, Cell-Signaling) and  $\beta$ -actin (42 kDa, pan Ab-5, Neomarkers)<sup>30</sup>. 200,000 CD canine CLCs (mixture of the previously used CD canine donors) were plated per well (6-wells plate, 657160, Greiner CELLSTAR®) in expansion medium. After 5 days, the cells received 3 mL chondrogenic culture medium with/without CSD. The following conditions were tested: T<sub>2</sub>, T<sub>2</sub>C<sub>10</sub>, T<sub>2</sub>C<sub>25</sub>, T<sub>10</sub>, T<sub>10</sub>C<sub>10</sub> and T<sub>10</sub>C<sub>25</sub>. After 24 hours of treatment, protein samples were obtained and homogenized in RIPA buffer containing 0.6 mM phenylmethylsulphonyl fluoride, 17  $\mu$ g/ml aprotinin and 1 mM sodium orthovanadate (Sigma-Aldrich). Protein concentrations were measured using the Qubit® Protein Assay Kit (Q32851, Invitrogen) according to the manufacturer's instructions. The mean volume of the protein bands on the blots was determined by volumetric (INT\*mm<sup>2</sup>) band analysis using Quantity One software. The mean volume of pSmad2 was divided by the mean volume of  $\beta$ -actin (pSmad2/ $\beta$ -actin ratio) to correct for different protein concentrations applied to the membranes.

### Statistical analysis

Statistical analysis was performed using IBM SPSS (version 22) and R Studio (version 0.96). All data were examined for normal distribution (Shapiro Wilks test). Kruskal Wallis and Mann-Whitney U tests were performed on non-normally distributed data, whereas general linear regression models based on ANOVAs were used for normally distributed data. A cox proportional hazard model was used for genes with undetectable expression (Ct-value >40). To find correlations between the caveolin-1/TUNEL ratio and IVD degeneration score, partial correlations (corrected for donor) were determined. All above-mentioned tests were followed by a Benjamini & Hochberg False Discovery Rate *post-hoc* correction for multiple comparisons. A *p*-value < 0.05 was considered significant.

## Results

### The effect of *in vivo* caveolin-1 inactivation on the murine nucleus pulposus

*In vivo* caveolin-1 loss did not affect the morphometry of the murine IVDs (Supplementary File 3). However, there was a distinct difference in morphology between NP cells of WT and caveolin-1 null mice. The NP of WT mice was rich in large, vacuolated NCs, whereas the NP of caveolin-1 null mice contained relatively few, smaller, non-vacuolated chondrocyte- and fibroblast-like cells at every studied age (Figure 1a). NCs were diffusely scattered throughout the NP of 1.5-month old WT mice, whereas they were mainly located in the center of the NP surrounded by a rim of chondroid matrix in 3- and 6-month old WT mice. WT mice NP cell numbers did not considerably change during ageing, whereas NP cell numbers of caveolin-1 null mice decreased over time with significantly less cells at 1.5 and 6 months of age (Figure 1b,  $p < 0.05$ ). At the ages tested, the proportion of positively stained TUNEL cell nuclei (TUNEL ratio) was significantly higher in the NP of caveolin-1 null mice than in WT mice (Figure 1b,  $p < 0.05$ ), indicating that the *in vivo* loss of caveolin-1 induced apoptosis of murine NP cells leading to lower cell numbers. *In vivo* caveolin-1 loss did not affect the expression of the cell proliferation associated protein Ki-67: there was no positive Ki-67 staining in WT or caveolin-1 null mice NPs (data not shown). In the caveolin-1 null mice, GAGs and collagen type II were abundantly present in the extracellular matrix (ECM), whereas it was present to a lesser extent in WT NPs (Figure 2).

Immunofluorescent staining confirmed that caveolin-1 null NP cells expressed no caveolin-1 at the protein level, whereas NCs of WT mice abundantly expressed caveolin-1 in their cytoplasm and cell membrane at every studied age (Figure 3). *In vivo* caveolin-1 inactivation increased the expression of NPPC markers Tie2 (differentiation marker for dormant NPPCs<sup>31</sup>) and GD2 (NPPC proliferation marker<sup>31</sup>): caveolin-1 null NP cells abundantly expressed these markers at every studied age, whereas WT NCs only expressed Tie2 at 1.5 months of age and GD2 at 1.5 and 6 months of age (Figure 3). GD2 was intracellularly compartmentalized in caveolin-1 null NP cells, but localized in the cell membrane of WT mice NCs. Moreover, the percentage of cells expressing nuclear pSmad2 protein was significantly higher in the 1.5-month-old murine caveolin-1 null NPs compared with murine WT NPs of the same age. The percentage of cells expressing pSmad2 was significantly increased in the 3-month-old WT NPs compared with the 1.5-month-old WT NPs. At 3 and 6 months of age, WT and caveolin-1 null NP cells showed a similar percentage of pSmad2 positive stained nuclei, indicating comparable levels of activated Smad2 TGF- $\beta$  signaling (Figure 4,  $p < 0.05$ ).

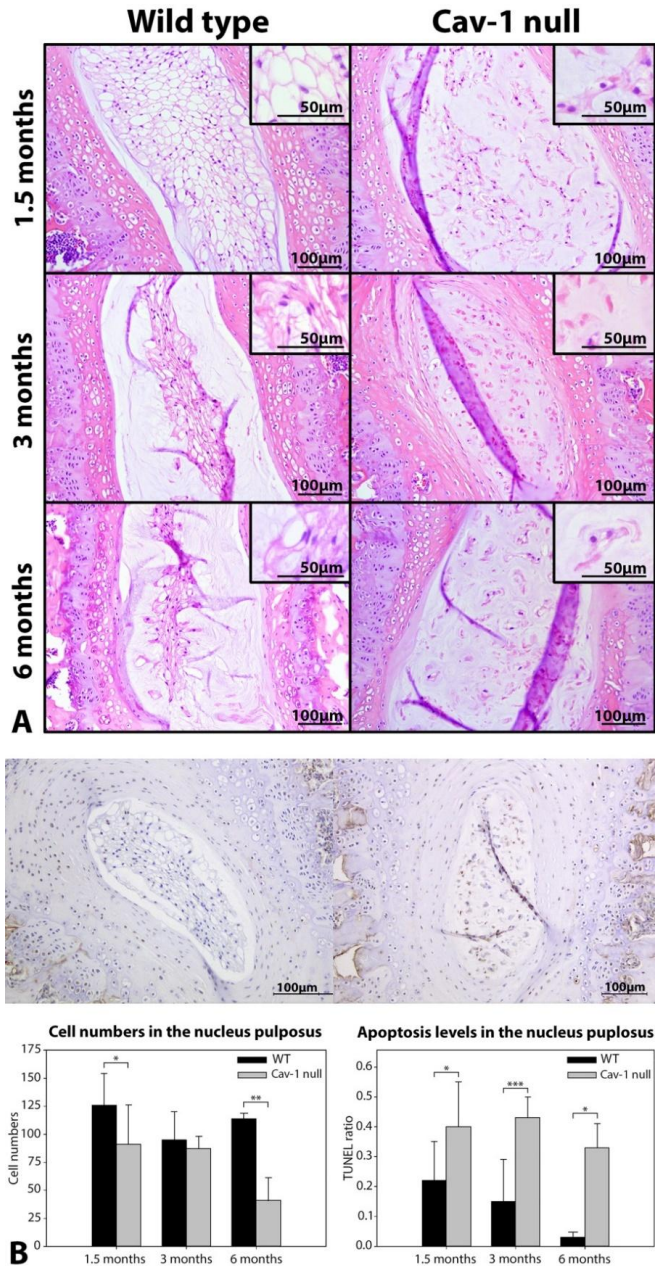


**Figure 1. Effect of *in vivo* caveolin-1 inactivation on morphology and apoptosis of murine nucleus pulposus cells.** (a) H&E stained nucleus pulposus sections of wild type (WT) and caveolin-1 null mice at 1.5, 3, and 6 months of age. Typical large, vacuolated NCs are present in the NP of WT mice, whereas smaller, non-vacuolated CLCs are present in the NP of caveolin-1 null mice. (b) The IVD of a 1.5-month-old WT mice stained with a TUNEL assay shows only some brown apoptotic cell nuclei, whereas the IVD of a 1.5-month-old caveolin-1 null mice shows many positive nuclei. NP cell numbers are significantly lower in caveolin-1 null mice than in WT mice at 1.5 and 6 months of age. The proportion of apoptotic cell nuclei (TUNEL ratio) is significantly higher in the NP of caveolin-1 null mice than in the NP of WT mice at every tested age. WT: wild type. \*: $p < 0.05$ , \*\*:  $p < 0.01$ , \*\*\*:  $p < 0.001$ .  $n = 4-9$  per age group and condition (WT or caveolin-1 null mice).

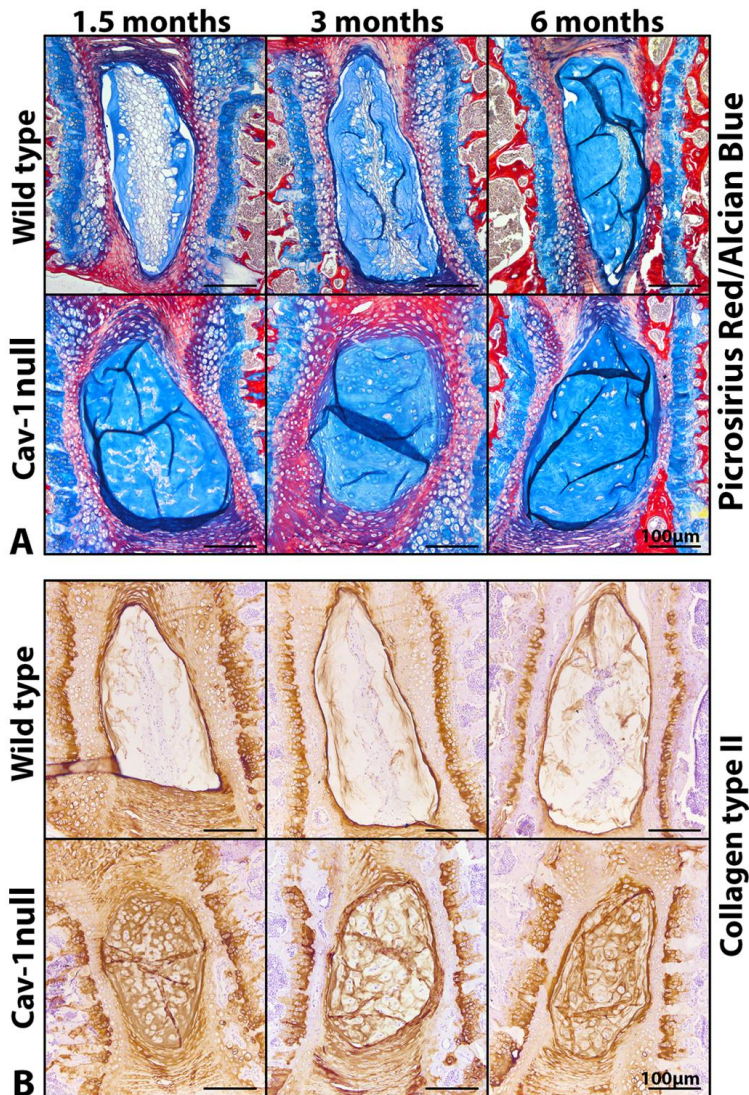


**Figure 2.** Effect of *in vivo* caveolin-1 inactivation on extracellular matrix production of the murine nucleus pulposus. Picosirius Red/Alcian Blue staining and immunohistochemistry for collagen type II on the nucleus pulposus of wild type (WT) and caveolin-1 null mice. GAGs and collagen type II are abundantly present in the extracellular matrix of caveolin-1 null mice NPs, whereas it was present to a lesser extent in WT mice NPs. Bars indicate 100 µm.  $n=4-9$  per age group and condition (WT or caveolin-1 null mice).

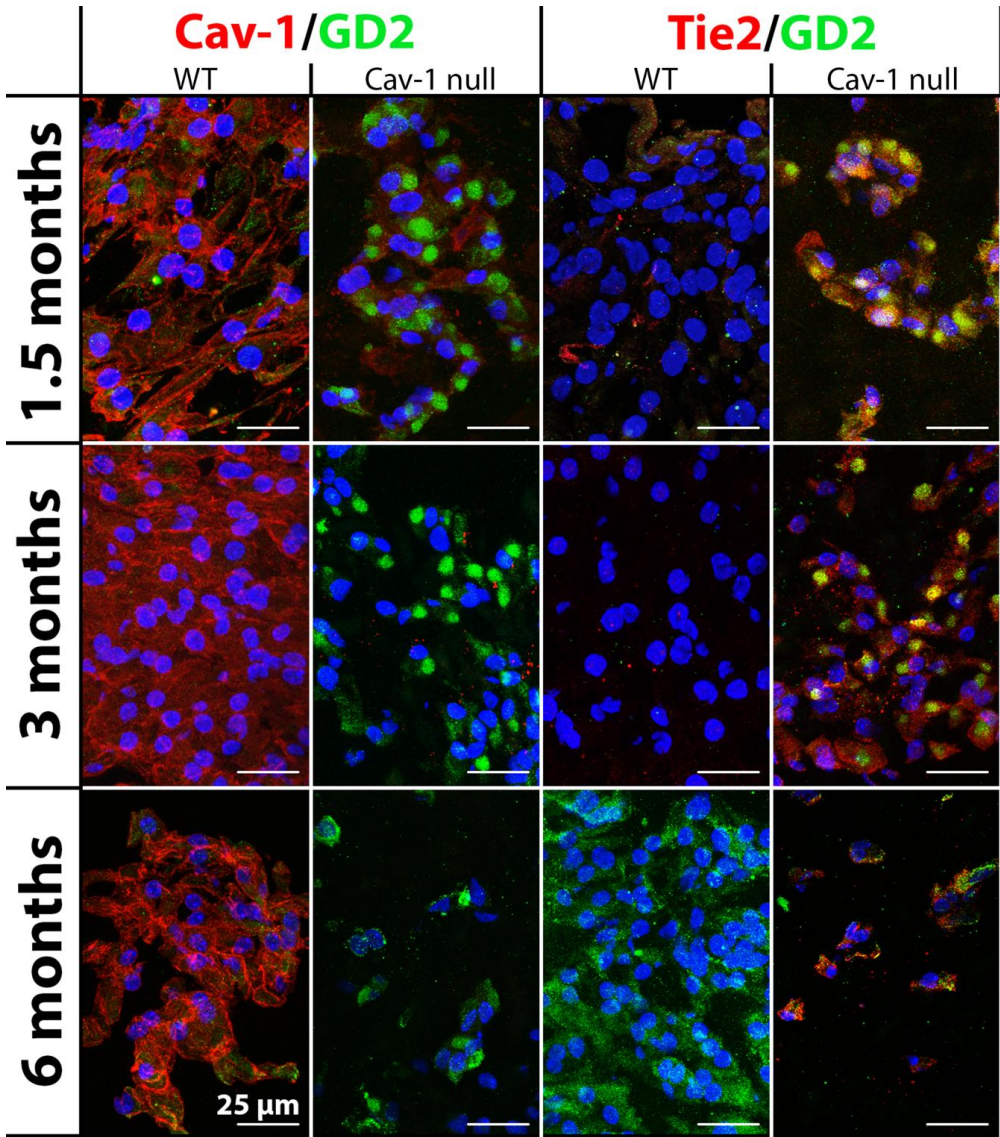


**Figure 3. GD2 and Tie2 expression is increased in caveolin-1 null mice.** Immunofluorescent staining for caveolin-1 (red), GD2 (green) and Tie2 (red) on the nucleus pulposus of wild type (WT) and caveolin-1 null mice. The cell nuclei were stained with DAPI (blue). WT: wild type. Bars indicate 25  $\mu$ m.  $n=2-5$  per age group and condition (WT or caveolin-1 null mice).

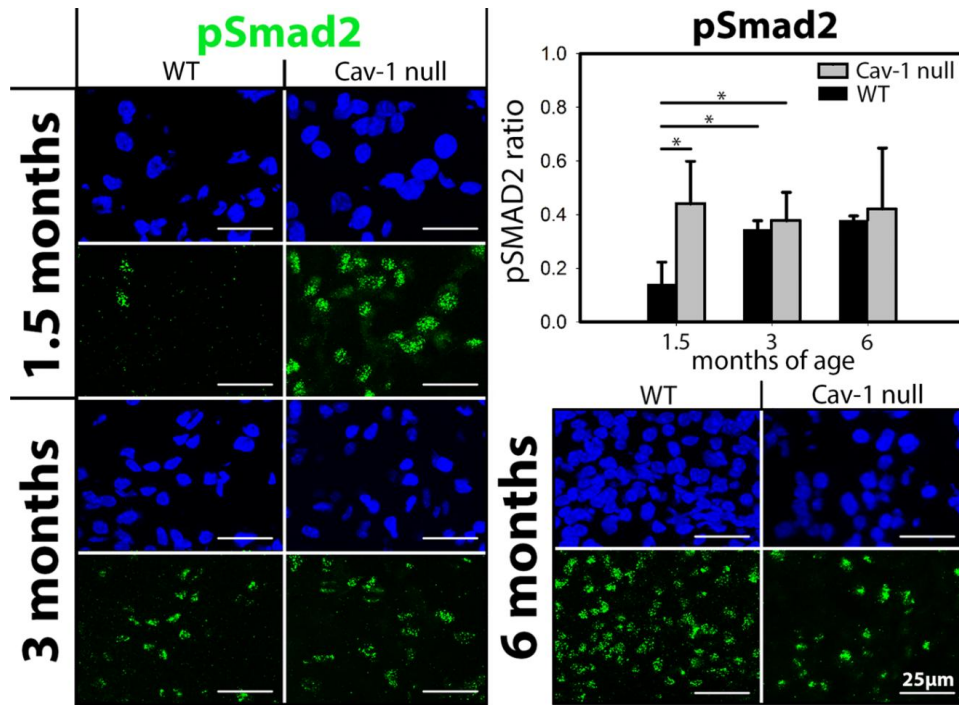
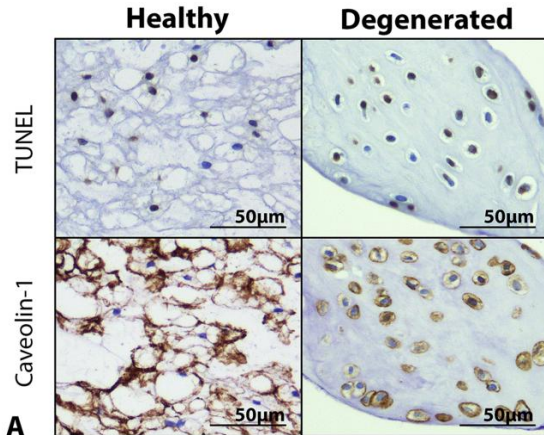


**Figure 4. Phosphorylated Smad2 (pSmad2) expression is lower in young wild type than in young caveolin-1 null mice.** Immunofluorescent staining for pSmad2 (green) on the nucleus pulposus of wild type (WT) and caveolin-1 null mice. The cell nuclei were stained with DAPI (blue). pSmad2 protein expression (pSmad2 ratio) is significantly lower in the murine WT nucleus pulposus (NP) at 1.5 months of age than in the murine WT NP at 3 months of age and the murine caveolin-1 null NP at 1.5 and 3 months of age. WT: wild type. Bars indicate 25  $\mu$ m.  $n=2-5$  per age group and condition (WT or caveolin-1 null mice).  $^*p<0.05$ .

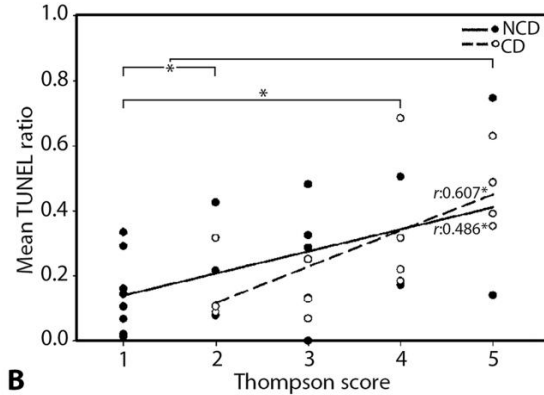
### Caveolin-1 expression and apoptosis during canine IVD degeneration

Apoptotic (TUNEL positive) cell nuclei were observed in healthy NC-containing NPs and in degenerated CLC-containing NPs (Figure 5a). NPs obtained from IVDs with Thompson score IV and V demonstrated significantly more apoptotic cells than healthy and early degenerated NPs (Thompson score I and II) in CD and NCD dogs (Figure 5b,  $p<0.05$ ). Also, there was a significant positive correlation between apoptosis levels and IVD degeneration grade in CD and NCD dogs (Figure 5B,  $r:0.607$  and  $r:0.486$ , respectively,  $p<0.05$ ). There were no statistically significant differences between CD and NCD dogs for apoptosis levels per Thompson score. Caveolin-1 expression was localized in the cytoplasm and cell membrane of NCs from healthy NPs and in CLCs from (severely) degenerated NPs (Figure 5a). No correlation between caveolin-1 expression and donor age was encountered (data not shown). Also, there were no statistically significant differences between CD and NCD dogs for caveolin-1 expression per Thompson score. The expression of caveolin-1 significantly increased during IVD degeneration in CD dogs (Figure 5c,  $p<0.05$ ). Caveolin-1 expression and IVD degeneration grade (Thompson score I-V) did not correlate in NCD dogs ( $r:-0.247$ ), while in CD dogs there was a strong positive correlation between caveolin-1 expression and IVD degeneration grade (Figure 5c,  $r:0.719$ ,  $p<0.01$ ). However, given that NC-rich Thompson score I IVDs were only available from NCD dogs, when excluding those Thompson score I

IVDs, caveolin-1 expression weakly correlated with IVD degeneration for the range of Thompson score II-V in the NCD dogs (Figure 5c,  $r:0.349$ ). No statistically significant correlation between caveolin-1 expression and apoptosis levels was found in CD or NCD canine NPs (data not shown).



**A** Apoptosis levels in canine IVD degeneration



**B** Caveolin-1 expression in canine IVD degeneration

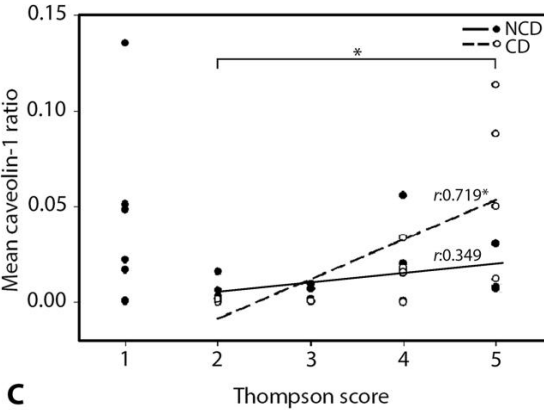


**Figure 5. Caveolin-1 expression and apoptosis levels are increased during canine intervertebral disc degeneration.**

(a) TUNEL assay and immunohistochemical staining for caveolin-1. Part of a healthy canine NP (Thompson score I) and a severely degenerated canine NP (Thompson score V) with brown apoptotic NC nuclei (TUNEL) and brown NC membranes and cytoplasm (caveolin-1). (b) The mean TUNEL ratio (the proportion of positively stained TUNEL nuclei in the NP) per Thompson degeneration score of canine IVDs. Apoptosis levels increase during canine IVD degeneration in CD and NCD dogs. The  $r$ -values indicate the partial correlation between the mean TUNEL ratio and IVD degeneration grade (Thompson score range I-V) for CD and NCD dogs. \*:  $p < 0.05$  (significance indicated for changes related to Thompson score). (c) The mean caveolin-1 ratio (the proportion of the total NP surface area that stained positive for caveolin-1) per Thompson degeneration score of canine IVDs. The  $r$ -values indicate the partial correlation between the mean caveolin-1 ratio and IVD degeneration grade (Thompson score range II-V) for CD and NCD dogs. Caveolin-1 protein expression increases during canine IVD degeneration in CD and NCD dogs. \*:  $p < 0.05$  (significance indicated for changes related to Thompson score).  $n=37$  IVD samples from 16 dogs.

### ***In vitro* effects of caveolin-1 on human and canine CLCs**

#### *The effect of caveolin-1 silencing in canine CLCs in vitro*

With a clinical directive in mind, caveolin-1 was silenced and caveolin-1 scaffolding domain (CSD) peptide (which mimics the function of caveolin-1<sup>8, 9, 32-34</sup>) was added to canine and human CLCs derived from degenerated IVDs to determine whether caveolin-1 modifies TGF- $\beta$  signaling in CLCs with concurrent effects on extracellular matrix level.

*CAV1* mRNA knockdown in the caveolin-1 silenced CLCs was 70% compared with mock-treated CLCs at day 4 ( $p < 0.001$ , Figure 6a). CSD treatment upregulated *CAV1* mRNA expression in canine CLCs silenced for caveolin-1 ( $p < 0.05$ ). Caveolin-1 protein knockdown was 53% compared with mock-treated CLCs at day 7 and 48% at day 14 (Figure 6a). While *PAI1* expression was decreased in caveolin-1 silenced CLCs compared with mock-treated CLCs ( $p < 0.05$ ), *ALK5* and *PAI1* expression was increased by CSD treatment of these CLCs ( $p < 0.01$ , Figure 6b), which indicated activated TGF- $\beta$ /Smad2/3 signaling under the influence of CSD at least at gene expression level. Expression of the anti-apoptotic *BCL2* gene was decreased by caveolin-1 silencing, whereas the addition of CSD reversed this effect ( $p < 0.05$ , Figure 6b). Gene expression of *MMP13*, *ACAN* (Figure 6b), *COL1A1*, *COL2A1*, *SOX9*, *TIMP1*, *ALK1*, *ID1*, *CCND1*, *BAX* and *CASP3* (data not shown) was not significantly different between the conditions.

Caveolin-1 silenced CLCs showed increased *ADAMTS5* expression compared with mock-treated CLCs ( $p < 0.05$ ), whereas CSD treatment reversed this effect ( $p < 0.01$ , Figure 6b). Also, the GAG content of caveolin-1 silenced micro-aggregates was significantly lower than in mock-treated micro-aggregates at day 7 (17%,  $p < 0.05$ ), but not at day 14 (10%, Figure 6c). CSD treatment increased the GAG content of caveolin-1 silenced micro-aggregates at day 14 (14%,  $p < 0.05$ ). GAG release into the culture medium (data not shown) and the DNA content (Figure 6c) of the micro-aggregates was not considerably different between the conditions.

All CLC micro-aggregates stained positive for GAGs, collagen type I and II (Figure 6c). In the mock-treated micro-aggregates and mainly in the caveolin-1 silenced micro-aggregates supplemented with CSD, a collagen type II positive rim was present, but not in the caveolin-1 silenced micro-aggregates not supplemented with CSD.

#### *The dose-response effect of caveolin-1 peptide on canine and human CLCs in vitro*

Since CSD treatment rescued the effects of caveolin-1 silencing and exerted anabolic effects on canine CLCs by modifying TGF- $\beta$  signaling at gene expression level, different concentrations, *i.e.* 2 ng/mL TGF- $\beta_1$  ( $T_2$ ), 10 ng/mL TGF- $\beta_1$  ( $T_{10}$ ), 10  $\mu$ M CSD ( $C_{10}$ ), and 25  $\mu$ M CSD ( $C_{25}$ ) were tested to determine the additive effect of CSD on TGF- $\beta_1$  treatment of human, CD and NCD canine CLCs. The DNA content of CD and NCD canine  $T_{10}$ -treated micro-aggregates was significantly higher than that of  $T_2$ -treated micro-aggregates ( $p < 0.05$ ), whereas this was not observed in human micro-aggregates (Figure 7). Only in NCD canine donors,  $T_2C_{25}$ -treated micro-aggregates showed an increased DNA content compared with  $T_2C_{10}$ -treated micro-aggregates ( $p < 0.05$ ). CSD treatment did not affect the DNA content of human and CD canine micro-aggregates.

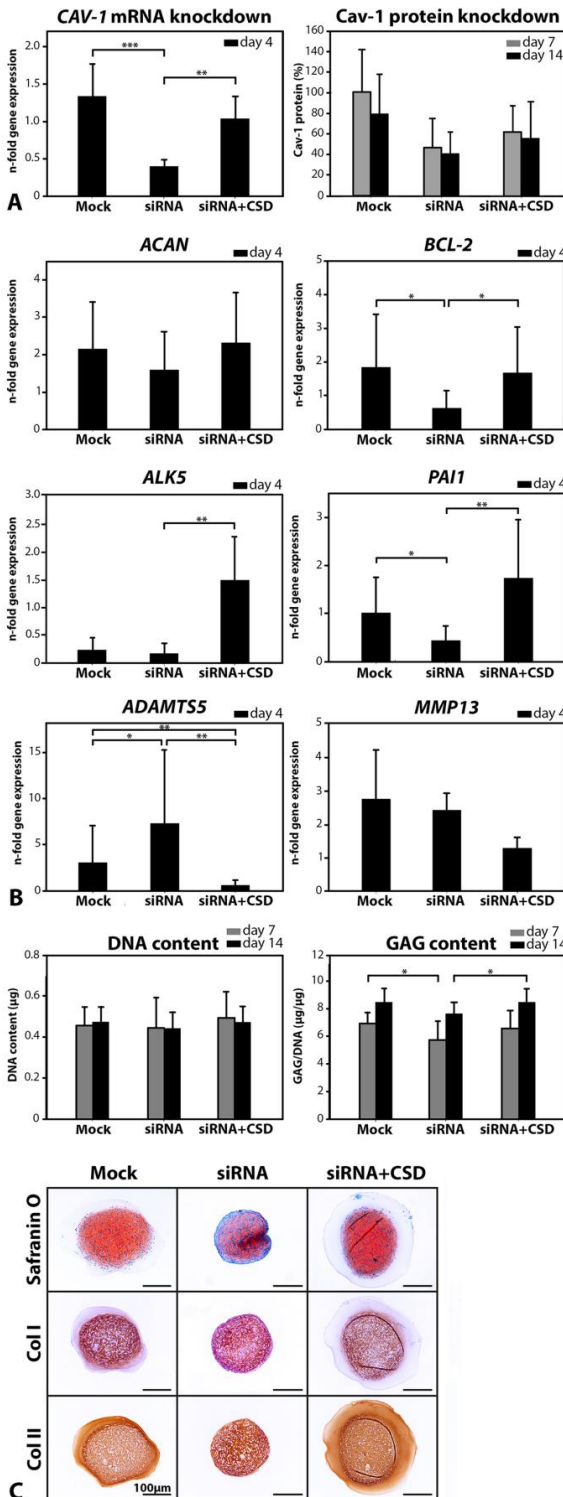


**Figure 6. The effect of *in vitro* caveolin-1 silencing on CLCs from chondro-dystrophic dogs.** *In vitro* caveolin-1 silencing decreased TGF- $\beta$ / Smad2/3 signaling and canine CLC ECM deposition, while CSD supplementation rescued this effect. (a) Caveolin-1 mRNA (n-fold change + SD) and protein knockdown by caveolin-1 siRNA. The caveolin-1 protein level in the mock-treated micro-aggregates at day 7 was set at 100%. (b) RT-qPCR results (n-fold change + SD). Gene expression in the non-treated CLC micro-aggregates was set at 1. (c) DNA and GAG content (corrected for DNA content) of the canine CLC micro-aggregates with corresponding Safranin O/Fast Green, collagen type I and II IHC stained sections. Bars indicate 100 $\mu$ m.  $n=6$ . \*:  $p<0.05$ , \*\*:  $p<0.01$ , \*\*\*:  $p<0.001$ . siRNA: micro-aggregates silenced for caveolin-1, CSD: 10  $\mu$ M caveolin-1 scaffolding domain peptide, Col I: collagen type I, Col II: collagen type II.

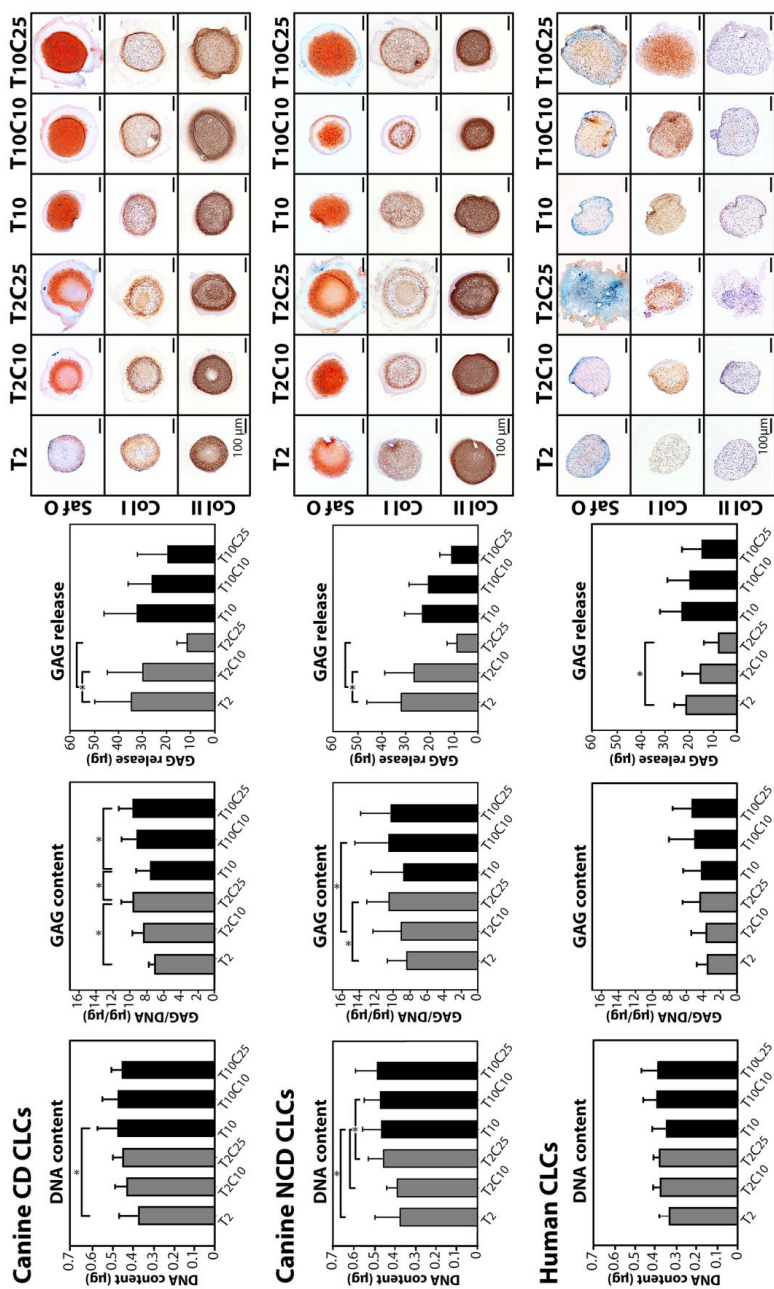


**Figure 7. The dose-response effect of caveolin-1 on canine and human CLCs *in vitro*.** DNA content, GAG content (corrected for DNA content) and GAG release into the culture medium of human, CD and NCD canine CLC micro-aggregates with corresponding Safranin O/Fast Green, collagen type I and II IHC stained sections. Generally, the GAG content was increased in the micro-aggregates treated with 25µM CSD, whereas the GAG release in the culture medium was decreased in these 25µM CSD-treated micro-aggregates. T<sub>2</sub>: 2 ng/mL TGF-β<sub>1</sub>, T<sub>10</sub>: 10 ng/mL TGF-β<sub>1</sub>, C<sub>10</sub>: 10µM CSD, C<sub>25</sub>: 25µM CSD, Bars indicate 100µm. n=5 (canine chondrodystrophic (CD) and non-chondrodystrophic (NCD)) and n=3 (human); two micro-aggregates were analyzed per donor and condition. \*:p<0.05.

In CD and NCD donors, the GAG content of the T<sub>2</sub>C<sub>25</sub>-treated micro-aggregates was significantly higher (35% for CD, 25% for NCD) than the GAG content of T<sub>2</sub>-treated micro-aggregates (Figure 7). Additionally, only in CD donors, the GAG content of the T<sub>10</sub>C<sub>25</sub>-treated micro-aggregates was significantly higher (26%) than the GAG content of the T<sub>10</sub>-treated micro-aggregates. GAG release in the culture medium was approximately three times decreased in T<sub>2</sub>C<sub>25</sub>-treated CLC micro-aggregates compared with T<sub>2</sub>-treated CLC micro-aggregates in all species ( $p < 0.05$ , Figure 7). Total GAG production (GAG content in the micro-aggregates plus GAG release into the culture medium) appeared to be 20-40% decreased by 25  $\mu$ M CSD treatment in all species and was significantly decreased in T<sub>2</sub>C<sub>25</sub>-treated CD and NCD canine CLCs compared with T<sub>2</sub>- and T<sub>2</sub>C<sub>10</sub>-treated CD and NCD canine CLCs ( $p < 0.05$ ), but not significantly different between the differentially treated human CLCs (data not shown). The GAG content of human CLC micro-aggregates was lower than the GAG content of CD and NCD canine micro-aggregates. In contrast to canine CLC micro-aggregates, human CLC micro-aggregates demonstrated no collagen type II protein deposition (Figure 7). Furthermore, CSD treatment increased collagen type I deposition in human CLC micro-aggregates, whereas this was not observed in canine CLC micro-aggregates.

Western blot analysis demonstrated that pSmad2 protein expression was 1.7 times higher in CD canine CLCs treated with 2 ng/mL TGF- $\beta$ <sub>1</sub> than in those treated with 10 ng/mL TGF- $\beta$ <sub>1</sub> (Figure 8). pSmad2 protein expression was 1.3-1.5 times higher in the canine CLCs treated with 10 or 25  $\mu$ M CSD and 2 ng/mL TGF- $\beta$ <sub>1</sub> than those only treated with 2 ng/mL TGF- $\beta$ <sub>1</sub> (Figure 8). Furthermore, pSmad2 protein expression was 1.1-1.2 times higher in the CLCs treated with 10 or 25  $\mu$ M CSD and 10 ng/mL TGF- $\beta$ <sub>1</sub> than in those only treated with 10 ng/mL TGF- $\beta$ <sub>1</sub> (Figure 8). Altogether, this indicates that CSD peptide treatment enhanced TGF- $\beta$ /pSmad2 signaling.

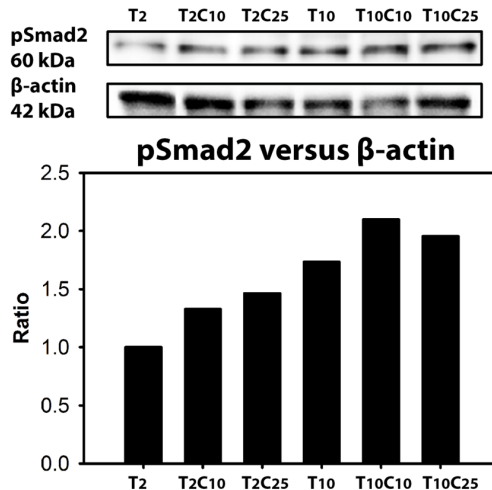


**Figure 8. Caveolin-1 enhances TGF- $\beta$ / pSmad2 signaling in canine CLCs *in vitro*.** Western blot analysis for pSmad2 and  $\beta$ -actin protein expression in CD canine CLCs after 24 hours of treatment, expressed as pSmad2/ $\beta$ -actin ratio. T<sub>2</sub>: 2 ng/mL TGF- $\beta$ <sub>1</sub>, T<sub>10</sub>: 10 ng/mL TGF- $\beta$ <sub>1</sub>, C<sub>10</sub>: 10  $\mu$ M CSD, C<sub>25</sub>: 25  $\mu$ M CSD. The pSmad2/ $\beta$ -actin ratio in the T<sub>2</sub>-treated CLCs was set at 1.

## Discussion

The present study demonstrates that caveolin-1 plays a role in IVD degeneration. *In vivo* studies with murine caveolin-1 null NPs demonstrated that caveolin-1 was essential for NC preservation. Furthermore, we demonstrated that caveolin-1 expression and apoptosis levels significantly increased during CD canine IVD degeneration. In addition, *in vitro* caveolin-1 silencing decreased CLC ECM deposition, while CSD supplementation increased TGF- $\beta$ / pSmad2 signaling at gene and protein expression level and enhanced the anabolic effects of TGF- $\beta$ 1 on CLCs resulting in higher extracellular matrix deposition. Taken together, this may indicate that the increased caveolin-1 expression during IVD degeneration facilitates an anabolic reparative response of the CLCs at least by modifying TGF- $\beta$  signaling rather than being merely correlated with CLC apoptosis.

### Caveolin-1 is essential for NC physiology

Histological analysis of caveolin-1 null NPs revealed that apoptotic cells were present in the healthy WT murine NP at 1.5, 3 and 6 months of age, implying that during IVD tissue homeostasis, there is physiologic turnover of NP cells (they proliferate and undergo apoptosis). Affirmatively, previous work already demonstrated apoptotic cells in IVDs from two-week-old WT mice<sup>35</sup>. Caveolin-1 null NPs showed the absence of typical NCs in favor of chondrocyte/fibroblast-like cells with an increased apoptotic activity, suggesting that caveolin-1 is essential for NC preservation. In line with this thought, NPs of NCD dogs with Thompson grade I, rich in NC cells, abundantly expressed caveolin-1, while the caveolin-1 null mice had lost their NCs already when they were skeletally mature (young adult), which is rather comparable with the loss of NCs in young adult CD dogs and humans. In the NP of 1.5-month-old caveolin-1 null mice (with lower total NP cells numbers than WT mice), Tie2<sup>+</sup>/GD2<sup>+</sup> progenitor cells were present, and TGF- $\beta$  signaling mediated by pSmad2 probably facilitated abundant ECM deposition. Affirmatively, Tie2/GD2 positive NP cells have been shown to possess superior ECM production, self-renewal, multipotent differentiation and proliferation capacity<sup>31</sup>. Increased cell proliferation is associated with late stage IVD degeneration<sup>36</sup>. Notably, the NPPC proliferation marker GD2 was expressed in caveolin-1 null and WT mice NPs, but Ki-67 positivity was not detected. The short Ki-67 protein half-life (90 minutes) and nutritionally deprived NP environment may explain the absence of Ki-67 in murine NPs<sup>36</sup>. GD2 appeared intracellularly compartmentalized in caveolin-1 null NP cells, but localized to the cell membrane of WT NCs. We hypothesize that in the caveolin-1 null NP phenotype, GD2 may not mark proliferating cells *per se* if the different localization could render GD2 inactive, but future studies should look into the functionality of GD2 in caveolin-1 null NP cells.

Altogether, caveolin-1 plays a role in the preservation of healthy NCs, since *in vivo* inactivation of caveolin-1 induced a change in cell phenotype from NCs towards CLCs with a high apoptotic activity in mice. Activated NPPCs and TGF- $\beta$ / pSmad2 signaling probably resulted into GAG- and collagen-rich ECM deposition in the caveolin-1 null mice NP. The caveolin-1 null mice showed several metabolic/endocrine disorders<sup>37-39</sup> that could have influenced their NP phenotype, *e.g.* insulin resistance leading to diabetes mellitus, which has been associated with premature NC senescence and apoptosis<sup>40</sup>. Further studies need to concentrate at earlier stages of development in order to delineate how caveolin-1

preserves NCs, including modification of MAPK/ERK, Wnt<sup>15</sup>, Indian/Sonic Hedgehog signaling pathways<sup>41, 42</sup> and/or glucose transportation<sup>43, 44</sup>.

### **Caveolin-1 increases during IVD degeneration mediating a reparative response**

Caveolin-1 is known to induce apoptosis via - amongst others - cell cycle arrest in the G2/M phase<sup>45</sup> and by influencing the expression of the anti-apoptosis protein survivin<sup>46, 47</sup>. Caveolin-1 may induce senescence in CLCs given that in NPs derived from degenerated CD canine and human IVDs, caveolin-1 expression<sup>16</sup> and apoptosis levels were positively correlated with IVD degeneration grade. However, a causative relationship in the IVD remains to be determined. Based on the results of the present study, it is tempting to hypothesize that the increased caveolin-1 expression in degenerated IVDs may be part of an ultimate attempt of (unsuccessful) repair. With a clinical directive in mind (degenerated human and canine IVDs contain almost 100% CLCs), the effect of caveolin-1 was investigated in human and canine CLCs derived from degenerated IVDs by silencing for caveolin-1 and/or supplementing with CSD peptide. Caveolin-1 silencing decreased anti-apoptotic *BCL-2* expression, whereas CSD addition increased it to baseline levels again, opposing the hypothesis that caveolin-1 itself induces CLC apoptosis. Furthermore, caveolin-1 silencing increased *ADAMTS5* expression and decreased the GAG content of the micro-aggregates, whereas when the canine CLCs were treated with CSD, *ADAMTS5* expression decreased and the GAG content was restored. In line with this, GAG release was decreased in 25  $\mu$ M CSD-treated human and canine CLCs. Notably, caveolin-1 silencing and CSD supplementation did not influence collagen type I deposition by canine CLCs, while its deposition was increased by CSD treatment in human CLCs. It is plausible that caveolin-1 exerts a protective effect by decreasing ECM degradation, given its well described anti-inflammatory properties<sup>48-50</sup>. This altogether implies that decreased GAG degradation resulted in the significantly increased GAG content of CSD-treated canine CLCs. The underlying mechanisms for the latter could be decreased ECM degradation and/or more collagen type II protein expression that enables the deposition<sup>51</sup> and prevents the release of GAGs.

The results of this study imply that caveolin-1 regulates TGF- $\beta$  signaling in CLCs *in vitro*: caveolin-1 silencing decreased, whereas CSD supplementation increased TGF- $\beta$ / Smad2 signaling at gene and protein expression level. TGF- $\beta$  signals through two membrane TGF- $\beta$  receptors type I (ALK1 and ALK5) and one TGF- $\beta$  receptor type II. These TGF- $\beta$  receptors have been demonstrated to colocalize with caveolin-1<sup>20</sup>. TGF- $\beta$  receptor type II phosphorylates TGF- $\beta$  receptor type I. When ALK5 is phosphorylated, Smad2/3 signaling becomes activated and ECM is produced. However, when ALK1 is phosphorylated, Smad1/5/8 signaling becomes activated, which inhibits Smad2/3 signaling and ECM production<sup>52, 53</sup>. In this study we demonstrate that CSD enhanced the anabolic effect of TGF- $\beta$ <sub>1</sub> in terms of ECM deposition in the micro-aggregates. Caveolin-1 silencing decreased *PAI1* (a classical readout for activated Smad2/3 TGF- $\beta$  signaling<sup>27-29</sup>) gene expression, while CSD supplementation increased *ALK5* and *PAI1* gene expression, did not influence *ALK1* or *ID1* (readout for activated Smad1/5/8 signaling) gene expression and increased pSmad2 protein expression. This all indicates that caveolin-1 indeed enhanced TGF- $\beta$ -induced Smad2/3 signaling.

There is evidence that caveolin-1 acts differently according to stimulating/inhibiting signals and cellular context, e.g. cell type, age, and disease/health stage of the tissue<sup>7, 11, 54</sup>. In the present study, caveolin-1 enhanced TGF- $\beta$  signaling mediated by pSmad2 in CLCs from degenerated IVDs *in vitro*, while the opposite is true for earlier reports<sup>14, 55-57</sup>. In line with our results, however, TGF- $\beta$  signaling is reduced in caveolin-1-deficient fibroblasts<sup>58</sup> and regenerating hepatocytes of caveolin-1 null mice<sup>20</sup>. Notably, in caveolin-1 silenced canine CLCs, ECM production was decreased, whereas in caveolin-1 null mice, which initially contained primarily NCs, abundant ECM was deposited. This implies that caveolin-1 may indeed have different functions in NCs and CLCs: caveolin-1 is required for NC preservation, whereas in CLCs it may be related with apoptosis and/or it may influence signaling pathways (such as TGF- $\beta$ ) that support ECM deposition.

## Conclusions

The current study demonstrates that caveolin-1 plays a role in IVD degeneration. The abundant expression of caveolin-1 in NCs from NCD dogs and the loss of healthy NCs in the NP of caveolin-1 null mice indicate that caveolin-1 supports preservation of the NC phenotype. In the CD canine NP, both caveolin-1 expression and apoptosis levels had a positive correlation with IVD degeneration grade, indicating that caveolin-1 may be related with CLC apoptosis. Nevertheless, ECM deposition was decreased by *in vitro* caveolin-1 silencing of canine CLCs, whereas CSD peptide increased TGF- $\beta$ / pSmad2 signaling at gene and protein expression level and enhanced the anabolic effects of TGF- $\beta$ <sub>1</sub> with concomitant increased extracellular matrix deposition. This implies that the increased caveolin-1 expression during IVD degeneration may be an anabolic repair response rather than being merely correlated with CLC apoptosis. Further studies are needed to investigate how caveolin-1 modifies other signaling pathways and facilitates IVD repair.

## Acknowledgements

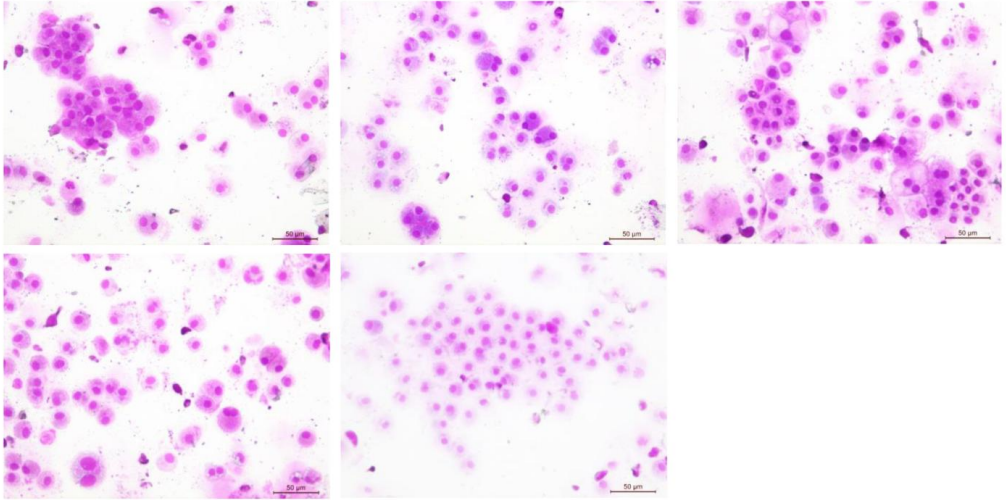
The authors would like to thank Anita Krouwels for supplying the human CLCs and Willem de Jong, Bianca Kuster, Dirk Vestjens and Birgit Seubers for assistance during the execution of experiments.

## References

1. Murray CJ, Vos T, Lozano R, et al. 2012. Disability-adjusted life years (DALYs) for 291 diseases and injuries in 21 regions, 1990-2010: A systematic analysis for the global burden of disease study 2010. *Lancet* 380: 2197-2223.
2. Freemont AJ. 2009. The cellular pathobiology of the degenerate intervertebral disc and discogenic back pain. *Rheumatology (Oxford)* 48: 5-10.
3. Bergknut N, Rutges JP, Kranenburg HJ, et al. 2012. The dog as an animal model for intervertebral disc degeneration? *Spine (Phila Pa 1976)* 37: 351-358.
4. Smolders LA, Bergknut N, Grinwis GC, et al. 2013. Intervertebral disc degeneration in the dog. part 2: Chondrodystrophic and non-chondrodystrophic breeds. *Vet J* 195: 292-299.
5. Bach FC, Willems N, Penning LC, et al. 2014. Potential regenerative treatment strategies for intervertebral disc degeneration in dogs. *BMC Vet Res* 10: 3-6148-10-3.
6. Head BP, Hu Y, Finley JC, et al. 2011. Neuron-targeted caveolin-1 protein enhances signaling and promotes arborization of primary neurons. *J Biol Chem* 286: 33310-33321.
7. Baker N, Tuan RS. 2013. The less-often-traveled surface of stem cells: Caveolin-1 and caveolae in stem cells, tissue repair and regeneration. *Stem Cell Res Ther* 4: 90.
8. Tourkina E, Richard M, Gooz P, et al. 2008. Antifibrotic properties of caveolin-1 scaffolding domain in vitro and in vivo. *Am J Physiol Lung Cell Mol Physiol* 294: L843-61.
9. Zhang GY, Yu Q, Cheng T, et al. 2011. Role of caveolin-1 in the pathogenesis of tissue fibrosis by keloid-derived fibroblasts in vitro. *Br J Dermatol* 164: 623-627.
10. Zou H, Stoppani E, Volonte D, Galbiati F. 2011. Caveolin-1, cellular senescence and age-related diseases. *Mech Ageing Dev* 132: 533-542.
11. Mercier I, Jasmin JF, Pavlides S, et al. 2009. Clinical and translational implications of the caveolin gene family: Lessons from mouse models and human genetic disorders. *Lab Invest* 89: 614-623.
12. Okamoto T, Schlegel A, Scherer PE, Lisanti MP. 1998. Caveolins, a family of scaffolding proteins for organizing "preassembled signaling complexes" at the plasma membrane. *J Biol Chem* 273: 5419-5422.
13. Hult J, Bash T, Fu M, et al. 2000. The cyclin D1 gene is transcriptionally repressed by caveolin-1. *J Biol Chem* 275: 21203-21209.
14. Gvaramia D, Blaauboer ME, Hanemaaijer R, Everts V. 2013. Role of caveolin-1 in fibrotic diseases. *Matrix Biol* 32: 307-315.
15. Smolders LA, Meij BP, Onis D, et al. 2013. Gene expression profiling of early intervertebral disc degeneration reveals a down-regulation of canonical wnt signaling and caveolin-1 expression: Implications for development of regenerative strategies. *Arthritis Res Ther* 15: R23.
16. Heathfield SK, Le Maitre CL, Hoyland JA. 2008. Caveolin-1 expression and stress-induced premature senescence in human intervertebral disc degeneration. *Arthritis Res Ther* 10: R87.
17. Le Maitre CL, Freemont AJ, Hoyland JA. 2007. Accelerated cellular senescence in degenerate intervertebral discs: A possible role in the pathogenesis of intervertebral disc degeneration. *Arthritis Res Ther* 9: R45.
18. Dai SM, Shan ZZ, Nakamura H, et al. 2006. Catabolic stress induces features of chondrocyte senescence through overexpression of caveolin 1: Possible involvement of caveolin 1-induced down-regulation of articular chondrocytes in the pathogenesis of osteoarthritis. *Arthritis Rheum* 54: 818-831.
19. Zhao W, Wang T, Luo Q, et al. 2015. Cartilage degeneration and excessive subchondral bone formation in spontaneous osteoarthritis involves altered TGF-beta signaling. *J Orthop Res* 34(5):763-70.
20. Mayoral R, Valverde AM, Llorente Izquierdo C, et al. 2010. Impairment of transforming growth factor beta signaling in caveolin-1-deficient hepatocytes: Role in liver regeneration. *J Biol Chem* 285: 3633-3642.
21. Gruber HE, Ingram J, Hanley EN, Jr. 2002. An improved staining method for intervertebral disc tissue. *Biotech Histochem* 77: 81-83.
22. Bergknut N, Grinwis G, Pickee E, et al. 2011. Reliability of macroscopic grading of intervertebral disk degeneration in dogs by use of the thompson system and comparison with low-field magnetic resonance imaging findings. *Am J Vet Res* 72: 899-904.
23. Bergknut N, Meij BP, Hagman R, et al. 2013. Intervertebral disc disease in dogs - part 1: A new histological grading scheme for classification of intervertebral disc degeneration in dogs. *Vet J* 195: 156-163.
24. Rutges JP, Nikkels PG, Oner FC, et al. 2010. The presence of extracellular matrix degrading metalloproteinases during fetal development of the intervertebral disc. *Eur Spine J* 19: 1340-1346.
25. Willems N, Bach FC, Plomp SG, et al. 2015. Intradiscal application of rhBMP-7 does not induce regeneration in a canine model of spontaneous intervertebral disc degeneration. *Arthritis Res Ther* 17: 137-015-0625-2.
26. Bach FC, de Vries SA, Krouwels A, et al. 2015. The species-specific regenerative effects of notochordal cell-conditioned medium on chondrocyte-like cells derived from degenerated human intervertebral discs. *Eur Cell Mater* 30: 132-147.
27. Mallat Z, Tedgui A. 2002. The role of transforming growth factor beta in atherosclerosis: Novel insights and future perspectives. *Curr Opin Lipidol* 13: 523-529.
28. Cunha SI, Pietras K. 2011. ALK1 as an emerging target for antiangiogenic therapy of cancer. *Blood* 117: 6999-7006.
29. Vaughan DE. 2006. PAI-1 and TGF-beta: Unmasking the real driver of TGF-beta-induced vascular pathology. *Arterioscler Thromb Vasc Biol* 26: 679-680.

30. Spee B, Arends B, van den Ingh TS, et al. 2006. Transforming growth factor beta-1 signalling in canine hepatic diseases: New models for human fibrotic liver pathologies. *Liver Int* 26: 716-725.
31. Sakai D, Nakamura Y, Nakai T, et al. 2012. Exhaustion of nucleus pulposus progenitor cells with ageing and degeneration of the intervertebral disc. *Nat Commun* 3: 1264.
32. Bernatchez PN, Bauer PM, Yu J, et al. 2005. Dissecting the molecular control of endothelial NO synthase by caveolin-1 using cell-permeable peptides. *Proc Natl Acad Sci U S A* 102: 761-766.
33. Bucci M, Gratton JP, Rudic RD, et al. 2000. In vivo delivery of the caveolin-1 scaffolding domain inhibits nitric oxide synthesis and reduces inflammation. *Nat Med* 6: 1362-1367.
34. Miyasato SK, Loeffler J, Shohet R, et al. 2011. Caveolin-1 modulates TGF-beta1 signaling in cardiac remodeling. *Matrix Biol* 30: 318-329.
35. Dahia CL, Mahoney EJ, Durrani AA, Wylie C. 2009. Postnatal growth, differentiation, and aging of the mouse intervertebral disc. *Spine (Phila Pa 1976)* 34: 447-455.
36. Johnson WE, Eisenstein SM, Roberts S. 2001. Cell cluster formation in degenerate lumbar intervertebral discs is associated with increased disc cell proliferation. *Connect Tissue Res* 42: 197-207.
37. Pojoga LH, Underwood PC, Goodarzi MO, et al. 2011. Variants of the caveolin-1 gene: A translational investigation linking insulin resistance and hypertension. *J Clin Endocrinol Metab* 96: E1288-92.
38. Senou M, Costa MJ, Massart C, et al. 2009. Role of caveolin-1 in thyroid phenotype, cell homeostasis, and hormone synthesis: In vivo study of caveolin-1 knockout mice. *Am J Physiol Endocrinol Metab* 297: E438-51.
39. Le Lay S, Kurzchalia TV. 2005. Getting rid of caveolins: Phenotypes of caveolin-deficient animals. *Biochim Biophys Acta* 1746: 322-333.
40. Jiang L, Zhang X, Zheng X, et al. 2013. Apoptosis, senescence, and autophagy in rat nucleus pulposus cells: Implications for diabetic intervertebral disc degeneration. *J Orthop Res* 31: 692-702.
41. Karpen HE, Bukowski JT, Hughes T, et al. 2001. The sonic hedgehog receptor patched associates with caveolin-1 in cholesterol-rich microdomains of the plasma membrane. *J Biol Chem* 276: 19503-19511.
42. Dahia CL, Mahoney E, Wylie C. 2012. Shh signaling from the nucleus pulposus is required for the postnatal growth and differentiation of the mouse intervertebral disc. *PLoS One* 7: e35944.
43. Zhang QQ, Huang L, Han C, et al. 2015. Caveolin-1 and glucose transporter 4 involved in the regulation of glucose-deprivation stress in PC12 cells. *Sheng Li Xue Bao* 67: 349-356.
44. Gonzalez-Munoz E, Lopez-Iglesias C, Calvo M, et al. 2009. Caveolin-1 loss of function accelerates glucose transporter 4 and insulin receptor degradation in 3T3-L1 adipocytes. *Endocrinology* 150: 3493-3502.
45. Kang J, Park JH, Lee HJ, et al. 2015. Caveolin-1 modulates docetaxel-induced cell death in breast cancer cell subtypes through different mechanisms. *Cancer Res Treat* 48(2):715-26.
46. Zhang M, Lin L, Lee SJ, et al. 2009. Deletion of caveolin-1 protects hyperoxia-induced apoptosis via survivin-mediated pathways. *Am J Physiol Lung Cell Mol Physiol* 297: L945-53.
47. Torres VA, Tapia JC, Rodriguez DA, et al. 2007. E-cadherin is required for caveolin-1-mediated down-regulation of the inhibitor of apoptosis protein survivin via reduced beta-catenin-tcf/lef-dependent transcription. *Mol Cell Biol* 27: 7703-7717.
48. Feng H, Guo L, Song Z, et al. 2010. Caveolin-1 protects against sepsis by modulating inflammatory response, alleviating bacterial burden, and suppressing thymocyte apoptosis. *J Biol Chem* 285: 25154-25160.
49. Yuan K, Huang C, Fox J, et al. 2011. Elevated inflammatory response in caveolin-1-deficient mice with pseudomonas aeruginosa infection is mediated by STAT3 protein and nuclear factor kappaB (NF-kappaB). *J Biol Chem* 286: 21814-21825.
50. Wang P, Zhu F, Tong Z, Konstantopoulos K. 2011. Response of chondrocytes to shear stress: Antagonistic effects of the binding partners toll-like receptor 4 and caveolin-1. *FASEB J* 25: 3401-3415.
51. Yuan M, Leong KW, Chan BP. 2011. Three-dimensional culture of rabbit nucleus pulposus cells in collagen microspheres. *Spine J* 11: 947-960.
52. Blaney Davidson EN, Remst DF, Vitters EL, et al. 2009. Increase in ALK1/ALK5 ratio as a cause for elevated MMP-13 expression in osteoarthritis in humans and mice. *J Immunol* 182: 7937-7945.
53. Kwon YJ, Lee JW, Moon EJ, et al. 2013. Anabolic effects of peniel 2000, a peptide that regulates TGF-beta1 signaling on intervertebral disc degeneration. *Spine (Phila Pa 1976)* 38: E49-58.
54. Boscher C, Nabi IR. 2012. Caveolin-1: Role in cell signaling. *Adv Exp Med Biol* 729: 29-50.
55. Meyer C, Liu Y, Kaul A, Peipe I, Dooley S. 2013. Caveolin-1 abrogates TGF-beta mediated hepatocyte apoptosis. *Cell Death Dis* 4: e466.
56. Razani B, Zhang XL, Bitzer M, et al. 2001. Caveolin-1 regulates transforming growth factor (TGF)-beta/SMAD signaling through an interaction with the TGF-beta type I receptor. *J Biol Chem* 276: 6727-6738.
57. Del Galdo F, Sotgia F, de Almeida CJ, et al. 2008. Decreased expression of caveolin 1 in patients with systemic sclerosis: Crucial role in the pathogenesis of tissue fibrosis. *Arthritis Rheum* 58: 2854-2865.
58. Samarakoon R, Chitnis SS, Higgins SP, et al. 2011. Redox-induced src kinase and caveolin-1 signaling in TGF-beta1-initiated SMAD2/3 activation and PAI-1 expression. *PLoS One* 6: e22896.

**Supplementary File 1. Cytospins of canine CLC donors**



Cytospins of the 5 canine NCD donors used in the study: 100% CLCs were present, and no NCs with the typical vacuolated appearance.

## Supplementary 2. Primers used for quantitative PCR of canine samples

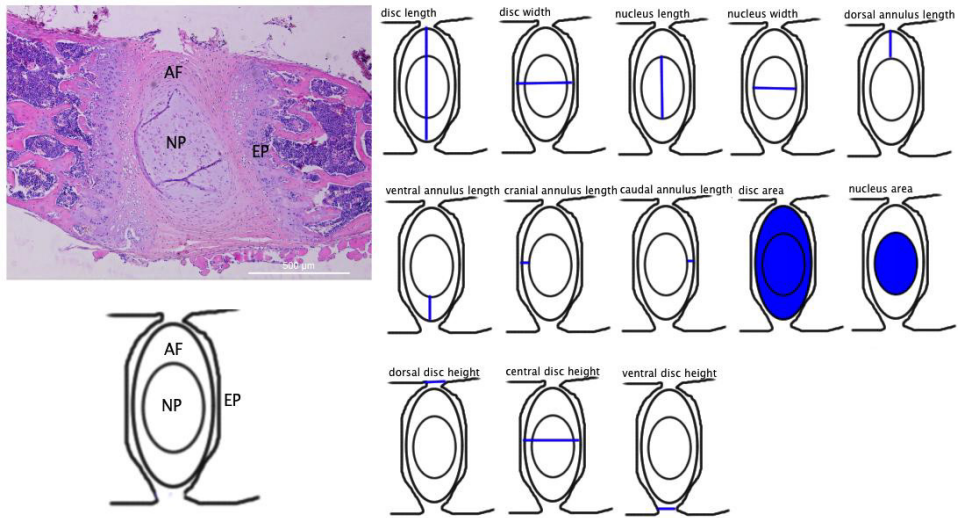
Genes	Forward sequence 5' → 3'	Reverse sequence 5' → 3'	Amplicon size	Annealing temp (°C)
<b>Reference genes</b>				
<i>GAPDH</i>	TGTCCCCACCCCAATGTATC	CTCCGATGCCTGCTTCACTACCTT	100	58
<i>HPRT</i>	AGCTTGCTGGTGAAAAGGAC	TTATAGTCAAGGGCATATCC	104	58
<i>RPS19</i>	CCTTCTCAAAAAGTCTGGG	GTTCTCATCGTAGGGAGCAAG	95	61
<i>SDHA</i>	GCCTTGGATCTCTTGATGGA	TTCTTGGCTTATGCGATG	92	56.5
<b>Target genes</b>				
<i>ACAN</i>	GGCACTCCTTGCAATTTGAG	GTCATTCCTCTCCCTTCTC	111	62
<i>ADAMTS5</i>	CTACTGCACAGGGAAGAG	GAACCCATTCCACAATGTC	149	61
<i>ALK1</i>	CCTTTGGTCTGGTGCTGTG	CGAAGCTGGGATCATTGGG	107	61
<i>ALK5</i>	GAGGCAGAGATTATCAGACC	ATGATAATCTGACCAACCAG	116	59.5
<i>BAX</i>	CCTTTTGCTTCAGGGTTTCA	CTCAGCTTCTTGGTGGATGC	108	58
<i>BCL2</i>	TGGAGAGVGTCAACCGGAGATGT	AGGTGTGCAGATGCCGGTTCAGGT	87	62
<i>CASP3</i>	ATCACTGAAGATGGATGGTTGGGT	TGAAAGGAGCATGTTCTGAAGTAGCACT	139	58
<i>CAV1</i>	CGCACCAAGGAAATCG	AAATCAATCTTGACCACGTCG	72	60
<i>COL1A1</i>	GTGTGTACAGAACGGCCTCA	TCGCAATCACGTCATCG	109	61
<i>COL2A1</i>	GCAGCAAGCAAGGAC	TTCTGAGAGCCCTCGGT	151	62
<i>CCND1</i>	GCCTCGAAGATGAAGGAGAC	CAGTTTGTTCACCAGGAGCA	117	60
<i>ID1</i>	CTCAACGGCGAGATCAG	GAGCACGGGTTCTTCTC	135	59.5
<i>MMP13</i>	CTGAGGAAGACTTCCAGCTT	TTGGACCCTTGAGAGTTCG	250	65
<i>PAI1</i>	AAACCTGGCGACTTCTC	ACTGTGCCACTCTCATTAC	98	61.5
<i>SOX9</i>	CGCTCGCAGTACGACTACAC	GGGGTTCATGTAGGTGAAGG	105	62
<i>TIMP1</i>	GGCGTTATGAGATCAAGATGAC	ACCTGTGCAAGTATCCGC	120	66

All primers were designed in-house using Perlprimer except for *MMP-13*<sup>1</sup> and *BAX*<sup>2</sup>.

## References

1. Muir P, Danova NA, Argyle DJ, Manley PA, Hao Z. 2005. Collagenolytic protease expression in cranial cruciate ligament and stifle synovial fluid in dogs with cranial cruciate ligament rupture. *Vet Surg* 34: 482-490.
2. Mahmoudabady M, Niazmand S, Shafei MN, McEntee K. 2013. Investigation of apoptosis in a canine model of chronic heart failure induced by tachycardia. *Acta Physiol Hung* 100: 435-444.

### Supplementary File 3. Histomorphometrical measurements of the IVD, AF, and NP of WT and caveolin-1 null mice



Measurement	WT 1.5 months	Cav-1 null 1.5 months	WT 3 months	Cav-1 null 3 months	WT 6 months	Cav-1 null 6 months
IVD length ( $\mu\text{m}$ )	915 $\pm$ 207	964 $\pm$ 152	1,139 $\pm$ 151	1,149 $\pm$ 55	1,209 $\pm$ 251	984 $\pm$ 111
IVD width ( $\mu\text{m}$ )	359 $\pm$ 51	383 $\pm$ 53	356 $\pm$ 42	376 $\pm$ 80	347 $\pm$ 50	391 $\pm$ 45
Dorsal IVD height ( $\mu\text{m}$ )	298 $\pm$ 57	349 $\pm$ 113	313 $\pm$ 50	235 $\pm$ 71	306 $\pm$ 40	297 $\pm$ 23
Ventral IVD height ( $\mu\text{m}$ )	508 $\pm$ 124	463 $\pm$ 148	570 $\pm$ 150	554 $\pm$ 80	482 $\pm$ 75	495 $\pm$ 89
Central IVD height ( $\mu\text{m}$ )	359 $\pm$ 51	383 $\pm$ 55	356 $\pm$ 41	377 $\pm$ 78	364 $\pm$ 51	391 $\pm$ 41
IVD area ( $\mu\text{m}^2$ )	343,231 $\pm$ 89,733	398,678 $\pm$ 95,096	431,116 $\pm$ 105,283	402,970 $\pm$ 74,510	440,733 $\pm$ 130,238	358,400 $\pm$ 77,423
NP length ( $\mu\text{m}$ )	597 $\pm$ 196	520 $\pm$ 183	738 $\pm$ 75	671 $\pm$ 123	817 $\pm$ 213	584 $\pm$ 78
NP width ( $\mu\text{m}$ )	248 $\pm$ 77	294 $\pm$ 119	337 $\pm$ 39	360 $\pm$ 108	346 $\pm$ 50	349 $\pm$ 87
NP area ( $\mu\text{m}^2$ )	134,884 $\pm$ 84,690	138,704 $\pm$ 77,067	200,078 $\pm$ 37,215	193,994 $\pm$ 75,365	234,358 $\pm$ 82,046	168,230 $\pm$ 49,878
Dorsal AF length ( $\mu\text{m}$ )	134 $\pm$ 56	264 $\pm$ 133	119 $\pm$ 32	177 $\pm$ 107	127 $\pm$ 64	190 $\pm$ 55
Ventral AF length ( $\mu\text{m}$ )	178 $\pm$ 62	179 $\pm$ 39	278 $\pm$ 64	293 $\pm$ 57	258 $\pm$ 52	201 $\pm$ 52
Cranial AF length ( $\mu\text{m}$ )	38 $\pm$ 31	49 $\pm$ 52	6.5 $\pm$ 5.7	8.1 $\pm$ 14.0	0 $\pm$ 0	18 $\pm$ 24
Caudal AF length ( $\mu\text{m}$ )	69 $\pm$ 53	38 $\pm$ 29	12.4 $\pm$ 18.4	6.7 $\pm$ 11.7	0 $\pm$ 0	23 $\pm$ 33

Histomorphometrical measurements of the murine intervertebral disc (IVD). No statistically significant histomorphometrical differences in the IVD/NP/AF between WT and caveolin-1 null mice at 1.5, 3, and 6 months of age. WT: wild type, IVD: intervertebral disc, NP: nucleus pulposus, AF: annulus fibrosus. IVD morphometry was performed on the raw images using Image J software (Rasband NIH).

**Part III – What can we learn from developmental biology?**



**The Paracrine Feedback Loop Between Vitamin D<sub>3</sub> (1,25(OH)<sub>2</sub>D<sub>3</sub>) and PTHrP in Prehypertrophic Chondrocytes**

Frances C. Bach<sup>1</sup>, Kirsten R.T. Rutten<sup>1</sup>, Kristyanne Hendriks<sup>1</sup>, Frank M. Riemers<sup>1</sup>, Peter Cornelissen<sup>2</sup>, Alain de Bruin<sup>2</sup>, Ger J.A. Arkesteijn<sup>3</sup>, Richard W. Wubbolts<sup>4</sup>, William A. Horton<sup>5,6</sup>, Louis C. Penning<sup>1</sup>, Marianna A. Tryfonidou<sup>1</sup>

<sup>1</sup>Department of Clinical Sciences of Companion Animals, Faculty of Veterinary Medicine, Utrecht University, Utrecht, the Netherlands

<sup>2</sup>Department of Pathobiology, Faculty of Veterinary Medicine, Utrecht University, Utrecht, the Netherlands

<sup>3</sup>Department of Immunology, Faculty of Veterinary Medicine, Utrecht University, Utrecht, the Netherlands

<sup>4</sup>Department of Biochemistry and Cell Biology, Faculty of Veterinary Medicine, Utrecht University, Utrecht, the Netherlands

<sup>5</sup>Research Center, Shriners Hospital for Children, Portland, Oregon, USA

<sup>6</sup>Department of Molecular and Medical Genetics, Oregon Health and Science University, Portland, Oregon, USA

## Abstract

The endocrine feedback loop between vitamin D<sub>3</sub> (1,25(OH)<sub>2</sub>D<sub>3</sub>) and parathyroid hormone (PTH) plays a central role in skeletal development. PTH-related protein (PTHrP) shares homology and its receptor (PTHR1) with PTH. The aim of this study was to investigate whether there is a functional paracrine feedback loop between 1,25(OH)<sub>2</sub>D<sub>3</sub> and PTHrP in the growth plate, in parallel with the endocrine feedback loop between 1,25(OH)<sub>2</sub>D<sub>3</sub> and PTH. This was investigated in ATDC5 cells treated with 10<sup>-8</sup> M 1,25(OH)<sub>2</sub>D<sub>3</sub> or PTHrP, Col2-pd2EGFP transgenic mice, and primary Col2-pd2EGFP growth plate chondrocytes isolated by FACS, using RT-qPCR, Western blot, PTHrP ELISA, chromatin immunoprecipitation (ChIP) assay, silencing of the 1,25(OH)<sub>2</sub>D<sub>3</sub> receptor (VDR), immunofluorescent staining, immunohistochemistry, and histomorphometric analysis of the growth plate. The ChIP assay confirmed functional binding of the VDR to the PTHrP promoter, but not to the PTHR1 promoter. Treatment with 1,25(OH)<sub>2</sub>D<sub>3</sub> decreased PTHrP protein production, an effect which was prevented by silencing of the VDR. Treatment with PTHrP significantly induced VDR production, but did not affect 1 $\alpha$ - and 24-hydroxylase expression. Hypertrophic differentiation was inhibited by PTHrP and 1,25(OH)<sub>2</sub>D<sub>3</sub> treatment. Taken together, these findings indicate that there is a functional paracrine feedback loop between 1,25(OH)<sub>2</sub>D<sub>3</sub> and PTHrP in the growth plate. 1,25(OH)<sub>2</sub>D<sub>3</sub> decreases PTHrP production, while PTHrP increases chondrocyte sensitivity to 1,25(OH)<sub>2</sub>D<sub>3</sub> by increasing VDR production. In light of the role of 1,25(OH)<sub>2</sub>D<sub>3</sub> and PTHrP in modulating chondrocyte differentiation, 1,25(OH)<sub>2</sub>D<sub>3</sub> in addition to PTHrP could potentially be used to prevent undesirable hypertrophic chondrocyte differentiation during cartilage repair or regeneration.

## Introduction

Longitudinal bone growth occurs at the growth plate, a highly organized cartilage structure that contains proliferating chondrocytes. These cells undergo a maturation process involving hypertrophy followed by apoptosis, thereby facilitating bone formation<sup>1, 2</sup>. Some changes that occur in cartilage after injury or osteoarthritis (OA) resemble the processes that occur during the differentiation of growth plate chondrocytes<sup>3, 4</sup>. In healthy articular cartilage, chondrocytes resist proliferation and terminal differentiation. In contrast, cartilage damage caused by injuries or OA reactivates chondrocyte hypertrophy as part of a repair mechanism, accompanied by acquisition of an autolytic phenotype and cartilage degradation<sup>3-5</sup>. Ultimately, the hypertrophic chondrocytes undergo apoptosis to enable bone deposition<sup>5</sup>. The inferior quality of the repaired cartilage suggests that the inhibition of chondrocyte hypertrophy could be a target of treatment to improve cartilage repair<sup>4</sup>.

Chondrocyte proliferation and differentiation at the growth plate is regulated through the interaction of systemic hormones (endocrine level) and locally produced growth factors (autocrine and/or paracrine level). The endocrine feedback loop between the active metabolite of vitamin D<sub>3</sub> (1,25(OH)<sub>2</sub>D<sub>3</sub>) and parathyroid hormone (PTH) plays a central role in calcium and phosphate homeostasis during skeletal growth<sup>2</sup>. Vitamin D<sub>3</sub> is hydroxylated in the liver to 25-hydroxycholecalciferol (25(OH)D<sub>3</sub>), which is thereafter hydroxylated in various target cells into 1,25(OH)<sub>2</sub>D<sub>3</sub> by the enzyme 1 $\alpha$ -hydroxylase<sup>6</sup>. 1,25(OH)<sub>2</sub>D<sub>3</sub> in turn can be deactivated and catabolized by the enzyme 24-hydroxylase<sup>7, 8</sup>. It has been shown that 1,25(OH)<sub>2</sub>D<sub>3</sub> exerts its genomic effects by binding to its nuclear receptor (VDR), and that this complex then binds to vitamin D<sub>3</sub> response elements (VDREs) in the promoter region of various target genes<sup>6, 9, 10</sup>.

Both 1,25(OH)<sub>2</sub>D<sub>3</sub> and PTH are also active at the growth plate and play an important autocrine and/or paracrine role during chondrocyte proliferation and/or differentiation<sup>11-13</sup>. Growth plate chondrocytes express the VDR and the enzymes 1 $\alpha$ -hydroxylase and 24-hydroxylase *in vitro* as well as *in vivo*<sup>2, 6, 14-16</sup>. PTH-related protein (PTHrP) resembles PTH in genetic sequence and structure and both PTH and PTHrP share the same receptor: PTHR1<sup>4, 17</sup>. PTHR1 is expressed in low levels by proliferating chondrocytes and in high levels by pre/early hypertrophic chondrocytes<sup>4, 18, 19</sup>. PTHrP is produced by proliferative growth plate chondrocytes and prevents proliferative cells from leaving the proliferating pool. In this way, hypertrophic chondrocyte differentiation is delayed<sup>4, 18-20</sup>.

Understanding the processes behind chondrocyte differentiation is crucial, not only from a developmental point of view. Regenerative strategies for bone and cartilage make use of mesenchymal stromal (stem) cells undergoing chondrogenic differentiation. The growth plate can be used as a model to study these processes, mainly because it has a highly organized structure, with chondrocytes undergoing differentiation in an orderly fashion<sup>1, 2, 21</sup>. Therefore, the main aim of this study was to investigate whether there is a functional paracrine feedback loop between 1,25(OH)<sub>2</sub>D<sub>3</sub> and PTHrP in prehypertrophic growth plate chondrocytes, in parallel to the well-known endocrine 1,25(OH)<sub>2</sub>D<sub>3</sub>-PTH feedback loop.

We hypothesized that PTHrP increases the sensitivity of growth plate chondrocytes to  $1,25(\text{OH})_2\text{D}_3$  either by increasing  $1,25(\text{OH})_2\text{D}_3$  production by upregulating  $1\alpha$ -hydroxylase, and/or decreasing the catabolism of  $1,25(\text{OH})_2\text{D}_3$  by downregulating 24-hydroxylase, and/or by upregulating VDR expression (Supplementary File 1). The feedback loop is closed by the inhibition of PTHrP and/or PTHR1 transcription by the binding of  $1,25(\text{OH})_2\text{D}_3$  to a VDRE located in the promoter region of (one of) these target genes.

## Material and Methods

### *In vitro* studies with the ATDC5 cell line

#### *Cell culture and experimental design*

The murine chondrogenic ATDC5 cell line was kindly provided by Dr. T. Welting (UMC Maastricht, the Netherlands). Cell culture was performed as described previously<sup>22</sup>. Standard differentiation culture medium was supplemented with 0.2 mM L-ascorbic acid 2-phosphate (AsAP, Sigma, A8960) to reduce the time in culture until prehypertrophic differentiation<sup>23</sup>. Cells grown in a standard differentiation medium were compared with cells grown in a standard differentiation medium supplemented with  $10^{-8}$  M PTHrP (pTH-Related Protein (1-34) amide, Bachem, H-9095) or  $10^{-8}$  M  $1,25(\text{OH})_2\text{D}_3$  (kindly provided by Dr. C.Veldhuizen, Dishman, the Netherlands). Stripped fetal bovine serum (FBS) was used, which is devoid of vitamin  $\text{D}_3$  metabolites and growth factors. ATDC5 cells were plated on 24-well plates (Greiner Cellstar®) at a density of 6,400 cells/cm<sup>2</sup>. Six hours later, cell differentiation was induced (day 0). The three different culture groups were studied from differentiation day 7 until day 10 (prehypertrophic phase) at the following time points:  $T_0$ ,  $T_1$ ,  $T_2$ ,  $T_4$ ,  $T_8$ ,  $T_{24}$ ,  $T_{28}$ ,  $T_{48}$ , and  $T_{72}$  (the digits indicate the number of hours after PTHrP or  $1,25(\text{OH})_2\text{D}_3$  was first added to the cell culture medium). At  $T_0$ ,  $T_{24}$ , and  $T_{48}$ ,  $10^{-8}$  M PTHrP or  $1,25(\text{OH})_2\text{D}_3$  was added to the experimental plates. The experiment was repeated at least six times for each time point and culture condition.

#### *RNA isolation and cDNA synthesis*

Total RNA was extracted with the aid of the RNeasy® Mini kit (Qiagen, 74104), according to the manufacturer's protocol. An additional DNA digestion step with DNase (RNase-Free DNase Set, Qiagen, 79254) was included to ensure DNA removal. Total RNA was quantified with a Nanodrop® ND-1000 spectrophotometer (Thermo Scientific). cDNA was synthesized using the iScript™ cDNA Synthesis Kit (Bio-Rad, Veenendaal, the Netherlands, 170-8891), according to the manufacturer's instructions.

#### *Quantitative determination of the expression of target genes*

Primer nucleotide sequences for all reference genes were obtained from the Eccles Lab Reference Gene List ([http://openwetware.org/wiki/Eccles:QPCR\\_reference\\_genes](http://openwetware.org/wiki/Eccles:QPCR_reference_genes)). Most primer nucleotide sequences for the target genes were obtained from PrimerBank. For the other target genes, primer sequences were designed using PerlPrimer. Subsequently, M-fold version 3.2 was used to check for secondary structure formation<sup>24</sup>. Primer uniqueness and specificity was determined using BLAST<sup>25</sup>. Annealing temperatures were established by performing a temperature gradient PCR on a 16-fold dilution series. Amplicons were validated by sequence analysis using an ABI Prism 3130XL genetic analyzer (Applied Biosystems). All primers were purchased from Eurogentec (Maastricht, the Netherlands). An

overview of the primer pairs used is given in Supplementary File 2. In order to normalize the relative expression of the target genes, a set of 10 reference genes was evaluated: *Hspca*, *Rpl32*, *Rps19*, *Ywhaz*, *B2m*, *Gapdh*, *Hbms*, *Hprt-1*, *Sdha*, and *Tbp*. The geNorm program was used to evaluate the stability of the housekeeping genes<sup>26</sup>. The three most stably expressed reference genes in the ATDC5 cell line, *Rpl32*, *Rps1*, and *Sdha*, were chosen to normalize gene expression. However, *Sdha* was not used as a reference gene in the experiment in which the VDR was silenced, because *Sdha* gene expression was not sufficiently stable under the experimental conditions used. RT-qPCR was performed using the iQ™ SYBR Green Supermix Kit (Bio-Rad, Veenendaal, the Netherlands) and the MyiQ™ single color Real-Time PCR Detection System (Bio-Rad, Veenendaal, the Netherlands).

#### *Protein isolation and Western blot*

Semi-quantitative protein expression of the VDR and collagen type X was determined using Western blot. Protein was extracted from the ATDC5 cells with 50 µL RIPA buffer per well, and protein concentration was determined with a Lowry assay (Bio-Rad, Veenendaal, the Netherlands, 500-0116). Thereafter, 30 µg protein was subjected to 12% SDS-PAGE, and electroblotted onto a Hybond-C nitrocellulose membrane (Amersham Biosciences, RPN203C). Only one SDS-PAGE gel and membrane was used per target protein. The membrane was blocked for 60 minutes, followed by overnight incubation at 4°C with the first antibody (Supplementary File 3). Thereafter, the membrane was washed and incubated for 60 minutes with a horseradish peroxidase (HRP)-conjugated second antibody. Protein was detected by enhanced chemiluminescence (Molecular Imager ChemiDoc XRS System, Bio-Rad, Veenendaal, the Netherlands). Control experiments were included in which the first antibody was omitted. After completion of Western blotting of the target proteins, the membranes were stripped using Stripping Buffer (Restore™ Western Blot Stripping Buffer, Thermo Scientific, 21059), and β-actin protein expression was determined. The mean volume of the protein bands was determined with Quantity One software using volumetric band analysis. The mean volume of the target gene was divided by the mean volume of β-actin (target gene/β-actin ratio), to correct for different protein concentrations applied to the membranes. Western blot images were prepared using Adobe Photoshop CS5.1. Linear adjustment of brightness, contrast, and color balance was applied to every pixel in the image.

#### *PTHrP ELISA*

The concentration of PTHrP in the cell lysate and culture media (which was stored at -70°C) was measured with an ELISA (ELISA kit for mouse PLP, USCN E90819Mu), according to the manufacturer's instructions.

#### *mRNA superinduction*

mRNA and protein samples were taken from the control cultures and the 10<sup>-8</sup> M 1,25(OH)<sub>2</sub>D<sub>3</sub>-treated cultures on differentiation day 7 at T<sub>0</sub>, T<sub>1</sub>, T<sub>2</sub>, T<sub>4</sub>, T<sub>8</sub>, T<sub>12</sub>, and T<sub>24</sub>. RNA isolation, cDNA synthesis, RT-qPCR for *Pthrp* and a PTHrP ELISA were performed as described previously.

#### *DNA quantification*

DNA was quantified using the Quant-iT™ PicoGreen® dsDNA Assay Kit (Invitrogen, P11496).

### Silencing RNA

Stealth RNAi™ siRNA Duplex (Invitrogen, 10620312) was used to silence the ATDC5 VDR. The siRNA oligonucleotide sequence used for the mouse VDR (nm\_009504) was: 5' CCCUCAAUGGAGAUUGCCGCAUCA 3' (ORF, GC percentage estimated at 52%). A Stealth RNAi™ Control Duplex (Invitrogen) sequence 5' CCCUAAACGAGGGUUA CGCCAUUUCA 3' (scrambled mock, GC percentage estimated at 52%) was used to determine the effect of Stealth RNAi™ siRNA Duplex versus background. Lipofectamine™ RNAiMAX (Invitrogen, 13778-075) was used as transfection reagent. ATDC5 cells were plated on 24-well plates (Greiner Cellstar®) at a standard density of 6,400/cm<sup>2</sup>. Six hours later, ATDC5 cell differentiation was induced (day 0). On differentiation day 4, RNA in the approximately 100% confluent ATDC5 cells was silenced (Lipofectamine™ RNAiMAX concentration of 5.3 μL/mL, siRNA VDR-oligo (Stealth RNAi™ siRNA Duplex)/scrambled mock (Stealth RNAi™ siRNA Control Duplex) concentration of 50 nM). After siRNA transfection medium was added to the experimental plates, the ATDC5 cells were incubated for 48 hours at 37°C in 5% CO<sub>2</sub> before the siRNA transfection medium was replaced by normal differentiation medium. On day 7 of differentiation (which was 72 hours after siRNA initiation), 10<sup>-8</sup> M PTHrP or 1,25(OH)<sub>2</sub>D<sub>3</sub> was added to determine whether the effects of PTHrP and 1,25(OH)<sub>2</sub>D<sub>3</sub> on the ATDC5 cells could be prevented by VDR silencing. From differentiation day 7 until day 10 (i.e., 72-144 hours after siRNA initiation), the different culture groups were studied at the time points T<sub>0</sub>, T<sub>24</sub>, T<sub>48</sub>, and T<sub>72</sub> (the digits indicate the number of hours after PTHrP or 1,25(OH)<sub>2</sub>D<sub>3</sub> was first added to the cell culture medium). 10<sup>-8</sup> M PTHrP or 1,25(OH)<sub>2</sub>D<sub>3</sub> was added at T<sub>0</sub>, T<sub>24</sub>, and T<sub>48</sub>. Nine different cell culture conditions (control, control + scrambled mock, control + VDR-oligo, PTHrP, PTHrP + scrambled mock, PTHrP + VDR-oligo, 1,25(OH)<sub>2</sub>D<sub>3</sub>, 1,25(OH)<sub>2</sub>D<sub>3</sub> + scrambled mock and 1,25(OH)<sub>2</sub>D<sub>3</sub> + VDR-oligo) were studied and compared.

### Chromatin immunoprecipitation (ChIP) Assay

The sequence and location of the VDREs in the PTHrP promoter region have only been determined in the rat<sup>27, 28</sup>. The *Mus musculus* and *Rattus norvegicus* PTHrP promoter regions were BLASTed<sup>25</sup> to determine their homology (Supplementary File 4). Primers were designed and validated for the two VDRE regions of the mouse PTHrP promoter (Supplementary File 4, Figure 3a). As a negative control, primers were designed at 1000 bp upstream of VDRE2.

To date, there is no VDRE reported for the PTHR1 gene. The PTHR1 gene has two promoter regions, P1 and P2 (Figure 3c). In bone and cartilage, the P2 promoter controls *Pthr1* gene expression, and therefore we searched for possible VDREs in this P2 promoter with the aid of the core binding motif consensus sequence RGKTS (R=A or G, K=G or T, S=C or G)<sup>29</sup>. This motif was included in two six-nucleotide sequences in the region upstream of U3: AGGTGA and GGTTGA, which are 2092 and 2027 bp upstream of the transcription start site (TSS), respectively. The distance between these sequences was 104 bp. The consensus is that a VDRE has normally three to six nucleotides between the two motif sequences<sup>30</sup>. We cannot exclude that the area between these two sequences loops back to bring the sequences close together, enabling the VDR to bind. For this reason, primers were designed for each six-nucleotide sequence (VDRE1 and VDRE2), but also for the region containing these two core binding motif consensus sequences (VDRE combination). As negative and positive controls, primers were designed at 1000 bp upstream of the expected VDREs and for one of the VDREs of the 24-hydroxylase promoter, respectively (Supplementary File 4). VDREs for 24-hydroxylase have been identified in the rat<sup>31</sup>, and therefore the rat promoter region was

BLASTed against the mouse 24-hydroxylase promoter region. Both VDREs revealed 100% alignment. Primers were designed for the VDRE 5' CGCACCCGCTGAACC 3'.

The ChIP assay was performed as described previously<sup>32</sup>, with minor modifications. Briefly, ATDC5 cells were seeded in Falcon Primaria petri dishes (BD Biosciences, 353803) at a density of 6,400 cells/cm<sup>2</sup> and cultured for 7 days (approximately 22\*10<sup>6</sup> cells per dish), as described earlier in this section. Cells were treated with 10<sup>-8</sup> M 1,25(OH)<sub>2</sub>D<sub>3</sub> for 24 hours. For immunoprecipitation, rat anti-VDR (Affinity Bioreagents, MA1-710) was used, whereas an equal amount of rat IgG (Chemicon, IgG2b, CBL606) was used as a normalization control. For more detailed information on the ChIP assay, see Supplementary File 5.

### Statistical analysis

For determination of relative quantitative gene expression, the corrected  $\Delta$ Ct method was used<sup>33</sup>.  $\Delta$ Ct-values were determined for each time point by subtracting the mean reference gene Ct-value at the time point of interest from the target gene Ct-value at the same time point:  $\Delta$ Ct = Ct<sub>target</sub> - Ct<sub>mean ref.</sub>. Subsequently, all values were related to the T<sub>0</sub> time point by subtracting the  $\Delta$ Ct-value for T<sub>0</sub> from the  $\Delta$ Ct-value for T<sub>x</sub>, the time point of interest:  $\Delta$ Ct<sub>T<sub>x</sub></sub> -  $\Delta$ Ct<sub>T<sub>0</sub></sub>. For each individual experiment, target gene expression per time point of interest (n-fold change) was determined separately. Afterwards, for each target gene, the mean n-fold changes and standard deviations in gene expression per time point of interest were calculated. In the silencing study, VDR knockdown percentages in the siRNA VDR-oligo cultures were determined by subtracting the VDR Ct-value from the mean reference gene Ct-value for each time point: Ct<sub>ref</sub> - Ct<sub>vdr</sub>. Subsequently, this value was subtracted from the value for the siRNA scrambled mock cultures or the value for the control cultures, to obtain  $\Delta$ Ct-values. VDR knockdown percentages were calculated using the formula:  $100 * 1 - (1/E_{vdr}^{\Delta Ct})$ .

Statistical analysis was performed using R Studio (version 0.96, <http://www.rstudio.com>) and R (version 2.15.2)<sup>34</sup>. To determine whether the enrichment in the ChIP experiments was statistically significant, the data were examined for normal distribution, and a one-way ANOVA with Benjamini-Hochberg correction was used. For the rest of the data (target gene and PTHrP protein production), a mixed model for dependent data was used. This mixed model was optimized per target gene/protein and comparison. After it was determined whether the data were normally distributed, the random part of the model was determined (e.g. with random slopes and/or random intercepts). Thereafter, the fixed part of the model was optimized. Interaction of time and treatment (culture condition) appeared necessary in all cases. In the above mentioned tests, a *p*-value < 0.05 was considered significant.

## In vivo studies

### Animals

The animal studies were approved by the institutional animal care committee (DEC 2008.III.03.024), as required by Dutch law. The colony of the transgenic Col2-pd2EGFP reporter mice was maintained at the SPF facilities with approval from the Dutch ministry of Infrastructure and Environment (DEM/SAS IG 99-057/03). The Col2-pd2EGFP transgenic mouse is appropriate for visualizing *Col2a1* expression, for monitoring chondrocyte

differentiation, and for isolating murine growth plate chondrocytes by fluorescence activated cell sorting (FACS)<sup>35</sup>.

### *Diets*

Vitamin D<sub>3</sub> sufficient (control, TD 07370, 0.47% Ca, 0.3% P, 2,200 IU/kg vitamin D<sub>3</sub>) and deficient (TD 89123, 0.47% Ca, 0.3% P, 0 IU/kg vitamin D<sub>3</sub>) diets were purchased from Teklad Harlan SD (Indianapolis, Indiana). The vitamin D<sub>3</sub> content of these diets was re-analyzed by an independent laboratory (TNO Nutrition and Food Research, Zeist, the Netherlands); the vitamin D<sub>3</sub>-sufficient diet contained 1,900 IU/kg and the vitamin D<sub>3</sub>-deficient diet less than 20 IU/kg.

### *Experimental design*

The mice were kept under standard conditions in the experimental animal facility of the University of Utrecht. Control offspring were obtained from dams maintained on the vitamin D<sub>3</sub>-sufficient diet. Vitamin D<sub>3</sub>-deficient pups were obtained by feeding the dams a vitamin D<sub>3</sub>-deficient diet, from 2 weeks prior to mating until weaning. The weaned offspring were given the vitamin D<sub>3</sub>-deficient diet until euthanasia at 6 weeks of age. In order to ensure vitamin D<sub>3</sub> deficiency, the pregnant females and their offspring were housed in filter-top cages, in which all fluorescent light was shielded, thereby preventing the endogenous production of vitamin D<sub>3</sub>. Only those pups that had a weight within 2 S.D. of the mean at 3 weeks of age were included. The pups were weaned at approximately 3 weeks of age, depending on whether they could feed independently. Weaned pups were housed in groups according to diet and gender (in order to prevent mating): vitamin D<sub>3</sub> sufficient (VitD+), vitamin D<sub>3</sub> deficient (VitD-), and vitamin D<sub>3</sub> deficient supplemented with 1,25(OH)<sub>2</sub>D<sub>3</sub> (VitD-;+1,25D). The animals were weighed every week at fixed times. At 3 weeks of age, the vitamin D<sub>3</sub>-deficient pups were given either 50 ng 1,25(OH)<sub>2</sub>D<sub>3</sub> (VitD-;+1,25D, intraperitoneal (IP), 1 ng/μL in sterilized peanut oil; mean dose 5 ng/g body weight, BW) or placebo (VitD-, sterilized peanut oil). Thereafter, the dose of vitamin D<sub>3</sub> metabolite was adjusted weekly, based on the mean body weight of the respective group. The vitamin D<sub>3</sub>-sufficient mice (VitD+) received placebo (sterilized peanut oil) IP. The IP administration was performed five times a week, *lege artis*, by the animal caretakers. At 6 weeks of age, blood (as much as possible) was obtained by cardiac puncture under general anesthesia, followed by cervical dislocation.

### *Serum biochemistry*

Blood samples for the measurement of calcium (Ca), inorganic phosphate (P), and vitamin D<sub>3</sub> metabolites were collected in heparin-coated mini-collection-tubes (Greiner bio-one, REF 450479). For the measurement of PTH, blood was collected in EDTA-coated mini-collection tubes (Greiner bio-one, REF 450475). Samples were immediately placed on ice until centrifugation and plasma was stored at -20°C until further analysis. Ca and P levels were measured according to standard procedures. Plasma 25(OH)D<sub>3</sub> levels were measured to verify vitamin D<sub>3</sub> deficiency in the respective groups. 25(OH)D<sub>3</sub> was extracted from 25 μL plasma with the Bligh and Dyer method<sup>36</sup> and quantified with the aid of a competitive binding assay. Thereafter, plasma samples for pairs of mice were pooled within the ascribed group (due to sample volume limitations) and vitamin D<sub>3</sub> metabolites were extracted from the pooled plasma using acetonitrile followed by a two-step phase extraction (C18 and Silicagel cartridge) and separated by straight phase HPLC. 25(OH)D<sub>3</sub> was quantitatively determined using a competitive protein binding assay with a sensitivity of 2 nmol/L and

1,25(OH)<sub>2</sub>D<sub>3</sub> was quantitatively determined with a radioreceptor assay<sup>37</sup>, with a sensitivity of 40 pmol/L. Levels were corrected for procedural losses (recovery) with the aid of the specific 3H-labeled vitamin D<sub>3</sub> metabolite. PTH was determined according to the manufacturer's instructions (intact PTH mouse EIA, Alpco diagnostics Salem NH).

#### *Growth plate histology*

After euthanasia, the right tibia was removed and fixed in 4% formaldehyde (pH = 7.4, 4°C) for 24 hours and decalcified in 0.5 M EDTA in Ca-Mg free Hanks solution (pH = 7.8, 4°C) for 7 days. After demineralization, the bones were washed and bisected in the sagittal plane. One half was embedded in Tissue Tek (O.C.T. compound, Sakura Fine Technical Co. Ltd. Tokyo, Japan) and stored at -70°C until further processing. The other half of the tibia was embedded in paraffin and stored at 4°C until further processing.

#### *Quantitative determination of the expression of target genes*

From each mouse, growth plate chondrocytes were isolated as described previously<sup>35</sup>. Briefly, after euthanasia, the long bones and rib cartilage (except for the right tibia) were removed and submerged in cold (4°C) Hanks + 2% pen/strep. The growth plate and adjacent tissue from each animal was dissected with the aid of a stereoscope and scalpel blade, pooled, and digested overnight at 37°C 5% CO<sub>2</sub> with collagenase II (Worthington, 4176). After digestion, cells were suspended in DMEM/F12 + glutamine (Gibco, without phenol red) with 10% FCS (PAA) and 2% pen/strep. The cell solution was individually run through a FACS (BD Influx cell sorter, BD Biosciences, USA) with a nozzle of 100 µm. After collection, the cells were lysed in 350 µL RLT buffer (Qiagen, Valencia, CA) containing 1% β-mercaptoethanol and stored at -70°C until further processing. RNA isolation, cDNA production, and RT-qPCR were performed as described for the *in vitro* studies. The relative level of gene expression of *Pthrp*, *Pthr1*, *Vdr*, and *ColX* was determined (Supplementary File 2).

#### *Immunofluorescent staining*

Immunofluorescent staining of bone for collagen type X was performed as described previously<sup>35</sup> on 10-µm cryosections, in order to define the pattern of GFP expression in relation to the phase of differentiation of growth plate chondrocytes. Briefly, after sections were rinsed with PBS, antigen retrieval with 4 mg/mL bovine hyaluronidase (450 IU/mg, Sigma-Aldrich St. Louis, MO, USA) was performed. After blockade of aspecific binding sites with 10% goat serum, sections were incubated with rabbit polyclonal anti-mouse collagen type X (PXNC2, 1:100) overnight at 4°C<sup>38</sup>. Goat anti-rabbit ALEXA 568 (1:100, Invitrogen) was used as second antibody. Nuclear counterstaining was performed with TO-PRO<sup>®</sup>-3, and the slides were mounted in Prolong Gold anti-fade reagent (Invitrogen). Confocal microscopy was performed using a Leica TCS SP confocal laser scanning microscope. Immunofluorescent staining images were prepared using Adobe Photoshop CS5.1. Linear adjustment of brightness, contrast, and color balance was applied to every pixel in the image.

#### *Immunohistochemistry*

Paraffin sections of 4 µm were cut and mounted on Microscope KP plus slides (Klinipath B.V., Duiven, the Netherlands). Each slide contained three sections: one section of each group in an ad random order. Slides were deparaffinized through xylene (2 times 5 minutes) and graded ethanol (96%, 80%, 70%, 60%, 30%; 5 minutes each), followed by two rinses with PBS. Mid-sagittal sections of the three samples representing each group were included in the

same Pap-pen circle and were thus incubated under identical conditions. Thereafter, antigen retrieval was performed (Supplementary File 3). After inhibition of endogenous peroxidase for 5 minutes, sections were preincubated with blocking buffer for 30 minutes at room temperature (RT). The sections were incubated overnight with first antibody at 4 °C. For further processing, depending on the first antibody, either the EnVision™ –HRP detection system (Dako), the goat ImmunoCruz™ system (sc-2053, Santa Cruz biotechnology Inc.), or specific second antibody was applied for 30 minutes at RT, followed by incubation with streptavidin-conjugated with HRP for 30 minutes at RT. All antibodies were visualized with the liquid DAB+ substrate chromogen system (K3468, Dako). In control experiments, the first antibody was omitted and, depending on the antibody, either substitution of the first antibody with its respective serum, and/or competition of the first antibody with corresponding peptides available for PTHR1 (sc-12777 P) was performed. Raw images were made using a Colorview IIIU digital camera (Olympus, Zoeterwoude, the Netherlands) mounted to a BX-40 microscope (Olympus). Histomorphometry was performed on the raw images with Image J software package (Rasband NIH, Bethesda, ML). The mean width of the growth plate (GPI.Th.) was calculated from the width of the growth plate at 20 set locations. The mean width of the proliferative (GPI.Th.<sub>pr</sub>) and hypertrophic zone (GPI.Th.<sub>hp</sub>) was determined in a similar way. The proliferative zone comprised the region containing columnar chondrocytes of constant size, whereas the hypertrophic zone was defined by collagen type X staining.

A custom-made color range selection optimized for each immunohistochemical stain was used to determine the area within the growth plate that stained positive. For each growth plate section, the proportion of the surface area of the growth plate that stained positively for the respective protein was calculated, as were the mean gray value and integrated density. Quantitative image analysis of the nuclear VDR area that stained positive was performed using the Image J plugin ImmunoRatio, which calculates the percentage of positively stained nuclear area (labeling index) by using a color deconvolution algorithm for separating the staining components (diaminobenzidine and hematoxylin) and adaptive thresholding for nuclear area segmentation.

### ***In vitro* studies with primary growth plate chondrocytes**

#### *Cell culture and experimental design*

The isolation of primary growth plate chondrocytes from the limbs of three 9-day-old Col2-pd2EGFP mice was performed as described previously<sup>35</sup>. Approximately 26% of the selected population was positive for GFP. On differentiation day 0 (T<sub>0</sub>), droplets of 10 μL (containing approximately 20,000 cells) were placed on a Falcon Primaria petri dish (BD Biosciences, 353803), not touching each other to create multiple high-density micro-cultures. After 2 hours, 10 mL differentiation medium was added as describe previously, and after 2 days (T<sub>2</sub>), 10<sup>-8</sup> M 1,25(OH)<sub>2</sub>D<sub>3</sub> (Dishman Netherlands BV) was daily added to the 1,25(OH)<sub>2</sub>D<sub>3</sub>-treated cultures. In a similar manner, high-density microcultures on chamber slides (Lab-Tek®) were studied from differentiation day 0 until day 7. At the time points T<sub>0</sub>, T<sub>3</sub>, T<sub>5</sub>, and T<sub>7</sub> (the digits indicate the number of days after differentiation culture medium was first added to the wells), medium for PTHrP ELISA and cells for RNA isolation were obtained, and formalin-fixed slices were stained for collagen type X (as described previously). Confocal microscopy was performed using a Leica SPEll confocal laser-scanning microscope (Leica Microsystems,

Germany). The concentration of PTHrP in culture media was measured with an ELISA (ELISA kit for mouse PLP, USCN E90819Mu), according to the manufacturer's instructions.

#### *Chromatin immunoprecipitation (ChIP) Assay*

The ChIP analysis of the cultured primary growth plate chondrocytes (Falcon Primaria petri dish) was performed as described for the *in vitro* studies.

#### *Quantitative determination of the expression of target genes*

RNA isolation, cDNA production, and RT-qPCR were performed as described for the *in vitro* studies. Ultimately, the relative gene expression of *Pthrp*, *Pthr1*, *Vdr*, and *ColX* was determined (Supplementary File 2).

#### *Statistical analysis*

After it was determined that the data had a normal distribution, a one-way ANOVA with Benjamini-Hochberg correction was used to analyze the significance of differences in the mean (+ S.D.) width of the growth plate (including the proliferative and hypertrophic zone), plasma parameters, target gene expression, and ChIP assay results between the different groups. For body weight and PTHrP protein levels, a mixed model for dependent data was used as described at the *in vitro* studies. In the above-mentioned tests, a *p*-value <0.05 was considered significant.

## Results

### ***In vitro* studies with the ATDC5 cell line**

#### *The effect of PTHrP on the vitamin D<sub>3</sub> pathway*

Protein and mRNA expression of 1 $\alpha$ - and 24-hydroxylase was stable during culture and appeared not affected by treatment with 10<sup>-8</sup> M PTHrP (data not shown). At all time points, *Vdr* gene expression was significantly higher in the PTHrP-treated cultures than in the control cultures (*p*<0.01, Figure 1a). After the first addition of PTHrP at T<sub>0</sub>, *Vdr* gene expression increased significantly to reach a maximum at T<sub>4</sub> and declined thereafter. At T<sub>28</sub>, 4 hours after the second addition of PTHrP, *Vdr* gene expression was significantly higher than that at T<sub>24</sub> (*p*<0.01), but significantly lower than that at T<sub>4</sub> (*p*<0.001). *Vdr* gene expression did not change substantially after T<sub>28</sub>. VDR protein levels were also significantly higher at time points T<sub>24</sub> and T<sub>48</sub> in the PTHrP-treated cultures than in the control cultures (*p*<0.01, Figure 1b). Altogether, these data indicate that PTHrP treatment increased ATDC5 chondrocyte sensitivity for 1,25(OH)<sub>2</sub>D<sub>3</sub> by upregulating VDR expression and not by influencing 1 $\alpha$ - and/or 24-hydroxylase expression.

#### *The effect of vitamin D<sub>3</sub> on the PTHrP pathway*

Treatment of ATDC5 chondrocytes with 10<sup>-8</sup> M 1,25(OH)<sub>2</sub>D<sub>3</sub> increased the activity of the vitamin D<sub>3</sub> pathway<sup>39</sup>, as evidenced by a more than 1000 times increased expression of the 24-OHase gene compared with control cultures (data not shown). 10<sup>-8</sup> M 1,25(OH)<sub>2</sub>D<sub>3</sub> treatment also significantly increased VDR expression in ATDC5 chondrocytes in the prehypertrophic phase of differentiation (*p*<0.05, Figure 1a, b)<sup>40-42</sup>.

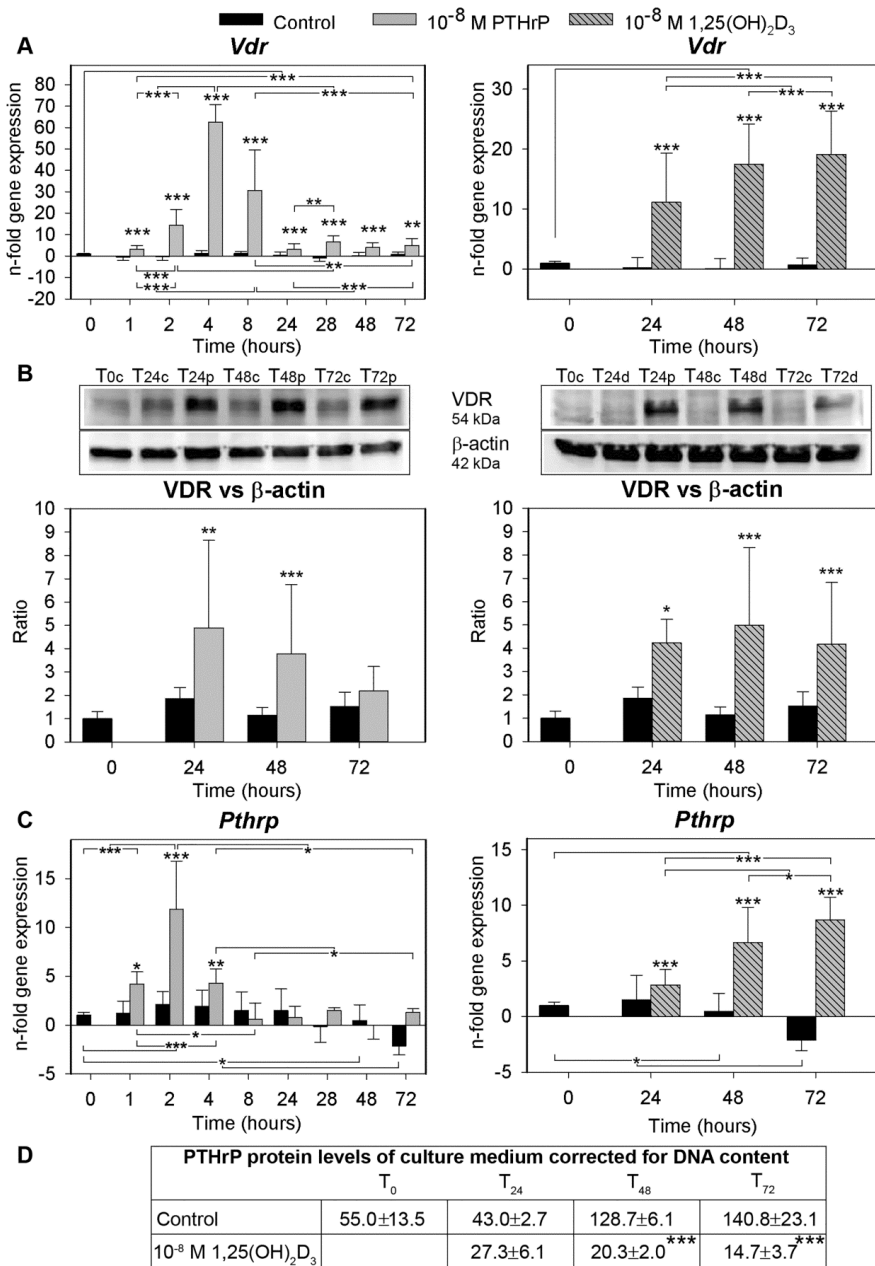


**Figure 1.** VDR and PTHrP expression in  $1,25(\text{OH})_2\text{D}_3$ - and PTHrP-treated ATDC5 chondrocytes in the prehypertrophic phase of differentiation. ATDC5 cells were treated starting from day 7 of differentiation (T<sub>0</sub>) with  $10^{-8}$  M PTHrP or  $1,25(\text{OH})_2\text{D}_3$  at T<sub>0</sub>, T<sub>24</sub>, and T<sub>48</sub>. (a) Relative *Vdr* gene expression (mean + SD); T<sub>0</sub> in the control culture was set at 1. n=8. (b) VDR protein expression expressed as VDR/ $\beta$ -actin ratio; T<sub>0</sub> in the control culture was set at 1. c = control culture, p =  $10^{-8}$  M PTHrP-treated culture, d =  $10^{-8}$  M  $1,25(\text{OH})_2\text{D}_3$ -treated culture. The error bars indicate experimental replicates. n=6. (c) Relative *Pthrp* gene expression (mean + SD). T<sub>0</sub> in the control culture was set at 1. n=8. (d) PTHrP protein levels (mean + SD) corrected for DNA content (pg PTHrP/ng DNA) in ATDC5 culture media of control cultures and  $10^{-8}$  M  $1,25(\text{OH})_2\text{D}_3$ -treated cultures, determined using a PTHrP ELISA. n=4. \*:  $p < 0.05$ , \*\*:  $p < 0.01$ , \*\*\*:  $p < 0.001$ .

*Pthrp* gene expression was significantly higher in the 10<sup>-8</sup> M 1,25(OH)<sub>2</sub>D<sub>3</sub>-treated cultures than in the control cultures at all time points ( $p < 0.001$ , Figure 1c). In contrast, the PTHrP protein content of the medium from 1,25(OH)<sub>2</sub>D<sub>3</sub>-treated cultures was significantly lower than that of medium from the control cultures at T<sub>48</sub> and T<sub>72</sub> ( $p < 0.001$ , Figure 1d). This seemingly contradictory result could be attributed to a phenomenon called ‘mRNA superinduction’. It has been reported that the inhibition of PTHrP protein synthesis leads to the induction of *Pthrp* mRNA expression (‘mRNA superinduction’) in a number of cell lines<sup>43</sup>. We explored this possibility in the ATDC5 cell line by measuring PTHrP mRNA and protein levels (in culture medium and cell lysate, corrected for DNA content) in the first 24 hours after treatment with 1,25(OH)<sub>2</sub>D<sub>3</sub>. PTHrP protein production decreased by 10<sup>-8</sup> M 1,25(OH)<sub>2</sub>D<sub>3</sub> treatment from T<sub>4</sub>/T<sub>8</sub> onward ( $p < 0.01$ , Figure 2b, c) and remained lower in the 10<sup>-8</sup> M 1,25(OH)<sub>2</sub>D<sub>3</sub>-treated cultures than in the control cultures until T<sub>72</sub> (Figure 1d). In contrast, *Pthrp* mRNA expression significantly increased from T<sub>24</sub> onward by 10<sup>-8</sup> M 1,25(OH)<sub>2</sub>D<sub>3</sub> treatment (Figure 2a, 1c). Given the time line of these events, where the increase in *Pthrp* mRNA expression (T<sub>24</sub>) is preceded by an initial significant decrease in PTHrP protein production (T<sub>4</sub>/T<sub>8</sub>), it seems reasonable to assume that the increased *Pthrp* mRNA levels were due to the ‘mRNA superinduction’ phenomenon. To determine whether this observed effect was physiological or pharmacological, we conducted an additional experiment investigating the time line of PTHrP mRNA and protein expression in the presence of 10<sup>-8</sup>, 10<sup>-10</sup>, and 10<sup>-12</sup> M 1,25(OH)<sub>2</sub>D<sub>3</sub>. PTHrP protein levels were dose-dependently influenced by 1,25(OH)<sub>2</sub>D<sub>3</sub> treatment (Figure 2b, c). Moreover, the increased *Pthrp* mRNA expression observed in the 10<sup>-8</sup> M 1,25(OH)<sub>2</sub>D<sub>3</sub>-treated ATDC5 chondrocytes (at T<sub>24</sub>), was not observed in the 10<sup>-10</sup> and 10<sup>-12</sup> M 1,25(OH)<sub>2</sub>D<sub>3</sub>-treated cells. This indicates that the ‘*Pthrp* mRNA superinduction’ phenomenon, only observed in the 10<sup>-8</sup> M 1,25(OH)<sub>2</sub>D<sub>3</sub>-treated ATDC5 chondrocytes, is pharmacological and can be avoided with lower physiological 1,25(OH)<sub>2</sub>D<sub>3</sub> regimes.

#### *Functional binding of 1,25(OH)<sub>2</sub>D<sub>3</sub> to the promoter region of the PTHrP gene*

Computational analysis of the PTHrP promoter revealed the presence of two VDR binding elements (Figure 3a). ChIP experiments showed a significant 2-fold enrichment of VDRE1 ( $p < 0.01$ ) and a 1.6-fold enrichment of VDRE2 (n.s.) in the PTHrP promoter (Figure 3b). No enrichment was observed in the PTHrP negative control (sequence 1000 bp upstream of VDRE2) and a significant 2.5-fold enrichment was observed in the positive control (24-hydroxylase promoter,  $p < 0.05$ , Figure 3b). Altogether, this indicates that in ATDC5 chondrocytes in the prehypertrophic phase of differentiation, 1,25(OH)<sub>2</sub>D<sub>3</sub> binds to its nuclear receptor, the VDR, and together they bind to a 1,25(OH)<sub>2</sub>D<sub>3</sub>-responsive region (VDRE1) in the PTHrP promoter. In this way, 1,25(OH)<sub>2</sub>D<sub>3</sub> directly regulates *Pthrp* expression via genomic effects.

Computational analysis of the PTHR1 promoter revealed the presence of two VDREs (Figure 3c). ChIP experiments showed a 1.4-fold enrichment of both VDRE1 and VDRE2, and a 2.1-fold enrichment of the VDRE combination (region containing both the expected VDRE1 and VDRE2) in the PTHR1 promoter (Figure 3d). However, these results were not significant and the PTHR1 negative control (sequence 1000 bp upstream of the expected VDREs) also revealed a 1.5-fold enrichment of the VDR antibody. Altogether, this indicates that there is no functional binding of 1,25(OH)<sub>2</sub>D<sub>3</sub> and the VDR to a VDRE in the PTHR1 promoter of ATDC5 chondrocytes in the prehypertrophic phase of differentiation.

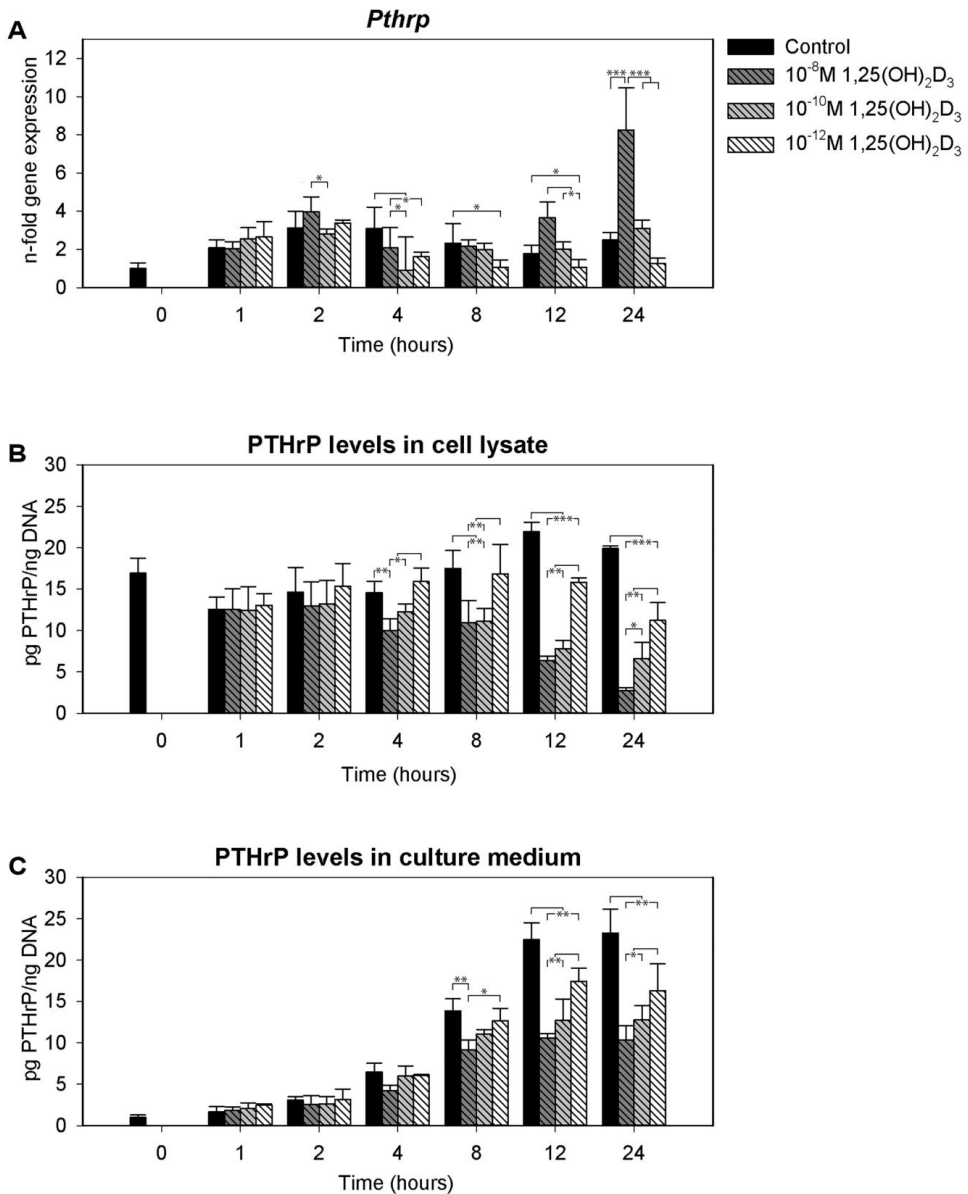


**Figure 2. *Pthrp* mRNA superinduction phenomenon.**  $10^{-8}$ ,  $10^{-10}$ , and  $10^{-12}$  M  $1,25(\text{OH})_2\text{D}_3$ -treated ATDC5 cell cultures were compared with control cultures. At  $T_0$  (on day 7 of differentiation, i.e. the prehypertrophic phase of the ATDC5 chondrocytes),  $1,25(\text{OH})_2\text{D}_3$  was added to the culture medium and the respective PTHrP gene (a) and protein content (mean + SD) of cell lysates (b) and culture media (c), respectively, were determined at  $T_{1-24}$  after  $1,25(\text{OH})_2\text{D}_3$  treatment. Relative *Pthrp* gene expression at  $T_0$  in the control culture was set at 1. The pharmacological '*Pthrp* mRNA superinduction' phenomenon is only observed in the  $10^{-8}$  M  $1,25(\text{OH})_2\text{D}_3$ -treated ATDC5 chondrocytes, and can be avoided with lower physiological regimes.  $n=6$  (control and  $10^{-8}$  M  $1,25(\text{OH})_2\text{D}_3$  cultures) and  $n=4$  ( $10^{-10}$  and  $10^{-12}$  M  $1,25(\text{OH})_2\text{D}_3$  cultures). \*:  $p < 0.05$ , \*\*:  $p < 0.01$ , \*\*\*:  $p < 0.001$ .

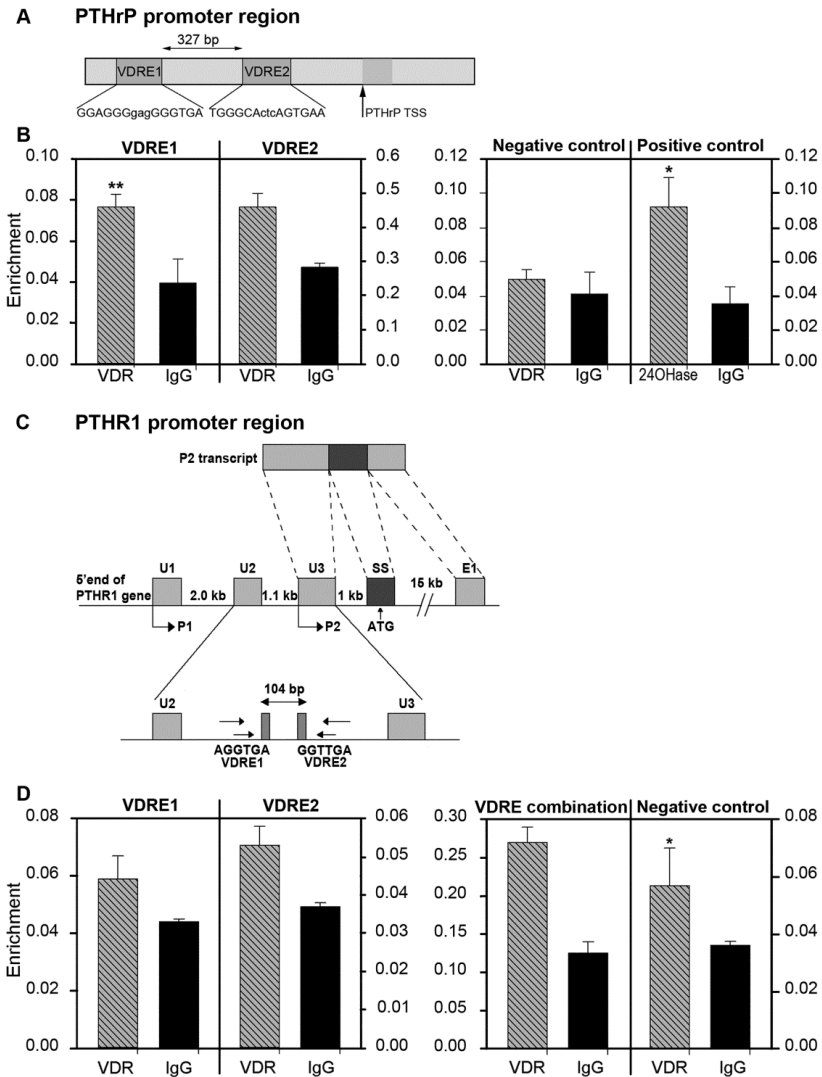


**Figure 3. Identification of a functional vitamin D<sub>3</sub> response element (VDRE) in the PTHrP and PTHR1 promoter region.** (a) Schematic presentation of the mouse PTHrP promoter region with location of the vitamin D<sub>3</sub> response elements (VDREs). Primers were designed for VDRE1 and VDRE2. The location of VDRE1 and VDRE2 upstream from TSS is 913 and 571 bp, respectively. bp: base pairs, TSS: transcription start site. (b) VDR ChIP assay performed on ATDC5 cells in the prehypertrophic phase of differentiation. Cells were fixed after 24 hours of treatment with 10<sup>-8</sup> M 1,25(OH)<sub>2</sub>D<sub>3</sub>. IgG was used as normalization control and a sequence 1000 bp upstream of VDRE2 was used as a negative control. Enrichment is given as mean + SD. The results are representative for four separate experiments and indicate functional binding of 1,25(OH)<sub>2</sub>D<sub>3</sub> and its receptor, the VDR, to the PTHrP promoter region. (c) Overview of expected VDREs in the PTHR1 promoter region. The PTHR1 gene has two promoter regions, P1 and P2. In bone and cartilage, the P2 promoter controls PTHR1 expression, whereas expression of P1 is restricted mainly to the kidney. The location of the expected VDRE1 (AGGTGA) and VDRE2 (GGTTGA) is 2092 and 2027 bp upstream from TSS, respectively. The arrows indicate the position of the primers used in this study. bp: base pairs, TSS: transcription start site. (d) VDR ChIP assay performed on ATDC5 cells in the prehypertrophic phase of differentiation. The VDRE combination contains both the expected VDRE1 and VDRE2 sequence. The same conditions apply as described with A. n=8. \*: p<0.05, \*\*: p<0.01.

### *Determination of the role of the VDR in the paracrine feedback loop between PTHrP and 1,25(OH)<sub>2</sub>D<sub>3</sub>*

To clarify the role of the VDR in the paracrine feedback loop between PTHrP and 1,25(OH)<sub>2</sub>D<sub>3</sub>, we successfully silenced the VDR in 100% confluent ATDC5 chondrocytes in the prehypertrophic phase of differentiation; significant VDR knockdown was seen at all time points in the control + VDR-oligo cultures and the 1,25(OH)<sub>2</sub>D<sub>3</sub> + VDR-oligo cultures ( $p < 0.05$ , Figure 4a,c).

Up- and downregulated PTHrP protein production in the scrambled mock cultures compared with the control cultures was observed at several time points (both with and without 1,25(OH)<sub>2</sub>D<sub>3</sub> supplementation, Figure 4d), which can be explained by off-target effects of the scrambled mock siRNA sequence<sup>44</sup>. The culture medium PTHrP protein content increased over time in the control cultures, whereas it decreased over time in the 1,25(OH)<sub>2</sub>D<sub>3</sub>-treated cultures, the difference being significant at T<sub>24</sub>-T<sub>72</sub> ( $p < 0.05$ , Figure 4d). At T<sub>48</sub> and T<sub>72</sub>, PTHrP protein levels in the 1,25(OH)<sub>2</sub>D<sub>3</sub> + VDR-oligo cultures were significantly higher than in the 1,25(OH)<sub>2</sub>D<sub>3</sub> cultures ( $p < 0.05$ ), indicating that VDR silencing counteracted the 1,25(OH)<sub>2</sub>D<sub>3</sub>-mediated inhibitory effect on PTHrP protein production in ATDC5 chondrocytes in the prehypertrophic phase of differentiation.

### *The role of the paracrine PTHrP-1,25(OH)<sub>2</sub>D<sub>3</sub> feedback loop in hypertrophic chondrocyte differentiation*

1,25(OH)<sub>2</sub>D<sub>3</sub> treatment of the prehypertrophic ATDC5 cultures decreased the DNA content by about 40% whereas the addition of PTHrP increased the DNA content by about 30% compared with the control cultures (data not shown). Gene expression of the (pre)hypertrophic differentiation markers *Col9*, *ColX*, and *Pthr1* increased significantly over time in the control cultures ( $p < 0.05$ ), but not in the PTHrP- and 1,25(OH)<sub>2</sub>D<sub>3</sub>-treated cultures (Figure 5a). Generally, *Pthr1*, *Col9* and *ColX* gene expression was higher in the control cultures than in the PTHrP- or 1,25(OH)<sub>2</sub>D<sub>3</sub>-treated cultures at all time points. However, western blot analysis indicated that only on differentiation day 14 (T<sub>168</sub>), collagen type X protein expression was significantly lower in the PTHrP- and 1,25(OH)<sub>2</sub>D<sub>3</sub>-treated cultures than in the control cultures ( $p < 0.001$ , Figure 5b), but not on differentiation day 10 (T<sub>72</sub>). This indicates that both 1,25(OH)<sub>2</sub>D<sub>3</sub> and PTHrP treatment inhibited hypertrophic differentiation of the ATDC5 chondrocytes, which was noticed earlier at the mRNA than at the protein level.

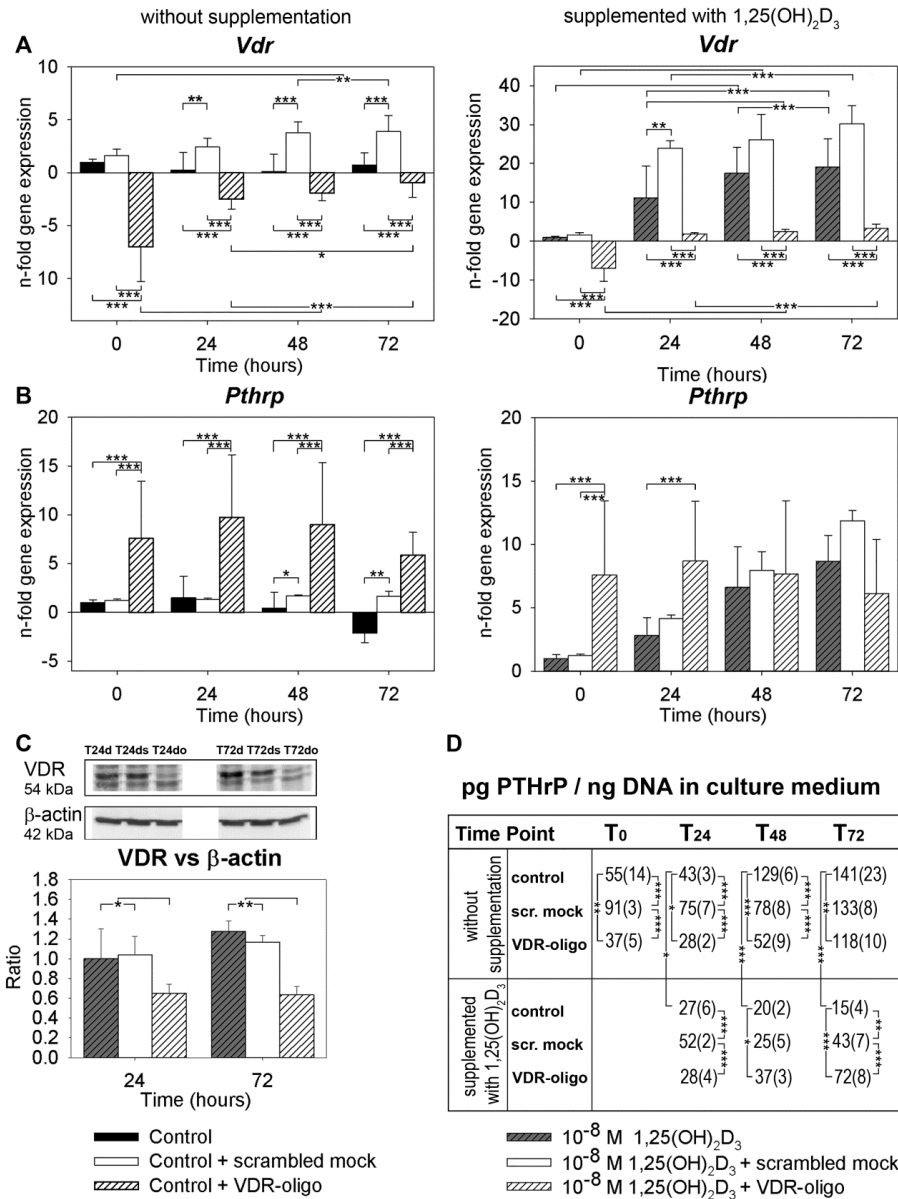


**Figure 4. The role of VDR in the paracrine feedback loop between PTHrP and 1,25(OH)<sub>2</sub>D<sub>3</sub>.** Relative *Vdr* (a) and *PTHrP* (b) gene expression (mean + SD) in ATDC5 cells in the prehypertrophic phase of differentiation. In the VDR-oligo groups, silencing of the VDR was performed on differentiation day 4. At T<sub>0</sub> (day 7 of differentiation), T<sub>24</sub>, and T<sub>48</sub>, 10<sup>-8</sup> M 1,25(OH)<sub>2</sub>D<sub>3</sub> was added to the three 1,25(OH)<sub>2</sub>D<sub>3</sub>-treated culture groups. Relative target gene expression at T<sub>0</sub> in the control culture was set at 1. n=6. (c) Western blot confirming the successful siRNA transfection in 10<sup>-8</sup> M 1,25(OH)<sub>2</sub>D<sub>3</sub>-treated prehypertrophic ATDC5 cells with approximately 50% downregulation of VDR production. Time is shown in hours after 1,25(OH)<sub>2</sub>D<sub>3</sub> was first added and the VDR/β-actin ratio in the 1,25(OH)<sub>2</sub>D<sub>3</sub> culture at T<sub>24</sub> was set at 1. d = 10<sup>-8</sup> M 1,25(OH)<sub>2</sub>D<sub>3</sub>-supplemented culture, ds = 1,25(OH)<sub>2</sub>D<sub>3</sub> + scrambled mock culture, do = 1,25(OH)<sub>2</sub>D<sub>3</sub> + VDR-oligo culture. The error bars indicate experimental replicates. n=3. D. PTHrP protein levels (mean + SD) corrected for DNA content in ATDC5 culture media, determined using a PTHrP ELISA. n=3. \*: p<0.05, \*\*: p<0.01, \*\*\*: p<0.001.

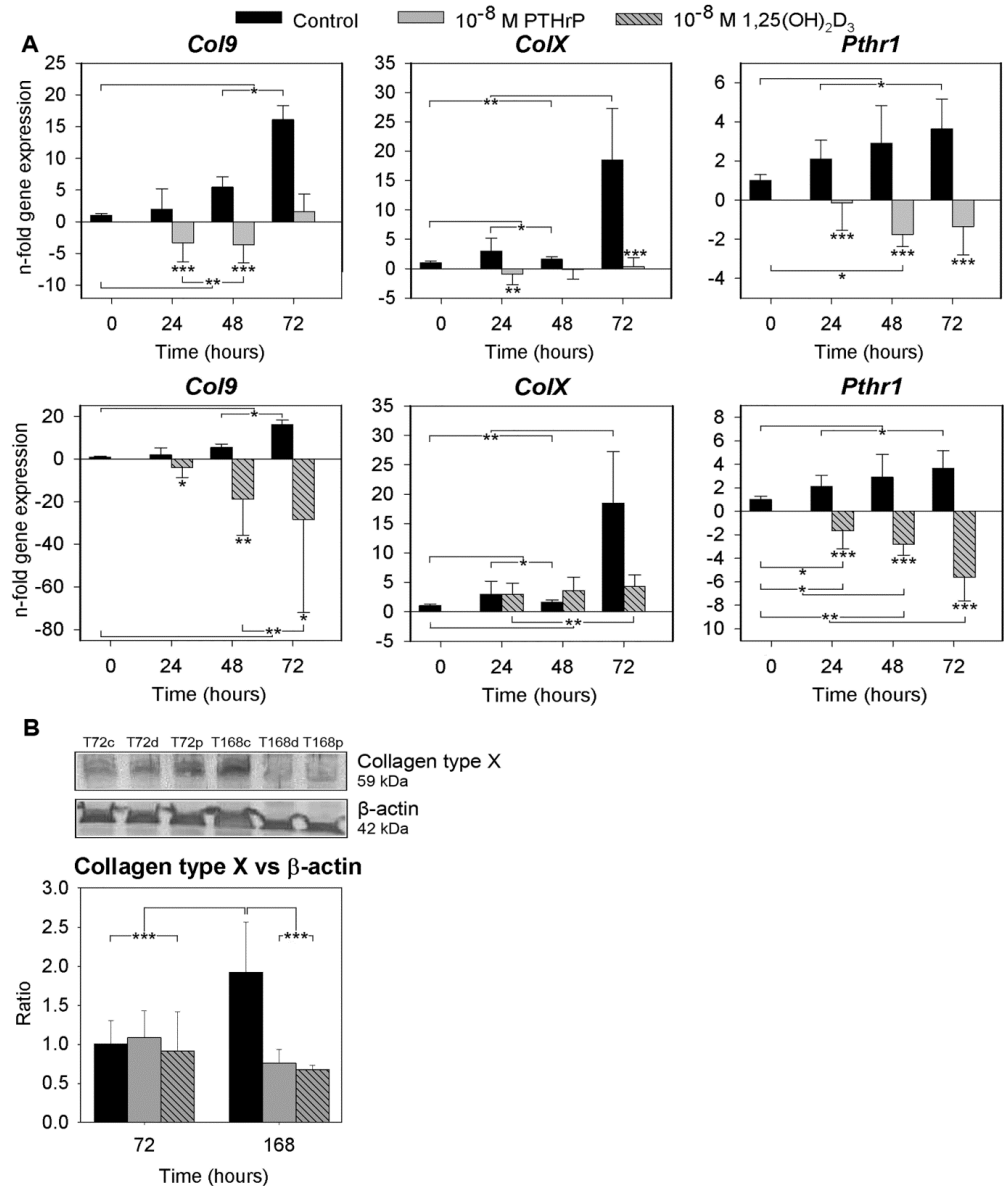


**Figure 5. The role of the paracrine PTHrP- $1,25(\text{OH})_2\text{D}_3$  feedback loop in hypertrophic chondrocyte differentiation.** (a) Relative (mean + SD) *Col9*, *Col10*, and *Pthr1* gene expression in PTHrP- or  $1,25(\text{OH})_2\text{D}_3$ -treated ATDC5 cell cultures compared with control cultures.  $10^{-8}$  M PTHrP or  $1,25(\text{OH})_2\text{D}_3$  was added daily from  $T_0$ , which was day 7 of differentiation, i.e. the prehypertrophic phase of the ATDC5 chondrocytes. Relative target gene expression at  $T_0$  in the control culture was set at 1.  $n=8$ . (b) Collagen type X protein expression expressed as Collagen type X/ $\beta$ -actin ratio. Time is shown in hours after PTHrP/ $1,25(\text{OH})_2\text{D}_3$  was first added to the culture medium on differentiation day 7.  $T_{72}$  in the control culture was set at 1. c = control culture, p =  $10^{-8}$  M PTHrP-treated culture, d =  $10^{-8}$  M  $1,25(\text{OH})_2\text{D}_3$ -treated culture. The error bars indicate experimental replicates.  $n=3$ . \*:  $p<0.05$ , \*\*:  $p<0.01$ , \*\*\*:  $p<0.001$ .

To clarify the role of the paracrine feedback loop between PTHrP and 1,25(OH)<sub>2</sub>D<sub>3</sub> in growth plate chondrocyte differentiation, we silenced the VDR in ATDC5 chondrocytes in the prehypertrophic phase of differentiation. In the control + scrambled mock and the control + VDR-oligo cultures, *ColX* gene expression did not increase over time, in contrast to what was observed in the control cultures (Figure 6a). For the PTHrP- and 1,25(OH)<sub>2</sub>D<sub>3</sub>-treated ATDC5 cultures, no significant differences in collagen type X expression between the non-silenced (PTHrP/1,25(OH)<sub>2</sub>D<sub>3</sub>) and the VDR silenced (PTHrP/1,25(OH)<sub>2</sub>D<sub>3</sub> + VDR-oligo) cultures were observed (Figure 6a,b), indicating that VDR silencing did not counteract the PTHrP/1,25(OH)<sub>2</sub>D<sub>3</sub>-mediated inhibitory effect on collagen type X expression in ATDC5 chondrocytes in the prehypertrophic phase of differentiation. In contrast, *Pthr1* expression was significantly upregulated in the 1,25(OH)<sub>2</sub>D<sub>3</sub> + VDR-oligo cultures at T<sub>48</sub> and T<sub>72</sub> ( $p < 0.01$ , Figure 6), indicating that VDR silencing counteracted the 1,25(OH)<sub>2</sub>D<sub>3</sub>-mediated inhibitory effect on *Pthr1* expression in ATDC5 chondrocytes in the prehypertrophic phase of differentiation.

Generally, *ColX* and *Vdr* gene expression was significantly higher in the scrambled mock cultures than in the non-silenced control cultures, whereas the scrambled mock treatment did not affect *Pthr1* and *Pthrp* expression (Figure 4a,b and 6a). The difference in *ColX* and *Vdr* gene expression was, however, not accompanied with differences in VDR and collagen type X protein expression between the scrambled mock and the non-silenced control cultures (Figure 4c and 6b), indicating that the scrambled mock-induced upregulated mRNA expression was not translated into increased protein expression. Most probably, the upregulated *ColX* and *Vdr* mRNA expression can be attributed to off-target effects of the scrambled mock sequence<sup>44</sup>.

## **In vivo studies**

### *Animals and biochemistry*

From 4 weeks of age onward, the control vitamin D<sub>3</sub>-sufficient (VitD+) mice weighed significantly more than the VitD- mice ( $p < 0.001$ , Supplementary file 6a). Plasma 25(OH)D<sub>3</sub> levels confirmed vitamin D<sub>3</sub> deficiency in VitD- mice ( $p < 0.001$ , Supplementary file 6a). As expected, the plasma concentration of 1,25(OH)<sub>2</sub>D<sub>3</sub> was significantly higher in VitD-;+1,25D mice than in VitD+ and VitD- mice ( $p < 0.01$ ). Plasma calcium (Ca) levels were significantly lower in VitD- mice than in VitD+ mice ( $p < 0.01$ ), but were significantly higher in VitD-;+1,25D mice than in VitD- and VitD+ mice ( $p < 0.01$ ). Inorganic phosphate (P) plasma levels were not significantly different between groups, but PTH levels were significantly higher in VitD- mice than in VitD+ and VitD-;+1,25D mice ( $p < 0.001$ ).

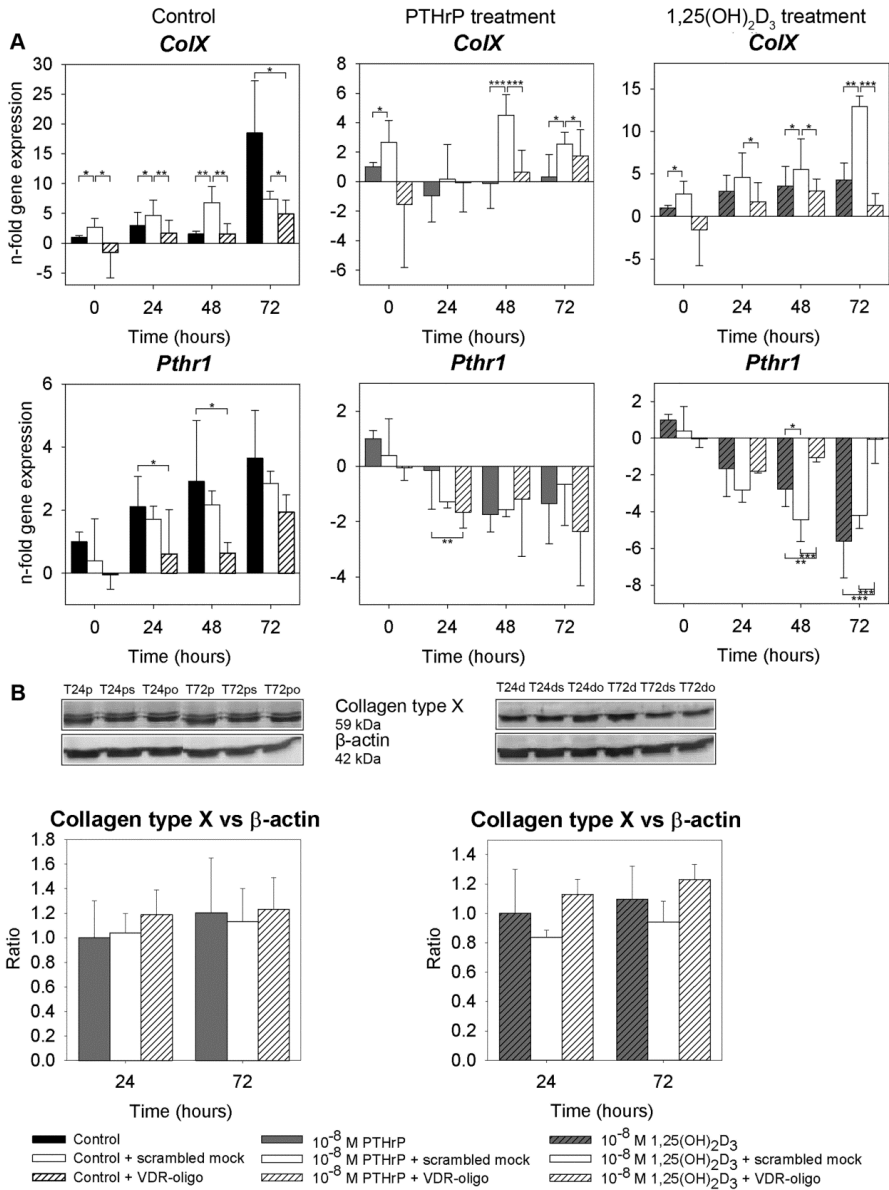


**Figure 6. The role of the VDR in the paracrine PTHrP-1,25(OH)<sub>2</sub>D<sub>3</sub> feedback loop during hypertrophic chondrocyte differentiation.** (a) Relative (mean ± SD) *Col1X* and *Pth1r* gene expression corrected for reference genes in ATDC5 cells in the prehypertrophic differentiation phase. In the VDR-oligo groups, silencing of the VDR was performed on differentiation day 4. 10<sup>-8</sup> M PTHrP or 1,25(OH)<sub>2</sub>D<sub>3</sub> was added daily, starting at T<sub>0</sub>, which was day 7 of differentiation. Relative target gene expression at T<sub>0</sub> in the control culture was set at 1. n=6. (b) Collagen type X protein expression in 10<sup>-8</sup> M PTHrP- and 1,25(OH)<sub>2</sub>D<sub>3</sub>-treated ATDC5 cells silenced for the VDR. Time is shown in hours after PTHrP/1,25(OH)<sub>2</sub>D<sub>3</sub> was first added to the culture medium on differentiation day 7. The collagen type X/β-actin ratio in the PTHrP/1,25(OH)<sub>2</sub>D<sub>3</sub> culture at T<sub>24</sub> was set at 1. p = PTHrP culture, pm = PTHrP + scrambled mock culture, po = PTHrP + VDR-oligo culture, d = 1,25(OH)<sub>2</sub>D<sub>3</sub> culture, dm = 1,25(OH)<sub>2</sub>D<sub>3</sub> + scrambled mock culture, do = 1,25(OH)<sub>2</sub>D<sub>3</sub> + VDR-oligo culture. The error bars indicate experimental replicates. n=3. \*: p<0.05, \*\*: p<0.01, \*\*\*: p<0.001.

### *Growth plate histomorphometry*

The mean growth plate height (GPI.Th) was significantly higher in VitD<sup>-</sup> mice than in VitD<sup>+</sup> and VitD<sup>-</sup>;+1,25D mice ( $p < 0.001$ , Figure 7a). The mean GPI.Th.<sub>pr</sub> did not differ between groups, whereas the GPI.Th.<sub>p2</sub>/GPI.Th ratio was significantly lower in VitD<sup>-</sup> mice than in the other groups ( $p < 0.05$ ). The mean GPI.Th.<sub>hyp</sub> and the ratio of GPI.Th.<sub>hyp</sub>/GPI.Th were significantly higher in VitD<sup>-</sup> mice than in VitD<sup>+</sup> or VitD<sup>-</sup>;+1,25D mice ( $p < 0.05$ ). The standard deviation of GPI.Th.<sub>hyp</sub>, a measure of the irregularity of the hypertrophic zone, was also significantly higher in VitD<sup>-</sup> mice than in VitD<sup>+</sup> and VitD<sup>-</sup>;+1,25D mice ( $p < 0.01$ , Figure 7a). The Col2-pd2EGFP vitamin D<sub>3</sub>-deficient mice thus showed the classical signs of low body weight, hypocalcemia, hyperparathyroidism, and rickets with an enlarged growth plate. The latter was mainly due to an increased and irregular hypertrophic zone<sup>45</sup>. Their vitamin D<sub>3</sub>-deficient phenotype was successfully reversed by 1,25(OH)<sub>2</sub>D<sub>3</sub> supplementation.

### *Gene and protein expression of primary growth plate chondrocytes*

Col2-pd2EGFP-positive growth plate chondrocytes were sorted and processed for RNA isolation on an individual basis. The number of positive Col2-pd2EGFP chondrocytes was  $5.1 \cdot 10^5 \pm 3.1 \cdot 10^5$ ,  $1.4 \cdot 10^6 \pm 8.1 \cdot 10^5$ , and  $3.3 \cdot 10^5 \pm 2.1 \cdot 10^5$  for the VitD<sup>+</sup>, VitD<sup>-</sup>, and VitD<sup>-</sup>;+1,25D mice, respectively. Hypertrophic differentiation marker (*ColX* and *Pthr1*) gene expression was significantly higher in VitD<sup>-</sup> mice than in mice from the two other groups ( $p < 0.01$ , Figure 7b). Furthermore, *Vdr* gene expression was significantly higher in VitD<sup>-</sup> mice than in VitD<sup>+</sup> mice ( $p < 0.05$ ) and *Pthrp* gene expression was significantly higher in VitD<sup>-</sup>;+1,25D mice than in VitD<sup>+</sup> mice ( $p < 0.05$ , Figure 7b).

Confocal imaging of tibial growth plates from Col2-pd2EGFP transgenic mice indicated that VitD<sup>+</sup> and VitD<sup>-</sup>;+1,25D mice had less Col2-pd2EGFP than VitD<sup>-</sup> mice (Figure 7a). Nuclear VDR protein expression was highest in VitD<sup>-</sup> mice and lowest in VitD<sup>+</sup> mice (n.s., Supplementary file 6b). Within the proliferative and hypertrophic zones, the percentage area staining for PTHrP (over the total surface of the growth plate, and thus corrected for the larger surface of the growth plate in VitD<sup>-</sup> mice), the integrated density, and mean gray value did not differ between groups (Supplementary file 6b). However, in accordance with gene expression levels, immunohistochemical staining showed that PTHR1 was produced in all zones of the growth plate and in greater amounts in VitD<sup>-</sup> mice than in mice from the other two groups (n.s., Supplementary file 6b).

### ***In vitro studies with primary growth plate chondrocytes***

As other signaling pathways may interfere with the interpretation of the *in vivo* results, an *in vitro* study was performed with primary Col2-pd2EGFP growth plate chondrocytes. Vitamin D<sub>3</sub>-deficient primary growth plate chondrocytes (controls) were compared with  $10^{-8}$  M 1,25(OH)<sub>2</sub>D<sub>3</sub>-treated primary growth plate chondrocytes over 7 days. *ColX* gene expression decreased with time and was lower in 1,25(OH)<sub>2</sub>D<sub>3</sub>-treated primary growth plate chondrocytes than in control primary growth plate chondrocytes at all time points (Figure 7C). In line with our hypothesis, *Pthrp* gene expression was lower and *Vdr* gene expression was higher in 1,25(OH)<sub>2</sub>D<sub>3</sub>-treated primary growth plate chondrocytes compared with control primary growth plate chondrocytes at all time points (Figure 7C).

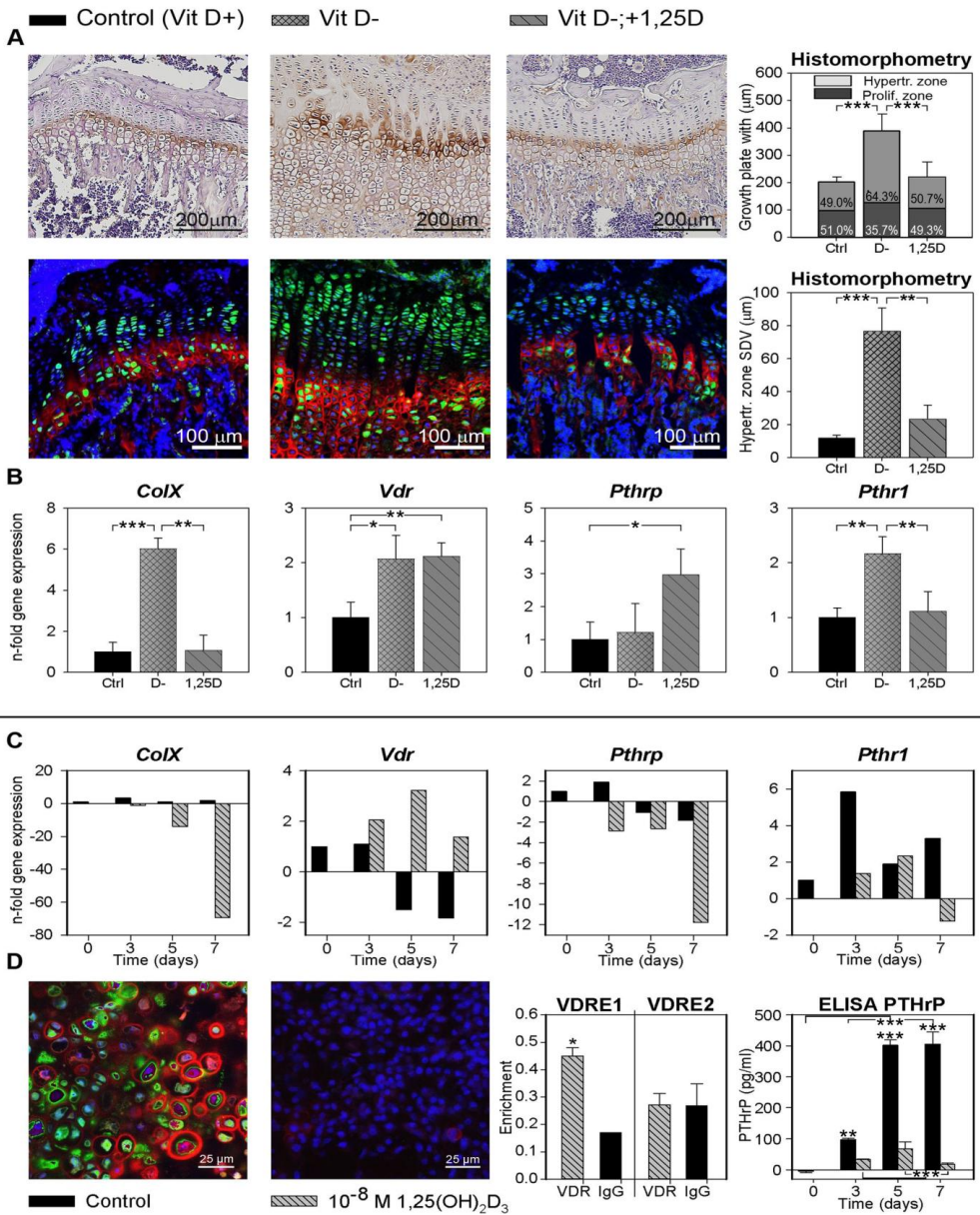


**Figure 7. Results of the *in vivo* study and the primary cell culture of Col2-pd2EGFP transgenic mice growth plate chondrocytes.** (a) Histomorphometry (H&E) and immunofluorescent staining for collagen type X (red) of tibial growth plates from Col2-Col2-pd2EGFP transgenic mice (6 weeks of age) indicating that vitamin D<sub>3</sub> deficient mice (VitD<sup>-</sup>) developed rickets. Supplementation with 1,25(OH)<sub>2</sub>D<sub>3</sub> (VitD<sup>-</sup>;+1,25D) reversed the rachitic phenotype as compared with controls (VitD<sup>+</sup>). Note that Col2-pd2EGFP fluorescence (green) is native. *n*=7. (b) Relative (mean + SD) *ColIX*, *Vdr*, *Pthrp*, and *Pthr1* gene expression corrected for reference genes in sorted Col2-pd2EGFP positive growth plate chondrocytes after termination of the study, at 6 weeks of age. Relative target gene expression in the growth plate of control (VitD<sup>+</sup>) mice was set at 1. *n*=6. (c) Relative *ColIX*, *Vdr*, *Pthrp*, and *Pthr1* gene expression corrected for reference genes in control or 1,25(OH)<sub>2</sub>D<sub>3</sub>-treated cultured primary Col2-pd2EGFP growth plate chondrocytes. Time is shown in days after the start of differentiation (T<sub>0</sub>, T<sub>3</sub>, T<sub>5</sub> and T<sub>7</sub>). From T<sub>2</sub> onward, 10<sup>-8</sup> M 1,25(OH)<sub>2</sub>D<sub>3</sub> was daily added to the culture medium. Relative target gene expression at

T<sub>0</sub> in the control culture was set at 1. These data were not subjected to statistical analysis due to the small sample size. *n*=1. (d) From left to right: Immunofluorescent staining for collagen type X and native expression of Col2-pd2EGFP in control and 10<sup>-8</sup> M 1,25(OH)<sub>2</sub>D<sub>3</sub>-treated cultured primary Col2-pd2EGFP growth plate chondrocytes. Transcription of collagen type 2 (green) and hypertrophic differentiation of chondrocytes (red) were detected in control cultures, whereas the 10<sup>-8</sup> M 1,25(OH)<sub>2</sub>D<sub>3</sub>-treated cells expressed no Col2-pd2EGFP and only occasionally collagen type X immunofluorescence in their pericellular matrix. A ChIP assay revealed enrichment of PTHrP VDRE1, but not the VDRE2. A PTHrP ELISA performed on culture media revealed decreased PTHrP production in the 10<sup>-8</sup> M 1,25(OH)<sub>2</sub>D<sub>3</sub>-treated primary growth plate chondrocytes compared with control cultures. *n*=4. \*: *p*<0.05, \*\*: *p*<0.01, \*\*\*: *p*<0.001.

Confocal imaging of native Col2-pd2EGFP fluorescence and staining for collagen type X revealed transcription of collagen type II and hypertrophic differentiation of the control cultures at T<sub>7</sub>, whereas 1,25(OH)<sub>2</sub>D<sub>3</sub>-treated primary growth plate chondrocytes showed no Col2-pd2EGFP fluorescence and collagen type X staining in their pericellular matrix (Figure 7d), which was in line with our hypothesis and confirms the reported gene expression profiles.

ChIP assays showed no enrichment of VDRE1, VDRE2, or the negative control in the PTHR1 promoter (data not shown), indicating that there is no functional binding of 1,25(OH)<sub>2</sub>D<sub>3</sub> and the VDR to a VDRE in the PTHR1 promoter of primary Col2-pd2EGFP growth plate chondrocytes. However, in parallel with what was found in the chondrogenic ATDC5 cell line, ChIP assays on sorted Col2-pd2EGFP growth plate chondrocytes showed a significant 2.6-fold enrichment of VDRE1 (*p*<0.05), and no enrichment of VDRE2 or the negative control in the PTHrP promoter (Figure 7d). Furthermore, PTHrP production in 1,25(OH)<sub>2</sub>D<sub>3</sub>-treated primary growth plate chondrocytes was significantly lower than in control cultures at all time points (*p*<0.01, Figure 7d). These results indicate that also in primary Col2-pd2EGFP growth plate chondrocytes, 1,25(OH)<sub>2</sub>D<sub>3</sub> and the VDR together bind to a 1,25(OH)<sub>2</sub>D<sub>3</sub>-responsive region (VDRE1) in the PTHrP promoter. In this way, 1,25(OH)<sub>2</sub>D<sub>3</sub> directly inhibits PTHrP production via the VDR.

## Discussion

The regulation of chondrocyte differentiation is a key event in skeletal development. Regenerative strategies for cartilage engineering use mesenchymal stem cells (MSCs), but are hampered by the inherent capacity of chondrogenically differentiating MSCs to undergo hypertrophic differentiation<sup>46</sup>. Hence, understanding the processes that regulate chondrocyte differentiation is crucial to further fine-tune regenerative strategies for cartilage and bone engineering. In order to do so, we used growth plate chondrocytes, which undergo differentiation in an orderly fashion. We used complementary *in vitro* (ATDC5 and primary growth plate chondrocytes) and *in vivo* (Col2-pd2EGFP mice) models and demonstrated that there is a functional paracrine feedback loop between 1,25(OH)<sub>2</sub>D<sub>3</sub> and PTHrP in prehypertrophic growth plate chondrocytes (Figure 8).

### The effect of PTHrP on the vitamin D<sub>3</sub> pathway

We hypothesized that in growth plate chondrocytes, PTHrP treatment would increase vitamin D<sub>3</sub> activity, either by interference with the key enzymes of vitamin D<sub>3</sub> metabolism (1 $\alpha$ - and 24-hydroxylase) or by a direct effect on the VDR (Supplementary File 1). In the kidney, PTH stimulates 1 $\alpha$ -hydroxylase and inhibits 24-hydroxylase<sup>47, 48</sup>. The subcutaneous administration of PTHrP to healthy women increased plasma 1,25(OH)<sub>2</sub>D<sub>3</sub> levels, but did not affect endogenous PTH levels, indicating that - at an endocrine level - PTHrP stimulates 1 $\alpha$ -hydroxylase in the kidney in the same way that PTH does<sup>49</sup>. However, in the current study, PTHrP did not significantly affect the expression of 1 $\alpha$ - and 24-hydroxylase in ATDC5 chondrocytes in the prehypertrophic phase of differentiation. Although we did not determine the actual activity of the respective enzymes, it is tempting to speculate that PTH and PTHrP influence 1 $\alpha$ - and 24-hydroxylase expression in a tissue/cell-specific manner.

We found that PTHrP significantly increased VDR expression. *Vdr* gene expression was upregulated 4 hours after initiation of PTHrP treatment (T<sub>4</sub>), whereas repeated treatment resulted in a lower increase in *Vdr* gene expression at T<sub>28</sub>. Desensitization of the PTH-induced cAMP response<sup>50</sup> might explain the decreased response of the ATDC5 cells to PTHrP after the second addition of PTHrP (at T<sub>24</sub>) compared with the first addition (at T<sub>0</sub>). Previous studies found a PTH/PTHrP-mediated decreased VDR expression in renal, intestinal, and osteoblast-like cells<sup>10, 51, 52</sup>, but increased VDR expression in growth plate chondrocytes and osteoblast-like cells<sup>53, 54</sup>. A possible explanation for these contradictory results is again a cell-line/tissue specific effect.

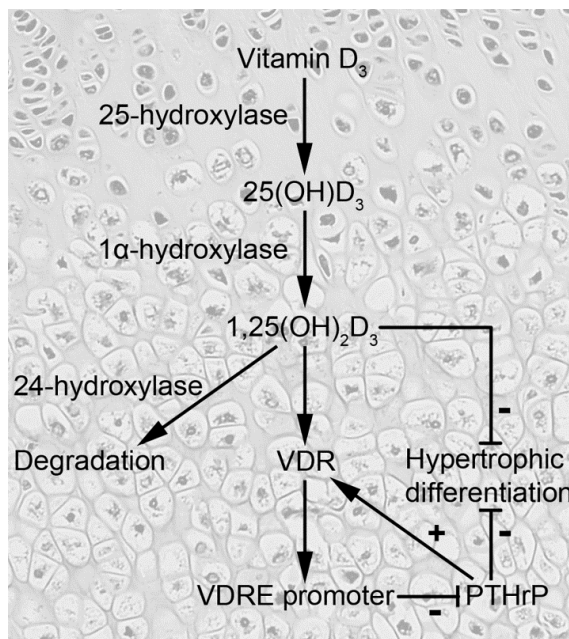


**Figure 8. The paracrine feedback loop between PTHrP and 1,25(OH)<sub>2</sub>D<sub>3</sub> in prehypertrophic growth plate chondrocytes.** 1,25(OH)<sub>2</sub>D<sub>3</sub> inhibits PTHrP production through a VDRE in the PTHrP promoter, and PTHrP increases chondrocyte sensitivity to 1,25(OH)<sub>2</sub>D<sub>3</sub> via increased VDR expression.

### The effect of vitamin D<sub>3</sub> on the PTHrP pathway

We hypothesized that treatment with 1,25(OH)<sub>2</sub>D<sub>3</sub> would decrease PTHrP production, because *Pthrp* expression is reported to be suppressed by 1,25(OH)<sub>2</sub>D<sub>3</sub> in several other cell types<sup>27, 55, 56</sup>. In contrast to our hypothesis, in the *in vivo* studies with the Col2-pd2EGFP mouse model, *Pthrp* gene expression was increased in Col2-pd2EGFP growth plate chondrocytes from VitD<sup>-</sup>;+1,25D mice compared with VitD<sup>-</sup> or VitD<sup>+</sup> mice. However, these *in vivo* studies are limited by several factors. First, growth plate chondrocytes were isolated on the basis of FACS of Col2-pd2EGFP-positive chondrocytes and, hence, may not be representative of the total population of growth plate chondrocytes. Second, the altered calcium homeostasis in the vitamin D<sub>3</sub>-deficient mice treated with 1,25(OH)<sub>2</sub>D<sub>3</sub> resulted in hypercalcemia, which could have attributed to the increased *Pthrp* and *Vdr* expression in VitD<sup>-</sup>;+1,25D mice. Calcium has been shown to regulate PTHrP secretion<sup>57, 58</sup> and to have an additive effect on the homologous upregulation of VDR expression during treatment with 1,25(OH)<sub>2</sub>D<sub>3</sub><sup>40-42</sup>. To exclude the effects of interfering factors, we also performed *in vitro* studies with ATDC5 and primary Col2-pd2EGFP growth plate chondrocytes and studied the pattern of expression of target genes and proteins in the presence and absence of 1,25(OH)<sub>2</sub>D<sub>3</sub>. In line with our hypothesis, PTHrP gene and protein expression was lower in the 1,25(OH)<sub>2</sub>D<sub>3</sub>-treated primary Col2-pd2EGFP growth plate chondrocytes compared with control cultures. Also in prehypertrophic ATDC5 chondrocytes, PTHrP protein production was decreased by 1,25(OH)<sub>2</sub>D<sub>3</sub>-treatment. The counterintuitive increase of *Pthrp* gene expression in 10<sup>-8</sup> M 1,25(OH)<sub>2</sub>D<sub>3</sub>-treated ATDC5 cultures compared with control cultures from 24 hours of treatment onward could be explained by '*Pthrp* mRNA superinduction'<sup>43</sup>, which is only provoked by the preceding decreased PTHrP protein expression in 10<sup>-8</sup> M 1,25(OH)<sub>2</sub>D<sub>3</sub>-treated prehypertrophic ATDC5 chondrocytes, and not at lower dosages.

We furthermore silenced the VDR to clarify its role in the regulation of PTHrP expression by 1,25(OH)<sub>2</sub>D<sub>3</sub>. VDR silencing counteracted the inhibitory effect of 1,25(OH)<sub>2</sub>D<sub>3</sub> on PTHrP protein production. In addition, we observed significant enrichment of the PTHrP VDRE1 in 1,25(OH)<sub>2</sub>D<sub>3</sub>-treated ATDC5 and primary growth plate chondrocytes in the prehypertrophic phase of differentiation. This is the first study to report functional binding of 1,25(OH)<sub>2</sub>D<sub>3</sub> through its receptor to the promoter region of the PTHrP gene in growth plate chondrocytes. The 1,25(OH)<sub>2</sub>D<sub>3</sub>-responsive region (VDRE) in the PTHrP promoter has already been characterized in other tissues<sup>27, 28, 55</sup>. Taken together, these findings prove that in the growth plate, the functional paracrine feedback loop between PTHrP and 1,25(OH)<sub>2</sub>D<sub>3</sub> is closed by the inhibition of PTHrP transcription by the binding of 1,25(OH)<sub>2</sub>D<sub>3</sub> to a VDRE located in the PTHrP (and not the PTHR1) promoter region.

### The role of the paracrine PTHrP-1,25(OH)<sub>2</sub>D<sub>3</sub> feedback loop in hypertrophic chondrocyte differentiation

Having established that there is a functional paracrine feedback loop between PTHrP and 1,25(OH)<sub>2</sub>D<sub>3</sub> in growth plate chondrocytes, we wanted to define the role of this feedback loop in hypertrophic chondrocyte differentiation. Both 1,25(OH)<sub>2</sub>D<sub>3</sub> and PTHrP affected the proliferation and differentiation of growth plate chondrocytes. 1,25(OH)<sub>2</sub>D<sub>3</sub> treatment resulted in a decreased DNA content of the prehypertrophic ATDC5 chondrocytes, indirectly indicating that 1,25(OH)<sub>2</sub>D<sub>3</sub> had an anti-proliferative effect, which is in line with previous reports<sup>12</sup>. Moreover, 1,25(OH)<sub>2</sub>D<sub>3</sub> had an inhibitory effect on chondrocyte hypertrophy,

based on the reduced *Col9*, *ColX*, and *Pthr1* gene expression and collagen type X protein expression in 1,25(OH)<sub>2</sub>D<sub>3</sub>-treated ATDC5 and primary Col2-pd2EGFP positive growth plate chondrocytes. This is by no means a new finding, since 1,25(OH)<sub>2</sub>D<sub>3</sub> has been shown to inhibit terminal chondrocyte differentiation both *in vitro* and *in vivo*<sup>11, 13, 59</sup>. In addition, VDR silencing in 1,25(OH)<sub>2</sub>D<sub>3</sub>-treated ATDC5 cells only partially reversed the anti-hypertrophic effects of 1,25(OH)<sub>2</sub>D<sub>3</sub>: it prevented the inhibitory effect of 1,25(OH)<sub>2</sub>D<sub>3</sub> on *Pthr1* gene expression, but it did not affect collagen type X expression. In unpublished studies, we found that treatment with 10<sup>-10</sup> M and 10<sup>-12</sup> M 1,25(OH)<sub>2</sub>D<sub>3</sub> decreased the expression of (pre)hypertrophic differentiation markers, and hence VDR silencing may have been ineffective in counteracting the strong inhibitory effect of 10<sup>-8</sup> M 1,25(OH)<sub>2</sub>D<sub>3</sub> on hypertrophic differentiation. An alternative explanation is that 1,25(OH)<sub>2</sub>D<sub>3</sub> also exerts effects by binding to a membrane-associated receptor PDIA3<sup>65, 60</sup>.

PTHrP is a well-known suppressor of hypertrophic chondrocyte differentiation<sup>1, 61-63</sup>. Accordingly, in the control ATDC5 cultures, *Col9* gene and collagen type X gene and protein expression increased with time, but this increase was prevented by the addition of PTHrP. Furthermore, the addition of PTHrP to ATDC5 cells in a prehypertrophic differentiation phase significantly downregulated the expression of the gene for the receptor of PTHrP, *Pthr1*, which is also in line with previous reports<sup>64, 65</sup>. This homologous downregulation of *Pthr1* is possibly a measure to prevent overstimulation, but another explanation lies in the physiological role of PTHrP, namely, to prevent proliferative cells leaving the proliferating pool. In this way, hypertrophic chondrocyte differentiation - and thus PTHR1 production - is delayed<sup>4, 18-20</sup>. Taken together, the results of our study indicate that PTHrP could be used clinically to inhibit undesirable hypertrophic chondrocyte differentiation. Accordingly, *in vitro* work has already demonstrated that PTHrP successfully inhibited hypertrophic differentiation of articular chondrocytes<sup>66, 67</sup> and cartilage constructs engineered from bone marrow-derived mesenchymal stem cells (BMSCs), without losing cartilage-specific matrix proteins (US patent 20080318859<sup>68</sup>). Moreover, *in vivo*, intra-articular PTHrP injection together with collagen-silk scaffold implantation (4-6 weeks post-injury) inhibited terminal differentiation and enhanced chondrogenesis in induced osteochondral defects in rabbits<sup>67</sup>. In contrast, in chondrogenically differentiated BMSC pellets, PTHrP could not diminish the T<sub>3</sub>-induced enhancement of hypertrophy<sup>69</sup>. Despite significant reduction of some hypertrophic markers, the absolute level of expression was still high compared with articular chondrocyte-based cartilage constructs<sup>46</sup>. Furthermore, PTHrP has even been reported to suppress chondrogenic differentiation of BMSC pellets<sup>70</sup>. Noteworthy is the fact that above mentioned studies started the PTHrP treatment at different time points, *i.e.* before or after manifestation of hypertrophy. Thus, the use of PTHrP needs to be further investigated with regard to the inhibition of hypertrophic chondrocyte differentiation, articular cartilage repair, and the generation of stable engineered cartilage from MSCs<sup>4</sup>.

In order to further study how the interaction between 1,25(OH)<sub>2</sub>D<sub>3</sub> and PTHrP influences hypertrophic chondrocyte differentiation, we evaluated whether PTHrP prevents the differentiation of chondrocytes through a VDR-dependent mechanism. For this purpose, the VDR was successfully silenced in PTHrP-supplemented cultures, but the expression of *Pthr1* gene and collagen type X protein was hardly influenced. As it is not possible to discuss these results in the light of earlier reports, we can only postulate that the anti-hypertrophic effect of PTHrP is independent of the VDR. This indicates that 1,25(OH)<sub>2</sub>D<sub>3</sub> and PTHrP individually

influence hypertrophic chondrocyte differentiation and thus may have a synergistic effect in suppressing hypertrophic differentiation.

## Conclusions

Taken together, the data obtained using an integrative approach involving *in vitro* studies with ATDC5 and primary growth plate chondrocytes and *in vivo* studies with Col2-pd2EGFP transgenic mice led us to conclude that there is a functional paracrine feedback loop between PTHrP and 1,25(OH)<sub>2</sub>D<sub>3</sub> in prehypertrophic growth plate chondrocytes. 1,25(OH)<sub>2</sub>D<sub>3</sub> inhibits PTHrP production through a functional binding place (VDRE) in the PTHrP promoter, and PTHrP increases chondrocyte sensitivity to 1,25(OH)<sub>2</sub>D<sub>3</sub> by increasing VDR production. The results of this study furthermore indicate that 1,25(OH)<sub>2</sub>D<sub>3</sub> and PTHrP individually influence chondrocyte hypertrophy and, hence, may have the potential to inhibit undesirable hypertrophic chondrocyte differentiation during cartilage repair or engineering. To our knowledge, the effect of 1,25(OH)<sub>2</sub>D<sub>3</sub> and the synergistic effect of a combination of PTHrP and 1,25(OH)<sub>2</sub>D<sub>3</sub> on MSC-based cartilage regeneration has not yet been evaluated and might provide leads for new strategies to improve the quality of engineered cartilage.

## Acknowledgements

We are grateful to Rob Bleumink for assistance with microscopy, Jan Jaap Stevenhagen (TNO Nutrition and Food Research) for the vitamin D<sub>3</sub> content analysis, and Mr. Hans Vernooij (Utrecht University, the Netherlands) for assistance in statistical analysis. Furthermore, we thank Dr. G. P. Lunstrum (Oregon Health Sciences University), Dr. T. Welting (UMC Maastricht) and Dr. C.Veldhuizen (Dishman, the Netherlands) for their generous gifts.

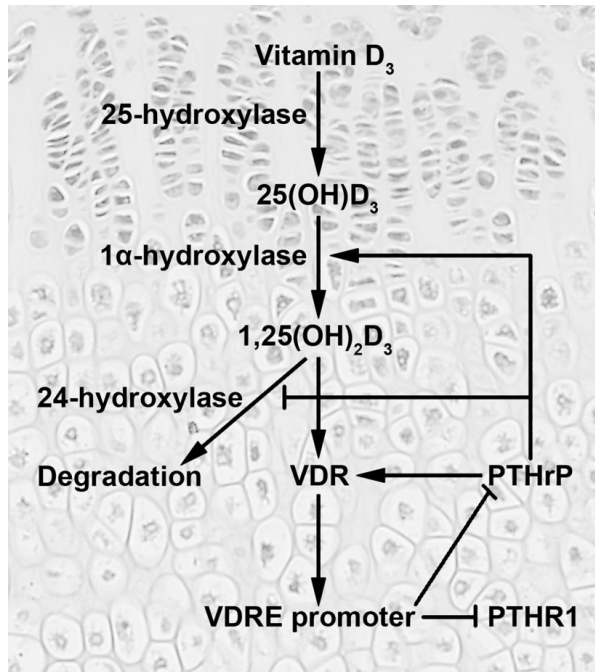
## References

1. Brochhausen C, Lehmann M, Halstenberg S, et al. 2009. Signalling molecules and growth factors for tissue engineering of cartilage-what can we learn from the growth plate? *Journal of tissue engineering and regenerative medicine* 3: 416-29.
2. Nilsson O, Marino R, De Luca F, Phillip M, Baron J. 2005. Endocrine regulation of the growth plate. *Hormone research* 64: 157-65.
3. Dreier R. 2010. Hypertrophic differentiation of chondrocytes in osteoarthritis: The developmental aspect of degenerative joint disorders. *Arthritis Res Ther* 12: 216.
4. Zhang W, Chen J, Zhang S, Ouyang HW. 2012. Inhibitory function of parathyroid hormone-related protein on chondrocyte hypertrophy: The implication for articular cartilage repair. *Arthritis Res Ther* 14: 221.
5. van der Kraan PM, van den Berg WB. 2012. Chondrocyte hypertrophy and osteoarthritis: Role in initiation and progression of cartilage degeneration? *Osteoarthritis Cartilage* 20: 223-232.
6. St-Arnaud R, Naja RP. 2011. Vitamin D metabolism, cartilage and bone fracture repair. *Mol Cell Endocrinol* 347: 48-54.
7. Akeno N, Saikatsu S, Kawane T, Horiuchi N. 1997. Mouse vitamin D-24-hydroxylase: Molecular cloning, tissue distribution, and transcriptional regulation by 1 $\alpha$ ,25-dihydroxyvitamin D<sub>3</sub>. *Endocrinology* 138: 2233-40.
8. Tryfonidou MA, Oosterlaken-Dijksterhuis MA, Mol JA, et al. 2003. 24-hydroxylase: Potential key regulator in hypervitaminosis D<sub>3</sub> in growing dogs. *Am J Physiol Endocrinol Metab* 284: E505-13.
9. Healy KD, Zella JB, Prahl JM, DeLuca HF. 2003. Regulation of the murine renal vitamin D receptor by 1,25-dihydroxyvitamin D<sub>3</sub> and calcium. *Proc Natl Acad Sci U S A* 100: 9733-7.
10. Healy KD, Vanhooke JL, Prahl JM, DeLuca HF. 2005. Parathyroid hormone decreases renal vitamin D receptor expression in vivo. *Proc Natl Acad Sci U S A* 102: 4724-8.
11. Kato Y, Shimazu A, Iwamoto M, et al. 1990. Role of 1,25-dihydroxycholecalciferol in growth-plate cartilage: Inhibition of terminal differentiation of chondrocytes in vitro and in vivo. *Proc Natl Acad Sci U S A* 87: 6522-6526.
12. Klaus G, Meinhold-Heerlein R, Milde P, Ritz E, Mehls O. 1991. Effect of vitamin D on growth cartilage cell proliferation in vitro. *Pediatr Nephrol* 5: 461-466.
13. Drissi H, Pouliot A, Kooloos C, et al. 2002. 1,25-(OH)<sub>2</sub>-vitamin D<sub>3</sub> suppresses the bone-related Runx2/Cbfa1 gene promoter. *Exp Cell Res* 274: 323-333.
14. Hugel U, Weber L, Reichrath J, Mehls O, Klaus G. 2004. Rat growth plate chondrocytes express low levels of 25-hydroxy-1 $\alpha$ -hydroxylase. *J Steroid Biochem Mol Biol* 89-90: 143-7.
15. Naja RP, Dardenne O, Arabian A, St Arnaud R. 2009. Chondrocyte-specific modulation of Cyp27b1 expression supports a role for local synthesis of 1,25-dihydroxyvitamin D<sub>3</sub> in growth plate development. *Endocrinology* 150: 4024-4032.
16. Boyan BD, Sylvia VL, Dean DD, Del Toro F, Schwartz Z. 2002. Differential regulation of growth plate chondrocytes by 1 $\alpha$ ,25-(OH)<sub>2</sub>D<sub>3</sub> and 24R,25-(OH)<sub>2</sub>D<sub>3</sub> involves cell-maturation-specific membrane-receptor-activated phospholipid metabolism. *Crit Rev Oral Biol Med* 13: 143-54.
17. Schipani E, Provot S. 2003. PTHrP, PTH, and the PTH/PTHrP receptor in endochondral bone development. *Birth Defects Res C Embryo Today* 69: 352-62.
18. Kronenberg HM. 2003. Developmental regulation of the growth plate. *Nature* 423: 332-6.
19. Mak KK, Kronenberg HM, Chuang PT, Mackem S, Yang Y. 2008. Indian hedgehog signals independently of PTHrP to promote chondrocyte hypertrophy. *Development* 135: 1947-56.
20. Hirai T, Chagin AS, Kobayashi T, Mackem S, Kronenberg HM. 2011. Parathyroid hormone/parathyroid hormone-related protein receptor signaling is required for maintenance of the growth plate in postnatal life. *Proc Natl Acad Sci U S A* 108: 191-196.
21. Denison TA, Koch CF, Shapiro IM, Schwartz Z, Boyan BD. 2009. Inorganic phosphate modulates responsiveness to 24,25(OH)<sub>2</sub>D<sub>3</sub> in chondrogenic ATDC5 cells. *J Cell Biochem* 107: 155-62.
22. Caron MM, Emans PJ, Surtel DA, et al. 2012. Activation of NF- $\kappa$ B/p65 facilitates early chondrogenic differentiation during endochondral ossification. *PLoS One* 7: e33467.
23. Altaf FM, Hering TM, Kazmi NH, Yoo JU, Johnstone B. 2006. Ascorbate-enhanced chondrogenesis of ATDC5 cells. *European cells & materials* 12: 64-70.
24. Zuker M. 2003. Mfold web server for nucleic acid folding and hybridization prediction. *Nucleic Acids Res* 31: 3406-3415.
25. Altschul SF, Madden TL, Schaffer AA, et al. 1997. Gapped BLAST and PSI-BLAST: A new generation of protein database search programs. *Nucleic Acids Res* 25: 3389-3402.
26. Vandesompele J, De Preter K, Pattyn F, et al. 2002. Accurate normalization of real-time quantitative RT-PCR data by geometric averaging of multiple internal control genes. *Genome Biol* 3: RESEARCH0034.
27. Falzon M. 1996. DNA sequences in the rat parathyroid hormone-related peptide gene responsible for 1,25-dihydroxyvitamin D<sub>3</sub>-mediated transcriptional repression. *Mol Endocrinol* 10: 672-681.
28. Kremer R, Sebag M, Champigny C, et al. 1996. Identification and characterization of 1,25-dihydroxyvitamin D<sub>3</sub>-responsive repressor sequences in the rat parathyroid hormone-related peptide gene. *J Biol Chem* 271: 16310-16316.
29. Toell A, Polly P, Carlberg C. 2000. All natural DR3-type vitamin D response elements show a similar functionality in vitro. *Biochem J* 352 Pt 2: 301-309.
30. Carlberg C. 1995. Mechanisms of nuclear signalling by vitamin D<sub>3</sub>. Interplay with retinoid and thyroid hormone signalling. *Eur J Biochem* 231: 517-527.

31. Zierold C, Darwish HM, DeLuca HF. 1995. Two vitamin D response elements function in the rat 1,25-dihydroxyvitamin D 24-hydroxylase promoter. *J Biol Chem* 270: 1675-1678.
32. Pandit SK, Westendorp B, Nantasanti S, et al. 2012. E2F8 is essential for polyploidization in mammalian cells. *Nat Cell Biol* 14: 1181-1191.
33. Pfaffl MW. 2001. A new mathematical model for relative quantification in real-time RT-PCR. *Nucleic Acids Res* 29: e45.
34. R Core Team. 2012. R: A language and environment for statistical computing. R Foundation for Statistical Computing, Vienna, Austria. ISBN 3-900051-07-0.
35. Tryfonidou MA, Lunstrum GP, Hendriks K, et al. 2011. Novel type II collagen reporter mice: New tool for assessing collagen 2alpha1 expression in vivo and in vitro. *Dev Dyn* 240: 663-673.
36. Bligh EG, Dyer WJ. 1959. A rapid method of total lipid extraction and purification. *Can J Biochem Physiol* 37: 911-917.
37. Reinhardt TA, Horst RL, Orf JW, Hollis BW. 1984. A microassay for 1,25-dihydroxyvitamin D not requiring high performance liquid chromatography: Application to clinical studies. *J Clin Endocrinol Metab* 58: 91-98.
38. Lunstrum GP, Keene DR, Weksler NB, et al. 1999. Chondrocyte differentiation in a rat mesenchymal cell line. *J Histochem Cytochem* 47: 1-6.
39. Armbrecht HJ, Boltz MA. 1991. Expression of 25-hydroxyvitamin D 24-hydroxylase cytochrome P450 in kidney and intestine. effect of 1,25-dihydroxyvitamin D and age. *FEBS Lett* 292: 17-20.
40. Klaus G, Weber L, Rodriguez J, et al. 1998. Interaction of IGF-I and 1 alpha, 25(OH)2D3 on receptor expression and growth stimulation in rat growth plate chondrocytes. *Kidney Int* 53: 1152-1161.
41. Davoodi F, Brenner RV, Evans SR, et al. 1995. Modulation of vitamin D receptor and estrogen receptor by 1,25(OH)2-vitamin D3 in T-47D human breast cancer cells. *J Steroid Biochem Mol Biol* 54: 147-153.
42. Healy KD, Frahm MA, DeLuca HF. 2005. 1,25-dihydroxyvitamin D3 up-regulates the renal vitamin D receptor through indirect gene activation and receptor stabilization. *Arch Biochem Biophys* 433: 466-473.
43. Ikeda K, Lu C, Weir EC, Mangin M, Broadus AE. 1990. Regulation of parathyroid hormone-related peptide gene expression by cycloheximide. *J Biol Chem* 265: 5398-5402.
44. Persengiev SP, Zhu X, Green MR. 2004. Nonspecific, concentration-dependent stimulation and repression of mammalian gene expression by small interfering RNAs (siRNAs). *RNA* 10: 12-18.
45. Donohue MM, Demay MB. 2002. Rickets in VDR null mice is secondary to decreased apoptosis of hypertrophic chondrocytes. *Endocrinology* 143: 3691-3694.
46. Hellingman CA, Koevoet W, van Osch GJ. 2012. Can one generate stable hyaline cartilage from adult mesenchymal stem cells? A developmental approach. *J Tissue Eng Regen Med* 6: e1-e11.
47. Xue Y, Karaplis AC, Hendy GN, Goltzman D, Miao D. 2005. Genetic models show that parathyroid hormone and 1,25-dihydroxyvitamin D3 play distinct and synergistic roles in postnatal mineral ion homeostasis and skeletal development. *Human molecular genetics* 14: 1515-28.
48. Zierold C, Mings JA, DeLuca HF. 2003. Regulation of 25-hydroxyvitamin D3-24-hydroxylase mRNA by 1,25-dihydroxyvitamin D3 and parathyroid hormone. *J Cell Biochem* 88: 234-7.
49. Henry JG, Mitnick M, Dann PR, Stewart AF. 1997. Parathyroid hormone-related protein-(1-36) is biologically active when administered subcutaneously to humans. *J Clin Endocrinol Metab* 82: 900-6.
50. Jongen JW, Willemstein-van Hove EC, van der Meer JM, et al. 1996. Down-regulation of the receptor for parathyroid hormone (PTH) and PTH-related peptide by PTH in primary fetal rat osteoblasts. *J Bone Miner Res* 11: 1218-25.
51. Reinhardt TA, Horst RL. 1990. Parathyroid hormone down-regulates 1,25-dihydroxyvitamin D receptors (VDR) and VDR messenger ribonucleic acid in vitro and blocks homologous up-regulation of VDR in vivo. *Endocrinology* 127: 942-8.
52. Sriussadaporn S, Wong MS, Whitfield JF, Tembe V, Favus MJ. 1995. Structure-function relationship of human parathyroid hormone in the regulation of vitamin D receptor expression in osteoblast-like cells (ROS 17/2.8). *Endocrinology* 136: 3735-42.
53. Klaus G, May T, Hugel U, et al. 1997. Parathyroid hormone prevents 1,25 (OH)2D3 induced down-regulation of the vitamin D receptor in growth plate chondrocytes in vitro. *Kidney Int* 52: 45-51.
54. Pols H, et al. 1988. Heterologous up-regulation of the 1,25-dihydroxyvitamin D3 receptor by parathyroid hormone (PTH) and PTH-like peptide in osteoblast-like cells. *Biochem. Biophys. Res. Commun.* 156: 588-594.
55. Kremer R, Karaplis AC, Henderson J, et al. 1991. Regulation of parathyroid hormone-like peptide in cultured normal human keratinocytes. effect of growth factors and 1,25 dihydroxyvitamin D3 on gene expression and secretion. *J Clin Invest* 87: 884-893.
56. Sepulveda VA, Weigel NL, Falzon M. 2006. Prostate cancer cell type-specific involvement of the VDR and RXR in regulation of the human PTHrP gene via a negative VDRE. *Steroids* 71: 102-115.
57. Chattopadhyay N, Evliyaoglu C, Heese O, et al. 2000. Regulation of secretion of PTHrP by ca(2+)-sensing receptor in human astrocytes, astrocytomas, and meningiomas. *Am J Physiol Cell Physiol* 279: C691-9.
58. Kremer R, Woodworth CD, Goltzman D. 1996. Expression and action of parathyroid hormone-related peptide in human cervical epithelial cells. *Am J Physiol* 271: C164-71.
59. Idelevich A, Kerschmitzki M, Shahar R, Monsonego-Ornan E. 2011. 1,25(OH)2D3 alters growth plate maturation and bone architecture in young rats with normal renal function. *PLoS One* 6: e20772.
60. Boyan BD, Wang L, Wong KL, Jo H, Schwartz Z. 2006. Plasma membrane requirements for 1alpha,25(OH)2D3 dependent PKC signaling in chondrocytes and osteoblasts. *Steroids* 71: 286-290.
61. van der Eerden BC, Karperien M, Wit JM. 2003. Systemic and local regulation of the growth plate. *Endocr Rev* 24: 782-801.

62. Ballock RT, O'Keefe RJ. 2003. Physiology and pathophysiology of the growth plate. *Birth Defects Res C Embryo Today* 69: 123-43.
63. Hoogendam J, Farih-Sips H, van Beek E, et al. 2007. Novel late response genes of PTHrP in chondrocytes. *Horm Res* 67: 159-70.
64. Wealhall RJ. 2009. In vitro regulation of proliferation and differentiation within a postnatal growth plate of the cranial base by parathyroid hormone-related peptide (PTHrP). *J Cell Physiol* 219: 688-697.
65. Weisser J, Riemer S, Schmidl M, et al. 2002. Four distinct chondrocyte populations in the fetal bovine growth plate: Highest expression levels of PTH/PTHrP receptor, indian hedgehog, and MMP-13 in hypertrophic chondrocytes and their suppression by PTH (1-34) and PTHrP (1-40). *Experimental cell research* 279: 1-13.
66. Wang D, Taboas JM, Tuan RS. 2011. PTHrP overexpression partially inhibits a mechanical strain-induced arthritic phenotype in chondrocytes. *Osteoarthritis Cartilage* 19: 213-221.
67. Zhang W, Chen J, Tao J, et al. 2013. The promotion of osteochondral repair by combined intra-articular injection of parathyroid hormone-related protein and implantation of a bi-layer collagen-silk scaffold. *Biomaterials* 34: 6046-6057.
68. Kafienah W, Mistry S, Dickinson SC, et al. 2007. Three-dimensional cartilage tissue engineering using adult stem cells from osteoarthritis patients. *Arthritis Rheum* 56: 177-187.
69. Mueller MB, Fischer M, Zellner J, et al. 2013. Effect of parathyroid hormone-related protein in an in vitro hypertrophy model for mesenchymal stem cell chondrogenesis. *Int Orthop* 37: 945-951.
70. Weiss S, Hennig T, Bock R, Steck E, Richter W. 2010. Impact of growth factors and PTHrP on early and late chondrogenic differentiation of human mesenchymal stem cells. *J Cell Physiol* 223: 84-93.

**Supplementary File 1. The proposed feedback loop between vitamin D<sub>3</sub> (1,25(OH)<sub>2</sub>D<sub>3</sub>) and PTHrP in the growth plate**



We hypothesized that PTHrP increases the sensitivity of growth plate chondrocytes to 1,25(OH)<sub>2</sub>D<sub>3</sub> either by increasing 1,25(OH)<sub>2</sub>D<sub>3</sub> production by upregulating the 1 $\alpha$ -hydroxylase enzyme, and/or decreasing the catabolism of 1,25(OH)<sub>2</sub>D<sub>3</sub> by downregulating the 24-hydroxylase enzyme, and/or by upregulating vitamin D<sub>3</sub> receptor (VDR) expression. Furthermore, we hypothesized that the feedback loop is closed by the inhibition of PTHrP and/or PTHrP receptor (PTHr1) transcription by the binding of 1,25(OH)<sub>2</sub>D<sub>3</sub> to a vitamin D<sub>3</sub> response element (VDRE) located in the promoter region of (one of) these target genes.

## Supplementary File 2. Primers for the used reference and target genes in the *in vivo* and *in vitro* RT-qPCR

Reference gene	Amplicon Size (bp)	Forward and reverse primer 5'-3'	Exon	Tm (°C)	Protocol
<i>Hspca</i>	111	Fw:AATTGCCCGATTAATGTCCTTGA	2	60	2-step
		Rv:TCGTAACGGATTTATCCAGAGC	3		
<i>Rpl32</i>	100	Fw:TTAAGCGAAACTGGCGGAAAC	2/3	64	2-step
		Rv:TTGTTGCTCCATAACCGATG	3		
<i>Rps19</i>	72	Fw:CAGCAGGAGTTCGTCCAGAGC	1	56	3-step
		Rv:CACCCATTCGGGGACTTTCA	1		
<i>Ywhoz</i>	120	Fw:AACAGCTTTCGATGAAGCCAT	5/6	64	2-step
		Rv:TGGGTATCCGATGTCACAAT	6/7		
<i>B2m</i>	194	Fw:TTCTGGTGCTTGCTCACTGA	2	64	2-step
		Rv:CAGTATGTTCCGCTTCCCATTC	4		
<i>Gapdh</i>	165	Fw:GGAGTCCACTGGCGTCTTAC	5	58	2-step
		Rv:GAGGCATTGCTGATGATCTTGAGG	6/7		
<i>Hbms</i>	101	Fw:ACTCTGCTTCGTCGATTG	11	58	2-step
		Rv:AGTTGCCCATCTTTCATCACTG	12/13		
<i>Hprt-1</i>	142	Fw:TCAGTCAACGGGGACATAAA	4	64	2-step
		Rv:GGGGCTGTACTGCTTAACCAG	6		
<i>Sdha</i>	106	Fw:GGAACACTCAAACAGACCT	2	57	3-step
		Rv:CCACCACTGGGTATTGAGTAGAA	3		
<i>Tbp</i>	167	Fw:GGCCTCTCAGAAGCATCACTA	2/3	66	2-step
		Rv:GCCAAGCCTGAGCATAA	3		

Target Gene	Amplicon Size (bp)	Forward and reverse primer 5'-3'	Exon	Tm (°C)	Protocol
<i>lhh</i> <sup>#</sup>	171	Fw:CAGCCTGCCACCTGCTCTTC	1	64	2-step
		Rv:TGGGCTGCTGGTCTGTATGATTGTC	2		
<i>Pthc</i> <sup>#</sup>	164	Fw:AAAGAACTGCGCAAGTTTTTG	2	65	2-step
		Rv:CTTCTCTATCTTCTGACGGGT	3		
<i>Pthrp</i> <sup>#</sup>	172	Fw: GTTCAGCAGTGGAGTGTCT	2	61	2-step
		Rv: GATGGTGGAGGAAGAAACG	3		
<i>Pthr1</i> <sup>#</sup>	125	Fw:CAGGCGCAATGTGACAAGC	5	58	2-step
		Rv:TTTCCGGTGCCTTCTCTTTC	6		
<i>Vdr</i> <sup>#</sup>	165	Fw:ACCCTGGTGACTTTGACCG	3	62	2-step
		Rv:GGCAATCTCCATTGAAGGGG	4		
<i>24-(OH)ase</i> <sup>#</sup>	148	Fw:CTGCCCAATTGACAAAAGGC	1	68	2-step
		Rv:CTCACCGTCGGTCATCAGC	1		
<i>1<math>\alpha</math>-(OH)ase</i> <sup>#</sup>	125	Fw:TCCTGGCTGAACTCTTCTGC	1	68	2-step
		Rv:GGCAACGTAAACTGTGCGAA	2		
<i>Collagen X*</i>	177	Fw:GCAGCATTACGACCCAAGAT	3	60	2-step
		Rv:CCTGAAGCCTGATCCAGGTA	3		
<i>Collagen II</i>	103	Fw: ACCATGAACGGTGGCTTCCA	52	64	2-step
		Rv: AGCCCTCAGTGGACAGTAGA	53		
<i>Collagen IX</i>	352	Fw: CTGTGTGTGCAGTTGTCTGG	2	64	2-step
		Rv: CCAGTGCTTTTCAAGTGTGC	5		

bp: base pairs, Tm: melting temperature.

([http://openwetware.org/wiki/Eccles:QPCR\\_reference\\_genes](http://openwetware.org/wiki/Eccles:QPCR_reference_genes),\*(adapted from <sup>1</sup>),

<sup>#</sup><http://pga.mgh.harvard.edu/primerbank>)

### Reference

1. Lafont J, Jacques C, Le Dreau G, et al. 2005. New target genes for NOV/CCN3 in chondrocytes: TGF-beta2 and type X collagen. *J Bone Miner Res* 20: 2213-2223.

### Supplementary File 3. Details of the primary and secondary antibodies used in the Western blot and immunohistochemistry protocols

#### Western blot

Target protein	Primary Antibody	Secondary Antibody	Washing	Block
1 $\alpha$ -hydroxylase	CYP27B1 (M-100): sc-67260, Santa Cruz Biotechnology (0.2 mg/mL) 1:500	Goat anti-rabbit IgG, R&D systems, HAF008 1:20,000	TBST0.1%	4% ECL Blocking Solution powder, (Amersham ECL™ Advance Western Blotting Detection Kit, RPN2108)
24-hydroxylase	ANTI-CYP24A1, Sigma Prestige Antibodies, HPA022261 (0.4 mg/mL) 1:1000	Goat anti-rabbit IgG, R&D systems, HAF008 1:20,000	TBST0.1%	4% ECL Blocking Solution powder, (Amersham ECL™ Advance Western Blotting Detection Kit, RPN2108)
$\beta$ -actin	Pan Actin Ab-5 (ACTN05), NeoMarkers, MS-1295-P1 (0.2 mg/mL) 1:1000	Goat anti-mouse IgG, R&D Systems, HAF007 1:20,000	TBST0.1%	4% ECL Blocking Solution powder, (Amersham ECL™ Advance Western Blotting Detection Kit, RPN2108)
Col X	pXNC1* (0.36 mg/mL) 1:1000	Goat anti-rabbit IgG, R&D Systems, HAF008 1:20,000	TBST0.1%	4% ECL Blocking Solution powder, (Amersham ECL™ Advance Western Blotting Detection Kit, RPN2108)
PTHrP	PTH-rP (N-19): sc-9680, Santa Cruz Biotechnology (0.2 mg/mL) 1:250	Chicken anti-goat IgG-HRP: sc-2961, Santa Cruz Biotechnology 1:20,000	TBST0.3%	4% ECL Blocking Solution powder, (Amersham ECL™ Advance Western Blotting Detection Kit, RPN2108)
VDR	Anti-VDR, MA1-710, Affinity Bioreagents (1 mg/mL) 1:500	IHC Select® Secondary Goat Anti-Rat IgG, Millipore, 21543 1:10,000	TBST0.3%	1% BSA (Albumin from Bovine Serum, Sigma, A3059)

#### Immunohistochemistry

Name	Manufacturer	Origin	Ab Ig fraction	Antigen retrieval	Block	Dilution 1 <sup>st</sup> Ab	2 <sup>nd</sup> Ab
Col X, clone PXNC2 (0.36 mg/mL)	Greg Lunstrum	Mouse	Pab rabbit IgG	Hyaluronidase 37°C, 30 min	1:10 goat serum / PBST	1:800 in PBST	EnVision K4011
VDR MAB 1360, clone 9A7 (1 mg/mL)	Millipore	human and chicken 89-105	Mab rat IgG2b	Citrate, 70°C, 60 min	1:5 goat serum / PBST	1:600 in 1%BSA/PBST	RTU 21543, Chemicon
PTHLP, PC09 (0.1 mg/mL)	Calbiochem	human recombinant 34-53	Pab rabbit IgG	Trypsin 37°C, 30 min	1:10 goat serum / PBST	1:75 in 1%BSA/ PBST	EnVision K4011
PTH/PTHrP-R (E-17), sc-12777 (0.2 mg/mL)	Santa Cruz	N-terminus human	Pab goat IgG	Citrate, 70°C, 60 min	Donkey serum	1:100 in serum block	sc-2053

\* The pXNC1 antibody against collagen type X was kindly provided by Dr. Gregory P. Lunstrum (Lunstrum GP, Keene DR, Weksler NB, et al. 1999. Chondrocyte differentiation in a rat mesenchymal cell line. J Histochem Cytochem 47: 1-6) Mab: monoclonal antibody, Pab: polyclonal antibody, Hyaluronidase: bovine hyaluronidase 450 IU/mg, 4 mg/mL adjust to pH 5 with 0.1M HCl, Citrate buffer: 10mM citrate, buffer adjusted to pH 6, Trypsin: 0.1% in 0.1% CaCl<sub>2</sub> working solution adjusted to pH 7.8, PBST: Phosphate buffered saline 0.1% Tween-20.

## Supplementary File 4. Chromatin immunoprecipitation (ChIP) analysis - VDRE locations in the PTHrP promoter and primer details

VDRE locations in the PTHrP gene of rats and mice, upstream from the transcription start site (TSS) of the PTHrP promoter <sup>1,2</sup>

PTHrP DRE	Species	Location upstream from TSS
VDRE1	Rat	1403 GGGTGGAGAGGGGTGA 1387
	Mouse	1128 GGGAGGGGAGGGGTGA 1111
VDRE2	Rat	1076 AGTTACTCAGTGAA 1061
	Mouse	783 TGGGCACTCAGTGAA 768

Primer sequences of the used target genes in the ChIP analysis

Target	Amplification Size (bp)	Forward and reverse primer 5'-3'	Tm (°C)
PTHrP VDRE1	147	Fw: CAAGGAAAGAGACAAGGGC	57
		Rv: TGATGCTCTACAGACTTCTGG	
PTHrP VDRE2	184	Fw: CACCTCTAGACCCACAATCAG	54.5
		Rv: GATCACAGACGACCTGGA	
PTHrP negative control	150	Fw: ATTTCTGAATGAGACTGACAGG	61.5
		Rv: AGAGAAACTATGGACAATGAGG	
PTHR1 VDRE1	144	Fw: AAACCTCATTCCCATCACG	59
		Rv: CTACAAGACTCGGGTTCAG	
PTHR1 VDRE2	108	Fw: ATCGAAGAACCAAGGGATGC	62
		Rv: TCTGGACCTTCGTTGGAC	
PTHR1 VDRE combination	202	Fw: GGAGGATAACATGATGGAGGG	59
		Rv: TCTGGACCTTCGTTGGAC	
PTHR1 negative control	150	Fw: CCCAGAGACCCATGCTGATCTA	61.5
		Rv: GCAGCAAGTTAAGGTGCCAGAGC	
24-OHase VDRE	151	Fw: GTCCTCAGGAACCTTGC	63
		Rv: TAACCTGAGAAAGCGAG	

Forward (Fw) and Reverse (Rv) primer pairs used for DNA analysis of the PTHrP, PTHR1 and 24-hydroxylase promoter. bp: base pairs, Tm: melting temperature, TSS: transcription start site, VDRE: vitamin D response element.

### References

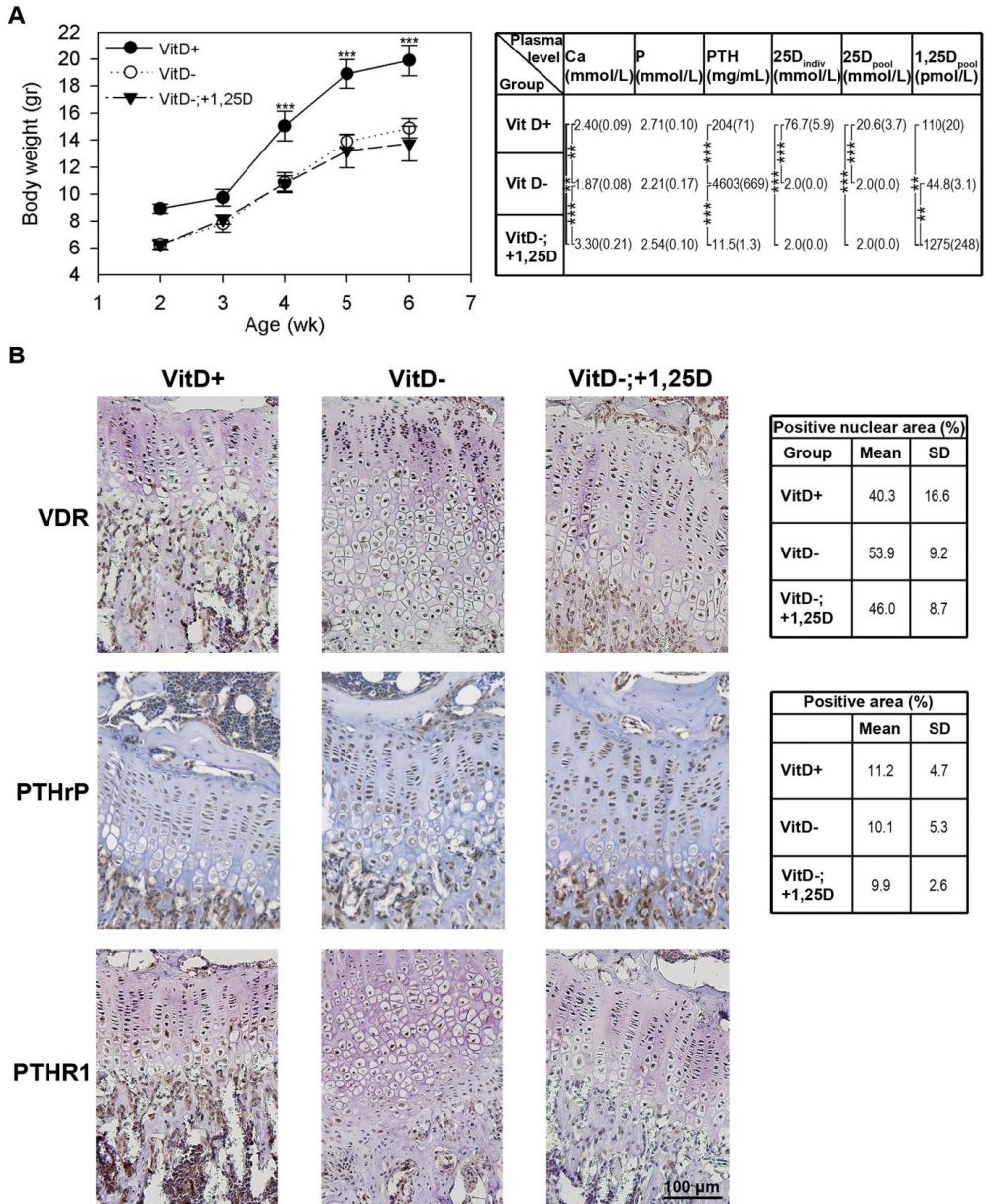
- Falzon M. 1996. DNA sequences in the rat parathyroid hormone-related peptide gene responsible for 1,25-dihydroxyvitamin D3-mediated transcriptional repression. *Mol Endocrinol* 10: 672-681.
- Kremer R, Sebag M, Champigny C, et al. 1996. Identification and characterization of 1,25-dihydroxyvitamin D3-responsive repressor sequences in the rat parathyroid hormone-related peptide gene. *J Biol Chem* 271: 16310-16316.

**Supplementary File 5. Detailed protocol of the ChIP assay**

ATDC5 cells were seeded in Falcon primary petri dishes (BD Biosciences, 353803) at a density of 6,400 cells/cm<sup>2</sup> and differentiated for 7 days. On differentiation day 7, each petri dish contained approximately 22\*10<sup>6</sup> cells. Cells were treated with 10<sup>-8</sup> M 1,25(OH)<sub>2</sub>D<sub>3</sub> for 1, 4, and 24 hours. At these time points, protein and DNA were cross-linked by adding 37% formaldehyde solution (Merck, 104003) in a final concentration of 1%; culture dishes were incubated for 10 minutes at room temperature on a swirl plate. The reaction was stopped by the addition of glycine in a final concentration of 0.125 M and dishes were incubated for 5 minutes. Cells were washed with cold Hanks (Sigma, D8537) twice and scraped into 1 mL SDS lysis buffer (1% SDS, 10 mM EDTA, 50 mM Tris-HCl pH 8.1) containing a protease inhibitor cocktail (Roche, 11873580001). Thereafter, cells were sonicated on a Soniprep 150 MSE for 10 seconds at power level 24-26 in order to homogenize the lysate. Then 500 µL of the lysate was diluted with 500 µL SDS lysis buffer and further sonicated eleven times with 10-second pulses for 50 seconds at power level 24-26. After centrifugation for 10 minutes (4 °C, 16.1 rpm), aliquots of 150 µL were stored at -20 °C. Each aliquot was brought up to 1.5 mL by adding ChIP dilution buffer (0.01% SDS, 1.1% Triton X 100, 1.2 mM EDTA, 167 mM NaCl, 16.7 Tris-HCl, pH 8.1) containing a protease inhibitor cocktail. The chromatin was precleared with 30 µg Protein G Agarose beads (92590, Millipore) per immunoprecipitation, and incubated for 1 hour at 4 °C with rotation. Beads were removed by centrifugation for 3 minutes (6.6 rpm). Input controls were collected at this time and stored at 4°C. Then 2 µg of rat anti-VDR (Affinity Bioreagents, MA1-710) and rat IgG (Chemicon, IgG2b, CBL606) antibodies were added to each pre-cleared sample and samples were rotated overnight at 4°C. Antibodies were pelleted by the addition of 30 µg protein G beads and rotation for 1 hour at 4°C. The bead-antibody-protein-DNA complexes were pelleted by cooled centrifugation (6.6 rpm) for 2 minutes and washed by 5 minute rotation with 1 mL of the following wash buffers: once with low salt buffer (0.1% SDS, 1% Triton X 100, 2 mM EDTA, 20 mM Tris-HCl pH 8.1, 150 mM NaCl); once with high salt buffer (1% SDS, 1% Triton X 100, 2 mM EDTA, 20 mM Tris-HCl pH 8.1, 500 mM NaCl); once with LiCl buffer (0.25 M LiCl, 1% NP40, 1% deoxycholate, 1 mM EDTA, 10 mM Tris-HCl pH 8.1), and twice with TE buffer (10 mM Tris-HCl pH 8.1, 1 mM EDTA). The samples were cooled and centrifuged after each washing step for 1 minute (6.6 rpm). Beads were eluted by two times after a 15-minute incubation at room temperature in 200 µL elution buffer (1% SDS, 0.1 M NaHCO<sub>3</sub>). Protein-DNA crosslinking was reversed by incubation of eluates with 0.19 M NaCl final concentration at 65°C overnight. RNA was digested by adding 1 µL RNase A to each sample and incubation for 30 minutes at 37°C. Thereafter 4 µL 0.5 M EDTA, 8 µL 1 M Tris pH 8.1, and 1 µL proteinase K were added to each sample and samples were incubated for 2 hours at 45°C. DNA purification (Qiagen PCR cleanup kit, 28106) was performed according to manufacturer's instruction. Eluates were used as templates in the real-time qPCR.

ChIP experiments were analyzed with real-time qPCR in an iCycler iQ real-time PCR detection system (Bio-Rad, Veenendaal, the Netherlands). Two microliters of purified DNA was used, to which 13 µL SYBR green supermix (Bio-Rad, Veenendaal, the Netherlands, IQ 10003253), 12 µL MQ and 1.2 µL forward and reverse primer were added. As a normalization method, 'signal over background' was used. First, the value of input minus sample was calculated, and the power of two was calculated for this value. Thereafter, the correction for the input percentage was performed. Lastly, the difference between normalization control (IgG) and antibody were calculated, representing the n-fold enrichment.

**Supplementary File 6. Biochemistry and immunohistochemistry of the *in vivo* studies with transgenic Col2-pd2EGFP reporter mice**



(a) From left to right: Significantly increased body weight in VitD+ mice compared with VitD- mice from 4 weeks of age onward. Plasma levels of Ca, P, PTH (all individual), 25(OH)D<sub>3</sub> (individual and pooled), and 1,25(OH)<sub>2</sub>D<sub>3</sub> (pooled) for the three different groups revealing the typical signs of rickets with hypocalcemia and hyperparathyroidism in Vitamin D<sub>3</sub> deficient mice (VitD-) compared with controls (VitD+). Supplementation with 1,25(OH)<sub>2</sub>D<sub>3</sub> (VitD-;+1,25D) reversed the vitamin D<sub>3</sub>-deficient phenotype. \*:p<0.05, \*\*:p<0.01, \*\*\*:p<0.001. (b) Immunohistochemical staining for VDR, PTHrP, and PTHR1 in VitD+, VitD-, and VitD-;+1,25D mice quantified with the aid of Image J.

**IHH and PTHrP are implicated in degeneration of the intervertebral disc**

Frances C. Bach<sup>1</sup>, Kim M. de Rooij<sup>1</sup>, Joseph W. Snuggs<sup>2</sup>, Willem A.M. de Jong<sup>1</sup>, Ying Zhang<sup>3</sup>, Laura B. Creemers<sup>4</sup>, Danny Chan<sup>3</sup>, Christine Le Maitre<sup>2</sup>, Marianna A. Tryfonidou<sup>1\*</sup>

<sup>1</sup> Department of Clinical Sciences of Companion Animals, Faculty of Veterinary Medicine, Utrecht University, Utrecht, the Netherlands

<sup>2</sup> Biomolecular Sciences Research Centre, Sheffield Hallam University, Sheffield, United Kingdom

<sup>3</sup> School of Biomedical Sciences, The University of Hong Kong, Pokfulam, Hong Kong, China

<sup>4</sup> Department of Orthopedics, University Medical Center Utrecht, Utrecht, the Netherlands

*Submitted to Oncotarget (revisions)*

## Abstract

Humans and dogs experience back pain related to intervertebral disc (IVD) degeneration. Parathyroid hormone related protein (PTHrP) and Indian hedgehog (IHH) play a role in chondrocyte (hypertrophic) differentiation and degeneration, but their role in IVD degeneration and calcification is unknown. A better understanding of their involvement may provide therapeutic clues. Therefore, this study aimed to explore their expression in the postnatal IVD during the maturation and degeneration phase. IHH, PTHrP and related receptor expression were studied during IVD maturation, defined as notochordal cell (NC) to chondrocyte-like cell (CLC) transition: *i.e.* in healthy and matured canine IVDs, canine NCs that lost their phenotype during culture, and caveolin-1 null IVDs known to undergo accelerated IVD maturation. Additionally, their expression was determined during IVD degeneration: in matured until severely degenerated canine and human IVDs. Correlations were determined between IHH, PTHrP, and related receptor expression and calcification levels. Lastly, the effect of IHH and PTHrP on CLCs was determined *in vitro*. The expression of IHH, PTHrP and related receptors decreased during IVD maturation, while their expression and calcium deposition increased during IVD degeneration. IHH and PTHrP receptor immunopositivity was increased in nucleus pulposus tissue with abundant calcification versus no/low calcification. Additionally, PTHrP decreased glycosaminoglycan production in 3D-cultured CLCs, while IHH facilitated calcification in 2D-cultured CLCs. In conclusion, IHH and PTHrP expression is present in healthy and degenerated IVDs. IHH had the propensity to induce calcification in CLCs from degenerated IVDs, indicating that inhibiting IHH signaling could be a therapeutic approach to inhibit calcification during IVD degeneration.

## Introduction

Low back pain is a major health problem, since over eighty percent of the human population experiences this during their lifetime<sup>1</sup>. An important cause for low back pain is degeneration of the intervertebral disc (IVD)<sup>2</sup>. The IVD, situated between the vertebral bodies, provides flexibility to the spine. The IVD consists of an inner gelatinous nucleus pulposus (NP) and outer fibrous annulus fibrosus. During IVD maturation, large, vacuolated notochordal cells (NCs) are replaced by smaller, non-vacuolated chondrocyte-like cells (CLCs), a process that in the human NP has come to near completion already at birth<sup>3</sup>. The healthy NP contains a high glycosaminoglycan (GAG) content that attracts water, whereas during IVD degeneration, the NP GAG and water content decreases and denatured collagen content increases<sup>4</sup>. These adverse changes result in formation of a more rigid extracellular matrix (ECM), NP dehydration, and decreased disc height. Additionally, hypertrophic differentiation and calcification can occur in the degenerated IVD<sup>5</sup>. The avascular IVD exhibits inadequate repair, leading to a vicious circle. Hereby, the IVD weakens and encounters increased vulnerability to damage by physiologic loading. Consequently, loss of mechanical function, traumatic damage, and pain develops<sup>6</sup>.

Current treatments for IVD disease are primarily aimed at relieving symptoms. Therefore, there is an urgent need for agents stimulating biological repair of the IVD<sup>7</sup>. To develop such treatments, further knowledge of the pathogenesis of IVD degeneration is required. Numerous signaling pathways have been proposed to play a role in IVD degeneration, including: Wnt/ $\beta$ -catenin; Sonic hedgehog (SHH); and Hypoxia-inducible factor signaling<sup>8-10</sup>. However, the role of the Parathyroid hormone-related protein (PTHrP) and Indian hedgehog (IHH) pathway in the postnatal IVD remains elusive. It is known that IHH and PTHrP form a growth-restraining feedback loop during endochondral ossification in the embryonic and early postnatal growth plate, in which PTHrP inhibits IHH and IHH stimulates PTHrP production<sup>11-13</sup>. IHH, produced by prehypertrophic growth plate chondrocytes, promotes proliferation and differentiation and stimulates calcification independently from PTHrP<sup>14</sup>. Together with SHH, IHH belongs to the hedgehog family, which plays a crucial role in embryonic development. In the absence of hedgehogs, their receptor Patched (PTCH) interacts with transmembrane protein Smoothed (SMO), thereby inhibiting downstream hedgehog signaling. In the presence of hedgehog proteins, SMO is released upon their binding to PTCH. This activates downstream hedgehog signaling, including activated target gene expression through three GLI transcription factors. GLI1 functions as transcriptional activator, whereas GLI2 and GLI3 act as either positive or negative regulators, depending on posttranscriptional and translational processing<sup>11, 12, 14-16</sup>. PTHrP, produced by periarticular chondrocytes, prevents proliferative cells from leaving the proliferating pool. In this way, hypertrophic chondrocyte differentiation and IHH production is delayed. PTHrP has an auto- and paracrine function in various tissues and resembles parathyroid hormone (PTH) in genetic sequence and structure. In addition, PTHrP and PTH share their receptor: PTHR1<sup>12, 17, 18</sup>.

IHH and PTHrP are extensively studied in joint cartilage, but their function in the postnatal IVD is largely unexplored. Previous work indicated a positive correlation between IHH expression and osteoarthritis (OA)<sup>19-22</sup>, a process resembling IVD degeneration<sup>5</sup>. Furthermore, IHH promotes chondrocyte hypertrophy and calcification<sup>19</sup>, which also occurs

during IVD degeneration<sup>5</sup>. In line with this, disrupted IHH signaling prevented hypertrophic chondrocyte differentiation and osteophyte formation in OA cartilage<sup>23, 24</sup>, indicating that inhibition of IHH signaling could be a therapeutic approach to prevent or retard degeneration. Additionally, previous research demonstrated that PTHrP expression was decreased in OA chondrocytes<sup>25</sup>, that PTHrP suppressed chondrocyte mineralization and hypertrophy<sup>26</sup> and that PTH inhibited progression of OA<sup>27</sup>.

Only scarce and fragmented information is available regarding the role of PTHrP and IHH in the IVD. Previous work indicates that PTCH<sup>10, 28</sup> and SHH<sup>10, 29, 30</sup> are expressed in the postnatal murine IVD, whereas PTHrP was absent<sup>10</sup>. Furthermore, PTH has been shown to increase *ACAN* and *COL2A1* expression in ovariectomized rat NPs<sup>31</sup>. In addition, it partially recovered NC numbers compared with non-treated CLC-containing ovariectomized rat NPs<sup>31</sup>. In line with this, PTH also increased collagen type II expression and suppressed calcification in degenerated human CLCs<sup>32</sup>.

Altogether, results from previous research imply that IHH and PTHrP could potentially be targets for IVD repair, but that their effect has not been determined on postnatal IVDs that can suffer from clinical IVD disease. Therefore, in the current study, the expression and possible role of PTHrP and IHH in the IVD was determined in two different phases: during the transition from NCs to CLCs (maturation phase) and in matured IVDs, to determine the effects of degeneration (degeneration phase). The setup of the current study is presented in Figure 1, and a schematic overview of the results in Table 2.

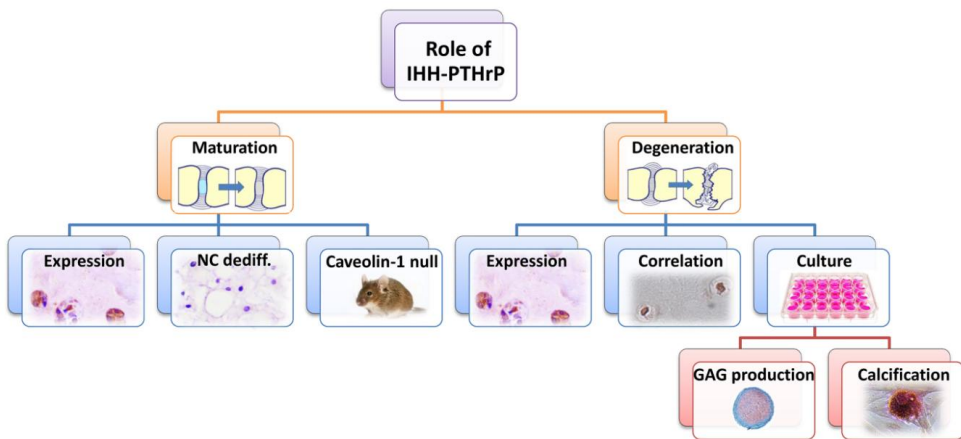


**Figure 1. Schematic setup of the study.** The role of Indian hedgehog (IHH) and Parathyroid hormone related protein (PTHrP) in the intervertebral disc (IVD) was determined in two different phases: during the transition from vacuolated notochordal cells (NCs) to chondrocyte-like cells (CLCs) (maturation phase) and in matured until severely degenerated IVDs (degeneration phase). IHH- and PTHrP-related protein expression was determined using immunohistochemistry in canine and human NPs from healthy until severely degenerated IVDs. To further elucidate the expression of IHH and PTHrP in IVD maturation, IHH- and PTHrP-related gene and protein expression was studied in NCs from healthy canine IVDs that dedifferentiated during monolayer culture and in murine WT and caveolin-1 null NPs. Both models are representative for the transition of NCs towards CLCs (maturation phase). To determine the role of IHH and PTHrP in IVD degeneration, the correlation between PTHrP and IHH (receptor) expression and calcification was determined in surgically removed human NP samples across the range of histological IVD degeneration. Lastly, the effect of IHH and PTHrP was determined on GAG production and calcification of canine CLCs *in vitro*.

## Materials and Methods

### Study design

In this study, IHH, PTHrP and related receptor expression and function was determined in two different phases: during the transition from NCs to CLCs (maturation phase) and in matured until severely degenerated IVDs (degeneration phase) (Figure 1). To determine the expression of IHH and PTHrP in IVD maturation, IHH- and PTHrP-related gene and protein expression was studied in healthy-matured canine IVDs, NCs from healthy NCD canine IVDs, and in murine WT and caveolin-1 null NPs. The canine NCs lose their typical vacuolated phenotype and characteristics during monolayer culture<sup>33</sup>. Caveolin-1 null mice are known to undergo accelerated IVD maturation: the large, vacuolated NCs are replaced by smaller, non-vacuolated chondrocyte- and fibroblast-like cells<sup>34</sup>. Therefore, both models are representative for the transition of NCs towards CLCs, which occurs during IVD maturation.

To determine the role of IHH and PTHrP in IVD degeneration, IHH- and PTHrP-related protein expression was studied in matured until severely degenerated canine and human IVDs. Additionally, the correlation between IHH, PTHrP and related receptor expression and calcification was determined in surgically removed human NP tissue across the range of histological IVD degeneration. Lastly, the effect of IHH and PTHrP was determined on chondrogenic matrix deposition and calcification of canine CLCs from degenerated IVDs *in vitro*.

### IHH-PTHrP expression in healthy until severely degenerated canine and human NPs

IHH- and PTHrP-related immunopositivity was determined in canine and human NPs from healthy until severely degenerated (Thompson score I-V) IVDs. All dogs had been euthanized in unrelated experiments, approved by the Utrecht University Animal Ethics Committee, or were client-owned dogs that were submitted for necropsy to the Faculty of Veterinary Medicine, Utrecht University. Thirty-seven thoracolumbar or lumbosacral IVDs from dogs of various breeds (5 CD, 11 NCD), age (1-16 years) and gender (11 female, 5 male) were studied (Supplementary File 1). The samples were divided into five different grades of degeneration based on gross morphology of midsagittal sections (Thompson grading): score I is healthy and score V represents end stage degeneration<sup>35,36</sup>. IVD donors were chosen based on equal representation of all Thompson scores ( $n=8-7-8-7-7$  for grade I-V, respectively). Tissue was obtained within 24 h after death, and IVD slices were decalcified in 0.5M EDTA (pH 7.0) for three months as previously described<sup>37</sup>. Sections were dehydrated and rinsed in xylene before being embedded in paraffin wax.

Human IVDs were obtained during standard postmortem diagnostics. The L2-L5 part of the spine was collected (<48 hours after death), as approved by the scientific committee of the Pathology department (University Medical Centre Utrecht (UMCU)). Anonymous use of redundant tissue for research purposes is a standard treatment agreement with UMCU patients (Local Medical Ethical Committee number 12-364). IVDs were used in line with the code 'Proper Secondary Use of Human Tissue', installed by the Federation of Biomedical Scientific Societies. Also the human IVDs were chosen based on approximately equal representation of all Thompson scores ( $n=5-4-4-5-4$  for grade I-V, respectively, Supplementary File 1). IVD tissues were decalcified in Kristensen's solution (50% formic acid

and 68 g/L sodium formate) in a microwave oven at 150 W and 50°C for 6 h as previously described<sup>38, 39</sup>. Sections were dehydrated and rinsed in xylene before embedding in paraffin wax and after an H&E staining histologically graded<sup>40, 41</sup>. Briefly, sections were scored numerically between 0 and 12 based on the presence of cell clusters, fissures, loss of demarcation and haematoxophilia (indicating reduced proteoglycan content).

For both canine and human samples, 5 µm midsagittal sections were mounted on Microscope KP+ slides (KP-3056, Klinipath) and immunohistochemically stained for IHH, PTCH, SMO, PTHrP and PTHR1 (Table 1) using the ImmunoCruz™ goat LSAB Staining System (sc-2053, Santa Cruz) with citrate buffer (10 mM, pH 6) antigen retrieval (30 minutes, 70°C). Negative control sections stained with blocking peptides for the specific target proteins did not show staining. End plates of each section served as internal positive control. Raw images were made with a Leica DFC420C digital camera (Leica Microsystems) mounted to a BX60 microscope (Olympus) and Leica Application Suite (V4.2) software package. (Positively stained) cell numbers in each NP were manually counted. Adobe Photoshop CS6 was used to manually count (positively stained) cell numbers in four (canine) or six (human) randomly selected NP areas per IVD section as described previously<sup>34</sup>. The mean percentage of cells that stained positive over the total number of cells present (ratio) was determined per Thompson score for every target protein. Immunopositivity thus indicates ratio of positive cells, not intensity of the staining.

**Table 1. Details of the immunohistochemistry protocols**

Target protein	Manufacturer	Concentration Ab murine	1 <sup>st</sup> Concentration 1 <sup>st</sup> Ab canine	Concentration 1 <sup>st</sup> Ab human
IHH	Santa cruz, sc-1196	2 µg/mL	2 µg/mL	4 µg/mL
PTCH	Santa cruz, sc-6149	4 µg/mL	4 µg/mL	4 µg/mL
SMO	Santa cruz, sc-6366	8 µg/mL	4 µg/mL	8 µg/mL
PTHrP	Santa cruz, sc-9680	8 µg/mL	4 µg/mL	8 µg/mL
PTHR1	Santa cruz, sc-12777	8 µg/mL	10 µg/mL	10 µg/mL
Collagen type X	2031501005, Quartett	Not done	1:50 (actual concentration not known)	Not done

Antibodies for target proteins and concentrations that were applied per species.

Only in young canine donors with healthy (Thompson score I) IVDs, PTHrP was highly expressed, whereas this was considerably lower in older canine donors with healthy IVDs. This indicates that PTHrP was present in NCs from healthy canine IVDs, but that its expression decreased during ageing. To confirm this, Thompson score I IVDs of younger canine and human donors were also studied. NPs from 8 canine (1 day - 6 weeks of age) and 12 human (21 weeks of gestation - 3 months of age, postnatal) donors were fixed in 4% neutral buffered formaldehyde, embedded in paraffin, and 5 µm sections were mounted. PTHrP IHC was performed as described previously (Table 1).

### IHH-PTHrP expression in cultured NC clusters

To study IHH and PTHrP in IVD maturation, IHH- and PTHrP-related gene expression was studied in NCs from healthy NCD canine IVDs that lost their typical vacuolated phenotype and characteristics during monolayer culture<sup>33</sup>. This model thus also represents the transition of NCs towards CLCs (IVD maturation).

All dogs had been euthanized in unrelated experiments, approved by the Utrecht University Animal Ethics Committee. The cervical and thoracolumbar spines were collected from 8 NCD (mixed breed, 13-60 months). NC clusters were obtained as described previously<sup>33</sup> and cultured in their original cluster-like formation. To imitate NC dedifferentiation, the NC clusters from each donor were plated in 6-wells and cultured for 4 days at 37°C, 5% CO<sub>2</sub>, 21% O<sub>2</sub> in DMEM-F12 (10565018, Gibco), 10% Fetal Bovine Serum (FBS, 16000-044, Life Technologies) and 1% penicillin/streptomycin (P/S, P11-010, PAA Laboratories). During monolayer culture, the NCs lost their specific phenotype and marker (*brachyury*, *cytokeratin 8*) expression<sup>33</sup>. Samples for RT-qPCR were collected at day 0, 2, and 4. RNA was isolated and cDNA was generated from the cultured NCs (*n*=8) and native NPs (*n*=6) as described previously<sup>33</sup>. RT-qPCR for Indian hedgehog (*IHH*), Sonic hedgehog (*SHH*), Patched (*PTCH*), Smoothed (*SMO*), Parathyroid hormone-related protein (*PTHrP*), Parathyroid hormone receptor-1 (*PTHr1*) and transcription factors *GLI1*, *GLI2*, and *GLI3* was performed and analyzed as described previously<sup>3</sup> (Supplementary File 2).

### IHH-PTHrP expression in murine caveolin-1 null and WT NPs

To further study IHH and PTHrP during IVD maturation, IHH- and PTHrP-related protein expression was studied in murine WT and caveolin-1 null NPs. Caveolin-1 null mice are known to undergo accelerated IVD maturation: the large, vacuolated NCs are replaced by smaller, non-vacuolated chondrocyte- and fibroblast-like cells<sup>34</sup>. As such, this model is representative for the transition of NC towards CLCs, which occurs during IVD maturation. Experimental procedures were performed according to guidelines of the Utrecht University Ethics Committee (DEC 2008.III.01.001). Lumbar spines of 1.5-, 3-, and 6-month-old caveolin-1 null (*Cav<sup>tm1Mls</sup>*, JAX®, the Jackson Laboratory) and WT mice (B6129SF2, JAX®) were fixed in 4% neutral buffered formaldehyde, decalcified (7 days, 10% EDTA) and embedded in paraffin. Five µm midsagittal sections were immunohistochemically stained as described for the canine and human IVDs, with adjusted antibody dilution (Table 1). All IVDs were evaluated, yielding 3-4 IVDs per lumbar spine. (Positively stained) cell numbers in each NP were manually counted as described previously. The percentage of positively stained cells over the total number of cells present was determined for every NP.

### Correlation between PTHrP-IHH expression and calcification in human NPs

Surgically removed NP tissue was fixed in 10% v/v neutral buffered formalin and processed to paraffin wax. Following embedding, 4 µm sections were cut and histologically graded using the previously published criteria<sup>40, 41</sup>. To determine the frequency of calcium deposition in the NP of human IVDs, initial work investigated Alizarin Red S staining on 113 human NP samples with different grades of degeneration (Supplementary File 1). Calcium deposition was then manually scored on a grade of 0-3 where 0 was no calcium deposits present and 3 was intense calcium (Figure 6a). To enable comparison of low versus high calcium deposition, percentage of samples from non-degenerate, mid-grade degenerate, and high grade degenerate discs were then determined for those scoring ≤1 (low) and >1

(high) calcium staining intensity. Thereafter, the correlation between PTHrP, IHH and related receptor expression (ratio) and calcification staining intensity was determined in a smaller subset of 30 surgically removed human NP samples with different degeneration grades and calcium deposition (Supplementary File 1). IHH, PTCH, SMO, PTHrP and PTHR1 IHC and Alizarin Red S staining<sup>42</sup> was performed as described previously. Since we observed a trend towards higher IHH immunopositivity with high NP calcium levels ( $p=0.14$ , medium effect size), the sample size was increased ( $n=56$ ). Thereafter, the trend was confirmed with statistical significance ( $p=0.003$ , large effect size).

### **The effects of IHH and PTHrP on canine CLCs *in vitro***

To further elucidate the role of IHH and PTHrP in the IVD degeneration phase, the effect of IHH and PTHrP was determined on chondrogenic matrix deposition, hypertrophic differentiation and calcification of CLCs from degenerated IVDs *in vitro*.

#### *The effect of IHH and PTHrP on chondrogenic matrix production and target gene expression*

CLCs from six canine donors (Beagles, 2-6 years of age) were obtained from degenerated IVDs (Thompson score II-III) and expanded as described previously<sup>3</sup> in expansion medium containing hgDMEM+Glutamax (31966, Invitrogen) with 10% FBS, 1% P/S, 0.1 mM Ascorbic acid 2-phosphate (Asap, A8960, Sigma-Aldrich),  $10^{-8}$  M dexamethasone (AD1756, Sigma-Aldrich) and 1 ng/mL bFGF (PHP105, AbD Serotec). Passage 2 CLCs were plated in 96-well plates (7007, Corning Life Sciences) at 5% O<sub>2</sub>, 5% CO<sub>2</sub>, 37°C at a density of 35,000 cells/well in 50 µL basal culture medium, composed of hgDMEM+Glutamax, 1% P/S, 1% ITS+ premix (354352, Corning Life Sciences), 0.04 mg/mL L-proline (P5607, Sigma-Aldrich), 0.1 mM Asap, and 1.25 mg/mL bovine serum albumin (A9418, Sigma-Aldrich). Micro-aggregate formation was induced by centrifuging the 96-well plates at 50g for 5 minutes. After one day, basal culture medium was replaced by basal culture medium (control) supplemented with/without 0.1 or 1 µg/mL IHH (1705-HH, R&D Systems) or  $10^{-7}$  or  $10^{-8}$  M PTHrP (PTH-Related Protein (1-34) amide, H-9095, Bachem). Concentrations were chosen based on previous research<sup>17, 43</sup>. After 24 hours of treatment, micro-aggregates were collected for RT-qPCR (Supplementary File 2; *IHH*, *PTCH*, *SMO*, *PTHrP*, *PTHR1*). RNA isolation, cDNA synthesis, and RT-qPCR was performed as described previously<sup>3</sup>. After two weeks, micro-aggregates were collected for histology, DNA and GAG content measurements (*in duplo*) as described previously<sup>3</sup>. The micro-aggregates' GAG content and release in culture medium were measured using a dimethyl methylene blue assay<sup>44</sup>. The DNA content was measured using the Qubit® dsDNA High Sensitivity Assay Kit (Q32851, Invitrogen). For histology, micro-aggregates were fixed in 4% neutral buffered formaldehyde for 24 hours and embedded in alginate and processed in paraffin. Five µm sections were mounted and Safranin O/Fast Green staining was performed as described previously<sup>3</sup>.

#### *Induction of hypertrophic differentiation and calcification*

To test the effect of PTHrP and IHH on hypertrophic differentiation and calcification, hypertrophy needed to be induced in CLCs. Several approaches were tested. First, a previously described setup for hypertrophic MSC differentiation was followed<sup>45</sup>. Passage 2 canine CLCs from 6 Beagles with degenerated IVDs (2-6 years of age, Thompson score II-III) were cultured in micro-aggregates subjected to basal culture medium supplemented with 10 ng/mL TGF-β<sub>1</sub> (R&D Systems, 240-B-010) for one week, followed by hypertrophic induction medium (consisting of hgDMEM+Glutamax, 1% P/S, 1% ITS+ premix, 0.1 mM Asap,  $10^{-9}$  M

dexamethasone, 10 mM  $\beta$ -glycerolphosphate (G9422, Sigma-Aldrich), and 1 nM 3,3',5-triiodo-L-thyronine (T3, T6397, Sigma-Aldrich)) for three weeks. Control micro-aggregates only received basal culture medium with 10 ng/mL TGF- $\beta_1$  during the entire culture period. To determine the most optimal hypertrophic CLC differentiation condition, micro-aggregates were cultured in normoxia (21% O<sub>2</sub>, 5% CO<sub>2</sub>, 37°C) and hypoxia (5% O<sub>2</sub>, 5% CO<sub>2</sub>, 37°C). PTHR1 and collagen type X IHC<sup>3</sup> (Table 1) and Alizarin Red S<sup>42</sup> staining were performed as described previously.

With abovementioned setup, only prehypertrophic CLC differentiation was achieved and was most outspoken in normoxia. Therefore, in a follow-up experiment, passage 2 canine CLCs (same donors) and passage 3 human CLCs (5 male, 1 female, 44-72 years of age, Thompson grade III) from degenerated IVDs were cultured in micro-aggregates at 21% O<sub>2</sub>, 5% CO<sub>2</sub>, 37°C. Again, these human IVDs (L2-L5) were obtained during standard postmortem diagnostics <48 hours after death, as approved by the scientific committee of the Pathology department (UMCU, Local Medical Ethical Committee number 12-364). The micro-aggregates were subjected to basal culture medium supplemented with 10 ng/mL TGF- $\beta_1$  for one week, followed by hypertrophic induction medium for six weeks. IHH (0.1 or 1  $\mu$ g/mL) or PTHrP (10<sup>-8</sup> or 10<sup>-7</sup> M) was supplemented from culture week 4 onwards. Culture medium was changed twice a week. With this second setup, hypertrophic induction medium alone did not induce calcification. Therefore, in the last experiment the CLCs were cultured in monolayers, since previous work indicated that calcium deposition could be induced in short-term CLC monolayer cultures<sup>32, 46</sup>.

#### *The effect of IHH and PTHrP on calcification in CLC monolayers*

Passage 2 CLCs from 4 canine donors (3 Beagles, 1 Cocker Spaniel, 2-6 years of age) were plated at a density of 10,000 cells/well in 12-wells plates (665180, Greiner) in expansion medium at 21% O<sub>2</sub>, 5% CO<sub>2</sub>, 37°C. After one week, expansion medium was replaced by hypertrophic induction medium supplemented with/without IHH or PTHrP. Trying to facilitate hypertrophic CLC differentiation and calcification, CLCs from the same donors were also seeded in osteogenic culture medium (consisting of hgDMEM+Glutamax, 10% FBS, 1% P/S, 0.1 mM Asap, 10<sup>-7</sup> M dexamethasone and 10 mM  $\beta$ -glycerolphosphate)<sup>42</sup> supplemented with/without 1  $\mu$ g/mL IHH or 10<sup>-7</sup> M PTHrP. After 14 days, monolayers were fixed in 4% neutral buffered formaldehyde for 2 hours. Alizarin Red S staining was performed as described previously.

#### **Statistical analysis**

Statistical analysis was performed using IBM SPSS (version 22). All data were examined for normal distribution (Shapiro Wilks test). Kruskal Wallis and Mann-Whitney U tests were performed on non-normally distributed data, whereas general linear regression models based on ANOVAs were used for normally distributed data. To find correlations between protein immunopositivity and IVD degeneration score, partial correlations (corrected for donor) were determined. Benjamini & Hochberg False Discovery Rate *post-hoc* corrections for multiple comparisons were performed. A *p*-value <0.05 was considered significant. A Chi-squared test was performed to determine whether calcium deposition ( $\leq 1$  and  $> 1$  intensity) increased per histologic degeneration grade ( $\leq 4$ , 4.1-7, and  $> 7$ ).

## Results

### Expression of IHH and PTHrP during IVD maturation

To study the IVD maturation phase (defined by the NC to CLC transition), IHH, PTHrP, and related receptor immunopositivity was studied in canine IVDs. Furthermore, IHH and PTHrP signaling-related gene and protein expression was studied in NCs from canine IVDs that dedifferentiated during monolayer culture<sup>33</sup> and in murine caveolin-1 null NPs that demonstrate accelerated IVD maturation compared with wild type (WT) mice<sup>34</sup>. Both models are considered representative for the transition of NCs towards CLCs (maturation phase).

#### *IHH and PTHrP immunopositivity in canine IVD maturation*

Canines experience back pain and IVD degeneration with similar characteristics as humans and are considered a suitable translational animal model<sup>47,48</sup>. Dog breeds can be classified as chondrodystrophic (CD) or non-chondrodystrophic (NCD)<sup>49</sup>. CD and NCD dogs demonstrate distinct differences in clinical IVD disease which correlate with their physical appearance and are defined by their genetic background. In CD dogs, NCs are replaced by CLCs around one year of age and back pain due to IVD degeneration usually develops around 3–7 years of age. In NCD dogs, NCs can remain the predominant cell type during life and if low back pain develops, it occurs around 6–8 years of age<sup>49</sup>.

IHH- and PTHrP-related protein expression was determined in canine NPs from healthy, Thompson<sup>36</sup> score I until severely degenerated, Thompson score V IVDs (Figure 2). Thompson score I IVDs were only available from NCD dogs, not CD dogs. To determine potential changes in IHH- and PTHrP-related protein expression in the IVD maturation phase, NC-containing NPs from healthy, Thompson score I IVDs were compared to NPs from matured, Thompson score II canine IVDs. In healthy, Thompson score I NPs, only NC cell clusters were detected (Figure 2f). In matured, Thompson score II IVDs, mainly CLCs were present; only one NCD canine NP also contained some NCs. Both cell phenotypes were present in clusters and as single cells within the same NP.

Immunopositivity (ratio of positive cells) for IHH, PTCH, SMO, PTHrP, or PTHR1 was identified in both single cells and clusters (where present). No clear pattern in spatial distribution was detected; where immunopositive cells were present, they were scattered throughout the NP. Immunopositivity for IHH, PTCH, and SMO was significantly higher in NP tissues from healthy, Thompson score I NC-rich IVDs than in NP tissue from matured, Thompson score II CLC-rich IVDs ( $p < 0.05$ , Figure 2a-c), suggesting higher expression in NCs than CLCs. PTHrP and PTHR1 immunopositivity did not differ between NPs from healthy and matured canine IVDs (Figure 2d-e).

Notably, PTHrP immunopositivity in healthy canine IVDs seems to depend on age: PTHrP was detected in more than 10% of the NCs of 7- and 16-month-old canine donors, whereas this was 0-5% in older (17 until 96-month-old) canine donors (Figure 2). This indicates that PTHrP was present in NCs from young, healthy canine IVDs, but that its expression decreased during ageing (in contrast to the expression of PTHR1, IHH, PTCH and SMO). To confirm this, Thompson score I IVDs of younger canines (1 day - 6 weeks of age) were also investigated together with human (21 weeks of gestation – 3 months of age) donors as comparators. The canine NPs contained approximately 100% NCs, mainly present in clusters (Supplementary

File 3). In contrast, the human NPs also contained, smaller fibroblast- and chondrocyte-like cells in clusters and single cells, in addition to the typical NCs (Supplementary File 3). All young canine donors showed abundant PTHrP immunopositivity in their NCs, with no clear pattern in spatial distribution. In contrast, only 7 out of 12 young human donors showed PTHrP immunopositivity in both NC and CLC clusters and single cells (no spatial distribution; Supplementary File 3). Taken together, this indicates that PTHrP expression is present in young, healthy NPs, but that its expression considerably decreases in older, healthy NPs, in line with results obtained using equine chondrocytes<sup>50</sup>.

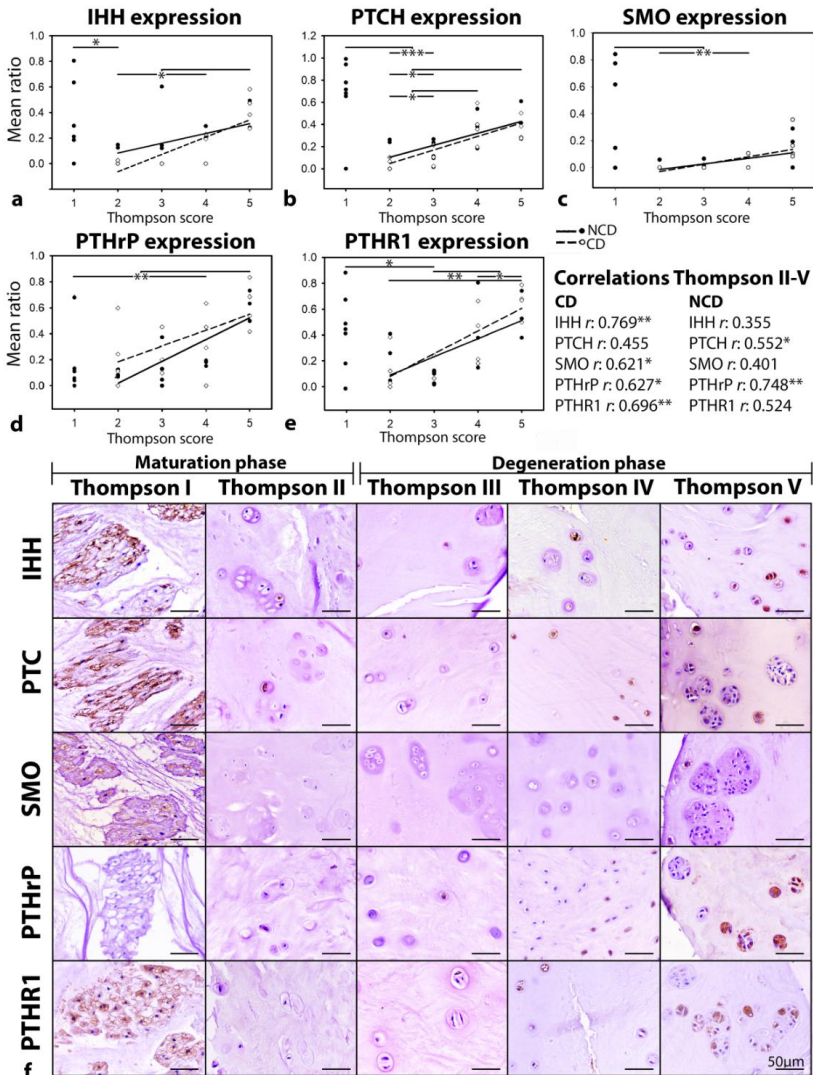


**Figure 2. IHH and PTHrP signaling-related immunopositivity in canine intervertebral discs with different degeneration grades.** Both signaling pathways are activated in healthy IVDs and increase with degeneration. IHH: Indian hedgehog, PTCH: Patched, SMO: Smoothened, PTHrP: Parathyroid hormone-related protein, PTHR1: PTHrP receptor 1. CD: chondrocytic, NCD: non-chondrocytic. *n*=7-8 per Thompson score. \*, \*\*, \*\*\*: *p*<0.05, *p*<0.01 and *p*<0.001, respectively.

### IHH and PTHrP signaling-related gene expression during *in vitro* canine NC differentiation

IHH- and PTHrP signaling-related mRNA expression was studied in native (non-cultured) NCD canine NC-rich NP tissue and 0-4 day cultured NC clusters (derived via digestion of healthy NCD canine NP tissue). The NCs lose their typical phenotype and characteristics during culture<sup>33</sup>, providing an *in vitro* model to study the IVD maturation phase. On the overall, the mRNA expression pattern of both IHH and PTHrP-signaling related genes resembled the protein expression pattern of maturing canine IVDs, *i.e.* reduced mRNA levels coincided with the loss of the NC phenotype.

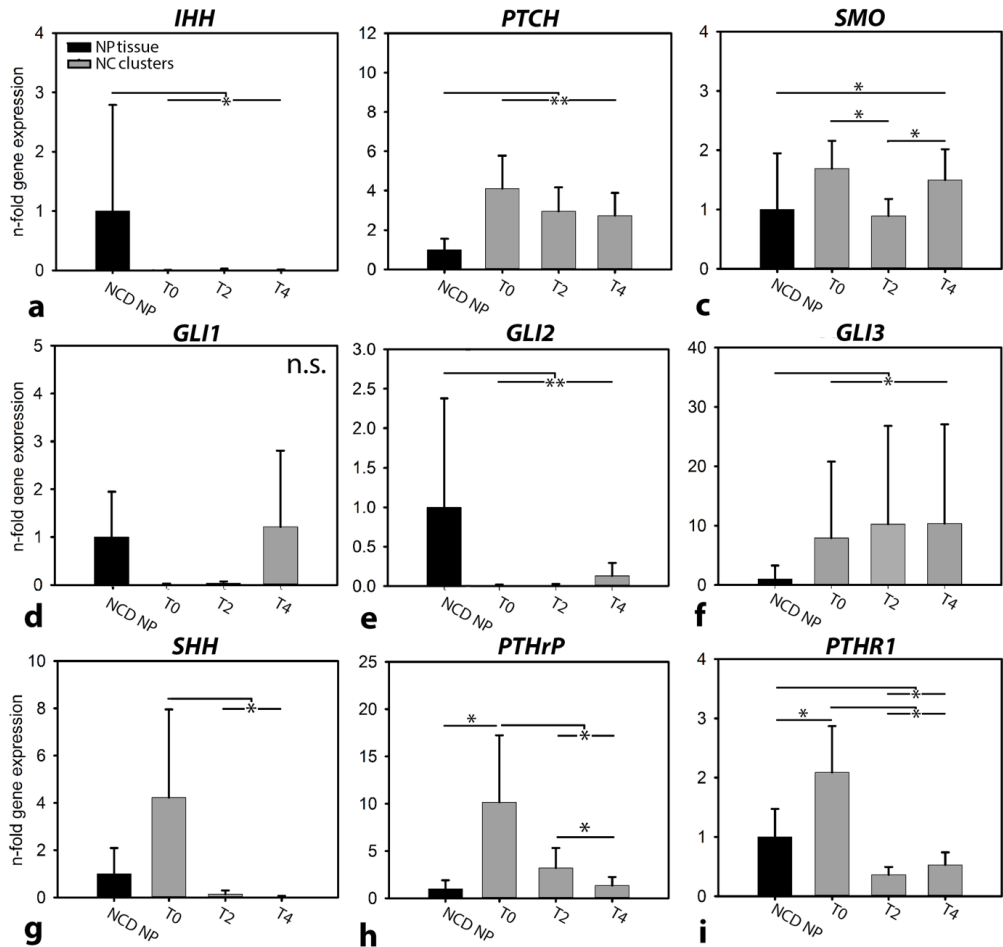


**Figure 3.** IHH and PTHrP signaling-related mRNA expression in canine nucleus pulposus (NP) tissue and cultured notochordal cell (NC) clusters. The NC clusters lose their typical vacuolated phenotype and characteristics during 4-day monolayer culture. Therefore, this model is representative for the transition of NCs towards CLCs (IVD maturation phase). mRNA expression of both the IHH and PTHrP signaling pathway decreases with NC dedifferentiation. *IHH*: Indian hedgehog, *PTCH*: Patched, *SMO*: Smoothed, *SHH*: Sonic hedgehog, *PTHrP*: Parathyroid hormone-related protein, *PTHR1*: PTHrP receptor. NCD: non-chondrodystrophic.  $n=6$  (NP tissue) – 8 (NC clusters). T0, T2, T4: NC clusters at culture day 0, 2, and 4, respectively. \*, \*\*:  $p<0.05$  and  $p<0.01$ , respectively. n.s.: not significant.

*IHH* mRNA expression was significantly higher in NCD canine NP tissue than in 0-4 day cultured NCs ( $p < 0.05$ ), where it was hardly detectable (Figure 3a). *PTCH* mRNA expression was significantly lower in NCD NP tissue than in 0-4 day cultured NCs ( $p < 0.01$ , Figure 3b). *SMO* mRNA expression decreased from day 0 until day 2 and thereafter increased again, and was significantly higher in 4-day cultured NCs than in NCD NP tissue ( $p < 0.05$ , Figure 3c). mRNA of transcription factor *GLI1*, target gene of IHH signaling, was hardly detectable at T0 and T2, and was not differentially expressed between groups (Figure 3d). *GLI2* mRNA was expressed at significantly higher levels in NCD NP tissue than in 0-4 day cultured NCs ( $p < 0.01$ ), where it was hardly detectable (Figure 3e). mRNA expression of *GLI3* was significantly lower in NCD NP tissue than in 0-4 day cultured NCs ( $p < 0.05$ , Figure 3f). *SHH* mRNA expression was significantly higher in non-cultured NCs (culture day 0) and decreased rapidly during culture ( $p < 0.05$ , Figure 3g). Taken together, although *PTCH* and *SMO* mRNA was expressed, mRNA of *IHH*, *SHH* (both hedgehog ligands) and their transcription factors *GLI1* and *GLI2* was hardly detectable in canine NCs that lost their typical vacuolated morphology during culture.

*PTHrP* mRNA expression was significantly higher in freshly isolated NCs than in native tissue ( $p < 0.05$ ) and decreased rapidly during NC culture ( $p < 0.05$ , Figure 3h). Also *PTHR1* mRNA expression decreased from day 0 to day 2 and 4 in culture ( $p < 0.01$ , Figure 3i). Furthermore, it was significantly lower in 2- and 4-day cultured NCs than in NCD NP tissue ( $p < 0.05$ ).

#### *IHH and PTHrP expression in murine caveolin-1 null and WT NPs*

IHH- and PTHrP-related protein expression was further studied using immunohistochemistry in NPs derived from 1.5-, 3-, and 6-month-old WT and caveolin-1 null mice to investigate protein expression levels during the maturation phase. NP tissues of WT mice from all ages contain large, vacuolated NCs. In contrast, 1.5-month-old caveolin-1-null NPs already contain fewer, smaller, non-vacuolated CLCs, fibroblast-like cells and only some NCs (Figure 4f)<sup>34</sup> while maintaining a GAG- and collagen type II-rich matrix. As such, the caveolin-1 null NPs provide an *in vivo* model for accelerated IVD maturation.

The murine immunopositivity profiles resembled the mRNA and protein profiles observed in the canine NP samples. Caveolin-1 null mice displayed lower immunopositivity for IHH- and PTHrP-related proteins than WT animals. The number of IHH immunopositive cells was significantly higher in WT than in caveolin-1 null mice in all ages investigated ( $p < 0.05$ , Figure 4a). Even more so, IHH immunopositivity decreased during ageing in both WT and caveolin null NPs ( $p < 0.05$ ). Immunopositivity for the receptor of IHH (PTCH), also decreased during ageing in WT mice ( $p < 0.05$ ), but not in caveolin-1 null mice (Figure 4b). However, at 1.5 and 3 months of age, more PTCH immunopositive cells were observed in WT mice than in caveolin-1 null mice ( $p < 0.05$ ). At 1.5 months of age, *SMO* immunopositivity was significantly higher in WT than in caveolin-1 null NPs ( $p < 0.01$ ), whereas *SMO* immunopositivity was not different at 3 and 6 months of age (Figure 4c).

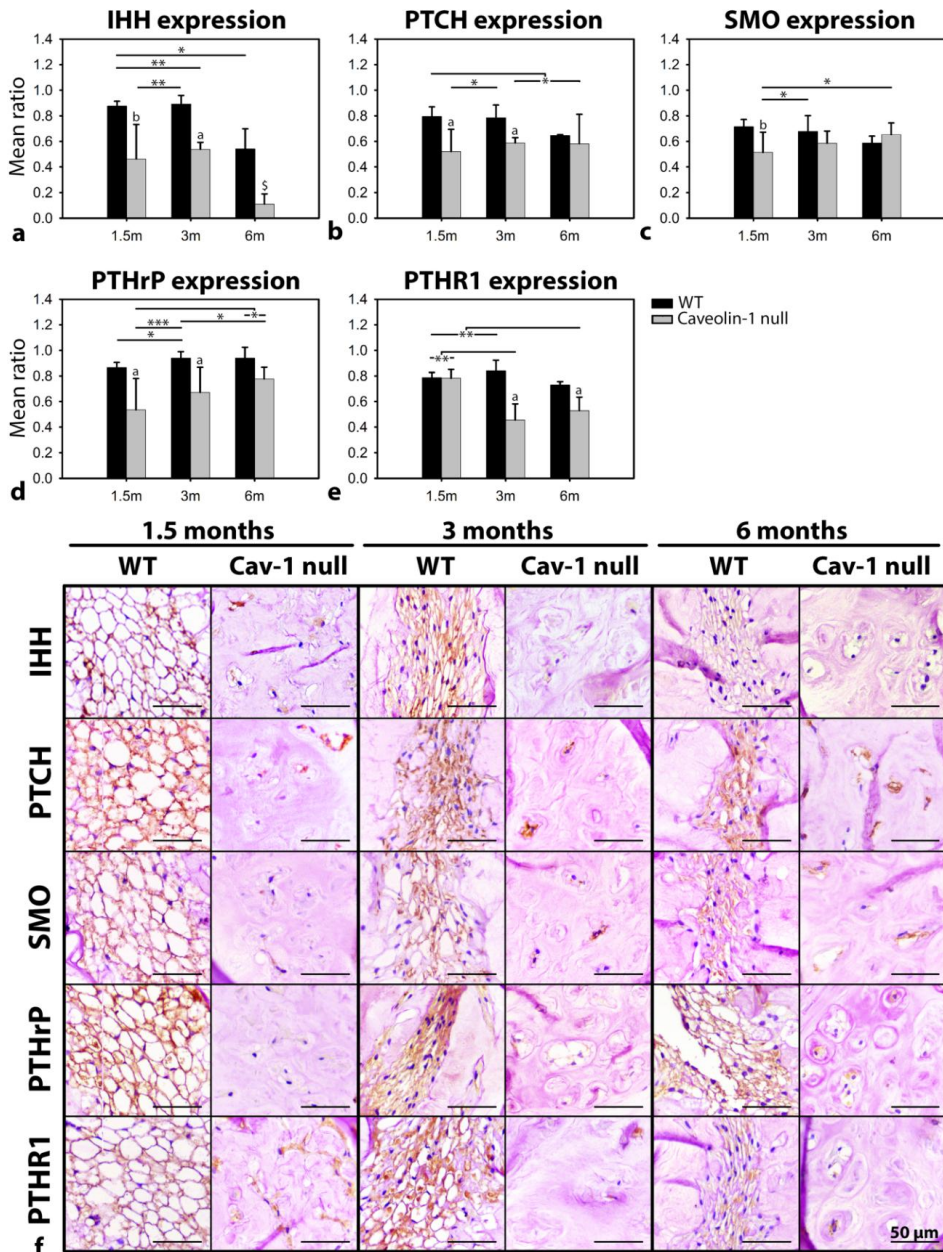


**Figure 4. IHH and PTHrP signaling-related immunopositivity in intervertebral discs of caveolin-1 null and wild type mice at 1.5, 3, and 6 months of age.** In murine caveolin-1 null NPs, the large, vacuolated NCs, are replaced by smaller, non-vacuolated chondrocyte- and fibroblast-like cells. Thus, this model shows accelerated IVD degeneration and is representative for the transition of NCs towards CLCs (IVD maturation phase). Protein expression of both the IHH and PTHrP signaling pathway is decreased in caveolin-1 null versus WT mice IVDs. IHH: Indian hedgehog, PTCH: Patched, SMO: Smoothed, PTHrP: Parathyroid hormone-related protein, PTHR1: PTHrP receptor 1, WT: wild type.  $n=4-10$  per age group and condition (WT or caveolin-1 null mice). a, b: significantly different from WT ( $p<0.05$ ,  $p<0.01$ , respectively);  $\$$ : significantly different from all other conditions ( $p<0.05$ ); \*, \*\*, \*\*\*:  $p<0.05$ ,  $p<0.01$  and  $p<0.001$ , respectively.

At 1.5 and 3 months of age, immunopositivity for PTHrP was significantly higher in WT than in caveolin-1 null NPs ( $p < 0.05$ ) and increased during ageing in both WT and caveolin null NPs ( $p < 0.05$ , Figure 4d). Immunopositivity for the receptor of PTHrP, PTHR1, did not alter during ageing in WT NPs, but significantly decreased with increasing age in caveolin-1 null NPs ( $p < 0.05$ , Figure 4e). PTHR1 immunopositivity was significantly higher in WT than in caveolin-1 null NPs at 3 and 6 months of age ( $p < 0.05$ ).

### **IHH and PTHrP in human and canine IVD degeneration**

Protein expression of IHH, PTHrP, and related receptors was studied throughout the IVD degeneration process in both canines and humans. Furthermore, the correlation between PTHrP and IHH (receptor) expression and calcification was determined in surgically removed human NP samples across the range of histological IVD degeneration. Lastly, the effect of IHH and PTHrP was determined on GAG production and calcification of canine CLCs *in vitro*.

#### *IHH and PTHrP expression in canine IVD degeneration*

To determine IHH- and PTHrP-related protein expression in the IVD degeneration phase, we focus in this part of the manuscript on Thompson score II/III (matured) until Thompson score V (severely degenerated) canine IVDs (Figure 2). Also correlations between protein immunopositivity and macroscopic IVD degeneration grade were determined for (CLC-rich) NPs from Thompson score II-V IVDs. In Thompson score III-V NPs, only CLCs were encountered in single cells and clusters, with increased cluster numbers and sizes seen in severely degenerated Thompson score V IVDs. Although the current study demonstrates some differences in IHH-PTHrP (related) expression between CD and NCD dogs, which may be related with their differential genetic background, the direction of the correlation between protein expression and IVD degeneration grade was similar.

Immunopositivity for IHH was significantly higher in NPs from severely degenerated grade V IVDs than in NPs from matured - moderately degenerated grade II-IV IVDs ( $p < 0.05$ , Figure 2a). CD dogs showed a significant, strong positive correlation between IHH immunopositivity and macroscopic IVD degeneration grade ( $p < 0.01$ ,  $r: 0.769$ ), whereas NCD dogs did not. PTCH immunopositivity was significantly higher in NPs from Thompson score IV-V IVDs than in NPs from Thompson score II-III IVDs ( $p < 0.05$ , Figure 2b). Only NCD dogs showed a positive correlation between PTCH immunopositivity and macroscopic IVD degeneration grade (Thompson score II-V,  $p < 0.05$ ,  $r: 0.552$ ), whereas only CD dogs showed a positive correlation between SMO immunopositivity and macroscopic IVD degeneration grade ( $p < 0.05$ ,  $r: 0.621$ ).

PTHrP immunopositivity significantly increased during canine IVD degeneration ( $p < 0.01$ , Figure 2d). In both CD and NCD dogs, a positive correlation between PTHrP immunopositivity and macroscopic IVD degeneration grade was observed ( $p < 0.05$ ,  $r: 0.627$  (CD) and  $p < 0.01$ ,  $r: 0.748$  (NCD)). Immunopositivity for PTHR1 increased from NPs of matured, Thompson score II-III IVDs to severely degenerated, Thompson score V IVDs ( $p < 0.05$ , figure 2e). Only CD dogs showed a positive correlation between PTHR1 immunopositivity and macroscopic IVD degeneration grade ( $p < 0.01$ ,  $r: 0.696$ ).

*IHH and PTHrP expression in human IVD degeneration*

In NPs from healthy, Thompson score I human IVDs, mainly CLCs and only some NCs were detected, mainly as single cells, but also in clusters (Figure 5g). In NPs from Thompson score II-V IVDs, only CLCs were encountered in single cells and clusters. Again, correlations between protein expression and IVD degeneration grade were only determined for CLC-rich NPs from Thompson score II-V IVDs. CLC clusters were more abundant and larger in NPs from Thompson score IV and V IVDs. Immunopositivity, where present for all proteins, was identified in both single cells and clusters without an evident spatial distribution pattern.

As expected, a strong, positive correlation was found between the macroscopic Thompson and the histologic IVD degeneration score<sup>40, 41</sup> of the human samples ( $r:0.907$ ,  $p<0.001$ ; Figure 5f). To be able to relate these results to the follow-up study (determining the relationship between PTHrP/IHH immunopositivity and calcification in surgically removed human NP samples), correlation are given in relation to the histological IVD degeneration grade. A significant positive correlation between IHH, PTCH, SMO and PTHrP immunopositivity and histologic IVD degeneration grade was encountered ( $p<0.05$ ,  $r:0.679$ ,  $0.577$ ,  $0.502$ , and  $0.848$ , respectively; Figure 5a-d). There was, however, no significant correlation between PTHR1 immunopositivity and histologic IVD degeneration grade (Figure 5e).

*PTHrP decreases chondrogenic matrix production, whereas IHH does not influence this in canine CLCs*

To further study the effect of IHH and PTHrP in the IVD degeneration phase, PTHrP or IHH were supplemented to CD canine CLCs from matured IVDs *in vitro*. IHH treatment significantly induced mRNA expression of its target genes *PTHrP* and *PTCH* ( $p<0.05$ ; Supplementary File 4a,b). *SMO* mRNA expression was not significantly influenced by the different treatments (data not shown), while *PTHR1* and *IHH* mRNA was not detected in any samples regardless the culture condition. PTHR1 immunopositivity was, however, present in  $10^{-8}$  and  $10^{-7}$  M PTHrP-treated micro-aggregates (Supplementary File 4c), indicating that PTHrP exerted its effects via this receptor.

After 14 days of culture, the DNA content of  $10^{-7}$ M PTHrP-treated micro-aggregates was significantly decreased compared with controls ( $p<0.05$ ; Supplementary File 5a) and remained unaffected in the other culture conditions. IHH and PTHrP treatment did not influence the GAG content of canine CLC micro-aggregates (Supplementary File 5b). However,  $10^{-7}$  and  $10^{-8}$  M PTHrP treatment significantly decreased GAG release and subsequently total GAG production compared with controls ( $p<0.05$ ; Supplementary File 5c,d).

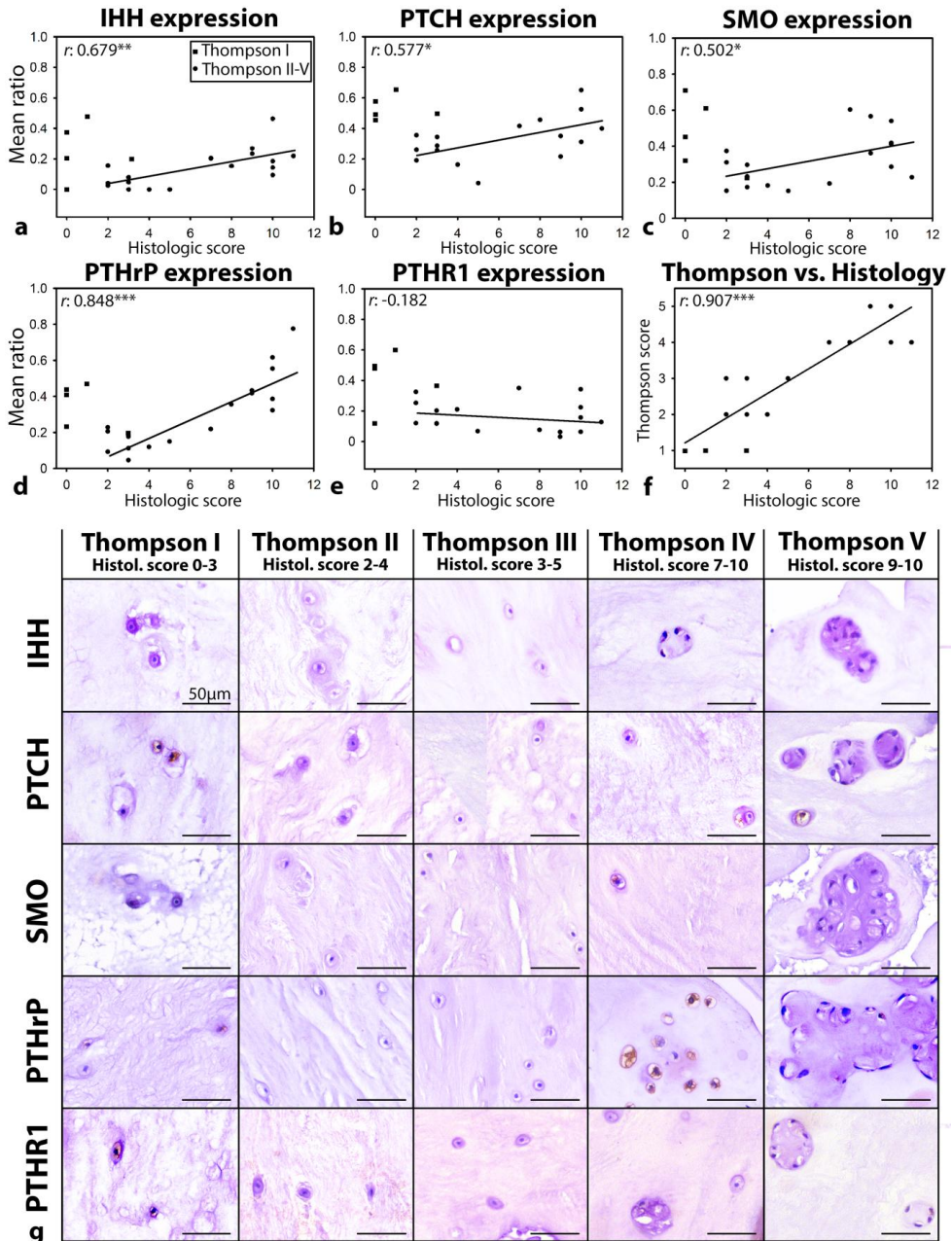


**Figure 5. IHH and PTHrP signaling-related immunopositivity in human intervertebral discs with different degeneration grades.** The samples were graded according to the macroscopic Thompson score and histologic degeneration score. These scores strongly correlated with each other. Both signaling pathways are increasingly activated with progress of degeneration. IHH: Indian hedgehog, PTCH: Patched, SMO: Smoothed, PTHrP: Parathyroid hormone-related protein, PTHR1: PTHrP receptor 1.  $n=4-5$  per Thompson score. \*, \*\*, \*\*\*:  $p<0.05$ ,  $p<0.01$  and  $p<0.001$ , respectively.

## IHH and PTHrP in IVD calcification

### *Correlation between IHH and PTHrP expression and calcification*

IHH and PTHrP have well-known effects on calcification of joint cartilage<sup>19-21, 26</sup>, which can also occur during the later stages of IVD degeneration<sup>5, 51-53</sup>. To determine the association between IHH/PTHrP-related protein expression and calcification, IHC for IHH, PTCH, SMO, PTHrP and PTHR1 and Alizarin Red S staining were performed on surgically removed human NP tissue across the range of histological IVD degeneration<sup>40, 41</sup>. The morphological assessment of the calcium staining intensity was divided in two groups ( $\leq 1$  and  $> 1$  staining intensity; Figure 6a). The percentage of human NP tissue samples with high calcium deposition significantly increased with the histologic IVD degeneration grade (Figure 6b;  $p < 0.05$ ). Moreover, the number of cells with PTHR1 and IHH and immunopositivity was significantly higher in the NP tissues associated with high calcium deposition ( $p < 0.01$ ; Figure 6c-d). In contrast, no difference in number of immunopositive cells for PTHrP (Figure 6c-d), PTCH and SMO was observed between the NPs with low and high calcium deposition.

### *Induction of hypertrophic CLC differentiation*

To study the effect of PTHrP and IHH on hypertrophic CLC differentiation and calcification *in vitro*, first hypertrophy was induced using methodology to induce hypertrophic differentiation in mesenchymal stromal cells (MSC)<sup>45</sup>. Given that IVD cells maintain their disc phenotype better in a 3D than 2D environment<sup>54, 55</sup>, canine CLC micro-aggregates were subjected to TGF- $\beta_1$ -supplemented basal culture medium for one week and subsequently to hypertrophic induction medium for three weeks in hypoxia (5% O<sub>2</sub>) and normoxia (21% O<sub>2</sub>). The latter was employed as an extra condition given that normoxia facilitated hypertrophic differentiation of MSCs<sup>45</sup>. Immunopositivity for the prehypertrophic differentiation protein PTHR1<sup>56, 57</sup> was not present in controls, and most abundant in micro-aggregates cultured in hypertrophic induction medium in normoxia (Supplementary File 6a). Collagen type X was not expressed in any samples (Supplementary File 6a) and Alizarin Red S staining did not show calcifications (data not shown). Thus, with this setup, only prehypertrophic, but not complete hypertrophic differentiation was achieved. Therefore, in follow-up experiments, canine and human CLC micro-aggregates were subjected to TGF- $\beta_1$ -supplemented basal culture medium for one week, followed by hypertrophic induction medium for six weeks, while 0.1 or 1  $\mu\text{g}/\text{mL}$  IHH or  $10^{-8}$  or  $10^{-7}$  M PTHrP was supplemented from week 4 onwards. After 7 weeks, while PTHR1 was abundantly present in the hypertrophic culture conditions, collagen type X was not deposited regardless the treatment group (data not shown) and hypertrophic induction medium alone did not induce calcification (Supplementary File 6b). In one out of six canine and in one out of six human CLC donors treated with hypertrophic induction medium supplemented with 1  $\mu\text{g}/\text{mL}$  IHH, however, calcification was induced (Supplementary File 6b).

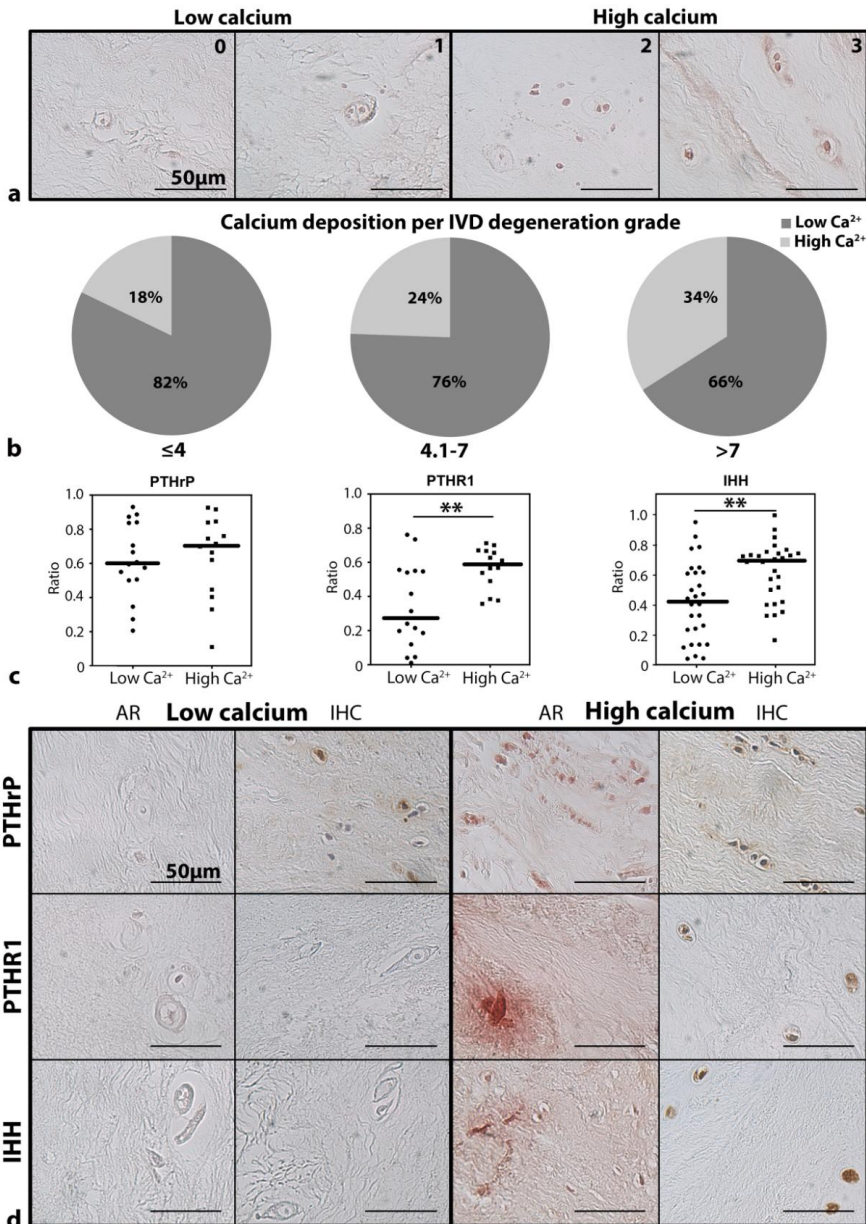


**Figure 6.** PTHrP, PTHR1, and IHH immunopositivity and calcium deposition in surgically removed human nucleus pulposus tissue across the range of histological IVD degeneration. The degree of histologic IVD degeneration was divided in three groups ( $\leq 4$ , 4.1-7, and  $>7$ ), while calcium deposition was divided in low ( $\leq 1$ ) and high ( $\geq 1$ ) intensity. (a) Alizarin Red S staining of representative samples with different calcium staining intensity (0-3). (b) Calcium deposition increases with the degree of histologic IVD degeneration.  $n=133$  (c) PTHrP, PTHR1, and IHH immunopositivity (ratio) versus calcium deposition (low ( $\leq 1$ ) and high ( $\geq 1$ ) intensity). Bars indicate median.  $n=30$  (PTHrP, PTHR1) - 56 (IHH) (d) Alizarin Red S staining (AR; left) and immunohistochemistry (IHC; right) for PTHrP, PTHR1, and IHH for representative human NP samples with low ( $\leq 1$ ) and high ( $\geq 1$ ) calcium deposition. IHH: Indian hedgehog, PTHrP: Parathyroid hormone-related protein, PTHR1: PTHrP receptor 1, \*\*:  $p < 0.01$ .

*IHH facilitates calcification in CLC monolayers, whereas PTHrP does not*

Given the challenges we encountered during the induction of hypertrophy of CLCs in 3D culture, we opted to investigate whether IHH augmented calcification in canine CLC monolayer culture. Previous work indicated that short-term CLC monolayer culture enabled calcium deposition<sup>32, 46</sup> and this may be explained by the fact that CLC need the stiffness of culture plastic to differentiate<sup>58</sup>. Interestingly, the canine CLCs seeded in osteogenic culture medium did not thrive; they failed to attach to culture plastic and died within 24 hours. Hypertrophic induction medium alone induced calcification in only one out of four canine CLC donors (Figure 7). In the other three donors, IHH supplementation was required for the development of calcified nodules. As expected, PTHrP supplementation did not influence calcification compared with hypertrophic induction medium alone (data not shown).

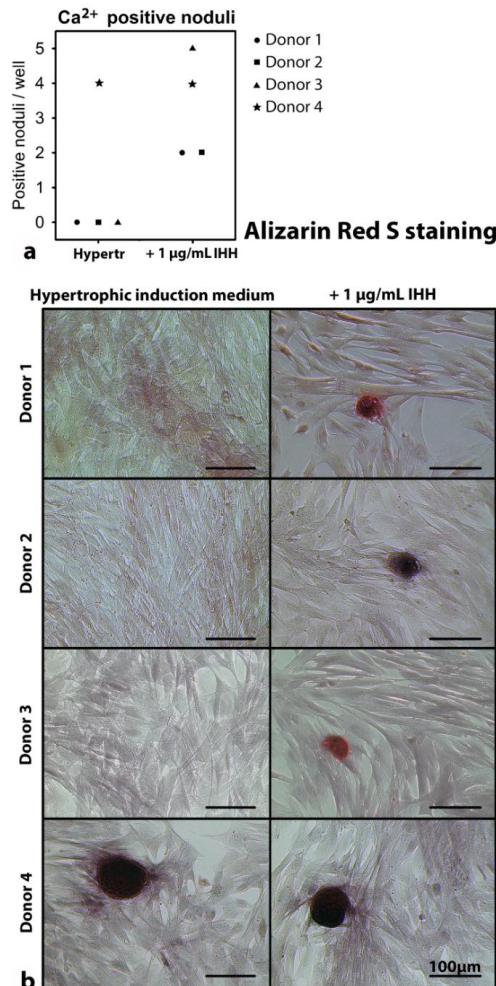


**Figure 7. Indian hedgehog facilitates calcification in chondrocyte-like cells *in vitro*.** Alizarin Red S staining on canine CLC monolayers treated with hypertrophic induction medium supplemented with/without 1 µg/mL IHH for 7 days. (a) Number of Alizarin Red S positive nodules per well. (b) Alizarin Red S staining results for all donors. IHH: Indian hedgehog.  $n=4$

**Table 2. IHH, PTHrP and related receptor expression during IVD maturation and degeneration**

Model	IHH	PTCH	SMO	PTHrP	PTHR1
<b>IVD maturation</b>					
IHC on canine NP tissue	↓	↓	↓	+/-	+/-
Canine NC dedifferentiation	↓	+/-	+/-	↓	↓
Caveolin-1 null mice	↓	↓	↓	↓	↓
<b>IVD degeneration</b>					
IHC on canine NP tissue	↑ <sup>§</sup>	↑*	↑ <sup>§</sup>	↑	↑ <sup>§</sup>
IHC on human NP tissue	↑	↑	↑	↑	+/-

IHH, PTHrP and related receptor expression was studied during intervertebral disc (IVD) maturation (the transition from vacuolated notochordal cells (NCs) to chondrocyte-like cells (CLCs)) using three different models. IHH- and PTHrP-related protein expression was determined using immunohistochemistry in nucleus pulposus (NP) tissue from healthy (Thompson score I) until matured (Thompson score II) canine IVDs and in murine wild type (WT) and caveolin-1 null NPs. Caveolin-1 null IVDs undergo accelerated maturation. Additionally, IHH- and PTHrP-related mRNA expression was studied in NCs from healthy canine IVDs that dedifferentiated and lost their typical vacuolated phenotype and characteristics during monolayer culture. Additionally, IHH, PTHrP and related receptor expression was studied during IVD degeneration using immunohistochemistry in NPs from matured (Thompson score II) until severely (Thompson score V) degenerated canine and human IVDs. \*: only in NCD dogs, <sup>§</sup>: only in CD dogs, +/-: not significantly affected.

## Discussion

Treatment strategies leading to functional IVD restoration can benefit from in depth knowledge of the pathways involved in IVD degeneration. Therefore, this study focused on the largely unexplored role of PTHrP and IHH in the postnatal IVD that can suffer from clinical IVD disease. The current manuscript provides a first step towards a better understanding of the possible role of PTHrP and IHH in IVD (patho)physiology.

### IHH and PTHrP expression decreases during IVD maturation

To study IHH- and PTHrP-related mRNA and protein expression during NC towards CLC transition (IVD maturation), NC-rich healthy and CLC-rich matured canine IVDs, canine NCs that lost their specific phenotype and characteristics during monolayer culture<sup>3</sup>, and caveolin-1 null NPs demonstrating accelerated IVD maturation<sup>34</sup> were studied. The results from all three models indicate that the expression of IHH, PTHrP and their receptors was high in healthy, NC-containing NPs, but decreased with the transition towards matured, CLC-containing NPs. Whether the observed changes in expression are a cause or consequence of the maturation process, play a role in preservation of NCs, or are related to NP differentiation remains to be determined with the aid of antagonists or functional knockout/in models.

### IHH and PTHrP expression increases from matured towards severely degenerated IVDs

The current study demonstrates that PTHR1 immunopositivity increased from matured to severely degenerated canine, but not human IVDs, possibly due to species differences. It can, however, not be excluded that the different decalcification procedures may have affected the results<sup>59</sup>. Nonetheless, IHH, PTCH, and PTHrP expression increased during the IVD degeneration process in both species. This result is in line with the positive correlation between IHH expression and OA<sup>19-22</sup>, a process resembling IVD degeneration<sup>5</sup>. The results

from the current study may indicate that IHH and PTHrP induce/facilitate IVD degeneration, or reflect an attempt of repair. Therefore, functional *in vitro* studies were performed to elucidate the role of increased PTHrP and IHH expression in degenerated IVDs.

### **PTHrP, but not IHH, decreases GAG production by CLCs**

NP cell cluster formation (associated with cell proliferation<sup>60</sup>) is most marked in degenerated IVDs<sup>61</sup>. This could imply that increased IHH and PTHrP expression in the degenerated IVD promotes CLC proliferation (*e.g.* as an attempt at matrix repair), in line with their well-known effect on chondrocytes<sup>12</sup>. Moreover, IHH also increased GAG production in chondrocytes<sup>62, 63</sup> and PTHrP increased the GAG and DNA content of chondrogenically differentiated MSC pellets<sup>43, 64</sup>. Lastly, PTH treatment increased *ACAN* and *COL2A1* expression in NC-rich rat IVDs<sup>31</sup>. To test this hypothesis, the effect of IHH and PTHrP on CLC chondrogenic ECM production was determined *in vitro*. Neither IHH nor PTHrP, however, increased the DNA content of the canine CLC micro-aggregates. Additionally, GAG production was not influenced by IHH, whereas it was decreased by PTHrP. This indicates that the effects of IHH and PTHrP are tissue and context dependent. Previous work demonstrates that an anabolic response is induced during canine IVD maturation<sup>8</sup>. PTHrP expression is low in this anabolic maturation phase and increases during the later stages of IVD degeneration, where the GAG content of the NP decreases<sup>4, 65</sup>. Thus, this further supports the notion that PTHrP may negatively affect GAG production in degenerated CLCs.

### **Calcium levels increase in the human NP during IVD degeneration**

Based on their well described role in chondrocytes<sup>19-21, 26</sup>, IHH and PTHrP could be involved in hypertrophic CLC differentiation and calcification, processes that are known to occur during the later stages of IVD degeneration<sup>5, 51-53</sup>. The current study confirmed a positive correlation between human NP calcification levels and IVD degeneration grade. A significant, positive correlation between IHH immunopositivity and calcification was detected in human NP tissue. In line with this, previous work displayed a significant association between those two in OA samples<sup>19-21</sup>. PTHR1 immunopositivity was also significantly higher in NPs with abundant calcification versus those with no/low calcification, which can be explained by the cellular phenotype: PTHR1 is mainly expressed in prehypertrophic cells<sup>56</sup> and calcium is most likely deposited in severely degenerated IVDs<sup>5, 51, 52</sup> with (pre)hypertrophically differentiated CLCs. PTHrP immunopositivity was not upregulated in NPs with abundant calcification. Previous work showed that PTHrP inhibits calcification in chondrocytes<sup>26</sup>. Moreover, PTH inhibits terminal differentiation of chondrocytes<sup>27</sup> and calcification in CLCs<sup>32</sup>. Assuming that PTHrP indeed inhibits the IVD calcification process, the absence of PTHrP upregulation in later stages of degeneration may allow for NP calcification in the process of degeneration.

### **IHH induces calcification in CLCs, while PTHrP does not influence this**

In contrast to PTHrP, IHH is known to promote chondrocyte hypertrophy and calcification in OA<sup>19-21</sup>. To our knowledge, this is the first study to demonstrate that IHH also has the propensity to induce calcification in CLCs from degenerated IVDs *in vitro*. Interestingly, collagen type X was not detected, suggesting that calcification can occur without simultaneous collagen type X expression or hypertrophic differentiation, as shown previously<sup>51, 66</sup>. Together with the increased IHH expression in IVDs with high levels of calcium, this may suggest a possible role for IHH in calcification during IVD degeneration. In line with this thought, disrupted IHH signaling prevented hypertrophic chondrocyte

differentiation and osteophyte formation in OA cartilage<sup>23, 24</sup>. Possibly, this could also be a therapeutic approach to prevent or retard these processes during IVD degeneration.

## Conclusions

Expression of IHH, PTHrP and their receptors was high in NCs from young, healthy IVDs, decreased during the transition towards matured IVDs, and increased again in the advanced stages of IVD degeneration. *In vitro* studies indicated that PTHrP decreased chondrogenic matrix production in CLCs from degenerated IVDs *in vitro*, whereas IHH did not influence this. While PTHrP did not induce hypertrophic differentiation, IHH had the propensity to facilitate calcification in canine CLCs *in vitro*. Taken together with the increased IHH expression in IVDs with high levels of calcium deposition, this may indicate that inhibition of IHH signaling could be a therapeutic approach to inhibit CLC calcification in IVD degeneration.

## Acknowledgments

The authors would like to thank Anneleen Tuinman for help with the execution of experiments.

## References

1. Walker BF. 2000. The prevalence of low back pain: A systematic review of the literature from 1966 to 1998. *J Spinal Disord* 13: 205-217.
2. Mok FP, Samartzis D, Karppinen J, et al. 2016. Modic changes of the lumbar spine: Prevalence, risk factors, and association with disc degeneration and low back pain in a large-scale population-based cohort. *Spine J* 16: 32-41.
3. Bach FC, de Vries SA, Krouwels A, et al. 2015. The species-specific regenerative effects of notochordal cell-conditioned medium on chondrocyte-like cells derived from degenerated human intervertebral discs. *Eur Cell Mater* 30: 132-47.
4. Bergknut N, Smolders LA, Grinwis GC, et al. 2013. Intervertebral disc degeneration in the dog. part 1: Anatomy and physiology of the intervertebral disc and characteristics of intervertebral disc degeneration. *Vet J* 195: 282-291.
5. Rutges JP, Duit RA, Kummer JA, et al. 2010. Hypertrophic differentiation and calcification during intervertebral disc degeneration. *Osteoarthritis Cartilage* 18: 1487-1495.
6. Colombini A, Lombardi G, Corsi MM, Banfi G. 2008. Pathophysiology of the human intervertebral disc. *Int J Biochem Cell Biol* 40: 837-842.
7. Bach FC, Willems N, Penning LC, et al. 2014. Potential regenerative treatment strategies for intervertebral disc degeneration in dogs. *BMC Vet Res* 10: 3-6148-10-3.
8. Smolders LA, Meij BP, Onis D, et al. 2013. Gene expression profiling of early intervertebral disc degeneration reveals a down-regulation of canonical wnt signaling and caveolin-1 expression: Implications for development of regenerative strategies. *Arthritis Res Ther* 15: R23.
9. Hiyama A, Sakai D, Mochida J. 2013. Cell signaling pathways related to pain receptors in the degenerated disk. *Global Spine J* 3: 165-174.
10. Dahia CL, Mahoney EJ, Durrani AA, Wylie C. 2009. Intercellular signaling pathways active during intervertebral disc growth, differentiation, and aging. *Spine (Phila Pa 1976)* 34: 456-462.
11. van der Eerden BC, Karperien M, Wit JM. 2003. Systemic and local regulation of the growth plate. *Endocr Rev* 24: 782-801.
12. Kronenberg HM. 2006. PTHrP and skeletal development. *Ann N Y Acad Sci* 1068: 1-13.
13. Chau M, Forcinito P, Andrade AC, et al. 2011. Organization of the indian hedgehog--parathyroid hormone-related protein system in the postnatal growth plate. *J Mol Endocrinol* 47: 99-107.
14. Kobayashi T, Soegiarto DW, Yang Y, et al. 2005. Indian hedgehog stimulates periarticular chondrocyte differentiation to regulate growth plate length independently of PTHrP. *J Clin Invest* 115: 1734-1742.
15. Rohatgi R, Scott MP. 2007. Patching the gaps in hedgehog signalling. *Nat Cell Biol* 9: 1005-1009.
16. Rimkus TK, Carpenter RL, Qasem S, Chan M, Lo HW. 2016. Targeting the sonic hedgehog signaling pathway: Review of smoothed and GLI inhibitors. *Cancers (Basel)* 8: 10.3390/cancers8020022.
17. Bach FC, Rutten K, Hendriks K, et al. 2014. The paracrine feedback loop between vitamin D(3) (1,25(OH)(2)D(3)) and PTHrP in prehypertrophic chondrocytes. *J Cell Physiol* 229: 1999-2014.
18. Zhang W, Chen J, Zhang S, Ouyang HW. 2012. Inhibitory function of parathyroid hormone-related protein on chondrocyte hypertrophy: The implication for articular cartilage repair. *Arthritis Res Ther* 14: 221.
19. Wei F, Zhou J, Wei X, et al. 2012. Activation of indian hedgehog promotes chondrocyte hypertrophy and upregulation of MMP-13 in human osteoarthritic cartilage. *Osteoarthritis Cartilage* 20: 755-763.
20. Lin AC, Seeto BL, Bartoszko JM, et al. 2009. Modulating hedgehog signaling can attenuate the severity of osteoarthritis. *Nat Med* 15: 1421-1425.
21. Zhou J, Wei X, Wei L. 2014. Indian hedgehog, a critical modulator in osteoarthritis, could be a potential therapeutic target for attenuating cartilage degeneration disease. *Connect Tissue Res* 55: 257-261.
22. Shuang F, Zhou Y, Hou SX, et al. 2015. Indian hedgehog signaling pathway members are associated with magnetic resonance imaging manifestations and pathological scores in lumbar facet joint osteoarthritis. *Sci Rep* 5: 10290.
23. Ruiz-Heiland G, Horn A, Zerr P, et al. 2012. Blockade of the hedgehog pathway inhibits osteophyte formation in arthritis. *Ann Rheum Dis* 71: 400-407.
24. Zhou J, Chen Q, Lanske B, et al. 2014. Disrupting the indian hedgehog signaling pathway in vivo attenuates surgically induced osteoarthritis progression in Col2a1-CreERT2; ihhfl/fl mice. *Arthritis Res Ther* 16: R11.
25. Becher C, Szuwart T, Ronstedt P, et al. 2010. Decrease in the expression of the type 1 PTH/PTHrP receptor (PTH1R) on chondrocytes in animals with osteoarthritis. *J Orthop Surg Res* 5: 28-799X-5-28.
26. Jiang J, Leong NL, Mung JC, Hidaka C, Lu HH. 2008. Interaction between zonal populations of articular chondrocytes suppresses chondrocyte mineralization and this process is mediated by PTHrP. *Osteoarthritis Cartilage* 16: 70-82.
27. Chang JK, Chang LH, Hung SH, et al. 2009. Parathyroid hormone 1-34 inhibits terminal differentiation of human articular chondrocytes and osteoarthritis progression in rats. *Arthritis Rheum* 60: 3049-3060.
28. DiPaola CP, Farmer JC, Manova K, Niswander LA. 2005. Molecular signaling in intervertebral disk development. *J Orthop Res* 23: 1112-1119.
29. Dahia CL, Mahoney E, Wylie C. 2012. Shh signaling from the nucleus pulposus is required for the postnatal growth and differentiation of the mouse intervertebral disc. *PLoS One* 7: e35944.
30. Winkler T, Mahoney EJ, Sinner D, Wylie CC, Dahia CL. 2014. Wnt signaling activates shh signaling in early postnatal intervertebral discs, and re-activates shh signaling in old discs in the mouse. *PLoS One* 9: e98444.

31. Jia H, Ma J, Lv J, et al. 2016. Oestrogen and parathyroid hormone alleviate lumbar intervertebral disc degeneration in ovariectomized rats and enhance wnt/beta-catenin pathway activity. *Sci Rep* 6: 27521.
32. Madiraju P, Gawri R, Wang H, Antoniou J, Mwale F. 2013. Mechanism of parathyroid hormone-mediated suppression of calcification markers in human intervertebral disc cells. *Eur Cell Mater* 25: 268-283.
33. Smolders LA, Meij BP, Riemers FM, et al. 2012. Canonical wnt signaling in the notochordal cell is upregulated in early intervertebral disk degeneration. *J Orthop Res* 30: 950-957.
34. Bach FC, Zhang Y, Miranda-Bedate A, et al. 2016. Increased caveolin-1 in intervertebral disc degeneration facilitates repair. *Arthritis Res Ther* 18: 59-016-0960-y.
35. Bergknut N, Meij BP, Hagman R, et al. 2013. Intervertebral disc disease in dogs - part 1: A new histological grading scheme for classification of intervertebral disc degeneration in dogs. *Vet J* 195: 156-163.
36. Bergknut N, Grinwis G, Pickee E, et al. 2011. Reliability of macroscopic grading of intervertebral disk degeneration in dogs by use of the thompson system and comparison with low-field magnetic resonance imaging findings. *Am J Vet Res* 72: 899-904.
37. Willems N, Bach FC, Plomp SG, et al. 2015. Intradiscal application of rhBMP-7 does not induce regeneration in a canine model of spontaneous intervertebral disc degeneration. *Arthritis Res Ther* 17: 137-015-0625-2.
38. Kristensen HK. 1948. An improved method of decalcification. *Stain Technol* 23: 151-154.
39. Rutges JP, Duit RA, Kummer JA, et al. 2013. A validated new histological classification for intervertebral disc degeneration. *Osteoarthritis Cartilage* 21: 2039-2047.
40. Binch AL, Cole AA, Breakwell LM, et al. 2014. Expression and regulation of neurotrophic and angiogenic factors during human intervertebral disc degeneration. *Arthritis Res Ther* 16: 416-014-0416-1.
41. Le Maitre CL, Freemont AJ, Hoyland JA. 2005. The role of interleukin-1 in the pathogenesis of human intervertebral disc degeneration. *Arthritis Res Ther* 7: R732-45.
42. Malagola E, Teunissen M, van der Laan LJ, et al. 2015. Characterization and comparison of canine multipotent stromal cells derived from liver and bone marrow. *Stem Cells Dev* 25(2):139-50.
43. Handorf AM, Chamberlain CS, Li WJ. 2015. Endogenously produced indian hedgehog regulates TGFbeta-driven chondrogenesis of human bone marrow stromal/stem cells. *Stem Cells Dev* 24: 995-1007.
44. Farndale RW, Sayers CA, Barrett AJ. 1982. A direct spectrophotometric microassay for sulfated glycosaminoglycans in cartilage cultures. *Connect Tissue Res* 9: 247-248.
45. Gawlitta D, van Rijen MH, Schrijver EJ, Alblas J, Dhert WJ. 2012. Hypoxia impedes hypertrophic chondrogenesis of human multipotent stromal cells. *Tissue Eng Part A* 18: 1957-1966.
46. Illien-Junger S, Torre OM, Kindschuh WF, et al. 2016. AGEs induce ectopic endochondral ossification in intervertebral discs. *Eur Cell Mater* 32: 257-270.
47. Bergknut N, Rutges JP, Kranenburg HJ, et al. 2012. The dog as an animal model for intervertebral disc degeneration? *Spine (Phila Pa 1976)* 37: 351-358.
48. Tellegen AR, Willems N, Beukers M, et al. 2017. Intradiscal application of a PCLA-PEG-PCLA hydrogel loaded with celecoxib for the treatment of back pain in canines: What's in it for humans? *J Tissue Eng Regen Med*, Epub ahead of print.
49. Smolders LA, Bergknut N, Grinwis GC, et al. 2013. Intervertebral disc degeneration in the dog. part 2: Chondrodystrophic and non-chondrodystrophic breeds. *Vet J* 195: 292-299.
50. Semevolos SA, Nixon AJ, Fortier LA, Strassheim ML, Haupt J. 2006. Age-related expression of molecular regulators of hypertrophy and maturation in articular cartilage. *J Orthop Res* 24: 1773-1781.
51. Melrose J, Burkhardt D, Taylor TK, et al. 2009. Calcification in the ovine intervertebral disc: A model of hydroxyapatite deposition disease. *Eur Spine J* 18: 479-489.
52. Hristova GI, Jarzem P, Ouellet JA, et al. 2011. Calcification in human intervertebral disc degeneration and scoliosis. *J Orthop Res* 29: 1888-1895.
53. Grant MP, Epure LM, Bokhari R, et al. 2016. Human cartilaginous endplate degeneration is induced by calcium and the extracellular calcium-sensing receptor in the intervertebral disc. *Eur Cell Mater* 32: 137-151.
54. Lee JY, Hall R, Pelinkovic D, et al. 2001. New use of a three-dimensional pellet culture system for human intervertebral disc cells: Initial characterization and potential use for tissue engineering. *Spine (Phila Pa 1976)* 26: 2316-2322.
55. Maldonado BA, Oegema TR, Jr. 1992. Initial characterization of the metabolism of intervertebral disc cells encapsulated in microspheres. *J Orthop Res* 10: 677-690.
56. Lee K, Deeds JD, Segre GV. 1995. Expression of parathyroid hormone-related peptide and its receptor messenger ribonucleic acids during fetal development of rats. *Endocrinology* 136: 453-463.
57. Mak KK, Kronenberg HM, Chuang PT, Mackem S, Yang Y. 2008. Indian hedgehog signals independently of PTHrP to promote chondrocyte hypertrophy. *Development* 135: 1947-56.
58. Ye K, Cao L, Li S, Yu L, Ding J. 2016. Interplay of matrix stiffness and cell-cell contact in regulating differentiation of stem cells. *ACS Appl Mater Interfaces* 8: 21903-21913.
59. Binch AL, Cole AA, Breakwell LM, et al. 2015. Nerves are more abundant than blood vessels in the degenerate human intervertebral disc. *Arthritis Res Ther* 17: 370-015-0889-6.
60. Johnson WE, Eisenstein SM, Roberts S. 2001. Cell cluster formation in degenerate lumbar intervertebral discs is associated with increased disc cell proliferation. *Connect Tissue Res* 42: 197-207.
61. Sharp CA, Roberts S, Evans H, Brown SJ. 2009. Disc cell clusters in pathological human intervertebral discs are associated with increased stress protein immunostaining. *Eur Spine J* 18: 1587-1594.

62. Kellner K, Lang K, Papadimitriou A, et al. 2002. Effects of hedgehog proteins on tissue engineering of cartilage in vitro. *Tissue Eng* 8: 561-572.
63. Zhang W, Chen J, Tao J, et al. 2013. The promotion of osteochondral repair by combined intra-articular injection of parathyroid hormone-related protein and implantation of a bi-layer collagen-silk scaffold. *Biomaterials* 34: 6046-6057.
64. Kim YJ, Kim HJ, Im GI. 2008. PTHrP promotes chondrogenesis and suppresses hypertrophy from both bone marrow-derived and adipose tissue-derived MSCs. *Biochem Biophys Res Commun* 373: 104-108.
65. Willems N, Tellegen AR, Bergknut N, et al. 2016. Inflammatory profiles in canine intervertebral disc degeneration. *BMC Vet Res* 12: 10-016-0635-6.
66. Sasano Y, Takahashi I, Mizoguchi I, et al. 1998. Type X collagen is not localized in hypertrophic or calcified cartilage in the developing rat trachea. *Anat Embryol (Berl)* 197: 399-403.

## Supplementary File 1 . Canine and human IVD donors for immunohistochemistry

## Canine IVD donors for IHH-PTHrP-related IHC

Dog number	IVD level	Age (months)	CD/NCD	Breed
<b>Thompson score I</b>				
1	T12/T13	16	NCD	Flatcoated retriever
2	T11/T12	7	NCD	Mongrel
3	T12/T13	36	NCD	Kerry beagle
4	L7/S1	36	NCD	Kerry beagle
5	L5/L6	96	NCD	Kerry beagle
3	L4/L5	36	NCD	Kerry beagle
2	T13/L1	16	NCD	Mongrel
6	L4/L5	17	NCD	Mongrel
<b>Thompson score II</b>				
7	L7/S1	25	CD	Beagle
2	L4/L5	16	NCD	Mongrel
8	L6/L7	28	CD	Beagle
9	L4/L5	84	NCD	Foxhound
10	L3/L4	25	CD	Beagle
9	L5/L6	84	NCD	Foxhound
7	L3/L4	25	CD	Beagle
<b>Thompson score III</b>				
11	L7/S1	117	CD	Beagle
11	L6/L7	117	CD	Beagle
9	T13/L1	84	NCD	Foxhound
12	T12/T13	120	NCD	Foxhound
12	L2/L3	120	NCD	Foxhound
7	T13/L1	25	CD	Beagle
12	T13/L1	120	NCD	Foxhound
13	L7/S1	142	NCD	Bouvier
<b>Thompson score IV</b>				
9	L7/S1	84	NCD	Foxhound
14	L2/L3	120	CD	Beagle
15	L7/S1	108	NCD	Foxhound
14	T13/L1	120	CD	Beagle
12	T11/T12	120	NCD	Foxhound
14	L7/S1	120	CD	Beagle
14	L1/L2	120	CD	Beagle
<b>Thompson score V</b>				
14	L5/L6	120	CD	Beagle
14	T11/T12	120	CD	Beagle
14	T12/T13	120	CD	Beagle
16	L7/S1	192	CD	Welsh Terriër
16	L1/L2	192	CD	Welsh Terriër
14	L4/L5	120	CD	Beagle
16	T11/T12	192	CD	Welsh Terriër

## Human IVD donors for IHH/PTHrP-related IHC (level L3-L4)

Number	Age (years)	Gender	Histologic score
<b>Thompson score I</b>			
1	17	Male	0
2	21	Female	0
3	14	Female	1
4	14	Male	0
5	18	Female	3
<b>Thompson score II</b>			
6	63	Male	4
7	35	Male	3
8	50	Female	2
9	39	Male	2
<b>Thompson score III</b>			
10	73	Female	5
11	80	Female	3
12	46	Female	3
13	59	Female	4
<b>Thompson score IV</b>			
14	88	Female	10
15	73	Female	7
16	84	Male	11
17	70	Female	8
18	77	Male	10
<b>Thompson score V</b>			
19	62	Female	10
20	59	Male	10
21	71	Male	9
22	88	Female	9

**Human NP tissue donors for Alizarin Red and IHH/PTHrP-related IHC**

Number	Source	Age	IVD Level	Histological Grade	Classification	Alizarin Red	IHC
1	Surgical	42	L4/L5	3	Non-degenerate	✓	✓
2	Surgical	40	L5/S1	3.9	Non-degenerate	✓	
3	Surgical	25	L4/L5	4.8	Degenerate	✓	
4	Surgical	50	L4/L5	4	Non-degenerate	✓	✓
5	Surgical	33	L5/S1	9	Degenerate	✓	✓
7	Surgical	47	C6/C7	5	Degenerate	✓	✓
8	Surgical	70	L4/L5	7.5	Degenerate	✓	
9	Surgical	32	L5/S1	5	Degenerate	✓	
15	Surgical	34	L4/L5	7.5	Degenerate	✓	✓
19	Surgical	36	L5/S1	9	Degenerate	✓	
24	Surgical	35	L4/L5	2	Non-degenerate	✓	✓
27	Surgical	73	L4/L5	4.7	Degenerate	✓	
30	Postmortem	45	L5/S1	2	Non-degenerate	✓	✓
31	Postmortem	45	L3/L4	1	Non-degenerate	✓	✓
32	Postmortem	45	L3/L4	4	Non-degenerate	✓	✓
33	Surgical	48	L4/L5	8	Degenerate	✓	
36	Surgical	33	L5/S1	9	Degenerate	✓	✓
37	Postmortem	74	L5/S1	3	Non-degenerate	✓	
38	Postmortem	74	L4/L5	5	Degenerate	✓	✓
39	Postmortem	74	L3/L4	11.5	Degenerate	✓	✓
40	Postmortem	74	L2/L3	11	Degenerate	✓	✓
44	Surgical	42	L5/S1	2	Non-degenerate	✓	✓
45	Surgical	36	L5/S1	8	Degenerate	✓	
46	Surgical	41	L5/S1	8.5	Degenerate	✓	
52	Surgical		L4/L5	9	Degenerate	✓	
53	Surgical	38	L5/S1	7	Degenerate	✓	
55	Surgical		L5/S1	6	Degenerate	✓	
56	Surgical	43	L5/S1	8	Degenerate	✓	✓
57	Surgical	44	L5/S1	9	Degenerate	✓	✓
60	Surgical	38	L5/S1	6	Degenerate	✓	✓
63	Surgical	42	L5/S1	5	Degenerate	✓	
65	Surgical	43	L4/L5	10	Degenerate	✓	✓
66	Surgical	62	L3/L4	10	Degenerate	✓	
67	Surgical	39	L4/L5	5	Degenerate	✓	
68	Surgical	62	L4/L5	9	Degenerate	✓	✓
69	Surgical	37	L5/S1	8.5	Degenerate	✓	
70	Surgical	39	L5/S1	7.5	Degenerate	✓	
71	Surgical	42	L5/S1	3	Non-degenerate	✓	
72	Surgical		C5/C6	9.5	Degenerate	✓	
74	Surgical		L4/L5	7.5	Degenerate	✓	

75	Surgical	40	L3/L4	11	Degenerate	✓	✓
78	Surgical	54	C3/C4	10	Degenerate	✓	
80	Surgical	33	L5/S1	5	Degenerate	✓	✓
84	Surgical	38	C6/C7	5	Degenerate	✓	✓
85	Surgical	85	L2/L3	8	Degenerate	✓	
86	Surgical	40	L5/S1	9	Degenerate	✓	
89	Surgical	21	L5/S1	4	Non-degenerate	✓	✓
90				11	Degenerate	✓	✓
93	Surgical	38	L5/S1	12	Degenerate	✓	✓
95	Surgical	38	L5/S1	6	Degenerate	✓	✓
97	Surgical	46	L5/S1	10	Degenerate	✓	
100	Surgical	43	L5/S1	7	Degenerate	✓	✓
101	Surgical	54	C5/C6	4.5	Degenerate	✓	✓
103	Surgical	45	C5/C6	9.5	Degenerate	✓	✓
104	Surgical	33	L5/S1	5.5	Degenerate	✓	
109	Surgical	29	L4/L5	7	Degenerate	✓	
110	Surgical	24	L3/L4	3	Non-degenerate	✓	
111	Surgical	68	L4/L5	8	Degenerate	✓	
112	Surgical	42	L5/S1	11	Degenerate	✓	✓
118	Surgical	27	L4/L5	8	Degenerate	✓	
121	Surgical	27	L4/L5	3	Non-degenerate	✓	✓
122	Surgical	29	L4/L5			✓	
124	Surgical	40	L4/L5	3.5	Non-degenerate	✓	✓
127	Surgical	27	L5/S1	4	Non-degenerate	✓	
133	Surgical	35	L4/L5	7	Degenerate	✓	
134	Surgical	54	C5/C6	9	Degenerate	✓	
136	Surgical	33	L4/L5			✓	
144	Surgical	37	L5/S1	9	Degenerate	✓	✓
145	Surgical	38	L4/L5	11	Degenerate	✓	✓
146	Surgical	47	L5/S1	7	Degenerate	✓	
154	Surgical	52	L4/L5	11	Degenerate	✓	
157	Surgical	31	L5/S1	5	Degenerate	✓	
159	Surgical	39	L4/L5	9	Degenerate	✓	
161	Surgical	39	C6/C7	7	Degenerate	✓	✓
170	Surgical		L5/S1	10	Degenerate	✓	✓
174	Surgical	29	L5/S1	6	Degenerate	✓	
175	Surgical	37	L5/S1	7	Degenerate	✓	
177	Surgical	51	L4/L5	2	Non-degenerate	✓	✓
179	Surgical	79	C4/C5	4	Non-degenerate	✓	✓
184	Surgical	49	L4/L5	5	Degenerate	✓	✓
192	Surgical	29	L5/S1	8	Degenerate	✓	
194	Surgical	35	L4/L5	11	Degenerate	✓	
197	Surgical	42	L4/L5	8	Degenerate	✓	✓

203	Surgical	45	L5/S1	4	Non-degenerate	✓	
207	Surgical	38	L5/S1	8	Degenerate	✓	
225	Surgical	36	L5/S1	10	Degenerate	✓	✓
228	Surgical			7	Degenerate	✓	
229	Surgical	56	L4/L5	6	Degenerate	✓	
230	Surgical	56	L5/S1	8.5	Degenerate	✓	
231	Surgical	56	L4/L5	5	Degenerate	✓	
232	Surgical	58	L5/S1	8	Degenerate	✓	
233	Surgical	44	L5/S1	10	Degenerate	✓	✓
234	Surgical	54	L5/S1	9	Degenerate	✓	✓
243	Surgical	28	L4/L5	6	Degenerate	✓	
244	Surgical	43	L4/L5	4	Non-degenerate	✓	✓
245	Surgical	80	L4/L5	4	Non-degenerate	✓	✓
253	Surgical	63	C5/C6	4	Non-degenerate	✓	
254	Surgical	47	L4/L5	6	Degenerate	✓	✓
257	Surgical	46	L5/S1	3	Non-degenerate	✓	✓
263				9	Degenerate	✓	✓
264	Surgical	65	C3/C5	6	Degenerate	✓	
266	Surgical	27	L5/S1	4	Non-degenerate	✓	
272	Surgical	26	L5/S1	4.5	Degenerate	✓	
276	Surgical	71	C5/C6	6	Degenerate	✓	✓
288	Surgical	73	C6/C7	5	Degenerate	✓	
292	Surgical	23	L2/L3	4	Non-degenerate	✓	
310	Surgical	37	L4/L5	5	Degenerate	✓	
319	Surgical	47	L5/S1	5	Degenerate	✓	
320	Surgical	68	L4/L5	4	Non-degenerate	✓	✓
322	Surgical	48	L4/L5	5	Degenerate	✓	✓
321	Surgical	22	L4/L5	4	Non-degenerate	✓	
328	Surgical	38	L5/S1	6	Degenerate	✓	✓
329	Surgical	48	L5/S1	5	Degenerate	✓	
330	Surgical	32	L5/S1	5.5	Degenerate	✓	
332	Surgical	24	L5/S1	10	Degenerate	✓	
336	Surgical	40	L5/S1	7	Degenerate	✓	✓
337	Surgical	24	L5/S1	7	Degenerate	✓	
338	Surgical	29	L5/S1	8	Degenerate	✓	
340	Surgical	42	L5/S1	7	Degenerate	✓	✓
342	Surgical	18	L4/L5	6	Degenerate	✓	✓
346	Surgical	46	C5/C6	6	Degenerate	✓	
348	Surgical	67	C4/C5	9	Degenerate	✓	✓
350	Surgical	38	L4/L5	9	Degenerate	✓	
352	Surgical	82	L4/L5	8	Degenerate	✓	
355	Surgical	33	L4/L5	5	Degenerate	✓	
356	Surgical	26	L5/S1	4	Non-degenerate	✓	

<b>357</b>	Surgical	53	L4/L5	4	Non-degenerate	✓
<b>360</b>	Surgical	50	C6	5.5	Degenerate	✓
<b>374</b>	Surgical	37	L4/L5	4	Non-degenerate	✓
<b>375</b>	Surgical	41	L5/S1	6	Degenerate	✓
<b>379</b>	Postmortem	33	L3/L4	5	Degenerate	✓
<b>384</b>	Surgical	47	L5/S1	5	Degenerate	✓
<b>388</b>	Surgical	54	C6/C7	6	Degenerate	✓

✓: only used for IHH IHC

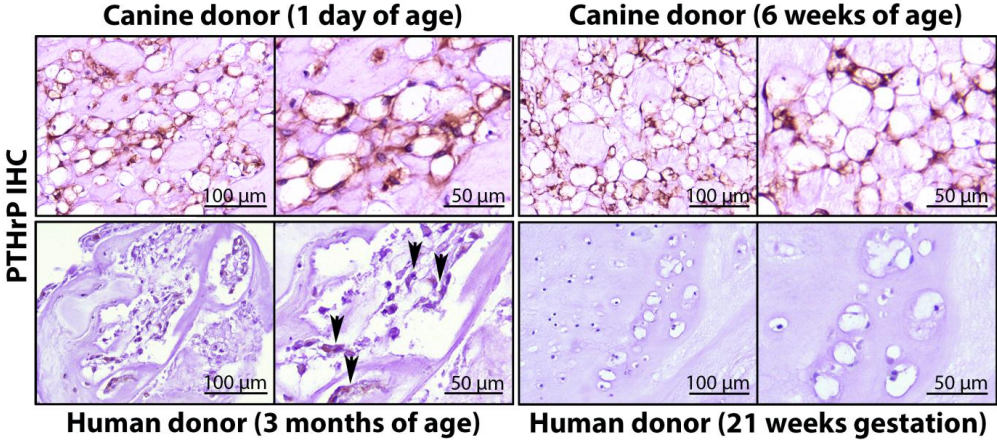
✓: used for PTHrP, PTHR1, IHH, SMO, and PTCH IHC

## Supplementary File 2. Primers used for quantitative PCR

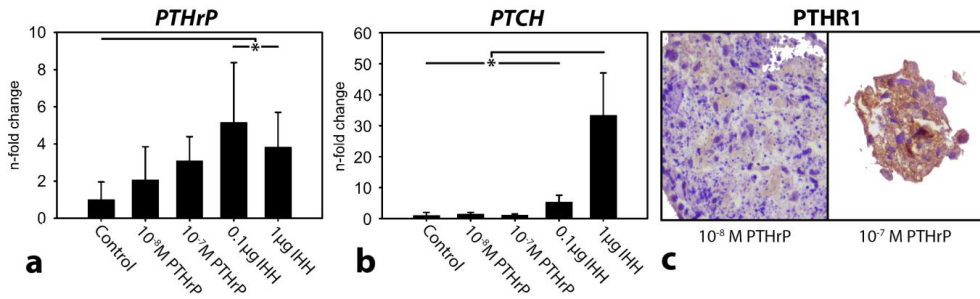
## Primers used for quantitative PCR of canine samples

Genes	Forward sequence 5' → 3'	Reverse sequence 5' → 3'	Amplicon size
<b>Reference genes</b>			
<i>GAPDH</i>	TGTCCCAACCCCAATGTATC	CTCCGATGCCTGCTTCACTACCTT	100
<i>HPRT</i>	AGCTTGCTGGTGAAAAGGAC	TTATAGTCAAGGGCATATCC	104
<i>RPS19</i>	CCTTCCTCAAAAAGTCTGGG	GTTCTCATCGTAGGGAGCAAG	95
<i>SDHA</i>	GCCTTGGATCTCTTGATGGA	TTCTTGGCTCTTATGCGATG	92
<b>Target genes</b>			
<i>GLI1</i>	TCAAGGCTCAGTACATGCTG	ATGGCTTCTCATTGGAGTGG	240
<i>GLI2</i>	CACGCTCTGGGAAATGAGG	CGGGCATCAGCAACATG	145
<i>GLI3</i>	CCAGCAGGAACAGCCAG	GAACTCCTTCTTCGCCG	190
<i>IHH</i>	TCACCACTCAGAGGAGTCG	GTGCTCAGACTTGACGGAG	172
<i>PTCH</i>	CCTCCTCATATTTGGGGC	CACCTTCTTCTTCGGGG	158
<i>PTHrP</i>	GTGTTCTGCTGAGCTACTCG	ATGGGTGGTCGCCTTCTA	451
<i>PTHR1</i>	GACCACATCCTTTGCTGG	CAAACACCTCCCGTTCAC	217
<i>SHH</i>	CAGTGGAAGATACGAAGGA	TTGCCTTGACACCTCTGAG	140
<i>SMO</i>	CTATGTGCTGTGCCAG	ATCACTCTGCCAGTC	214

**Supplementary File 3. PTHrP protein expression in young canine and human nucleus pulposus tissue**

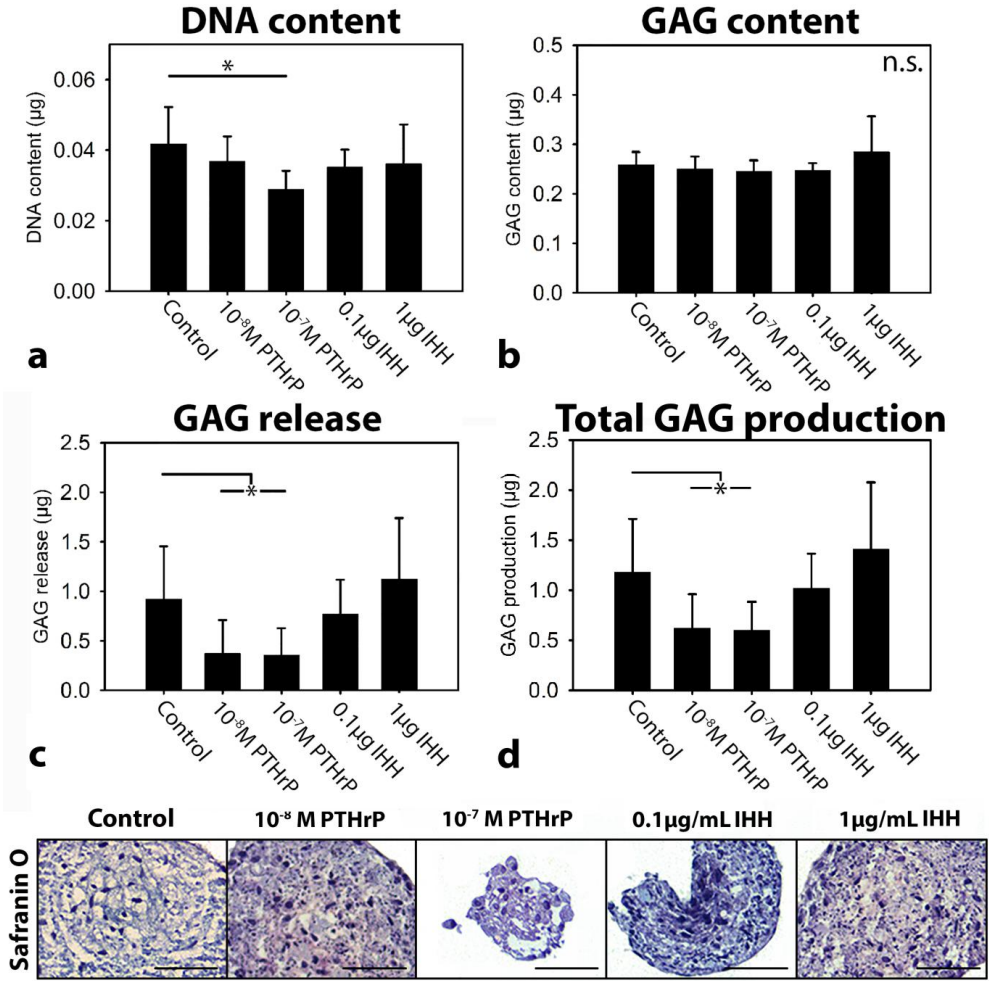


PTHrP: Parathyroid hormone-related protein. *n*=8 (canine), 12 (human). Human NP tissue with some PTHrP expression is shown in the lower left panel, whereas the lower right picture shows human NP tissue not expressing PTHrP. In every panel, the right picture is a two times magnified version of the left picture.

Supplementary File 4. The effect of IHH and PTHrP on canine CLC gene expression *in vitro*

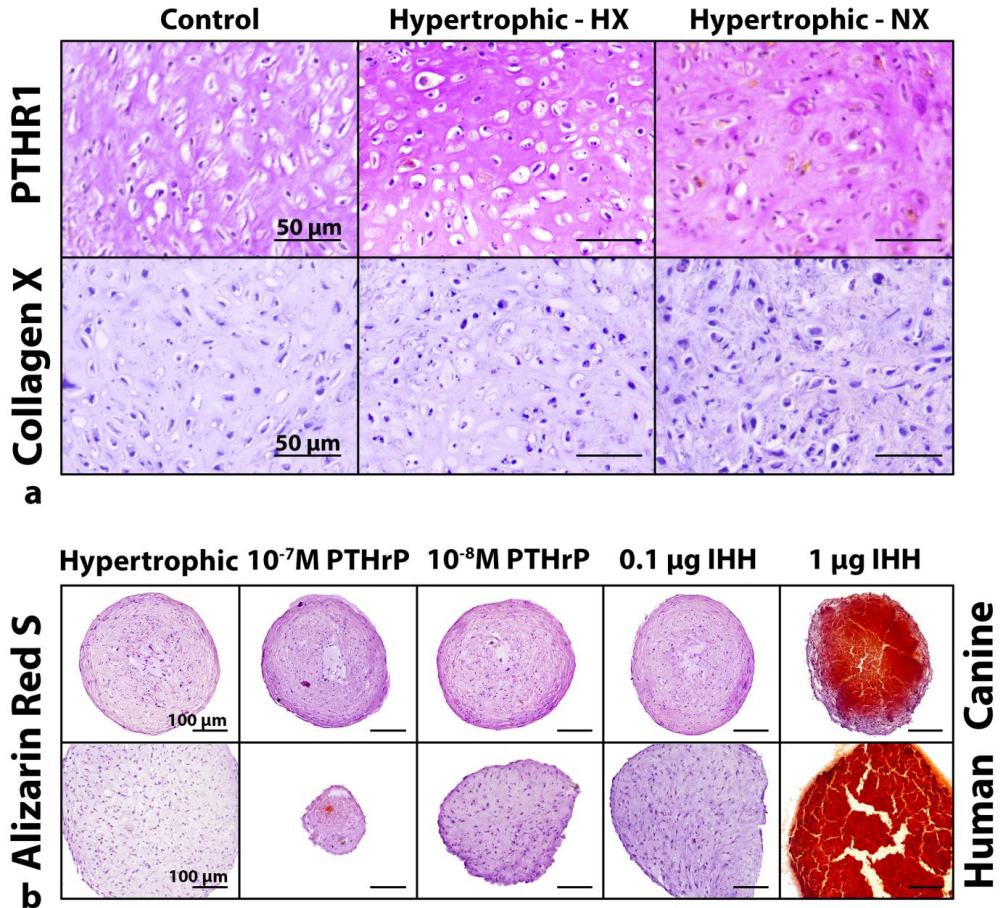
Gene expression levels of canine CLC micro-aggregates cultured for 24 hours in basal culture medium (control), supplemented with/without 0.1 or 1  $\mu$ g/mL IHH or  $10^{-8}$  or  $10^{-7}$  M PTHrP in hypoxia (5% O<sub>2</sub>). Relative *PTHrP* (a) and *PTCH* (b) gene expression (mean + SD) of the micro-aggregates. Control micro-aggregates were set at 1. \*:  $p < 0.05$ .  $n = 6$ . IHH: Indian hedgehog; PTHrP: Parathyroid hormone-related protein; GAG: glycosaminoglycan. n.s.: not significant. (c) PTHR1 immunopositivity in 14-day  $10^{-8}$  and  $10^{-7}$  M PTHrP-treated canine CLC micro-aggregates. IHH: Indian hedgehog; PTHrP: Parathyroid hormone-related protein, PTHR1: PTHrP receptor, PTCH: patched.

**Supplementary File 5. The effect of IHH and PTHrP on GAG production of canine CLCs *in vitro***



DNA content, GAG content and release (mean + SD) and histological evaluation of canine CLC micro-aggregates treated with basal culture medium (control), supplemented with 10<sup>-8</sup> or 10<sup>-7</sup> M PTHrP or 0.1 or 1 µg/mL IHH for 14 days in hypoxia (5% O<sub>2</sub>). DNA content (a), GAG content (b), GAG release (c), total GAG production (d) and representative histological images of the Safranin O/Fast Green staining. \*: *p*<0.05. *n*=6 (in duplo). IHH: Indian hedgehog; PTHrP: Parathyroid hormone-related protein; GAG: glycosaminoglycan. n.s.: not significant. Scale bar represents 50 µm.

Supplementary File 6. The effect of IHH and PTHrP on hypertrophic CLC differentiation *in vitro*



(a) Normoxia facilitates hypertrophic CLC differentiation compared with hypoxia. PTHR1 and collagen type X expression in canine CLC micro-aggregates that were cultured for 4 weeks in basal culture medium supplemented with 10 ng/mL TGF-β<sub>1</sub> (control) or micro-aggregates that were cultured for 1 week in basal culture medium with 10 ng/mL TGF-β<sub>1</sub>, followed by a 3-week culture in hypertrophic induction medium. HX: hypoxia, NX: normoxia. *n*=6. (b) IHH facilitates calcification. Alizarin Red S staining of canine and human CLC micro-aggregates cultured for 1 week in basal culture medium with 10 ng/mL TGF-β<sub>1</sub>, followed by a 6-week culture in hypertrophic induction medium (hypertrophic). 0.1 or 1 μg/mL IHH and 10<sup>-8</sup>M or 10<sup>-7</sup>M PTHrP were supplemented after 4 weeks of culture. *n*=6; IHH: Indian hedgehog; PTHrP: Parathyroid hormone-related protein.



## Chapter 12

### Summarizing discussion

Back pain due to intervertebral disc (IVD) degeneration (IVD disease) is a major health problem in both humans and dogs<sup>1-4</sup>. Current treatments are only symptomatic, and therefore, regenerative treatment strategies, aiming to biologically repair the IVD at an earlier stage, are emerging. Research in the field of regenerative medicine increases the understanding of disease processes. Outcomes may ultimately be translated into minimally invasive therapeutic interventions for both veterinary and human patients according to the 'One Health' principle. There are indications that at least in the dog, IVD degeneration starts in the nucleus pulposus (NP)<sup>5</sup>. Therefore, the studies described in this thesis investigated new strategies to regenerate the NP, as a treatment for human and canine IVD degeneration, by focusing on developmental biology. Results, challenges, and future perspectives are discussed below.

## Notochordal cell-based treatment strategies

Loss of the notochordal cell (NC) population in the NP is associated with the development of IVD degeneration, indicating that NCs may play an important role in maintaining healthy NP tissue<sup>6</sup>. Work performed by others indeed indicates that NCs secrete bioactive factors with regenerative potential when used to treat NP-derived chondrocyte-like cells (CLCs)<sup>7-13</sup> and mesenchymal stromal cells (MSCs)<sup>12, 14-20</sup>. The work described in this thesis not only confirms these findings, but also adds new insights to the field. We were the first to compare the regenerative potential of NC-conditioned medium (NCCM) from different (human, canine, porcine) species (**Chapter 2**), and found that the NC-secreted bioactive factors exert cross-species effects. The regenerative effect of porcine and canine NCCM, however, appeared more potent than that of human NCCM. In addition, based on ethical considerations and the fact that healthy canine and especially porcine NP tissue is more easily obtained than healthy human NP tissue, we mainly concentrated on canine and porcine NC-rich NP tissue in follow-up studies.

In our second NCCM-based study, we performed mass spectrometry to identify the bioactive components secreted by NCs (**Chapter 3**), but mainly identified extracellular matrix (ECM)-related proteins and no growth factors. This is in contrast with previous studies that were able to detect specific (growth) factors<sup>10, 15, 21, 22</sup>. Most of these studies, however, generated NCCM from isolated NCs, whereas we employed whole NC-rich NP tissue. Potential growth factors may therefore be overshadowed by large quantities of ECM-related proteins. For future studies, it is therefore recommended to first fractionate NCCM (thereby separating large ECM proteins such as proteoglycans ( $\pm$  220 kDa) from smaller growth factors (30-50 kDa)) and thereafter perform mass spectrometry on the obtained fractions. Besides ECM-related proteins, we also identified membrane bound vesicle proteins, indicating that extracellular vesicles (EVs) might be present in NCCM. By carrying bioactive molecules, EVs serve in intracellular signaling and can be involved in tissue regeneration<sup>23</sup>. We were the first to show that NCCM indeed contains EVs that exert regenerative effects on canine and human CLCs (**Chapter 4**). As a future perspective, the regenerative potential of NC-derived EVs versus CLC-derived EVs should be compared to gain more fundamental knowledge on the IVD degeneration process. Besides, the role of EVs as carriers need to be elucidated to fully exploit their regenerative potential. The next recommended step is the identification of the bioactive substances which are transported with the EVs. First, these factors and the

subsets of EVs that contain them should be identified (*e.g.* using lipidomics, mass spectrometry and/or RNA sequencing). Thereafter, the EV subsets of interest or the recombinantly synthesized variant of identified factors could be used to perform functional *in vivo* studies.

Phenotypically, NCs contain large, membrane-bound cytoplasmic vesicles<sup>24</sup>. These cytoplasmic vesicles are generated by post-Golgi trafficking pathways: cargo is synthesized within the endoplasmic reticulum (ER) and transported into the Golgi apparatus, after which the cargo is sorted and delivered to endosomes and finally lysosomes, or routed into secretory granules or plasma membrane for release<sup>25, 26</sup>. Indeed, NC cytoplasmic vesicles are lysosome-related organelles failing to vacuolate when ER to Golgi transport is blocked<sup>27</sup>. In **Chapter 4** of this thesis, we show that EVs are abundantly secreted by NCs. Since EVs are also membrane-bound and can also have an endosomal origin<sup>28</sup>, they could well be related to the vacuoles. The sorting mechanism through which cargo is transported into vacuoles rather than lysosomes as well as the content of the NC vacuoles are still unclear<sup>29</sup>. The vacuoles are electron-lucent and stain negative for eosin, Periodic Acid-Schiff, Oil Red O, and Alcian Blue, suggesting that they could contain water<sup>27, 29-31</sup> and are possibly involved in osmoregulation<sup>31</sup>. Since NC vacuoles are versatile organelles in the embryonic notochord and postnatal NP, they might also be involved in the NC-mediated regenerative effects. In line with this, during IVD maturation, vacuolated NCs are replaced by non-vacuolated CLCs<sup>24</sup>. Assuming that the NC vacuoles indeed have regenerative potential, the absence of vacuoles in CLCs may explain their lower regenerative potential. Taken together, studying the NC vacuoles may provide novel information, possibly enabling guidance for NC-based IVD regeneration. For this reason, future studies should elucidate the content and the specific role of the NC vacuoles. Lastly, it would be worthwhile studying the exact relationship between the EVs and vacuoles of NCs.

**Chapters 2-4** demonstrate the challenges in identifying and isolating NC-secreted bioactive factors. A more straightforward approach for IVD regeneration was investigated by applying whole NC-derived matrix (NCM) derived from healthy porcine NPs (**Chapter 5**). NCM (10 mg/mL) demonstrated a promising regenerative potential *in vitro* and *in vivo*. We can only hypothesize what the mechanism of action of NCM is. Presumably, the ECM present in NCM provides a beneficial niche for the CLCs, enabling them to proliferate and produce healthy ECM themselves. Besides, NCM may serve as 'instructive matrix', locally releasing growth factors, similarly as cartilage oligomeric matrix protein (COMP)<sup>32, 33</sup> or demineralized bone matrix (DBM)<sup>34, 35</sup>. Because of the high ECM concentration of NCM (about five times higher than NCCM), it should first be fractionated to be able to identify growth factors and/or EVs if present. A different approach would be to culture CLCs or IVD explants in NCM and determine (phosphorylated) proteins that are up- or down-regulated in the NCM-treated cells/tissue, respectively. In this way, clues for signalling pathways that are activated by NCM can be obtained. Besides identifying the working mechanism of NCM, higher concentrations could be tested and, if feasible, intradiscally applied in hydrogels, thereby reducing the change of leakage. Follow-up *ex vivo* (whole organ IVD spinal units in bioreactors) or *in vivo* studies (in animal models) should focus on dose finding and subsequent translation from bench-to bedside, *e.g.* by using veterinary patients suffering from spontaneously developed clinical IVD disease. Safety aspects including methods to remove nucleic acids from NCM

without affecting its biologic activity should be optimized before NCM can be applied clinically in human and veterinary patients.

## Stem cell-based treatment strategies

MSCs are an emerging target for regenerative medicine, since they can easily be isolated from a variety of tissues, can differentiate into different cell types, have immunosuppressive properties, and secrete trophic factors<sup>36-38</sup>. The effect of canine MSCs was tested on canine CLCs in **Chapter 7** and on degenerated canine IVDs in **Chapter 5**. In both the *in vitro* (28 days) and the *in vivo* (six months) study, however, the MSCs did not exert beneficial effects. These results are in contrast with previous *in vitro*<sup>39,40</sup> and *in vivo*<sup>41-43</sup> studies and might be due to the heterogeneity of the MSC population<sup>44</sup>. Previous work indicated that the percentage of senescent MSCs increased linearly with culture time in all tested canine breeds<sup>45</sup>. Additionally, canine MSCs were not always able to chondrogenically differentiate, with differentiation potential differences between breeds<sup>45</sup>. Taken together, the studies described in this thesis show that the quality of MSC-based treatment strategies is not easily guaranteed in veterinary medicine. Therefore, future studies are warranted to optimize conditions that enable survival and differentiation of canine MSCs.

A better alternative to bone marrow-derived MSCs could be the tissue specific progenitor cells. Local Tie2 expressing NP progenitor cells (NPPCs) were first described in humans and mice<sup>46</sup>, and later in bovines<sup>47</sup>, indicating that they are preserved throughout species. Tie2<sup>+</sup> NP cells possess superior ECM production, self-renewal, multipotent differentiation and proliferation capacity<sup>46</sup>. The young, healthy NP itself may thus represent a niche of precursor cells for IVD regeneration superior to MSCs. Preliminary work in collaboration with the research group of Daisuke Sakai (Tokyo, Japan) has demonstrated that Tie2<sup>+</sup> cells are present in fetal-young human, canine and porcine NPs (**Figure 1**). Future studies should explore the presence of NPPCs in different canine species (chondrodystrophic and non-chondrodystrophic dogs) in health and IVD disease. Besides, it should be determined whether NPPCs exert regenerative effects in NPPC:CLC co-cultures or by applying conditioned medium generated from NPPCs. If a pronounced regenerative effect of NPPCs is detected *in vitro*, it could be investigated whether intradiscal NPPC delivery is also able to induce regenerative effects in species suffering from clinical IVD disease *in vivo*. A challenge for the clinical use of NPPCs, however, is their yield, since the NPPC population decreases with IVD ageing and degeneration<sup>46</sup>. Since both NCs and NPPCs are lost with degeneration, there may be an instructive role of either NCs on NPPCs or *vice versa*. In this respect, the instructive roles of NC-derived and NPPC-derived bioactive factors should be investigated. Furthermore, since NPPC expansion seems inevitable to obtain sufficient numbers for intradiscal injection, it should be elucidated whether NPPCs from species with clinical IVD disease lose their characteristics during expansion and which conditions best preserve their progenitor criteria. In this respect, it has already been demonstrated that addition of FGF2 and hypoxia preserved bovine NPPCs in monolayer culture for 7 days<sup>47</sup>.

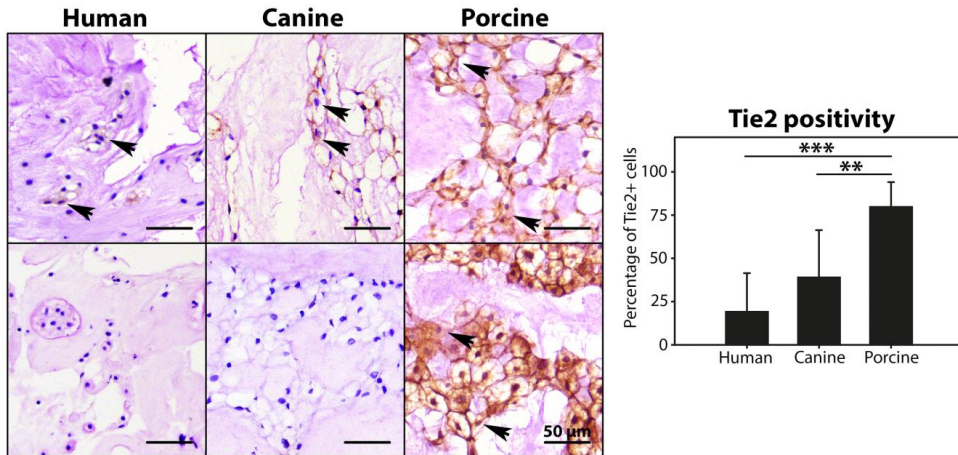


**Figure 1.** Tie2 expression in nucleus pulposus tissue from young human (20 weeks of pregnancy–3 months postnatal,  $n=15$ ), canine (stillborn,  $n=11$ ) and porcine (1.5 months postnatal,  $n=9$ ) donors. The percentage of Tie2 positive cells is significantly higher in young porcine than the percentages found in young human and canine nucleus pulposus tissue. Tie2 immunopositivity (present in the cell membrane) varies considerably in young human (0–57%) and canine (0–83%) donors, but less in young porcine (66–93%) donors. The upper and lower picture represent the nucleus pulposus of two donor examples per species. Bars represent 50  $\mu\text{m}$ . (Positive) cell numbers were manually counted in each NP using Photoshop CC and the percentage of Tie2 positive cells was calculated per donor. \*\*:  $p<0.01$ , \*\*\*:  $p<0.001$ .

## Growth factor-based treatment strategies

Besides cell-based therapies, regenerative medicine also focuses on the use of growth factors to stimulate cell proliferation and/or healthy ECM synthesis. The studies described in **Chapter 6** tested bone morphogenetic protein-7 (BMP7) (which has previously been shown to stimulate ECM production in IVD cells *in vitro*<sup>48, 49</sup> and in animal models of induced IVD degeneration *in vivo*<sup>50–52</sup>) in a canine model with spontaneous IVD degeneration. No beneficial effects were found. The results of this chapter demonstrate that (a) promising *in vitro* results (increased cell proliferation and glycosaminoglycan (GAG) synthesis) do not always result in beneficial results *in vivo*, (b) side effects that develop *in vivo* (e.g. extradiscal bone formation) cannot always be predicted from *in vitro* studies, and (c) the effect of a regenerative treatment may differ between animal models in which degeneration is induced and animals with spontaneously developed IVD degeneration.

**The question remains how adequately animal models, with induced IVD degeneration, represent the human situation.** This dilemma is further highlighted by the studies described in **Chapter 8**. Herein, the effect of Link-N and short (s)Link-N was studied on canine CLCs to facilitate translation of Link-N into the clinic by using the dog as large animal model for human IVD degeneration. No relevant effect of canine or human (s)Link-N was detected on canine CLCs, however, in contrast to the beneficial effect observed in human CLCs. Thus, although both dogs and humans spontaneously develop IVD degeneration with similar characteristics<sup>1</sup>, the dog is not always the best suited model for studying human IVD degeneration. The studies in **Chapter 7** confirm this, since CLCs from chondrodystrophic

dogs, non-chondrodystrophic dogs, and humans did not always similarly respond to growth factor treatment *in vitro*.

In the continuing search for a valid large animal model for Link-N treatment of human IVD degeneration, we recently employed CLCs from six sheep by using the same set up as for the other species. Surprisingly, the ovine donors showed a variable chondrogenic response to basal culture medium with/without TGF- $\beta_1$  or (s)Link-N, which may be attributed to their genetic background. In the Netherlands, Swifter sheep are available for experimental studies. These sheep have been crossed with New-Zealand Texel sheep, which possess a quantitative trait locus mapping to the growth differentiation factor-8 (GDF8 or myostatin) gene, a potent negative regulator of skeletal muscle growth<sup>53</sup>. Myostatin induces atrophy by inhibiting the AKT pathway, which promotes protein synthesis, and increasing the activity of the ubiquitin-proteasome system<sup>53</sup>. In Texel sheep, a single G to A transition in the 3' untranslated region of GDF8 creates a target site for microRNAs (*e.g.* *miR1* and *miR206*), thereby inhibiting transcription of GDF8 and promoting muscle hypertrophy<sup>54</sup>. The latter is beneficial from an economic animal production standpoint. Additionally, GDF8 has been suggested to inhibit chondrogenesis by suppressing *SOX9* and collagen type II expression in MSCs<sup>55</sup>. However, the role of GDF8 in IVD (patho)physiology has not been explored yet. To determine whether the genotype can explain the variable chondrogenic capacity of the ovine donors, the presence of the polymorphism was investigated in the Swifter sheep population. Forty-one sheep were screened, of which 40% carried two copies (AA) and 40% carried one copy of the A allele (AG), whereas 20% did not carry the polymorphism (GG). Interestingly, the number of A copies correlated with the chondrogenic capacity of the donors: AA donors were able to produce GAG-rich matrix in basal culture medium, while GG donors were not able to produce GAG-rich matrix in the absence of growth factors, and the AG donors responded intermediately (**Figure 2**). The results of these preliminary studies thus imply that the regenerative capacity of ovine donors is dependent on their genotype. Moreover, only AA and AG donors were able to respond to (s)Link-N, indicating that GDF8 signalling influences (s)Link-N signalling. Considering the fact that the human population does not carry this polymorphism, GG sheep seem to better represent the human situation and should be used in experimental animal studies. Lastly, GDF8 could be a valuable target to further explore in the search for a regenerative treatment for IVD degeneration and ongoing studies explore this possibility.

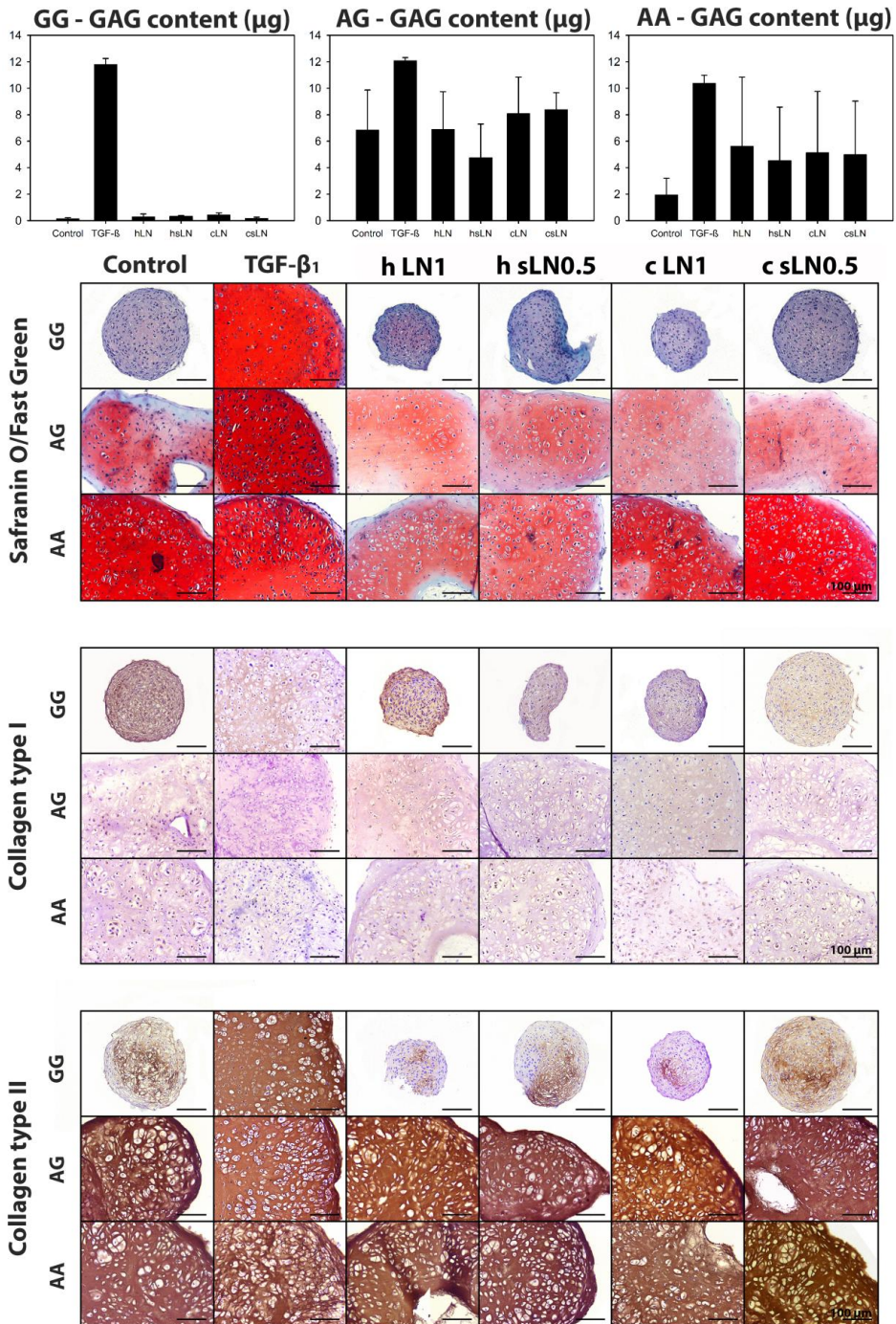


**Figure 2. Effect of the GDF8 polymorphism on extracellular matrix production.** Histological images of the Safranin O/Fast green staining and collagen type I and II IHC of ovine CLC micro-aggregates treated with basal culture medium (control), supplemented with 10 ng/mL TGF- $\beta_1$ , 1  $\mu$ g/mL (1) human (h)/canine (c) Link-N (LN), or 0.5  $\mu$ g/mL (0.5) short Link-N (sLN) for 28 days in hypoxia.  $n=2$  ovine donors per condition.

Taken together, the studies described in abovementioned chapters demonstrate the importance of sharing side effects and ‘negative’ results to the field to prevent others from performing otiose (animal) experiments<sup>56</sup>. This moral obligation not only concerns researchers, but also journal editors and reviewers, when reviewing studies with ‘negative results’. Follow-up animal experiments carried out by researchers that are not informed by negative results (because they are not publishable) cause unnecessary animal suffering and are in direct contrast with the obligation of every researcher that uses animals, *e.g.* looking for means to reduce, refine, and replace animal experiments. The unexpected loss of a dog’s life that we experienced early in the study described in **Chapter 5** gave us valuable baseline information and made that particular dog an important part of the study. Moreover, the multispecies (s)Link-N study described in **Chapter 8** stresses the importance of choosing a proper animal model to test a regenerative treatment, *e.g.* taking into consideration the genetic background of the animals.

The studies described in **Chapter 5** and **Chapter 6** furthermore demonstrate that no adverse effects were observed due to the intradiscal injections themselves, indicating that even in small Beagle IVDs, low volumes can be safely injected under fluoroscopic guidance using 25-27 G needles. This is significant and important information, consistent with previous findings by our group using the intradiscal delivery route<sup>57-59</sup> and contradicts with the conclusions of another study<sup>60</sup>. The latter study has influenced many follow-up studies in the spine research field in the last decade and refrained researchers to use the intradiscal injection route to deliver regenerative strategies to the NP. It has even driven research into other more invasive approaches, *e.g.* perforation of the end plate<sup>61</sup>.

## What can we learn from developmental biology?

The studies described in **Chapter 9** of this thesis demonstrate that the membrane protein caveolin-1 was able to exert growth factor-like effects by augmenting TGF- $\beta$  signaling. Interestingly, since caveolin-1 is present in membranes, it might also be involved in the EV-mediated regenerative effects we observed in **Chapter 4**, and future studies should elaborate on this. Furthermore, it appeared that caveolin-1 was involved in the preservation of the NC phenotype, since the NP of wild type mice was rich in NCs, whereas the NP of caveolin-1 null mice contained CLCs and fibroblast-like cells.

At this moment, we can only speculate how caveolin-1 mediates the maintenance of the NC phenotype. Glucose deprivation has been shown to stimulate caveolin-1 and glucose transporter 4 (GLUT4) expression, while caveolin-1 depletion caused a decreased GLUT4 expression in several cell types<sup>62, 63</sup>. Therefore, a protective role for caveolin-1 was suggested during nutrient deprivation. NCs are more metabolically active and more susceptible to nutrient deprivation than CLCs<sup>64</sup>. Furthermore, the change in NP cell phenotype from NCs towards CLCs (*i.e.* IVD maturation) coincides with a decreased vascular supply to the growing human IVD<sup>65</sup>, also implying that decreased nutrient availability might be a main factor involved in the disappearance of NCs from the IVD. Moreover, canine IVD maturation (when NCs are replaced with CLCs) involved a significant down-regulation of caveolin-1 expression<sup>66</sup>. Thus, perhaps caveolin-1 helps to maintain an adequate nutrient (glucose) uptake in NCs. A second option would be that caveolin-1 mediates its effects via

influencing signaling pathways such as Wnt signaling, since caveolin-1 co-localizes with  $\beta$ -catenin in NC membranes<sup>66</sup>. Maturation of the canine IVD involved a significant down-regulation of caveolin-1 and *AXIN2* expression<sup>66</sup>. As Wnt signaling regulates the fate of the notochord and stem cell renewal and apoptosis, decreased Wnt signaling (*i.e.* during IVD maturation and in the caveolin-1 null IVD) may result in increased apoptosis and decreased self-renewal of NCs<sup>66</sup>. Lastly, caveolin-1 may possibly preserve the NC phenotype via hedgehog signaling, since it co-localizes with the indian hedgehog (IHH)/sonic hedgehog (SHH) receptor patched (PTCH) in the cell membrane<sup>67</sup>.

The IHH-Parathyroid hormone-related protein (PTHrP) pathway is known to play a role in chondrocyte differentiation and osteoarthritis<sup>68-73</sup>, but their role in the IVD is largely unknown. The studies described in **Chapter 10** investigated the effect of PTHrP on the growth plate, a proper model to study chondrocyte differentiation<sup>74-76</sup>, and found that PTHrP was able to suppress hypertrophic differentiation of growth plate chondrocytes. This may suggest that PTHrP could potentially be used to prevent this undesirable process in regeneration of cartilage, but also in regeneration of the IVD, since hypertrophic differentiation and calcification can also develop during IVD degeneration<sup>77</sup>. Previous work indicated that calcium is able to induce degenerative responses in IVD organ cultures<sup>78</sup>. Based on the outcomes of **Chapter 10**, the studies described in **Chapter 11** determined the expression and possible role of PTHrP and IHH in the postnatal IVD. IHH, PTHrP and related receptor expression as well as calcification levels increased during IVD degeneration. Moreover, IHH had the propensity to facilitate calcification in canine CLCs *in vitro*, in line with results on chondrocytes<sup>70</sup>. In contrast with the results of **Chapter 10**, however, PTHrP was not able to suppress calcification in CLC cultures, but this was merely due to the fact that induction of calcification in CLCs *in vitro* appeared challenging, *i.e.* almost impossible without IHH supplementation. Taken together, the results of **Chapter 10 and 11** may imply that supplementing PTHrP or inhibiting IHH signalling could in the future be a therapeutic approach to inhibit hypertrophic differentiation and calcification during IVD degeneration.

Lastly, the expression of IHH and PTCH was decreased in murine caveolin-1 null NPs compared with wild type NPs and IHH showed a similar expression pattern as caveolin-1 in the postnatal IVD, *i.e.* decreased during IVD maturation, and increased during IVD degeneration. Taken together, this may suggest that caveolin-1 and IHH indeed interact, possibly via PTCH. Future studies are needed to elucidate the precise interaction between caveolin-1 and the IHH-PTHrP signaling pathway, as they are both intriguing targets for the development of regenerative therapies for IVD degeneration. In this respect, the expression and role of SHH, another hedgehog ligand, should also be determined in the postnatal IVD of species suffering from clinical IVD disease, since SHH was found to be important for notochord development and postnatal growth and differentiation of the murine IVD<sup>79-81</sup>.

## General conclusions

In this thesis, new cell- and growth factor-based regenerative strategies for the treatment of human and canine intervertebral disc degeneration were investigated. In this respect, the value of studying developmental biology was demonstrated, as interesting targets were identified, *e.g.* caveolin-1, PTHrP and IHH. Not all proposed agents appeared to exert a positive effect *in vitro* (MSCs, Link-N, TGF- $\beta_1$ ), and promising *in vitro* results did not always translate to beneficial effects *in vivo* (BMP7). However, notochordal cell-based therapies induced regenerative effects across species susceptible for intervertebral disc disease. While identifying the bioactive factors secreted by notochordal cells is challenging, it is valuable from a fundamental perspective and will provide innovative insights for the improvement of regenerative treatment strategies. However, a more straightforward alternative for bench to (veterinary) bedside translation is the application of notochordal cell-derived matrix, which exerted regenerative effects on intervertebral disc (cells) *in vitro* and *in vivo*.

## Key points

### Notochordal cell-based strategies

- Factors secreted from human, canine, and porcine NC-rich NPs exerted regenerative effects on human CLCs. This result indicates a cross-species effect and supports further research into NC-based treatment strategies employing canine or porcine models for translation into humans.
- By mass spectrometry of porcine, canine, and human NCCM, mainly ECM-related proteins were identified, but also membrane-bound vesicle proteins, indicating that NCs secrete EVs.
- Porcine NCCM contained a considerable amount of EVs with regenerative potential upon human and canine CLCs. The EV-mediated effects may be influenced by proteins present in NCCM.
- The application of NC-derived matrix from healthy porcine NPs induced an anabolic, anti-catabolic, anti-apoptotic, and proliferative effect on human and canine CLCs *in vitro*. When intradiscally applied in canine IVDs with moderate (induced) degeneration, NCM exerted beneficial effects on macroscopic, MRI, biochemical and histologic level and ameliorated local inflammation. This indicates that intradiscal NCM injection could be a promising treatment for IVD disease, circumventing the cumbersome identification of bioactive NC-secreted substances.
- No beneficial effect of canine MSCs was detected upon canine CLCs *in vitro* or on degenerated canine IVDs *in vivo*, indicating that the quality of an MSC-based treatment strategy is not easily guaranteed in veterinary medicine.

### Growth factor based strategies

- BMP7 stimulated healthy ECM production of canine CLCs from early degenerated IVDs *in vitro*. When intradiscally applied in spontaneously, early degenerated canine IVDs, however, BMP7 exerted no regenerative effects, but induced extensive extradiscal bone formation. This implies that a bolus injection of BMP7 alone cannot be used as a treatment for IVD disease in human or canine patients.
- TGF- $\beta_1$  and BMP2 increased proliferation and ECM deposition of human and canine CLCs. BMP2-mediated Smad1 signaling was associated with collagen type II production, whereas TGF- $\beta_1$ -mediated Smad2 signaling was associated with fibrotic CLC (re)differentiation.
- Human and canine (short) Link-N exerted species-specific effects on human, bovine, and canine CLCs from early degenerated IVDs. Both variants, however, lacked the potency as canine IVD regeneration agent.
- Caveolin-1 plays a role in preservation of the NC phenotype and may be related with CLC apoptosis given its increased expression in degenerated IVDs. Since caveolin-1 scaffolding domain increased TGF- $\beta$ /pSmad2 signaling and healthy ECM deposition in CLCs *in vitro*, however, increased caveolin-1 expression in degenerated IVDs may also facilitate an attempt of repair.

**What can we learn from developmental biology?**

- There is a functional paracrine feedback loop between vitamin D<sub>3</sub> and PTHrP in the growth plate: vitamin D<sub>3</sub> decreased PTHrP production, while PTHrP increased chondrocyte sensitivity to vitamin D<sub>3</sub> by increasing vitamin D<sub>3</sub> receptor production. Undesirable hypertrophic chondrocyte differentiation was inhibited by PTHrP and vitamin D<sub>3</sub> *in vitro*.
- The expression of IHH, PTHrP and related receptors decreased during IVD maturation, while their expression and calcium deposition increased during IVD degeneration. PTHrP decreased healthy ECM production, while IHH facilitated calcification in canine CLCs *in vitro*. The latter indicates that inhibiting IHH signaling could be a therapeutic approach to inhibit calcification during IVD degeneration.

## References

1. Bergknut N, Rutges JP, Kranenburg HJ, et al. 2012. The dog as an animal model for intervertebral disc degeneration? *Spine (Phila Pa 1976)* 37: 351-358.
2. Katz JN. 2006. Lumbar disc disorders and low-back pain: Socioeconomic factors and consequences. *J Bone Joint Surg Am* 88 Suppl 2: 21-24.
3. Andersson GB. 1999. Epidemiological features of chronic low-back pain. *Lancet* 354: 581-585.
4. Bergknut N, Smolders LA, Grinwis GC, et al. 2013. Intervertebral disc degeneration in the dog. part 1: Anatomy and physiology of the intervertebral disc and characteristics of intervertebral disc degeneration. *Vet J* 195: 282-291.
5. Bergknut N, Meij BP, Hagman R, et al. 2013. Intervertebral disc disease in dogs - part 1: A new histological grading scheme for classification of intervertebral disc degeneration in dogs. *Vet J* 195: 156-163.
6. Kim JH, Deasy BM, Seo HY, et al. 2009. Differentiation of intervertebral notochordal cells through live automated cell imaging system in vitro. *Spine (Phila Pa 1976)* 34: 2486-2493.
7. Abbott RD, Purmessur D, Monsey RD, Iatridis JC. 2012. Regenerative potential of TGFbeta3 + dex and notochordal cell conditioned media on degenerated human intervertebral disc cells. *J Orthop Res* 30: 482-488.
8. Aguiar DJ, Johnson SL, Oegema TR. 1999. Notochordal cells interact with nucleus pulposus cells: Regulation of proteoglycan synthesis. *Exp Cell Res* 246: 129-137.
9. Erwin WM, Inman RD. 2006. Notochord cells regulate intervertebral disc chondrocyte proteoglycan production and cell proliferation. *Spine (Phila Pa 1976)* 31: 1094-1099.
10. Matta A, Karim MZ, Isenman DE, Erwin WM. 2017. Molecular therapy for degenerative disc disease: Clues from secretome analysis of the notochordal cell-rich nucleus pulposus. *Sci Rep* 7: 45623.
11. Potier E, de Vries S, van Doeselaar M, Ito K. 2014. Potential application of notochordal cells for intervertebral disc regeneration: An in vitro assessment. *Eur Cell Mater* 28: 68-81.
12. de Vries SA, Potier E, van Doeselaar M, et al. 2015. Conditioned medium derived from notochordal cell-rich nucleus pulposus tissue stimulates matrix production by canine nucleus pulposus cells and bone marrow-derived stromal cells. *Tissue Eng Part A* 21: 1077-1084.
13. de Vries SA, van Doeselaar M, Meij BP, Tryfonidou MA, Ito K. 2016. The stimulatory effect of notochordal cell-conditioned medium in a nucleus pulposus explant culture. *Tissue Eng Part A* 22: 103-110.
14. Korecki CL, Taboas JM, Tuan RS, Iatridis JC. 2010. Notochordal cell conditioned medium stimulates mesenchymal stem cell differentiation toward a young nucleus pulposus phenotype. *Stem Cell Res Ther* 1: 18.
15. Purmessur D, Schek RM, Abbott RD, et al. 2011. Notochordal conditioned media from tissue increases proteoglycan accumulation and promotes a healthy nucleus pulposus phenotype in human mesenchymal stem cells. *Arthritis Res Ther* 13: R81.
16. Chen S, Emery SE, Pei M. 2009. Coculture of synovium-derived stem cells and nucleus pulposus cells in serum-free defined medium with supplementation of transforming growth factor-beta1: A potential application of tissue-specific stem cells in disc regeneration. *Spine (Phila Pa 1976)* 34: 1272-1280.
17. Yang SH, Wu CC, Shih TT, Sun YH, Lin FH. 2008. In vitro study on interaction between human nucleus pulposus cells and mesenchymal stem cells through paracrine stimulation. *Spine (Phila Pa 1976)* 33: 1951-1957.
18. Allon AA, Butcher K, Schneider RA, Lotz JC. 2012. Structured coculture of mesenchymal stem cells and disc cells enhances differentiation and proliferation. *Cells Tissues Organs* 196: 99-106.
19. Xie LW, Fang H, Chen AM, Li F. 2009. Differentiation of rat adipose tissue-derived mesenchymal stem cells towards a nucleus pulposus-like phenotype in vitro. *Chin J Traumatol* 12: 98-103.
20. Lu ZF, Zandieh Doulabi B, Wuisman PI, Bank RA, Helder MN. 2007. Differentiation of adipose stem cells by nucleus pulposus cells: Configuration effect. *Biochem Biophys Res Commun* 359: 991-996.
21. Gantenbein B, Calandriello E, Wuertz-Kozak K, et al. 2014. Activation of intervertebral disc cells by co-culture with notochordal cells, conditioned medium and hypoxia. *BMC Musculoskelet Disord* 15: 422-2474-15-422.
22. Erwin WM, Ashman K, O'Donnell P, Inman RD. 2006. Nucleus pulposus notochord cells secrete connective tissue growth factor and up-regulate proteoglycan expression by intervertebral disc chondrocytes. *Arthritis Rheum* 54: 3859-3867.
23. Malda J, Boere J, van de Lest CH, van Weeren P, Wauben MH. 2016. Extracellular vesicles - new tool for joint repair and regeneration. *Nat Rev Rheumatol* 12: 243-249.
24. Hunter CJ, Matyas JR, Duncan NA. 2003. The notochordal cell in the nucleus pulposus: A review in the context of tissue engineering. *Tissue Eng* 9: 667-677.
25. Paczkowski JE, Richardson BC, Fromme JC. 2015. Cargo adaptors: Structures illuminate mechanisms regulating vesicle biogenesis. *Trends Cell Biol* 25: 408-416.
26. Szul T, Sztul E. 2011. COPII and COPI traffic at the ER-golgi interface. *Physiology (Bethesda)* 26: 348-364.
27. Ellis K, Bagwell J, Bagnat M. 2013. Notochord vacuoles are lysosome-related organelles that function in axis and spine morphogenesis. *J Cell Biol* 200: 667-679.
28. Thery C, Zitvogel L, Amigorena S. 2002. Exosomes: Composition, biogenesis and function. *Nat Rev Immunol* 2: 569-579.
29. Wang F, Gao ZX, Cai F, et al. 2017. Formation, function, and exhaustion of notochordal cytoplasmic vacuoles within intervertebral disc: Current understanding and speculation. *Oncotarget* 8: 57800-57812.
30. Hunter CJ. 2003. The three-dimensional architecture of the notochordal nucleus pulposus: Novel observations on cell structures in the canine intervertebral disc. *J. Anat.* 202: 279-291.

31. Hunter CJ, Bianchi S, Cheng P, Muldrew K. 2007. Osmoregulatory function of large vacuoles found in notochordal cells of the intervertebral disc running title: An osmoregulatory vacuole. *Mol Cell Biomech* 4: 227-237.
32. Haudenschild DR, Hong E, Yik JH, et al. 2011. Enhanced activity of transforming growth factor beta1 (TGF-beta1) bound to cartilage oligomeric matrix protein. *J Biol Chem* 286: 43250-43258.
33. Ishida K, Acharya C, Christiansen BA, et al. 2013. Cartilage oligomeric matrix protein enhances osteogenesis by directly binding and activating bone morphogenetic protein-2. *Bone* 55: 23-35.
34. Holt DJ, Grainger DW. 2012. Demineralized bone matrix as a vehicle for delivering endogenous and exogenous therapeutics in bone repair. *Adv Drug Deliv Rev* 64: 1123-1128.
35. Gruskin E, Doll BA, Futrell FW, Schmitz JP, Hollinger JO. 2012. Demineralized bone matrix in bone repair: History and use. *Adv Drug Deliv Rev* 64: 1063-1077.
36. Bartholomew A, Sturgeon C, Siatskas M, et al. 2002. Mesenchymal stem cells suppress lymphocyte proliferation in vitro and prolong skin graft survival in vivo. *Exp Hematol* 30: 42-48.
37. Meirelles Lda S, Fontes AM, Covas DT, Caplan AI. 2009. Mechanisms involved in the therapeutic properties of mesenchymal stem cells. *Cytokine Growth Factor Rev* 20: 419-427.
38. Tse WT, Pendleton JD, Beyer WM, Egalka MC, Guinan EC. 2003. Suppression of allogeneic T-cell proliferation by human marrow stromal cells: Implications in transplantation. *Transplantation* 75: 389-397.
39. Vadala G, Studer RK, Sowa G, et al. 2008. Coculture of bone marrow mesenchymal stem cells and nucleus pulposus cells modulate gene expression profile without cell fusion. *Spine (Phila Pa 1976)* 33: 870-876.
40. Sobajima S, Vadala G, Shimer A, et al. 2008. Feasibility of a stem cell therapy for intervertebral disc degeneration. *Spine J* 8: 888-896.
41. Ganey T, Hutton WC, Moseley T, Hedrick M, Meisel HJ. 2009. Intervertebral disc repair using adipose tissue-derived stem and regenerative cells: Experiments in a canine model. *Spine (Phila Pa 1976)* 34: 2297-2304.
42. Hiyama A, Mochida J, Iwashina T, et al. 2008. Transplantation of mesenchymal stem cells in a canine disc degeneration model. *J Orthop Res* 26: 589-600.
43. Serigano K, Sakai D, Hiyama A, et al. 2010. Effect of cell number on mesenchymal stem cell transplantation in a canine disc degeneration model. *J Orthop Res* 28: 1267-1275.
44. Phinney DG. 2012. Functional heterogeneity of mesenchymal stem cells: Implications for cell therapy. *J Cell Biochem* 113: 2806-2812.
45. Bertolo A, Steffen F, Malonzo-Marty C, Stoyanov J. 2015. Canine mesenchymal stem cell potential and the importance of dog breed: Implication for cell-based therapies. *Cell Transplant* 24: 1969-1980.
46. Sakai D, Nakamura Y, Nakai T, et al. 2012. Exhaustion of nucleus pulposus progenitor cells with ageing and degeneration of the intervertebral disc. *Nat Commun* 3: 1264.
47. Tekari A, Chan SC, Sakai D, Grad S, Gantenbein B. 2016. Angiopoietin-1 receptor Tie2 distinguishes multipotent differentiation capability in bovine coccygeal nucleus pulposus cells. *Stem Cell Res Ther* 7: 75-016-0337-9.
48. Imai Y, Miyamoto K, An HS, et al. 2007. Recombinant human osteogenic protein-1 upregulates proteoglycan metabolism of human annulus fibrosus and nucleus pulposus cells. *Spine (Phila Pa 1976)* 32: 1303-9.
49. Masuda K, Takegami K, An H, et al. 2003. Recombinant osteogenic protein-1 upregulates extracellular matrix metabolism by rabbit annulus fibrosus and nucleus pulposus cells cultured in alginate beads. *J Orthop Res* 21: 922-930.
50. Masuda K, Imai Y, Okuma M, et al. 2006. Osteogenic protein-1 injection into a degenerated disc induces the restoration of disc height and structural changes in the rabbit annular puncture model. *Spine (Phila Pa 1976)* 31: 742-754.
51. An HS, Takegami K, Kamada H, et al. 2005. Intradiscal administration of osteogenic protein-1 increases intervertebral disc height and proteoglycan content in the nucleus pulposus in normal adolescent rabbits. *Spine (Phila Pa 1976)* 30: 25-32.
52. Chubinskaya S, Kawakami M, Rappoport L, et al. 2007. Anti-catabolic effect of OP-1 in chronically compressed intervertebral discs. *J Orthop Res* 25: 517-530.
53. Rodriguez J, Vernus B, Chelh I, et al. 2014. Myostatin and the skeletal muscle atrophy and hypertrophy signaling pathways. *Cell Mol Life Sci* 71: 4361-4371.
54. Clop A, Marcq F, Takeda H, et al. 2006. A mutation creating a potential illegitimate microRNA target site in the myostatin gene affects muscularity in sheep. *Nat Genet* 38: 813-818.
55. Elkasrawy M, Fulzele S, Bowser M, Wenger K, Hamrick M. 2011. Myostatin (GDF-8) inhibits chondrogenesis and chondrocyte proliferation in vitro by suppressing sox-9 expression. *Growth Factors* 29: 253-262.
56. Li P, Zhang R, Gan Y, et al. 2017. Effects of osteogenic protein-1 on intervertebral disc regeneration: A systematic review of animal studies. *Biomed Pharmacother* 88: 260-266.
57. Tellegen AR, Willems N, Beukers M, et al. 2017. Intradiscal application of a PCLA-PEG-PCLA hydrogel loaded with celecoxib for the treatment of back pain in canines: What's in it for humans? *J Tissue Eng Regen Med*, Epub ahead of print.
58. Willems N, Bach FC, Plompp SG, et al. 2015. Intradiscal application of rhBMP-7 does not induce regeneration in a canine model of spontaneous intervertebral disc degeneration. *Arthritis Res Ther* 17: 137-015-0625-2.
59. Willems N, Mihov G, Grinwis GC, et al. 2017. Safety of intradiscal injection and biocompatibility of polyester amide microspheres in a canine model predisposed to intervertebral disc degeneration. *J Biomed Mater Res B Appl Biomater* 105: 707-714.
60. Carragee EJ, Don AS, Hurwitz EL, et al. 2009. 2009 ISSLS prize winner: Does discography cause accelerated progression of degeneration changes in the lumbar disc: A ten-year matched cohort study. *Spine (Phila Pa 1976)* 34: 2338-2345.
61. Vadala, G, Russo, F, Musumeci, M et al. 2015. Intervertebral disc regeneration using mesenchymal stem/stromal cells transplanted via the end-plate route in a large animal model. ORS Annual Meeting abstract.

62. Gonzalez-Munoz E, Lopez-Iglesias C, Calvo M, et al. 2009. Caveolin-1 loss of function accelerates glucose transporter 4 and insulin receptor degradation in 3T3-L1 adipocytes. *Endocrinology* 150: 3493-3502.
63. Zhang QQ, Huang L, Han C, et al. 2015. Caveolin-1 and glucose transporter 4 involved in the regulation of glucose-deprivation stress in PC12 cells. *Sheng Li Xue Bao* 67: 349-356.
64. Guehring T, Wilde G, Sumner M, et al. 2009. Notochordal intervertebral disc cells: Sensitivity to nutrient deprivation. *Arthritis Rheum* 60: 1026-1034.
65. Taylor JR TL. 1986. The role of the notochord and blood vessels in vertebral column development and in the aetiology of schmorl's nodes. *Modern manual therapy*. Edinburgh: Churchill Livingstone: 21-29.
66. Smolders LA, Meij BP, Onis D, et al. 2013. Gene expression profiling of early intervertebral disc degeneration reveals a down-regulation of canonical wnt signaling and caveolin-1 expression: Implications for development of regenerative strategies. *Arthritis Res Ther* 15: R23.
67. Karpen HE, Bukowski JT, Hughes T, et al. 2001. The sonic hedgehog receptor patched associates with caveolin-1 in cholesterol-rich microdomains of the plasma membrane. *J Biol Chem* 276: 19503-19511.
68. Jiang J, Leong NL, Mung JC, Hidaka C, Lu HH. 2008. Interaction between zonal populations of articular chondrocytes suppresses chondrocyte mineralization and this process is mediated by PTHrP. *Osteoarthritis Cartilage* 16: 70-82.
69. Becher C, Suzwart T, Ronstedt P, et al. 2010. Decrease in the expression of the type 1 PTH/PTHrP receptor (PTH1R) on chondrocytes in animals with osteoarthritis. *J Orthop Surg Res* 5: 28-799X-5-28.
70. Wei F, Zhou J, Wei X, et al. 2012. Activation of indian hedgehog promotes chondrocyte hypertrophy and upregulation of MMP-13 in human osteoarthritic cartilage. *Osteoarthritis Cartilage* 20: 755-763.
71. Lin AC, Seeto BL, Bartoszko JM, et al. 2009. Modulating hedgehog signaling can attenuate the severity of osteoarthritis. *Nat Med* 15: 1421-1425.
72. Zhou J, Wei X, Wei L. 2014. Indian hedgehog, a critical modulator in osteoarthritis, could be a potential therapeutic target for attenuating cartilage degeneration disease. *Connect Tissue Res* 55: 257-261.
73. Shuang F, Zhou Y, Hou SX, et al. 2015. Indian hedgehog signaling pathway members are associated with magnetic resonance imaging manifestations and pathological scores in lumbar facet joint osteoarthritis. *Sci Rep* 5: 10290.
74. Brochhausen C, Lehmann M, Halstenberg S, et al. 2009. Signalling molecules and growth factors for tissue engineering of cartilage-what can we learn from the growth plate? *Journal of tissue engineering and regenerative medicine* 3: 416-29.
75. Nilsson O, Marino R, De Luca F, Phillip M, Baron J. 2005. Endocrine regulation of the growth plate. *Hormone research* 64: 157-65.
76. Denison TA, Koch CF, Shapiro IM, Schwartz Z, Boyan BD. 2009. Inorganic phosphate modulates responsiveness to 24,25(OH)2D3 in chondrogenic ATDC5 cells. *J Cell Biochem* 107: 155-62.
77. Rutges JP, Duit RA, Kummer JA, et al. 2010. Hypertrophic differentiation and calcification during intervertebral disc degeneration. *Osteoarthritis Cartilage* 18: 1487-1495.
78. Grant MP, Epure LM, Bokhari R, et al. 2016. Human cartilaginous endplate degeneration is induced by calcium and the extracellular calcium-sensing receptor in the intervertebral disc. *Eur Cell Mater* 32: 137-151.
79. Dahia CL, Mahoney E, Wylie C. 2012. Shh signaling from the nucleus pulposus is required for the postnatal growth and differentiation of the mouse intervertebral disc. *PLoS One* 7: e35944.
80. Winkler T, Mahoney EJ, Sinner D, Wylie CC, Dahia CL. 2014. Wnt signaling activates shh signaling in early postnatal intervertebral discs, and re-activates shh signaling in old discs in the mouse. *PLoS One* 9: e98444.
81. Dahia CL, Mahoney EJ, Durrani AA, Wylie C. 2009. Intercellular signaling pathways active during intervertebral disc growth, differentiation, and aging. *Spine (Phila Pa 1976)* 34: 456-462.



**Dutch summary/Nederlandse samenvatting**

## Achtergrond

Rug- en nekpijn komt veelvuldig voor bij zowel de mens als de hond en is sterk geassocieerd met degeneratie (slijtage) van de tussenwervelschijf (TWS). De huidige conservatieve en chirurgische therapieën voor TWS slijtage zijn vooral symptomatisch en leiden niet tot herstel van de TWS zelf. Om deze reden is de belangstelling voor regeneratieve therapieën, welke tot doel hebben de TWS in een vroeg stadium te repareren, toegenomen. Onderzoek binnen de regeneratieve geneeskunde vergroot onze kennis van ziekteprocessen. Het uiteindelijke doel is om de resultaten te vertalen naar minimaal invasieve therapieën voor zowel veterinaire als humane patiënten volgens het 'One Health' principe. In dit proefschrift worden daarom nieuwe regeneratieve strategieën (met nadruk op (notochordale) cellen en groeifactoren) voor de behandeling TWS slijtage bij de mens en hond onderzocht met als uitgangspunt de ontwikkelingsbiologie.

## Notochordale cellen

Gedurende maturatie (rijping) van de TWS (wat bij de mens al plaatsvindt gedurende de eerste levensjaren) verandert het celtype in het centrum van de TWS, de nucleus pulposus (NP): grote notochordale cellen (NCs) worden vervangen door kleinere chondrocyt-achtige NP cellen (NPCs). Het verlies van de NC populatie wordt geassocieerd met het ontwikkelen van TWS slijtage, wat impliceert dat NCs een belangrijke rol spelen in het behoud van gezond NP weefsel. Eerder onderzoek toont aan dat NCs inderdaad bioactieve stoffen met regeneratieve eigenschappen uitscheiden. Het onderzoek dat wordt beschreven in dit proefschrift bevestigt deze eerdere bevindingen, maar voegt ook nieuwe inzichten toe. In **Hoofdstuk 2** wordt het regeneratieve effect van NC-geconditioneerd medium (NCGM) van verschillende diersoorten (mens, hond, varken) vergeleken. De bioactieve stoffen die door NCs worden uitgescheiden oefenden weliswaar een diersoort overschrijdend effect uit, maar varkens NCGM bleek met meest potent. Gebaseerd op deze bevindingen, de ethische overwegingen en het feit dat gezond TWS weefsel van honden en varkens makkelijker verkrijgbaar is dan gezond humaan TWS weefsel, werd besloten vervolgstudies voornamelijk te richten op gezonde honden en varkens TWS-en. In een tweede studie gebaseerd op NCGM (**Hoofdstuk 3**) werd getracht met behulp van massaspectrometrie bioactieve factoren te identificeren welke waren uitgescheiden door NCs. Echter, er werden voornamelijk matrix-gerelateerde eiwitten, maar geen specifieke groeifactoren gevonden, waarschijnlijk doordat gebruik werd gemaakt van geheel NP weefsel (en niet enkel NCs) om NCGM te maken. Naast matrix eiwitten werden ook membraanblaasjes-gerelateerde eiwitten gevonden, wat sterk suggereert dat membraanblaasjes aanwezig zijn in NCGM. Membraanblaasjes bevatten bioactieve moleculen en worden door cellen uitgescheiden om te communiceren met andere cellen. Op deze manier kan ook weefselregeneratie worden gestimuleerd. In **Hoofdstuk 4** laten we zien dat NCGM inderdaad membraanblaasjes bevat, welke regeneratieve effecten uitoefenen op NPCs van de mens en hond. In de toekomst kunnen de bioactieve moleculen van deze membraanblaasjes worden geïdentificeerd, waarna het effect van de recombinant gesynthetiseerde varianten van deze factoren kunnen worden getest in functionele studies.

**Hoofdstukken 2-4** van dit proefschrift demonstreren hoe moeilijk en bewerkelijk het is om de bioactieve factoren die door NCs worden uitgescheiden te identificeren en isoleren. Een eenvoudigere benadering voor TWS regeneratie werd daarom getest in **Hoofdstuk 5**, door gebruik te maken van NC-rijke matrix (NCM) van NP weefsel afkomstig van gezonde varkens. NCM (opgelost in een concentratie van 10 mg/mL) induceerde een anabool, anti-katabool en proliferatief effect in humane en honden NPCs en faciliteerde chondrogene differentiatie van mesenchymale stromale stamcellen (MSCs) *in vitro*. In de TWS-en van Beagles *in vivo* induceerde intradiscaal geïnjecteerd NCM een positief effect op de TWS, welke op MRI was te zien (o.a. toegenomen breedte van de TWS) en ook kon worden waargenomen met het blote oog (macroscopisch niveau). Tevens stimuleerde NCM de afzetting van gezonde matrix en oefende NCM een anti-inflammatoir effect uit. Het werkingsmechanisme van NCM is nog niet bekend, maar het zou kunnen zijn dat het vergelijkbaar is met gedemineraliseerd botmatrix, wat botregeneratie stimuleert door lokaal groeifactoren uit te scheiden. Naast onderzoek naar het exacte werkingsmechanisme zou vervolgonderzoek zich ook moeten richten op het testen van hogere concentraties NCM en de mogelijkheid tot het toedienen van NCM in hydrogel vorm, wat de kans op lekkage vermindert. Als laatste moet decellularisatie van NCM worden bewerkstelligd zonder verlies van biologische activiteit voordat deze veelbelovende therapeutische optie kan worden vertaald naar de humane en veterinaire kliniek. Concluderend kan worden gezegd dat intradiscale NCM injectie een veelbelovende therapie voor TWS slijtage kan zijn in de toekomst, waarmee de lastige identificatie van bioactieve stoffen die NCs uitscheiden omzeild kan worden.

## Mesenchymale stamcellen

MSCs zijn veelbelovende en vaak onderzochte celtypen in de onderzoekswereld gezien hun regeneratieve en immunosuppressieve eigenschappen. Het effect van MSCs is in dit proefschrift getest op honden NPCs *in vitro* (**Hoofdstuk 7**) en op TWS-en van Beagles *in vivo* (**Hoofdstuk 6**). De MSCs oefeneden echter zowel *in vitro* als *in vivo* geen regeneratief effect uit. Een mogelijke oorzaak kan de bekende heterogeniteit van MSC populaties zijn. De resultaten van deze hoofdstukken tonen dus aan dat een regeneratieve therapie voor slijtage van de TWS gebaseerd op MSCs (nog) niet kan worden gewaarborgd in de veterinaire geneeskunde. Vervolgonderzoek moet aantonen of lokale Tie2<sup>+</sup> NP progenitor cellen een goed alternatief zouden kunnen zijn voor MSCs in het kader van TWS regeneratie.

## Groeifactoren

De regeneratieve geneeskunde richt zich niet alleen op strategieën gebaseerd op cellen, maar ook op groeifactoren welke celproliferatie en matrixdepositie stimuleren. In **Hoofdstuk 6** werd het effect van de groeifactor bone morphogenetic protein-7 (BMP7) getest op TWS-en van Beagles met spontaan ontstane milde slijtage. Eerder was al aangetoond dat BMP7 afzetting van matrix stimuleert in diermodellen met geïnduceerde TWS slijtage. In onze studie oefende BMP7 geen regeneratief effect uit, maar stimuleerde wel extradiscale botformatie. Mogelijk verschilt de respons op groeifactoren tussen een TWS met geïnduceerde slijtage ten opzichte van een TWS met spontane slijtage. Dit toont eens te meer aan dat de keuze van het juiste representatieve diermodel van cruciaal belang is voor

het testen van een (regeneratieve) therapie. In **Hoofdstuk 8** wordt dit nogmaals benadrukt, aangezien Link-N (welke BMP-gemedieerde Smad1 signalering kan stimuleren) een regeneratief effect uitoefende op humane NPCs, terwijl het effect op honden NPCs nihil was. Alhoewel zowel de mens als de hond klinisch relevante TWS slijtage ontwikkelen, is hun respons op Link-N totaal verschillend. Om deze reden is de hond voor het testen van Link-N dan ook niet geschikt als diermodel voor de mens. Ook in **Hoofdstuk 7** vertoonden NPCs van de hond soms een verschillende respons op Transforming Growth Factor- $\beta$  (TGF- $\beta$ ) en BMP2 ten opzichte van NPCs van de mens. Concluderend kan worden gesteld dat **Hoofdstuk 6-8** het belang tonen van het delen van 'negatieve' resultaten en bijwerkingen van (regeneratieve) agentia ter voorkoming van het uitvoeren van overbodige (dier)experimenten en onnodig proefdiergebruik.

## Ontwikkelingsbiologie

In **Hoofdstuk 9** wordt gedemonstreerd dat het membraanewit caveolin-1 groeifactor effecten kan uitoefenen door TGF- $\beta$  signalering te bevorderen. Verder werd ook aangetoond dat caveolin-1 een rol speelt in het behoud van het NC fenotype, aangezien in de NP van wild type muizen veelal NCs werden waargenomen terwijl de NP van caveolin-1 knockout muizen voornamelijk NPCs en fibroblast-achtige cellen bevatte. Vervolgonderzoek zal moeten verduidelijken hoe caveolin-1 betrokken is bij het behoud van het NC fenotype. Mogelijk speelt hedgehog signalering hierbij een rol, aangezien caveolin-1 in het celmembraan co-lokaliseert met de Indian hedgehog (IHH) receptor Patched. Eerder onderzoek toonde al aan dat het IHH-Parathyroid hormone-related protein (PTHrP) pathway een rol speelt in chondrocyt differentiatie en artrose, maar hun rol in de TWS was nooit eerder onderzocht. Om deze reden werd in **Hoofdstuk 10** eerst het effect van PTHrP getest op de groeischijf, hetgeen een goed model is om chondrocyt differentiatie te bestuderen. PTHrP bleek de hypertrofische differentiatie van chondrocyten, zoals bij artrose voorkomt, te kunnen remmen. Aangezien hypertrofische differentiatie en calcificatie tevens voorkomt in versleten TWS-en, zou dit kunnen impliceren dat PTHrP deze pathologische processen ook zou kunnen inhiberen in TWS-en. Gebaseerd op deze hypothese werd vervolgens in **Hoofdstuk 11** de expressie en mogelijke rol van de PTHrP en IHH in de postnatale TWS onderzocht. Zowel de expressie van IHH, PTHrP en hun receptoren als calciumdepositie was toegenomen in versleten TWS-en. IHH faciliteerde bovendien calcificatie in honden NPCs *in vitro*, een fenomeen dat eerder was waargenomen in chondrocyten. PTHrP kon calcificatie echter niet remmen, waarschijnlijk doordat het induceren van calcificatie in NPCs *in vitro* vrijwel onmogelijk was zonder IHH suppletie. Al met al tonen de resultaten van **Hoofdstuk 10 en 11** het belang aan van het kijken naar de ontwikkelingsbiologie van (andere) weefsels. Op basis van dit principe werd gevonden dat suppletie van PTHrP of inhibitie van IHH mogelijk in de toekomst een therapeutische optie zou kunnen zijn om hypertrofische differentiatie en calcificatie gedurende TWS slijtage te remmen.

## Conclusies

De studies die in dit proefschrift zijn beschreven tonen de waarde aan van het bestuderen van de ontwikkelingsbiologie voor het ontwikkelen van (regeneratieve) therapieën. Op deze manier zijn mogelijk interessante agentia gevonden voor tussenwervelschijf regeneratie, zoals caveolin-1, PTHrP en IHH. Niet alle geopperde agentia bleken echter een positief effect te bewerkstelligen *in vitro* (MSCs, Link-N, TGF- $\beta_1$ ), en veelbelovende *in vitro* resultaten bleken niet altijd te leiden tot regeneratieve effecten *in vivo* (BMP7). Notochordale cellen bleken daarentegen een zeer interessante bron te zijn voor tussenwervelschijfregeneratie. Hoewel het identificeren van de bioactieve factoren welke worden uitgescheiden door deze notochordale cellen bewerkelijk is, kan het vanuit een fundamenteel perspectief waardevol zijn, omdat met deze kennis regeneratieve behandlungsstrategieën verbeterd kunnen worden. Om de lastige identificatie van bioactieve stoffen te omzeilen bleek de toepassing van notochordaal cel-rijke matrix een zeer potent alternatief te zijn voor het ontwikkelen van een regeneratieve therapie voor versleten tussenwervelschijven van zowel de mens als de hond.

## Belangrijkste bevindingen

### Strategieën gebaseerd op notochordale cellen

- Bioactieve factoren uitgescheiden door NCs van de mens, hond en varken oefenen een diersoort overschrijdend, regeneratief effect uit op humane NPCs. Dit ondersteunt verder onderzoek naar NC-gebaseerde strategieën die gebruik maken van varkens- en hondenmodellen voor translatie naar humane en veterinaire patiënten.
- Met behulp van massaspectrometrie zijn vooral matrix-gerelateerde eiwitten geïdentificeerd in NCGM van de mens, hond en varken, maar ook membraanblaasjes-gerelateerde eiwitten.
- Varkens NCGM bevat veel membraanblaasjes welke een regeneratief effect uitoefenen op humane en honden NPCs. Het effect van deze membraanblaasjes kan worden beïnvloed door de eiwitten die tevens aanwezig zijn in NCGM.
- Het toedienen van NC-rijke matrix van NP weefsel van gezonde varkens induceert een anabool, anti-katabool en proliferatief effect op humane en honden NPCs *in vitro*. Wanneer NCM geïnjecteerd wordt in matig gedegenererde honden TWS-en verbetert NCM het MRI beeld, oefent het een positief effect uit op macroscopisch, biochemisch en histologisch niveau en inhibeert het ontsteking. Dit impliceert dat een intradiscale NCM injectie in potentie een veelbelovende therapie voor TWS slijtage kan zijn in de toekomst, aangezien de lastige identificatie van bioactieve stoffen die NCs uitscheiden hiermee omzeild wordt.
- Er zijn geen positieve effecten van honden MSCs waargenomen op honden NPCs *in vitro* of op versleten TWS-en van honden *in vivo*. Dit impliceert dat een regeneratieve therapie voor TWS slijtage die gebaseerd is op MSCs (nog) niet goed kan worden gewaarborgd in de veterinaire geneeskunde.

### Strategieën gebaseerd op groeifactoren

- BMP7 stimuleert gezonde matrix productie in honden NPCs *in vitro*. Wanneer BMP7 intradiscaal geïnjecteerd wordt in versleten honden TWS-en oefent BMP7 geen regeneratief effect uit, maar induceert het extradiscale botnieuwvorming. Dit impliceert dat een bolusinjectie met alleen BMP7 niet geschikt is als therapie voor TWS slijtage.
- TGF- $\beta_1$  en BMP2 stimuleren proliferatie en matrixproductie in humane en honden NPCs *in vitro*. BMP2-gemedieerde Smad1 signalering induceert afzetting van collageen type II, terwijl TGF- $\beta_1$ -gemedieerde Smad2 signalering het ontstaan van fibrose stimuleert.
- De humane en honden variant van (short) Link-N oefenen diersoort specifieke effecten uit op NPCs van mens, rund en hond. Beide varianten hebben echter niet de potentie om regeneratie te induceren in honden NPCs.
- Caveolin-1 speelt een rol in het behoud van het NC fenotype en wordt tevens gerelateerd aan NPC apoptose, aangezien caveolin-1 verhoogd tot expressie komt in versleten TWS-en. Caveolin-1 induceert echter ook TGF- $\beta$ /Smad2 signalering en afzetting van gezonde matrix in NPCs *in vitro*, wat kan impliceren dat caveolin-1 reparatie faciliteert in versleten TWS-en.

### **Wat kunnen we leren van de ontwikkelingsbiologie?**

- In de groeischijf bestaat een functionele feedback loop tussen vitamine D<sub>3</sub> en PTHrP. Hypertrofische chondrocyt differentiatie wordt door zowel PTHrP als vitamine D<sub>3</sub> geremd.
- De expressie van IHH, PTHrP en hun receptoren neemt af gedurende maturatie (rijping) van de TWS, terwijl hun expressie en calciumdepositie toeneemt tijdens TWS slijtage. PTHrP remt de productie van gezonde matrix, terwijl IHH calcificatie faciliteert in honden NPCs *in vitro*. Dit impliceert dat het remmen van IHH signalering een therapeutische optie kan zijn om calcificatie te inhiberen gedurende TWS slijtage in de toekomst.



## List of abbreviations

1 $\alpha$ -OHase: 1 $\alpha$ -hydroxylase  
24-OHase: 24-hydroxylase  
ACAN: aggrecan  
ADAMT5: a disintegrin and metalloproteinase with thrombospondin motifs 5  
AF: annulus fibrosus  
Asap: ascorbic acid 2-phosphate  
ASC: adipose-derived stem cell  
BMP: bone morphogenetic protein  
Bp: base pairs  
BMSC: bone marrow-derived stem cells  
BW: body weight  
Ca: calcium  
CASP3: caspase 3  
Cav-1: caveolin-1  
CCND1: cyclin D1  
CD: chondrodystrophic  
ChIP: chromatin immunoprecipitation  
CLC: chondrocyte-like cell  
COL1A1: collagen type 1  
COL2A1: collagen type 2  
COL9: collagen type 9  
COL10: collagen type X  
CT: computer tomography  
CTGF: connective tissue growth factor  
DH: disc height  
DHI: disc height index  
DMMB: dimethyl methylene blue  
ECM: extracellular matrix  
EP: end plate  
ES: effect size  
EV: extracellular vesicles  
FACS: fluorescence-activated cell sorting  
FBS: fetal bovine serum  
FOXF1: Forkhead Box F1  
FSC: forward scatter  
GAG: glycosaminoglycan  
GDF: growth and differentiation factor  
GPI.Th: mean growth plate height  
GPI.Th.Pr: mean height of the proliferative growth plate zone  
GPI.Th.Hp: mean height of the hypertrophic growth plate zone  
ID1: DNA-binding protein inhibitor  
IGF: insulin-like growth factor  
IHC: immunohistochemistry  
IHH: indian hedgehog  
IL-1 $\beta$ : interleukin-1 $\beta$   
IVD: intervertebral disc  
HPRT: hypoxanthine-guanine phosphoribosyltransferase

HRP: horseradish peroxidase  
HYP: hydroxyproline  
HX: hypoxic  
KRT8: cytokeratin 8  
KRT18: cytokeratin 18  
KRT19: cytokeratin 19  
Mab: monoclonal antibody  
MMP13: matrix metalloproteinase 13  
MRI: magnetic resonance imaging  
MSC: mesenchymal stromal cell  
NC: notochordal cell  
NCCM: NC-conditioned medium  
NCD: non-chondrodystrophic  
NCM: NC-derived matrix  
NP: nucleus pulposus  
NPPC: nucleus pulposus progenitor cell  
n.s.: not significant  
NX: normoxic  
OA: osteoarthritis  
P: protein  
Pab: polyclonal antibody  
PAI1: plasminogen activator inhibitor type 1  
Pax-1: paired box protein-1  
PTCH: patched  
PTH: parathyroid hormone  
PTHR1: PTH/PTHrP receptor  
PTHrP: parathyroid hormone related protein  
RPS19: 40S ribosomal protein S19  
RT: room temperature  
rw-FSC: reduced wide-angle forward scatter  
S.D.: standard deviation  
SDHA: succinate dehydrogenase complex subunit A  
SEC: size-exclusion chromatography  
siRNA: silencing RNA  
SHH: sonic hedgehog  
SMO: smoothed  
SOX9: sex determining region Y-box 9  
SRY: sex-determining region of Y  
SSC: side scatter  
TBP: TATA-Box binding protein  
TGF- $\beta$ : transforming growth factor- $\beta$   
TIMP1: tissue inhibitor of metalloproteinases  
Tm: melting temperature  
TNF $\alpha$ : tumor necrosis factor  $\alpha$   
TSS: transcription start site  
UC: ultracentrifugation  
VDR: nuclear vitamin D3 receptor

Addendum

VDRE: vitamin D3 response element

VEGF: vascular endothelial growth factor

WT: wild type

YWHAZ: tyrosine 3-monooxygenase/tryptophan 5-monooxygenase activation protein zeta

## Acknowledgements/Dankwoord

Dit proefschrift was niet tot stand gekomen zonder de hulp van velen. Daarom maak ik van deze gelegenheid gebruik iedereen die heeft bijgedragen daarvoor te bedanken. Een (groot) aantal mensen zou ik in het bijzonder willen bedanken.

*Promotoren en copromotoren*

Geachte Prof. Dr. Meij, beste Björn,

Ten eerste wil ik je hartelijk bedanken dat ik ben geselecteerd voor deze PhD positie en voor al je input met betrekking tot de manuscripten in dit proefschrift. Met een scherp, kritisch en klinisch oog heb je dit proefschrift naar een hoger niveau gebracht. Ook waren zonder jou de intradiscale injecties en het induceren van tussenwervelschijf degeneratie niet gelukt. Als laatste wil ik je bedanken voor het vanuit de kliniek meedenken en -werken aan het onderzoek binnen deze faculteit: wanneer er waardevol materiaal beschikbaar komt bij jouw operaties zullen wij dit als onderzoeksgroep altijd direct horen!

Geachte Prof. Dr. Ito, dear Keita,

Thank you so much for giving me the chance to research this interesting subject and for bringing up NCM! Your ideas and input were of enormous value for this thesis. I really enjoyed our meetings and I am looking forward to our future collaboration.

Geachte Dr. Tryfonidou, beste Marianna,

Voor dit proefschrift ben ik jou zonder twijfel de meeste dank verschuldigd. Onze samenwerking begon al in 2009, tijdens mijn HP jaar. Wat was het fijn dat je mij niet uit het oog was verloren en mij hebt geselecteerd voor deze PhD plek. Wat waardeer ik je kwaliteiten als begeleider en onderzoeker (o.a. je gedrevenheid, kennis, enthousiasme, positiviteit en perfectionisme)! Je bent absoluut van enorm belang voor het onderzoek binnen de Faculteit Diergeneeskunde. Het vertrouwen dat je altijd in mij hebt uitgesproken was gedurende onze samenwerking van grote waarde voor mij. Ik waardeer het enorm dat je voor mij menigmaal je nek hebt uitgestoken en o.a. de uitwisseling met Hong Kong en Japan hebt mogelijk gemaakt. Je doet er alles aan om mij zo optimaal mogelijk voor te bereiden op een geslaagde wetenschappelijke carrière. Ik weet uit ervaring dat dit zeker niet 'de standaard' is, en mede daarom wil ik je hiervoor nogmaals danken. Ik waardeer onze samenwerking nog elke dag en kijk uit naar wat de toekomst ons mag brengen!

*Paranimfen*

Dan mijn paranimfen! Anna Tellegen en Michelle Teunissen, wij hebben als Ortho pods/Power girls/Spine girls (we moeten nog aan onze naam werken...) als vrouwen het CSI team veroverd! Mede door jullie aanwezigheid heb ik mijn PhD traject vooral als 'gezellig' ervaren. Anna, we hebben samen een hoop lief, leed en frustraties kunnen delen gedurende de jaren. Samen hebben we een hoop voor- en tegenspoed verwerkt op wetenschappelijk gebied. We vullen elkaar goed aan op *in vitro* en *in vivo* gebied. Ik wil je vooral enorm bedanken voor al je hulp met de *in vivo* studie, al helemaal toen je mijn studie noodgedwongen moest overnemen toen ik door longontsteking geveld in bed lag. Zonder jou was deze paper er niet geweest! Michelle, wat leuk dat je na je HP jaren terug bent gekomen voor jouw PhD! Het is enorm fijn je als collega te hebben. Je fungeert als wandelende MSC encyclopedie en bent een zeer waardevolle aanvulling binnen onze groep. Ik hoop dan ook dat je nog lang bij onze groep blijft! Dames, ik denk dat we naast collega's ook vriendinnen zijn geworden gedurende ons onderzoek en onder andere daarom heb ik

jullie als mijn paranimfen gevraagd. Ik kijk uit naar jullie promoties en zal jullie hierin steunen waar mogelijk, net als jullie voor mij hebben gedaan!

#### *Collega's Faculteit Diergeneeskunde*

Frank Riemers, ik heb veel respect voor het opzetten van alle lastige assays, Excell sheets en statistische scripts. Zonder jou waren er zeker 4 publicaties in deze thesis nu nog steeds niet af. Je bent van grote waarde voor ons orthopedie team!

Willem de Jong, wat heb jij veel voor mij (en anderen) gedaan. Door jouw efficiënte werk heeft mijn output denk ik wel kunnen verviervoudigen. Dank je wel voor het inwerken van tientallen studenten, het PCR-en van honderden platen en het analyseren van vele vele andere samples!

Alberto Mirada-Bedate, thank you for your scientific input in several manuscripts. It has improved the quality of this thesis significantly 😊.

Nicole Willems, mijn voorgangster! Ondanks dat het niet van een leien dakje ging heb je je kranig voor je promotie heen geslagen, met als resultaat prachtige (klinisch-georiënteerde) papers. Ik heb veel bewondering voor je doorzettingsvermogen. Dank je wel voor de prettige samenwerking, welke onder andere is bekroond met een review en de BMP7 paper.

Louis Penning, jij bent altijd in voor gezelligheid, zoals tijdens een borrel of feestje, maar hiernaast wil ik je ook bedanken voor je wetenschappelijke inbreng, onder andere op het gebied van myostatin (GDF8) bij de Texelaar. Hier ga je in de toekomst meer van horen!

Jeannette Wolfswinkel, dank je wel voor je hulp met de stamcellen voor de *in vivo* proef, en uiteraard ook voor alle bestellingen die je voor mij hebt afgehandeld. Zonder jou zou de Biochemie afdeling instorten!

Saskia Plomp, ondanks dat ik niet heel veel direct met je samenwerk hoor je er gewoon bij! Ik waardeer je gezelligheid, maar ook je toewijding aan je werk. Het lijkt me geweldig jou als analist in je team te hebben.

Maurits Olthof, fijn dat we een humane arts met bot-gerelateerd onderzoek binnen onze groep kregen voor wat verdieping op andere vlakken dan alleen tussenwervelschijf en kraakbeen. Ik heb respect voor het aantal uren dat jij per week aan je PhD besteedde.

Ben Gorissen en Nicoline Korthagen, dank jullie wel voor jullie waardevolle aandeel in de orthopedie meetings en voor onze gesprekken.

Elpetra Timmermans en Monique van Wolferen, ik weet nog goed dat ik bij jullie op de kamer werd geplaatst toen er nog geen echte orthopedie-kamer was. Ik voelde me er gelijk erg thuis. Dank voor jullie gezelligheid en interesse in mijn onderzoek.

Alle andere JDV collega's: hartelijk dank voor al jullie bijdrages, zowel op sociaal als wetenschappelijk gebied!

Martijn Beukers, Ank Wassink en de rest van het radiologie team, heel erg bedankt voor al jullie expertise en hulp bij het maken en beoordelen van de MRIs.

Harry van Engelen, ontzettend bedankt voor de hulp bij het verzamelen van alle weefsels die ik heb gebruikt voor dit proefschrift.

Marca Wauben, hartelijk dank voor de samenwerking met onze groep en het meedenken in de opzet van de EV paper. Uiteindelijk is het door de juiste controles mee te nemen een mooie en zeer complete paper geworden.

Janneke Boere en Sten Libregts, ik wil jullie heel erg bedanken voor alle hulp bij het opstarten van mijn EV avontuur. Door jullie zag ik door de bomen het bos in deze hele bijzondere wereld.

Rob Bleumink, bedankt voor het meedenken en -helpen bij het instellen van de camera!

Alle medewerkers pathologie (Ronald, Lotte, Henny *et al.*), hartelijk dank voor het verwerken van alle samples en het vrijhouden van het inbedapparaat tijdens jullie koffiepauzes voor mij!

Arie Doornenbal, heel erg bedankt voor alle hulp bij de computer gerelateerde issues.

Nico Atteveld, Jeroen van Ark, Helma Avezaat en alle andere GDL medewerkers, heel erg bedankt voor al jullie goede zorgen voor de Beagles en de hulp bij de operaties en medicatie. Alle medewerkers van de anesthesie, heel erg bedankt voor al jullie expertise en goede zorgen voor de Beagletjes.

Alle sterilisatie medewerkers, hartelijk dank voor het zo snel leveren van alle materialen gedurende de afgelopen vijf jaar.

### *Studenten*

Lucy Verdonschot, ondanks alle tegenslagen heeft jouw caveoline werk het begin kunnen vormen van een mooie paper. Heeft het verwerken van alle samples toch nog heel veel nut gehad!

Ferdi van Heel, zelden heb ik zo'n enthousiaste en goed voorbereide student op kennismakingsgesprek gehad. Ook gedurende het jaar heb je enorm bijgedragen in het onderzoek en daarbuiten, o.a. met goede gesprekken tijdens de autoritjes naar Brabant.

Lisanne Laagland, wat heb jij veel en goed kwalitatief werk verricht gedurende je HP jaar. Het effect van Link-N bleek marginaal op hondencellen, maar heeft desondanks een mooie paper opgeleverd, vooral dankzij jou. Ik hoop dat ik ooit nog eens jouw copromotor mag zijn. Kim de Rooij, dank je wel voor al het werk dat jij hebt verzet om het effect van PTHrP en IHH in de tussenwervelschijf te onderzoeken. Ook jouw bijdrage heeft geleid tot een mooi manuscript.

Stefan Wouters, Leili Ghazi, Dirk Vestjens, Bianca Kuster, Anneleen Tuinman, Lisa Hol, Sanne Loos, Janneke Oskam, Pascal Kamphuis, Amber van Heezen en Maxine Lourenburg, deze thesis was ook niet compleet geweest zonder jullie hulp. Bedankt voor al jullie afzonderlijke bijdrages!

Annemieke Vlijm, Eyleen de Poel, Margot Müller, Aileen Dessing, Joshka Wolfs, en Kaat Houben: alhoewel jullie niet in mijn "team" zaten heb ik toch enorm van jullie aanwezigheid genoten. Dank jullie allemaal voor de prettige samenwerking en heel veel succes in jullie verdere carrière!

### *Collega's Technische Universiteit Eindhoven*

Stefan de Vries, jij was al begonnen aan dit project voordat ik kwam. Ik heb bewondering voor je inzet gedurende je PhD. Ik heb onze samenwerking, welke uiteindelijk heeft geresulteerd in een aantal gezamenlijke manuscripten, als zeer prettig ervaren.

Marina van Doeselaar, dank je wel voor je hulp bij het PCR-en van de bovine samples en je inbreng tijdens onze meetings.

### *Collega's Universitair Medisch Centrum Utrecht*

Laura Creemers, dank je voor al je advies tijdens onze werkbijeenkomsten, bij presentaties en manuscripten en het mogelijk maken dat we in dit project ook humane samples konden gebruiken. Dit alles heeft dit proefschrift naar een hoger niveau getild.

Anita Krouwels en Imke Jansen, dank jullie wel voor het denken aan onze groep wanneer er samples beschikbaar waren. We hebben mooie manuscripten kunnen maken dankzij jullie. Als laatste ook bedankt voor de gezelligheid tijdens binnen- en buitenlandse congressen!

Simon Mastbergen en Katja Coeeveld, heel erg bedankt voor het advies bij en uitvoeren van de sulfaat incorporatie assay. Middels deze resultaten werd weer een stukje van de NCM puzzel duidelijk.

#### *International colleagues*

Danny Chan and Daisuke Sakai, thank you so much for giving me the possibility to visit your labs. It was a great experience and resulted in three nice papers.

Joyce Zhang, thank you for showing me downtown Hong Kong and your lab. I had a lot of fun! Thank you for your hard work on the caveolin-1 and PTHrP/IHH paper.

Sagawa, Jordi Schol and all other people in the Hong Kong and Tokai lab, thank you for your guidance and kindness.

Karin Benz, thank you for sending us all the hydrogel components and instruction and our nice collaboration in the BMP, NCCM, and NCM work.

Fackson Mwale and Michael Grant, thank you for the nice collaboration on human and canine (short) Link-N. The results were not exactly as we wished for, but I hope you still appreciate the manuscript.

Christine Le Maitre, Abbey Thorpe, and Joseph Snuggs, thank you for your work on the PTHrP-IHH manuscript.

#### *Vrienden*

Berit en Floor, in 2009 begonnen wij gezamenlijk ons ET jaar. We zijn allemaal een andere kant op gegaan (letterlijk en figuurlijk), maar zijn elkaar altijd blijven opzoeken. Berit, jij bent inmiddels ook aan het promoveren (en specialiseren) en Floor, misschien dat jij ook nog ooit weer naar het onderzoek terugkeert? Ik zal je dan in ieder geval aanbevelen ☺. Ik wil jullie bedanken voor alle gezellige etentjes, logeerpartijtjes, high teas en wijntjes, waardoor ik de nodige stress kwijt kon en me weer op kon laden voor een nieuwe dag/week op het lab!

Dan de rest van de Wulpse Berggeiten: Marleen, Monique, Suzanne, Eline en Klaske, we zijn onze studie gezamenlijk begonnen en hebben altijd contact gehouden. Ook jullie appjes, gesprekken en bezoekjes hebben me goed gedaan deze jaren!

BMW vriendinnen: het duurde even, maar ook ik ben dan eindelijk gepromoveerd! Naar jullie goede voorbeeld (en ondanks jullie horrorverhalen) ben ook ik mijn PhD track begonnen. Carola, respect voor de manier waarop je jouw promotie hebt afgerond. Ik ben blij te zien dat je helemaal je draai gevonden hebt in je werk (met direct gehonoreerde subsidie aanvragen!) en in je appartementje in Malden. Bedankt voor de belangstelling in mij en mijn onderzoek, maar ook je ziekenbezoekje(s). Je bent een ware vriendin in goede en slechtere tijden.

Floor, ook fijn om te zien dat jij na je promotie helemaal goed terecht bent gekomen als ambtenaar ☺. Ook jouw advies heeft me erg geholpen!

Lian, ondanks dat jij nu als enige geen ware dokter bent ('slechts' een humane arts) mag je toch wel in onze groep blijven :P Nee, juist fijn dat we er ook iemand bij hebben die geen PhD heeft gedaan, want anders waren AL onze gesprekken daarop uitgedraaid. Dank voor de afwisselingen in onze gesprekken, daardoor konden wij ons eigen onderzoek (en het falen daarvan) ook wel weer relativeren: er was inderdaad niemand dood gegaan...

Sjoukje, wij zijn samen onze differentiatie coschappen ingegaan en zijn sindsdien vrienden geworden en gebleven. Fijn dat we contact zijn blijven houden en elkaar in ieder geval een paar maal per jaar zien. Gelukkig konden Rob en Rik het ook goed vinden en wonen we nu wat meer bij elkaar in de buurt!

### *Familie*

Ary, hartelijk dank voor het ontwerpen van de omslag!

Tim en Anouk *et al.*, dank jullie wel voor jullie nieuwjaarskoppelpoging waar ik niets van wist! Anouk wist natuurlijk dat ik mijn PhD niet in m'n eentje zou overleven en heeft gelukkig ingegrepen. Dank daarvoor en uiteraard ook voor de befaamde BMW BBQs die jullie (dacht ik) geïntroduceerd hebben.

Gerard en Elly, dank jullie wel voor alle interesse in de voortgang van mijn promotie. Helaas heb ik nog steeds geen directe oplossing voor de rugproblemen van Gerard, maar ik hoop toch dat jullie dit proefschrift kunnen waarderen.

Remy, Lysanne, Juliette, Kiri, Chloe, Denise, Sander, Odessa, Jeffrey en Samantha, bedankt voor alle bezoeken en familiedagen de afgelopen jaren, waardoor ik me op kon laden en er weer vol tegenaan kon gaan.

Erik, wat is het handig dat ik nu raad kan vragen aan een fysiotherapeut, o.a. voor vragen over humane ruggen. Fijn dat jij je bij onze familie hebt gevoegd en mijn moeder blij maakt!

Pap en mam, ik ben jullie eeuwig dankbaar dat jullie mij altijd hebben gestimuleerd in het nastreven van mijn doelen. Ik mocht gaan studeren wat ik wilde, als ik maar mijn best deed. Jullie hebben mij altijd gesteund in al mijn beslissingen: om na een jaar BMW alsnog diergeneeskunde te gaan doen, het extra HP jaar en mijn beslissing om alsnog te gaan promoveren. Het proefschrift is er uiteindelijk gekomen (na een omweg – het had in principe drie jaar sneller gekund door niet van studie te wisselen). Toch heb ik van elk (extra) jaar genoten en ik hoop dat jullie tevreden zijn met het eindresultaat.

Last but definitely not least: Rik! Wat een toeval dat wij elkaar leerden kennen op de avond voordat ik aan mijn PhD traject begon. Ik ben je dankbaar voor de onvoorwaardelijke steun in goede en slechte tijden vanaf dag één en voor het in lekentaal uitleggen aan anderen waar ik nou in hemelsnaam mee bezig ben geweest al die jaren. We make a great team!

## Curriculum vitae



Frances Bach was born on the 8<sup>th</sup> of November 1985 in Zwolle, the Netherlands. After graduating from secondary school (Pantarijn, Wageningen, the Netherlands) in 2004, she studied Biomedical Sciences at the Radboud University (Nijmegen, the Netherlands). After obtaining her propedeutic diploma in Biomedical Sciences in 2005, she studied Veterinary Medicine (Utrecht University, the Netherlands). During her veterinary training, she was selected for the students Honours Program (HP) year (2009-2010), and researched the paracrine feedback loop between PTHrP and vitamin D<sub>3</sub> in the growth plate under the supervision of Dr. Marianna Tryfonidou (Faculty of Veterinary Medicine, Utrecht University, the Netherlands). After obtaining her veterinary degree in 2012, Frances started her PhD on intervertebral disc

regeneration under the supervision of Prof. Dr. Björn Meij (Utrecht University, the Netherlands) and Prof. Dr. Keita Ito (Eindhoven University of Technology, the Netherlands and University Medical Center Utrecht, the Netherlands). During her PhD project, she supervised about 15 master students and was a Veterinary PhD Council (2013-2016) and Veterinary Science Day board member (2015-2016). Additionally, she visited the laboratory of Prof. Dr. Danny Chan (Department of Biochemistry, The University of Hong Kong, China) and Prof. Dr. Daisuke Sakai (Department of Orthopedic Surgery, Tokai University School of Medicine, Japan), which resulted in three joint manuscripts. The work described in this thesis was presented by Frances at several national and international conferences. In April 2016, she won the award for best short talk at the World Forum for Spine Research (WFSR) of the Global Spine Congress in Dubai (UAE). In October 2017, she won the poster award at the 4<sup>th</sup> International Spine Research Symposium (Orthopaedic Research Society) in Philadelphia (USA). Currently, she continues her research at the Faculty of Veterinary Medicine (Utrecht University, the Netherlands).

